Different Mechanistic Aspects of Photoredox Catalysis and Its Application in Organic Transformations

विद्या वाचस्पति की
उपाधि की अपेक्षाओं की आंशिक पूर्ति में प्रस्तुत शोध प्रबंध

A thesis submitted in partial fulfillment of the requirements of the degree of Doctor of Philosophy

द्वारा / By

अनिंदिता भौमिक

Anindita Bhowmick

पंजीकरण सं. / Registration No.:

20183590

शोध प्रबंध पर्यवेक्षक / Thesis Supervisor:

Prof. Ramakrishna G. Bhat



भारतीय विज्ञान शिक्षा एवं अनुसंधान संस्थान पुणे

INDIAN INSTITUTE OF SCIENCE EDUCATION AND RESEARCH PUNE

2024

This thesis is dedicated to...

Ma, Baba,

Prakash, and

Family

भारतीय विज्ञान शिक्षा एवं अनुसंधान संस्थान पुणे
INDIAN INSTITUTE OF SCIENCE EDUCATION AND RESEARCH PUNE
IISER PUNE
An Autonomous Institution of the Ministry of Education, Govt. of India

Dr. Ramakrishna G. Bhat
Professor
Department of Chemistry
IISER Pune

CERTIFICATE

This is to certify that the research work incorporated in this thesis entitled ***"Different Mechanistic Aspects of Photoredox Catalysis and Its Application in Organic Transformations"*** submitted by **Anindita Bhowmick** and the research was carried out by the candidate at Indian Institute of Science Education and Research (IISER), Pune, under my supervision. The work presented here or any part of it has not been included in any other thesis submitted previously for the award of any degree or diploma from any other University or institution.

Date: 26/12/2023
Place: Pune (Maharashtra)

Prof. Ramakrishna G. Bhat
(Research supervisor)

rgb@iiserpune.ac.in • Ph: +91-20-25908092 • Fax: +91-20-25898022

DECLARATION

I declare that, this written submission represents my ideas in my own words and where others' ideas have been included; I have adequately cited and referenced the original sources. I also declare that I have adhered to all principles of academic honesty and integrity and have not misrepresented or fabricated or falsified any idea/data/fact/ source in my submission. I understand that violation of the above will be cause for disciplinary action by the Institute and can also evoke penal action from the sources which have thus not been properly cited or from whom proper permission has not been taken when needed.

Anindita Bhowmick.

Date: 26/12/2023.

Anindita Bhowmick

Place: Pune

(ID: 20183590)

Acknowledgements

I would like to extend my heartfelt gratitude and appreciation to Prof. Ramakrishna G. Bhat, my thesis supervisor, for his exceptional supervision, encouragement, and guidance throughout my doctoral research tenure. I am indebted to him for believing in my capabilities and allowing me the freedom to work independently during my Ph.D. His invaluable advice and suggestions while crafting my thesis, research papers, and preparing scientific presentations have been instrumental. I greatly admire his lessons on fostering independent thinking, honing soft skills, striving for perfection, and more, all of which have significantly contributed to shaping me as a researcher.

Beyond the realm of science, engaging in discussions about various historical events with him has been a fantastic experience. I am consistently amazed by his profound knowledge of literature and scripture. I consider myself extremely fortunate to have him as my advisor, and I appreciate the opportunity he provided me to work under his guidance. Finding the right words to convey my gratitude for his mentorship and keen interest, which made this work possible, is indeed a challenge.

I extend my sincere acknowledgment to Prof. Jayant B. Udgaonkar (Former Director, IISER-Pune) and Prof. Sunil S. Bhagwat (Director, IISER Pune) for furnishing outstanding infrastructure and cutting-edge research facilities at IISER-Pune, enabling me to conduct my doctoral research.

I express my gratitude to Prof. M. Jayakannan (Former Chair, Department of Chemistry, IISER Pune), Prof. Hosahudya N. Gopi (Former Chair, Department of Chemistry, IISER Pune), and Prof. Nirmalya Ballav (Chair of the Department of Chemistry, IISER Pune) for providing exceptional infrastructure and fostering a conducive research environment within the department.

I am very grateful to my research advisory committee (RAC) members Prof. V. G. Anand (IISER Pune) and Dr. J. Nithyanandhan (NCL-, Pune) for their valuable suggestions and feedback during RAC evaluations. I thank Prof. Srinivas Hotha and all faculty members of chemistry department for the valuable suggestion and discussions.

I take immense pleasure in expressing my gratitude to all the members of the laboratory. I extend my thanks to my senior colleagues, Dr. Tushar Khopade, Dr. Trimbak Mete, Dr. Rajesh, and Dr. Balu Navale, for their support and assistance at the commencement of my Ph.D. I also wish to acknowledge the post-doctoral project fellows, specifically Dr. Chennakesava Reddy, for engaging in both scientific and cultural discussions.

My sincere and heartfelt thanks go to Dr. Pankaj Dharpure, under whose guidance I completed my preliminary research and laboratory training. Working with him was always motivating, and I felt consistently encouraged. I am also grateful to Dr. Prakash Warghude, whose support and guidance proved invaluable throughout my Ph.D. His imparted skills, knowledge, and attitude will undoubtedly benefit me throughout my life. It was an honor to collaborate with him.

I feel fortunate to have shared moments with Dr. Vikas Khade (a gracious senior), Debasish (an excellent friend and a perfectionist), Javed (an inspiring personality), Abhijeet (a steadfast friend who is always there in any circumstances), Kajal (an intelligent and hardworking individual), Mousumi (a considerate and pure soul), Onkar (remarkably efficient, more like a brother), Sidharth (helpful, kind, and pure-hearted), Nitin (intelligent and hardworking), Saswata (smart and enthusiastic), Chhabi (adorable and lovable), Ganesh (smart and intelligent), Ajit (smart and well-behaved), Sachin (a great supportive person).

Their friendly discussions and unwavering support added joy to this journey, making it both memorable and enjoyable. A special mention goes to Sidharth for his assistance during my crucial research phases. I fondly recall the cheerful moments shared with energetic and high-spirited junior Shubhayan (i-PhD alumnus).

I extend my appreciation to the technical staff for their assistance in accessing various instruments: Mr. Ravinder and Mr. Parven Nasa (SCXRD), Dr. Sandeep Kanade (HRMS), Mr. Nitin Dalvi, Dr. Sandeep, Mr. Karan (NMR), and Mr. Mahesh Jadhav (HPLC). Gratitude is also owed to the entire IT department for their ongoing support. Special thanks go to Dr. V. S. Rao, Mr. Mayuresh Kulkarni, Mr. Tusharr Kulkarni, Ms. Dipali Dalvi, and the Dean of the Doctoral Studies Office for addressing academic and fellowship-related concerns.

I express my thanks to every individual in the administrative department, chemistry office staff, technical staff, security staff, and housekeeping for their invaluable assistance.

I express my gratitude to the Council of Scientific and Industrial Research (CSIR) and IISER-Pune for their provision of a research fellowship throughout the entirety of my research work. Additionally, I would like to appreciate DST-SERB and Infosys for granting the international travel support for attending an international conference.

I enjoyed wonderful moments with my friends at IISER, including Sarupa (A wonderful, intelligent, and supportive sister who graciously tolerates my tantrums) and Writakshi (friend who feel like family), Pulak (akin to a brother), Shankhajit (a lovable and adorable brother), and Dr. Ganesh Shinde (my companion for movies and tea), as well as the

entire chemistry department. I am grateful to Mr. Abhijit Chaterjee for his assistance in conducting mechanistic studies.

I have cherished and shared life experiences with my closest friends Madhumita, Lisha, Sayani, and Mampa. A heartfelt thanks goes to Biswadeep Majumder for being a steadfast presence during challenging phases of my life. Expressing gratitude to Mrs. Savita Basak, Mr. Arun Basak, and Mr. Ritabrota Basak is beyond mere words, as they have been like family, providing unwavering care and support for me. I would like to acknowledge Rakhi Di, my school teacher for her guidance and love.

I consider myself fortunate to have Prakash Warghude as not only my best friend but also my life partner. I am grateful for the care and support he extends, even amidst his demanding research schedule. His presence has consistently contributed to my calm and mature demeanor, and he remains a constant source of support through all the highs and lows. I am confident that we will continue to care for and support each other in all the stages of our future life.

Expressing my deepest gratitude for the blessings, love, and motivation from my parents (Mrs. Papiya Bhowmick, Mr. Arjun Bhowmick, Smt. Parwati Warghude, and Shri. Kashinath Warghude) and other family members, including Mrs. Nilima Mukherjee, Mrs. Rajlaxmi Bhowmick, Mr. Goutam Mukherjee, Mrs. Nupur Mukherjee, Mr. Biswanath Mukherjee, Mrs. Sandhya Mukherjee, Mrs. Shibani Banerjee, Mrs. Bhabani Bhowmick, Mrs. Shima Basak, Raja, Subrata (my spirited brother), Shreyasi, Rupsa (my lovely and spirited sister), Rohit, and Pritha. Their unconditional emotional support, encouragement, trust, patience, and sacrifices have been instrumental in making this journey possible. They are the primary reason and inspiration behind every success I have achieved and will continue to achieve in my future endeavors.

I extend my acknowledgment to those individuals whose names may have been inadvertently omitted, even though they provided unconditional assistance throughout my Ph.D. tenure. I always believe in following lines:

"Life is very interesting… In the end, some of your greatest pains, become your greatest streangths." *- Drew Barrymore*

Finally, I thank the almighty God for giving this wonderful life full of opportunities

Anindita Bhowmick

CONTENT

Contents……i

Abbreviations……..vi

Synopsis…….x

List of Publications……..…xxvi

Chapter 1: Photoredox Catalysis: Historical Evolution and Fundamental Mechanistic Pathways

1.1. General introduction to photoredox catalysis……...1

1.2. History of photoredox catalysis……....2

1.3. Mechanistic aspects of photoredox catalysis……....6

1.3.1. Single Electron Transfer (SET) catalysis……6

1.3.2. Hydrogen Atom Transfer (HAT) catalysis……..…11

1.3.3. Consecutive Photoinduced Electron Transfer (ConPET) catalysis……14

1.3.4. Reaction triggered by visible light in the absence of a photocatalyst……18

1.3.5. Visible light induced Electron Donor-Acceptor (EDA) Complex…….23

1.4. Conclusions……...…27

1.5. References……..28

Chapter 2: Direct Access to α-Acyloxy carbonyl Compounds and Esters via Oxidative Esterification of Aldehydes under Visible Light

2.1. Introduction……32

2.2. Previous work of esterification of aldehydes……..33

2.3. Our hypothesis and optimization of esterification……..…..35

2.4. Results and discussion……38

2.5. Control experiments and mechanistic study……..…..43

2.6. Conclusions…….……48

2.7. Experimental Section……..…49

2.7.1. General Information……49

2.7.2. Mechanistic study……49
2.7.2.1. Fluorescence Quenching Experiment……49
2.7.2.2. Control Experiments……51
2.7.3. General Procedure for the synthesis of α–acyloxy carbonyl compounds……53
2.7.4. Gram Scale Synthesis……54
2.7.5. Experimental data……55
2.8. Appendix II: ^{1}H, ^{13}C spectral data of representative compounds……70
2.9. References……79

Chapter 3: Visible Light Promoted Metal-Free Sustainable Reduction of α-Alkylidene Oxindoles/Succinimides

3.1. Introduction……82
3.2. Previous methods for the hydrogenation of different electron deficient alkene……84
3.3. Our hypothesis and optimization of hydrogenation of electron deficient alkenes……85
3.4. Results and discussion……88
3.5. Control experiments and mechanistic study……93
3.6. Conclusions……97
3.7. Experimental section……98
3.7.1. General information……98
3.7.2. Mechanistic study……99
3.7.2.1. Fluorescence Quenching Experiment……99
3.7.2.2. Stern-Volmer plot……100
3.7.2.3. Cyclic voltammetry (CV)…… 101
3.7.2.4. Radical trapping experiment…… 101
3.7.3. General procedure for the reduction of electron deficient alkenes……102
3.7.4. General procedure for the reduction of 1a in gram scale……102
3.7.5. Experimental data……104
3.8. Appendix III: ^{1}H, ^{13}C and ^{19}F spectra of representative compounds……121
3.9. References……128

Chapter 4: Synthesis of industrially significant glutaric acid diesters from aldehydes via sequential Giese-type addition under visible light illumination

4.1. Introduction……132
4.2. Previous report on the synthesis of dicarbonyl compound……..…133
4.3. Our hypothesis and optimization of glutaric acid diester synthesis……...……136
4.4. Results and discussion……...…139
4.5. Control experiments and mechanistic study……....…143
4.6. Conclusions……...…150
4.7. Experimental section…….…...151
4.7.1. General information……...…...151
4.7.2. General procedure for the synthesis of 3 (GP1)……..…….....151
4.7.3. General procedure for the synthesis of 3 under sunlight…….……152
4.7.4. Control Experiments……....153
4.7.4.1. Procedure for the preparation of 3f-D…….153
4.7.4.2. Procedure for the preparation of 3a-D_2……154
4.7.4.3. Procedure for the reaction using TEMPO……155
4.7.4.4. Procedure for the reaction using DMSO-D6……155
4.7.5. Procedure for the gram scale synthesis of 3a……...156
4.7.6. Mechanistic study……157
4.7.6.1. Fluorescence Quenching Experiment and Stern-Volmer plot……..157
4.7.6.2. UV-Visible absorption of Eosin Y and reaction mixture……..162
4.7.6.3. pH study of the reaction mixture during the course of the reaction…….163
4.8. Optimization table……164
4.9. Undesired transformation……165
4.10. Light Switch ON/OFF Experiment……..166
4.11. Quantum yield calculation of 3f……...167
4.12. NMR data of reaction of 2a and 1a in D_2O (3a-D_2)……169
4.13. Experimental data……170
4.14. Appendix IV: ^{1}H, ^{13}C and 2D spectral data of representative compounds……..193
4.15. References……212

Chapter 5: Photocatalyst-Free Visible Light Driven Synthesis of Anthranilic Acid and Quinoline Derivatives from 2-Phenylindole

5.1. Introduction……..….216
5.2. Results and discussion……218
5.3. Control experiments……...226
5.4. Conclusions……..…... 235
5.5. Experimental section……...…236
5.5.1. General information……...…..236
5.5.2. General procedure for the synthesis of 2 (GP1)……...…236
5.5.3. General procedure for the synthesis of 4 (GP2)……237
5.5.4. General procedure for the synthesis of 5 (GP3)…….…...…237
5.5.5. Procedure for the gram scale synthesis of 2a……237
5.5.6. Procedure for the synthesis of 2a under sunlight…….……..238
5.5.7. Optimisation table……238
5.5.7.1. Optimisation table for the synthesis of 4……..……238
5.5.7.1.1. Light optimisation table……..……239
5.5.7.1.2. Solvent optimisation table……..…….239
5.5.7.2. Optimisation table for the synthesis of quinoline derivative 5……240
5.5.7.2.1. Light optimisation table…….…240
5.5.7.2.2. Base optimisation table……...…240
5.5.7.2.3. Electrolyte optimisation table…….……241
5.5.7.2.4. Electrolyte mol% optimisation table……...…242
5.5.7.2.5. Control optimisation table……...…242
5.5.8. Control Experiments for the synthesis of anthranilic acid derivatives……243
5.5.8.1. Procedure for the radical quenching experiments with TEMPO……243
5.5.8.2. Procedure for the singlet oxygen quenching experiments……...…234
5.5.8.3. Procedure for the singlet oxygen trapping experiments……245
5.5.8.3.1. Oxygen trapping reaction with 9,10-Dimethylanthracene……..……245
5.5.8.3.2. Oxygen trapping reaction with 1,3-Diphenylisobenzofuran……..…245
5.5.8.4. Procedure for the detection of H_2O_2……..……246

5.5.9. Mechanistic study……..……247
5.5.9.1. UV-Visible experiment of the reaction mixture of the anthranilic acid derivatives…….……247
5.5.9.2. EPR Study……....248
5.5.10. Control Experiments for the synthesis of quinoline derivatives……...249
5.5.10.1. Procedure for the radical quenching experiments with TEMPO……..249
5.5.10.2. Procedure for the radical quenching experiments with BHT……..….250
5.5.10.3. Procedure for the generation and trapping of singlet carbene……...…251
5.5.10.4. Procedure for the NMR study…….……..…252
5.5.10.5. UV-Visible experiments of reaction mixture of the quinoline derivatives……..253
5.6. Experimental data…….……254
5.7. Appendix V: ^{1}H, ^{13}C spectral data of representative compounds……...…270
5.8. References……..……277

Summary……..……..……280

******

List of Abbreviations

Å	angstrom (s)
ACN	acetonitrile
Ag	argentums (Silver)
Ar	aryl
Ar-atm	Argon atmosphere
β-ICD	beta-isocupreidine
BHT	butylated hydroxytoluene
Bn	benzyl
^{t}Boc	*tert*-butoxycarbonyl
bs	broad singlet
C	carbon
°C	degree Celsius
Calcd.	calculated
Cat.	catalytic
ConPET	Consecutive Photoelectron Transfer
Cm^{-1}	wavenumber(s)
CV	Cyclic Voltametry
Cu	copper
d	day (s); doublet (spectral)
DCC	*N, N'*-dicyclohexylcarbodiimide
DCM	dichloromethane
dd	doublet of doublet
DABCO	1,4-diazabicyclo[2.2.2]octane
DBU	1,8-diazabicyclo(5.4.0)undec-7-ene
DFT	density functional theory
DMAP	*N*, *N'*-dimethylaminopyridine
DIPEA	*N*, *N*-diisopropylethylamine
DMF	dimethylformamide
DMSO	dimethylsulfoxide
dr	diastereomeric ratio

ee	enantiomeric excess
E	electrophile
equiv.	equivalent
EDA	Electron Donor-Acceptor
EnT	Energy transfer
EPR	Electron paramagnetic resonance
ESI	electrospray ionisation
EtOAc	ethyl acetate
EWG	electron withdrawing group
g	gram(s)
FTIR	fourier transform infrared
H	hydrogen
h	hour(s)
HAT	Hydrogen Atom Transfer
HPLC	high performance liquid chromatography
HRMS	high resolution mass spectrometry
Hz	hertz
^{i}Pr	isopropyl
J	Spin coupling constant
kcal	kilocalories
KBr	Potassium bromide
LEDs	light emitting diodes
M	multiplet (spectral)
m	meta
M	molar (mol L^{-1})
m/z	mass- to-charge ratio
Me	methyl
mg	milligram
min	minute(s)
mL	millilitres
mmL	microlitre
MS	molecular seives
mmol	millimole
mol	mole

m.p.	melting point
MTBE	methyl tert-butyl ether
N	nitrogen
Na	Sodium
NaN_3	Sodium azide
nEt_4NCl	Tetraethyl ammonium chloride
nBu_4NBr	Tetrabutyl ammonium bromide
NBS	N-bromosuccinimide
NMR	nuclear magnetic resonance
Nu	nucleophile
O	oxygen
o	ortho
p	para
P	phosphorus
PC	Photo-Catalyst
PCET	Proton-coupled electron transfer
PET	Photoinduced Electron Transfer
Ph	phenyl
ppm	parts per million
q	quartet
R_f	retention factor
rt	room temperature
S	sulphur
s	singlet (NMR)
SET	Single Electron transfer
t	triplet (NMR)
t-, tert-	tertiary (branched alkyl chain)
TCCA	Trichloroisocyanuric acid
Ti	Titanium
td	triplet of doublet
TEMP	2,2,6,6-Tetramethylpiperidine
TEMPO	2,2,6,6-Tetramethylpiperidin-1-yl)oxyl
TFA	Trifluoroacetic acid

THF	tetrahydrofuran
TPPT	2,4,6-triphenylpyrilium tetrafluoroborate
TLC	thin-layer chromatography
TMS	trimethylsilyl
TS	transition state
UV	ultraviolet
X	heteroatom
XRD	X-ray diffraction
W	Watt
δ	chemical shift in ppm downfield from trimethylsilane

SYNOPSIS

*The thesis entitled as "**Different Mechanistic Aspects of Photoredox Catalysis and Its Application in Organic Transformations**" comprises of five main chapters.*

CHAPTER 1: Photoredox Catalysis: Historical Evolution and Fundamental Mechanistic Pathways

In this introductory chapter, we have provided a concise introduction to various mechanistic aspects of photoredox catalysis and its utilization in the realm of organic synthesis driven by visible light. Photoredox catalysis is a form of catalytic process that harnesses the energy from light sources to facilitate redox chemical reactions in a catalytic manner. Photoredox catalysis triggered by visible light has rapidly risen to prominence as one of the most rapidly evolving fields in the realm of organic synthesis. In this process, a photoactive catalyst typically absorbs visible light and participates in single electron transfer interactions with organic substrates. This approach is characterized by its mildness, cost-effectiveness, and environmentally friendly nature, making it an efficient method for promoting radical-mediated organic transformations and potentially discovering innovative reaction pathways.

The mechanism of photoredox catalysis can vary depending on multiple factors, including differences in redox potential, reaction conditions, choice of solvents, bond dissociation energy, the pH of the reaction environment, and the type of catalyst utilized in the reaction medium.

Reactions carried out using visible light can be classified into two main categories based on their catalyst requirements.

i) Photoredox catalysis reaction in presence of photocatalyst
ii) Photoredox catalysis reaction in absence of photocatalyst.

In presence of photocatalyst the reaction traditionally follows different mechanistic pathway.

a) Single electron transfer (SET) catalysis
b) Hydrogen atom transfer (HAT) catalysis
c) Consecutive photoinduced electron transfer (ConPET) catalysis

a) Single electron transfer (SET) catalysis can be divided into two categories depending upon the difference between the redox potential of the starting materials and photocatalysts.

Reductive quenching cycle and ***Oxidative quenching cycle***

In the context of photocatalysis under visible light, the behavior of the excited state of a photocatalyst can be categorized into two main processes, depending on the role of a suitable reagent present in the reaction medium.

Reductive Quenching Cycle:

In the reductive quenching cycle, the excited state of the photocatalyst is effectively deactivated when it accepts an electron from a suitable reagent in the reaction medium. This electron transfer process occurs through a single electron transfer mechanism, where the reagent donates an electron to the photocatalyst in its excited state. As a result, the photocatalyst returns to its ground state. This process is called "reductive" because the excited state is reduced by gaining an electron.

Oxidative Quenching Cycle:

Conversely, in the oxidative quenching cycle, the excited state of the photocatalyst is quenched by a suitable reagent through a single electron transfer mechanism where the reagent accepts an electron from the photocatalyst in its excited state. This electron transfer causes the photocatalyst to return to its ground state. It is termed "oxidative" because the excited state of the photocatalyst gets oxidized as it loses an electron.

Both of these pathways are highly dependent on the difference in redox potential between the interactive substances involved. This redox potential difference plays a crucial role in governing the direction of electron transfer, either from the photocatalyst to the reagent (oxidative quenching) or from the reagent to the photocatalyst (reductive quenching), and ultimately influences the outcome of the photocatalytic reaction.

b) Hydrogen atom transfer (HAT) catalysis

The concept of hydrogen atom transfer (HAT) involves a coordinated mechanism that transfers both a proton and an electron. This transfer occurs from a donor (Y•) to an acceptor (X•) [$Y\bullet + H-X \rightarrow Y-H + X\bullet$], and it plays a vital role in a broader category known as proton-coupled electron transfer (PCET). PCET encompasses processes that involve the simultaneous movement of at least one electron and one proton.

For over a century, research has emphasized the significance of HAT in various processes, including hydrocarbon combustion, atmospheric chemistry, oxidative degradation, and catalysis. The presence of R-H bonds (where R can be C, Si, etc.) in organic compounds makes direct functionalization of these bonds an innovative approach to building and modifying complex molecules. In this context, intermolecular HAT is noteworthy as it enables

the direct activation of R-H bonds, eliminating the need for pre-functionalization or the use of directing groups. This method is highly efficient in terms of atom usage and provides an economical approach for R-H functionalization.Compared to photoinduced single electron transfer (SET) catalysis, photoinduced HAT has the advantage of not being limited by the redox potentials of the substrates. In a broader sense, HAT catalysis can drive organic transformations by involving a crucial step of either hydrogen atom abstraction or donation.

c) Consecutive photoinduced electron transfer (ConPET) catalysis

The concept of Consecutive Photoinduced Electron Transfer (ConPET) revolves around the formation of a highly reducing radical anion or anionic form of a photocatalyst in real-time. When this species is exposed to photoexcitation, it undergoes a transformation into an exceptionally powerful reducing chemical entity. This newly formed species possesses the unique capability to trigger the activation of substrates that require extremely negative reduction potentials, a capability that goes beyond what traditional photocatalysts can achieve. In simpler terms, Consecutive Photoinduced Electron Transfer (ConPET) involves creating a photocatalyst that, when exposed to light, transforms into an extremely powerful reducing agent. This agent can then activate substrates that demand exceptionally strong reducing conditions, surpassing the capabilities of standard photocatalysts.

In absence of photocatalyst the reaction traditionally follows different mechanistic pathway.

a) Taking advantage of the potential of visible light to initiate chemical reactions through suitable photocatalysts is an appealing strategy, primarily due to the environmentally friendly nature of visible light. However, the photoredox catalysts commonly used in such processes often come with high costs and potential safety concerns. Additionally, these catalysts tend to degrade when exposed to light for extended periods, leading to complex procedures for their removal or recovery from reaction mixtures.

   An innovative solution to address these issues involves a photocatalyst-free approach to visible light-mediated synthesis. This approach offers the advantage of using visible light for chemical transformations with reduced expenses and minimized environmental impact. It has been gaining momentum steadily, offering significant potential for groundbreaking advancements in the field. One strategy to eliminate the need for external photosensitizers involves directly incorporating a visible-light-absorbing functional group, often referred to as a "dyed auxiliary group," into the starting material.

b) ***Electron donor-acceptor (EDA) complex***: A significant method for achieving visible light-driven reactions without relying on a photocatalyst is through Electron Donor Acceptor (EDA) complexes. These complexes form when an electron-rich molecule (the donor, D) interacts with an electron-poor molecule (the acceptor, A) in their lowest energy state. EDA complexes can absorb visible light and facilitate electron transfer, even without a photocatalyst.

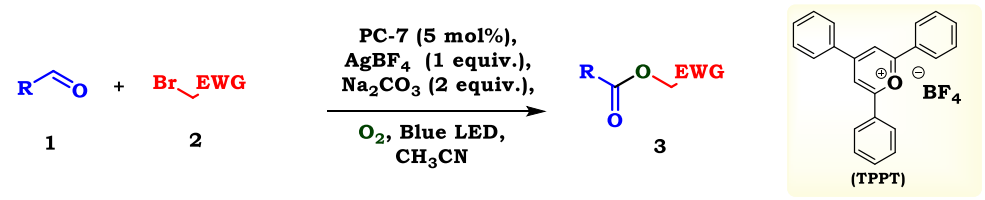
This process is adaptable to various reaction conditions. It involves a donor molecule (D), with electron-rich properties, acting as a reducing agent or nucleophile, and an acceptor molecule (A), with electron-poor attributes, serving as an oxidizing agent or electrophile. These molecules readily combine to create an initial complex known as [D, A] EDA, which is a reversible and transient association occurring in the ground state.

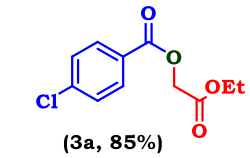
These interactions are more sensitive to changes in factors like temperature, solvent, and concentration compared to stronger interactions like hydrogen bonding. This sensitivity results in the appearance of a distinct absorption band called the charge-transfer band, which often shifts into the visible light range, giving the complex a characteristic color.

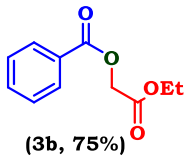
When illuminated with light matching its charge-transfer (CT) band, the [D, A] EDA complex transforms into a reactive excited complex ([D, A]*), initiating an electron-transfer process. This process leads to the formation of a radical ion pair ($[D^{\bullet+}, A^{\bullet-}]_{SOLV}$) within the surrounding solvent. The radical ion pair can follow various pathways, such as escaping the solvent cage to generate independent free radical ions or engaging in a reverse electron-transfer event.

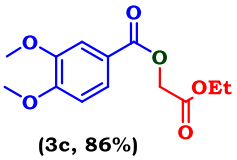
CHAPTER 2: Direct Access to α-Acyloxycarbonyl Compounds and Esters via Oxidative Esterification of Aldehydes Under Visible Light

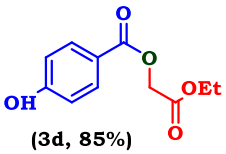
In this chapter, we detail the establishment of a highly effective method for synthesizing α–acyloxycarbonyl compounds and esters. This method directly starts from aldehydes(aromatic as well as aliphatic) **1** and α–bromoalkyl compounds **2**, benzyl bromide

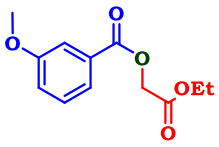


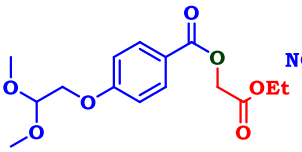

(3a, 85%)

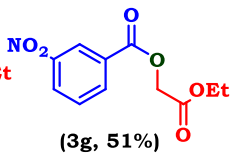

(3b, 75%)

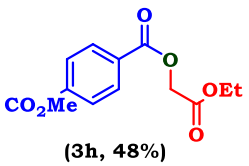

(3c, 86%)

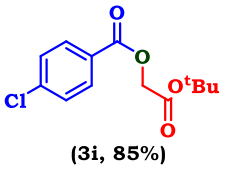

(3d, 85%)

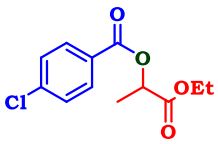

(3e, 81%)

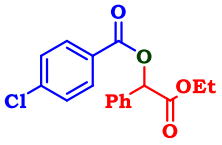

(3f, 52%)

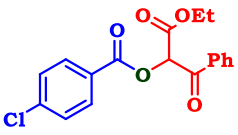

(3g, 51%)

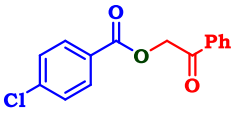

(3h, 48%)

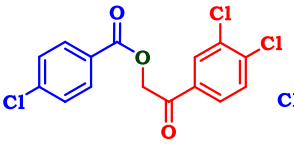

(3i, 85%)

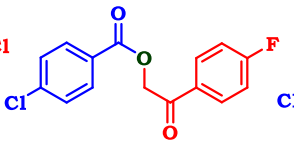

(3j, 82%)

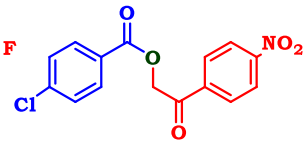

(3k, 70%)

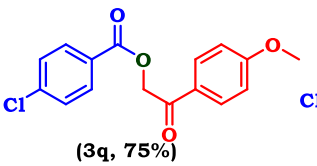

(3l, 56%)

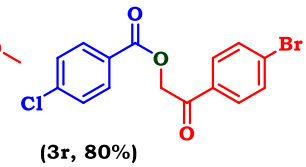

(3m, 74%)

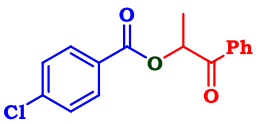

(3n, 85%)

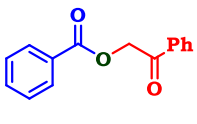

(3o, 90%)

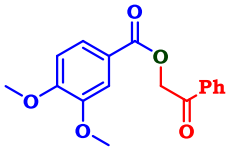

(3p, 91%)

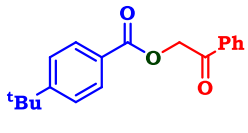

(3q, 75%)

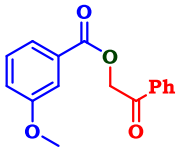

(3r, 80%)

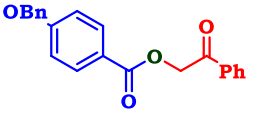

(3s, 90%)

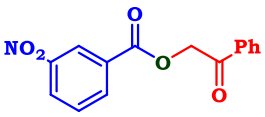

(3t, 80%)

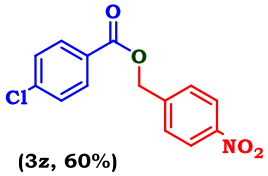

(3u, 90%)

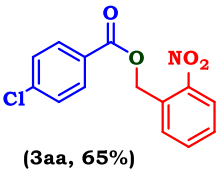

(3v, 86%)

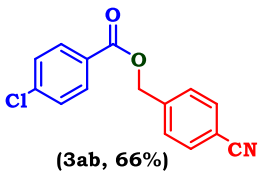

(3w, 90%)

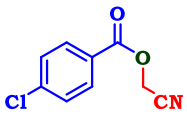

(3x, 87%)

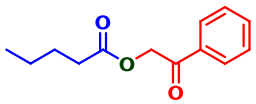

(3y, 65%)

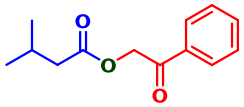

(3z, 60%)

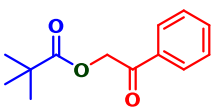

(3aa, 65%)

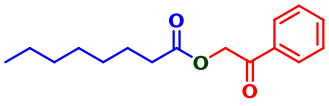

(3ab, 66%)

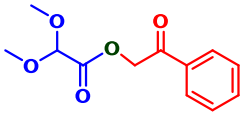

(3ac, 42%)


(3ad, 84%)


(3ae, 87%)


(3af, 85%)


(3ag, 88%)


(3ah, 40%)

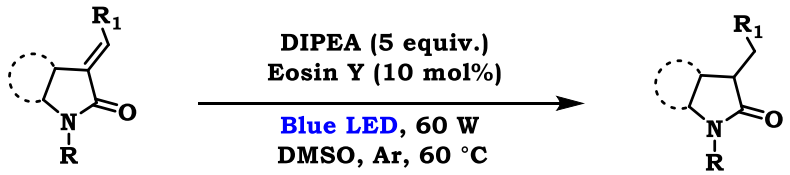
derivatives **2**, and bromo nitriles **2**. It leverages an organic photocatalyst in conjunction with silver tetrafluoroborate under visible light at room temperature. The chapter commences with a concise overview of the significance of α–acyloxycarbonyl compounds and esters, along with a discussion of a few notable approaches for their synthesis. These compounds are prevalent in various natural products and bioactive molecules. Given the substantial importance of α–acyloxycarbonyl compounds and esters, extensive efforts have been made to synthesize them through various routes. Although there are a few scarce references in the literature regarding the visible light-mediated esterification of aldehydes, it's worth highlighting that, as far as we know, the direct synthesis of α–acyloxycarbonyl compounds from aldehydes under visible light conditions has not been previously accomplished. In this regard, we reported the direct synthesis of various α–acyloxycarbonyl compounds and esters **3**, commencing from aldehydes **1** and α–bromoalkyl derivative **2** under visible light conditions. Having obtained the optimized protocol in hand, the scope esterification reaction was investigated by the different combination of various substituted aldehydes (**1a-1h**) and α–bromoethylacetate **2a** to afford the corresponding α–acyloxycarbonyl derivatives (**3a-3h**) (Table 2.1). Further, keeping the **1a** constant we have changed the α–bromoalkyl group (**2b-2v**) to derived the corresponding desired derivative (**3i-3ac**). And further we have explored aliphatic aldehydes (**1i-1m**) with **2f** to get the corresponding α–acyloxycarbonyl derivatives (**3ad-3ah**). Further we have performed mechanistic study and controlled experiments for the protocol. And based on that we have derived a plausible mechanism which follows reductive quenching photocatalytic cycle.

In summary, we have efficiently synthesized α–acyloxycarbonyl compounds and esters directly from aldehydes using visible light. This method is versatile, accommodating various functional groups and both aromatic and aliphatic aldehydes. We have synthesized a total of 34 of derivatives and the most plausible mechanism has been established based on several control experiments.

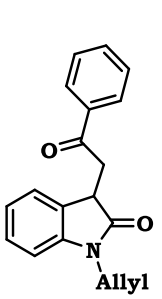
CHAPTER 3: Visible Light Promoted Metal-Free Sustainable Reduction of α-alkylidene Oxindoles/Succinimides

In this chapter, we have achieved a chemical reaction that selectively reduces activated double bonds using visible light, all without the need for metal catalysts. This was made possible through the use of photoredox catalysis, with Eosin Y serving as a highly effective catalyst. Specifically, we focused on reducing C-C double bonds in alkylidene oxindoles and succinimides under visible light. To facilitate this transformation, we employed DIPEA, a readily available compound, as a sacrificial electron donor. During the reaction, DIPEA's in-situ generated cationic radical acts as a reductant, enabling the process to take place. This method offers a promising and environmentally friendly approach to chemical transformations. Electron-deficient carbon-carbon double bond compounds, particularly α-alkylidene oxindoles and succinimides, are versatile precursors in organic synthesis, contributing to the production of numerous natural products and bioactive molecules. Hydrogenation of unsaturated organic compounds represents a fundamental and crucial process in organic synthesis. This indispensable transformation has found widespread utility in various industries, including chemistry, biochemistry, food production, agrochemicals, polymers, and pharmaceuticals. Achieving the selective hydrogenation of an electron deficient carbon-carbon double bond within a molecule is a particularly demanding and challenging task. While prior reports exist regarding the hydrogenation of α-alkylidene oxindoles and succinimides, no previous method has been established to accomplish the hydrogenation of both the α-alkylidene oxindoles and succinimides within a single protocol. Additionally, all of these methods relied on the use of metal catalysts, strong bases, or high-pressure hydrogen gas. The practicality of these approaches is limited due to their harsh reaction conditions and associated safety concerns. In this work, we presented a sustainable reduction method for activated C-C double bonds in α-alkylidene oxindoles and succinimides (**4**). This process is entirely free of metal catalysts and makes use of visible light, with DIPEA serving as both a sacrificial electron donor and a reducing agent, alongside Eosin Y as the photocatalyst.

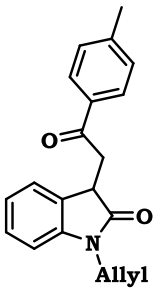
Table 3.1: Hydrogenation of α-alkylidene oxindole derivative es.



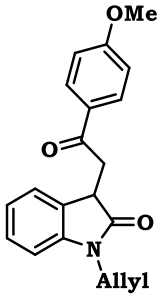
Reduction of α-akylidene oxindole derivatives



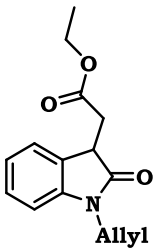
5a (75%)



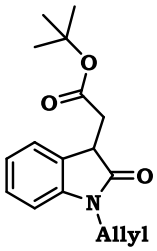
5b (80%)



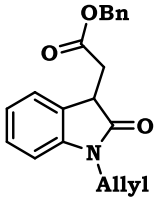
5c (81%)



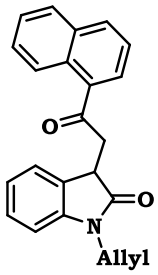
5d (80%)



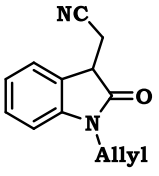
5e (78%)



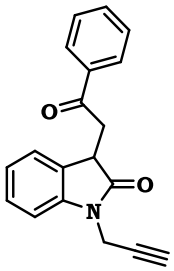
5f (82%)



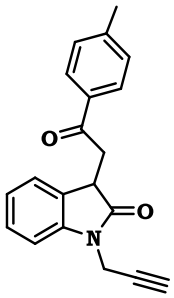
5g (80%)



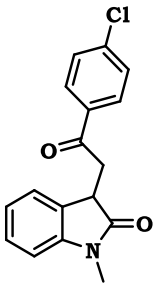
5h (74%)



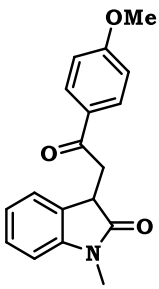
5i (77%)



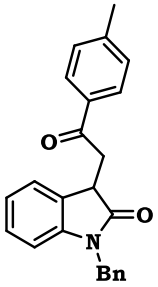
5j (79%)



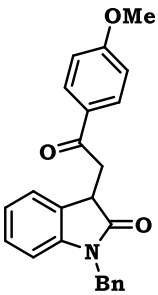
5k (61%)



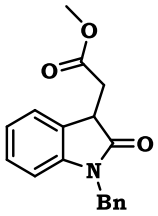
5l (72%)



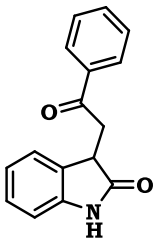
5m (81%)



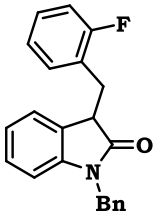
5n (78%)



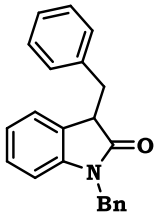
5o (75%)



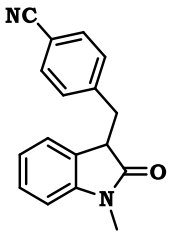
5p (76%)



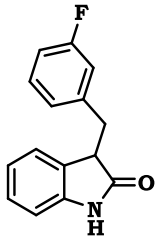
5q (70%)



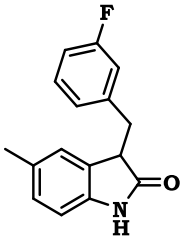
5r (70%)



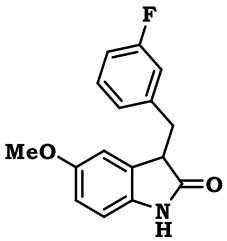
5s (50%)



5t (68%)



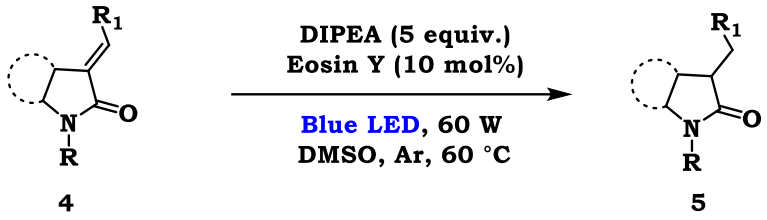
5u (60%)



5v (52%)

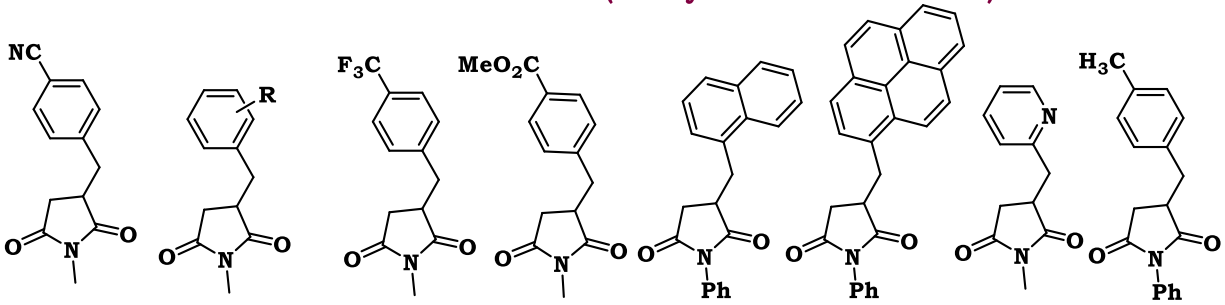
After developing the optimized procedure for hydrogenating α-alkylidene oxindoles and succinimides, we proceeded to apply this method to α-alkylidene oxindoles (**4a-4v**) to obtain their hydrogenated counterparts (**5a-5v**) (Table 3.1). Additionally, we extended this approach to the hydrogenation of α-alkylidene succinimides (**4w-4ae**), resulting in the formation of the reduced products (**5w-5ae**). (Table 3.2)

Table 3.2: Hydrogenation of α-alkylidene succinimides derivatives.



4 5

Reduction of Maleimide derived alkene (α-alkylidene succinimides) derivatives



5w (90%) 5x R= 3-F (78%) 5y R= 2-F(82%) 5z (81%) 5aa (69%) 5ab (78%) 5ac (74%) 5ad (80%) 5ae (70%)

We conducted additional investigations, including mechanistic studies and controlled experiments, to gain insights into the protocol. Based on these findings, we developed a plausible mechanism that aligns with the oxidative quenching photocatalytic cycle.

In conclusion, we have successfully established a protocol for the hydrogenation of derivatives of α-alkylidene oxindole and succinimides under metal-free conditions using visible light. This method is versatile, allowing for the incorporation of various functional groups. We have synthesized total of 31 of derivatives and presented a comprehensive mechanism to elucidate the process.

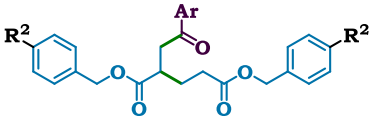
CHAPTER 4: Synthesis of Industrially Significant Glutaric Acid Diesters from Aldehydes via Sequential Giese-Type Addition Under Visible Light Illumination

In this chapter, we successfully carried out a chemical reaction that specifically abstracted a hydrogen atom from an aldehyde to create an acyl radical. This acyl radical was then subsequently added to two electron-deficient alkenes, resulting in the synthesis of α-substituted glutaric acid diesters. This achievement was facilitated by harnessing the hydrogen atom transfer (HAT) reactivity of Eosin Y and utilizing DIPEA while subjecting the reaction to visible light irradiation. Esters and their various forms are commonly found in a wide range of natural compounds, pharmaceuticals, polymer substances, and high-quality chemical products. Glutaric acid is a highly valuable compound, serving as a crucial starting material for the production of polymers like polyester polyols and polyamides. Glutaric acid, with its 1,5-dicarbonyl structure, can be prepared by subjecting butyrolactone and potassium cyanide to a ring-opening reaction at elevated temperatures. We developed a novel approach for synthesizing alpha-aroyl glutaric diesters. This method begins with aldehydes and acrylates and explored the hydrogen atom transfer (HAT) capability of Eosin Y to drive this reaction. It then utilizes photoredox catalysis without the need for metal catalysts to enable Giese-type 'consecutive addition. These Giese-type reactions lead to the formation of two new C–C bonds in a single reaction process. While many of the methods discussed are intriguing, they are constrained by their compatibility with only certain substrates, resulting in lower yields and the requirement for harsh reaction conditions. Moreover, a significant drawback is that many of these methods rely on the use of heavy transition metal reagents. In this context, there is a strong need for the creation and advancement of effective techniques that can produce alkyl radicals using readily accessible starting materials without the use of metal catalysts. Our journey to fine-tune the reaction conditions started with the use of benzyl acrylate **6a** and 4-chlorobenzaldehyde **7a** as representative substrates. After conducting a systematic and thorough investigation into the photocatalysis process, we determined that the combination of Eosin Y as a hydrogen atom transfer (HAT) catalyst and DIPEA as an additive in an anhydrous DMSO solvent, along with the utilization of blue LEDs emitting at 456 nm under an inert atmosphere, provided an excellent outcome, yielding the desired glutaric diester **8a** at an impressive rate of 80%.

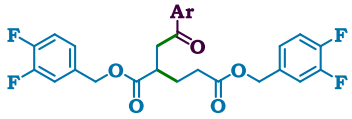
Having this optimised condition in hand, we moved towards the substrate scopes. We have kept **7a** constant and varied acrylates (**6a-6s**) derivatives to get the corresponding desired product with good yields (**8a-8s**) (**Table 4.1**).

Table 4.1: Substrate scopes with acrylate derivatives.

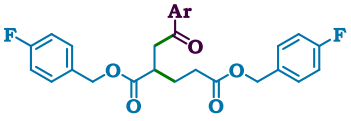
Acrylate Scope



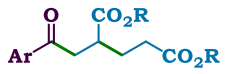
8a (80%), R^2 = H, Ar= 4-ClC_6H_4
8b (85%), R^2 = Me, Ar= 4-ClC_6H_4
8c (81%), R^2 = SMe, Ar= 4-ClC_6H_4



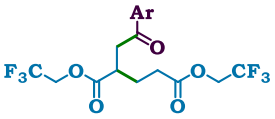
8d (79%), Ar= 4-ClC_6H_4



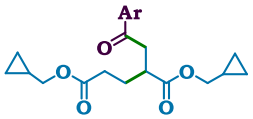
8e (82%),Ar= 4-ClC_6H_4



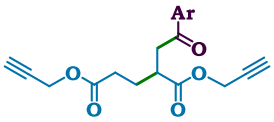
8f R= Et (70%), Ar= 4-ClC_6H_4
8g R= Me (68%), Ar= 4-ClC_6H_4
8h R= *t*-Bu (71%), Ar= 4-ClC_6H_4
8i R= *n*-Bu (72%), Ar= 4-ClC_6H_4
8j R= *i*-Bu (71%), Ar= 4-ClC_6H_4
8o[b] R=$C_{18}H_{37}$ (58%), Ar= 4-ClC_6H_4



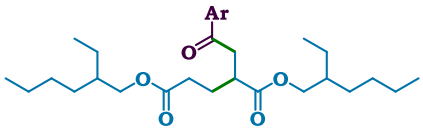
8k (69%), Ar= 4-ClC_6H_4



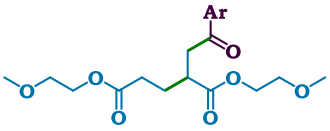
8l (71%)Ar= 4-ClC_6H_4



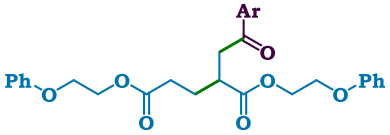
8m (70%), Ar= 4-ClC_6H_4



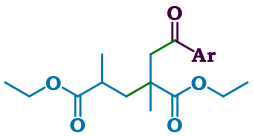
8n (72%), Ar= 4-ClC_6H_4



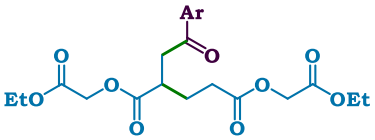
8p (70%), Ar= 4-ClC_6H_4



8q (75%), Ar= 4-ClC_6H_4



8r (72%), Ar= 4-ClC_6H_4



8s (71%), Ar= 4-ClC_6H_4

Further, we have explored the aldehyde scopes (**7b-7n**) with **6a** constant to get the desired product (**8t-8af**) (**Table 4.2**). After that, we have performed the reaction with **6a** and different complex acrylate derivatives (**6t-6v**) to synthesise the corresponding desired product (**8ag-8ai**) with satisfactory yield (**Table 4.3**). Further we have performed a detailed mechanistic study, controlled experiments to prove the HAT catalytic cycle of Eosin Y. And further we have performed light on/off experiments and quantum yield calculation to prove the reaction doesn't

proceed via radical chain mechanism. And further we have checked the synthetic utility of the desired product. Specifically needed to mention that 6,4- substituted 4,5-dihydropyridazin-3(2*H*)-one derivatives have been synthesized from our desired product **8**. 6,4- substituted 4,5-dihydropyridazin-3(2*H*)-one derivatives are recognized for their wide array of biological and pharmacological properties.

Table 4.2: Substrate scope with aldehyde derivatives.

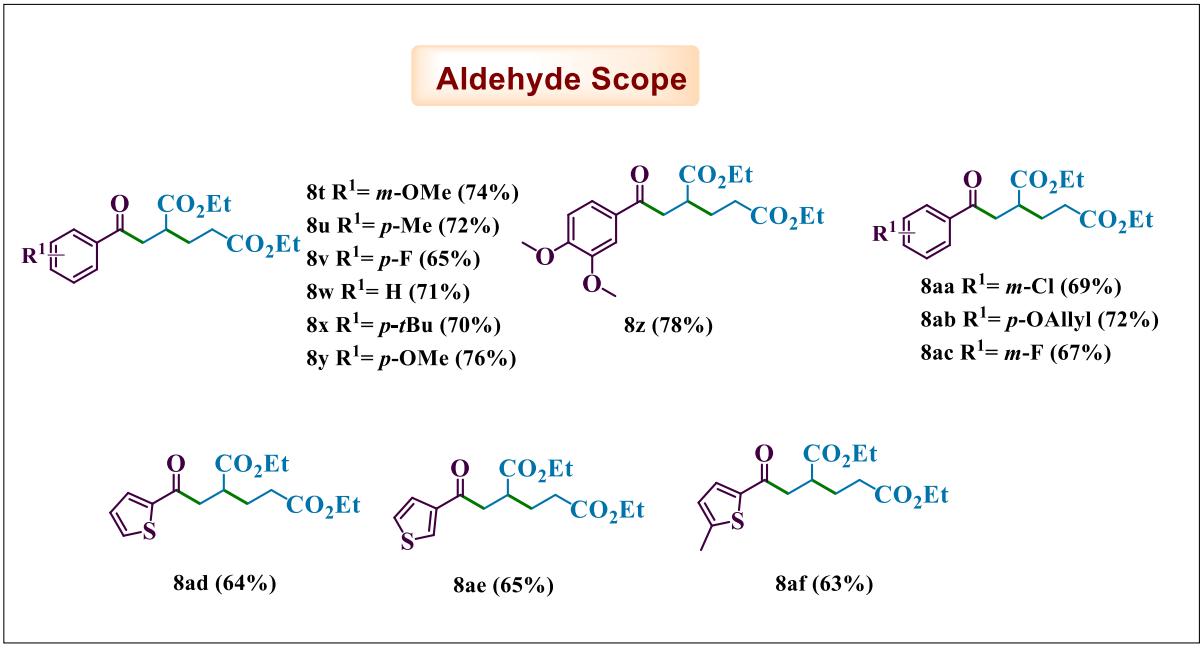
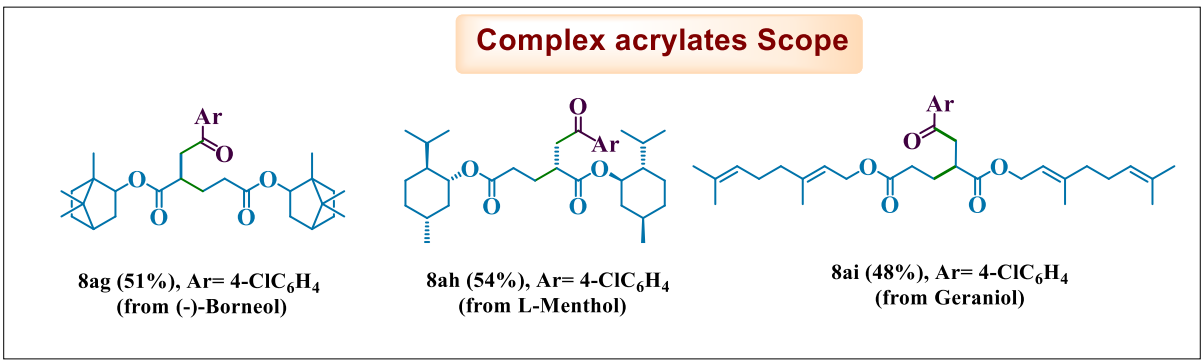


Table 4.3: Substrate scope with the complexed acrylate derivative.



In summary, we've developed a metal-free method for synthesizing alpha-substituted glutaric diesters directly from aldehydes and acrylates. It is scalable to gram quantities and can be conducted using natural sunlight, contributing to sustainability. Our study encompassed diverse experiments aimed at elucidating the underlying mechanism.

CHAPTER 5: Photocatalyst-Free Visible Light-Driven Synthesis of Anthranilic Acid and Quinoline Derivatives from 2-Phenylindole

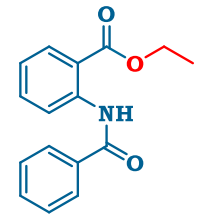
In this chapter, two successful solvent-dependent protocols have been developed, commencing from 2-Arylindole **9**. The choice of solvents plays a significant role in these reactions. When alcohol is employed as the solvent, anthranilic acid derivatives **10** are formed from 2-arylindole **9** through an oxidative ring-opening reaction, commonly known as the Wiktop oxidation, under visible light irradiation. In case of chloroform, the same reaction produces quinoline derivatives **11**. These methodologies were conducted under visible light irradiation and in the absence of a photocatalyst. Anthranilic acid and its analogues occupy a prominent role as central components in numerous bioactive compounds and approved pharmaceutical drugs. From an industrial perspective, anthranilic acid plays a pivotal role as a key intermediate in the production of azo dyes and saccharin. The quinoline structural motif is found in several naturally occurring bioactive compounds, including quinine, chloroquine, bulaquine, primaquine, and tafenoquine. These compounds are derived from Cinchona alkaloids. The de-aromatization of indole nuclei to generate difunctionally enriched products holds substantial significance, especially when carried out under mild reaction conditions. The de-aromatization of indole derivatives has been effectively achieved using diverse methods, such as borylation, hydrosilylation, trifluoromethylation, arylation, and allylation. These methods have limitations, involving significant metal waste, stoichiometric oxidants, or elevated temperatures. Amidst global energy and environmental challenges, there's a growing demand for eco-friendly synthetic methods. Visible light, an economical and environmentally friendly energy source, stands out as an excellent catalyst for organic transformations.

For the first time, we present a protocol for synthesizing anthranilic acid derivatives directly from 2-arylindole in a metal-free, photocatalyst-free condition under visible light irradiation. The reaction involves the oxidative ring opening of indole under oxygen through the nucleophilic addition of alcohol. When chloroform is utilized as a solvent instead of alcohol under the same conditions, quinoline derivatives are generated from 2-arylindole **9**. This alteration in product formation can be elucidated by the in-situ formation of dichlorocarbene from chloroform within the reaction conditions, subsequently reacting with 2-arylindole **9** to yield quinoline derivatives. Following detailed optimization, it was determined that the combination of K_2CO_3, nEt_4NCl, and (*E*)-1,4-diphenylbut-2-ene-1,4-dione in alcohol under

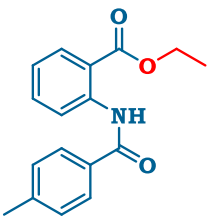
467 nm light irradiation provides the highest yield (74%) for synthesizing anthranilic acid derivative **10** from 2-arylindole **9**. For chloroform, the optimized conditions involve the combination of K_2CO_3 and nEt_4NCl under 427 nm light irradiation, resulting in the highest yield (76%) for the synthesis of quinoline derivatives **11**.

Table 5.1: Substrate scope for the synthesis of anthranilic acid derivatives.

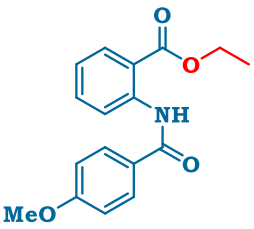
2-Arylindole scopes



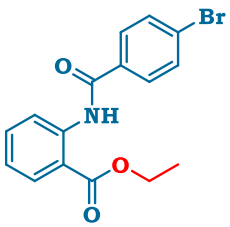
10a, (74%)



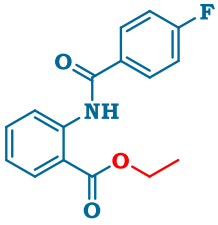
10b, (72%)



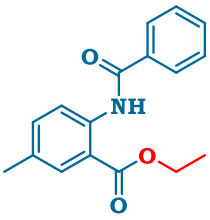
10c, (71%)



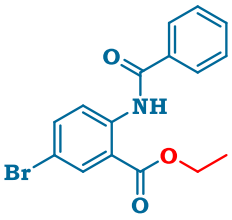
10d, (69%)



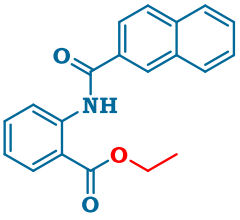
10e, (75%)



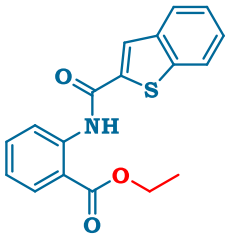
10f, (73%)



10g, (73%)

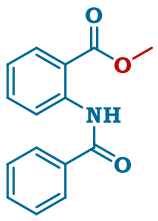


10h, (67%)

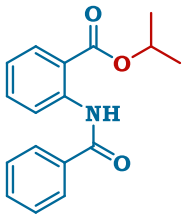


10i, (67%)

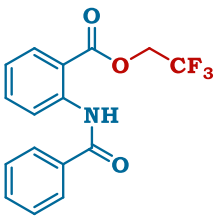
Nucleophile scope



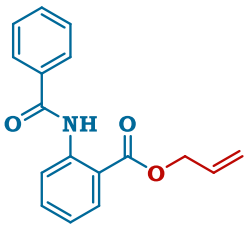
10j, (69%)



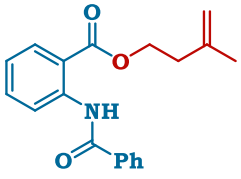
10k, (75%)



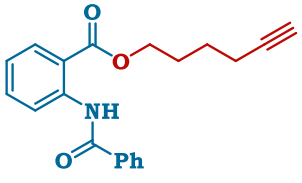
10l, (60%)



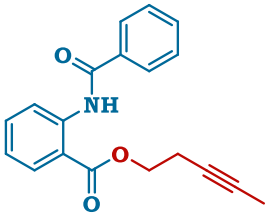
10m, (71%)



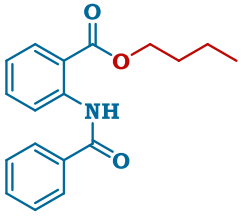
10n, (60%)
derived from Isoprenol



10o, (54%)



10p, (65%)

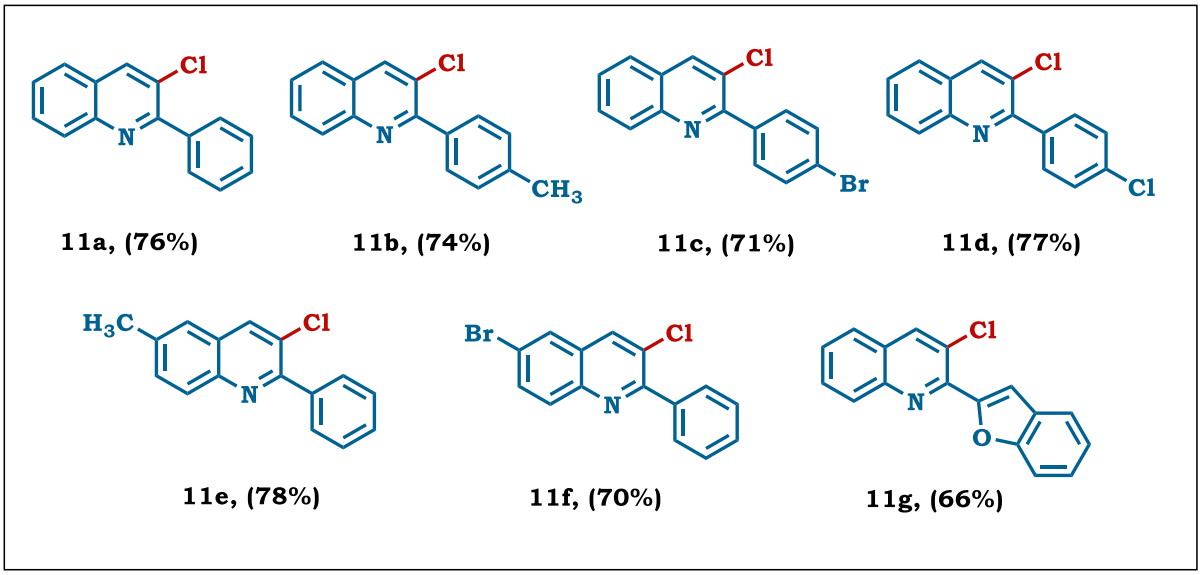


10q, (72%)

Having established optimized conditions, we proceeded to explore the substrate scope for anthranilic acid derivatives. Initially, we applied the protocol to various 2-arylindole derivatives, maintaining ethanol as a constant nucleophile and solvent source, resulting in the synthesis of different anthranilic acid derivatives (**10a-10i**) with moderate to good yields (**Table 5.1**). Furthermore, by keeping 2-phenylindole **9a** constant, we employed different alcohols to produce compounds **10j-10q** with moderate to good yields (**Table 5.1**).

Further in case of chloroform, we have synthesised seven derivatives of quinoline (**11a-11g**) using different 2-arylindole derivatives **9** using the optimised condition with moderate to good yield (**Table 5.2**).

Table 5.2: Substrate scope for the synthesis of quinoline derivatives.



Subsequently, we conducted a series of control experiments and spectroscopic analysis to validate the mechanisms of both protocols. In the alcohol-based protocol, the mechanistic study and controlled experiments elucidate that under visible light irradiation, molecular oxygen transforms into singlet oxygen, which serves as the active species facilitating the oxidation of indole. In the chloroform-based protocol, the mechanistic study establishes the formation of an Electron Donor-Acceptor (EDA) complex in the reaction medium. This complex absorbs light and progresses towards the desired transformation.

In summary, we have established a photocatalyst-free method for the direct synthesis of anthranilic acid derivatives from 2-arylindole derivatives in the presence of alcohol, conducted in a one-pot fashion under visible light irradiation. The mechanism has been validated through controlled experiments and a mechanistic study. Moreover, this protocol is applicable for gram-scale synthesis and is feasible under sunlight. In the presence of chloroform, the reaction mixture yields quinoline derivatives under visible light irradiation without the need for a photocatalyst. The mechanistic study confirms the formation of an Electron Donor-Acceptor (EDA) complex in the presence of chloroform in the reaction medium, progressing further under visible light irradiation.

*****

(*Numbers of substrates and products in the synopsis are different from those in thesis. Please note that compound numbers have been assigned for the convenience in every chapter and number of few compounds may vary from chapter to chapter*)

List of Publications

Included in the thesis

1. **Anindita Bhowmick**, Prakash K. Warghude, Pankaj D. Dharpure, Ramakrishna G. Bhat* "Direct Access to α-Acyloxycarbonyl Compounds and Esters via Oxidative Esterification of Aldehydes under Visible Light". *Org. Chem. Front*. **2021**, *8*, 4777.
2. **Anindita Bhowmick**, Prakash K. Warghude, Ramakrishna G. Bhat* "Visible Light Promoted Metal-Free Sustainable Reduction of α-Alkylidene Oxindoles/Succinimides". *Asian J. Org. Chem*. **2022**, *11*, e20220020.
3. **Anindita Bhowmick**, Abhijit Chatterjee, Sidharth S. Pathak, Ramakrishna G. Bhat, A Visible Light Driven Direct synthesis of Industrially Relevant Glutaric Acid Diesters from Aldehydes. *Chem. Commun*., **2023**, *59*, 11875-11878.

Not included in the thesis

4. Pankaj D. Dharpure, **Anindita Bhowmick**, Prakash K. Warghude, Ramakrishna G. Bhat* "Visible-light mediated facile dithiane deprotection under metalfree conditions". *Tetrahedron Lett*. **2020**, *61*, 151407.
5. Prakash K. Warghude, **Anindita Bhowmick**, Ramakrishna G. Bhat* "Direct access to spirooxindole dihydropyrrole fused pyrazolones and bis-spiropyrazolone derivatives". *Tetrahedron Lett*. **2022**, *97*, 153791.
6. Vikas V. Khade, **Anindita Bhowmick**, Archana S. Thube, Ramakrishna G. Bhat* "Direct Access to Strained Fused Dihalo Aziridino Quinoxalinones via C3-Alkylation Followed by Tandem Cyclization". *J. Org. Chem*. **2023**, *88*, 8010–8023.
7. Javed Y. Shaikh, **Anindita Bhowmick**, Abhijit Chatterjee, Nitin Thombare, Ramakrishna G. Bhat* "Transient Directing Group enabled C3-(sp^2)-H alkenylation of Five Membered Heterocyclic carbonyl compounds: An Easy Access to Mechanochromic Luminogens". *Adv. Synth. Catal*. **2023**, *365*, 2922–2928.
8. Javed Y. Shaikh, **Anindita Bhowmick**, Abhijit Chatterjee, Debasish Laha, Ramakrishna G. Bhat* "Palladium Catalyzed C3-(sp^2)-H Alkenylation of Pyrroles: A Direct Access to Novel Organic Thermally Activated Delayed Fluorescence (TADF) Materials" Chemrxiv, **2023**, Preprint *DOI:*10.26434/chemrxiv-2023-z95xl.

Book Chapter

1. **Anindita Bhowmick**, Mousumi Behera, Ramakrishna G. Bhat, Handbook of C-H-Functionalization – C-H Bond Functionalization by the Confluence of Organocatalysis and/or Transition Metal Catalysis with Photoredox Catalysis. DOI: 10.1002/9783527834242, ISBN: 9783527834242, Wiley Online Library, **2022**.

CHAPTER 1

Photoredox Catalysis: Historical Evolution and Fundamental Mechanistic Pathways

Abstract

In this chapter, we explore the historical development and progression of photoredox catalysis. Additionally, we delve into the conventional mechanistic pathways typically observed in visible light-induced photoredox catalysis. Reactions facilitated by light-induced photocatalysts traditionally adhere to Electron Transfer Processes (SET - Single Electron Transfer), Hydrogen Atom Transfer (HAT), and Consecutive Photoinduced Electron Transfer (ConPET). Conversely, light-induced reactions independent of photocatalysts generally operate through the Electron Donor-Acceptor (EDA) complex mechanism or involve participating reagents with inherent activity under light. Subsequent chapters delve into these reaction mechanisms in the context of novel organic transformations.



Photoredox Catalysis: Historical Evolution and Fundamental Mechanistic Pathways

1.1. General introduction to photoredox catalysis:

Advancement in the visible light mediated photoredox catalysis for realizing various organic transformations has made it as a powerful tool for organic synthesis over the recent years.[1]. Despite nearly half a century of existence, photoredox catalysis has been extensively applied in domains such as carbon dioxide reduction [2], water splitting [3], and the development of materials for solar cells [4]. It's only in recent times that these foundational principles have been adapted to generate radicals for chemical synthesis. This realization involves harnessing the capacity of visible light to transform into chemical energy, offering controlled and gentle synthetic applications [5]. Several factors have converged to facilitate this development: a heightened focus on enhancing energy efficiency in laboratory-scale reactions has pinpointed visible light as an ideal source. Progress in technology and the wide commercial availability of light-emitting diodes capable of delivering intense visible light within a narrow wavelength range for all colours have provided economical and energy-efficient light sources suitable for photocatalysis. The classical photochemistry utilizes ultraviolet light to directly excite organic compounds and is a well-established and extensively evolved field with a history spanning over a century.

With its reduced energy compared to classical ultraviolet irradiation, visible light frequently yields more selective, predictable, and manageable reactions. In addition to its lower energy, the straightforward and effective generation of reactive radical intermediates through visible light has rejuvenated the enthusiasm to strategize the radical reactions in organic synthesis. Using light-absorbing molecules, often termed as photoredox catalysts (PCs), a subsequent electron transfer mechanism either bimolecular or inner sphere is enabled, creating highly reactive open-shell intermediates that participate in further reactions [6]. Both of these reaction modes produce effective and practical ways to drive a variety of organic processes. The fact that photons can generate enough energy to trigger the appropriate reactivities without the need for high temperature or other severe conditions is a significant benefit of photoredox catalysis [6]. Owing to these advantages, the photoredox catalysis has been utilized not only to enhance several organic chemistry processes but also to create novel reactivity [7].

Since visible light falls within the spectral range where the Sun emits the most energy, its use is generally of great interest [8]. Reduced unwanted side effects brought on by the unintentional excitation of organic additives, substrates, and products are another benefit of using low-energy light for catalysis [1a]. In order to effectively engage in productive, diffusion-controlled bimolecular quenching reactions, it is crucial to design and employ PCs with strong absorption in the visible region of the spectrum, long enough lifetimes (ns-μs) of their excited states (ESs), and advantageous reversible redox chemistry of their ground states (GSs) and ESs.

1.2. History of photoredox catalysis:

The concept of utilizing visible light to drive organic transformations has a long history. To trace its origins, we need to journey back over a century. At the dawn of the previous century, Giacomo Ciamician [9], an Italian chemist at the University of Bologna, collaborated with his colleague Paul Silber to pioneer photochemical reactions employing visible light [**Figure 1**]. Utilizing sunlight, they conducted the reaction on the balcony of the Chemical Institute at the University of Bologna in Italy. Following that, a significant interval ensued during which the use of visible light in organic synthesis either lay dormant or certain unnoticed contributions were made, that did not gain attention within the synthetic community. Approximately five decades ago, the initial applications of photoredox catalysis in organic synthesis were documented. These pioneering works formed the bedrock upon which the contemporary advancements in the realm of modern photoredox catalysis have been built. In 1978, Kellogg exhibited that the photo-mediated reduction of sulfonium ions to their respective alkanes and thioethers, utilizing N-substituted 1,4-dihydropyridines as terminal reductants, could be enhanced through the addition of a catalytic quantity of $[Ru(bpy)_3]Cl_2$ [10] [**Scheme 1a**]. Subsequent reports from Fukuzumi and Tanaka [11], as well as Pac [12], demonstrated that analogous $[Ru(bpy)_3]Cl_2$-dihydropyridine catalyst systems could efficiently facilitate the reduction of a broad spectrum of organic substrates. These included electron-deficient olefins, aromatic ketones, and various halides on benzylic and phenacyl compounds.

In the 1980s and 1990s, the realm of organic synthesis saw investigations into photoredox catalysis. In 1984, Cano-Yelo and Deronzier documented the inaugural instance of a net oxidative photoredox-catalyzed reaction, employing aryldiazonium salts as the concluding oxidant to transform benzylic alcohols into their corresponding aldehydes [13]. Soon thereafter, they unveiled the premier redox-neutral photoredox-catalyzed alteration [14]. In this context, it was revealed that $[Ru(bpy)_3]Cl_2$ could catalyse the Pschorr reaction,

furnishing the phenanthrene product in a complete yield (**Scheme 1b**). Importantly, the reaction displayed significantly enhanced quantum efficiency under photoredox catalysis conditions in contrast to the direct photolysis of the reaction mixture. It's worth highlighting that during this period, India was also actively engaged in this field. In 1997, Indian scientist Prof. Ganesh Pandey and his research team documented a photocatalytic cycloaddition reaction employing light nearly within the visible range (395 nm) (**Scheme 1c**) [15].

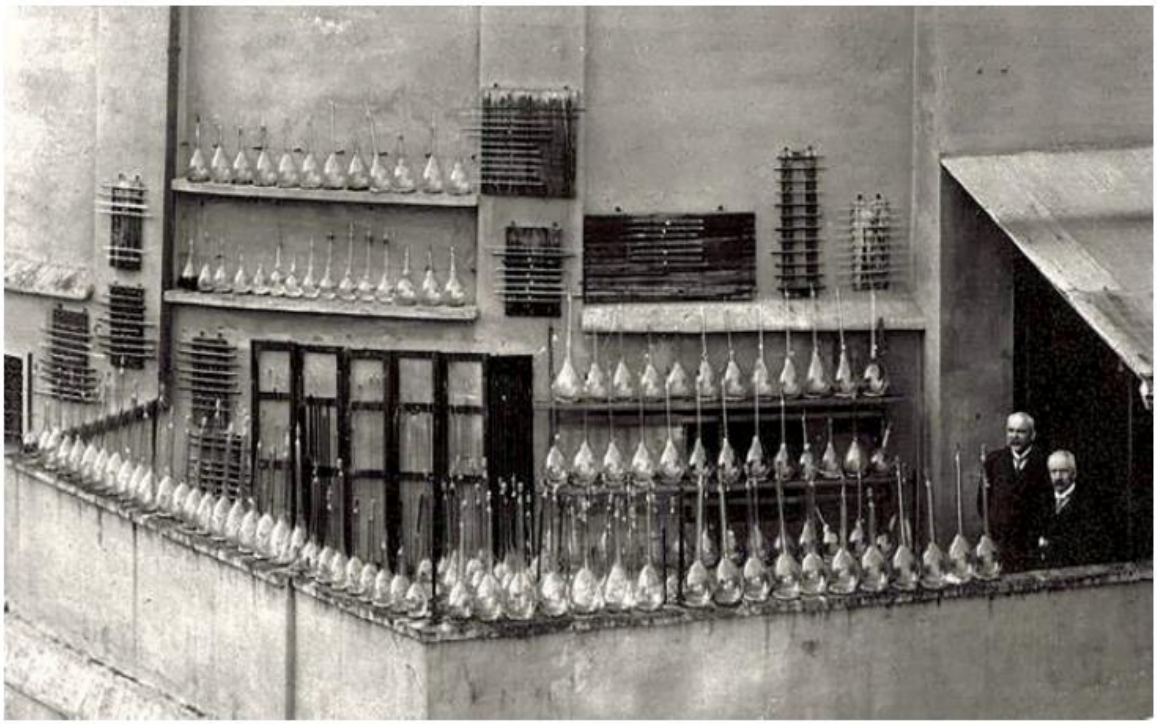
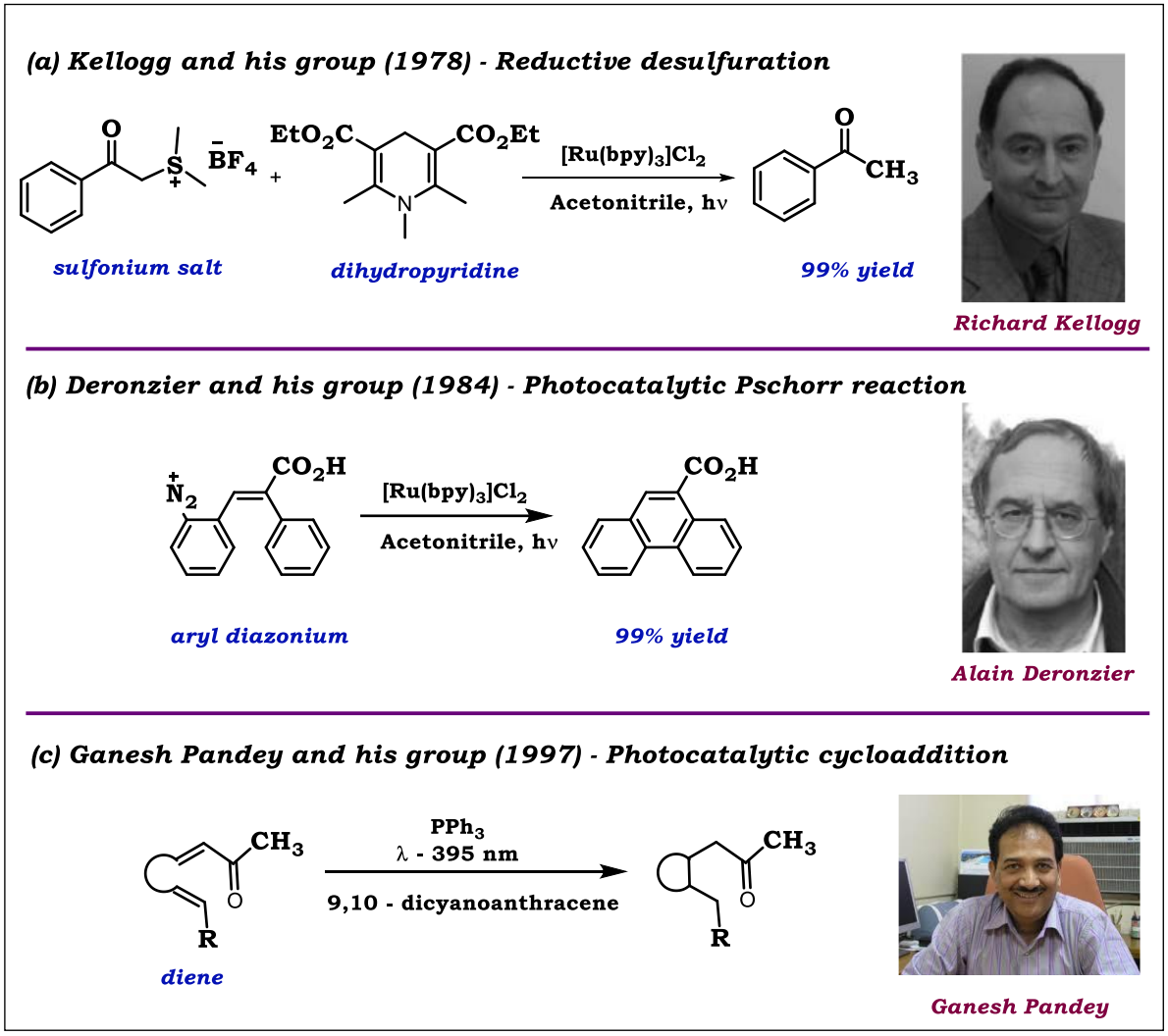


Figure 1: The historical aspiration of employing visible light in chemical reactions originated from Giacomo Ciamician and Paul Silber. They conducted reactions using sunlight on the balcony of the Chemical Institute at the University of Bologna, Italy. Reproduced with permission from the Chemistry Department, University of Bologna, Italy. (*Chem. Educator* **2007**, *12*, 362–369.)

Angelo Albini from Pavia and Vincenzo Balzani from Bologna from Italy, Janine Cossy from Paris, France and Frederick Lewis from Northwestern University in Illinois, USA, were among the many researchers who explored the incorporation of photoinduced electron-transfer processes in organic synthesis along with the various other investigations [16]. The method delineated in these reports signifies the first broad application of photoredox-mediated

substrate activation. Despite this early indication of the potential of photoredox catalysis in organic synthesis, its due recognition remained limited until the late 2000s.

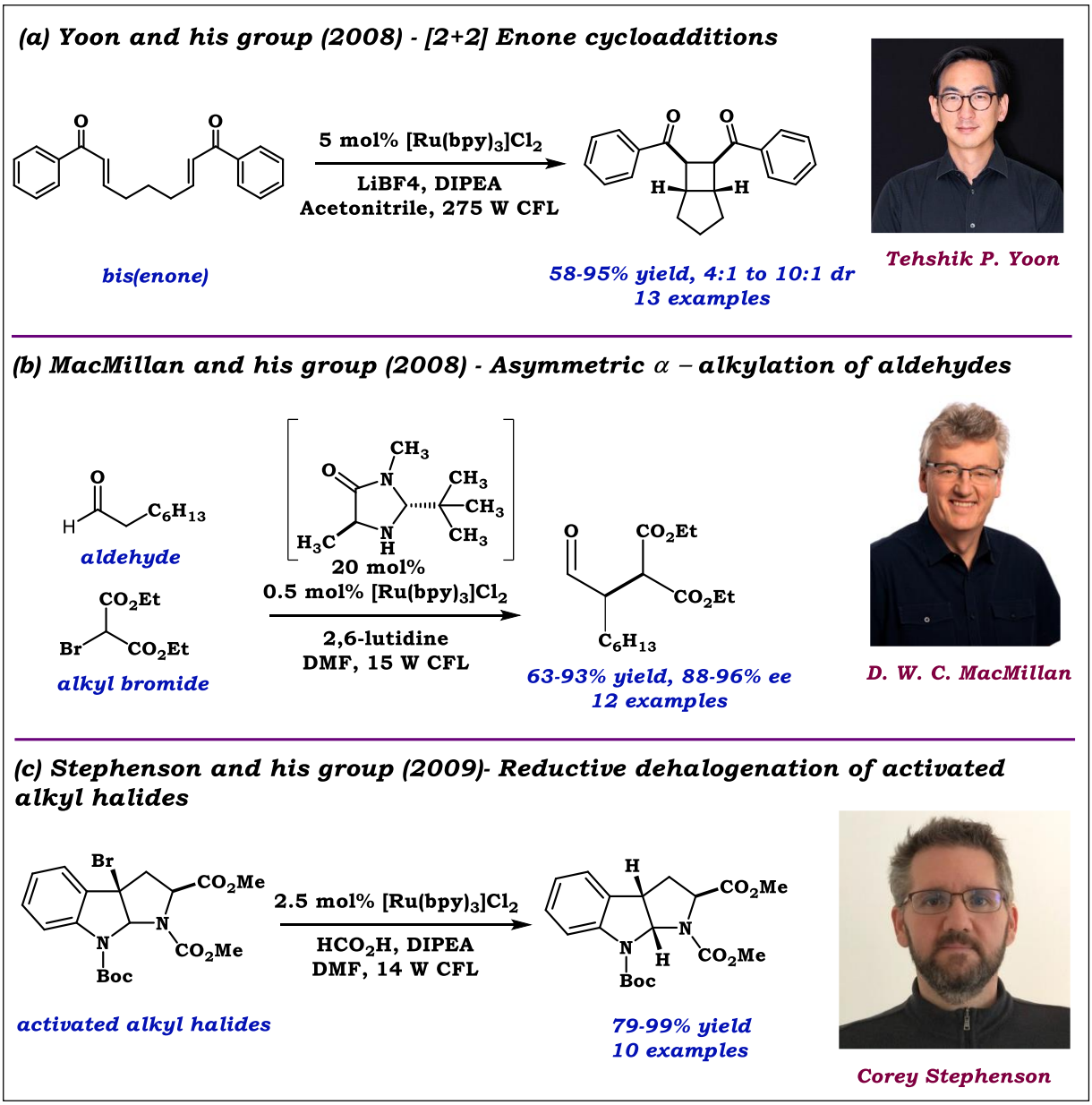
Scheme 1: Innovative and ground-breaking advances in the field of organic photoredox catalysis



A photoredox catalysed intramolecular [2 + 2] enone cycloaddition process was described by Yoon and colleagues in 2008 [17] (**Scheme 2a**). This groundbreaking study showed the advantages of integrating two activation modes in one sequence by using a Lewis acid addition to regulate the reactivity of the enone substrate. At the same time, the MacMillan group introduced a combined photoredox organocatalytic method to achieve enantioselective α-alkylation of aldehydes (**Scheme 2b**) [18]. This approach harnessed the unique properties of photoredox catalysis to generate electron-deficient radicals, which could then enantioselectively react with catalytically formed enamines. This inventive strategy addressed the longstanding challenge of achieving asymmetric α-carbonyl alkylation. Soon after,

Stephenson and his team presented a mild reductive dehalogenation protocol applicable to benzylic and α-acyl halides (**Scheme 2c**) [19].

Scheme 2: The scientific evolution of modern organic photoredox catalysis



This transformation could be executed using photoredox catalysis, circumventing the use of toxic tin reagents. These three reports together emphasized the promise of this activation method as a valuable catalytic platform for advancing organic reactions. This contribution also played a pivotal role in reigniting substantial progress in the domain of photoredox catalysis. Since these initial discoveries, other organic dyes and Rh- and Ir-polypyridyl complexes have been shown to function as effective photocatalysts for the conversion of visible light into chemical energy (**Figure 2**).

Based on these, a range of synthetic transformations have been carried out using photoredox catalysis. Its utility has been substantially increased due to the ability to modify the characteristics of metal complexes of the photocatalysts through alteration of the ligand backbone thus sparking additional interest in the area. The simplicity of the reaction setup, the ability to conduct reactions at room temperature, reduced toxicity, minimized waste generation, and the environmentally friendly nature of the reaction conditions have collectively contributed to the enhanced allure of this field [1].

1.3. Mechanistic aspects of photoredox catalysis:

Photocatalysts effectively convert light into chemical energy while selectively activating molecules through several prevalent mechanisms: (i) energy transfer, (ii) organometallic excitation, (iii) light-induced atom transfer, and (iv) photoredox catalysis.

In simpler terms, organic reactions conducted under visible light can be broadly divided into two classical versions. In one, the reaction takes place in the presence of a photocatalyst, while in the other, the reaction occurs without the use of a photocatalyst.

Upon absorbing visible light, the excited state of a photocatalyst can engage in distinct mechanistic pathways, including: i) Single Electron Transfer (**SET**), ii) Hydrogen Atom Transfer (**HAT**) catalysis, and iii) Consecutive Photoinduced Electron Transfer (**ConPET**).

In an alternative scenario, when the substrate possesses an absorbance within the visible region or when an intermediate formed in situ can absorb visible light and subsequently undergoing a transformation, the utilization of photocatalysts becomes dispensable. Under these circumstances, these reactions can be executed without the involvement of photocatalysts. In this chapter, I will provide an in-depth exploration of these categories.

1.3.1. Single Electron Transfer (SET) catalysis:

The process of Single Electron Transfer (SET) in photoredox catalysis entails an electron transfer that occurs either from the photoexcited catalyst to the reagents or starting material (SM) or conversely, from the reagents/SM to the catalyst. The direction of electron transfer is dictated by the disparity in redox potential between the two involved species [20].

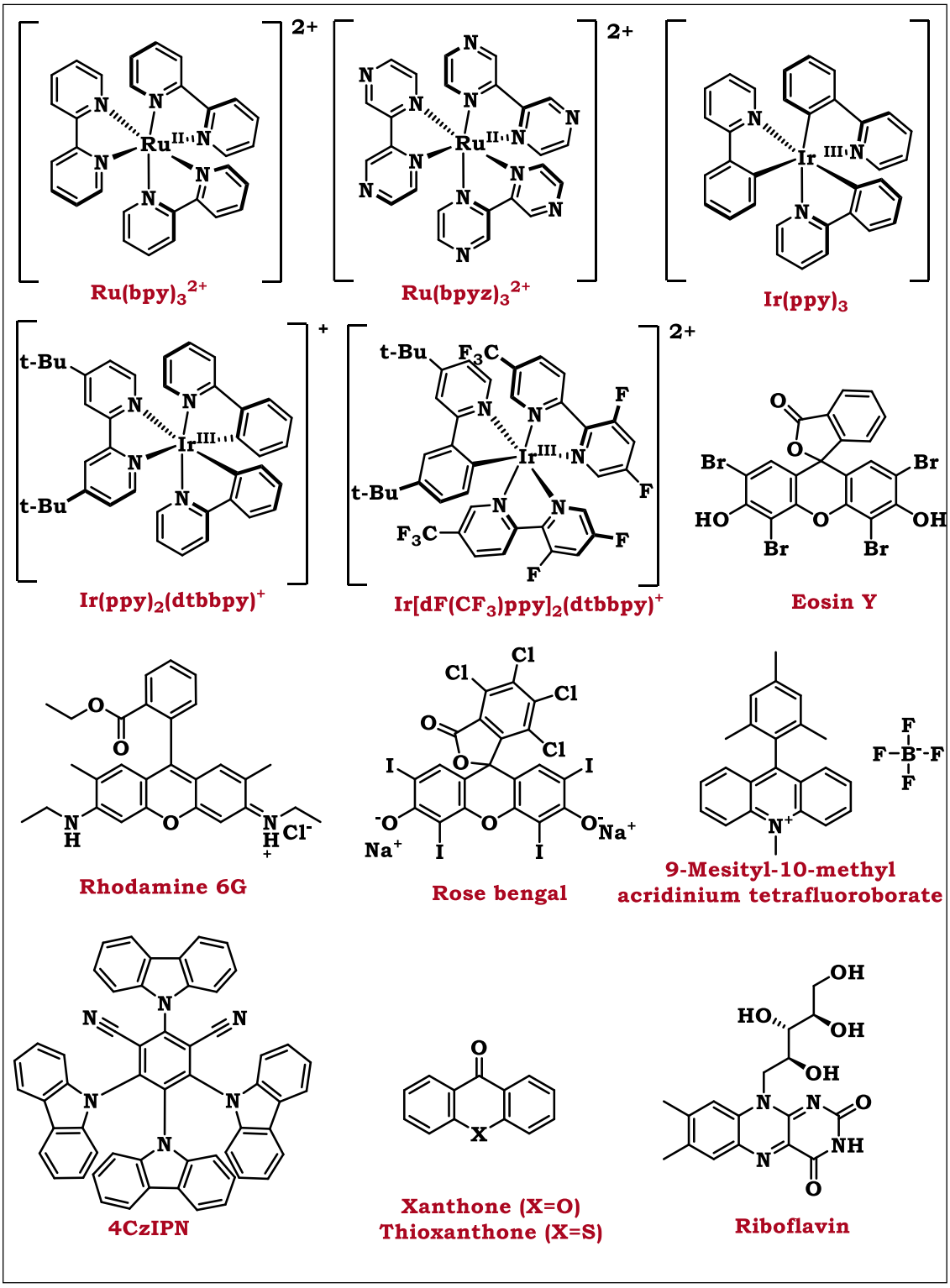
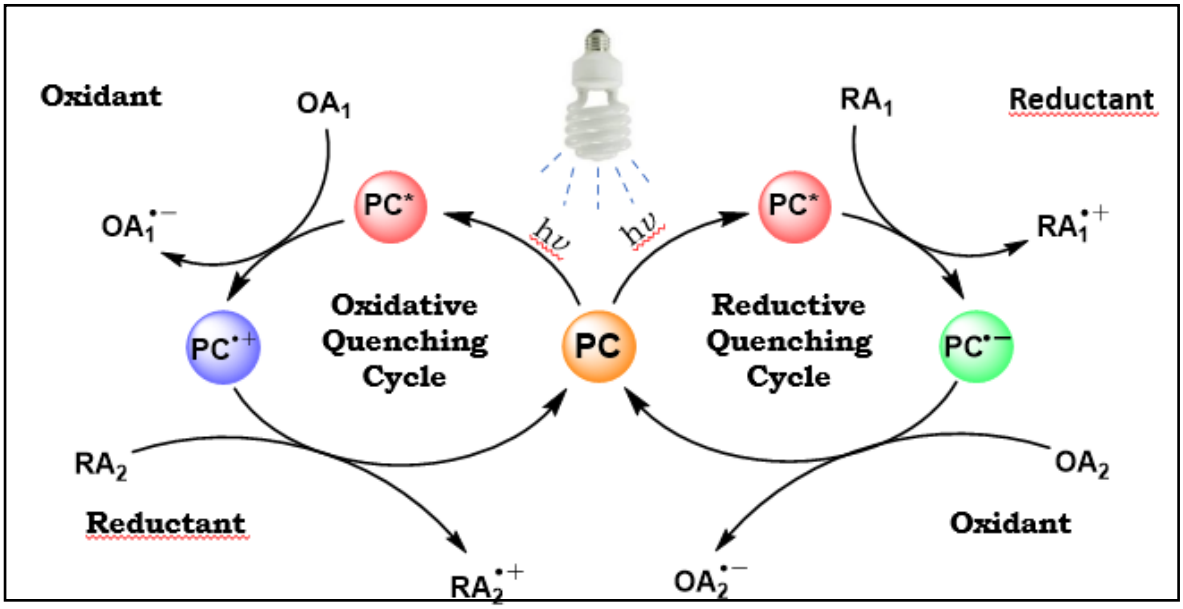


Figure 2: Molecular configurations of frequently encountered photoredox catalysts

Categorically, the catalytic cycle can be bifurcated into two types, contingent on the direction of electron movement and the mode of quenching of the excited state of photocatalysts: i) Oxidative quenching cycle and ii) Reductive quenching cycle.

Upon exposure to visible light, the photocatalyst transitions to its excited state. This excited state can undergo quenching by either accepting an electron from the substrate within the reaction medium, leading to ***reductive quenching*** (functioning as an ***oxidant***), or by donating an electron to the substrate within the reaction medium, resulting in ***oxidative quenching*** (functioning as a ***reductant***) (**Scheme 3**). The specific outcome is determined by the divergence in redox potential between the substrate and the excited state of the photocatalyst [20]. Ultimately, the radical anionic state of the photocatalyst, produced through reductive quenching, transfers an electron to an acceptor within the reaction medium. Conversely, the cationic state of the photocatalyst, generated through oxidative quenching, accepts an electron from a sacrificial donor in the reaction medium, subsequently returning to its original ground state and completes the whole catalytic cycle.

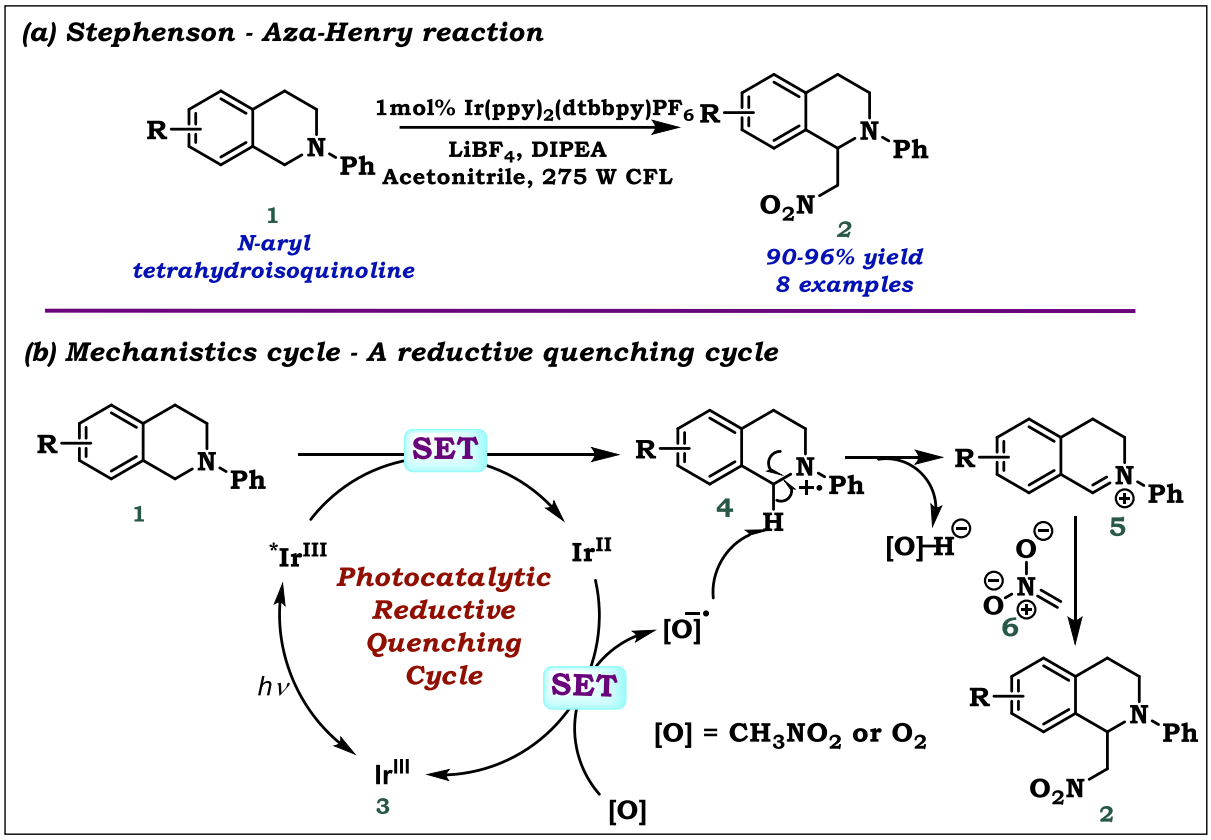
Scheme 3: Oxidative and reductive quenching cycle of photoredox catalysis



To illustrate the catalytic cycle of the mentioned Single Electron Transfer (SET) mechanism two examples have been highlighted (**Scheme 4 and 5**). In both cases, α-amino functionalization was achieved using Ir(III) photocatalysts. However, due to variations in the starting materials and the use of distinct sacrificial oxidants or reductants within the reaction medium, the mechanistic cycles differed [21]. This divergence occurred despite employing the same metal-based photocatalyst. In 2010, Stephenson and his group successfully pioneered Aza-Henry Reactions through C-H functionalization at the a-position of amines [21a] [**Scheme 4a**]. The comprehensive mechanisms of both these transformations have been briefly

highlighted (**Scheme 4b**). The radical cation **4** is generated through the reductive quenching of the excited state of **3** by **1**. This process leads to the formation of the highly potent reducing agent Ir^{2+}[Ir(III)/Ir(II) = -1.51 V vs SCE]. The catalyst in its reduced state returns to its initial ground state, which occurs through the reduction of nitromethane to its radical anion or due to incidental oxygen participation thus completing the catalytic cycle.

Scheme 4: Mechanistic cycle that follows reductive quenching cycle.

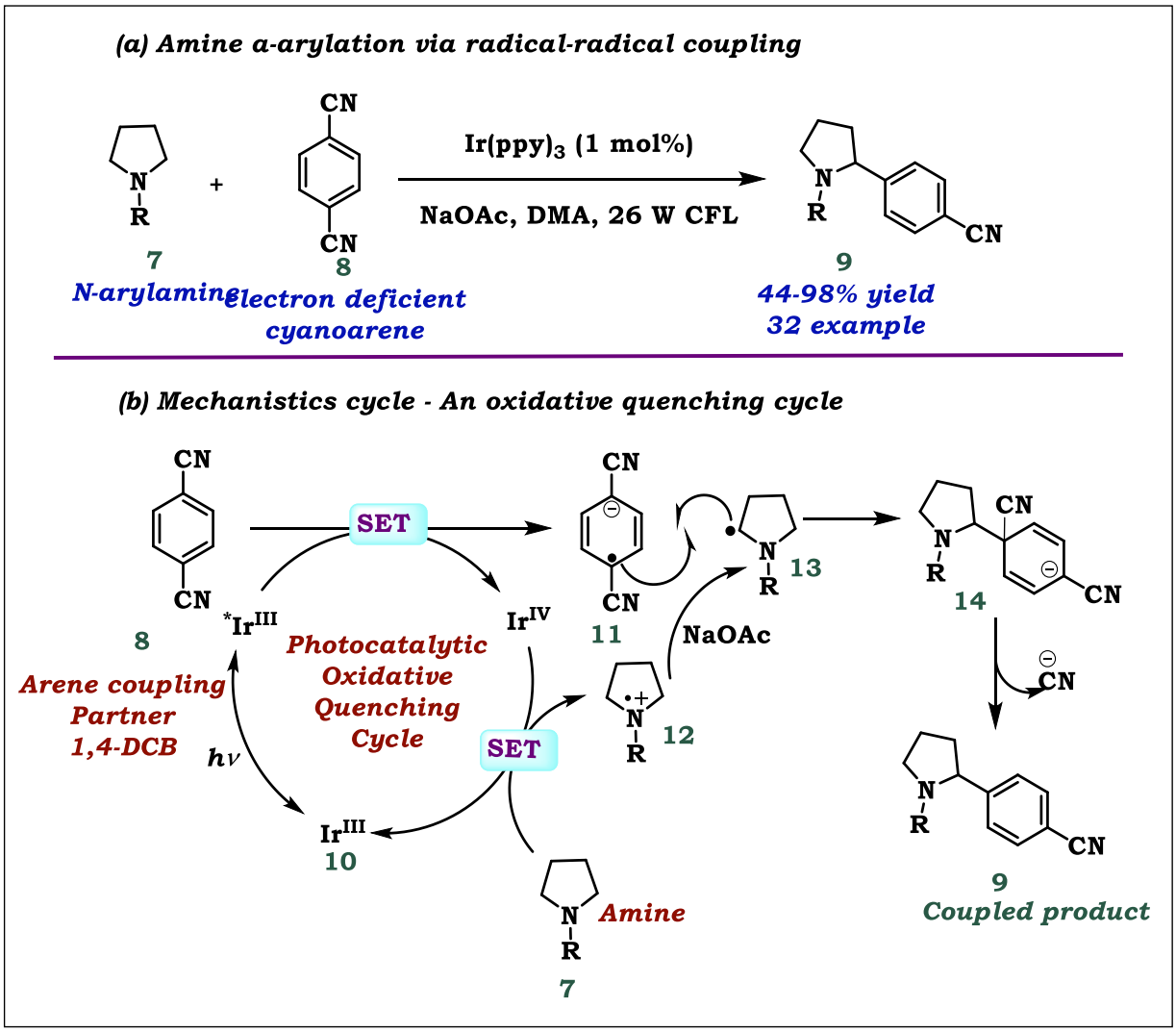


This radical anion might potentially extract a hydrogen atom from the radical cation of trialkylammonium, resulting in the creation of the targeted iminium ion **5**. Subsequently, the addition of compound **6** to this iminium ion leads to the formation of the observable product **2** (**Scheme 4b**). This mechanism follows a reductive quenching cycle pathway.

In 2011, MacMillan and his colleagues made a significant finding involving the α-arylation of amines through C-H bond activation, enabling the construction of benzylic amine derivatives using Irridium based photocatalysts [21b] [**Scheme 5a**]. The research team has put forward a mechanism for the C-H arylation process that aligns with the oxidative quenching pathway (**Scheme 5b**). Upon absorbing a photon from the 26 W light source, Ir(III) photocatalyst **10** gets into its excited state form, *Ir(III). The excited state *Ir(III) functions as a potent reductant with an oxidation potential ($E_{1/2ox}$) of -1.73 V versus a saturated calomel

electrode (SCE) in CH_3CN. Upon interaction with 1,4-dicyanobenzene **8** (1,4-DCB) possessing a reduction potential ($_{E1/2red}$) of -1.61 V versus SCE in CH_3CN, the complex could furnish an electron, leading to the formation of the corresponding arene radical anion **11**. Subsequently, Ir(IV) is generated, functioning as a strong oxidant with a reduction potential ($E_{1/2red}$) of +0.77 V versus SCE in CH_3CN. Subsequently, the complex Ir(IV) is capable of undergoing reduction to revert back to its initial form Ir(III), facilitated by the acceptance of an electron via SET mechanism from an amine molecule **7**. This electron transfer event gives rise to the formation of an amine radical cation **12**, culminating in the successful completion of the catalytic cycle. The adjacent C-H bonds to the nitrogen atom in species **12** experience a significant decrease in bond strength, amounting to approximately 40 kcal/mol.

Scheme 5: Mechanistic cycle that follows oxidative quenching cycle

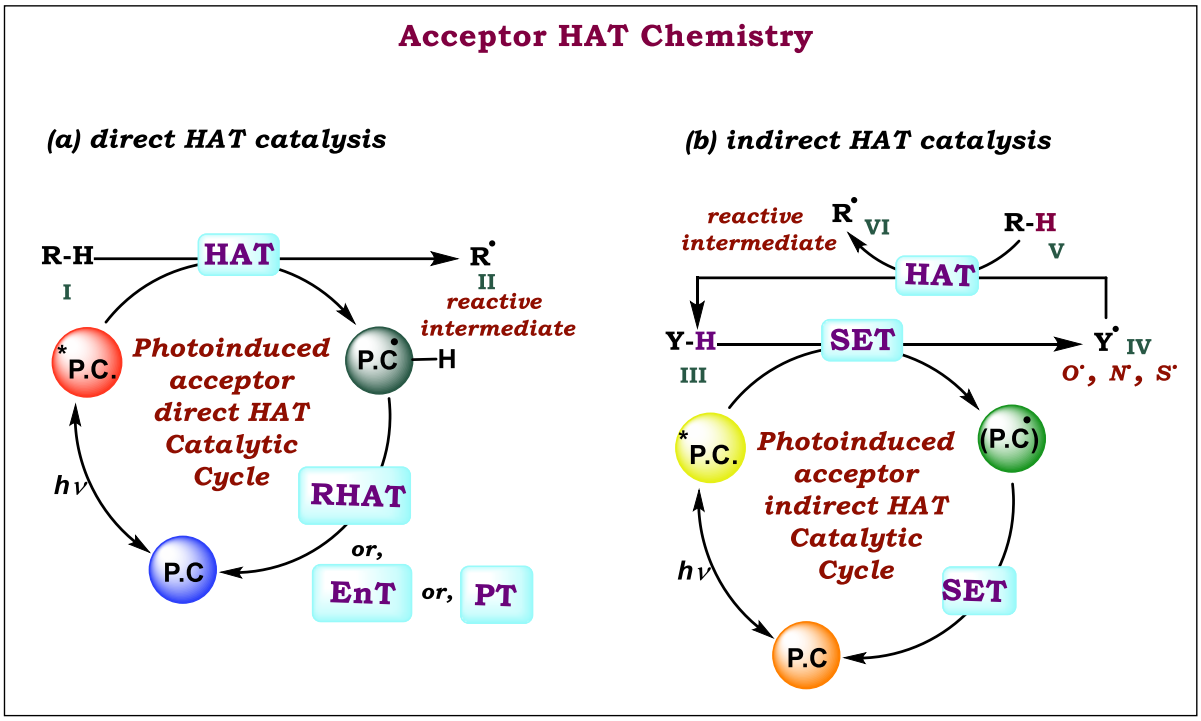


This makes it susceptible to deprotonation, a process facilitated by NaOAc (where OAc denotes an acetoxy group). The deprotonation event serves as the trigger for generating the α-amino radical **13**. Among all the steps the crucial importance is a phase involving a radical-radical coupling reaction that effectively combines intermediates **11** and **13**, constituting a fundamental bond-forming process. After this step, the elimination of CN anion from intermediate **14** furnishes the aromatized benzylic amine product **9**.

1.3.2. Hydrogen Atom Transfer (HAT) catalysis:

The concept of hydrogen atom transfer (HAT) [22] commonly refers to a coordinated mechanism that transfers both a proton and an electron moving from a lone donor to a sole acceptor ($Y\bullet+H-X\rightarrow Y-H+X\bullet$). The HAT process is one of the subsets of proton-coupled electron transfer (PCET) [23] which has been aptly defined by Hammes-Schifferas as "any process that entails the combined movement of at least one electron and one proton." [24]. Over the course of a century, research has emphasized the significance HAT in diverse processes, including hydrocarbon combustion, atmospheric chemistry, oxidative degradation, and catalysis [25]. Given the widespread presence of R-H bonds (where R = C, Si, etc.) in organic substrates, the direct functionalization of these bonds becomes a gateway to innovative pathways for building and modifying intricate molecules in later stages [26]. In this context, intermolecular HAT stands out by facilitating the direct activation of R-H bonds, eliminating the prerequisite of pre-functionalization or the use of directing groups. This approach stands as one of the most atom-efficient and step-economical strategies for the R-H functionalization. In contrast to photoinduced single electron transfer (SET) catalysis, photoinduced HAT exhibits the advantage of substrate activation not being restricted by redox potentials. In general, HAT catalysis can facilitate organic transformations by involving a pivotal step of either hydrogen atom abstraction or donation. These mechanisms can be further categorized as ***acceptor HAT chemistry*** and ***donor HAT chemistry*** respectively. Regarding ***acceptor HAT chemistry***, the photoinduced mechanism usually unfolds through two routes: ***direct*** and ***indirect HAT catalysis*** [27,28].

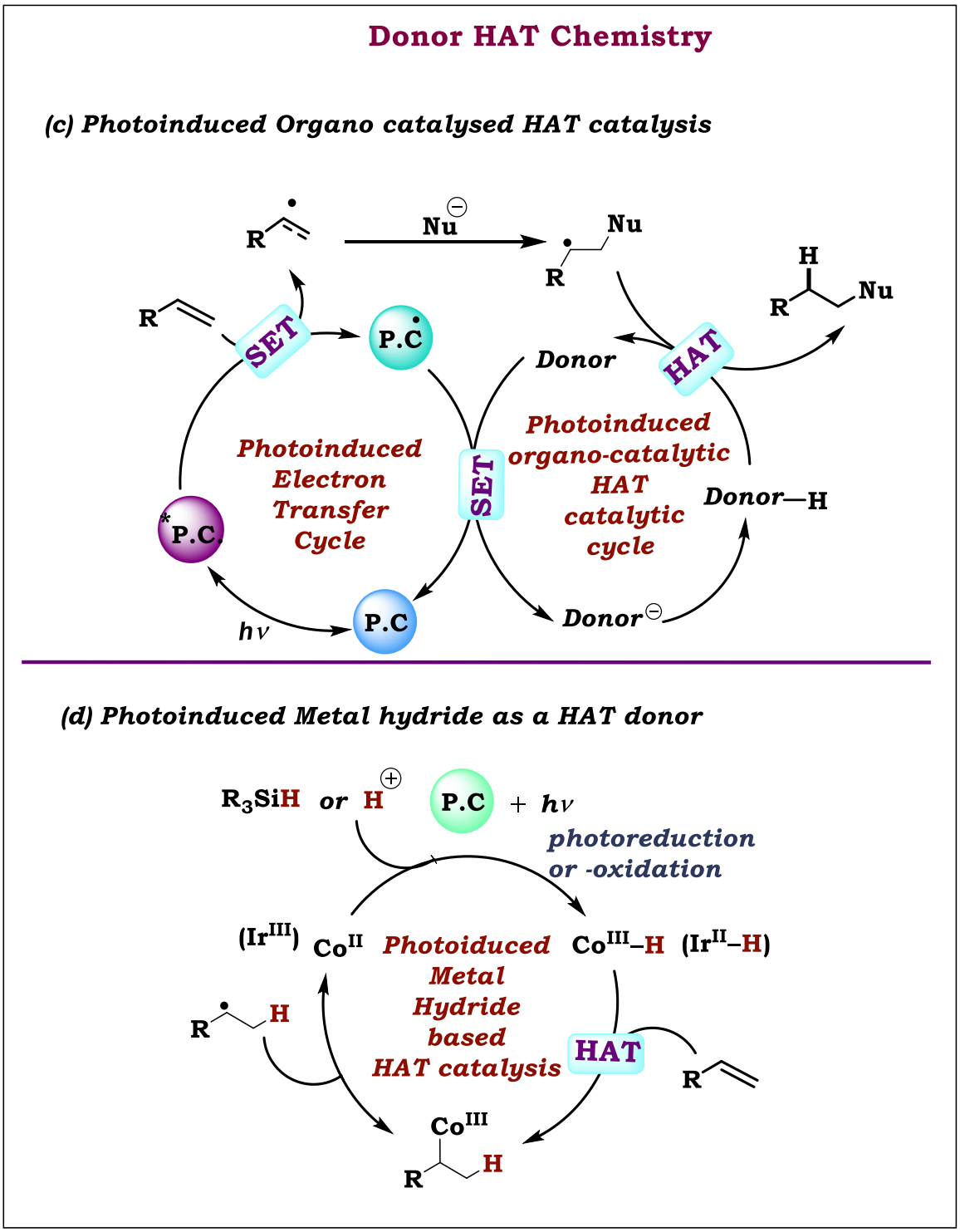
Scheme 6: Mechanistic cycle involving acceptor HAT catalytic cycle



In ***direct HAT catalysis*** (**Scheme 6a**), the photocatalyst (PC) transitions into an excited triplet state (PC*), enabling the direct abstraction of a hydrogen atom from R−H (**I**). This yields an alkyl radical R• (**II**) and (PC•)−H. The catalyst (PC) can then be regenerated from (PC•)−H via reverse hydrogen atom abstraction (RHAT), or through sequential processes involving electron transfer (EnT) and proton transfer (PT).

Indirect HAT catalysis (**Scheme 6b**) operates through a collaborative interaction between the photocatalyst (PC) and a co-catalyst Y−H (**III**). This synergy prompts the formation of heteroatom centered radicals Y• (**IV**) such as O•, S•, and N• from the co-catalyst Y−H (**III**). This process simultaneously activates the excited photocatalyst (PC*) via either single electron transfer (SET) or energy transfer (EnT). These heteroatoms centered radicals Y• (**IV**) are adept at abstracting hydrogen atoms from diverse R−H (**V**) bonds, producing alkyl radicals R• (**VI**) and rejuvenating the co-catalyst Y−H.

Scheme 7: Mechanistic cycle involving donor HAT catalytic cycle



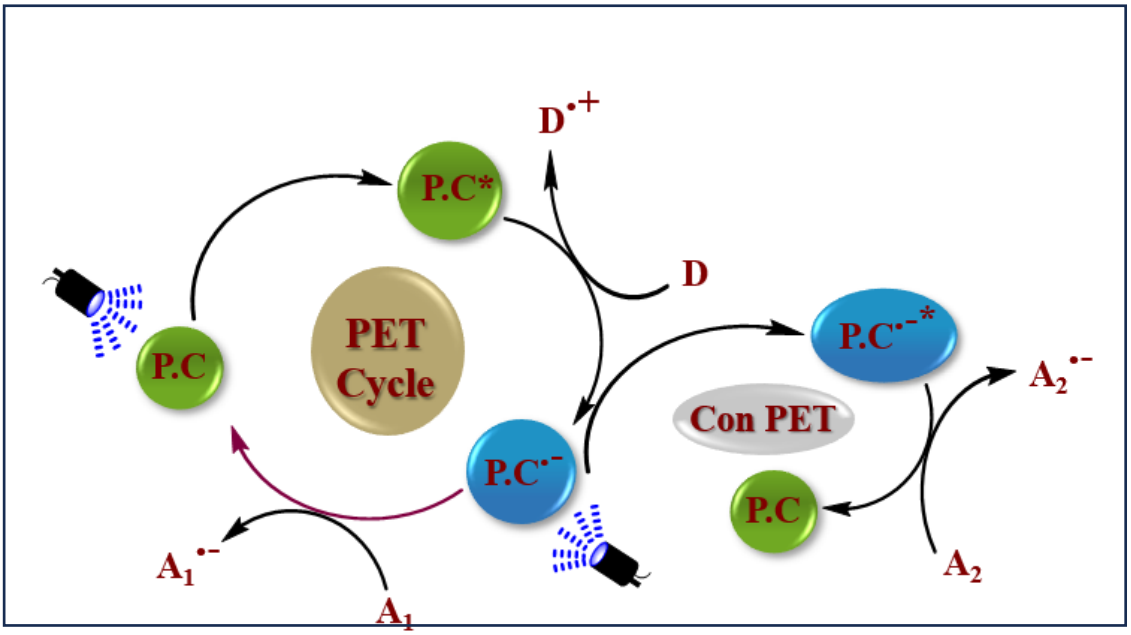
Donor HAT chemistry has found extensive investigation in the photocatalytic hydro functionalization of alkenes [29-33]. From a mechanistic perspective, the process of photoinduced HAT donation can be achieved through the utilization of either an organo-catalyst or a metal hydride as the HAT donor (**Scheme 7**). The mechanism centered around organic HAT donors has been comprehensively elucidated by Nicewicz and coworkers

(**Scheme 7a**) [29]. Within the catalytic cycle, the process of hydrogen atom donation plays a crucial role as a radical termination step in the hydro functionalization of alkenes. The HAT donor is subsequently regenerated via photoreduction and protonation. On the other hand, the metal-hydride mechanism produces an active HAT donor, Co (III)−H [or Ir(II)−H], through photoreduction or photooxidation. This HAT donor triggers the hydro functionalization of alkenes by generating a carbon centered radical (**Scheme 7b**) [30-33].

1.3.3. Consecutive Photoinduced Electron Transfer (ConPET) catalysis:

The Consecutive Photoinduced Electron Transfer (ConPET) concept involves the in-situ synthesis of the intrinsically reducing radical anion or anionic form of a photocatalyst (**Scheme 8**). Upon undergoing photoexcitation, this entity undergoes transformation into a profoundly reducing chemical species. This resultant species demonstrates the ability to initiate the activation of substrates mandating highly negative reduction potentials, a functionality beyond the scope of conventional photocatalysts. As an innovative exploration into the ConPET system, König and Ghosh and their colleagues documented the study involving perylene diimides (PDI) [34]. This class of fluorescent dyes, with applications ranging from pigments and colorants to photoreceptors and electronic materials, served as the focal point of their research.

Scheme 8: Mechanistic pathway of consecutive Photoinduced Electron Transfer (ConPET) catalysis



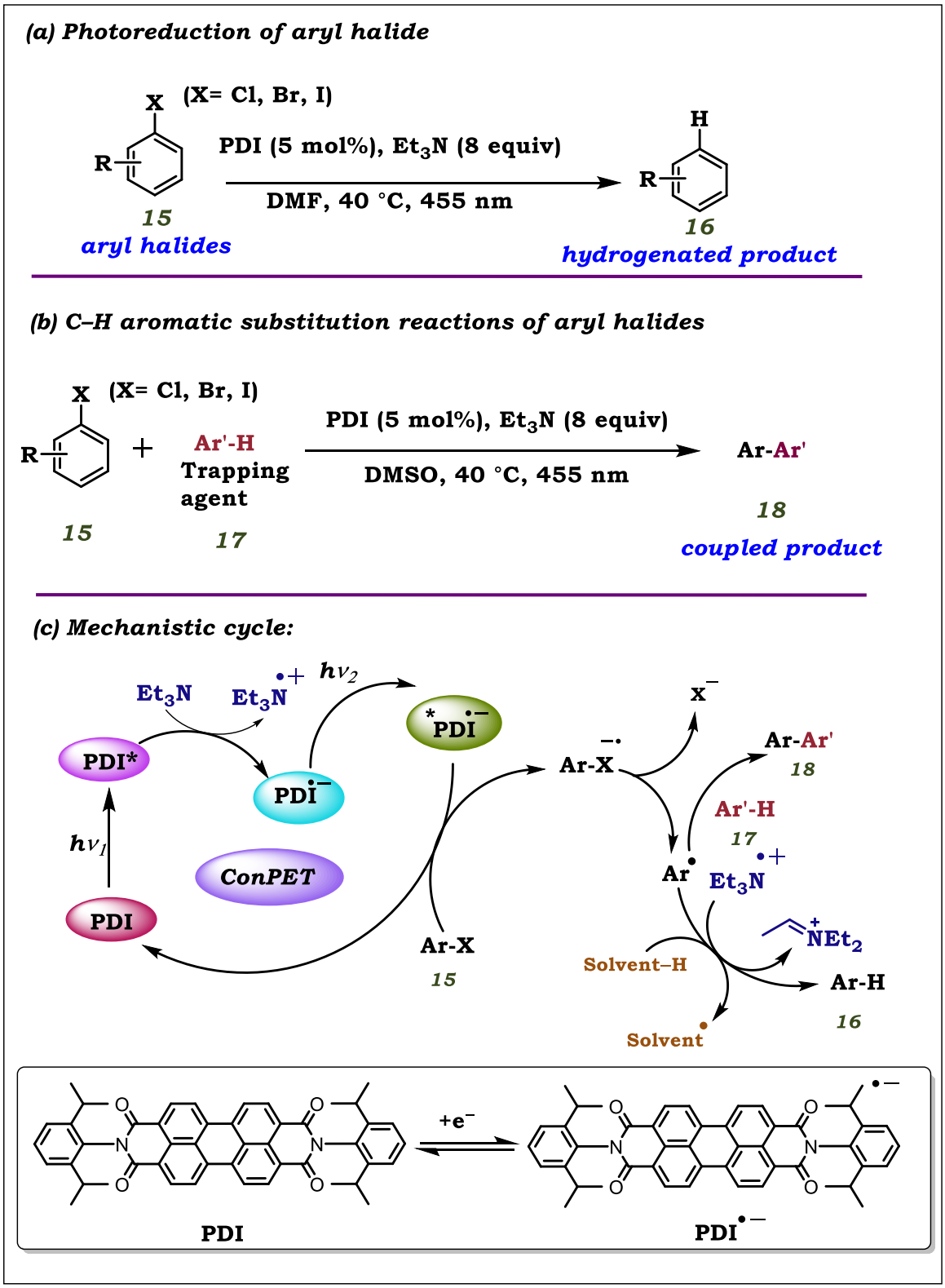
N,N-bis(2,6-diisopropylphenyl)perylene-3,4,9,10-bis(dicarboximide) (PDI) has been identified as a proficient photosensitizer for two distinct transformations.

In (**Scheme 9a**), it effectively facilitates the dehalogenative hydrogen transfer of aryl halide **15** to synthesize **16**, while in (**Scheme 9b**), it enables homolytic aromatic substitution (HAS)-type aryl-aryl cross-coupling between electron-deficient **15** and electron-rich heteroarene **17** to synthesize the coupled product **18**. During the progression of these reactions (**Scheme 9c**), a two-step photoexcitation process is initiated. In the first step ($h\nu_1$), the excited *PDI undergoes reductive quenching by Et_3N, leading to the formation of the radical anion $PDI^{\cdot-}$ as well as the radical cation of triethylamine ($Et_3N\cdot+$). Subsequently, the second excitation event ($h\nu_2$) of the electron-rich species (PDI·–) becomes pivotal. Notably, the ground state of PDI·– exhibits a sufficiently prolonged lifetime, allowing for further excitation, ultimately resulting in the generation of *[$PDI^{\cdot-}$].

In 2016, König et al. demonstrated that enhanced manipulation of the activation of redox-active chemical bonds can be attained through the utilization of a xanthene dye known as rhodamine 6G (see **Figure 2** for structure) [35]. By modulating the excitation wavelength, the reduction potential of the xanthene dye Rhodamine 6G (Rh-6G) can be adjusted within a range of approximately 2.4 V. This wavelength-dependent control of light colour facilitates the generation of distinct redox states in Rh-6G, allowing selective C-H arylations to produce functionalized arenes and heteroarenes [**Scheme 10**].

These transformations utilize readily accessible and stable starting materials. When subjected to green LEDs (λ_{Ex}= 530 nm) in the presence of a sacrificial electron donor (DIPEA), Rhodamine 6G (Rh-6G) generates its ground state radical anion (Rh-6G•−) through a photoinduced electron transfer (PET) process. Conversely, when blue LEDs (λ_{Ex}= 455 nm) are employed for photocatalyst excitation, the radical anion is re-excited. The significant difference in reduction potential between the excited and ground states of a redox-active species allows for precise control over the reactivity and resulting selectivity in this photocatalytic system by utilizing different light sources. Notably, unlike other types of organic dyes, the distinctive characteristic of light colour (wavelength)-regulated reactivity in xanthene dyes arises from the hypsochromic shift observed in the absorption spectra upon undergoing single-electron reduction.

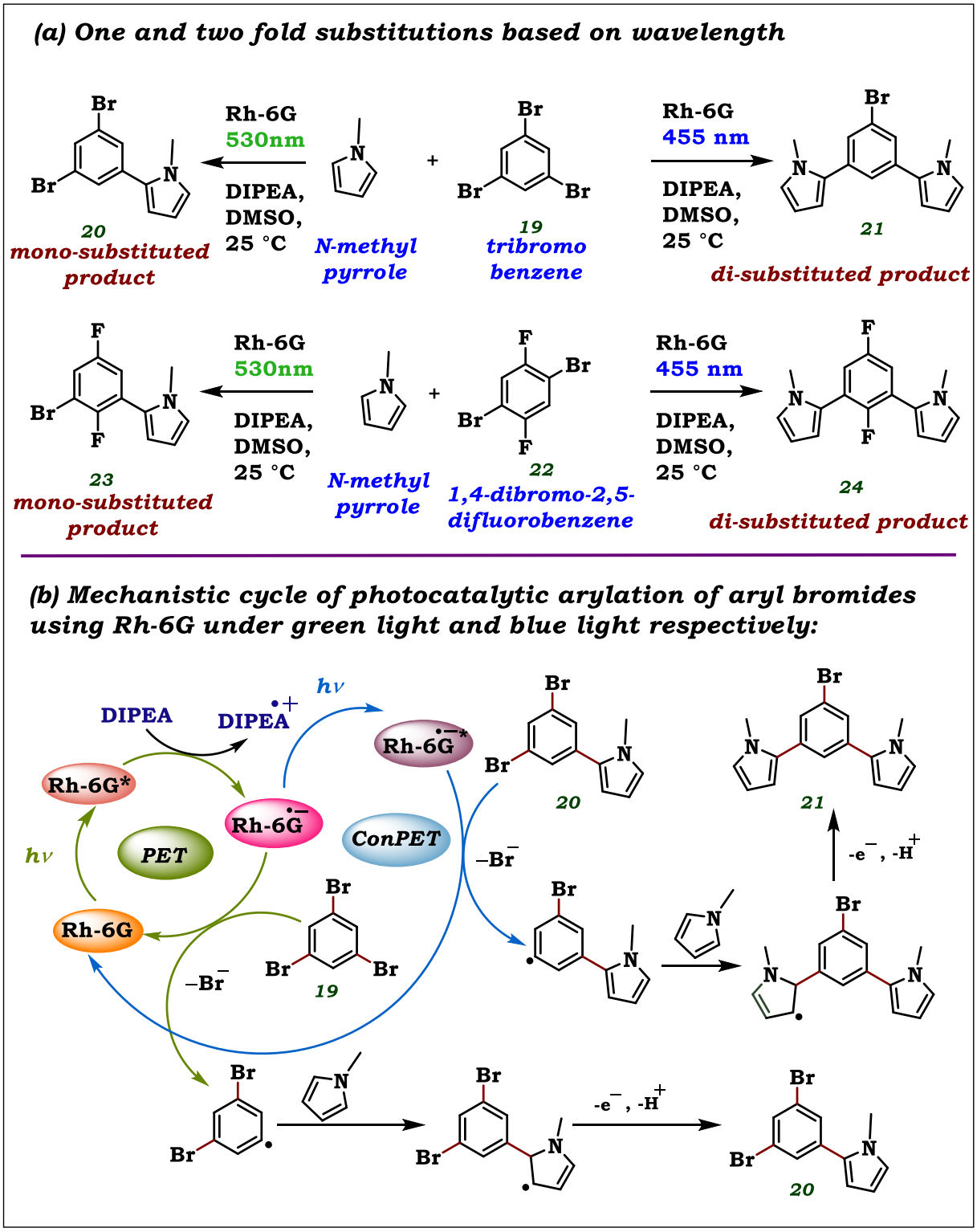
Scheme 9: Visible light induced photoreduction of aryl halides via ConPET pathway



This catalytic approach was employed to showcase a range of specific and consecutive bond activation processes. Upon exposure to green light, 1,3,5-tribromobenzene **19** and 1,4-dibromo-2,5-difluorobenzene **22**, each featuring three and two equivalent C−Br bonds respectively,

afforded selectively monosubstituted C−H arylated products **20**. Conversely, under blue light irradiation of the reaction mixtures, two aryl bromine bonds were triggered, leading to the formation of disubstituted C−H arylated products **21** and **24** respectively (**Scheme 10a**).

Scheme 10: Visible light induced wavelength dependent mono, and -di substitution of aryl bromides via ConPET mechanism



Upon exposure to either green (530 nm) or blue light (455 nm) for photoexcitation (**Scheme 10b**), Rhodamine 6G (Rh-6G) captures an electron from DIPEA, leading to the formation of a radical anion Rh-6G$^{\bullet-}$ and radical cation DIPEA$^{\bullet+}$. The radical anion, Rh-6G$^{\bullet-}$, in its ground state, becomes effective in instigating the activation of aryl bromide substrates that exhibit relatively moderate reduction potentials. Nevertheless, with the application of an irradiation wavelength at λ=455nm, Rh-6G$^{\bullet-}$ undergoes subsequent re-excitation [36, 37], thereby facilitating the activation of aryl bromide substrates characterized by comparably higher reduction potentials [38].

1.3.4. Reaction triggered by visible light in the absence of a photocatalyst:

Leveraging the potential of visible light to initiate chemical reactions using appropriate photocatalysts presents an attractive strategy, primarily due to the environmentally sustainable nature of visible light. Nonetheless, the photoredox catalysts commonly employed in such processes often come with a high cost and potential hazards. Moreover, these catalysts tend to degrade when exposed to light for extended periods, leading to complex procedures for their removal or recovery from reaction mixtures. An ingenious solution to address these issues involves a photocatalyst-free approach to visible light-mediated synthesis. This approach offers the advantage of utilizing visible light for chemical transformations with reduced expenses and minimized environmental contamination.

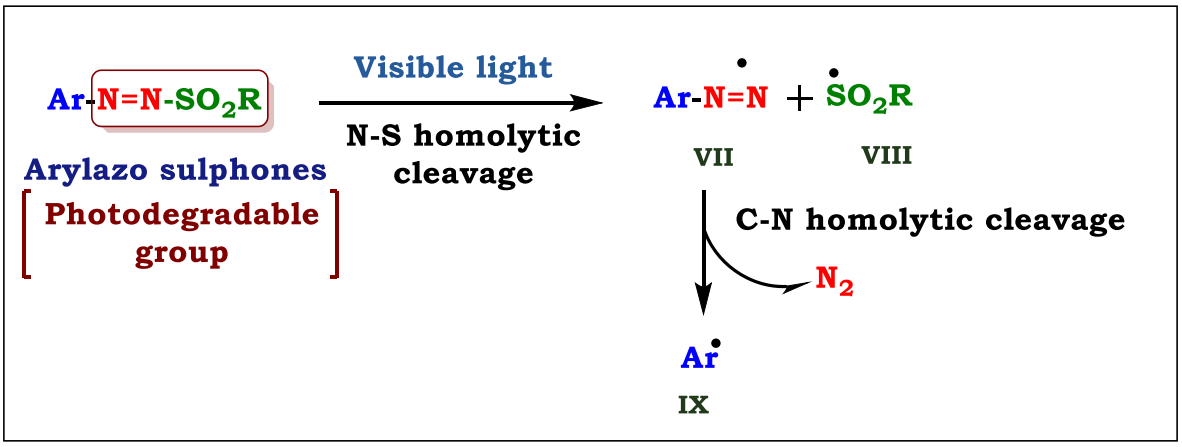


Figure 3: Arylazo sulfones act as precursors, yielding three distinct radicals when exposed to visible light

The approach has been steadily gathering momentum, offering significant potential for novel advancements in the field. One strategy to eliminate the need for external photosensitizers

involves incorporating a visible-light-absorbing functional group (referred to as a "dyed auxiliary group") directly into the starting material.

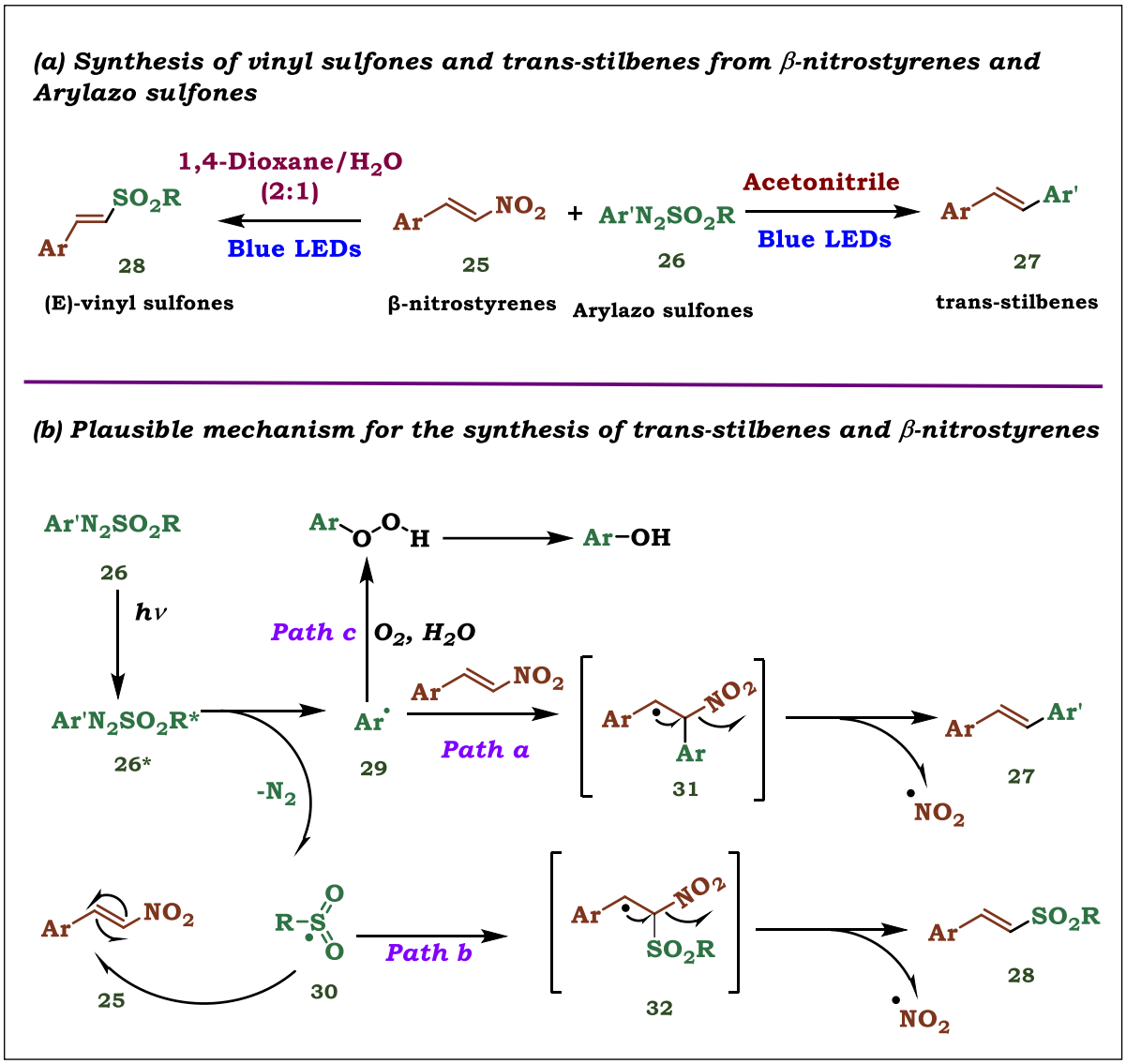
In this context, arylazo sulfones are intriguing photoactive compounds that are stable on the laboratory bench with shelf life and can be readily synthesized in two steps from anilines [39]. When exposed to visible light, these compounds can produce diazenyl **VII** [40], sulfonyl **VIII** [41], and aryl **IX** [42] radicals (**Figure 3**). Recently, this coloured reagent has been utilized as an arylating agent in various applications. For instance, it has been employed for the synthesis of heterobiaryls [42a], allylarenes [42b], arylboranes [42c], aromatic amides [42d], without the necessity of using metals, photocatalysts, or additives under visible light irradiation.

In 2021, Yadav and his group reported reactions mediated by visible light without the need for a photocatalyst, relying on the existence of a visible-light-absorbing functional group within the starting material itself. Arylazo sulfones **26** have been utilized as sources of aryl and sulfonyl radicals under blue LED irradiation, facilitating the synthesis of trans-stilbenes **27** in CH_3CN and (*E*)-vinyl sulfones **28** in dioxane/H_2O (2:1 ratio) [43] (**Scheme 11a**).

They have put forth a viable mechanism depicting the process of generating stilbenes **27** and vinyl sulfones **28** from β-nitrostyrenes **25** and arylazo sulfones **26**, as shown in **Scheme 11b**. Upon exposure to blue light (with a wavelength of 455 nm), arylazo sulfones **26** undergo excitation to a $^1n\pi^*$-state, denoted as **26***. This leads to subsequent homolytic breaking of their C-N, S–N bond, resulting in the creation of an aryl radical, designated as **29**, as well as a sulfonyl radical, referred to as **30**. These newly formed radicals are captured by nitroalkene **25**, resulting in the formation of β-nitro radicals **31** and **32**. Ultimately, these radicals transform into respective products **27** and **28**, accompanied by the emission of $NO2^{\bullet}$. In a solution comprising 1,4-dioxane and water in a 2:1 ratio, path b is the preferred route. This choice is due to the fact that the aryl radical **29** undergoes a transformation into a byproduct, phenol, in the presence of air and water (as indicated by path c).

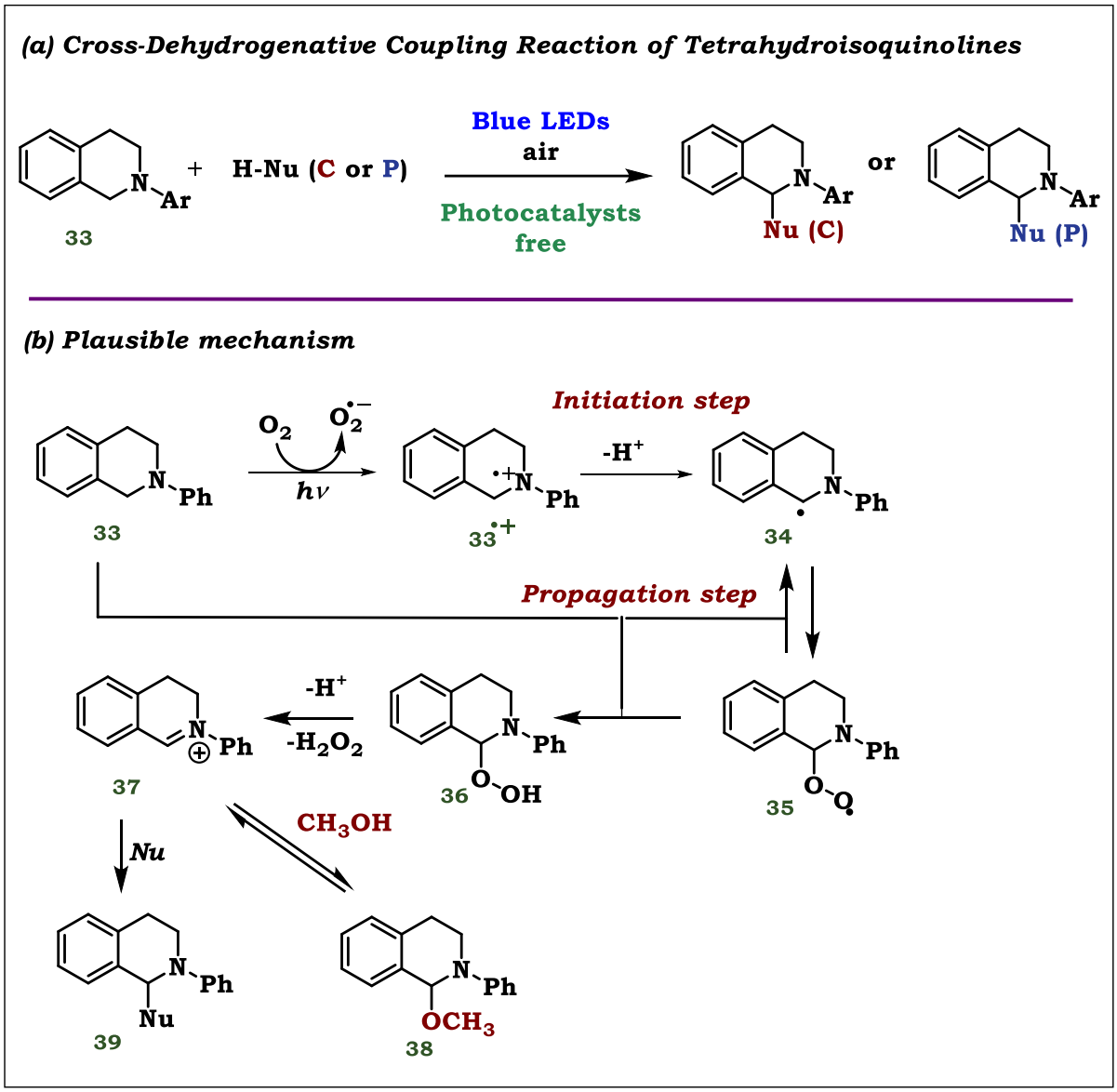
In 2021, Shi and colleagues have introduced an innovative photocatalyst-free approach for cross-dehydrogenative C−C and C−P coupling reactions. This method presents an efficient pathway for synthesizing diverse 1-substituted tetrahydroisoquinoline (THIQ) derivatives **33** [44]. The key feature of this protocol lies in the utilization of direct visible-light excitation of substrates, obviating the need for any photocatalyst (**Scheme 12a**).

Scheme 11: Visible light mediated synthesis of trans-stilbenes and vinyl sulfones



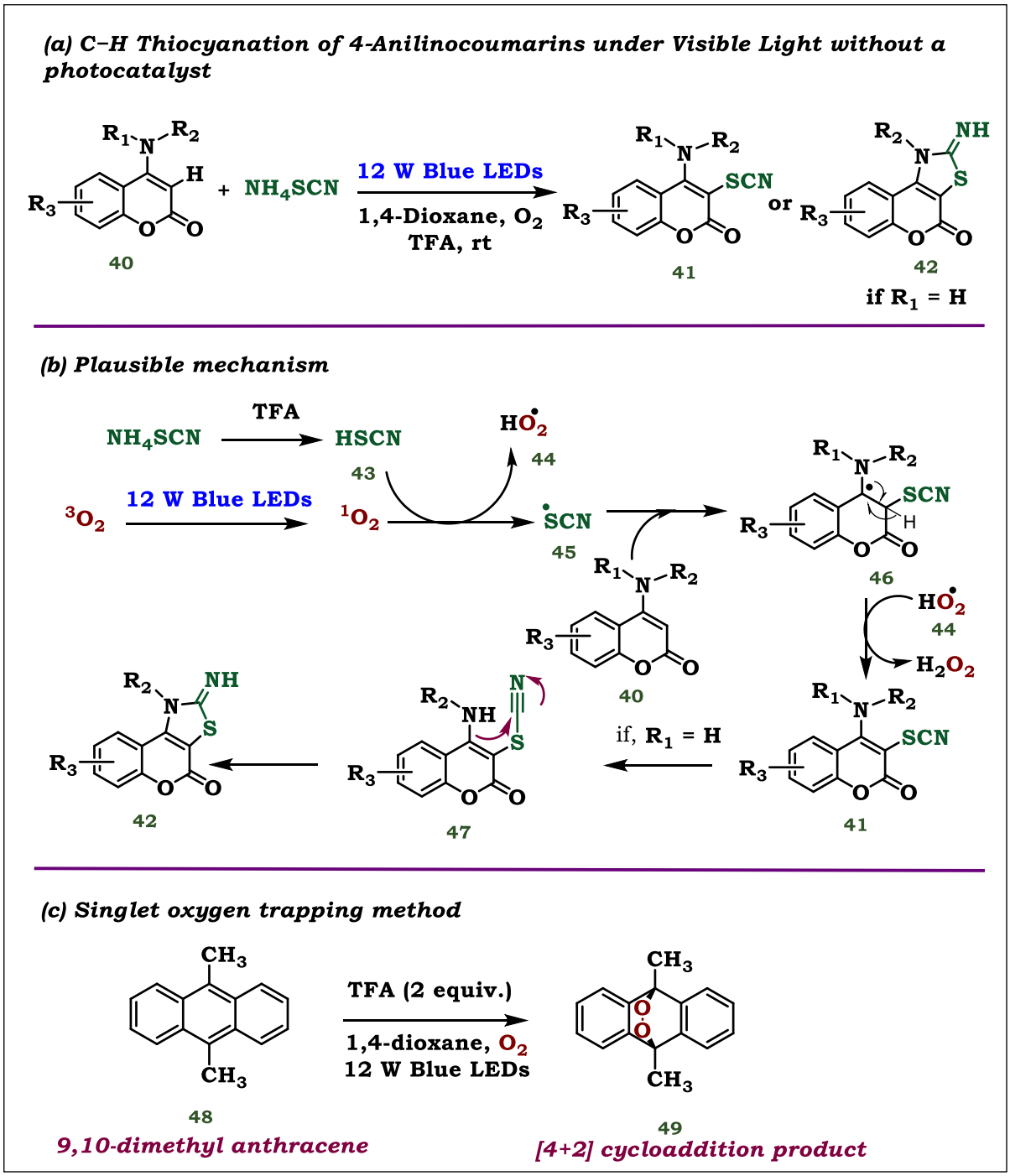
The authors have proposed the mechanism as depicted in **Scheme 12b**. Initially, the visible light-excited N-aryl THIQ (**33**) undergoes quenching by O_2, leading to the formation of radical cation $\mathbf{33}^{\bullet+}$ and superoxide radical anion $O_2^{\bullet-}$. These radicals subsequently combine to produce benzylic radical intermediate **34**. This radical intermediate **34** can then react with another O_2 to generate peroxyl radical **35**, followed by a step involving hydrogen atom abstraction from the initial material **33**, resulting in the regeneration of benzylic radical intermediate **34**. The formed peroxide **36** eventually transforms into an iminium- ion intermediate **37**, concurrently releasing hydrogen peroxide that is detectable using a KI/starch indicator. Methanol effectively stabilizes this intermediate by forming hemiaminal ethers through an off-cycle equilibrium **38**. Ultimately, the iminium-ion intermediate **37** is susceptible to addition by an active nucleophile, culminating in the formation of the coupling product **39**.

Scheme 12: Cross-dehydrogenative C−C and C−P coupling reactions



In 2019, Yang and colleagues reported a visible light-induced C(sp^2)−H thiocyanation reaction involving electron-rich heteroarenes and arenes, utilizing easily accessible ammonium thiocyanate [45] (**Scheme 13a**). Significantly, the reaction proceeded effectively without the need for utilizing any photocatalyst or strong oxidant, thereby significantly reducing the generation of chemical waste.

Scheme 13: Visible light-induced C(sp^2)–H thiocyanation reaction



In their mechanistic investigation (**Scheme 13b**), they determined that molecular oxygen serves as the active species under visible light. This involves its transition from the ground triplet state ($^3O_2$) to the excited singlet state ($^1O_2$). They successfully captured the singlet oxygen using 9,10-dimethylanthracene **48** through a [4+2] cycloaddition reaction **49** (**Scheme 13c**). Furthermore, the interaction between ammonium thiocyanate and trifluoroacetic acid (TFA)

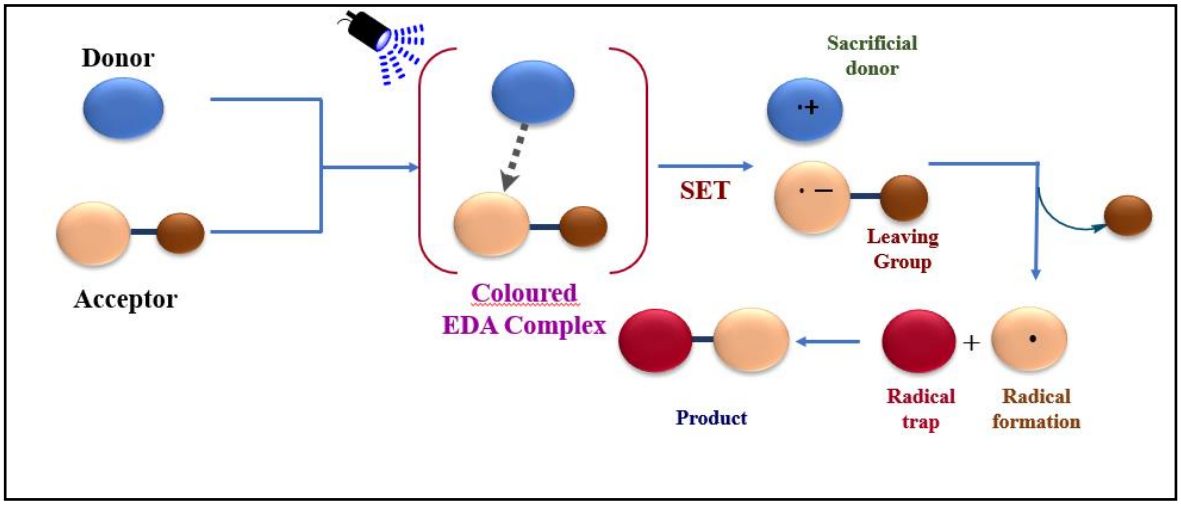
resulted in the formation of thiocyanic acid **43**. This acid reacted with the singlet oxygen $^1O_2$ to generate hydroperoxyl radical **44** and thiocyanate radical **45**. Selectively, thiocyanate radical **45** added to coumarin derivatives **40** to produce radical species **46**, which presumably transforms into the desired products **41** through a single electron transfer (SET) process involving hydroperoxyl radical **44**, consequently yielding hydrogen peroxide as a non-toxic byproduct. Furthermore, when R_2 is hydrogen (H) **47**, an intramolecular nucleophilic reaction involving NH to CN leads to the formation of the cyclization product **42 (Scheme 13b)**.

1.3.5. Visible light induced Electron Donor-Acceptor (EDA) Complex:

Another significant approach utilized for achieving visible light-driven reactions without the need for a photocatalyst is through the utilization of Electron Donor Acceptor (EDA) complexes [46] The interaction between an electron-rich molecule (referred to as the donor, D) and an electron-poor molecule (known as the acceptor, A) in their lowest energy state results in the formation of an electron donor-acceptor (EDA) complex. This complex may exhibit absorption of visible light and can facilitate electron transfer even in the absence of a photocatalyst (**Scheme 14**). The process is applicable under broad reaction conditions. The electron-transfer event can be outlined as follows: a donor molecule (D), characterized by electron-rich properties like low ionization potential, functioning as a reducing agent or nucleophile, and an acceptor molecule (A), possessing electron-poor attributes with high electron affinity as an oxidizing agent or electrophile, promptly combine within a solution or gas phase to create an initial complex known as [D, A] EDA. This initial interaction, known as an electron donor-acceptor (EDA) complex, or alternatively a charge-transfer (CT) complex, is a reversible and transient association taking place in the ground state [47]. Due to their comparatively weaker and less specific nature when compared to interactions like hydrogen bonding, [48] these associations are notably susceptible to alterations in temperature, solvent, and concentration [49]. Consequently, the resulting ensemble often displays a fresh absorption band referred to as the charge-transfer band. This distinct band, not evident in the UV-Vis absorption spectra of the individual constituents, usually shifts towards longer wavelengths, occasionally extending into the visible light spectrum. This shift leads to a pronounced characteristic coloration of the complex. When illuminated with light at the wavelength corresponding to its charge-transfer (CT) band, the [D, A] EDA complex undergoes a transformation. This transformation involves the formation of a reactive excited complex ([D, A]*), initiating an electron-transfer process. This process leads to the creation of a radical ion pair confined within the surrounding solvent environment, specifically denoted as

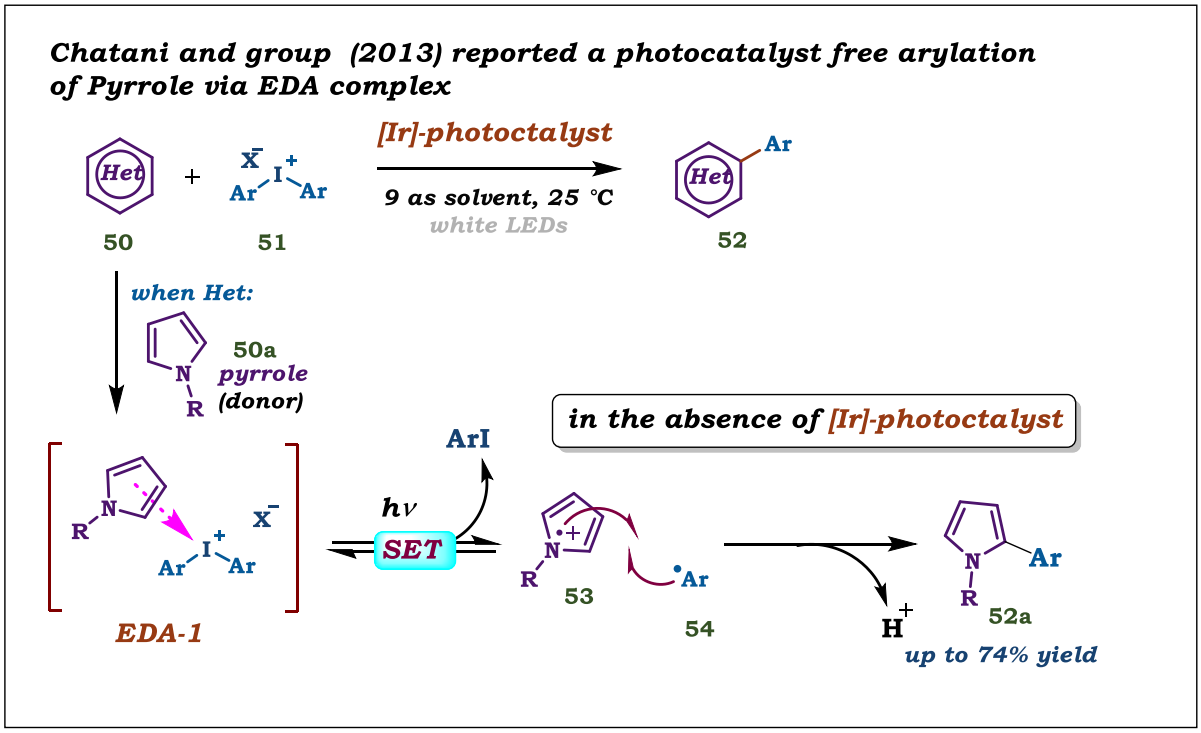
$[D^{\bullet+},A^{\bullet-}]_{SOLV}$. Subsequently, this radical ion pair has multiple possible courses of action, which encompass various reaction pathways. These options include breaking out of the solvent cage to generate independent free radical ions, or engaging in a reverse electron-transfer event.

Scheme 14: General mechanistic pathway of an EDA-complex



In order to understand the EDA complex and its functioning further a literature examples have been discussed. In 2013, both the Chatani group [50] and Melchiorre group [51] separately undertook endeavours to re-examine and re-introduce the photochemistry of EDA complexes as an effective approach for generating radicals in chemical synthesis (**Scheme 15** and **Scheme 16**). While developing a photoredox protocol for the arylation of heteroaromatics **50** using iodonium salts **51** (**Figure 3a**), Chatani and collaborators made an intriguing observation [50]. They noticed that when electron-rich pyrroles **50a** were employed as substrates, the resulting product **52a** could be obtained even without the addition of an external iridium photoredox catalyst. In their conventional approach, the photoredox catalyst facilitated the generation of aryl radicals through single-electron transfer (SET) reduction of **51**. However, in the case of pyrroles **50a**, the mere exposure of the substrates to visible light was sufficient to initiate the radical-forming process.

Scheme 15: Photocatalyst free arylation of pyrrole via Electron Donor-Acceptor (EDA) complex

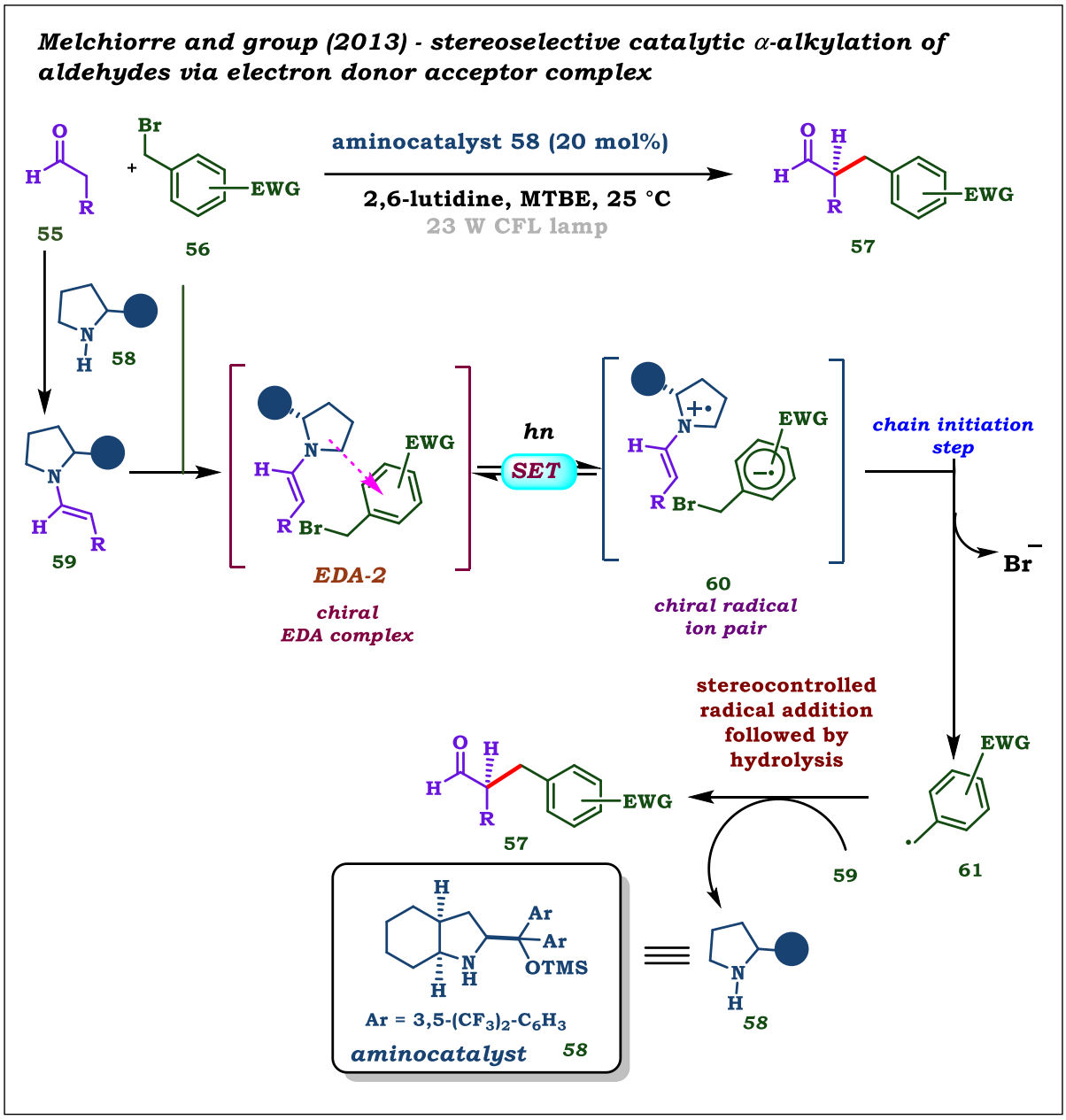


This unique reactivity was reasoned by the formation of an EDA complex, denoted as ***EDA-1*** (**Scheme 15**), exhibiting a yellow-orange hue. This complex was generated in the solution by the interaction between substrates **50a** and **51**. Verification through optical absorption spectroscopy confirmed the emergence of a fresh absorption band within the visible spectrum range, referred to as the charge-transfer band ($h\nu_{CT}$). The EDA complex (***EDA-1***), with its distinctive colour, upon light irradiation, underwent an irreversible aryl iodide extrusion process, giving rise to radical intermediates labeled as **53** and **54**. These intermediates played a role in furnishing the C2-arylated product **52a**.

Simultaneously, Melchiorre group investigated the direct α-alkylation of aldehydes **55** using electron-deficient alkyl bromides **56**, which included compounds like benzyl and phenacyl bromides, under the catalytic influence of the chiral amine **58** (**Scheme 16**). Prior investigations into analogous reactivity had indicated the necessity for a photoredox catalyst to generate radicals through the reductive cleavage of alkyl bromide **56** [18]. However, a controlled experiment brought to light that, for certain substrates **56**, the reaction could efficiently progress in a stereoselective manner without the addition of an external photoredox catalyst [51]. Notably, this chemistry remained unresponsive in the absence of light, and evidence supporting a radical-based mechanism was gathered.

Deeper mechanistic studies unveiled the capability of electron-rich chiral enamines **59**, formed upon the condensation of amine catalyst **58** with aldehyde **55**, to initiate the creation of EDA complexes (referred to as ***EDA-2***) with electron-deficient alkyl bromides **56**. When exposed to light, an intra-complex single-electron transfer (SET) process occurred within ***EDA-2***, leading to the formation of chiral radical ion pair **60**. This in turn facilitated the irreversible cleavage of the carbon-halogen bond within **60**, preventing unproductive processes and resulting in the formation of reactive open-shell intermediate **61**.

Scheme 16: α-alkylation of aldehyde via EDA complex formation



Experimental verification through optical absorption spectroscopy confirmed the existence of the enamine-based EDA complex ***EDA-2***, which displayed absorption in the visible frequency range, an ability lacking in its individual components (enamine **59** and bromide **56**). Quantitative measurements of quantum yield demonstrated [*52*] that the reaction unfolded through a self-propagating radical chain mechanism [53]. This indicated that the photochemical behavior of the enamine-based ***EDA-2*** complex acted as an initiation step to sustain a chain reaction process. The propagation process hinged on the capacity of the α-amino alkyl radical (not depicted in **Scheme 16**), emerging from the radical trap **61** of the ground-state chiral enamine **59**, to regenerate **61** through SET reduction of organic bromides **56**. In the forward step the coupling of **59** and **61** produces chiral α-alkylated aldehyde **57** with the regeneration of chiral amino catalyst **58**. This study underscored that transient catalytic intermediates, such as chiral enamines, can engage in the formation of photoactive EDA complexes, inciting asymmetric radical processes that conventional ground-state organocatalysis cannot achieve. Overall, this investigation demonstrated that the synthetic capabilities of organocatalysis can be elevated by amalgamating them with photochemical reactivity, thus unveiling reaction pathways that remain inaccessible via conventional thermal activation methods [54].

1.4. Conclusions:

The thesis on photoredox catalysis starts by tracing its historical evolution, merging photochemistry and catalysis to utilize visible light and catalysts for chemical transformations. Significant milestones, like discovering photochemical reactions and developing transition metal-based catalysts, highlight its importance in modern synthetic chemistry due to mild conditions, selectivity, and unconventional transformations. The introduction outlines mechanistic pathways, focusing on single electron transfer processes, such as reductive and oxidative quenching cycles, along with hydrogen atom transfer mechanisms. Some of the principles and mechanistic concepts described in this chapter have been explored for the development of newer transformations via visible light catalysis to access useful compounds of significance. The design and development of the methods have been described in detail in the subsequent chapters (two, three, and four). These chapters delve deeper into photocatalyst-based pathways, aiming for a comprehensive understanding of their applications. The final chapter introduces an innovative, photocatalyst-free protocol utilizing visible light for single oxygen generation and electron donor-acceptor complex formation an alternative avenue for light-induced chemical transformations.

1.5. References:

(1) a) Narayanam, J. M. R.; Stephenson, C. R. J. Visible Light Photoredox Catalysis: Applications in Organic Synthesis. *Chem. Soc. Rev*. **2011**, 40 (1), 102−113. b) Yoon, T. P.; Ischay, M. A.; Du, J. Visible Light Photocatalysis as a Greener Approach to Photochemical Synthesis. *Nat. Chem*. **2010**, 2 (7), 527−532. c) Marzo, L.; Pagire, S. K.; Reiser, O.; König, B. Visible-Light Photocatalysis: Does It Make a Difference in Organic Synthesis? *Angew. Chem. Int. Ed*. **2018**, *57*, (32), 10034−10072. d) Shaw, M. H.; Twilton, J.; MacMillan, D. W. C. Photoredox Catalysis in Organic Chemistry. *J. Org. Chem*. **2016**, 81 (16), 6898− 6926.

(2) Takeda, H. and Ishitani, O. (**2010**) Development of efficient photocatalytic systems for CO2 reduction using mononuclear and multinuclear metal complexes based on mechanistic studies. *Coord. Chem. Rev*. *254*, 346–354.

(3) Graetzel, M. (**1981**) Artificial photosynthesis: water cleavage into hydrogen and oxygen by visible light. *Acc. Chem. Rev*. 14, 376–384.

(4) Kalyanasundaram, K. and Grätzel, M. (**1998**) Applications of functionalized transition metal complexes in photonic and optoelectronic devices. Coord. *Chem. Rev*. 177, 347–414.

(5) a) Xuan, J. and Xiao, W.-J. Visible-light photoredox catalysis. *Angew. Chem. Int. Ed*. **2012**, 51, 6828–6838. b) Reckenthäler, M. and Griesbeck, A.G. Photoredox catalysis for organic syntheses. *Adv. Synth. Catal*. **2013**, 355, 2727–2744. c) Prier, C.K. et al. Visible light photoredox catalysis with transition metal complexes: applications in organic synthesis. *Chem. Rev*. **2013**, 113, 5322–5363. d) Schultz, D.M. and Yoon, T.P. Solar synthesis: prospects in visible light photocatalysis. *Science*, **2014**, 343, 1239176. e) Skubi, K.L. et al. Dual catalysis strategies in photochemical synthesis. *Chem. Rev*. **2016**, 116, 10035–10074.

(6) Crisenza, G. E. M.; Melchiorre, P. Chemistry Glows Green with Photoredox Catalysis. *Nat. Commun*. **2020**, 11 (1), 803.

(7) a) Douglas, J. J.; Sevrin, M. J.; Stephenson, C. R. J. Visible Light Photocatalysis: Applications and New Disconnections in the Synthesis of Pharmaceutical Agents. *Org. Process Res. Dev*. **2016**, 20 (7), 1134− 1147. (b) Nicholls, T. P.; Leonori, D.; Bissember, A. C. Applications of Visible Light Photoredox Catalysis to the Synthesis of Natural Products and Related Compounds. *Nat. Prod. Rep*. **2016**, 33 (11), 1248−1254. (c) McAtee,

R. C.; McClain, E. J.; Stephenson, C. R. J. Illuminating Photoredox Catalysis. *Trends Chem*. **2019**, 1 (1), 111−125.

(8) Gueymard, C. A. The Sun's Total and Spectral Irradiance for Solar Energy Applications and Solar Radiation Models. *Sol. Energy* **2004**, 76 (4), 423−453.

(9) G. Ciamician, *Science* **1912**, *36*, 385–394.

(10) (a) Hedstrand, D. M.; Kruizinga, W. M.; Kellogg, R. M. *Tetrahedron Lett*. **1978**, 19, 1255−1258. (b) van Bergen, T. J.; Hedstrand, D. M.; Kruizinga, W. H.; Kellogg, R. M. *J. Org. Chem*. **1979**, 44, 4953−4962.

(11) (a) Hironaka, K.; Fukuzumi, S.; Tanaka, T. *J. Chem. Soc*., *Perkin Trans*. 2 **1984**, 1705−1709. (b) Fukuzumi, S.; Koumitsu, S.; Hironaka, K.; Tanaka, T. *J. Am. Chem. Soc*. **1987**, *109*, 305−316. (c) Fukuzumi, S.; Mochizuki, S.; Tanaka, T. *J. Phys. Chem*. **1990**, *94*, 722−726.

(12) (a) Pac, C.; Ihama, M.; Yasuda, M.; Miyauchi, Y.; Sakurai, H. *J. Am. Chem. Soc*. **1981**, *103*, 6495−6497. (b) Pac, C.; Miyauchi, Y.; Ishitani, O.; Ihama, M.; Yasuda, M.; Sakurai, H. *J. Org. Chem*. **1984**, *49*, 26−34. (c) Ishitani, O.; Ihama, M.; Miyauchi, Y.; Pac, C. *J. Chem. Soc., Perkin Trans*. 1 **1985**, 1527−1531. (d) Ishitani, O.; Pac, C.; Sakurai, H. *J. Org. Chem*. **1983**, *48*, 2941−2942. (e) Ishitani, O.; Yanagida, S.; Takamuku, S.; Pac, C. *J. Org. Chem*. **1987**, *52*, 2790−2796.

(13) Cano-Yelo, H.; Deronzier, A. *Tetrahedron Lett*. **1984**, *25*, 5517− 5520.

(14) (a) Cano-Yelo, H.; Deronzier, A. *J. Chem. Soc., Perkin Trans*. 2 **1984**, 1093−1098. (b) Cano-Yelo, H.; Deronzier, A. *J. Photochem*. **1987**, *37*, 315−321.

(15) G. Pandey, S. Hajra, M. K. Ghorai, K. R. Kumar, *J. Am. Chem. Soc*. **1997**, *119*, 8777–8787.

(16) (a) P. S. Mariano (Ed.), Advances in Electron Transfer Chemistry, **1996**, JAI Press, London. (b) J. Mattay (Ed.), Photoinduced Electron Transfer V, Top. *Curr. Chem*. Vol. 168, **1993**, Springer, Stuttgart.

(17) Ischay, M. A.; Anzovino, M. E.; Du, J.; Yoon, T. P. *J. Am. Chem. Soc*. **2008**, *130*, 12886−12887.

(18) Nicewicz, D. A.; MacMillan, D. W. C. *Science* **2008**, *322*, 77−80.

(19) Narayanam, J. M. R.; Tucker, J. W.; Stephenson, C. R. J. *J. Am. Chem. Soc*. **2009**, *131*, 8756−8757.

(20) Bonardi, A.-H., Dumur, F., Noirbent, G. et al. *Beilstein J. Org. Chem*. **2018**,*14*, 3025–3046.

(21) (a) Condie, A. G.; Gonzalez-Gomez, J. C.; Stephenson, C. R. J.́ *J. Am. Chem. Soc*. **2010**, *132*, 1464−1465. b) McNally, A.; Prier, C. K.; MacMillan, D. W. C. *Science* **2011**, *334*, 1114−1117.

(22) (a) L. Capaldo and D. Ravelli, *Eur. J. Org. Chem*., **2017**, 2056–2071; (b) L. Capaldo, L. L. Quadri and D. Ravelli, *Green Chem*., **2020**, *22*, 3376–3396; (c) H. Cao, X. Tang, H. Tang, Y. Yuan and J. Wu, *Chem Catal*., **2021**, *1*, 523–598.

(23) (a) Hammes-Schiffer, S. *Acc. Chem. Res*. **2001**, *34*, 273−28. (b) Huynh, M. H. V.; Meyer, T. J. *Chem. Rev*. **2007**, *107*, 5004−5064. (c) Costentin, C. *Chem. Rev*. **2008**,*108*, 2145−2179.

(24) Warburton, R. E.; Soudackov, A. V.; Hammes-Schiffer, S. *Chem. Rev*. **2022**, *122*, 10599−10650.

(25) Darcy, J.W.; Koronkiewicz, B.; Parada, G.A. and Mayer, J.M. *Acc. Chem. Res*. **2018**, *51*, 2391–2399.

(26) Newhouse, T., and Baran, P.S. *Angew. Chem. Int. Ed. Engl*. **2011**, *50*, 3362–3374.

(27) Cao, H.; Tang, X.; Tang, H.; Yuan, Y.; Wu, J. *Chem. Catal*. **2021**,*1*, 523−598.

(28) Capaldo, L.; Ravelli, D.; Fagnoni, M. *Chem. Rev*. **2022**,*122*,1875−1924.

(29) Margrey, K. A.; Nicewicz, D. A. *Acc. Chem. Res*. **2016**, *49*, 1997−2006.

(30) Schreier, M. R.; Pfund, B.; Guo, X.; Wenger, O. S. *Chem. Sci*. **2020**, *11*, 8582−8594.

(31) Fang, X.; Zhang, N.; Chen, S. -C.; Luo, T. *J. Am. Chem. Soc*. **2022**, *144*, 2292−2300.

(32) Nakagawa, M.; Matsuki, Y.; Nagao, K.; Ohmiya, H., A. *J. Am. Chem. Soc*. **2022**, *144*, 7953−7959.

(33) Kamei, Y.; Seino, Y.; Yamaguchi, Y.; Yoshino, T.; Maeda, S.; Kojima, M.; Matsunaga, S. *Nat. Commun*. **2021**, *12*, 966.

(34) Ghosh, I.; Ghosh, T.; Bardagi, J. I.; Konig, B. *Science* **2014**, *346*, 725–728.

(35) Ghosh, I.; König, B. *Angew. Chem., Int. Ed*. **2016**, *55*, 7676−7679.

(36) van de Linde, S.; Lçschberger, A.; Klein, T.; Heidbreder, M.; Wolter, S.; Heilemann, M.; Sauer, M. *Nat. Protoc*. **2011**, *6*, 991–1009.

(37) van de Linde, S.; Krstić, I.; Prisner, T.; Doose, S.; Heilemann, M.; Sauer, M. *Photochem. Photobiol. Sci*. **2011**, *10*, 499–506.

(38) Costentin, C.; Robert, M.; Saveant, J. M. *J. Am. Chem. Soc*. **2004**, *126*, 16051–16057.

(39) (a) Kice, J. L.; Gabrielsen, R. S. *J. Org. Chem*., **1970**, *35*, 1010; (b) Rosini G.; Ranza, R. *J. Org. Chem*., **1971**, *36*, 1915.

(40) Abdulla, H. O.; Scaringi, S.; Amin, A. A.; Mella, M.; Protti S.; Fagnoni, M. *Adv. Synth. Catal*., **2019**, *362*, 2150.

(41) (a) Liu, Q.; Liu, F.; Yue, H.; Zhao, X.; Li, J.; Wei, W. *Adv. Synth. Catal*., **2019**, *361*, 5277; (b) Y. Lv, Q. Liu, F. Liu, H. Yue, J.-S. Li and W. Wei, Tetrahedron Lett., 2020, 61, 151335; (c) Chawla, R.; Jaiswal, S.; Dutta P. K.; Yadav, L. D. S. *Tetrahedron Lett*., **2020**, *61*, 151898.

(42) (a) Crespi, S.; Protti S.; Fagnoni, M. *J. Org. Chem*., **2016**, *81*, 9612; (b) Dossena, A.; Sampaolesi, S.; Palmieri, A.; Protti S.; Fagnoni, M. *J. Org. Chem*., **2017**, *82*, 10687; (c) Xu, Y.; Yang, X.; Fang, H. *J. Org. Chem*., **2018**, *83*, 12831; (d) Malacarne, M.; Protti S.; Fagnoni, M. *Adv. Synth. Catal*., **2017**, *359*, 3826.

(43) Chawla, R.; Jaiswal, S.; Dutta, P. K.; Yadav, L. D. S. *Org. Biomol. Chem*. **2021**, *19*, 6487−6492.

(44) Guo, X.; Shao, B.; Jiang, W. f; Shi, L. *J. Org. Chem*., **2021**, *86*, 15743–15752.

(45) Li, G.; Yan, Q.; Gong, X.; Dou, X.; Yang, D. *ACS Sustainable Chem. Eng*. **2019**, *7*, 14009−14015.

(46) Lima, C. G. S.; de M Lima, T.; Duarte, M.; Jurberg, I. D.; Paixao, M. W. *ACS Catal*. **2016**, *6*, 1389−1407.

(47) (a) Kochi, J. K. *Pure Appl. Chem*. **1991**, *63*, 255−264; (b) Foster, R. J. *Phys. Chem*. **1980**, *84*, 2135−2141.

(48) (a.) Zhao, G. J.; Han, K. L. *Acc. Chem. Res*. **2012**, *45*, 404−413 and references therein.. (b) Among others, such interactions can be seen as being of intermediate strength, between one extreme of a scale, attributable to forces of van der Waals, with values typically less than 1 kcal·mol−1, and the other extreme, where chemical bonds are, with values typically 50 kcal·mol^{-1}or more.

(49) Rosokha, S. V.; Kochi, J. K. *Acc. Chem. Res*. **2008**, *41*, 641−653.

(50) Tobisu, M.; Furukawa, T.; Chatani, N. *Chem. Lett*. **2013**, *42*, 1203−1205.

(51) Arceo, E.; Jurberg, I. D.; Á lvarez-Fernandez, A.; Melchiorre, P.́ *Nat. Chem*. **2013**, *5*, 750−756.

(52) Bahamonde, A.; Melchiorre, P. *J. Am. Chem. Soc*. **2016**, *138*, 8019−8030.

(53) Studer, A.; Curran, D. P. *Angew. Chem., Int. Ed*. **2016**, *55*, 58− 102.

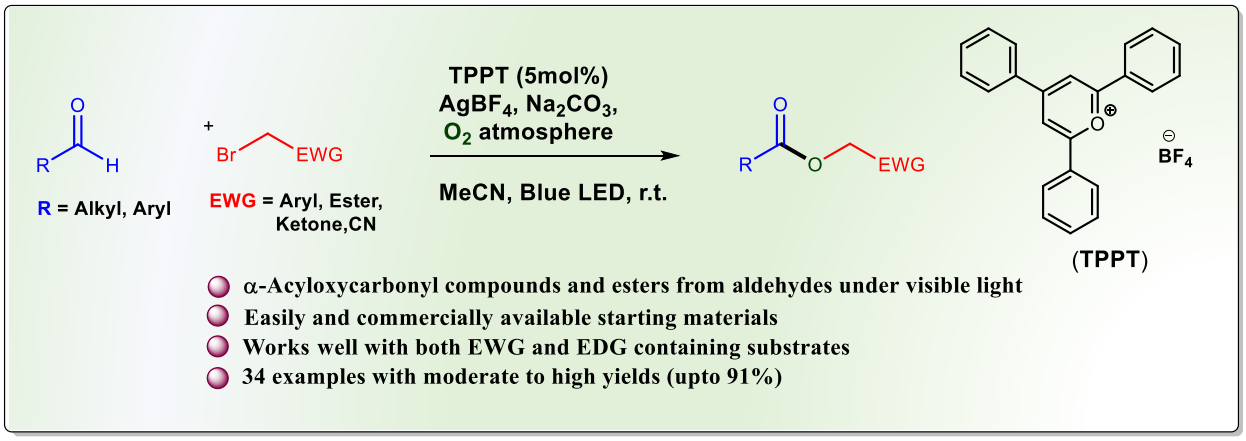
(54) Silvi, M.; Melchiorre, P. *Nature* **2018**, *554*, 41−49.

CHAPTER 2

Direct Access to α-Acyloxycarbonyl Compounds and Esters via Oxidative Esterification of Aldehydes Under Visible Light

Abstract

This chapter describes the effective synthesis of α-acyloxycarbonyl compounds and esters from aldehydes, α-bromocarbonyl compounds/benzyl bromide derivatives, and bromo nitriles at room temperature using an organic photocatalyst and silver tetrafluoroborate in the presence of visible light. The reaction has been successfully used to synthesize a wide range of compounds and is compatible with a wide range of functional groups. The labeling experiment and fluorescence spectroscopy data, along with other meticulously controlled tests, unmistakably demonstrated the reductive quenching of the photoredox catalytic cycle.



Bhowmick, A.; Warghude P. K.; Dharpure, P. D.; Bhat, R. G. *Org. Chem. Front.*, **2021**,*8*, 4777-4784.

Direct Access to α-Acyloxycarbonyl Compounds and Esters via Oxidative Esterification of Aldehydes Under Visible Light

2.1. Introduction:

α-Acyloxycarbonyl compounds and esters are prevalent in a wide range of natural products and bioactive molecules [1]. This group of compounds is celebrated for its remarkable properties, specifically its ability to combat microbial infections [2], fungal growth [3], and viral activity [4]. In other words, these compounds have demonstrated significant effectiveness in inhibiting the growth or activity of microorganisms, fungi, and viruses, making them valuable in various applications, including pharmaceuticals and medicine. These compounds are highly valuable starting materials and have been investigated for creating complex chiral molecules through a selective addition process, wherein chelation control plays a pivotal role [5]. Similarly, α-acyloxy ketones have been investigated for their utility in crafting valuable heterocyclic compounds, including derivatives of imidazole and oxazole [6]. Similarly, α-acyloxycarbonyl compounds have been employed in the construction of furans, cyclobutanes, and hydroxyketones [7]. Extensive studies have illustrated the utility of α-acyloxyketones as crucial intermediates in the synthesis of anti-inflammatory medications [8]. Numerous bioactive compounds feature the α-acyloxyketone functionality within their molecular structures (**Figure 1**) [7b].

Due to the significant relevance of α-acyloxycarbonyl compounds and esters, numerous endeavors have been undertaken to synthesize them through diverse pathways. Traditional approaches involve the reaction of alkaline carboxylates or carboxylic acids with α-halocarbonyl compounds [6a] or α-diazoesters [9]. Certain techniques within this category exhibit limited applicability to a range of substrates, while others necessitate the prior preparation of specific initial compounds. Traditional esterification processes like the Mitsunobu and Steglich reactions are known for producing substantial quantities of by-product waste. An alternative approach involves investigating the oxidative homocoupling of aryl ketones [10]. Additionally,

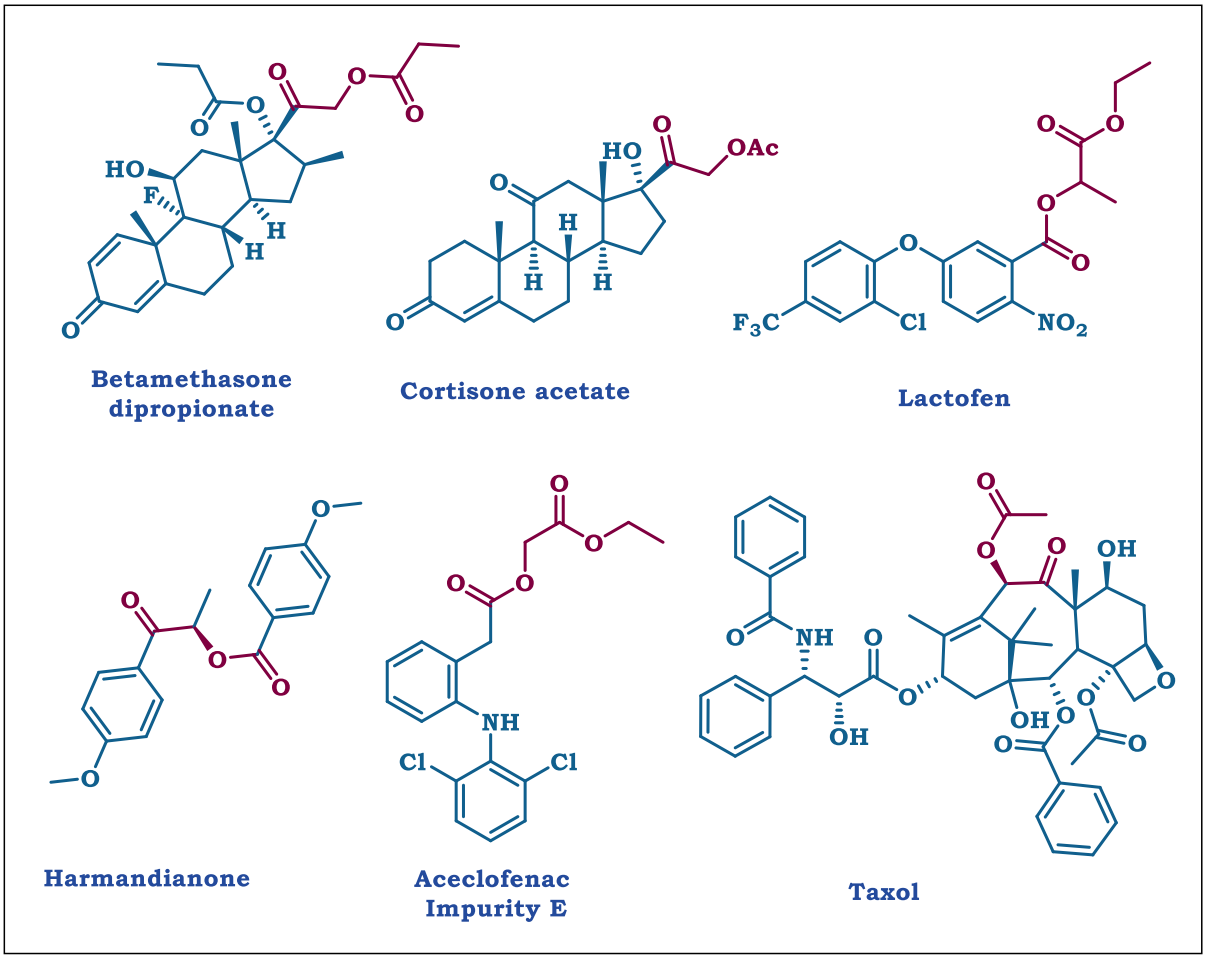


Figure 1. Bioactive compounds containing α-acyloxyketone moiety

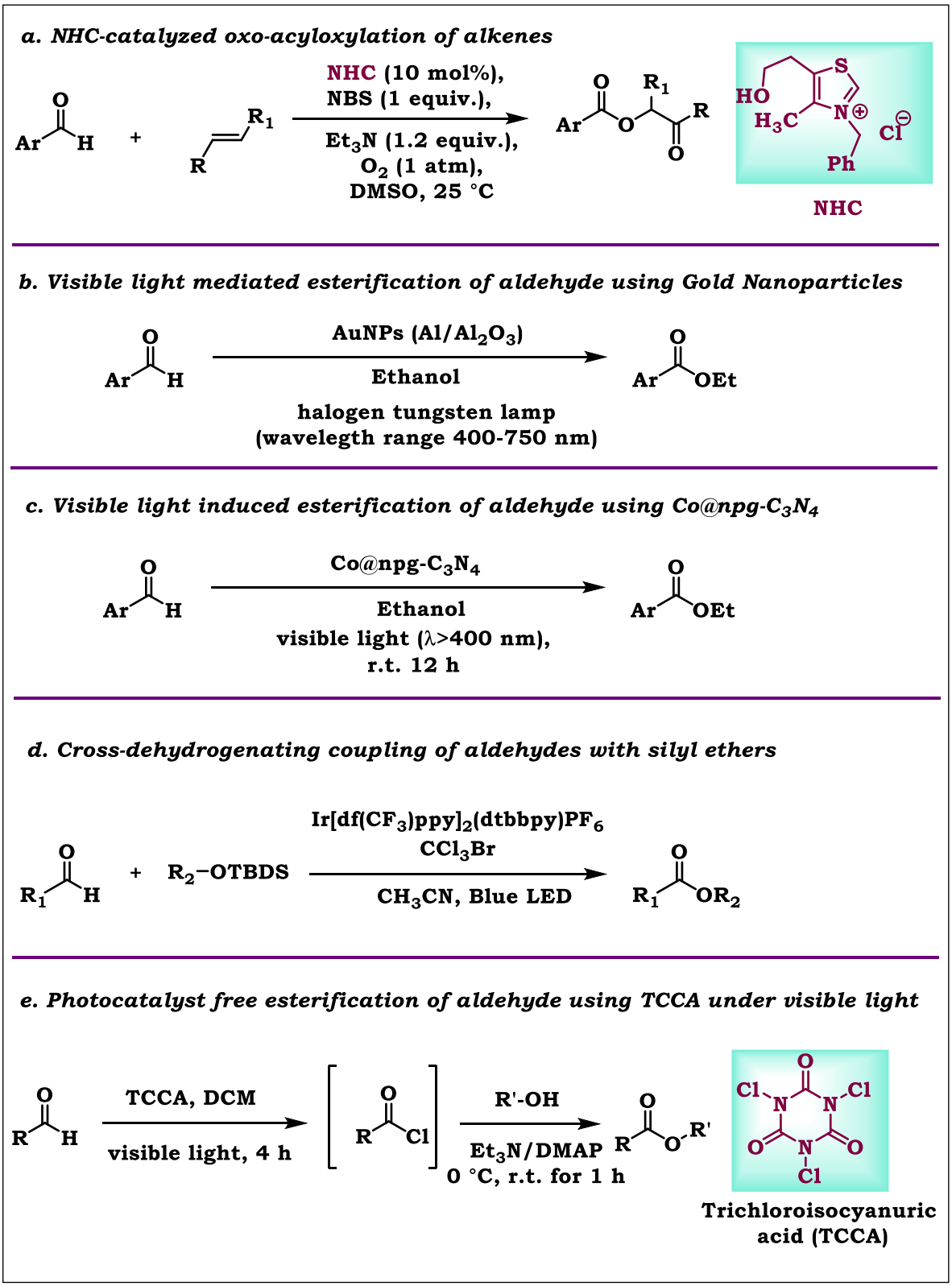
researchers have explored the utilization of hypervalent iodine catalysts for the direct oxidative coupling of ketones with carboxylic acids, employing co-oxidants to facilitate the synthesis of α-acyloxy ketones [11]. Over time, efforts have been made to directly access esters, starting from aldehydes, as these aldehydes are commercially viable and readily accessible starting materials, aiming to streamline the synthetic process and reduce the number of required steps [12].

2.2. Previous work of esterification of aldehydes:

Sudalai and his research team have reported a method for synthesizing α-acyloxyketones. This method commences with aldehydes and alkenes, utilizing NHC catalysis in the presence of an oxygen atmosphere (**Scheme 1a**) [13a]. This regioselective oxidative procedure utilizes *N*-bromosuccinimide (NBS) and triethylamine (Et_3N) in equal quantities, along with oxygen gas (1 atm) as an oxidizing agent, all under ambient conditions in dimethyl

sulfoxide (DMSO) as the solvent. Similarly, in 2010, Studer group have disclosed the NHC catalyzed oxidations of aldehydes to esters under mild reaction conditions [13b].

Scheme 1: Previously reported esterification of aldehydes



The utilization of visible light in organic compound synthesis has garnered significant interest within the synthetic organic community, primarily because it offers environmentally friendly and sustainable reaction conditions [14]. Several elegant approaches have been documented for the one-pot synthesis of esters, commencing with aldehydes, under visible light-driven conditions. In 2014, Zhu and co-workers introduced an innovative concept, the utilization of gold nanoparticles **AuNPs** (Au/Al_2O_3) to catalyse the esterification of aldehydes under visible light conditions (**Scheme 1b**) [15]. In 2017, Jain research group developed the method for the esterification of aromatic aldehydes [16]. They accomplished this under the influence of visible light, employing a cobalt complex ($Co@npg\text{-}C_3N_4$) based on carbon nitride as the photocatalyst (**Scheme 1c**). In 2018, Pandey and coworkers presented a method outlining the synthesis of amides, ureas and esters by cross dehydrogenative coupling between aldehydes (or amine carbaldehyde) and amines/silyl ethers (R-OTBS). This protocol utilized an iridium photocatalyst under visible light conditions (**Scheme 1d**) [17]. In a recent development, Luca and coworkers introduced a visible light-mediated approach for esterifying aldehydes, employing trichloroisocyanuric acid (TCCA) (**Scheme 1e**) [18]. The reaction pathway involved the generation of an acyl chloride intermediate in the presence of trichloroisocyanuric acid (TCCA) induced by visible light. Subsequently, this intermediate was used to produce esters, carboxylic anhydrides, or amides by employing alcohols, carboxylic acids, and amines, respectively.

While there is limited existing literature on the subject of visible light-mediated aldehyde esterification, as far as our current understanding goes, there has been no prior development of a method to directly synthesize α-acyloxycarbonyl compounds from aldehydes using visible light.

2.3. Our hypothesis and optimization of esterification:

We put forth a hypothesis suggesting that α-acyloxycarbonyl compounds and esters might be attainable through the reaction of aldehydes with α-bromocompounds under appropriate photocatalytic conditions. In this report, we are delighted to present the direct synthesis of various α-acyloxycarbonyl compounds, originating from aldehydes, employing visible light conditions.

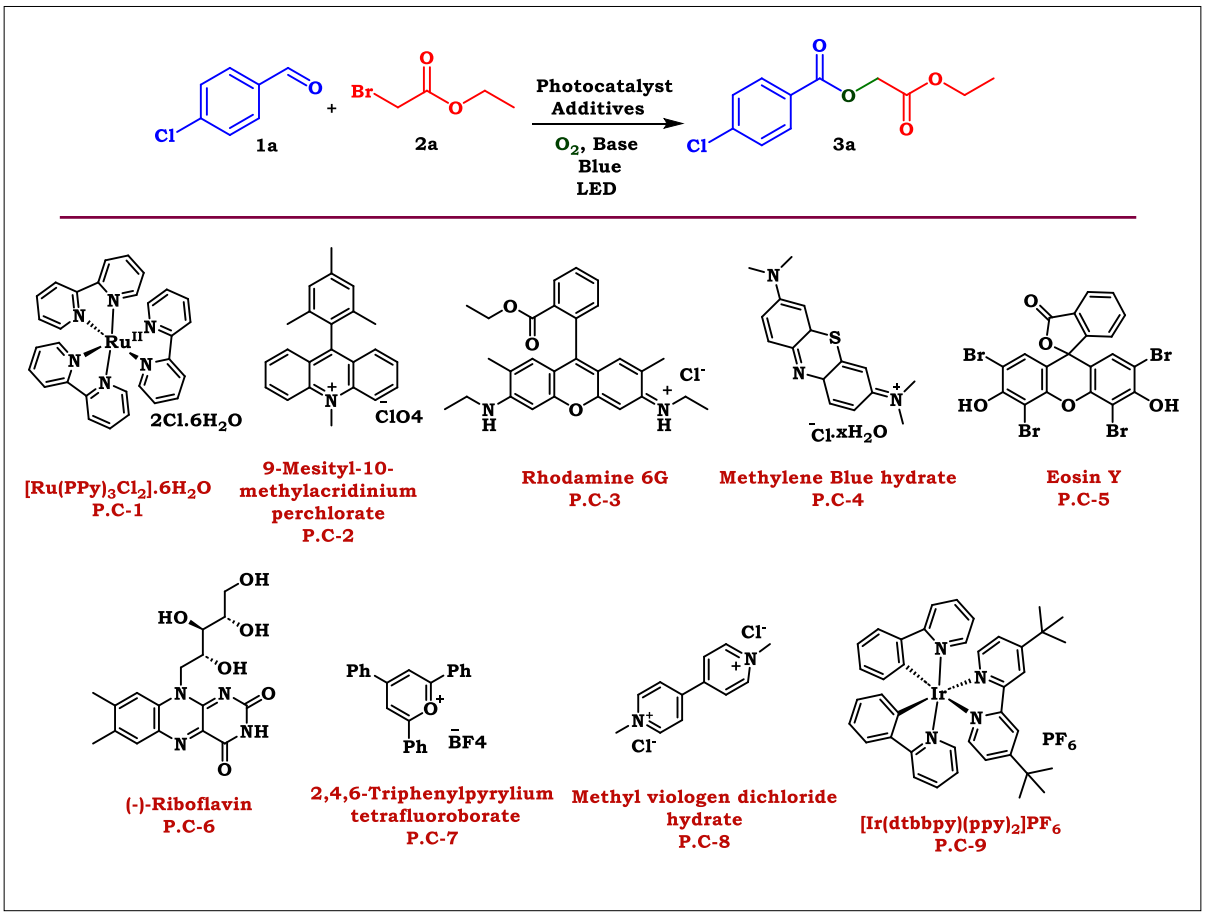


Figure 2. Structure of catalysts

To test our hypothesis, we initiated the experiment with the reaction involving 4-chlorobenzaldehyde **1a** and ethyl bromoacetate **2a** as our model substrates. Initially, we conducted the reaction of **1a** and **2a** using PC-1 [$Ru(PPy)_3Cl_2$] as the photoredox catalyst in DMF, with the addition of DIPEA (2 equiv.), all under blue LED irradiation. To our delight, we did obtain the desired product **3a**, albeit in a low yield, and there was also some unreacted aldehyde **1a** that remained (see **Table 1**, **Entry 1**). Encouraged by this preliminary outcome, we planned to test various catalysts and additives to fine-tune the reaction conditions under blue LED light. We systematically investigated the reaction between 4-chlorobenzaldehyde **1a** and ethyl bromoacetate **2a**, employing various photoredox catalysts in the presence of DIPEA (2 equiv.) within the solvent DMF (see**Table 1**, **Entries 2-9**). Our observations revealed that among the array of photoredox catalysts tested, 2,4,6-triphenylpyrilium tetrafluoroborate (TPPT; PC-7) demonstrated promising potential by yielding the desired product **3a** at 9% (**Table 1**, **Entry 7**). Further experimentation unveiled acetonitrile as the optimal solvent for this transformation, yielding compound **3a** at 15% yield (**Table 1**, **Entries 10-13**). To enhance the yield of **3a**, we explored the impact of different bases

Table 1. Optimization of reaction conditions[a]

Entry	Solvent	Catalyst	Base	Additive	Yield[e] (%)
1	DMF	PC-1	DIPEA	-	6
2	DMF	PC-2	DIPEA	-	6
3	DMF	PC-3	DIPEA	-	Trace
4	DMF	PC-4	DIPEA	-	N.R
5	DMF	PC-5	DIPEA	-	Trace
6	DMF	PC-6	DIPEA	-	N.R
7	DMF	PC-7	DIPEA	-	9
8	DMF	PC-8	DIPEA	-	N.R
9	DMF	PC-9	DIPEA	-	7
10	MeCN	PC-7	DIPEA	-	15
11	$CHCl_3$	PC-7	DIPEA	-	11
12	Dioxane	PC-7	DIPEA	-	12
13	Toluene	PC-7	DIPEA	-	13
14	MeCN	PC-7	Et_3N	-	11
15	MeCN	PC-7	Na_2CO_3	-	20
16	MeCN	PC-7	K_2CO_3	-	17
17	MeCN	PC-7	Na_2CO_3	$LiBF_4$	27
18	MeCN	PC-7	Na_2CO_3	$NaBF_4$	23
19	MeCN	PC-7	Na_2CO_3	$Sc(OTf)_3$	37
20	MeCN	PC-7	Na_2CO_3	$AgSbF_6$	60
21	MeCN	PC-7	Na_2CO_3	$AgBF_4$	82
22	MeCN	PC-7	Na_2CO_3	$AgNO_3$	30
23	MeCN	PC-7	Na_2CO_3	Ag_2CO_3	50
24[b]	MeCN	PC-7	Na_2CO_3	$AgBF_4$(1)	70
25[c]	MeCN	PC-7	Na_2CO_3	$AgBF_4$(0.5)	50
26[b]	MeCN	PC-7	Na_2CO_3	$AgBF_4(H_2O)$	Trace
27[b]	MeCN	PC-7	Na_2CO_3	$AgBF_4(O_2)$	85
28	MeCN	-	Na_2CO_3	$AgBF_4$	N.R
29	MeCN	PC-7	-	$AgBF_4$	N.R
30[d]	MeCN	PC-7	Na_2CO_3	$AgBF_4$	N.R

***Reaction conditions**: [a]Unless otherwise noted, all the reactions were carried out using 0.712 mmol of **1a**, 1.07 mmol of **2a**, 1.42 mmol of additive, 1.42 mmol of base and 0.0356 mmol (5 mol%) of photocatalyst under blue LED (15 W) irradiation at room temperature (27 °C two cooling fans used) 48 h. [b]Additive (1 equiv. $AgBF_4$); [c]Additive (0.5 equiv $AgBF_4$). All the reactions were carried out under blue LED (15 W) at room temperature (monitored); [d]reaction was carried out in dark (no light); [e]Isolated yield after the purification by column chromatography; N.R = no reaction.*

on the reaction (**Table 1**, **Entries 14-16**). Significantly, we achieved an incremental improvement in the yield, reaching 20%, when employing Na_2CO_3 as the base (**Table 1**, **Entry**

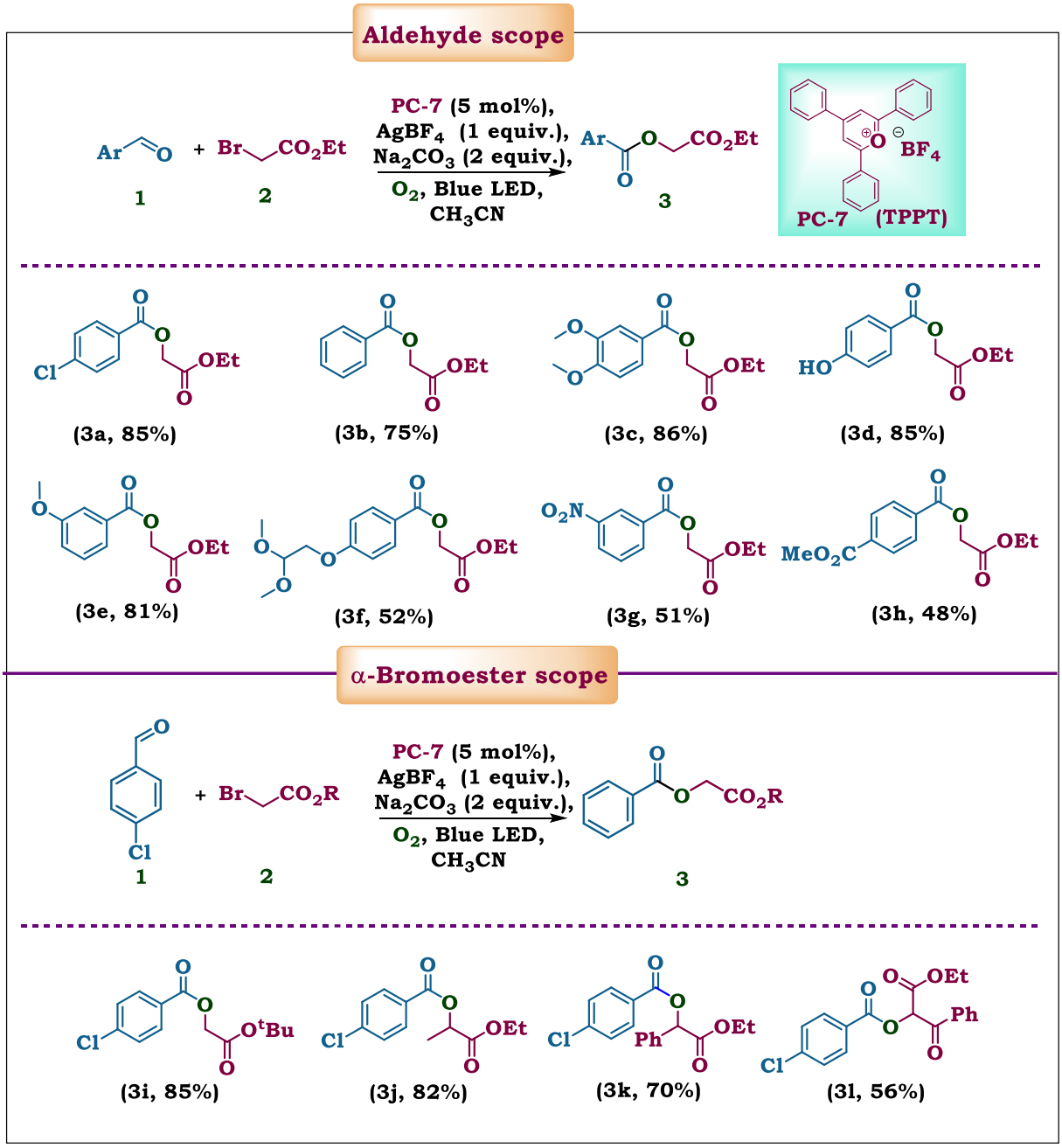
15). We then directed our focus towards exploring the incorporation of suitable additives to optimize the reaction conditions. We conducted the reaction between 4-chlorobenzaldehyde **1a** and ethyl bromoacetate **2a** in the presence of the photocatalyst TPPT (PC-7) in acetonitrile, incorporating various additives into the process (**Table 1**, **Entries 17-23**). Encouragingly, we observed a significant surge in the yield of **3a**, with complete consumption of aldehyde **1a** when $AgBF_4$ was introduced as an additive in the presence of TPPT in acetonitrile (resulting in an 82% yield, see **Table 1**, **Entry 21**). A further reduction in the quantity of $AgBF_4$ led to a notable decrease in the yield of **3a**, as observed in **Table 1**, **Entries 24-25**. To gain insights into the potential role of moisture in the reaction, we conducted the reaction in the presence of $AgBF_4$ and H_2O (**Table 1**, **Entry 26**). Interestingly, the presence of H_2O resulted in the formation of the desired product **3a** in only trace amounts. Considering that all our screening reactions had been conducted under open-air conditions, we grew curious about the potential role of oxygen in the reaction. In pursuit of this, we performed the reaction under an oxygen atmosphere (using an O_2 balloon) with a reduced loading of $AgBF_4$ (1 equiv.). Intriguingly, the reaction was completed in a relatively shorter time (15 hours) and afforded the desired product **3a** in a very good yield 85% (**Table 1**, **Entry 27)**.

The control experiments conducted in the absence of a photoredox catalyst, base, and light (blue LED) did not yield successful results (**Table 1**, **Entries 28-30)**. These outcomes unequivocally underscored the essential nature of the photoredox catalyst, base, and light for the desired transformation. Following our extensive screening, the optimal reaction conditions were determined to be as follows: 4-chlorobenzaldehyde **1a**, ethyl bromoacetate **2a**, 5 mol% of TPPT (PC-7), $AgBF_4$ (1 equiv.) as an additive, Na_2CO_3 (2 equiv.) in acetonitrile, under an oxygen atmosphere, and blue LED irradiation at room temperature (27 °C) (**Table 1**, **Entry 27)**.

2.4. Results and Discussion:

With the established and optimized reaction conditions in hand, we proceeded to investigate the broad substrate scope to assess the versatility of this protocol. To synthesize a range of α-acyloxy esters, we subjected ethyl bromoacetate **2a** to various aldehydes **1** under the optimized reaction conditions. Aromatic aldehydes with electron-donating groups (**1b-1f**) readily underwent the reaction with ethyl bromoacetate **2a** under the established conditions, yielding the respective α-acyloxy esters (**3b-3f**) in excellent yields (up to 86%), (**Scheme 2a**).

Scheme 2a: Substrate scopes of α-acyloxy ester[a]

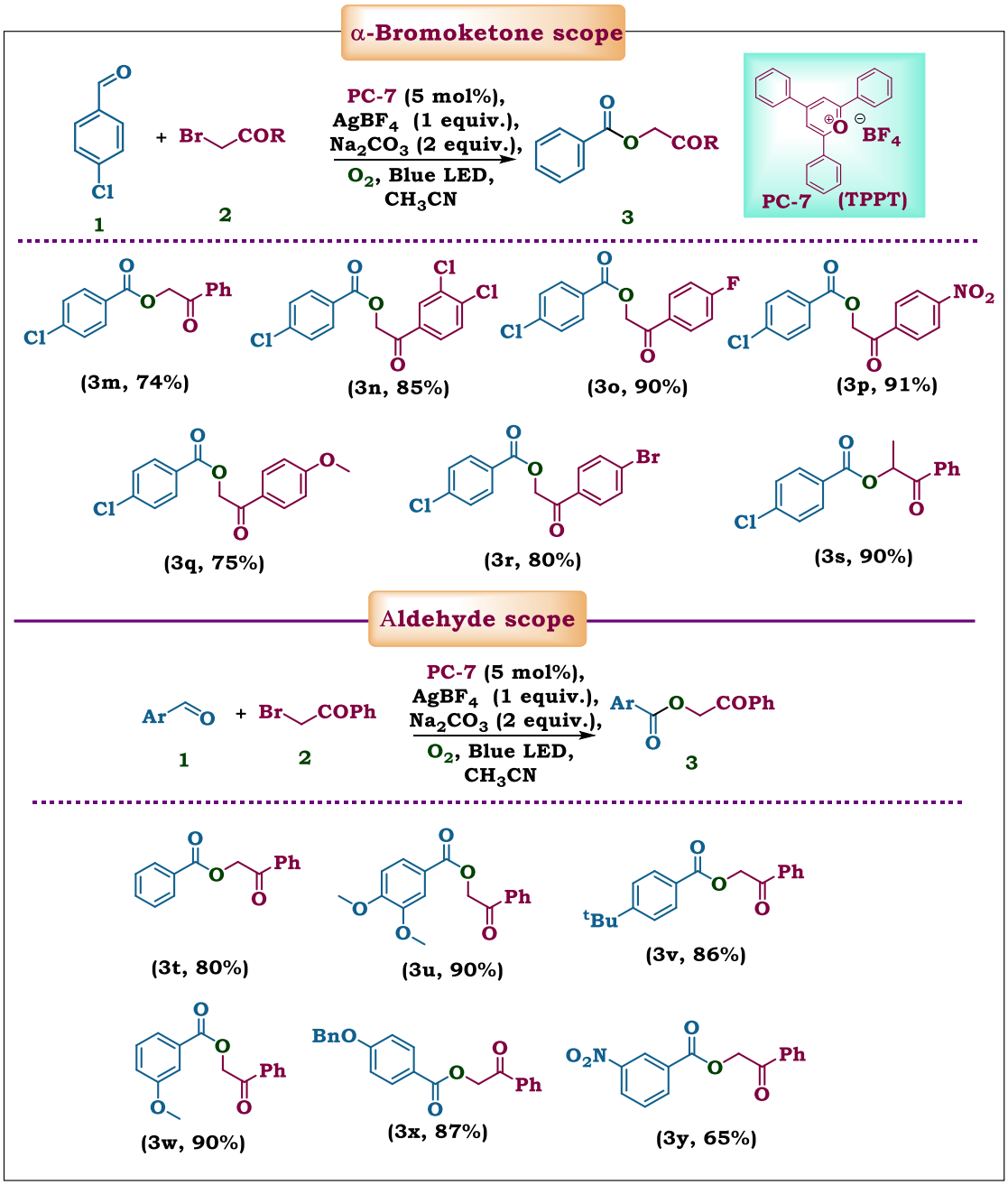


Reaction conditions: *[a]Unless otherwise noted, all the reactions were carried out using 50 mg of* ***1****, 1.5 equiv. of* ***2****, 1 equiv. of additive $AgBF_4$, 2 equiv. of Na_2CO_3 and 5 mol% of photoredox catalyst (TPPT) under blue LED (15 W) irradiation at room temperature (27 °C) 15-24 h (while, in case of* ***3m*** *to* ***3y*** *and* ***3ad*** *to* ***3ah****, 1.1 equiv. of* ***2*** *was used). All the reactions were carried out under blue LED (15 W) at room temperature (27 °C); Yields were calculated after the purification of the product by column chromatography.*

Aromatic aldehydes with electron-withdrawing or deactivating groups (**1g-1h**) produced the desired products (**3g-3h**) in moderate yields, as shown in **Scheme 2a**. What's particularly intriguing is that this protocol enables the direct one-pot synthesis of a diester (**3h**)

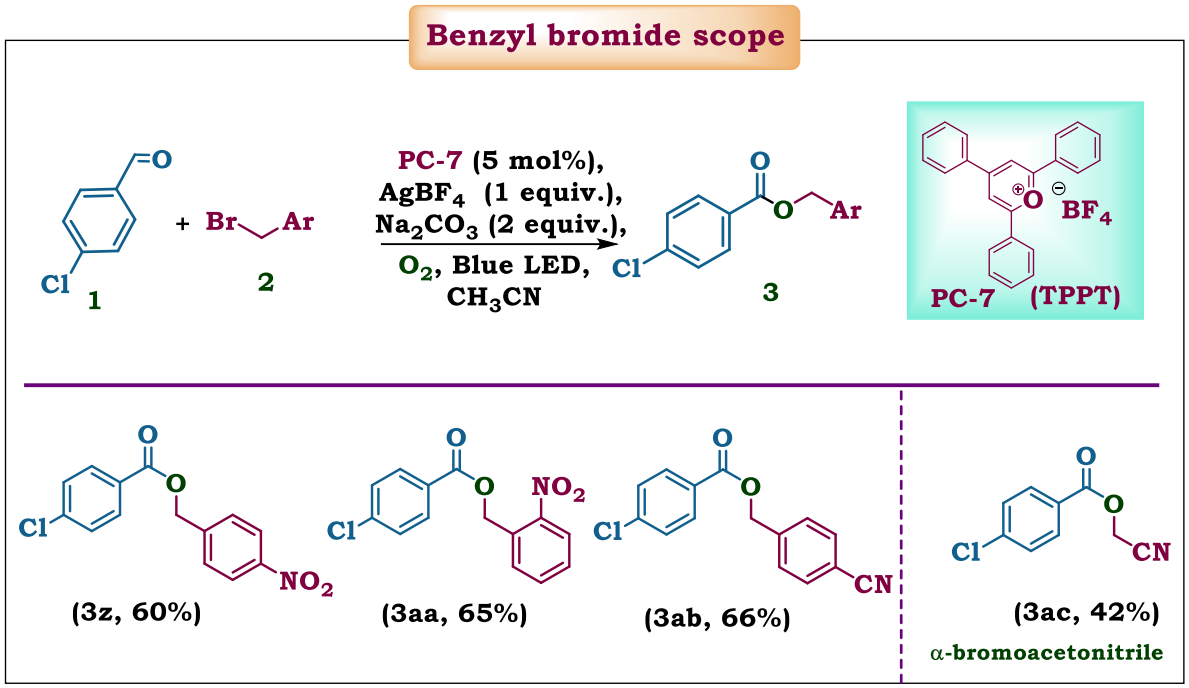
from an aldehyde, which can be quite challenging using alternative methods. Notably, we observed that aromatic aldehydes with electron-donating groups consistently provided higher yields compared to those with electron-withdrawing groups.

Scheme 2b: Substrate scopes for α-acyloxyketone[a]



Reaction conditions: [a]*Unless otherwise noted all the reactions were carried out using 50 mg of **1**, 1.5 equiv. of **2**, 1 equiv. of additive $AgBF_4$, 2 equiv. of Na_2CO_3 and 5 mol% of photoredox catalyst (TPPT) under blue LED (15 W) irradiation at room temperature (27 °C) 15-24 h (while, in case of **3m** to **3y** and **3ad** to **3ah**, 1.1 equiv. of **2** was used). All the reactions were carried out under blue LED (15 W) at room temperature; Yields were calculated after the purification of the product by column chromatography.*

Scheme 2c: Substrate scopes for ester[a]

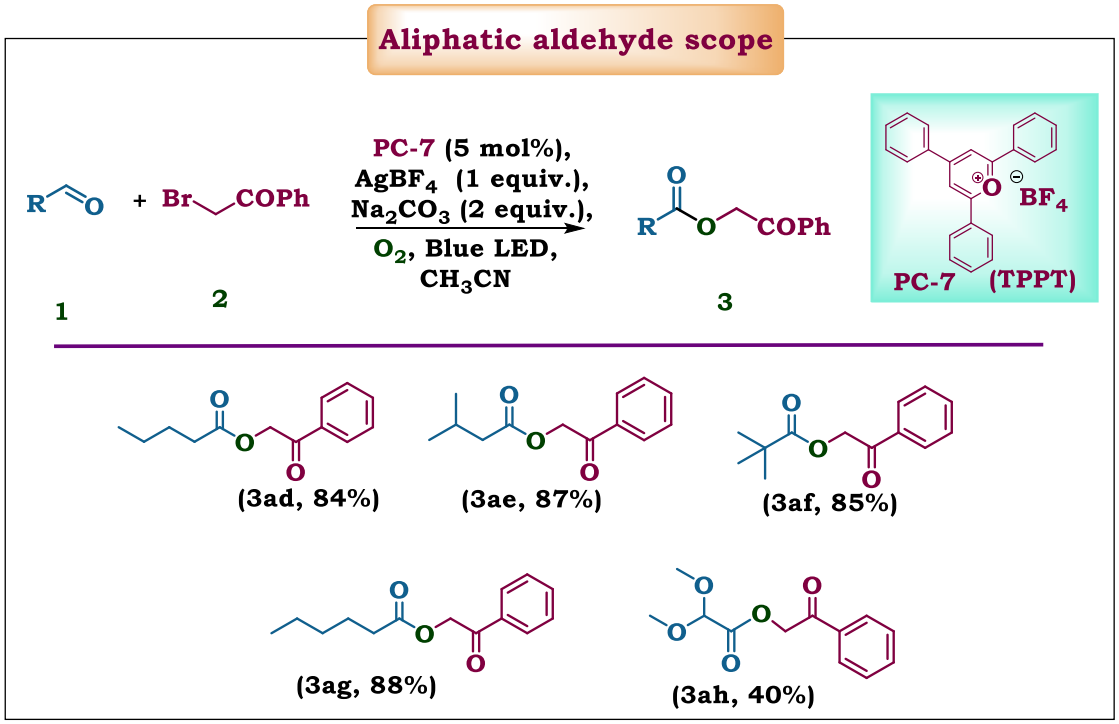


Reaction conditions: *[a]Unless otherwise noted all the reactions were carried out using 50 mg of **1**, 1.5 equiv. of **2**, 1 equiv. of additive $AgBF_4$, 2 equiv. of Na_2CO_3 and 5 mol% of photoredox catalyst (TPPT) under blue LED (15 W) irradiation at room temperature (27 °C) 15-24 h (while, in case of **3m** to **3y** and **3ad** to **3ah**, 1.1 equiv. of **2** was used). All the reactions were carried out under blue LED (15 W) at room temperature; Yields were calculated after the purification of the product by column chromatography.*

This phenomenon can likely be attributed to the fact that aromatic aldehydes containing electron-withdrawing groups typically possess higher oxidation potentials overall, which can make it challenging for them to undergo further oxidation, as discussed in prior studies.

To assess the practicality of our protocol, we treated various α-bromoesters (**2b-2e**) with 4-chlorobenzaldehyde **1a**. This resulted in the formation of the corresponding α-acyloxyesters (**3i-3l**) in yields ranging from moderate to very good, reaching up to 85% (**Scheme 2a**). We then shifted our focus towards synthesizing α-acyloxy ketones using different phenacyl bromides. Encouragingly, the reaction between 4-chlorobenzaldehyde **1a** and various phenacyl bromides (**2f-2l**) proceeded smoothly, yielding the respective α-acyloxy ketones (**3m-3s**) in good to excellent yields (up to 91%) (**Scheme 2b**).

Scheme 2d: Substrate scopes for aliphatic aldehyde based α-acyloxyketone[a]



Reaction conditions: *[a]Unless otherwise noted all the reactions were carried out using 50 mg of **1**, 1.5 equiv. of **2**, 1 equiv. of additive $AgBF_4$, 2 equiv. of Na_2CO_3 and 5 mol% of photoredox catalyst (TPPT) under blue LED (15 W) irradiation at room temperature (27 °C) 15-24 h (while, in case of **3m** to **3y** and **3ad** to **3ah**, 1.1 equiv. of **2** was used). All the reactions were carried out under blue LED (15 W) at room temperature; Yields were calculated after the purification of the product by column chromatography.*

In order to assess the reactivity of various aldehydes, we subjected phenacyl bromide **2f** to different aromatic aldehydes (**1b-1c, 1i, 1e, 1j, 1g**). This led to the formation of the desired products (**3t-3y**) moderate to excellent yield (up to 90%) (**Scheme 2b)**.

We further expanded the scope of our protocol by reacting 4-chlorobenzaldehyde **1a** with various benzylic bromides (**2m-2o**). To our satisfaction, we successfully obtained the corresponding benzyl esters (**3z**, **3aa-3ab**) in moderate yields. Remarkably, even bromoacetonitrile (**2p**) reacted smoothly under the reaction conditions with 4-chlorobenzaldehyde **1a**, yielding cyanomethyl ester **3ac** in a satisfactory yield (**Scheme 2c)**.

Later, we treated the various aliphatic aldehydes with phenacyl bromide under optimized reaction condition. Gratifyingly, all the reaction proceeded efficiently to deliver corresponding α-acyloxy carbonyl compounds (**3ad-3ah**) in very high yields (up to 87%) (**Scheme 2d**).

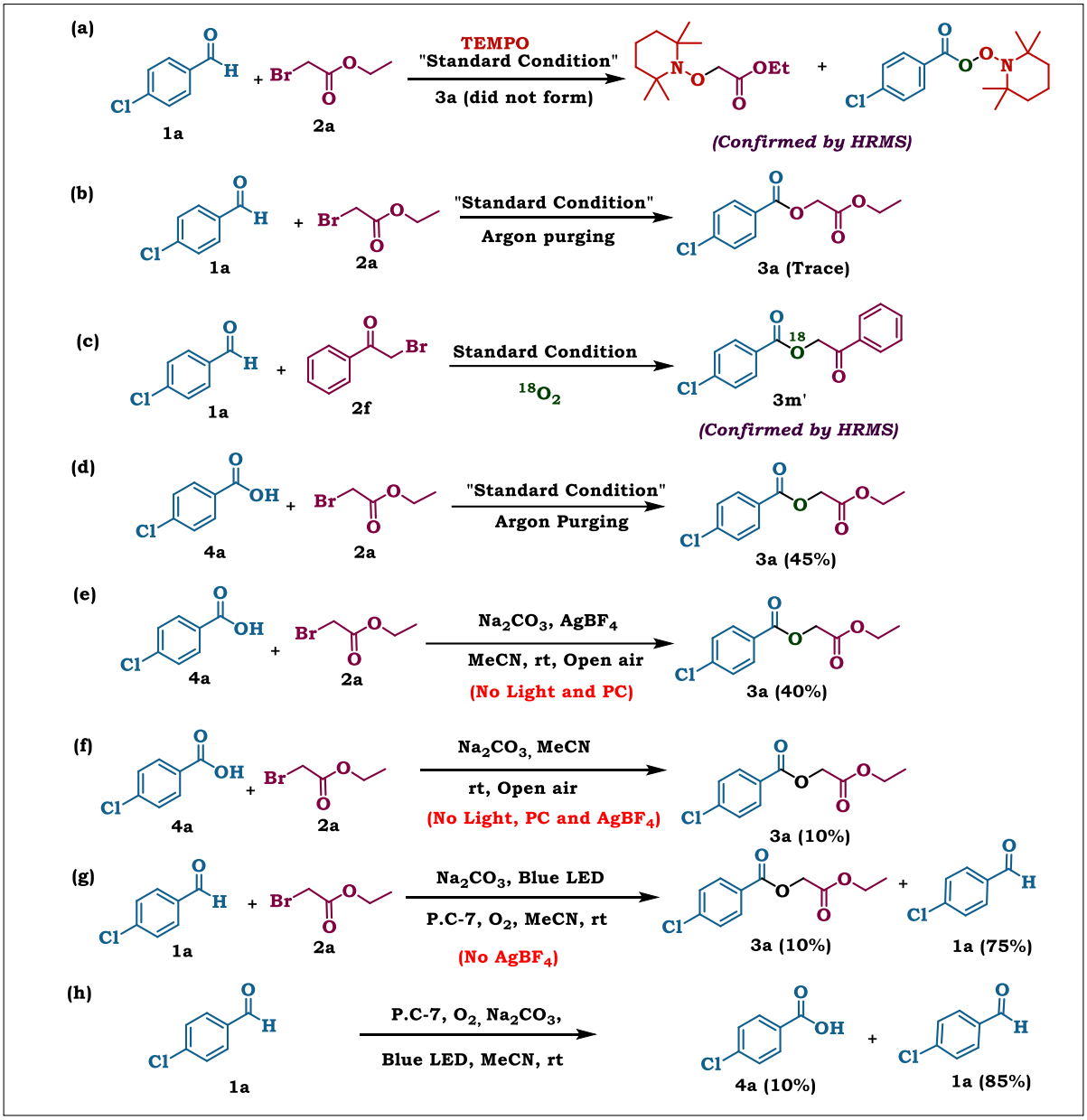
To illustrate the protocol's practicality, we effectively conducted a gram-scale synthesis of **3m**, commencing from **1a**, while adhering to the optimized reaction conditions. The gram scale reaction proceeded smoothly to deliver the desired product **3a** in 72% yield (*see experimental section 2.7.4, page no 54)*.

2.5. Control experiments and mechanistic study:

To gain a better understanding of the reaction mechanism, a series of systematic control experiments were conducted. Initially, when **1a** and **2a** were subjected to the reaction in the presence of the radical scavenger TEMPO, the desired product **3a** was not obtained. This observation strongly suggests the participation of radical intermediates in the reaction mechanism (**Scheme 3a**). Furthermore, the presence of TEMPO-trapped radical intermediates was proved through HRMS spectra. These results provided evidence for the in-situ generation of the carboxyl radical **1a'** and the ethyl acetate radical **2a'** originating from the aldehyde and ethyl bromoacetate, respectively, during the transformation (also refer to Scheme 4). In subsequent experiments, it was observed that the desired product **3a** was formed only in trace amounts when conducted under inert atmospheric conditions (**Scheme 3b**). This observation confirms the necessity of an oxygen atmosphere for the desired transformation. Furthermore, when the reaction was conducted in the presence of oxygen labelled with $^{18}O_2$, the resulting product **3m'** was found to contain the incorporated labelled oxygen, proves the necessity of the oxygen for the desired transformation (**Scheme 3c**). To investigate the potential in-situ formation of carboxylic acid from the aldehyde precursor, we conducted experiments using 4-chlorobenzoic acid **4a** and **2a** under the standard reaction conditions as well as under an argon atmosphere (in the absence of oxygen). Our observations revealed that the desired product **3a** was indeed formed, albeit in a moderate yield of approximately 43-45% (**Scheme 3d**). This experimental evidence suggests the involvement of an oxygen-dependent pathway in the formation of the carboxylic acid. This outcome strongly indicates that the reaction is likely not proceeding through the oxidation of an aldehyde to form a carboxylic acid, followed by the substitution of ethyl bromoacetate **2a**.

To confirm that this reaction represents a photocatalytic oxidative alkylation mechanism, rather than a photocatalytic oxidation of an aldehyde to form a carboxylic acid followed by nucleophilic substitution with ethyl bromoacetate, we devised a set of supplementary control experiments.

Scheme 3: Control Experiments



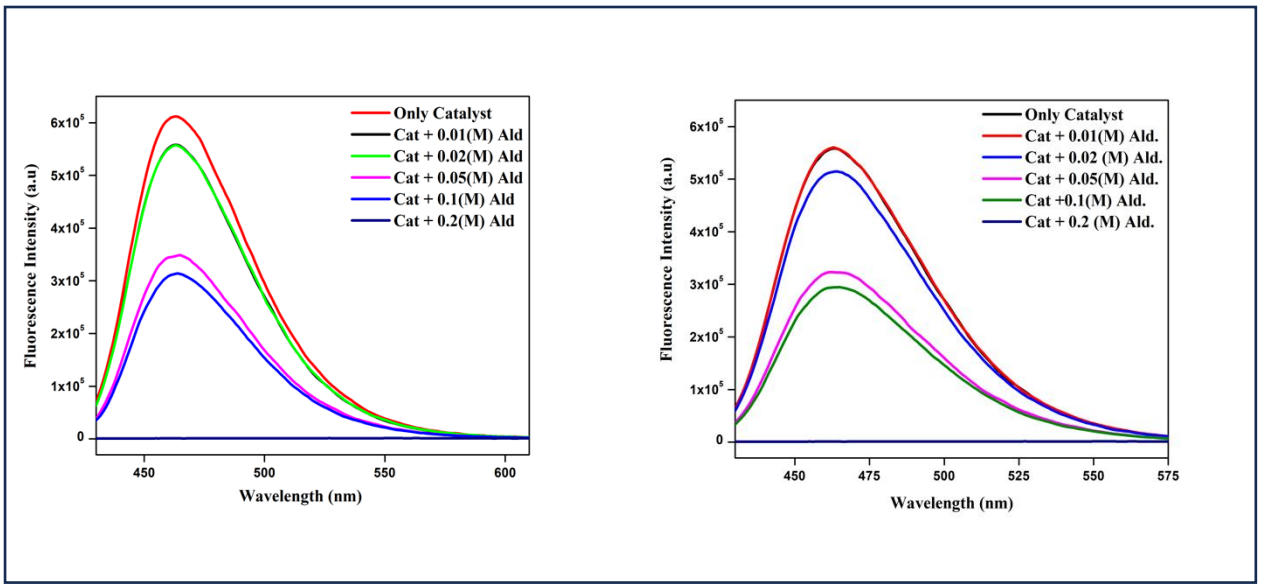
We initiated our investigation by conducting a reaction between 4-chlorobenzoic acid **4a** and ethyl bromoacetate **2a** using the standard conditions, but in the absence of both the blue LED and photocatalyst PC-7. Our observations revealed that the desired product **3a** was indeed formed, albeit in a moderate yield (**Scheme 3e**). Following that, we carried out the reaction between 4-chlorobenzoic acid **4a** and ethyl bromoacetate **2a** under the standard conditions, witout $AgBF_4$, the blue LED, and photocatalyst PC-7. To our surprise, the desired product **3a** was obtained in very low yield 10% (**Scheme 3f**). Subsequently, when we conducted the reaction between 4-chlorobenzaldehyde **1a** and ethyl bromoacetate **2a** under the standard

conditions, but excluding $AgBF_4$, we obtained the corresponding product **3a**, albeit in a low yield. Furthermore, we successfully isolated the unreacted 4-chlorobenzaldehyde **1a** in a yield of 75% (**Scheme 3g**). In our final experiment, we carried out the reaction involving 4-chlorobenzaldehyde **1a**, without the presence of ethyl bromoacetate **2a** and $AgBF_4$, under an oxygen atmosphere at room temperature. This resulted in the formation of a minimal amount of the corresponding 4-chlorobenzoic acid **4a**, with the unreacted 4-chlorobenzaldehyde **1a** being recovered in an 85% yield (as depicted in **Scheme 3h**).

The experimental observations from the **Scheme 3e-h** undeniably affirm the indispensable role played by the photocatalyst, light, oxygen, and $AgBF_4$ in facilitating the desired transformation. Furthermore, the results clearly indicate that $AgBF_4$ is not merely functioning as a Lewis acid but is actively driving and sustaining the photocatalytic cycle. These outcomes provide robust support for the photocatalytic oxidative alkylation mechanism rather than the conventional photocatalytic oxidation of an aldehyde.

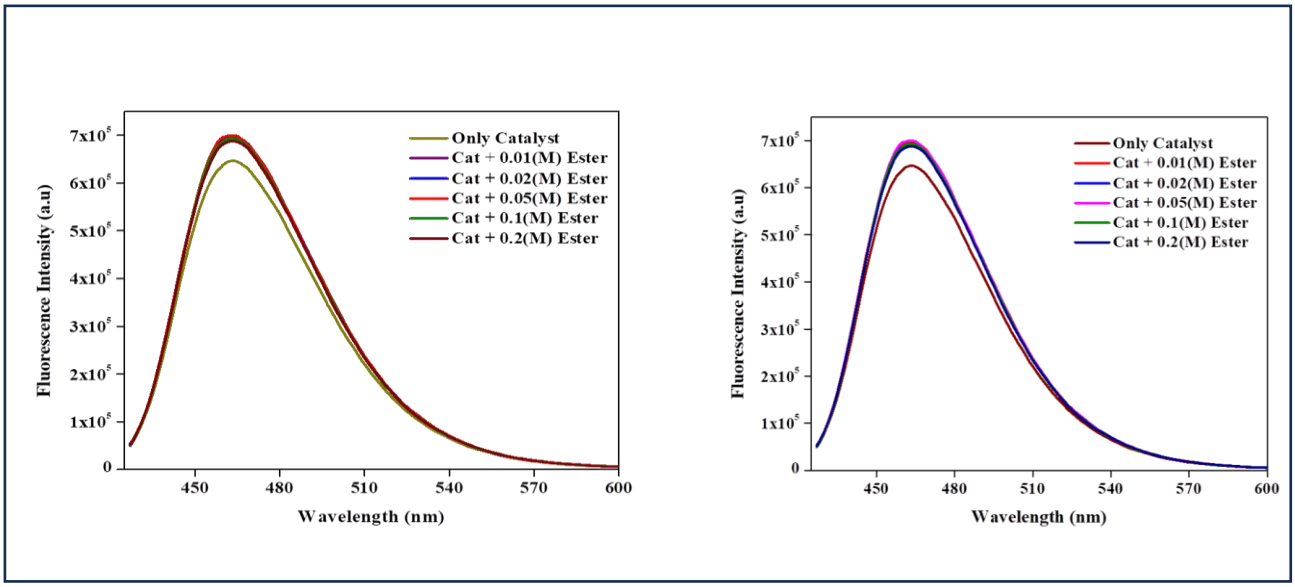
According to previous literature reports [20], it is established that reactions catalyzed by 2,4,6-triphenylpyrylium tetrafluoroborate (TPPT, PC-7) exclusively follow the reductive quenching cycle due to the electron-deficient nature of the catalyst. The oxidation potential of aldehyde is +1.34 V [21] and the excited state of TPT* is E_{red}* ($^3TPT^{+}$*/$TPT^{\bullet}$) = ca. +1.9 V [20]. These findings strongly indicate that the excited state of the photocatalyst can readily oxidize the aldehyde and subsequently undergo reduction. It is a well-established fact in the scientific literature that the generation of singlet oxygen ($^1O_2$) from molecular oxygen ($^3O_2$) through energy transfer from the triplet excited species $^3TPT^{+*}$ is improbable in this context. This is because the electron donor (aldehyde) present in the reaction mixture can efficiently quench the triplet excited state $^3TPT^{+*}$ at a much faster rate than $^3O_2$ [20].

To gain a more comprehensive understanding of the detailed mechanism, we conducted fluorescence quenching experiments separately in the presence of argon and oxygen. In both cases, we noticed a reduction in the fluorescence intensity of the PC-7 catalyst as the concentration of 4-chlorobenzaldehyde **1a** increased. Additionally, there were no notable differences observed in the fluorescence spectra between the two conditions (figure 3). In contrast, the presence of ethyl bromoacetate **2a** did not result in any reduction in the fluorescence intensity of the PC-7 catalyst (figure 4). These results indicates that oxygen is not directly engaged in the reductive quenching cycle, thus emphasizing the pivotal role played by 4-chlorobenzaldehyde **1a** in this reductive quenching process.



(a) **(b)**

Figure 3. Fluorescence quenching experiment using catalyst and aldehyde under (a) Argon and (b) Oxygen

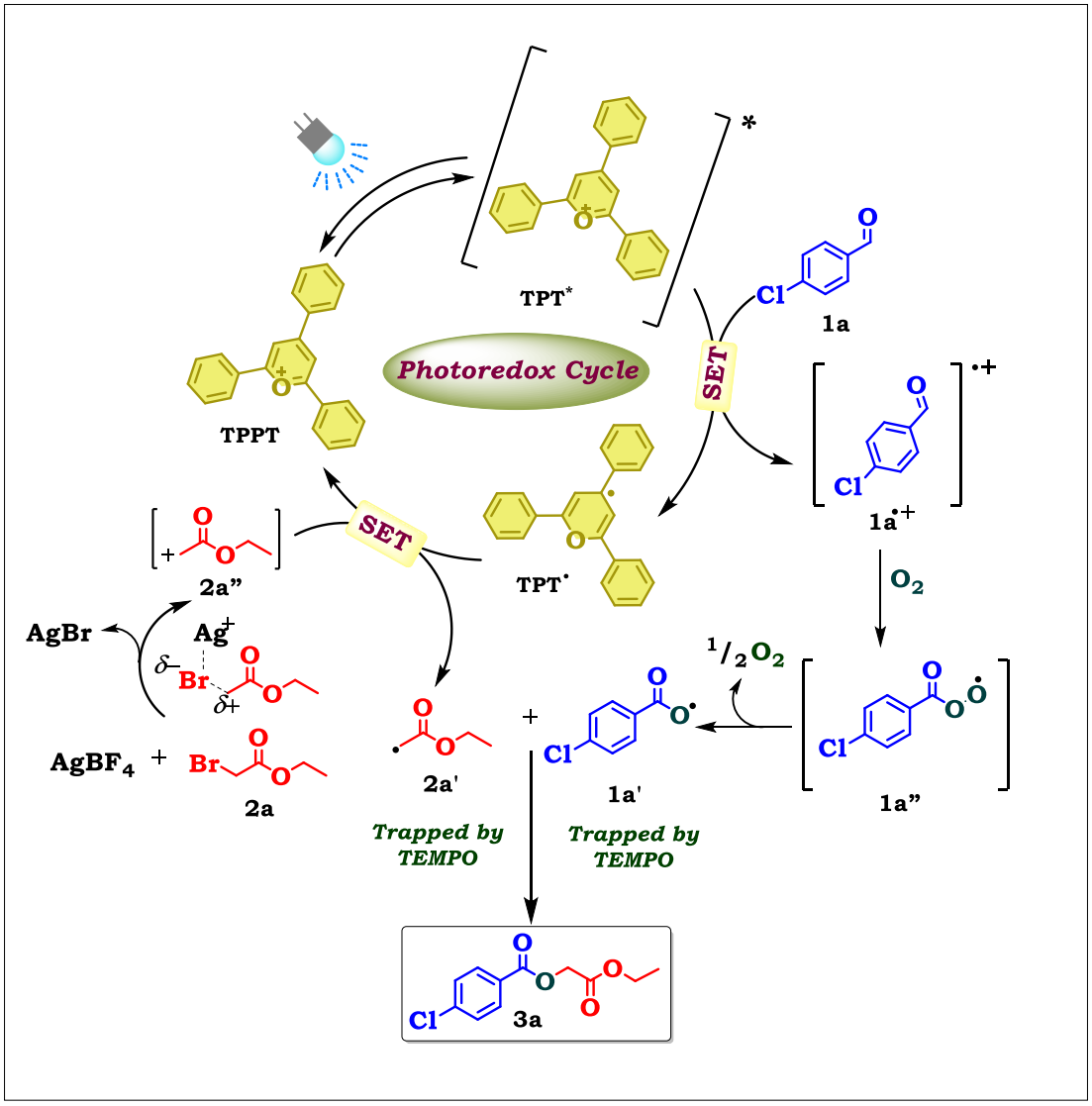


(a) **(b)**

Figure 4. Fluorescence quenching experiment using catalyst and ethyl bromoacetate (ester) under (a) Argon and (b) Oxygen

The reduction potentials for ethyl bromoacetate and TPPT are measured at -1.08 V and -0.28 V, respectively, relative to the standard calomel electrode (SCE) [22]. This value implies that TPPT, as a catalyst, encounters significant difficulty in reducing ethyl bromoacetate. To our surprise, we noted an increase in the yield of the desired product **3a** upon the addition of $AgBF_4$. Based on this experimental observation, it can be inferred that $AgBF_4$ potentially reduces the reduction potential of ethyl bromoacetate, possibly through the generation of the transient ethyl acetate cation $\mathbf{2a}^+$ or by augmenting the electrophilic nature of **2a** via coordination effects (**Scheme 4**). Considering the reduction potential data, it is reasonable to hypothesize that $TPPT^{\bullet}$ may potentially reduce the cationic species **2a''** or a highly polarized ethyl acetate through a Single Electron Transfer (SET) mechanism, giving rise to the formation of the ethyl acetate radical **2a'** (as illustrated in **Scheme 4**).

Scheme 4: Plausible mechanism



Based on the information gleaned from prior literature reports [21] and the control experiments conducted in our study, we have put forth the most plausible photoredox catalytic cycle, as depicted in **Scheme 4**. Upon exposure to visible light, the TPPT catalyst (PC-7) undergoes excitation, leading to the formation of TPT* through a photophysical process. Consequently, this excited state (TPT*) is being reductively quenched by 4-chlorobenzaldehyde **1a** through a single electron transfer (SET) mechanism, resulting in the formation of a carbonyl radical cation intermediate ($1a^{\bullet+}$) and the concurrent generation of reduced $TPT^{\bullet}$. Furthermore, the radical cation ($1a^{\bullet+}$) engages in a reaction with oxygen, leading to the formation of the reactive carboxyl radical **1a'**, likely through the intermediacy of the 4-chlorobenzoylperoxy radical **1a"**. In the presence of $AgBF_4$, it is hypothesized that ethyl bromoacetate **2a** undergoes reduction to form the ethyl acetate radical **2a'**. This transformation likely occurs through the mediation of cationic species **2a''** or a highly polarized ethyl acetate, interacting with $TPT^{\bullet}$ via a Single Electron Transfer (SET) mechanism, thus concluding the photoredox catalytic cycle. Ultimately, the desired product **3a** is formed through the radical-radical coupling of **1a'** and **2a'** [23].

2.6. Conclusions:

In summary, we have effectively demonstrated the direct synthesis of α-acyloxycarbonyl compounds and esters, commencing from aldehydes, under visible light conditions. The protocol's versatility was demonstrated through the synthesis of a wide range of α-acyloxy esters and α-acyloxy ketones. Both aromatic and aliphatic aldehydes proved to be highly effective in this process, and the reaction conditions were found to be compatible with a variety of functional groups. This indicates the broad applicability and robustness of the developed protocol for the synthesis of α-acyloxy esters and ketones, as it can accommodate different types of aldehydes and diverse chemical functionalities without significant interference or side reactions. Our success in utilizing this protocol across a diverse array of substrates, each featuring a variety of functional groups, highlights the robustness and versatility of our approach. This adaptability allows us to harness clean energy sources effectively to access valuable compounds, underscoring the strength and utility of our methodology. Drawing upon a series of meticulously designed control experiments (such as radical quenching experiments, isotope labelling experiment, and so on) and other pertinent observations (such as literature study and fluorescence quenching experiments), we have formulated a plausible reductive quenching photoredox catalytic cycle to elucidate the mechanism underlying this transformation.

2.7. Experimental section:

2.7.1. General information:

Unless otherwise noted, all the starting materials and reagents were purchased from commercial suppliers (Aldrich, TCI, and Alfa Aesar) and were used without further purification. Thin-layer chromatography (TLC) was performed using silica gel 60 GF_{254} pre-coated aluminum backed plates (2.5 mm). Visualization was accomplished by irradiation with UV light at 254 nm. Column chromatography was performed using silica gel (100–200 mesh) eluting with petroleum ether and ethyl acetate. The NMR spectra were recorded using tetramethylsilane as the internal standard. ^{1}H and $^{13}C\{^{1}H\}$ NMR were recorded on 400 MHz instrument (Bruker and Jeol). Chemical shifts (δ) are reported in ppm downfield from $CDCl_3$ (δ = 7.26 ppm) for ^{1}H NMR and relative to the central $CDCl_3$ resonance (δ = 77.16 ppm) for ^{13}C NMR spectroscopy. For ^{1}H NMR, data are reported as follows: chemical shift, multiplicity (s = singlet, d = doublet, dd = double doublet, t = triplet, q = quartet, br = broad, m = multiplet), coupling constants (*J*) are given in Hz and integration. Mass samples were analysed by high-resolution mass spectrometry (HRMS)-ESI TOF. Melting points were measured using BÜCHI M-560 melting point instrument and were uncorrected. Fluorescence spectra were recorded on Fluoromax-4 spectrofluorometer (Horiba Scientific, U.S.A.). All photocatalytic reactions were performed under blue LEDs (IBRA Pure30 W Blue LED Flood Light, IP Rating: IP66).

2.7.2. Mechanistic study:

A. Fluorescence Quenching Experiment:

Fluorescence quenching experiment was carried out using Fluorescence spectrophotometer, using 2.5 μM solution of 2, 4, 6-triphenylpyrylium tetrafluoroborate (TPPT) and variable. concentrations of (0.01, 0.02, 0.05, 0.1, 0.2 M) of 4-chlorobenzaldehyde **1a** in acetonitrile solvent. The sample was prepared in a 3 mL quartz cuvette and the flask was degasified with Argon before the spectra were recorded. Again, the same procedure was carried out in the presence of oxygen. The quenching plots of both the experiments are given in figure 5.

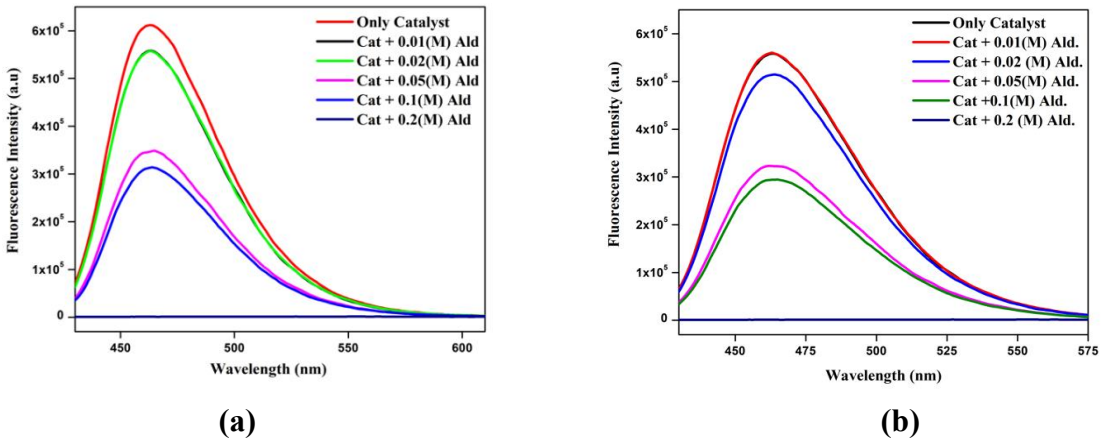


Figure 5. Fluorescence quenching experiment using catalyst and aldehyde under (a) Argon and (b) Oxygen

Fluorescence quenching experiment was carried out using Fluorescence spectrophotometer, using 2.5 μM solution of 2, 4, 6-triphenylpyrylium tetrafluoroborate (TPPT) and variable concentrations of (0.01, 0.02, 0.05, 0.1, 0.2 M) of Ethyl bromoacetate **2a** in acetonitrile solvent. The sample was prepared in a 3 mL quartz cuvette and the flask was degasified with Argon before the spectra were recorded. Again, the same procedure was carried out in presence of Oxygen. The quenching plots of both the experiments are given in figure 6.

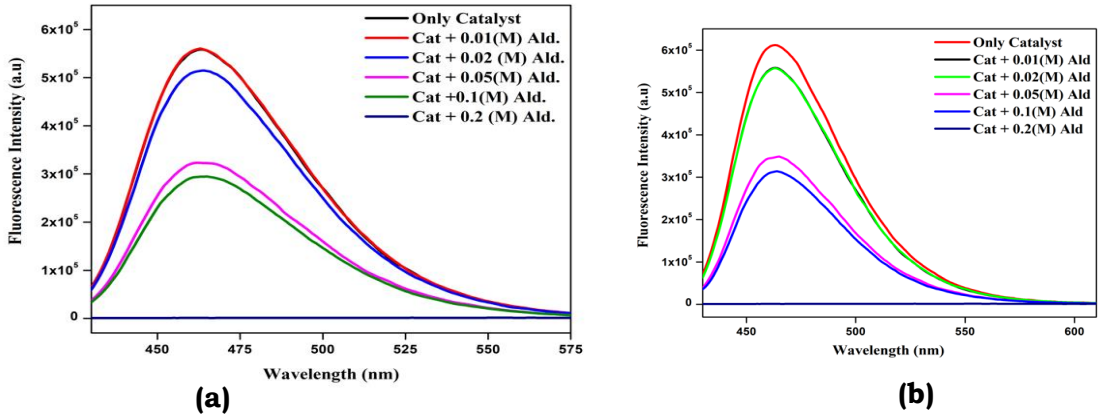
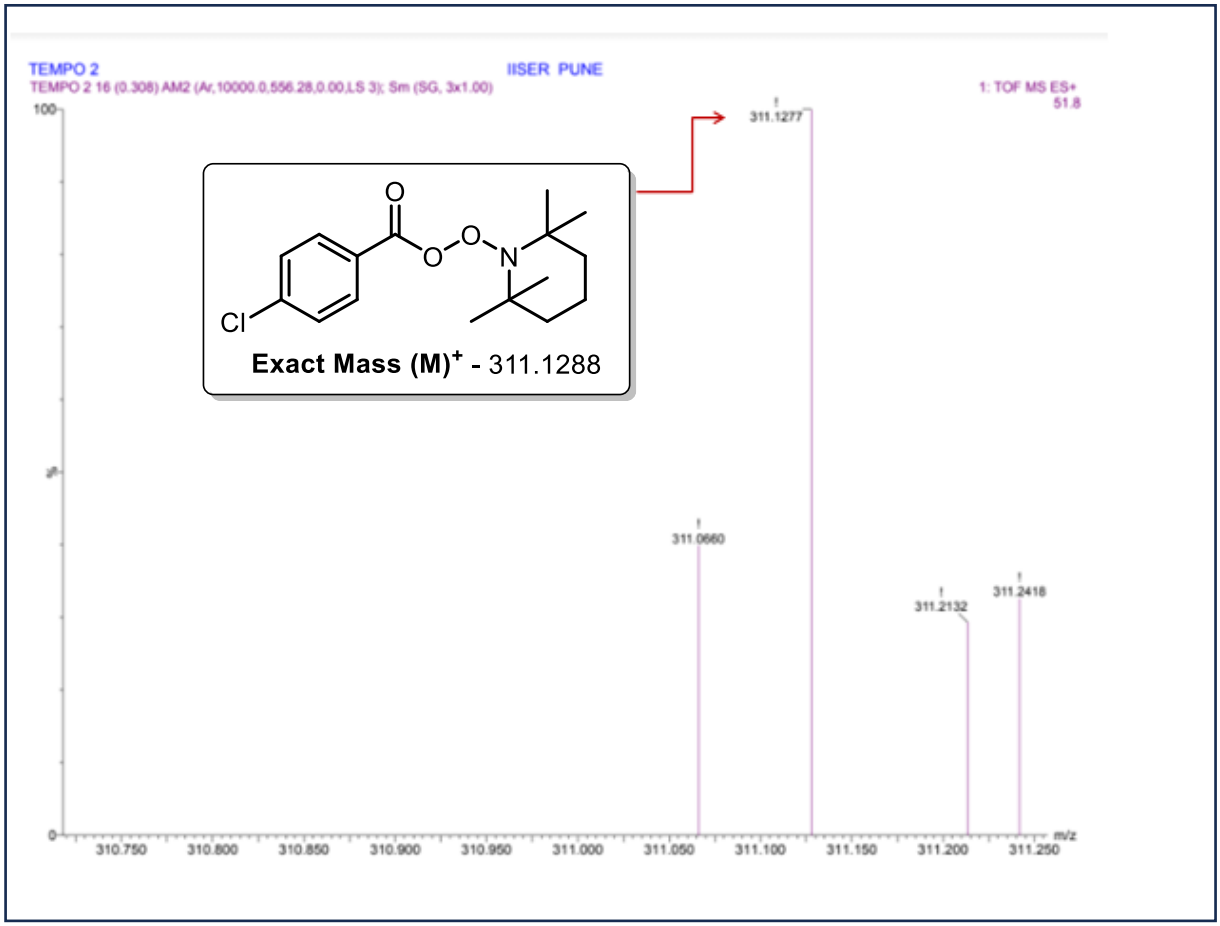


Figure 6. Fluorescence quenching experiment using catalyst and ethyl bromoacetate (ester) under (a) Argon and (b) Oxygen.

B. Control Experiments:

I. Radical quenching experiment:

To a solution of 4-chlorobenzaldehyde **1a** (50 mg, 1 equiv.) in 3 mL acetonitrile, ethyl bromoacetate (1.5 equiv.), Na_2CO_3 (2 equiv.) $AgBF_4$ (1 equiv.), TEMPO (2 equiv.) and photocatalyst TPPT (5 mol%) were added at room temperature under O_2 atmosphere using balloon and the reaction mixture was kept for stirring under Blue LED for 24 h. After the completion of the reaction (monitored by TLC), reaction mixture was filtered, the solvent was evaporated under vacuum and the residue was directly submitted for HRMS analysis. Based on the HRMS spectra we observed the TEMPO trapped radical intermediates (figure 7). These results supported the radical pathway during the course of the reaction.



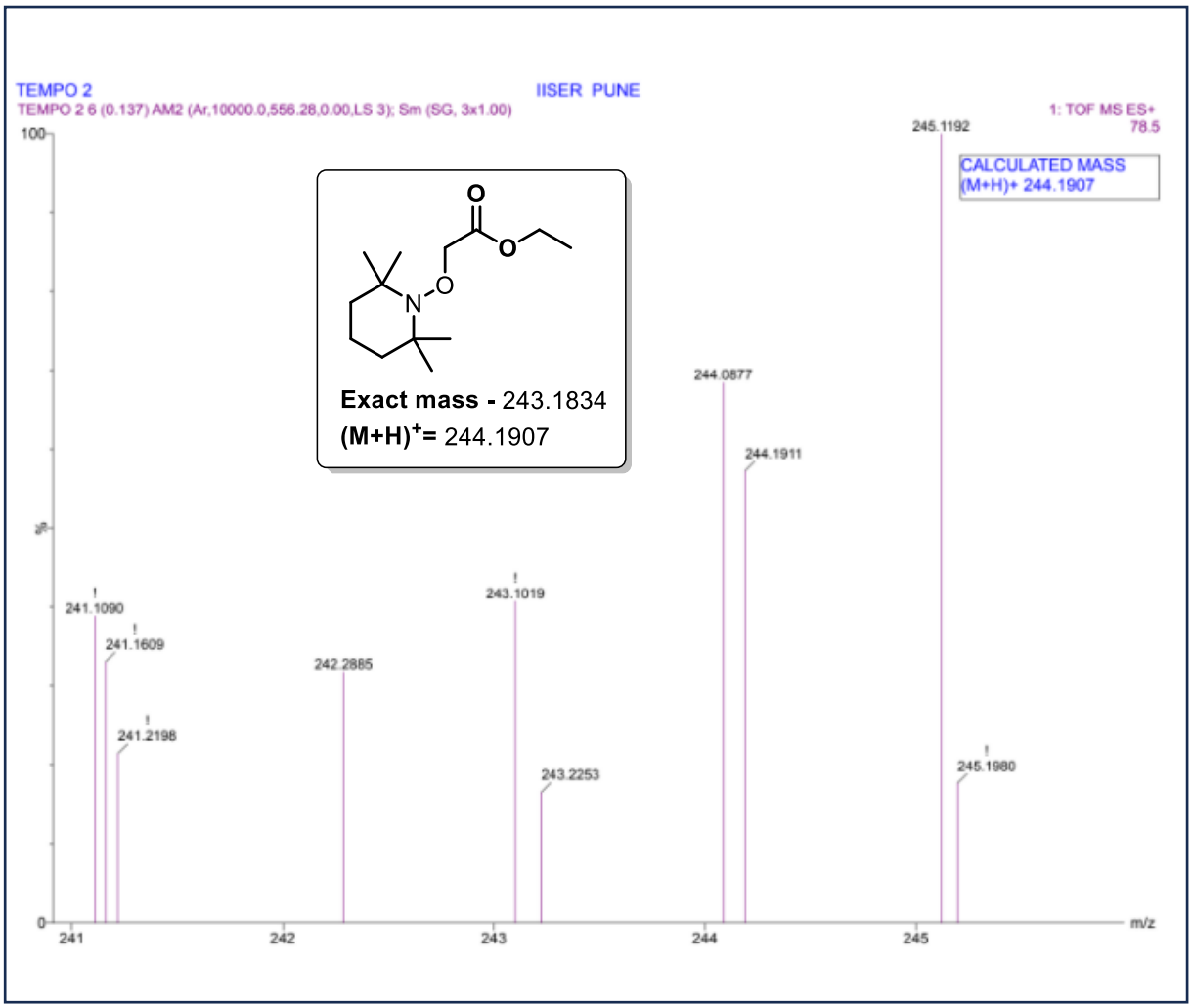


Figure 7. HRMS data of TEMPO trapped radical intermediates

II. $^{18}O_2$ labeling experiment:

To a solution of 4-chlorobenzaldehyde **1a** (50 mg, 1 equiv.) in 3 mL acetonitrile, 2-bromo-1-phenylethan-1-one **2f** (1.1 equiv.), Na_2CO_3 (2 equiv.) $AgBF_4$ (1 equiv.) and photocatalyst TPPT (5 mol%) were added at room temperature and the reaction mixture was degasified by purging with Argon. After which, $^{18}O_2$ was purged into the reaction mixture ($^{18}O_2$ cylinder) and the reaction mixture was kept for stirring under Blue LED for 24 h. After the completion of the reaction (monitored by TLC) the reaction mixture was filtered and immediately the solvent was reduced under vacuum. The residue was purified by column chromatography using silica gel 100-200 mesh using ethyl acetate/petroleum ether mixture (1:10) as an eluent to obtain the corresponding ^{18}O labelled product (**3m'**) (figure 8).

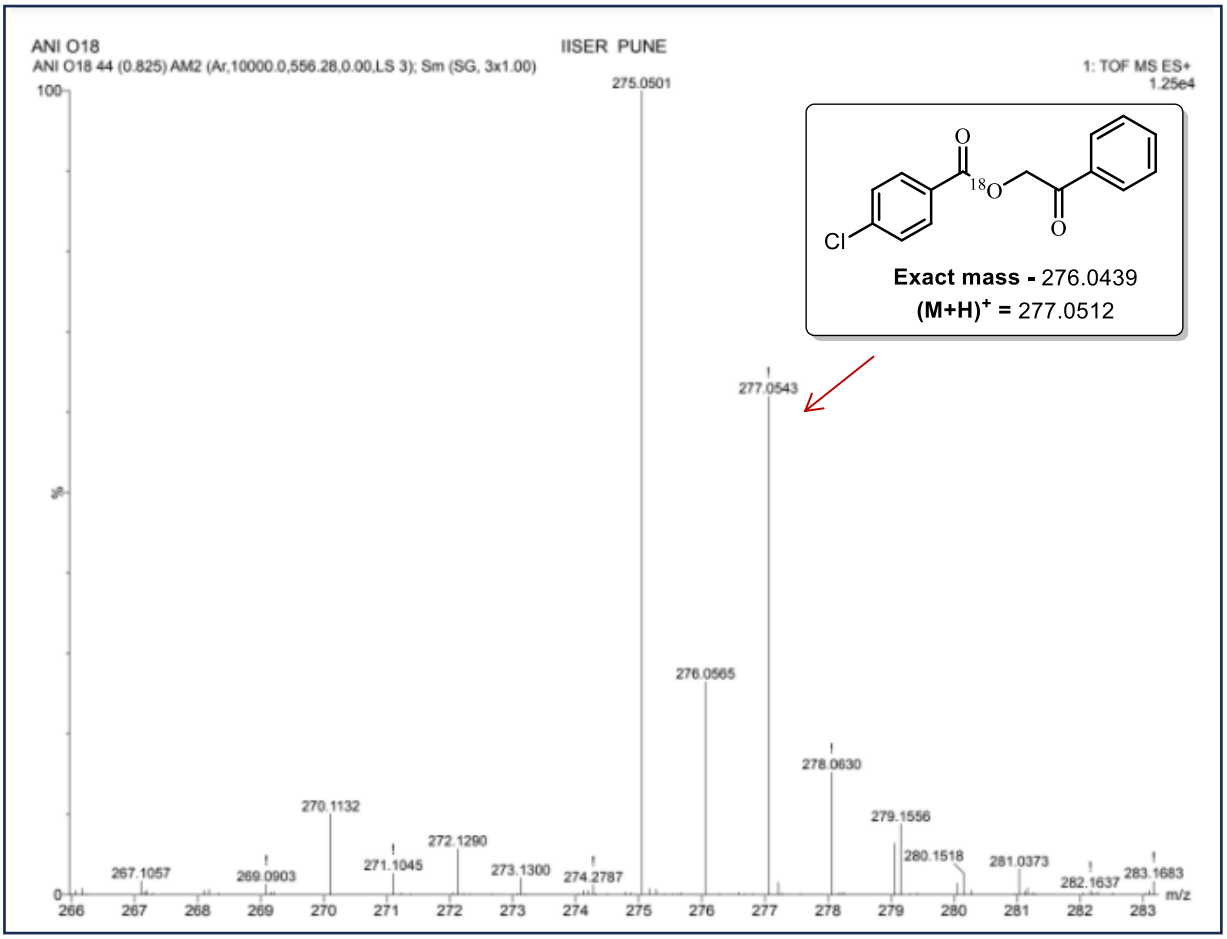
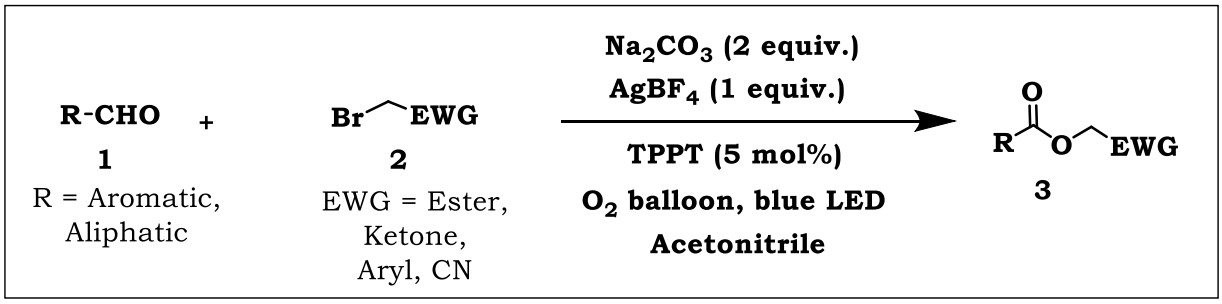


Figure 8. HRMS spectrum of $^{18}O_2$ labelled experiment

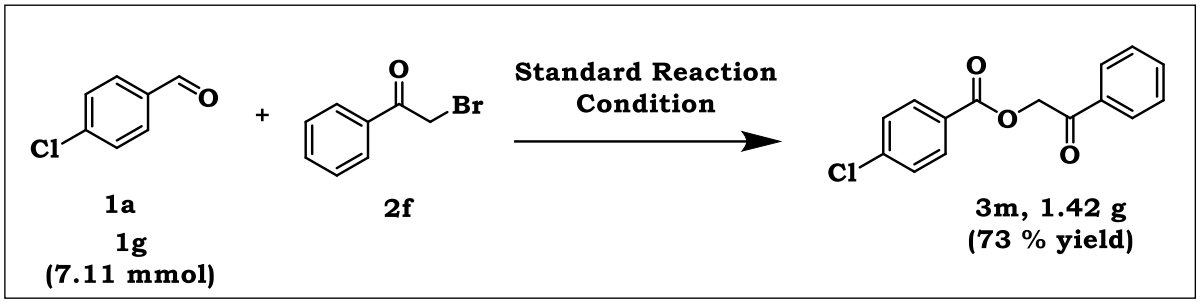
2.7.3. General Procedure for the synthesis of α–acyloxy carbonyl compounds:



To the round bottom flask containing solution of Aldehyde **1** (50 mg, 1 equiv.) in 3 mL, acetonitrile, α-bromoester **2** (1.5 equiv.)/ketone (1.1 equiv.)/substituted benzyl bromide (1.5 equiv.)/α-bromo acetonitrile (1.5 equiv.), Na_2CO_3 (2 equiv.) $AgBF_4$ (1 equiv.) and photocatalyst (TPPT, PC-7) (5 mol%) were added at room temperature under O_2 atmosphere and the reaction was kept for stirring under Blue LED for 15-24 h. After the completion of the reaction

(monitored by TLC), the reaction mixture was filtered, and the solvent was immediately evaporated under vacuum. The resultant residue was purified by column chromatography using silica gel 100-200 mesh using petroleum ether/ethyl acetate as an eluent system to obtain the corresponding α−acyloxy carbonyl compound **3**.

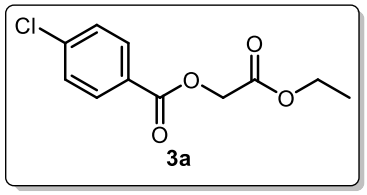
2.7.4. Gram Scale Synthesis:



To a solution of 4-chlorobenzaldehyde **1a** (1 g, 7.11 mmol) in 50 mL acetonitrile, 2-bromo-1-phenylethan-1-one **2f** (1.1 equiv.), Na_2CO_3 (2 equiv.) $AgBF_4$ (1 equiv.) and photocatalyst TPPT (5 mol%) were added at room temperature and the reaction mixture was kept for stirring under Blue LED (2 × 15 W) for 24 h. After the completion of the reaction (monitored by TLC), the reaction mixture was filtered and the solvent was removed under vacuum and the residue was purified by column chromatography using silica gel 100-200 mesh in petroleum ether/ethyl acetate as an eluent system to obtain the corresponding **3m** compound as white solid, 1.42 g, 73% yield.

2.7.5. Experimental data:

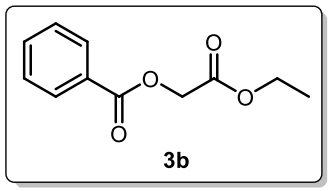
(2-ethoxy-2-oxoethyl 4-chlorobenzoate) (3a)[24]



3a

The compound **3a** was synthesized following the general procedure, starting from 4-chlorobenzadehyde **1a** (50 mg, 0.356 mmol, 1equiv.) and ethyl bromoacetate **2a** (59 µL, 0.534 mmol, 1.5 equiv.). The compound 3a was obtained as yellow oil, 73.5 mg, 85% yield. **^{1}H NMR (400 MHz, $CDCl_3$):** δ 8.03 (d, *J* = 8.8 Hz, 2H), 7.43 (d, *J* = 8.8 Hz, 2H), 4.83 (s, 2H), 4.25 (q, *J* = 7.1 Hz, 2H), 1.29 (t, *J* = 7.1 Hz, 3H). **^{13}C {^{1}H} NMR (100 MHz, $CDCl_3$)**: δ 167.7, 165.2, 140.0, 131.4, 128.9, 127.7, 61.6, 61.4, 14.2. **HRMS (ESI TOF)** *m/z* calcd. For $C_{11}H_{12}ClO_4$ [M + H]+ 243.0424; found 243.0421.

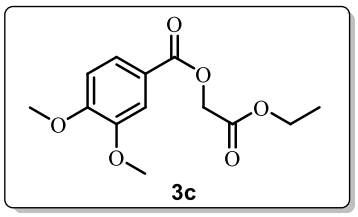
(2-ethoxy-2-oxoethyl benzoate) (3b) [24]



3b

The compound **3b** was synthesized following the general procedure, starting from benzaldehyde **1b** (50 mg, 0.471 mmol, 1 equiv.) and ethyl bromoacetate **2a** (78 µL,0.707 mmol, 1.5 equiv.). The **3b** was obtained as colorless oil, 74 mg, 75% yield. **FT-IR** (KBr): 2293, 1764, 1729, 1602, 1598, 1452, 1380, 1282, 1210, 1123, 1030, 712 cm^{-1}. **^{1}H NMR (400 MHz, $CDCl_3$):** δ 8.10 (d, *J* = 7.5 Hz, 2H), 7.58 (t, *J* = 7.4 Hz, 1H), 7.45 (t, *J* = 7.7 Hz, 2H), 4.84 (s, 2H), 4.25 (q, *J* = 7.1 Hz, 2H), 1.29 (t, *J* = 7.1 Hz, 3H). **^{13}C {^{1}H} NMR (100 MHz, $CDCl_3$):** δ 167.9, 166.1, 133.5, 130.0, 129.3, 128.5, 61.6, 61.3, 14.2. **HRMS (ESI TOF)** *m/z* calcd. For $C_{11}H_{12}O_4Na$ $[M + Na]^+$ 231.0633; found 231.0614.

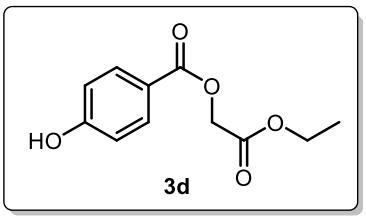
2-ethoxy-2-oxoethyl 3,4-dimethoxybenzoate (3c)



3c

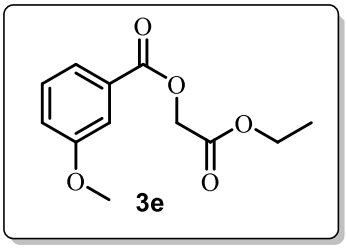
The compound **3c** was synthesized following the general procedure, starting from 3,4-dimethoxybenzaldehyde **1c** (50 mg, 0.301 mmol, 1 equiv.) and ethyl bromoacetate **2a** (50 µL, 0.451 mmol, 1.5 equiv.). The reaction mixture was stirring for 16 h. The compound **3c** was obtained as yellow oil, 69.5 mg, 86% yield. **^{1}H NMR (400 MHz, CDCl$_3$)**: δ 7.75 (dd, *J* = 8.4, 2.0 Hz, 1H), 7.58 (d, *J* = 2.0 Hz, 1H), 6.90 (d, *J* = 8.4 Hz, 1H), 4.81 (s, 2H), 4.25 (q, *J* = 7.1 Hz, 2H), 3.93 (s, 3H), 3.92 (s, 3H), 1.29 (t, *J* = 7.1 Hz, 3H). **^{13}C {^{1}H} NMR (100 MHz, CDCl$_3$):** δ 168.1, 165.9, 153.5, 148.8, 124.3, 121.7, 112.3, 110.4, 61.6, 61.2, 56.2, 56.1, 14.3. **HRMS (ESI TOF)** *m/z* calcd. For $C_{13}H_{17}O_6$ $[M + H]^+$ 269.1025; found 269.1031.

2-ethoxy-2-oxoethyl 4-hydroxybenzoate (3d)



The compound **3d** was synthesized following the general procedure, starting from 4-hydroxybenzaldehyde **1d** (50 mg, 0.409 mmol, 1 equiv.) and ethyl bromoacetate **2a** (68 µL, 0.614 mmol, 1.5 equiv.). The compound **3d** was obtained as colorless oil, 78 mg, 85% yield. **^{1}H NMR (400 MHz, CDCl$_3$):** δ 9.85 (s, 1H), 7.81 (d, *J* = 8.9 Hz, 2H), 6.97 (d, *J* = 8.8 Hz, 2H), 4.67 (s, 2H), 4.24 (q, *J* = 7.2 Hz, 2H), 1.26 (t, *J* = 7.2 Hz, 3H). **^{13}C {^{1}H} NMR (100 MHz, CDCl$_3$):** δ 190.8, 168.1, 162.7, 132.0, 130.8, 115.0, 65.3, 61.7, 14.2. **HRMS (ESI TOF)** *m/z* calcd. For $C_{11}H_{13}O_5$ $[M + H]^+$ 225.0763; found 225.0758.

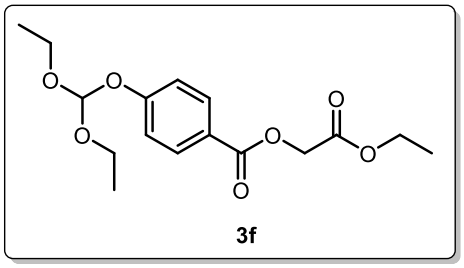
2-ethoxy-2-oxoethyl 3-methoxybenzoate (3e) [24]



The compound **3e** was synthesized following the general procedure, starting from 3-methoxybenzaldehyde **1e** (50 mg, 0.367mmol, 1 equiv.) and ethyl bromoacetate **2a** (61 µl, 0.551 mmol, 1.5 equiv.). The compound **3e** was obtained as Colorless oil, 71 mg, 81% yield.

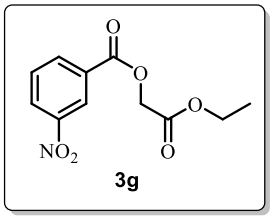
^{1}H NMR (400 MHz, $CDCl_3$): δ 7.69 (ddd, *J* = 7.7, 1.5, 1.0 Hz, 1H), 7.60 (dd, *J* = 2.7, 1.5 Hz, 1H), 7.36 (ddd, *J* = 8.2, 7.7, 0.4 Hz, 1H), 7.13 (ddd, *J* = 8.3, 2.7, 1.0 Hz, 1H), 4.83 (s, 2H), 4.26 (q, *J* = 7.1 Hz, 2H), 3.85 (s, 3H), 1.29 (t, *J* = 7.1 Hz, 3H). **^{13}C {^{1}H} NMR (100 MHz, $CDCl_3$):** δ 167.9, 166.0, 159.7, 130.6, 129.6, 122.5, 120.2, 114.3, 61.6, 61.4, 55.6, 14.3. **HRMS (ESI TOF)** *m/z* calcd. For $C_{12}H_{15}O_5$ $[M + Na]^+$ 261.0739; found 261.0735.

2-ethoxy-2-oxoethyl 4-(diethoxymethoxy)benzoate (3f)



The compound **3f** was synthesized following the general procedure, starting from 4-(diethoxymethoxy)benzaldehyde **1f** (50 mg, 0.223 mmol, 1 equiv.) and ethyl bromoacetate **2a** (37 μL, 0.334 mmol, 1.5 equiv.). The compound **3f** was obtained as colorless oil, 38 mg, 52% yield. **^{1}H NMR (400 MHz, $CDCl_3$):** δ 8.03 (d, *J* = 9.0 Hz, 2H), 6.95 (d, *J* = 9.0 Hz, 2H), 4.84 (t, *J* = 5.2 Hz, 1H), 4.80 (s, 2H), 4.24 (q, *J* = 7.1 Hz, 2H), 4.06 (d, *J* = 5.2 Hz, 2H), 3.77 (dq, *J* = 9.4, 7.1 Hz, 2H), 3.63 (dq, *J* = 9.4, 7.0 Hz, 2H), 1.26 (dt, *J* = 17.0, 7.1 Hz, 9H). **^{13}C {^{1}H} NMR (100 MHz, $CDCl_3$):** δ 168.1, 165.7, 162.9, 132.1, 122.0, 114.5, 100.5, 68.8, 63.0, 61.5, 61.2, 15.4, 14.3. **HRMS (ESI TOF)** *m/z* calcd. For $C_{16}H_{23}O_7$ $[M + H]^+$ 327.1444; found 327.1442.

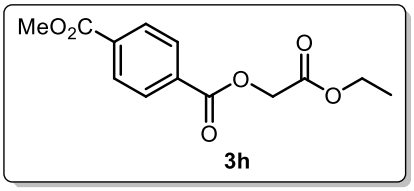
2-ethoxy-2-oxoethyl 3-nitrobenzoate (3g)



The compound **3g** was synthesized following the general procedure, starting from 3-nitrobenzaldehyde **1g** (50 mg, 0.331 mmol, 1 equiv.) and ethyl 2-bromoacetate **2a** (55 μL, 0.496 mmol, 1.5 equiv.). The reaction mixture was stirring for 16hrs. The compound **3g** was

obtained as colorless liquid, 43 mg, 51% yield. **^{1}H NMR (400 MHz, $CDCl_3$)**: δ 8.91 (td, *J* = 1.8, 0.9 Hz, 1H), 8.46 – 8.39 (m, 2H), 7.72 – 7.63 (m, 1H), 4.89 (s, 2H), 4.26 (q, *J* = 7.1 Hz, 2H), 1.30 (t, *J* = 7.1 Hz, 3H). **^{13}C {^{1}H} NMR (100 MHz, $CDCl_3$):** δ 167.4, 164.0, 148.4, 135.7, 131.1, 129.9, 128.0, 125.0, 61.9, 61.8, 14.2. **HRMS (ESI TOF)** *m/z* calcd. For $C_{11}H_{12}NO_6$ [M + H]$^+$ 254.0665; found 254.0658.

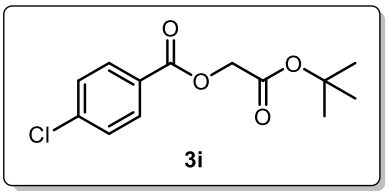
2-ethoxy-2-oxoethyl methyl terephthalate (3h) [24]



3h

The compound **3h** was synthesized following the general procedure, starting from methyl 4-formylbenzoate **1h** (50 mg, 0.305 mmol, 1 equiv.) and ethyl bromoacetate **2a** (37 μL, 0.457 mmol, 1.5 equiv.). The **3h** was obtained as colorless liquid, 39 mg, 48% yield. **^{1}H NMR (400 MHz, $CDCl_3$):** δ 8.14 (d, *J* = 8.9 Hz, 1H), 4.86 (s, 1H), 4.26 (q, *J* = 7.1 Hz, 1H), 3.95 (s, 1H), 1.30 (t, *J* = 7.1 Hz, 1H). **^{13}C {^{1}H} NMR (100 MHz, $CDCl_3$):** δ 167.7, 166.3, 165.3, 134.5, 133.1, 130.0, 129.8, 61.8, 61.6, 52.6, 14.3. **HRMS (ESI TOF)** *m/z* calcd. For $C_{13}H_{15}O_6$ [M + H]$^+$ 267.0869; found 267.0868.

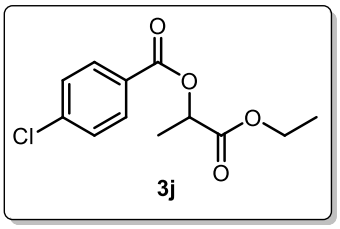
2-(tert-butoxy)-2-oxoethyl 4-chlorobenzoate (3i)



3i

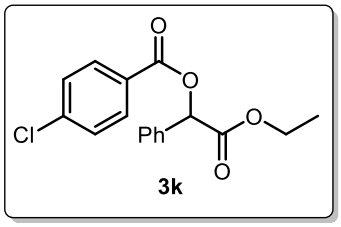
The compound **3i** was synthesized following the general procedure, starting from 4-chlorobenzaldehyde **1a** (50 mg, 0.356 mmol, 1 equiv.) and *tert*-butyl bromoacetate **2b** (104 mg, 0.534 mmol, 1.5 equiv.). The **3i** was obtained as colorless liquid, 82 mg, 85% yield. **^{1}H NMR (400 MHz, $CDCl_3$):** δ 8.05 (d, *J* = 8.8 Hz, 1H), 7.45 (d, *J* = 8.8 Hz, 1H), 4.75 (s, 2H), 1.51 (s, 9H). **^{13}C {^{1}H} NMR (100 MHz, $CDCl_3$)** δ 166.8, 165.3, 140.0, 131.4, 128.9, 128.0, 82.8, 61.9, 28.2. **HRMS (ESI TOF)** *m/z* calcd. For $C_{13}H_{15}ClO_4Na$ [M + Na]$^+$ 293.0557; found 293.0554.

1-ethoxy-1-oxopropan-2-yl 4-chlorobenzoate (3j)



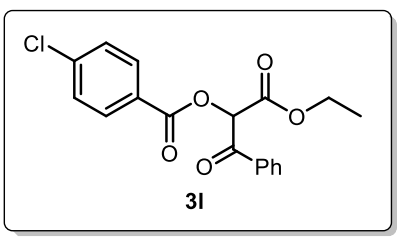
The compound **3j** was synthesized following the general procedure, starting from 4-chlorobenzaldehyde **1a** (50 mg, 0.356 mmol, 1 equiv.) and ethyl 2-bromopropanoate **2c** (105 mg, 0.534 mmol, 1.5 equiv.). The **3j** was obtained as colorless liquid, 75 mg, 82% yield. **^{1}H NMR (400 MHz, $CDCl_3$):** δ 8.01 (d, *J* = 8.8 Hz, 2H), 7.41 (d, *J* = 8.8 Hz, 2H), 5.29 (q, *J* = 7.1 Hz, 1H), 4.22 (q, *J* = 7.1 Hz, 2H), 1.61 (d, *J* = 7.1 Hz, 3H), 1.27 (t, *J* = 7.1 Hz, 3H). **^{13}C {^{1}H} NMR (100 MHz, $CDCl_3$):** δ 170.7, 165.2, 139.9, 131.3, 128.9, 128.1, 69.5, 61.6, 17.1, 14.2. **HRMS (ESI TOF)** *m/z* calcd. For $C_{12}H_{13}ClO_4Na$ $[M + Na]^+$ 279.0400; found 279.0387.

2-ethoxy-2-oxo-1-phenylethyl 4-chlorobenzoate (3k)[25]



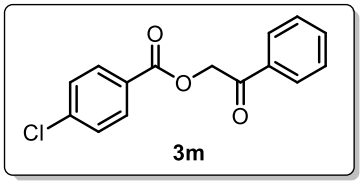
The compound **3k** was synthesized following the general procedure, starting from 4-chlorobenzaldehyde **1a** (50 mg, 0.356 mmol 1 equiv.) and ethyl 2-bromo-2-phenylacetate **2d** (130 mg, 0.534 mmol, 1.5 equiv.). The **3k** was obtained as colorless oil, 80 mg, 70% yield. **^{1}H NMR (400 MHz, $CDCl_3$):** δ 8.06 (d, *J* = 8.5 Hz, 2H), 7.57 (dd, *J* = 7.5, 1.9 Hz, 2H), 7.48 – 7.38 (m, 5H), 6.13 (s, 1H), 4.30 – 4.12 (m, 2H), 1.23 (t, *J* = 7.1 Hz, 3H). **^{13}C {^{1}H} NMR (100 MHz, $CDCl_3$):** δ (ppm) 168.8, 165.2, 140.1, 134.0, 131.5, 129.4, 129.0, 128.95, 127.9, 127.8, 75.3, 62.0, 14.1. **HRMS (ESI TOF)** *m/z* calcd. For $C_{17}H_{16}ClO_4$ $[M + H]^+$ 319.0737; found 319.0744.

1-ethoxy-1,3-dioxo-3-phenylpropan-2-yl 4-chlorobenzoate (3l)[26]



The compound **3l** was synthesized following the general procedure, starting from 4-chlorobenzaldehyde **1a** (50 mg, 0.356 mmol, 1 equiv.) and ethyl 2-bromo-3-oxo-3-phenylpropanoate **2e** (145 mg, 0.534 mmol, 1.5 equiv.). The compound **3l** was obtained as colorless oil, 69 mg, 56% yield. **^{1}H NMR (400 MHz, $CDCl_3$):** δ 8.12 – 8.08 (m, 2H), 8.07 (d, *J* = 1.4 Hz, 1H), 7.67 – 7.56 (m, 2H), 7.51 (t, *J* = 7.7 Hz, 2H), 7.45 (t, *J* = 7.7 Hz, 2H), 6.52 (s, 1H), 4.29 (q, *J* = 7.1 Hz, 2H), 1.25 (t, *J* = 7.1 Hz, 3H). **^{13}C{^{1}H} NMR (100 MHz, $CDCl_3$):** δ 189.9, 178.9, 165.4, 165.2, 134.4, 134.0, 132.9, 130.3, 130.2, 129.5, 129.4, 129.0, 128.7, 75.1, 62.7, 14.1. **HRMS (ESI TOF)** *m/z* calcd. For $C_{18}H_{16}ClO_5$ $[M + H]^+$ 347.0686; found 347.0687.

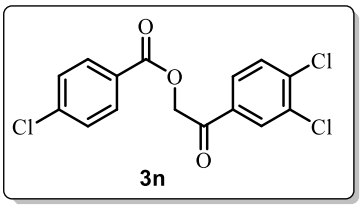
2-oxo-2-phenylethyl 4-chlorobenzoate (3m)[13]



3m

The compound **3m** was synthesized following the general procedure, starting from 4-chlorobenzaldehyde **1a** (50 mg, 0.356 mmol, 1 equiv.) and 2-bromo-1-phenylethan-1-one **2f** (78 mg, 0.391 mmol, 1.1 equiv.). The compound **3m** was obtained as white solid, 72 mg, 74% yield. M.P. 70 -72 °C. **^{1}H NMR (400 MHz, $CDCl_3$):** δ 8.10 – 8.07 (m, 2H), 7.99 – 7.94 (m, 2H), 7.65 – 7.60 (m, 1H), 7.51 (t, *J* = 7.7 Hz, 2H), 7.47 – 7.43 (m, 2H), 5.58 (s, 2H). **^{13}C {^{1}H} NMR (100 MHz, $CDCl_3$):** δ 192.0, 165.3, 140.0, 134.3, 134.1, 134, 133.5, 131.5, 130.1, 129.1, 129.04, 129, 128.6, 128, 127.98, 127.96, 66.7. **HRMS (ESI TOF)** *m/z* calcd. For $C_{15}H_{12}ClO_3$ $[M + H]^+$ 275.0475; found 275.0479.

2-(3,4-dichlorophenyl-2-oxoethyl 4-chlorobenzoate (3n)

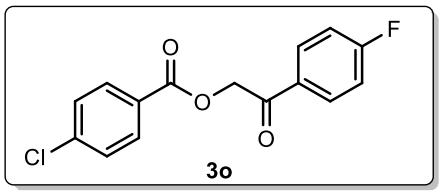


3n

The compound **3n** was synthesized following the general procedure, starting from 4-chlorobenzaldehyde **1a** (50 mg, 0.356 mmol, 1 equiv.) and 2-bromo-1-(3, 4-dichlorophenyl)ethan-1-one **2g** (105 mg, 0.391 mmol, 1.1 equiv.). The compound **3n** was obtained as white solid, 104 mg, 85% yield. M.P. 93-95 °C. **^{1}H NMR (400 MHz, $CDCl_3$):** δ 8.06 (s, 1H), 8.05 – 8.02 (m, 2H), 7.78 (dd, *J* = 8.4, 2.0 Hz, 1H), 7.59 (d, *J* = 8.3 Hz, 1H), 7.45

(d, *J* = 8.6 Hz, 2H), 5.50 (s, 2H). **^{13}C{^{1}H} NMR (100 MHz, $CDCl_3$):** δ 190.1, 165.2, 140.2, 138.9, 133.9, 133.8, 131.5, 131.2, 130.1, 130.0, 129.0, 128.7, 127.7, 126.9, 66.5. **HRMS (ESI TOF)** *m/z* calcd. For $C_{15}H_9Cl_3O_3Na$ $[M + Na]^+$ 364.9509; found 364.9441.

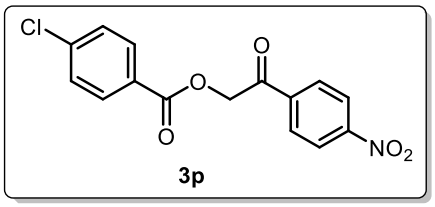
2-(4-fluorophenyl)-2-oxoethyl 4-chlorobenzoate (3o)



3o

The Compound **3o** was synthesized following the general procedure, starting from 4-chlorobenzaldehyde **1a** (50 mg, 0.356 mmol, 1 equiv.) and 2-bromo-1-(4-fluorophenyl)ethan-1-one **2h** (85 mg, 0.391 mmol, 1.1 equiv.). The compound **3o** was obtained as white solid, 94 mg, 90% yield. M.P. 110-111 °C. **^{1}H NMR (400 MHz, $CDCl_3$):** δ 8.07 (d, *J* = 8.5 Hz, 2H), 7.99 (dd, *J* = 8.7, 5.3 Hz, 2H), 7.45 (d, *J* = 8.5 Hz, 2H), 7.18 (t, *J* = 8.5 Hz, 2H), 5.53 (s, 2H). **^{13}C{^{1}H} NMR (100 MHz, $CDCl_3$):** δ 190.5, 166.3(d, $J_{(C-F)}$ = 255 Hz), 165.3, 140.1, 131.5, 130.8, 130.67 (d, $J_{(C-F)}$ = 9.5 Hz), 130.1, 129.0, 128.6, 127.9, 116.32 (d, $J_{(C-F)}$ = 22.1 Hz), 66.5. **^{19}F NMR (400 MHz, $CDCl_3$):** -103.1. **HRMS (ESI TOF)** *m/z* calcd. For $C_{15}H_{11}ClFO_3$ $[M + H]^+$ 293.0381; found 293.0334.

2-(4-nitrophenyl)-2-oxoethyl 4-chlorobenzoate (3p)

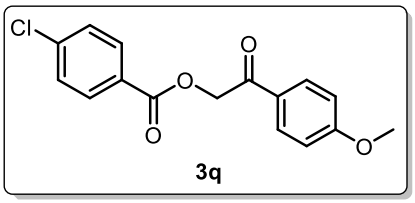


3p

The Compound **3p** was synthesized following the general procedure, starting from 4-chlorobenzaldehyde **1a** (50 mg, 0.356 mmol, 1 equiv.) and 2-bromo-1-(4-nitrophenyl)ethan-1-one **2i** (96 mg, 0.391 mmol, 1.1 equiv.). The **3p** was obtained as light yellow solid, 104 mg, 91% yield. M.P. 128-130 °C. **^{1}H NMR (400 MHz, $CDCl_3$):** δ 8.37 (d, *J* = 8.9 Hz, 2H), 8.13 (d, *J* = 8.9 Hz, 2H), 8.06 (d, *J* = 8.7 Hz, 2H), 7.47 (d, *J* = 8.7 Hz, 2H), 5.57 (s, 2H). **^{13}C {^{1}H} NMR (100 MHz, $CDCl_3$):** δ 191.0, 165.2, 151.0, 140.4, 138.7, 131.5, 130.1, 129.13, 129.11,

128.7, 127.5, 124.3, 66.8. **HRMS (ESI TOF)** *m/z* calcd. For $C_{15}H_{11}ClNO_5$ $[M + H]^+$ 320.0326; found 320.0329.

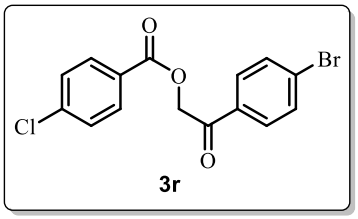
2-(4-methoxyphenyl)-2-oxoethyl 4-chlorobenzoate (3q)[27]



3q

The compound **3q** was synthesized following the general procedure, starting from 4-chlorobenzaldehyde **1a** (50 mg, 0.356 mmol, 1 equiv.) and 2-bromo-1-(4-methoxyphenyl)ethan-1-one **2j** (90 mg, 0.391 mmol, 1.1 equiv.). The **3q** was obtained as white solid, 81.5 mg, 75% yield. M.P. 124-126 °C. **^{1}H NMR (400 MHz, $CDCl_3$)**: δ 8.11 – 8.05 (m, 2H), 7.97 – 7.92 (m, 2H), 7.47 – 7.41 (m, 2H), 7.00 – 6.95 (m, 2H), 5.53 (s, 2H), 3.89 (s, 3H); **^{13}C{^{1}H} NMR (100 MHz, $CDCl_3$):** δ 190.4, 165.4, 164.3, 139.9, 131.5, 130.3, 128.9, 128.1, 127.3, 114.3, 66.5, 55.7. **HRMS (ESI TOF)** *m/z* calcd. For $C_{16}H_{14}ClO_4$ $[M + H]^+$ 305.0581; found 305.0587.

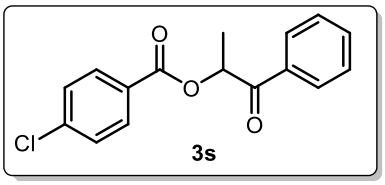
2-(4-bromophenyl)-2-oxoethyl 4-chlorobenzoate (3r)



3r

The compound **3r** was synthesized following the general procedure, starting from 4-chlorobenzaldehyde **1a** (50 mg, 0.356 mmol, 1 equiv.) and 2-bromo-1-(4-bromophenyl)ethan-1-one **2k** (109 mg, 0.391 mmol, 1.1 equiv.). The compound **3r** was obtained as White solid, 101 mg, 80% yield. M.P. 119-121 °C. **^{1}H NMR (400 MHz, $CDCl_3$):** δ 8.17 – 7.96 (m, 2H), 7.91 – 7.77 (m, 2H), 7.69 – 7.61 (m, 2H), 7.44 (d, *J* = 8.6 Hz, 1H), 5.52 (s, 2H). **^{13}C {^{1}H} NMR (100 MHz, $CDCl_3$):** δ 191.1, 165.2, 140.1, 133.0, 132.4, 132.37, 131.5, 130.1, 129.4, 129.39, 129.0, 128.6, 127.8, 66.5. **HRMS (ESI TOF)** *m/z* calcd. For $C_{15}H_{11}BrClO_3$ $[M + H]^+$ 352.9580; found 352.9582.

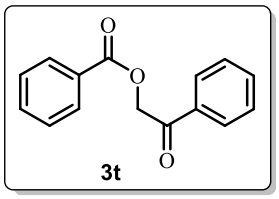
1-oxo-1-phenylpropan-2-yl 4-chlorobenzoate (3s)[28]



3s

The compound **3s** was synthesized following the general procedure, starting from 4-chlorobenzaldehyde **1a** (50 mg, 0.356 mmol, 1 equiv.) and 2-bromo-1-phenylpropan-1-one **2l** (83 mg, 0.391 mmol, 1.1 equiv.). The compound **3s** was obtained as white solid, 93 mg, 90% yield. M.P. 98-100 °C. **^{1}H NMR (400 MHz, $CDCl_3$):** δ 8.12 – 7.96 (m, 4H), 7.63 – 7.55 (m, 1H), 7.52 – 7.40 (m, 4H), 6.24 – 6.16 (m, 1H), 1.67 (dd, *J* = 7.0, 2.2 Hz, 3H). **^{13}C{^{1}H} NMR (100 MHz, $CDCl_3$):** δ 196.9, 196.6, 166.1, 165.3, 139.9, 134.6, 134.5, 133.8, 133.7, 133.4, 131.4, 130.0, 129.6, 129.0, 128.94, 128.91, 128.7, 128.6, 128.5, 128.1, 72.2, 72.0, 17.4, 17.3. **HRMS (ESI TOF)** *m/z* calcd. For $C_{16}H_{14}ClO_3$ $[M + H]^+$ 289.0631; found 289.0639.

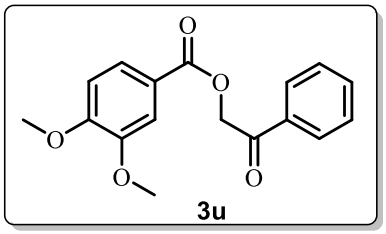
2-oxo-2-phenylethyl benzoate (3t)[11a]



3t

The compound **3t** was synthesized following the general procedure, starting from benzaldehyde **1b** (50 mg, 0.471 mmol, 1equiv.) and 2-bromo-1-phenylethan-1-one **2f** (103 mg, 0.518 mmol, 1.1 equiv.). The compound **3t** was obtained as white solid, 91 mg, 80% yield. **FT-IR** (KBr): 2719, 2598, 1719, 1698, 1594, 1452, 1286 cm^{-1}. M.P. 115 - 117 °C. **^{1}H NMR (400 MHz, $CDCl_3$):** δ 8.15 (dd, *J* = 8.3, 1.3 Hz, 1H), 7.98 (dd, *J* = 8.3, 1.2 Hz, 1H), 7.67 – 7.56 (m, 1H), 7.49 (dt, *J* = 13.9, 7.7 Hz, 2H), 5.58 (s, 1H). **^{13}C {^{1}H} NMR (100 MHz, $CDCl_3$):** δ 192.2, 166.2, 134.4, 134.0, 133.5, 130.1, 129.5, 129, 128.6, 128, 66.6. **HRMS (ESI TOF)** *m/z* calcd. For $C_{15}H_{12}O_3Na$ $[M + Na]^+$ 263.0684; found 263.0683.

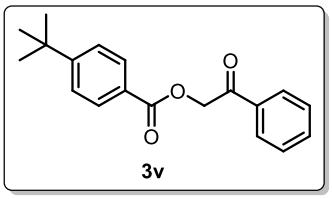
2-oxo-2-phenylethyl 3,4-dimethoxybenzoate (3u)



3u

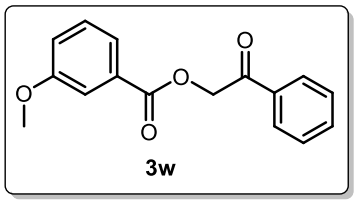
The compound **3u** was synthesized following the general procedure, starting from 3,4-dimethoxybenzaldehyde **1c** (50 mg, 0.301 mmol, 1 equiv.) and 2-bromo-1-phenylethan-1-one **2f** (66 mg, 0.331 mmol, 1.1 equiv.). The **3u** was obtained as white solid, 81 mg, 90% yield. M.P. 108-110°C. **^{1}H NMR (400 MHz, $CDCl_3$):** δ 7.99 – 7.95 (m, 2H), 7.80 (dd, *J* = 8.4, 2.0 Hz, 1H), 7.64 – 7.59 (m, 2H), 7.53 – 7.48 (m, 2H), 6.92 (d, *J* = 8.5 Hz, 1H), 5.55 (s, 2H), 3.95 (s, 3H), 3.93 (s, 3H). **^{13}C{^{1}H} NMR (100 MHz, $CDCl_3$):** δ (ppm) 192.5, 165.9, 153.4, 148.7, 134.4, 134.0, 129.0, 128.0, 124.3, 112.3, 110.4, 66.5, 56.2, 56.1. **HRMS (ESI TOF)** *m/z* calcd. For $C_{17}H_{17}O_5$ $[M + H]^+$ 301.1076; found 301.1078.

2-oxo-2-phenylethyl 4-(tert-butyl)benzoate (3v)[29]



The compound **3v** was synthesized following the general procedure, starting from 4-(tert-butyl)-benzadehyde **1i** (50 mg, 0.308 mmol, 1 equiv.) and 2-bromo-1-phenylethan-1-one **2f** (68 mg, 0.339 mmol, 1.1 equiv.). The compound **3v** was obtained as white solid, 79 mg, 86% yield. M.P. 64-66 °C. **^{1}H NMR (400 MHz, $CDCl_3$):** δ 8.10 – 8.07 (m, 2H), 7.97 (dd, *J* = 8.3, 1.2 Hz, 2H), 7.63 – 7.58 (m, 1H), 7.51 – 7.46 (m, 4H), 5.57 (s, 2H), 1.35 (s, 9H). **^{13}C {^{1}H} NMR (100 MHz, $CDCl_3$):** δ 192.3, 166.1, 157.1, 134.4, 133.9, 129.9, 128.9, 127.92, 127.91, 127.90, 127.89, 127.88, 126.7, 125.5, 66.4, 35.2, 31.2, 31.19, 31.18, 31.17, 31.16, 31.15, 31.14. **HRMS (ESI TOF)** *m/z* calcd. For $C_{19}H_{21}O_3$ $[M + H]^+$ 297.1491; found 297.1479.

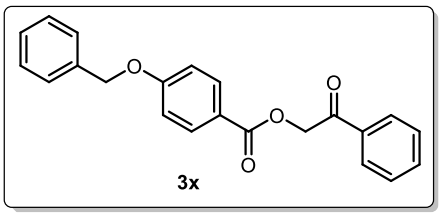
2-oxo-2-phenylethyl 3-methoxybenzoate (3w)[30]



The compound **3w** was synthesized following the general procedure, starting from 3-methoxybenzadehyde **1e** (50 mg, 0.367 mmol, 1 equiv.) and 2-bromo-1-phenylethan-1-one **2f**

(80 mg, 0.404 mmol, 1.1 equiv.). The compound **3w** was obtained as white solid, 89.5 mg, 90% yield. M.P. 80-81 °C. **^{1}H NMR (400 MHz, $CDCl_3$):** δ 7.97 (d, *J* = 7.4 Hz, 2H), 7.75 (d, *J* = 7.6 Hz, 1H), 7.69 – 7.58 (m, 2H), 7.51 (t, *J* = 7.7 Hz, 2H), 7.38 (t, *J* = 8.0 Hz, 1H), 7.14 (dd, *J* = 8.2, 2.4 Hz, 1H), 5.57 (s, 2H), 3.86 (s, 3H). **^{13}C{^{1}H} NMR (100 MHz, $CDCl_3$):** δ 192.2, 166.1, 159.7, 134.4, 134.0, 130.8, 130.0, 129.6, 129.1, 129.03, 129.0, 128.5, 128.0, 122.6, 120.2, 118.4, 114.3, 66.7, 55.6 **HRMS (ESI TOF)** *m/z* calcd. For $C_{16}H_{14}O_4Na$ [M + Na]$^+$ 293.0790; found 293.0790.

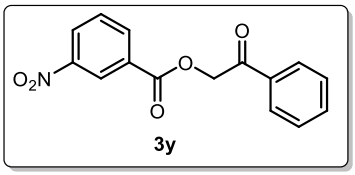
2-oxo-2-phenylethyl 4-(benzyloxy)benzoate (3x)



3x

The compound **3x** was synthesized following the general procedure, starting from 4-(benzyloxy)benzaldehyde **1j** (50 mg, 0.236 mmol, 1 equiv.) and 2-bromo-1-phenylethan-1-one **2f** (52 mg, 0.259 mmol, 1.1 equiv.). The compound **3x** was obtained as white solid, 71mg, 87%yield. M.P. 122-124 °C. **^{1}H NMR (400 MHz, $CDCl_3$):** δ 8.14 – 8.07 (m, 2H), 7.97 (dt, *J* = 8.4, 1.7 Hz, 2H), 7.67 – 7.58 (m, 1H), 7.56 – 7.47 (m, 2H), 7.47 – 7.34 (m, 5H), 7.05 – 7.00 (m, 2H), 5.55 (s, 2H), 5.14 (s, 2H). **^{13}C {^{1}H} NMR (100 MHz, $CDCl_3$):** δ 192.5, 165.8, 163.0, 136.3, 134.5, 134.0, 132.2, 129.0, 128.8, 128.4, 128.0, 127.6, 122.1, 114.7, 70.3, 66.4. **HRMS (ESI TOF)** *m/z* calcd. For $C_{22}H_{18}O_4Na$ [M + Na]$^+$ 369.1103; found 369.1096.

2-oxo-2-phenylethyl 3-nitrobenzoate (3y)

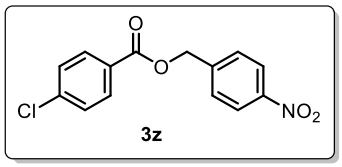


3y

The compound **3y** was synthesized following the general procedure, starting from 3-nitrobenzadehyde **1g** (50 mg, 1 equiv.) and 2-bromo-1-phenylethan-1-one **2f** (73 mg, 1.1equiv.). The compound **3y** was obtained as off-white solid, 61 mg, 65%. M.P. 87-89 °C.
^{1}H NMR (400 MHz, $CDCl_3$): δ 8.98 (t, *J* = 1.8 Hz, 1H), 8.49 – 8.45 (m, 2H), 8.01 – 7.93 (m, 2H), 7.74 – 7.61 (m, 2H), 7.58 – 7.49 (m, 2H), 5.66 (s, 2H). **^{13}C{^{1}H} NMR (100 MHz, $CDCl_3$):**

δ 191.4, 164.2, 148.5, 135.8, 134.3, 134.1, 131.4, 129.9, 129.2, 128.0, 127.9, 125.2, 67.2. **HRMS (ESI TOF)** *m/z* calcd. For $C_{15}H_{12}NO_5$ $[M + H]^+$ 286.0715; found 286.0721.

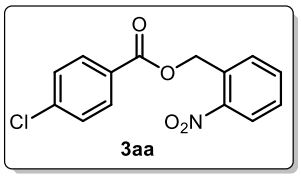
4-nitrobenzyl 4-chlorobenzoate (3z)



3z

The compound **3z** was synthesized following the general procedure, starting from 4-chlorobenzaldehyde **1a** (50 mg, 0.356 mmol, 1equiv.) and 1-(bromomethyl)-4-nitrobenzene **2m** (116 mg, 0.534 mmol, 1.5 equiv.). The compound **3z** was obtained as white solid, 62 mg, 60%yield. M.P. 122-124 °C. **^{1}H NMR (400 MHz, $CDCl_3$):** δ 8.25 (d, *J* = 8.7 Hz, 2H), 8.02 (d, *J* = 8.6 Hz, 2H), 7.60 (d, *J* = 8.9 Hz, 2H), 7.44 (d, *J* = 8.6 Hz, 2H), 5.45 (s, 2H). **^{13}C{^{1}H} NMR (100 MHz, $CDCl_3$):** δ 165.4, 147.9, 143.1, 140.1, 131.2, 129.0, 128.5, 128.0, 124.0, 65.5. **HRMS (ESI TOF)** *m/z* calcd. For $C_{14}H_{10}ClNO_4Na$ $[M + Na]^+$ 314.0196; Found - 314.0194.

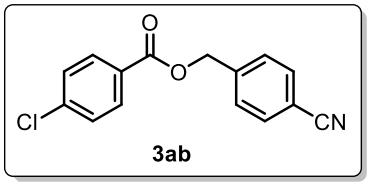
2-nitrobenzyl 4-chlorobenzoate (3aa)[31]



3aa

The compound **3aa** was synthesized following the general procedure, starting from 4-chlorobenzaldehyde **1a** (50 mg, 0.356 mmol, 1equiv.) and 1-(bromomethyl)-2-nitrobenzene **2n** (115 mg, 0.534 mmol, 1.5 equiv.). The compound **3aa** was obtained as grey colored solid, 68 mg, 65% yield. M.P. 90-92 °C. **^{1}H NMR (400 MHz, $CDCl_3$):** δ 8.28 – 8.09 (m, 1H), 8.06 – 7.91 (m, 2H), 7.72 – 7.59 (m, 2H), 7.56 – 7.46 (m, 1H), 7.46 – 7.40 (m, 2H), 5.77 (s, 2H). **^{13}C {^{1}H} NMR (100 MHz, $CDCl_3$):** δ 165.2, 147.8, 140.1, 133.9, 132.1, 131.3, 129.9, 129.2, 129.1, 129.07, 128.7, 128.1, 125.3, 63.7. **HRMS (ESI TOF)** *m/z* calcd. For $C_{14}H_{10}ClNO_4Na$ $[M + Na]^+$ 314.0196; found 314.0186.

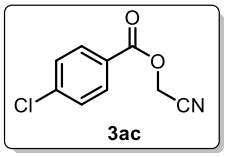
4-cyanobenzyl 4-chlorobenzoate (3ab)



3ab

The compound **3ab** was synthesized following the general procedure, starting from 4-chlorobenzaldehyde **1a** (50 mg, 0.356 mmol, 1 equiv.) and 1-(bromomethyl)-4-cyanobenzene **2o** (105 mg, 0.534 mmol, 1.5 equiv.). The compound **3ab** was obtained as white solid, 64 mg, 66% yield. M.P. 80-82 °C. **^{1}H NMR (400 MHz, $CDCl_3$):** δ 8.01 (d, *J* = 8.6 Hz, 2H), 7.73 – 7.64 (m, 2H), 7.54 (d, *J* = 8.1 Hz, 2H), 7.44 (d, *J* = 8.6 Hz, 2H), 5.41 (s, 2H). **^{13}C {^{1}H} NMR ($CDCl_3$, 100 MHz):** δ (ppm) 165.4, 141.2, 140.1, 133.6, 132.6, 131.2, 129.9, 129.0, 128.5, 118.6, 112.3, 77.5, 77.2, 76.8, 65.8 **HRMS (ESI TOF)** *m/z* calcd. For $C_{15}H_{11}ClNO_2$ $[M + H]^+$ 272.0478; found 272.0482.

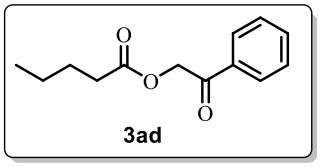
Cyanomethyl 4-chlorobenzoate (3ac)[32]



3ac

The compound **3ac** was synthesized following the general procedure, starting from 4-chlorobenzaldehyde **1a** (50 mg, 0.356 mmol, 1 equiv.) and 2-bromoacetonitrile **2p** (64 mg, 0.534 mmol, 1.5 equiv.). The **3ac** was obtained as light yellow liquid, 29 mg, 42% yield. **^{1}H NMR (400 MHz, $CDCl_3$):** δ 7.99 (d, *J* = 8.7 Hz, 2H), 7.46 (d, *J* = 8.7 Hz, 2H), 4.96 (s, 2H). **^{13}C {^{1}H} NMR (100 MHz, $CDCl_3$):** δ (ppm) 164.3, 141.0, 131.5, 130.2, 129.3, 128.8, 126.4, 114.4, 49.1. **HRMS (ESI TOF)** *m/z* calcd. For $C_9H_7ClNO_2$ $[M + H]^+$ 196.0165; found 196.0172.

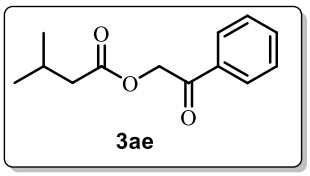
2-oxo-2-phenylethyl pentanoate (3ad)



3ad

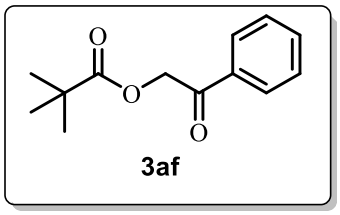
The compound **3ad** was synthesized following the general procedure, starting from pentanal **1k** (50 mg, 0.580 mmol, 1 equiv.) and 2-bromo-1-phenylethan-1-one **2f** (127 mg, 0.638 mmol, 1.1 equiv.). The compound **3ad** was obtained as yellow liquid, 108 mg, 84% yield. **^{1}H NMR (400 MHz, $CDCl_3$):** δ 8.01 – 7.82 (m, 2H), 7.61 (ddt, *J* = 8.6, 6.9, 1.3 Hz, 1H), 7.48 (ddd, *J* = 8.2, 6.7, 1.2 Hz, 2H), 5.34 (s, 2H), 2.67 – 2.28 (m, 2H), 1.87 – 1.58 (m, 2H), 1.50 – 1.34 (m, 2H), 0.94 (t, *J* = 7.4 Hz, 3H). **^{13}C {^{1}H} NMR (100 MHz, $CDCl_3$):** δ 192.5, 173.4, 134.4, 134.0, 129.0, 127.9, 66.0, 33.8, 27.1, 22.4, 13.9. **HRMS (ESI TOF)** *m/z* calcd. For $C_{13}H_{16}O_3Na$ [M + Na]$^+$ 243.0997; found 243.1005.

2-oxo-2-phenylethyl 3-methylbutanoate (3ae)



The compound **3ae** was synthesized following the general procedure, starting from 3-methylbutanal **1l** (50 mg, 0.580 mmol, 1 equiv.) and 2-bromo-1-phenylethan-1-one **2f** (127 mg, 0.638 mmol, 1.1 equiv.). The compound **3ae** was obtained as light-yellow liquid, 111 mg, 87% yield. **^{1}H NMR (400 MHz, $CDCl_3$):** δ 7.96 – 7.87 (m, 2H), 7.66 – 7.58 (m, 1H), 7.49 (ddt, *J* = 7.9, 6.7, 0.6 Hz, 2H), 5.35 (s, 2H), 2.38 (d, *J* = 7.1 Hz, 2H), 2.21 (ddq, *J* = 13.2, 7.4, 6.6 Hz, 1H), 1.05 (s, 3H), 1.03 (s, 3H). **^{13}C {^{1}H} NMR (100 MHz, $CDCl_3$):** δ 192.4, 172.6, 134.4, 133.9, 128.9, 127.9, 65.9, 43.1, 25.8, 22.5. **HRMS (ESI TOF)** *m/z* calcd. For $C_{13}H_{16}O_3Na$ [M + Na]$^+$ 243.0997; found 243.1002.

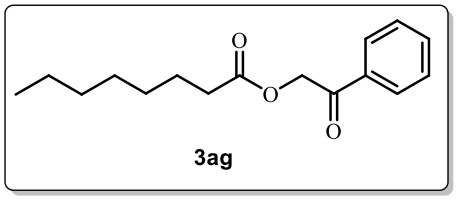
(2-oxo-2-phenylethyl pivalate (3af)[30]



The compound **3af** was synthesized following the general procedure, starting from pivalaldehyde **1m** (50 mg, 0.580 mmol, 1 equiv.) and 2-bromo-1-phenylethan-1-one **2f** (127 mg, 0.638 mmol, 1.1 equiv.). The compound **3af** was obtained as white solid, 109 mg, 85% yield. M.P. 54 - 55 °C. **^{1}H NMR (400 MHz, $CDCl_3$):** δ 7.94 – 7.83 (m, 2H), 7.65 – 7.54 (m, 1H), 7.48 (m, 2H), 5.31 (s, 2H), 1.30 (s, 9H). **^{13}C {^{1}H} NMR (100MHz, $CDCl_3$):** δ 192.6,

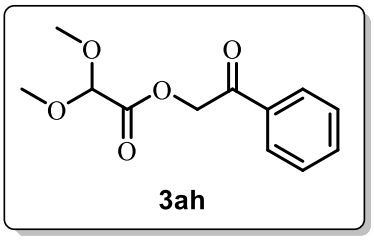
178.2, 134.5, 133.9, 129.0, 128.96, 127.9, 66.0, 39.0, 27.4. **HRMS (ESI TOF)** *m/z* calcd. For $C_{13}H_{17}O_3$ $[M + H]^+$ 221.1178; found 221.1159.

2-oxo-2-phenylethyl octanoate (3ag)



The compound **3ag** was synthesized following the general procedure, starting from octanal **1n** (50 mg, 0.390 mmol, 1 equiv.) and 2-bromo-1-phenylethan-1-one **2f** (85 mg, 0.429 mmol, 1.1 equiv.). The **3ag** was obtained as colorless liquid, 90 mg, 88% yield. **^{1}H NMR (400 MHz, $CDCl_3$):** δ 7.94 – 7.88 (m, 2H), 7.63 – 7.57 (m, 1H), 7.52 – 7.44 (m, 2H), 5.33 (s, 2H), 2.48 (t, *J* = 7.6 Hz, 2H), 1.69 (dd, *J* = 15.0, 7.3 Hz, 2H), 1.40 – 1.22 (m, 9H), 0.94 – 0.83 (m, 3H). **^{13}C {^{1}H} NMR (100 MHz, $CDCl_3$):** δ (ppm) 192.5, 173.4, 134.4, 133.9, 129.0, 128.9, 127.9, 66.0, 34.1, 31.8, 29.2, 29.0, 25.0, 22.7, 14.2. **HRMS (ESI TOF)** *m/z* calcd. For $C_{16}H_{22}O_3Na$ $[M + Na]^+$ 285.1467; found 285.1470.

2-oxo-2-phenylethyl 2,2-dimethoxyacetate (3ah)



The compound **3ah** was synthesized following the general procedure, starting from 2,2-dimethoxyacetaldehyde **1o** (50 mg, 0.480 mmol, 1 equiv.) and 2-bromo-1-phenylethan-1-one **2f** (105 mg, 0.582 mmol, 1.1 equiv.). The compound **3ah** was obtained as light-yellow liquid, 46 mg, 40% yield. **^{1}H NMR (400 MHz, $CDCl_3$):** δ 7.90 (dd, *J* = 8.4, 1.3 Hz, 2H), 7.63 – 7.57 (m, 1H), 7.51 – 7.46 (m, 2H), 5.45 (s, 2H), 5.01 (s, 1H), 3.50 (s, 6H). **^{13}C {^{1}H} NMR (100 MHz, $CDCl_3$):** δ 191.0, 166.7, 134.2, 134.0, 129.0, 127.9, 98.7, 66.7, 54.0. **HRMS (ESI TOF)** *m/z* calcd. For $C_{12}H_{14}O_5Na$ $[M + Na]^+$ 261.0739; found 261.0735.

2.8. Appendix II: ^{1}H, ^{13}C and IR spectral data of representative compounds

Compound No.	Figure AII.X	Data	Page No.
3a	Figure AII.1 and AII.2	^{1}H and ^{13}C	71
3l	Figure AII.3 and AII.4	^{1}H and ^{13}C	72
3m	Figure AII.5 and AII.6	^{1}H and ^{13}C	73
3z	Figure AII.7 and AII.8	^{1}H and ^{13}C	74
3ac	Figure AII.9 and AII.10	^{1}H and ^{13}C	75
3ad	Figure AII.11 and AII.12	^{1}H and ^{13}C	76
3b	Figure AII. 13	FT-IR	78
3t	Figure AII. 14	FT-IR	79



Figure AII.1 ^{1}H NMR (400 MHz, $CDCl_3$) spectrum of compound **3a**

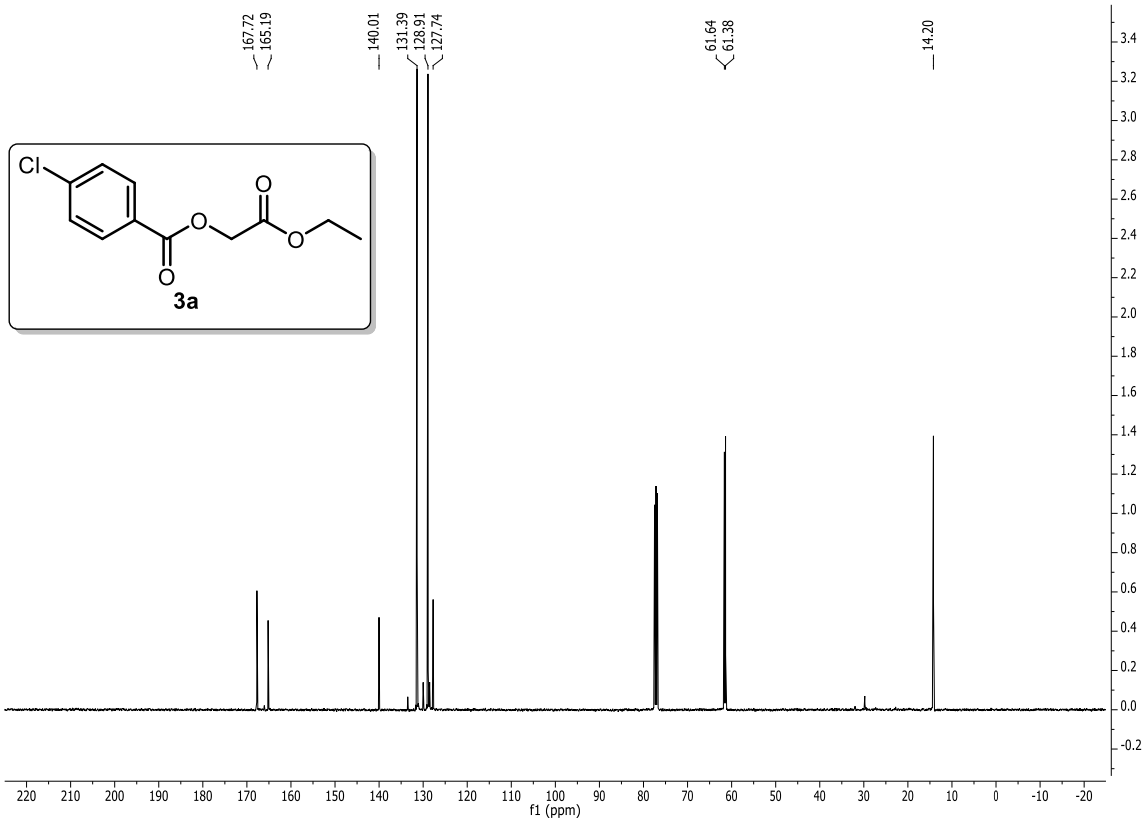


Figure AII.2 ^{13}C NMR (100 MHz, $CDCl_3$) spectrum of compound **3a**

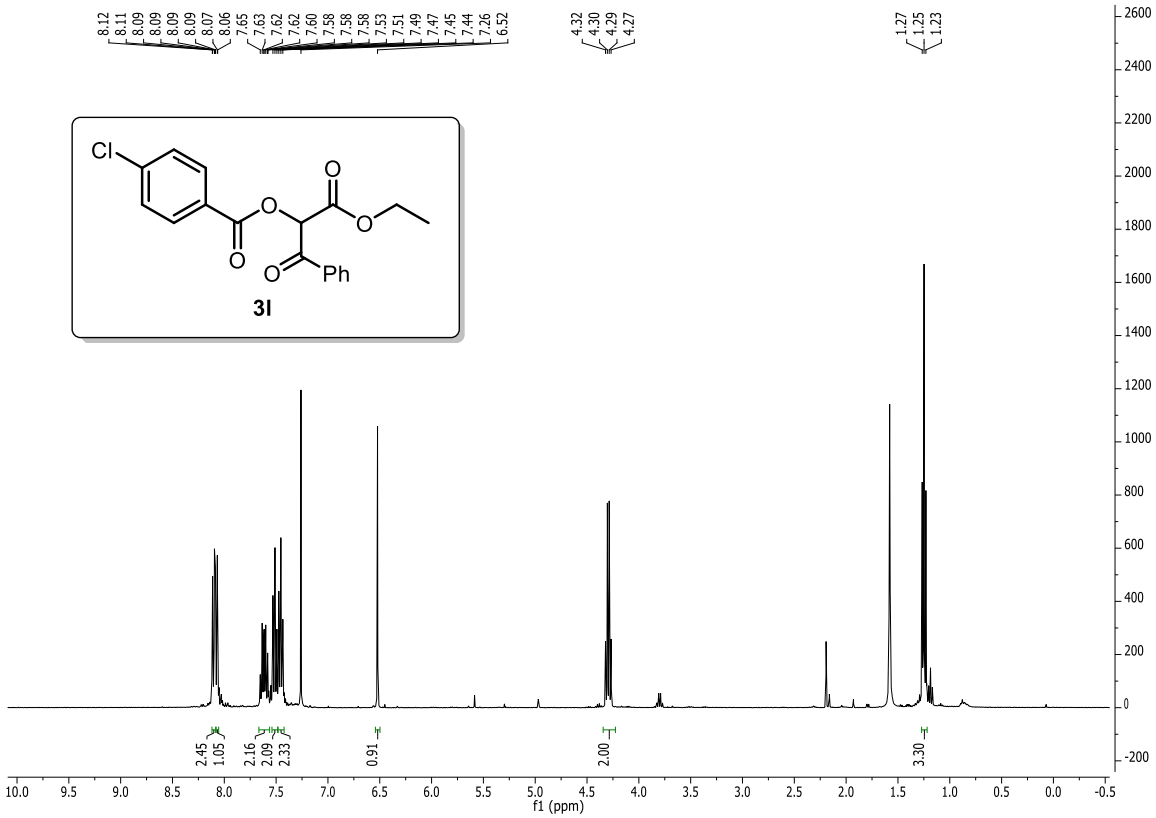


Figure AII.3 ^{1}H NMR (400 MHz, $CDCl_3$) spectrum of compound **3l**

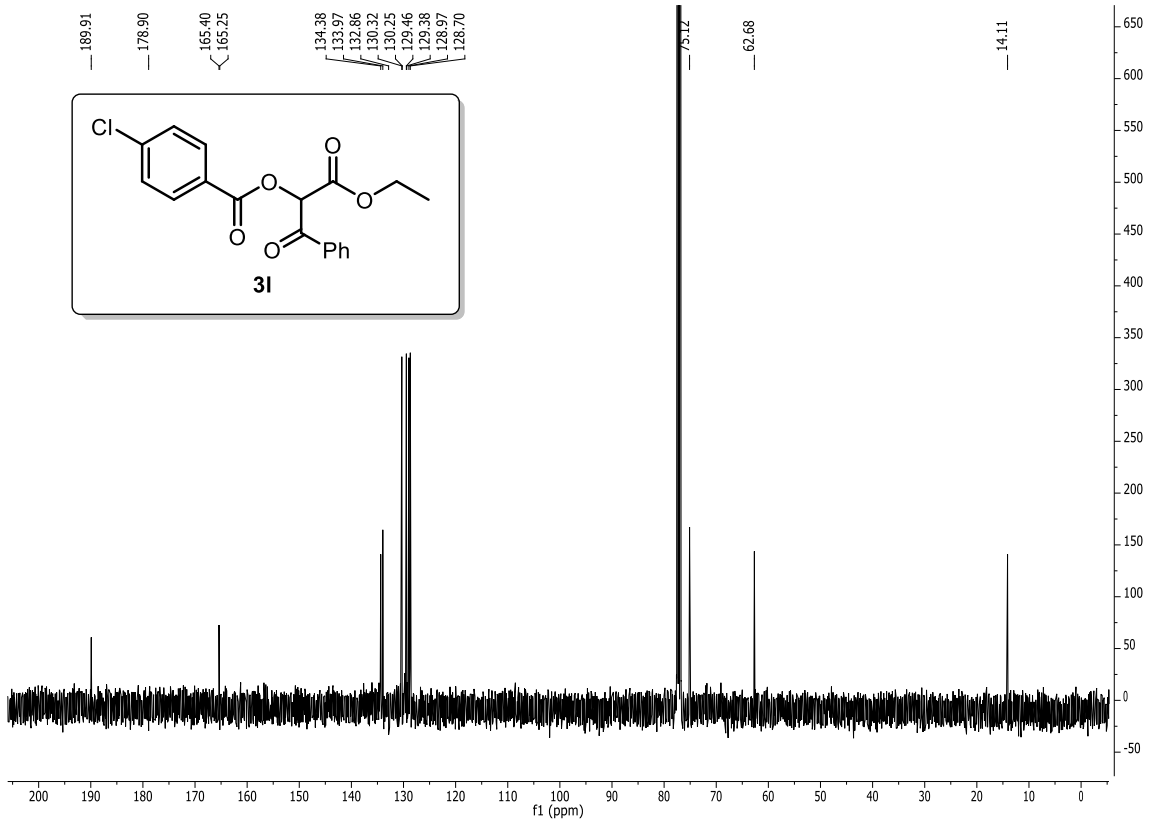


Figure AII.4 ^{13}C NMR (100 MHz, $CDCl_3$) spectrum of compound **3l**

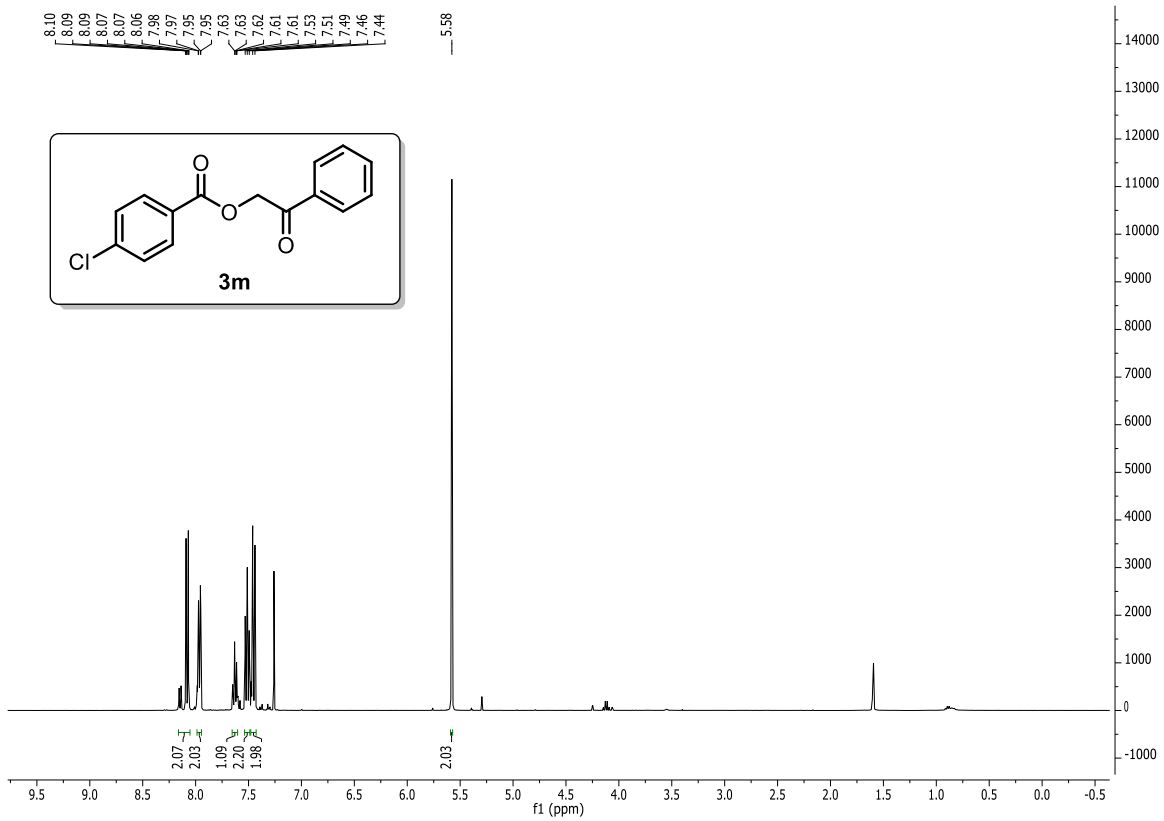


Figure AII.5 ^{1}H NMR (400 MHz, $CDCl_3$) spectrum of compound **3m**

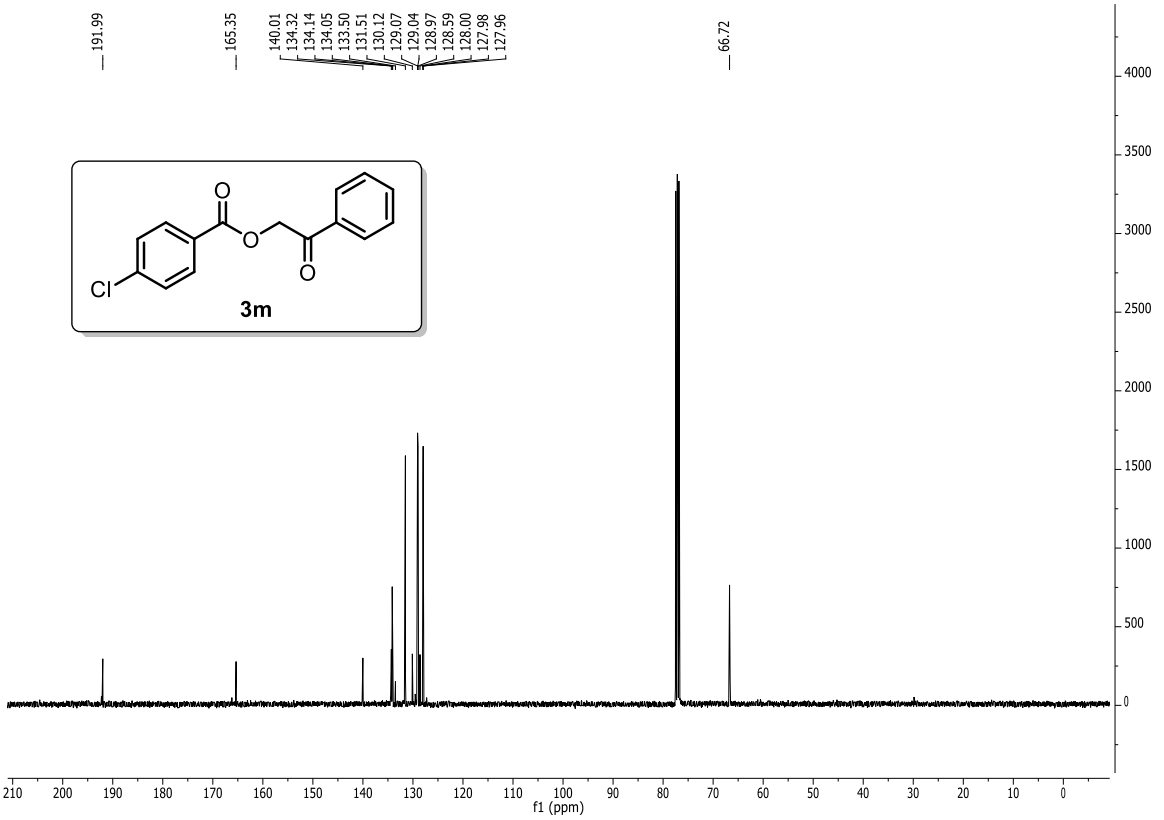


Figure AII.6 ^{13}C NMR (100 MHz, $CDCl_3$) spectrum of compound **3m**

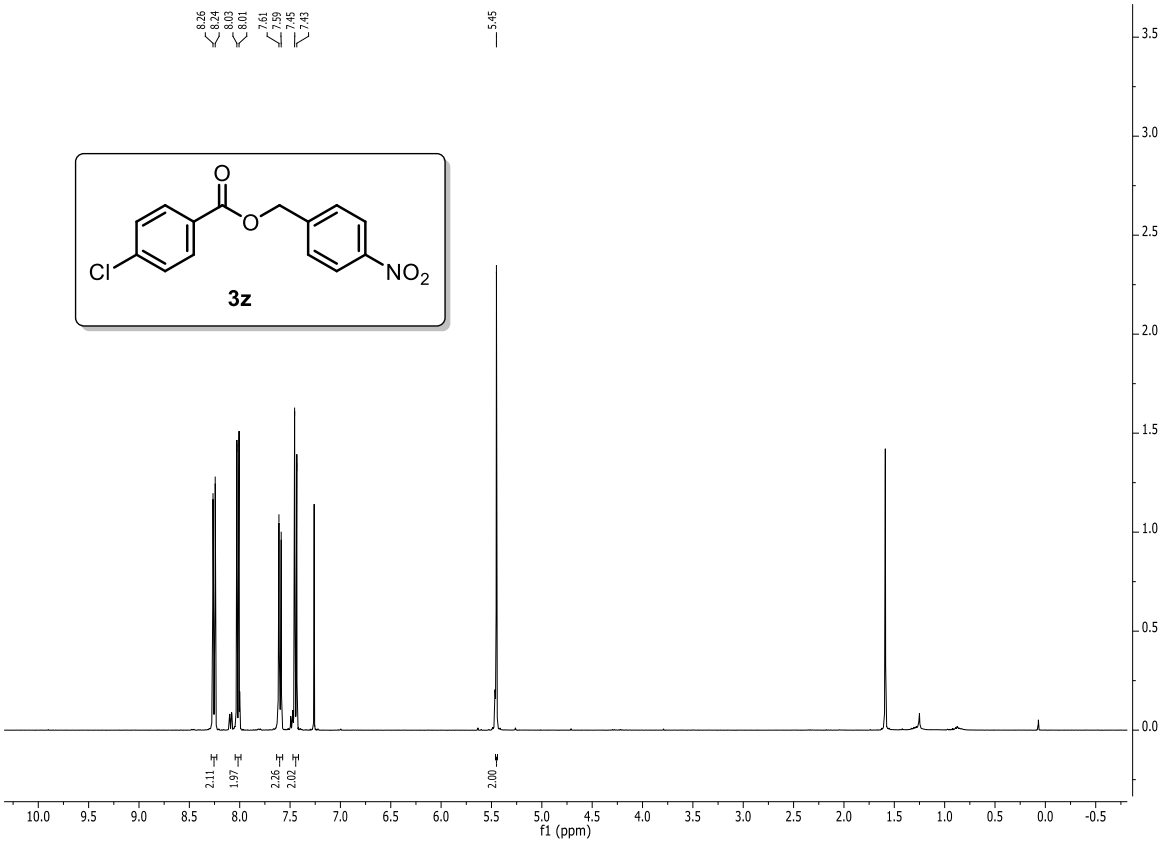


Figure AII.7 ^{1}H NMR (400 MHz, $CDCl_3$) spectrum of compound **3z**

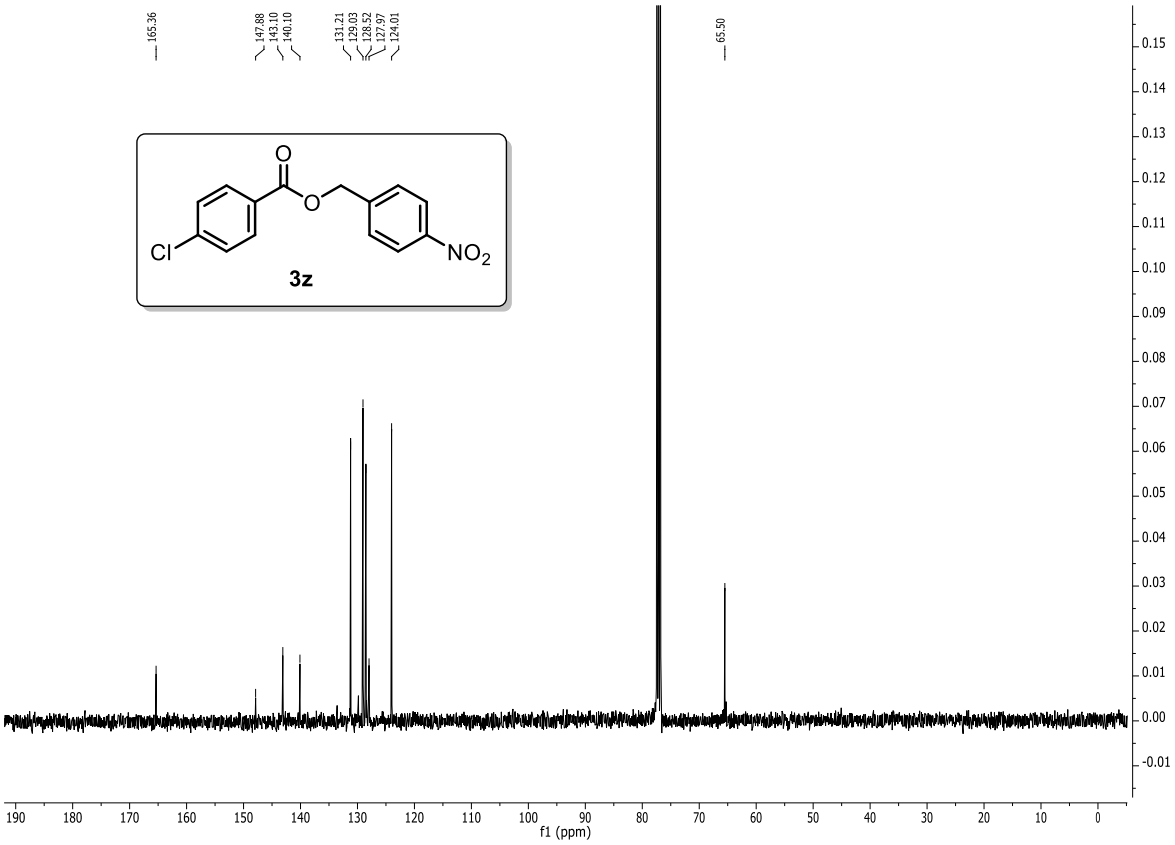


Figure AII.8 ^{13}C NMR (100 MHz, $CDCl_3$) spectrum of compound **3z**

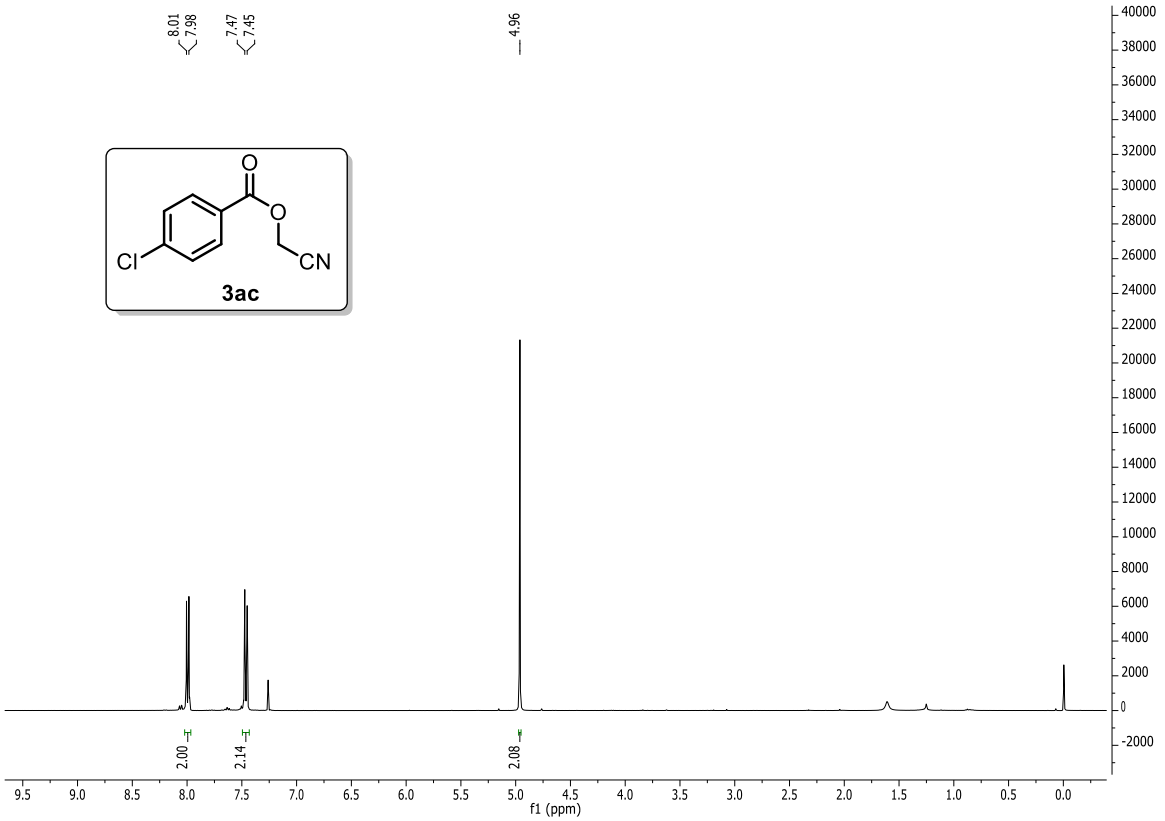


Figure AII.9 ^{1}H NMR (400 MHz, $CDCl_3$) spectrum of compound **3ac**

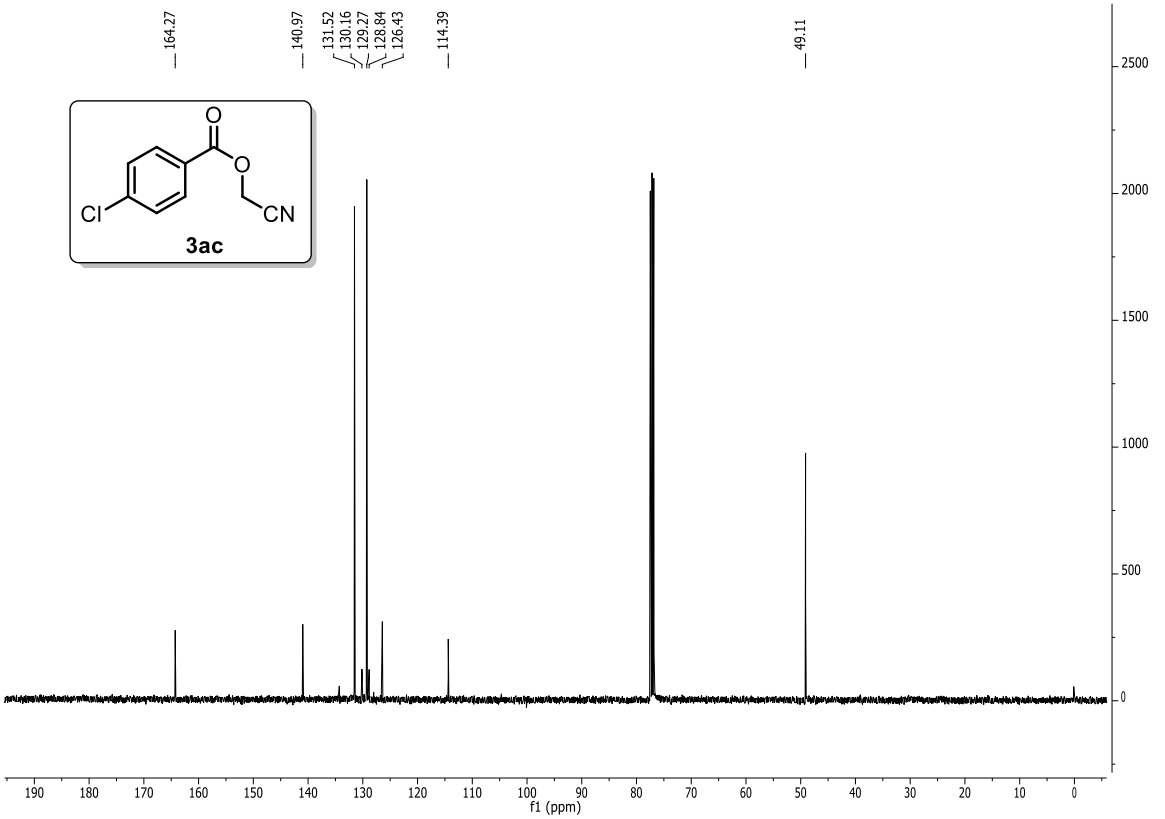


Figure AII.10 ^{13}C NMR (100 MHz, $CDCl_3$) spectrum of compound **3ac**

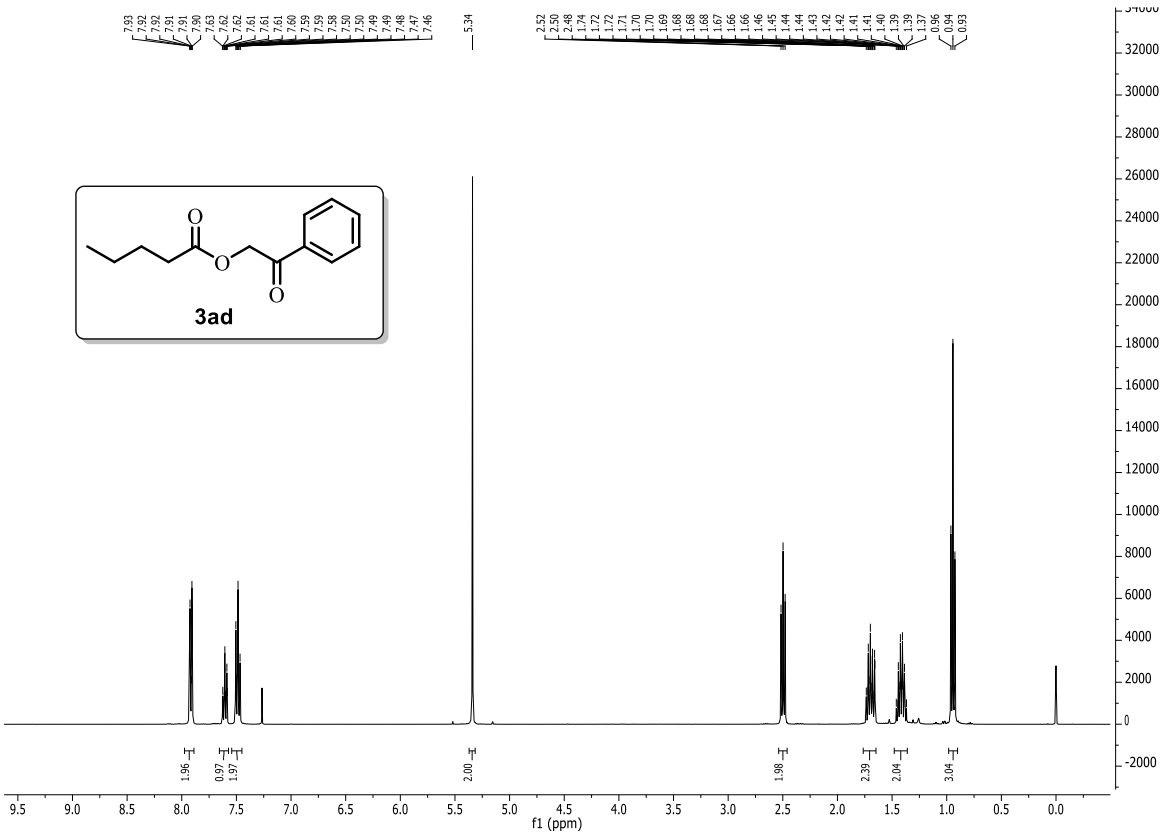


Figure AII.11 ^{1}H NMR (400 MHz, $CDCl_3$) spectrum of compound **3ad**

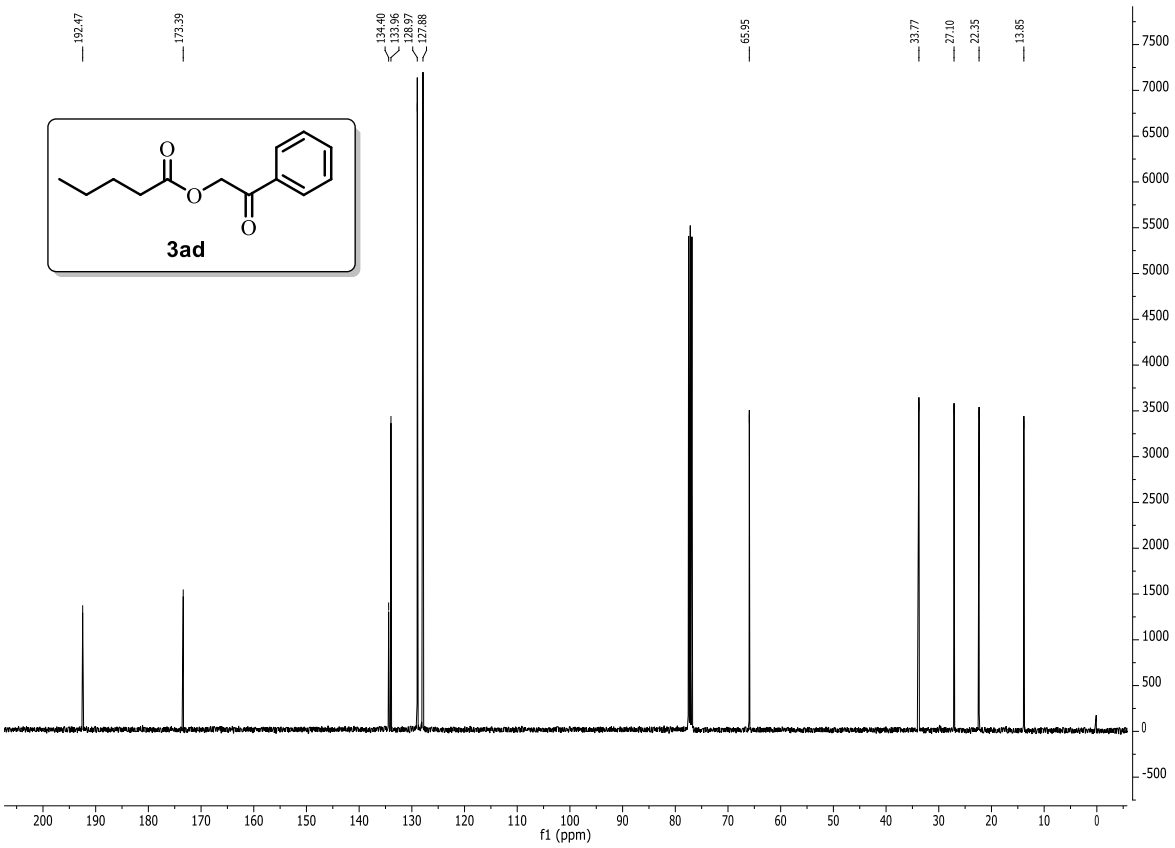


Figure AII.12 ^{13}C NMR (100 MHz, $CDCl_3$) spectrum of compound **3ad**

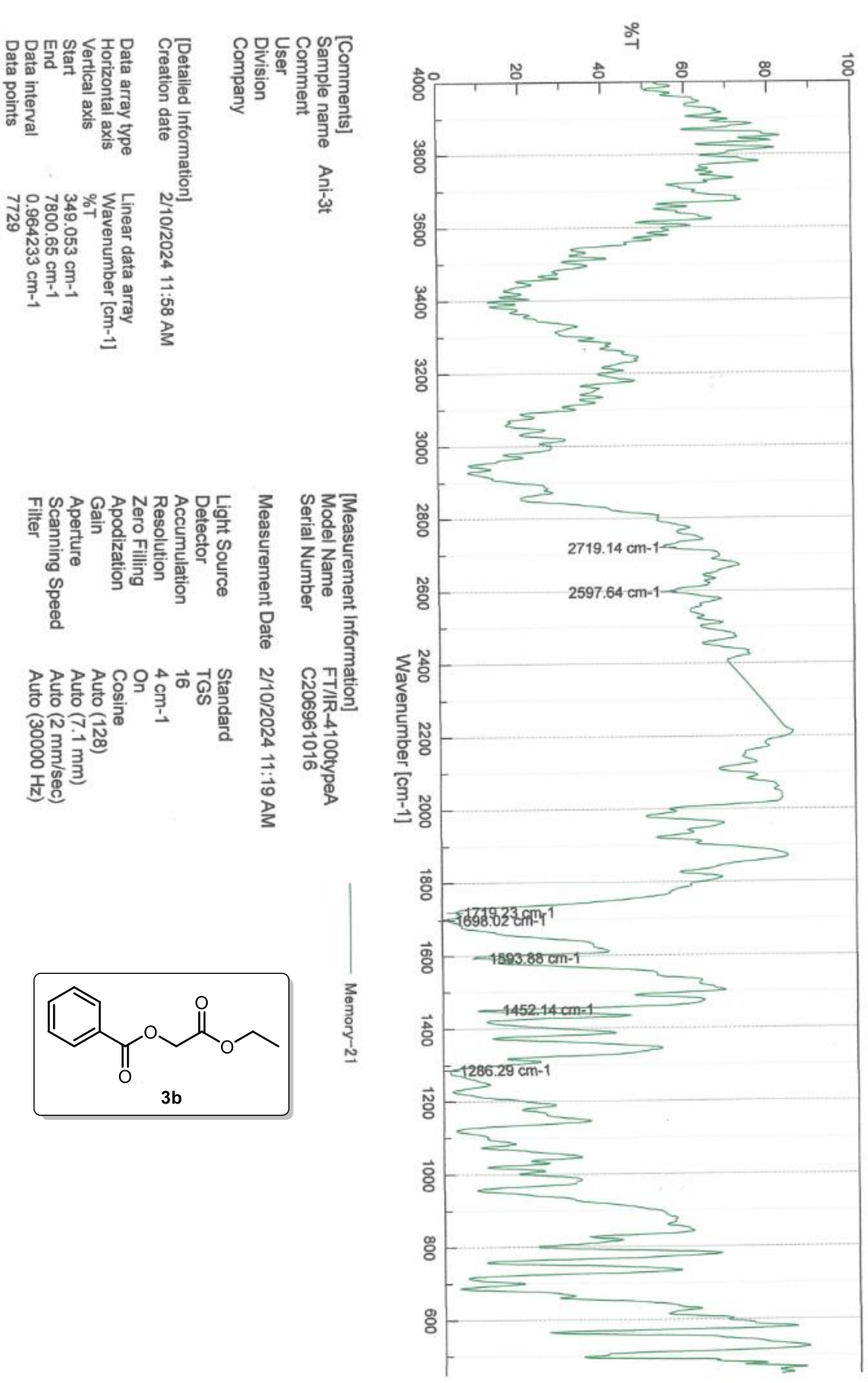


Figure AII.13 FT-IR spectrum of compound **3b**

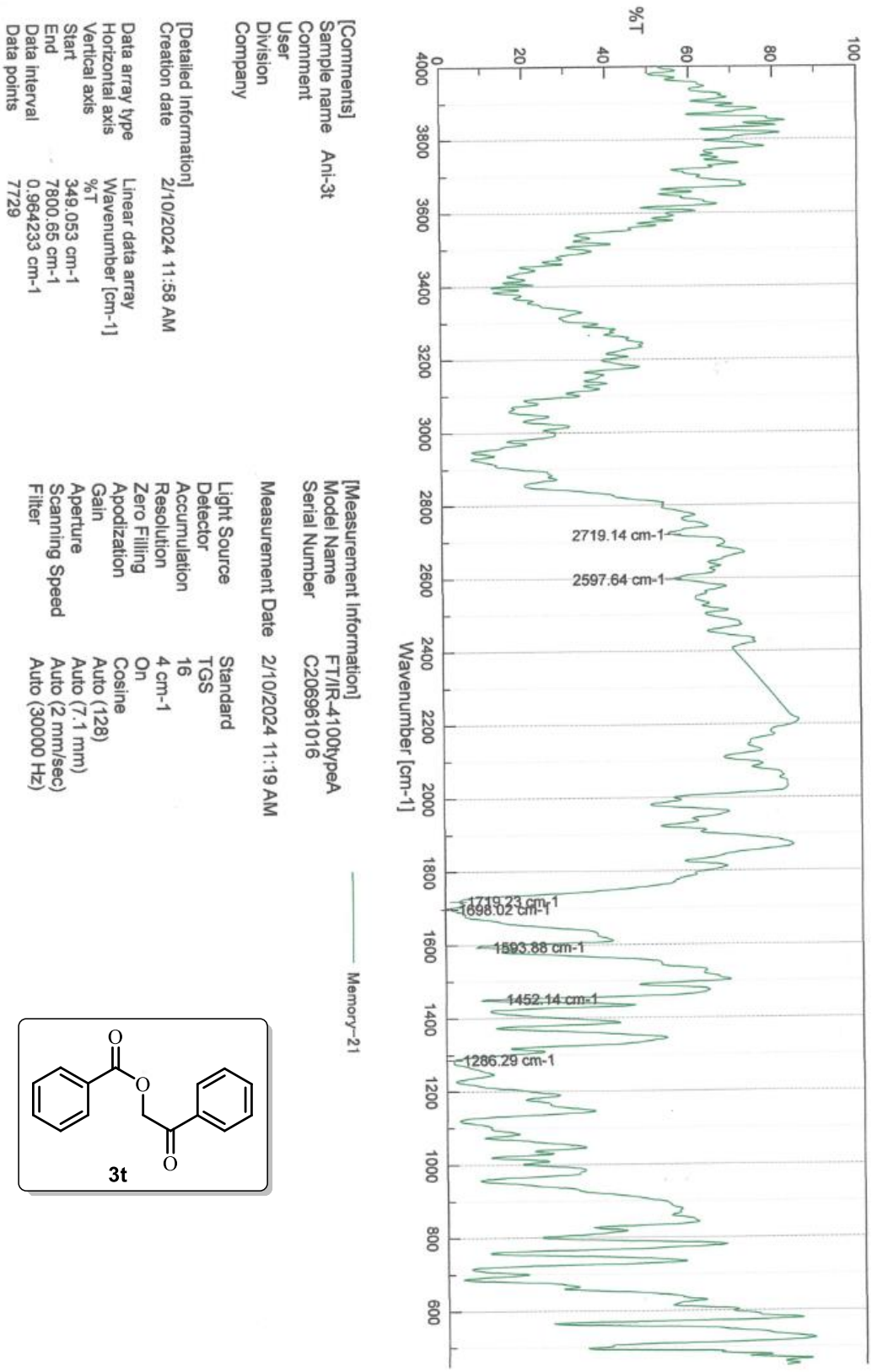


Figure AII.14 FT-IR spectrum of compound **3t**

2.9. References:

1. (a) Murahashi, S.; Saito, T.; Hanaoka, H.; Murakami, Y.; Naota, T.; Kumobayashi H.; Akutagawa, S. *J. Org. Chem*., **1993**, *58*, 2929-2930. (b) Gao, J. M.; Yang S. X.; Qin, J. C. *Chem. Rev*., **2013**, *113*, 4755−4811. (c) Sun, C.; Hunt, D. K.; Chen, C. L.; Deng, Y.; He, M.; Clark, R. B.; Fyfe, C.; Grossman, T. H.; Sutcliffe J. A.; Xiao, X. Y. *J. Med. Chem*., **2015**, *58*, 4703−4712. (d) Vida, J. A.; Samour, C. M.; O'Dea M. H.; Wang, T. S. T. *J. Med. Chem*., **1974**, *17*, 1194−1197. (e) Vida, J. A.; Samour, C. M.; O'Dea, M. H.; Wang, T. S. T.; Wilber W. R.; Reinhard, J. F. *J. Med. Chem*.,**1974**, *17*, 732−736.
2. (a) Che, Y.; Gloer, J. B.; Koster, B.; Malloch, D. *J. Nat. Prod*., **2002**, *65*, 916−919. (b) Wang, X.; Sena Filho, J. G.; Hoover, A. R.; King, J. B.; Ellis, T. K.; Powell, D. R.; Cichewicz, R. H. *J. Nat. Prod*. **2010**, *73*, 942−948. (c) Wang, P.; Kim, W.; Pickens, L. B.; Gao, X.; Tang, Y. *Angew. Chem., Int. Ed*., **2012**, *51*, 11136− 11140. (d) Wang, Z.; Sheng, Y.; Duan, H.; Yu, Q.; Shi, W.; Zhang, S. *RSC Adv*., **2014**, *4*, 53788−53794.
3. (a) Fukuda, T.; Matsumoto, A.; Takahashi, Y.; Tomoda, H.; Omura, S. *J. Antibiot*. **2005**, *58*, 252-259. (b) Lin, L.; Mul-holland, N.; Wu, Q.-Y.; Beattie, D.; Huang, S.-W.; Irwin, D.; Clough, J.; Gu, Y.-C.; Yang, G.-F. *J. Agric. Food Chem.*, **2012**, *60*, 4480−4491. (c) Yamazaki, H.; Omura, S.; Tomoda, H. *Chem. Pharm. Bull*., **2010**, *58*, 829−832.
4. (a) Wang, H.; Wang, Y.; Wang, W.; Fu, P.; Liu, P.; Zhu, W. *J. Nat. Prod*. **2011**, *74*, 2014−2018. (b) Sun, X.-L.; Hiroaki, T.; Keiichi, M.; Haruo, T.; Kimio, F.; Satoshi, O. *J. Antibiot*., **1996**, *49*, 689−692.
5. Yasuda, M.; Okamoto, K.; Sako, T.; Baba, A. *Chem. Commun*., **2001**, *2*, 157-158.
6. (a) Liu, L.; Feng, S.; Li, C. *ACS Sustain. Chem. Eng*., **2016**, *4*, 6754-6762. (b) Carneiro, P. F.; Gutmann, B.; de Souza, R. O. M. A.; Kappe, C. O. *ACS Sustain. Chem. Eng*., **2015**, *3*, 3445-3453.
7. (a) Cignarella, G.; Barlocco, D.; Pocar, D.; Clerici, F.; Curzu, M. M.; Gessa, G. L.; Fadda, F.; Serra, M.; Biggio, G. *Eur. J. Med. Chem*., **1995**, *30*, 721−726. (b) Prasad, P. K.; Reddi R. N.; Arumugam, S. *Org. Biomol. Chem*., **2018**, *16*, 9334-9348.
8. (a) Chen, J.; Liu, D.; Butt, N.; Li, C.; Fan, D.; Liu, Y.; Zhang, W. *Angew. Chem. Int. Ed*., **2013**, *52*, 11632 –11636. (b) Vigante, B.; Rucins, M.; Plotniece, A.; Pajuste, K.; Luntena, I.; Cekavicus, B.; Bisenieks, E.; Smits, R.; Duburs, G.; Sobolev, A. *Molecules*, **2015**, *20*, 20341–20354.
9. (a) Dumitrescu, L.; Azzouzi-Zriba, K.; Bonnet-Delpon, D.; Crousse, B. *Org. Lett*., **2011**, *13*, 692-695. (b) Wang, Y.; Cui, H.; Zhang, L.; Su, C.-Y. *ChemCatChem*, **2018**, *17*, 3901-3906.

10. Tan, L.; Chen, C.; Liu, W. *Beilstein J. Org. Chem*., **2017**, *13*, 1079–1084.
11. (a) Reddi, R. N.; Prasad, P. K.; Arumugam, S. *Org. Lett*., **2014**, *16*, 5674-5677. (b) Dohi, T.; Maruyama, A.; Yoshimura, M.; Morimoto, K.; Tohma, H.; Kita, Y. *Angew. Chem., Int. Ed*., **2005**, *44*, 6193-6196. (d) Ochiai, M.; Miyamoto, K. *Eur. J. Org. Chem*., **2008**, 4229-4239. (e) Huang, J.; Li, L.-T.; Li, H.-Y.; Husan, E.; Wang, P.; Wang, B. *Chem. Commun*., **2012**, *48*, 10204−10206. (f) Uyanik, M.; Suzuki, D.; Yasui, T.; Ishihara, K. *Angew. Chem., Int. Ed*., **2011**, *50*, 5331−5334. (g) Guo, S.; Yu, J. T.; Dai, Q.; Yang, H.; Cheng, J. *Chem. Commun*. **2014**, *50*, 6240-6242.
12. (a) Ekoue-Kovi, K.; Wolf, C. *Chem.-Eur. J*., **2008**, *21*, 6302-6315. (b) Feng, J. B.; Gong, J. L.; Wu, X. F. *Tetrahedron Lett*., **2014**, *9*, 1657-1659. (c) Green, R. A.; Pletcher, D.; Leach, S. G.; Brown, R. C. D. *Org. Lett*., **2015**, *17*, 3290-3293. (d) Gaspa, S.; Porcheddu, A.; De Luca, L. *Tetrahedron Lett*., **2016**, *31*, 3433-3440. (e) Jeong, D. J.; Lee, S. B.; Lee, J. C. *Lett. Org. Chem*., **2017**, *10*, 725-728. (f) Finney, E. E.; Ogawa, K. A.; Boydston, A. J. *J. Am. Chem. Soc*., **2012**, *134*, 12374-12377. (g) Marki, B. E.; Scheidt, K. A. *Org. Lett*., **2008**, *10*, 4331-4334. (h) Talukdar, D.; Sharma, K.; Bharadwaj, S. K.; Thakur, A. J. *Synlett*, **2013**, *24*, 963-966. (i) Mori N.; Togo, H. *Tetrahedron*, **2005**, *61*, 5915-5925. (j) Travis, B. R.; Sivakumar, M.; Hollist, G. O.; Borhan, B. *Org. Lett*., **2003**, *5*, 1031-1034. (k) Gaspa, S.; Porcheddu, A.; De Luca, L. *Org. Lett*., **2015**, *17*, 3666-3669. (l) Zhu, Y.; Yan, H.; Lu, L.; Liu, D.; Rong G.; Mao, J. *J. Org. Chem*. **2013**, *78*, 9898-9905. (m) De Sarkar, S.; Grimme, S.; Studer, A. *J. Am. Chem. Soc*., **2010**, *132*, 1190-1191. (n) Rout, S. K.; Guin, S.; Ghara, K. K.; Banerjee, A.; Patel, B. K. *Org. Lett*., **2012**, *14*, 3982-3985. (o) Lerebours, R.; Wolf, C. *J. Am. Chem. Soc*., **2006**, *128*, 13052-13053.
13. Reddi, R. N.; Malekar, P. V.; Arumugam, S. *Org. Biomol. Chem*., **2013**, *11*, 6477-6482.
14. (a) Liu Q.; Wu, L.-Z. *Nat. Sci. Rev*., **2017**, *4*, 359−380; (b) Marzo, L.; Pagire, S. K.; Reiser O.; König, B. *Angew. Chem., Int. Ed*., **2018**, *57*, 10034−10072; (c) Stephenson, C. R. J.; Yoon T. P.; MacMillan, D. W. C. Wiley-VCH, Weinheim, **2017**; (d) König, B. *Eur. J. Org. Chem*., **2017**, *15*, 1979−1981; (e) Tavakolian M.; Hosseini-Sarvari, M. *ACS Sustain. Chem. Eng*. **2021**, *9*, 4296−4323; (f) Gan, Z.; Li, G.; Yang, X.; Yan, Q.; Xu, G.; Li, G.; Jiang, Y.-Y.; Yang, D. *Sci. China: Chem*., **2020**, *63*, 1652–1658; (g) Cheng W.-M.; Shang, R. *ACS Catal*., **2020**, *10*, 9170–9196; (h) Xie, L.-Y.; Bai, Y.-S.; Xu, X.-Q.; Peng, X.; Tang, H.-S.; Huang, Y.; Lin, Y.-W.; Cao, Z.; He, W.-M. *Green Chem*., **2020**, *22*, 1720–1725.
15. Zhang, Y. L.; Xiao, Q.; Bao, Y. S.; Zhang, Y. J.; Bottle, S.; Sarina, S.; Zhaorigetu, B.; Zhu, H. Y. *J. Phys. Chem. C*, **2014**, *118*, 19062−19069.

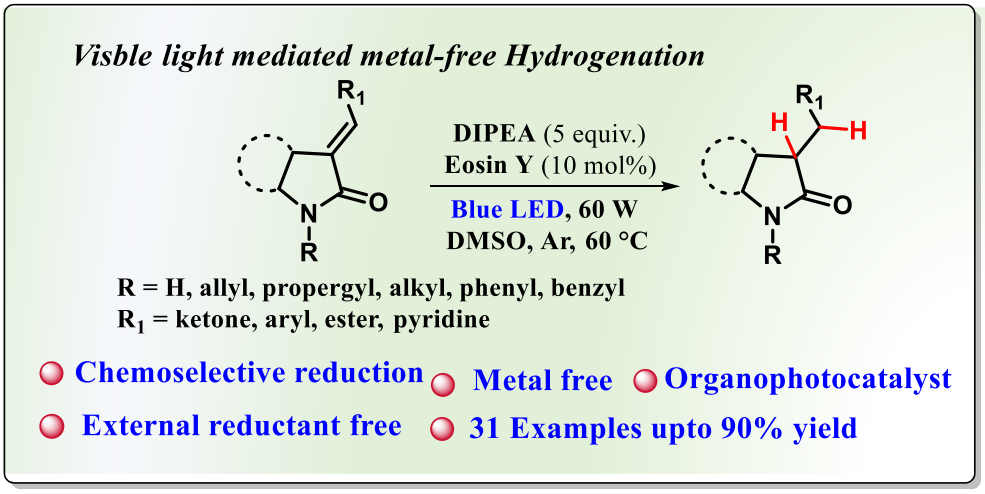
16. Kumar, A.; Kumar, P.; Pathak, A. K.; Chokkapu, A. N.; Jain, S. L. *ChemistrySelect* **2017**, *2*, 3437-3443.
17. Pandey, G.; Koley, S.; Talukdar, R.; Sahani, P. K. *Org. Lett*., **2018**, *20*, 5861−5865.
18. Gaspa, S.; Raposo, I.; Pereira, L.; Mulas, G.; Ricci, P. C.; Porcheddu A.; De Luca, L. *New J. Chem*., **2019**, *43*, 10711− 10715.
19. Pelzer, K. M.; Cheng L.; Curtiss, L. A. *J. Phys. Chem*. *C*, **2017**, *121*, 237−245.
20. (a) Romero N. A.; Nicewicz, D. A. *Chem. Rev*. **2016**, *116*, 10075−10166. And references cited therein. (b) Alfonzo, E.; Alfonso F. S.; Beeler, A. B. *Org. Lett*., **2017**, *19*, 2989−2992.
21. Adkins, H.; Elofson, R. M.; Rossow A. G.; Robinson, C. C. *J. Am. Chem. Soc*., **1949**, *71*, 3622-3629.
22. Roth, H. G.; Romero N. A.; Nicewicz, D. A. *Synlett* **2016**, *27*, 714-723.
23. For radical-radical coupling reactions under visible light (a) Santos, M. S.; Corrêa, A. G.; Paixão M. W.; König, B. *Adv. Synth. Catal*. **2020**, *362*, 2367-2372. (b) Berger, A. L.; Donabauer K.; Konig, B. *Chem. Sci*., **2018**, *9*, 7230. (c) Jeffrey, J. L.; Petronijevic F. R.; MacMillan, D. W. J. *Am. Chem. Soc*., **2015**, *137*, 8404–8407. (d) Cuthbertson J. D.; MacMillan, D. W. *Nature* **2015**, *519*, 74–77.
24. Ju, L.; Ma, C.; Tang, M.; Wang, Y.; Yu, X.; Ma, H. *Chin. J. Org. Chem*. **2018**, *38*, 3056–3062.
25. Zeng, L.; Sajiki, H.; Cui, S. *Org. Lett*. **2019**, *21*, 6423−6426.
26. Xiaoqing, L.; Can, Z.; Xiangsheng, X. *Arch. Org. Chem*. **2012**, 150−158.
27. Forte, G.; Chiarotto, I.; Inesi, A.; M. A. Loreto, M. A.; Feroci, M. *Adv. Synth.Catal*. **2014**, *356*, 1773–1781.
28. Li, C.; Jin, T.; Zhang,X.; Li, C.;Jia,X.; Li, J. *Org. Lett*. **2016**, *18*, 1916−1919.
29. Y. Hu, J. Chen, Z. G. Le, Z. C. Chen, Q. G. Zheng, Chin. Chem. Lett. **2005**, *16*, 903.
30. Chen, J.; Zhang,Z.; Liu, D.; Zhang,W. *Angew. Chem., Int. Ed*. **2016**, *55*, 844.
31. Duanmu, D.; Leong, P. K.; Jiang, Q. B., Yan, H. *Chin. J. Org. Chem.* **2017**, *37*, 2669–2677.
32. Ad, O.; Hoffman,K. S.; Cairns,A. G.; Featherston,A. L.; Miller,S. J.; Söll, D.; Schepartz,A. *ACS Cent.Sci*. **2019**, *5*, 1289−1294.

CHAPTER 3

Visible Light Promoted Metal-Free Sustainable Reduction of α-Alkylidene Oxindoles/Succinimides

Abstract

The chemoselective, metal-free hydrogenation of activated double bonds under visible light via photoredox catalysis has been successfully achieved. Eosin Y has demonstrated high efficiency as a catalyst for the reduction of C-C double bonds in alkylidene oxindoles and succinimides when exposed to visible light. In this process, the commercially available DIPEA serves as a sacrificial electron donor, and its in-situ generated cationic radical acts as the reductant for the transformation. Systematic and detailed mechanistic studies have unveiled the oxidative quenching of the photocatalyst by the activated double bond.



Bhowmick, A.; Warghude, P. K.; Bhat, R. G. *Asian J. Org. Chem*. **2022**, *11*, e20220020.

Visible Light Promoted Metal-Free Sustainable Reduction of α-Alkylidene Oxindoles/Succinimides

3.1. Introduction:

Hydrogenation of unsaturated organic compounds remains a pivotal and highly significant process in the realm of organic synthesis to this day [1]. Hydrogenation holds immense importance within the synthetic chemistry community and has found extensive use across various sectors, including chemical, biochemical, food, agrochemical, polymer, and pharmaceutical industries, due to its versatility and wide-ranging applications [2]. Selective reduction plays a significant role in numerous biosynthetic pathways. In the process of synthesizing fatty acids, the specific reduction of activated carbon-carbon double bonds is accomplished through enolate reductases, which are abundantly present in natural microorganisms [3]. In the domain of organic synthesis, conventional hydrogenation reactions typically involve the use of hydrogen gas along with either catalytic quantities of transition metals or stoichiometric amounts of metal hydrides [4]. In this context, sustainable transition metal-free reduction methods have been found, which are considered safer when compared to processes utilizing transition metals and highly reactive hydrogen gas. Hantzsch esters [5] and silanes [6] have both served as effective reactive organic reducing agents in the context of carbon-carbon double bond hydrogenation. Additionally, hydrogenation processes have been successfully accomplished through the utilization of frustrated Lewis pairs (FLPs) [7]. Chemoselective hydrogenation of unsaturated carbonyl compounds has been accomplished using alkyl phosphines and N-heterocyclic carbenes in certain cases [8]. Nevertheless, many hydrogenation methods depend on either transition metals along with hydrogen or costly, pyrophoric, and toxic metal-based reducing agents in stoichiometric quantities. Absolutely, the scientific pursuit of developing efficient and metal-free protocols for reducing C-C double bonds is a complex and rigorous endeavour.

In recent years, visible light photoredox catalysis has seen significant and rapid advancements, emerging as a promising field in organic synthesis. It offers a safer and more efficient alternative strategy for certain transformations that are challenging to achieve through traditional methods. Significantly, visible light-mediated transformations are often characterized by their non-toxic nature, environmental friendliness, and ease of handling, resulting in reduced waste generation [9]. In recent times, only a limited number of examples have emerged in which visible light-mediated cascade cross-coupling hydrogenation reactions

were conducted without the need for sacrificial oxidants. However, these transfer hydrogenation and semihydrogenation methods depend entirely on metal complexes to generate hydrogen in situ under visible light conditions [10]. In 1980s, the Sakurai research group pioneered visible light-mediated reduction procedures for alkenes using 1-benzyl-1,4-dihydronicotinamide in the presence of a ruthenium (Ru) catalyst [11].

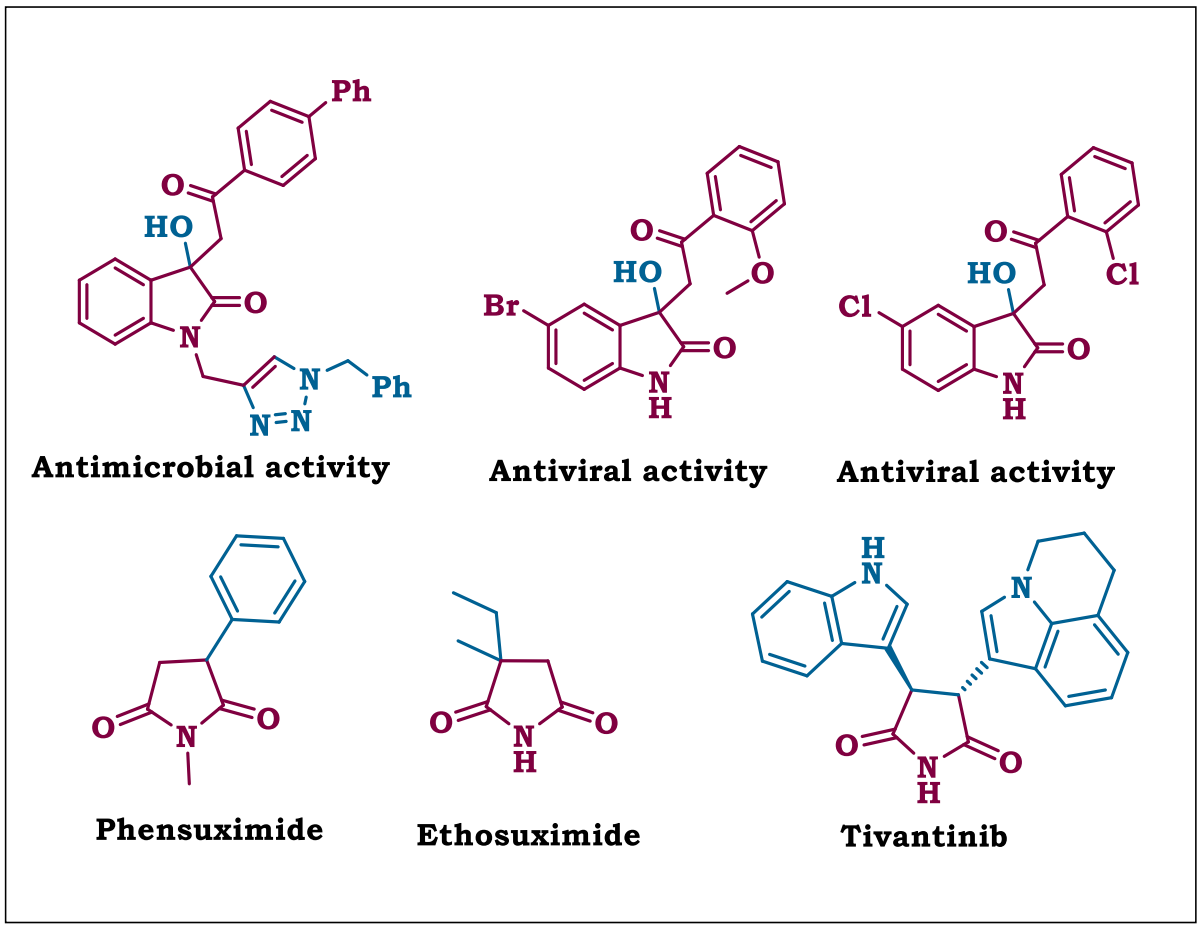


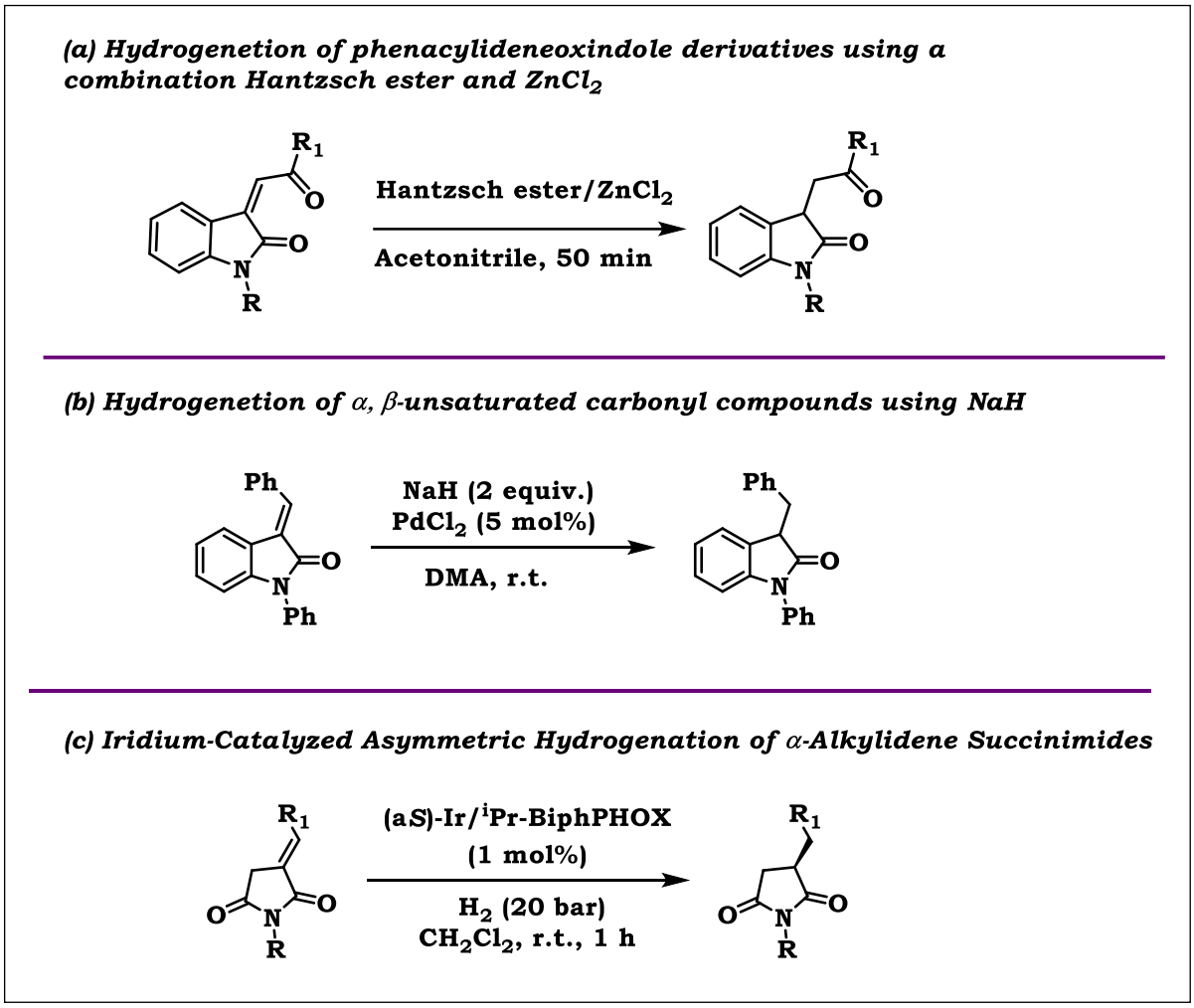
Figure 1: Synthetically and bioactive compounds containing oxindole and succinimide scaffolds

Despite these notable advancements, the need for a metal-free hydrogenation process under visible light irradiation remains highly desirable and necessary. Facilitating the selective hydrogenation of electron-deficient carbon-carbon double bonds within a molecule is a highly demanding and complex task. Within the category of molecules containing electron-deficient carbon-carbon double bonds, α-alkylidene oxindoles and unsaturated compounds based on succinimide are notably versatile and find extensive application in organic synthesis as they serve as precursors for numerous natural products and bioactive molecules (**Figure 1**) [12]. In this context, several research groups have undertaken efforts to selectively reduce electron-deficient or activated carbon-carbon double bonds.

3.2. Previous methods for the hydrogenation of different electron deficient alkene:

In 2019, Kasi Viswanath and co-workers have successfully and selectively reduced the exocyclic carbon carbon double bond present in phenacylideneoxindole **1** derivatives under mild reaction condition with high yields using a combination of inexpensive and ecofriendly Hantzsch ester and zinc chloride in acetonitrile at room temperature (**Scheme 1a**) [13].

Scheme 1: Previously reported hydrogenation of electron deficient alkenes



In the same year, Zhang and co-workers introduced a palladium-catalyzed hydrogenation method for *α, β*-unsaturated compounds, employing sodium hydride as a Michael donor, as illustrated in **Scheme 1b** [14]. Their discovery revealed that sodium hydride could function as a Michael donor in the 1, 4-conjugate reduction of various *α, β*-unsaturated carbonyl compounds, facilitated by palladium catalysis. This approach could be seamlessly integrated with processes such as alkylation, Michael addition, oxidation, or Dieckmann condensation in a one-pot cascade manner, allowing for the efficient synthesis of more complex compounds.

This procedure is characterized by its ease of use, gentle reaction conditions, high atom efficiency, and chemical specificity. It also boasts a broad range of applicable substrates, making it an appealing and robust choice for the hydrogenation of polarized alkenes in the realm of synthetic chemistry.

In 2013, Zhang and team reported an asymmetric hydrogenation process of α-alkylidene succinimide derivatives catalyzed by iridium, conducted under extremely high pressure (H_2, 20 bar), as depicted in **Scheme 1c** [15]. The described method outlines an effective asymmetric hydrogenation process for α-alkylidene succinimides, employing an IrI/iPr-BiphPHOX complex, resulting in the formation of hydrogenated products with excellent yields (>99%) and enantioselectivities (up to 99% *ee*).

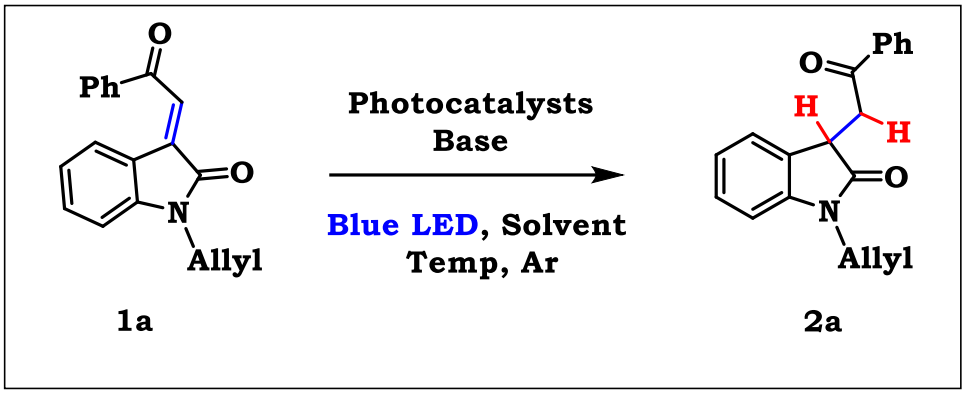
Nonetheless, all these approaches hinged upon the employment of metal catalysts, strong bases, or high-pressure hydrogen gas. The practicality of these methods is constrained by the rigorous reaction conditions and associated hazards. It would be highly intriguing to explore the reduction of activated C-C double bonds in alkylidene oxindoles/succinimides under entirely metal-free conditions. Additionally, it's worth noting that some of these scaffolds, which feature activated double bonds, are commonly utilized as intermediates in numerous transformations. Furthermore, they are readily synthesized and find widespread utility in various synthetic applications.

3.3. Our hypothesis and optimization of hydrogenation of electron deficient alkenes:

In this study, we aim to present a sustainable and metal-free reduction approach for activated C-C double bonds found in α-alkylidene oxindoles and succinimides. This method relies on visible light irradiation, with nitrogen-based amines serving as both a sacrificial electron donor and reducing agent, and a photocatalyst.

We initiated the process by subjecting compound **1a** to a reaction with DIPEA in the presence of a ruthenium catalyst (Ru cat.) in anhydrous acetonitrile. This reaction was carried out under blue LED irradiation (60 W) at 60 °C, employing an inert atmosphere. Encouragingly, we successfully obtained the desired reduction product, **2a**, with a moderate yield of 50% (refer to **Table 1, Entry 1**). Subsequently, we conducted a screening of the reaction involving **1a** with various photocatalysts (*fac*-Ir(PPy_3), Eosin Y, 4CzIPN, Rhodamine 6G, Acridinium) in the

Table 1: Optimization of reaction conditions[a]



Entry	Photocatalyst (mol %)	Base (equiv.)	Temp.	Light	Solvent	Yield (%)[g]
1	$Ru(bpy)_3Cl_2$	DIPEA	60 °C	60 W Blue LED	MeCN	50
2	*fac*-$Ir(PPy_3)$	DIPEA	60 °C	60 W Blue LED	MeCN	54
3	Eosin Y	DIPEA	60 °C	60 W Blue LED	MeCN	64
4	4CzIPN	DIPEA	60 °C	60 W Blue LED	MeCN	32
5	Rhodamine 6G	DIPEA	60 °C	60 W Blue LED	MeCN	NR
6	Acridinium	DIPEA	60 °C	60 W Blue LED	MeCN	NR
7	Eosin Y	DBU	60 °C	60 W Blue LED	MeCN	NR
8	Eosin Y	DABCO	60 °C	60 W Blue LED	MeCN	NR
9	Eosin Y	Et_3N	60 °C	60 W Blue LED	MeCN	46
10	Eosin Y	DIPEA	60 °C	60 W Blue LED	DMF	50
11	Eosin Y	DIPEA	60 °C	60 W Blue LED	THF	18
12	**Eosin Y**	**DIPEA**	**60 °C**	**60 W Blue LED**	**DMSO**	**75**
13	Eosin Y	^tBuOK	60 °C	60 W Blue LED	DMSO	NR
14	Eosin Y	Cs_2CO_3	60 °C	60 W Blue LED	DMSO	NR
15[b]	Eosin Y	DIPEA	60 °C	60 W Blue LED	DMSO	35
16	Eosin Y	DIPEA	r.t.	60 W Blue LED	DMSO	Trace

17	Eosin Y	DIPEA	60 °C	15 W Blue LED	DMSO	18
18	Eosin Y	DIPEA	60 °C	30 W Blue LED	DMSO	36
19	Eosin Y	DIPEA	40 °C	60 W Blue LED	DMSO	28
20	Eosin Y	DIPEA	50 °C	60 W Blue LED	DMSO	42
21	Eosin Y	DIPEA	80 °C	60 W Blue LED	DMSO	50
22	Eosin Y	DIPEA	60 °C	Green LED	DMSO	20
23	Eosin Y	DIPEA (1)	60 °C	60 W Blue LED	DMSO	30
24	Eosin Y	DIPEA (2)	60 °C	60 W Blue LED	DMSO	35
25	Eosin Y	DIPEA (3)	60 °C	60 W Blue LED	DMSO	50
26	Eosin Y	DIPEA (10)	60 °C	60 W Blue LED	DMSO	48
27	Eosin Y (1)	DIPEA	60 °C	60 W Blue LED	DMSO	38
28	Eosin Y (3)	DIPEA	60 °C	60 W Blue LED	DMSO	46
29	Eosin Y (5)	DIPEA	60 °C	60 W Blue LED	DMSO	58
30[c]	-	DIPEA	60 °C	60 W Blue LED	DMSO	NR
31[d]	Eosin Y	-	60 °C	60 W Blue LED	DMSO	NR
32[e]	Eosin Y	DIPEA	60 °C	-	DMSO	NR
33[f]	Eosin Y	DIPEA	60 °C	60 W Blue LED	DMSO	NR

Reaction Condition: *Unless otherwise noted. [a]all the reactions were carried out using 0.350 mmol of* ***1a****, 1.75 mmol of base and 35 μmol (10 mol%) of photocatalyst under blue LED (60 W) irradiation at 60 °C for 24 h. [b]10 equivalent of H_2O was added to the reaction mixture, [c]in absence of photocatalyst, [d]in absence of DIPEA, [e]in absence of light (in dark). [f]The reaction carried out in open air atmosphere [g]Isolated yield after the purification by column chromatography. Acridinium = 9-Mesityl- 10-methylacridinium perchlorate.*

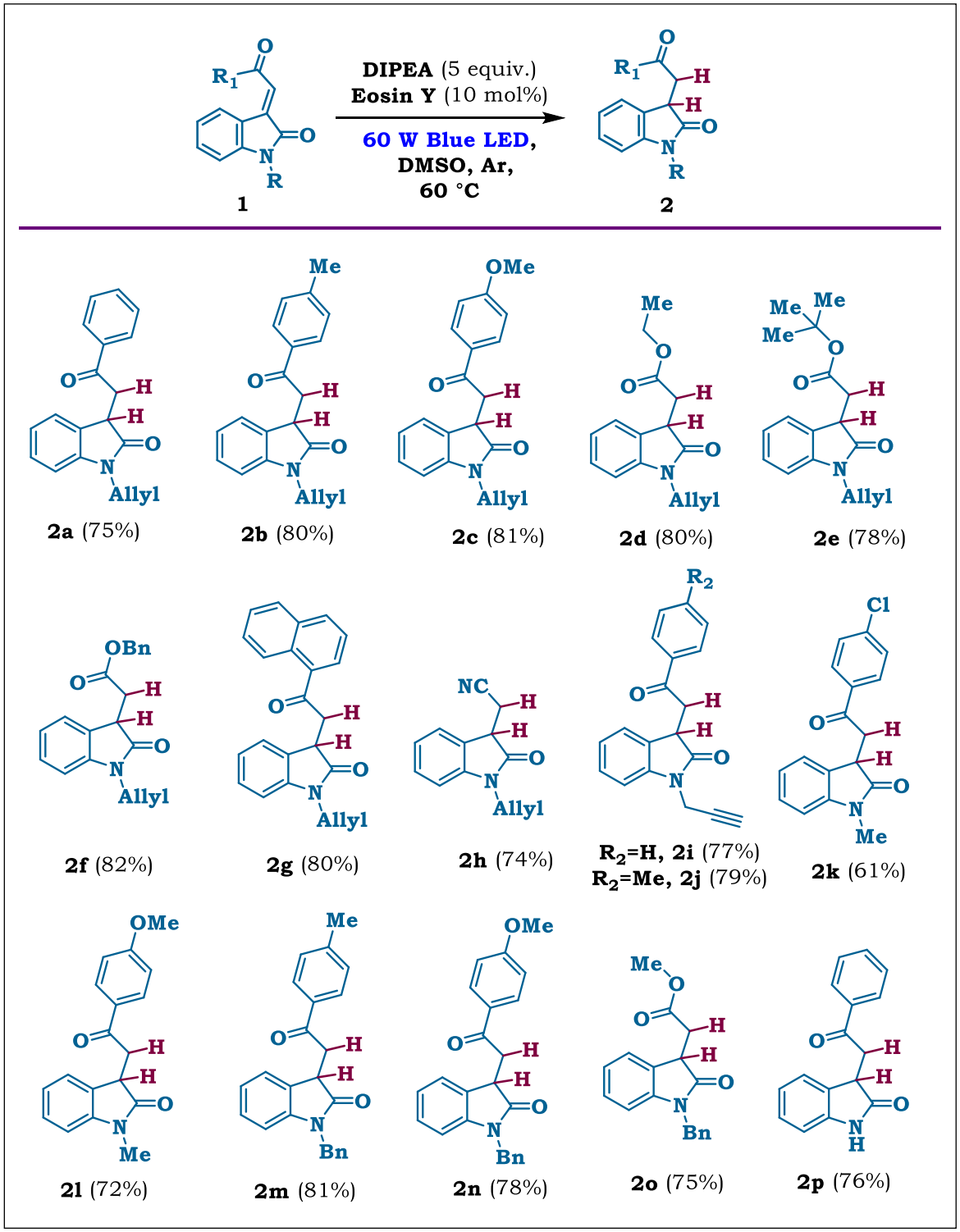
presence of DIPEA, as detailed in **Table 1**, **Entries 2 to 6**. Among the photocatalysts examined, Eosin Y demonstrated the highest efficiency, resulting in the desired reduced product **2a** with a yield of 64% (as indicated in **Table 1**, **Entry 3**). This outcome provided the motivation for us to conduct further optimization of the reaction conditions. To this end, we systematically examined the reaction with various organic and inorganic bases (DIPEA, DBU, DABCO, Et_3N, ^tBuOK,

Cs_2CO_3). Notably, our findings revealed that DIPEA emerged as the most effective base for producing the desired product, **2a** (**Table 1**, **Entries 1, 7-9, 13-14**). With the photocatalyst and base now optimized, we extended our screening efforts to various solvents in order to maximize the yield of the desired product, **2a** (as detailed in **Table 1**, **Entries 10-12**). Encouragingly, the reaction proceeded smoothly in dry DMSO, resulting in the desired reduction product **2a** with a good yield of 75% (as demonstrated in **Table 1**, **Entry 12**). To investigate the potential influence of water, we conducted the reaction involving **1a** with Eosin Y and DIPEA in DMSO, while introducing H_2O (10 equiv.). Notably, the presence of water led to a substantial reduction in the yield of **2a**, as evidenced in **Table 1**, **Entry 15**. Further we have optimised different LEDs of light (**Table 1, Entries 17-18, 22**) as well as we have performed the reaction at different temperatures (**Table 1, Entries 16, 19-21**) and 60 W blue LED at 60 °C temperature is the optimised condition (**Table 1, Entry 12**). We have varied the amount of DIPEA as well as Eosin Y (**Table 1, Entries 23-29**). Furthermore, we established that the presence of a photocatalyst, base, and light are all indispensable for the desired transformation to yield the desired product, **2a**. Notably, when any one of these three parameters was omitted individually, the reaction failed to proceed (**Table 1, Entries 30-33**). After an extensive screening process, it was ascertained that the most favorable conditions for achieving a higher yield of the desired product, **2a**, included the use of compound **1a** along with Eosin Y (10 mol%), DIPEA (5 equiv.) in dry DMSO, all under blue light irradiation (60 W) at 60 °C (**Table 1, Entry 12**).

3.4. Results and Discussion:

With the optimized reaction conditions in place, we embarked on a systematic exploration of the substrate scope for this visible light-mediated hydrogenation of electron-deficient alkenes. Initially, we synthesized a range of alkene derivatives, including isatin-based (**1a-1p**), oxindole-based (**1q-1v**), and maleimide-based (**1w-1ae**) compounds following literature procedure [16]. This was done to assess their reactivity and to explore the extensive substrate scope of the protocol. It was observed that all the substrates (**1a-1p**) underwent smooth reactions under the optimized conditions, resulting in the formation of the corresponding reduced products (**2a-2p**) with moderate to good yields (**Scheme 2a**).

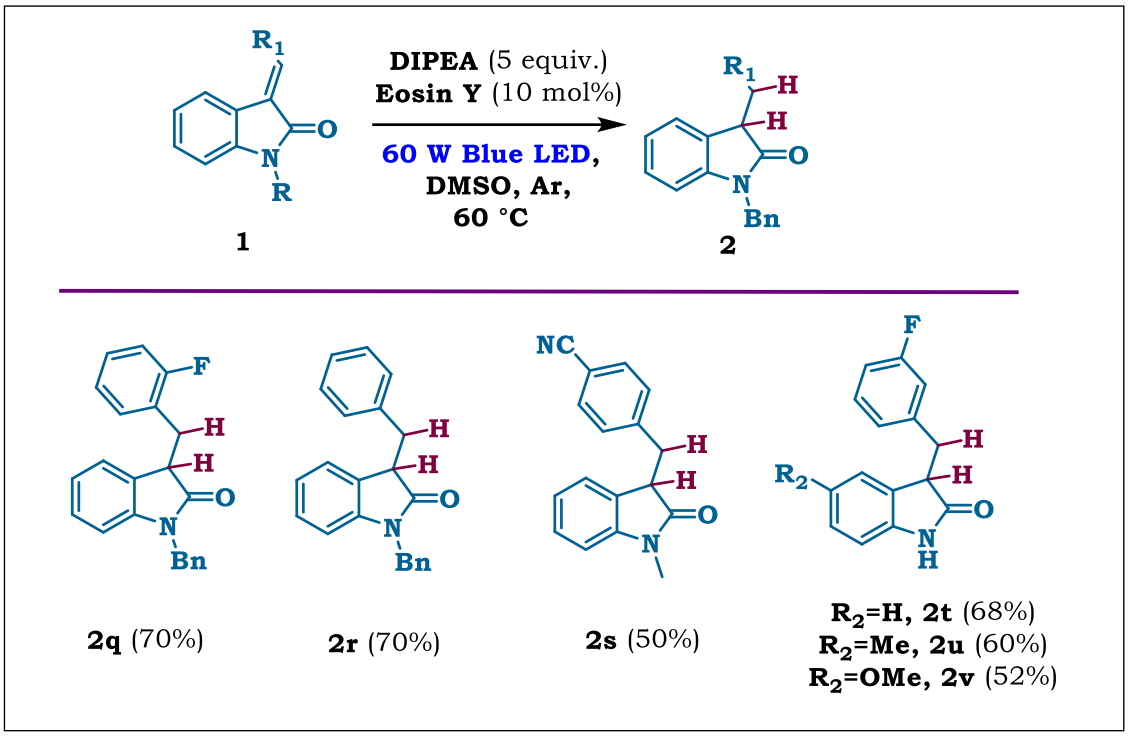
Scheme 2a: Substrate scopes for hydrogenation of isatin based alkene derivatives[a]



***Reaction Condition**: Unless otherwise noted. [a]all the reactions were carried out using 0.350 mmol of **1**, 1.75 mmol of base and 35 µmol (10 mol%) of photocatalyst under blue LED (60 W) irradiation at 60 °C for 24 h.*

Notably, it is worth emphasizing that all the substrates bearing N-allyl and N-propargyl protecting groups readily underwent reactions to yield the corresponding reduced products (**2a-2j**) with very good yields, reaching up to 82%. In the course of these reactions, we noted the selective reduction of electron-deficient alkenes, with the *N*-allyl or *N*-propargyl groups remaining unaffected. Additionally, *N*-methyl- and *N*-benzyl-protected isatin derivatives also exhibited efficient reactivity, yielding the desired reduced products (**2k-2o**) with moderate to good yields, with the highest yield reaching up to 81% (as depicted in **Scheme 2a**). It's notably remarkable that the substrate with an unprotected nitrogen atom underwent the reaction smoothly under the optimized conditions, yielding the corresponding reduced product **2p** in a good yield, and no side products were observed (as illustrated in **Scheme 2a**).

Scheme 2b: Substrate scopes for hydrogenation of oxiindole based alkene derivatives[a]

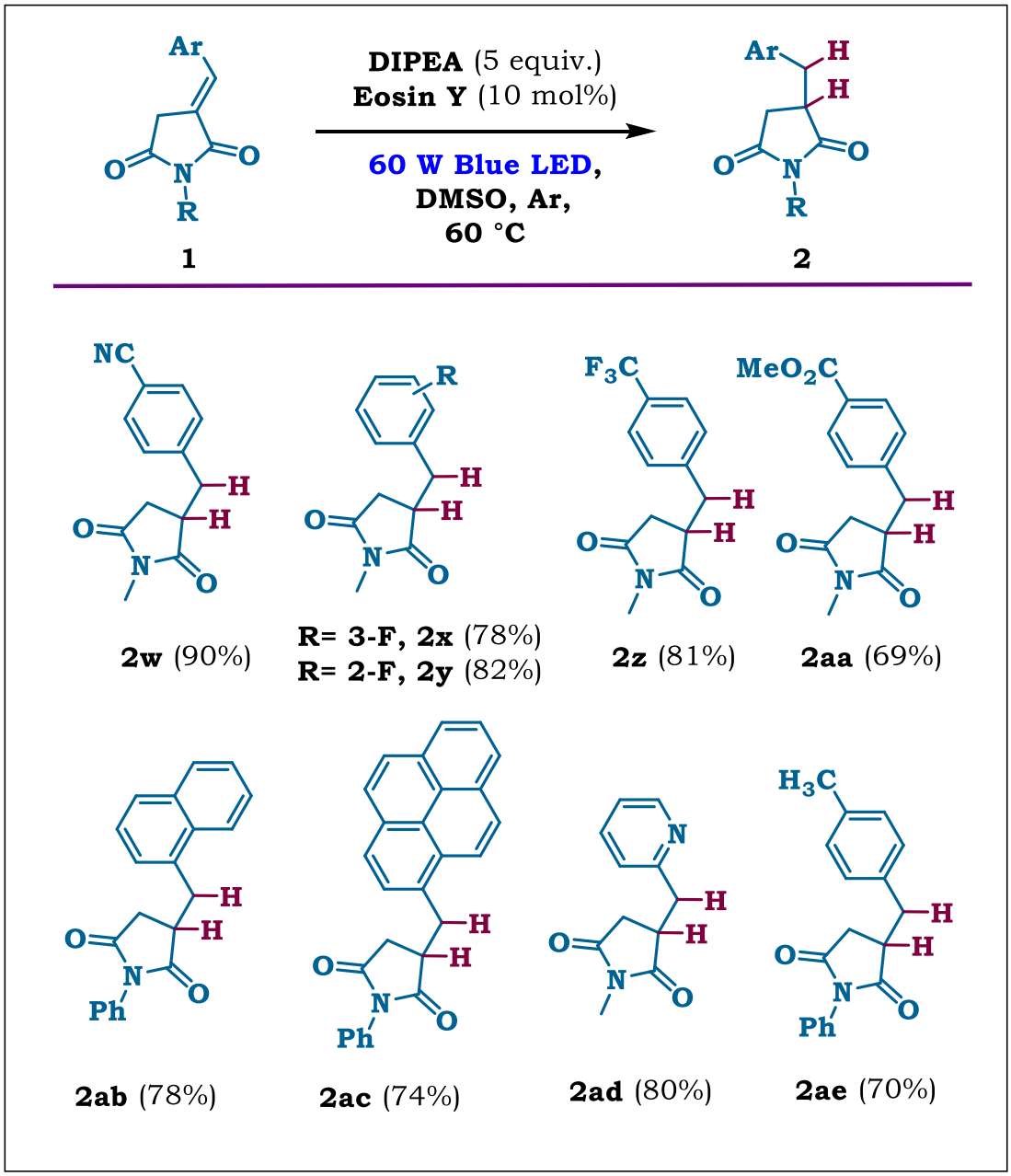


***Reaction Condition**: Unless otherwise noted. [a]all the reactions were carried out using 0.350 mmol of **1**, 1.75 mmol of base and 35 µmol (10 mol%) of photocatalyst under blue LED (60 W) irradiation at 60 °C for 24* h.

Subsequently, our focus shifted towards investigating the versatility of the protocol for reducing a range of alkylidene 2-oxindoles, encompassing various protecting groups and electron-withdrawing substituents. It was observed that 2-oxindole-based alkenes (**1q-1v**)

readily provided the corresponding reduced products (**2q-2v**) with moderate to good yields, achieving up to 70% yield (as depicted in **Scheme 2b**).

Scheme 2c: Reduction of Maleimide derived alkene (α-alkylidene succinimides) derivatives[a]

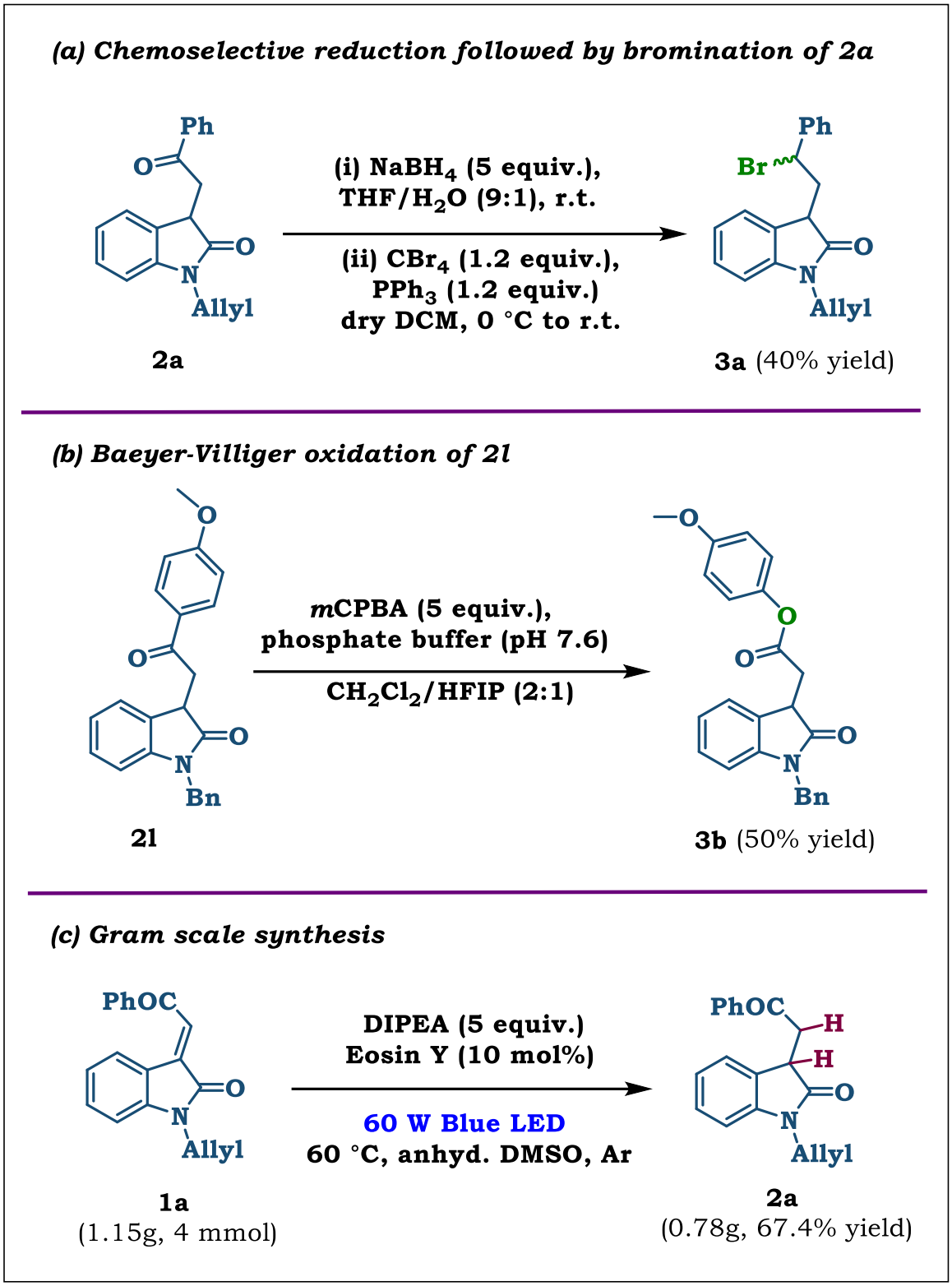


***Reaction Condition**: Unless otherwise noted. [a]all the reactions were carried out using 0.350 mmol of **1**, 1.75 mmol of base and 35 μmol (10 mol%) of photocatalyst under blue LED (60 W) irradiation at 60 °C for 24 h*

Following our initial success, we decided to extend the application of this photocatalyzed hydrogenation protocol to the reduction of α-alkylidene succinimides, which are derived from

maleimides. We found that various α-alkylidene succinimides (**1w–1ae**) exhibited excellent reactivity under the optimized reaction conditions, yielding the corresponding reduction products (**2w-2ae**) in moderate to very good yields (as illustrated in **Scheme 2c**).

Scheme 3: Further synthetic transformation and gram scale synthesis



Crucially, it is worth highlighting that the α-alkylidene succinimide derivatives, even those with electron-withdrawing groups (CN, F, CF_3, CO_2Me), fused aromatic rings, and heterocyclic moieties, exhibited excellent compatibility with the optimized reaction conditions. This resulted in the formation of the corresponding desired reduction products (**2w-2aa**, **2ab-2ac**, and **2ad**) in moderate to good yields, with the highest yield reaching up to 90% (as outlined in **Scheme 2c**). Furthermore, it's noteworthy that the α-alkylidene succinimide derivative with an electron-donating group was also well-tolerated under the standard reaction conditions, resulting in the desired reduction product **2ae** with a yield of 70% (as indicated in **Scheme 2c**).

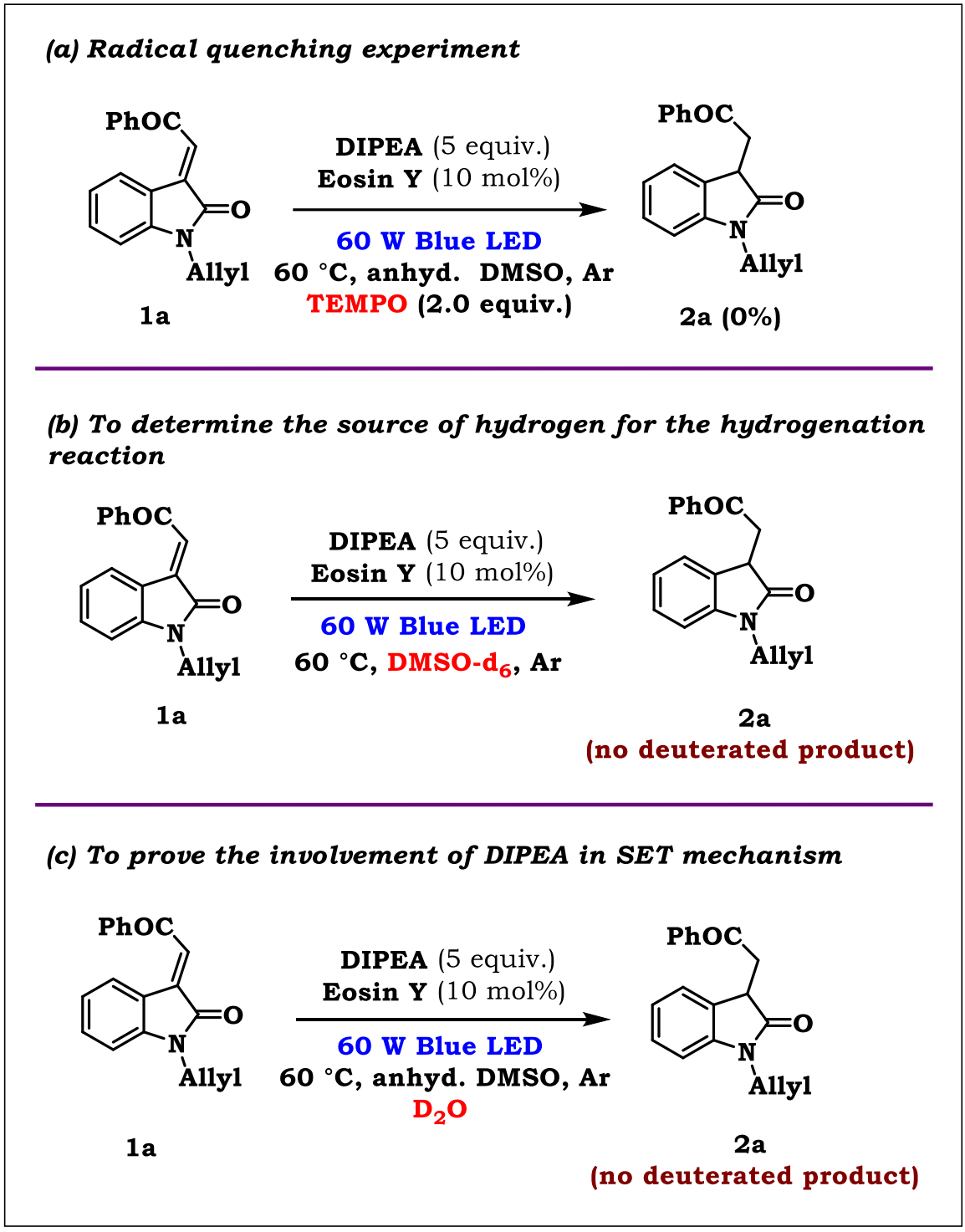
As an extension of our synthetic strategy, we conducted additional transformations using the final products **2a** and **2l** to showcase their versatility in organic synthesis (**Scheme 3**). Initially, we executed a chemo-selective reduction followed by bromination on the ketone group within **2a**, resulting in the synthesis of the corresponding brominated product, **3a** (**Scheme 3a**). Following this, we applied a Baeyer–Villiger oxidation to compound **2l**, yielding the corresponding ester, **3b**, as the final product (**Scheme 3b**). To establish the practical applicability of the protocol, we successfully performed a gram-scale synthesis of **2a**, obtaining 0.78 grams of the compound with a yield of 67% (**Scheme 3c**).

3. 5. Control experiments and mechanistic study:

To delve into the mechanistic aspects of this transformation, we systematically carried out a set of control experiments. We initiated this exploration by subjecting **1a** to the optimized reaction conditions in the presence of TEMPO as a radical quencher. Remarkably, even after an extended reaction time, the expected product **2a** did not form. This observation lends strong support to the notion that radical intermediates play a significant role in the progression of this reaction (**Scheme 4a**). In our pursuit to ascertain the origin of hydrogen in the reduction process, we conducted an experiment using DMSO-d6 as the solvent while subjecting **1a** to the optimized conditions (**Scheme 4b**). Surprisingly, we did not yield any deuterated reduced product. Instead, we exclusively obtained **2a**. This outcome definitively establishes that the solvent itself is not the supplier of hydrogen (**Scheme 4b**). Subsequently, to explore the feasibility of a visible light photoredox catalyzed successive single electron transfer process, we conducted an experiment involving the reaction of **1a** with D_2O (10 equivalents). This experiment was performed while keeping the optimized reaction conditions intact and maintaining an inert atmosphere. However, our observations revealed no deuterium

incorporation into the reduced product **2a**. This outcome effectively eliminates the possibility of a carbanion intermediate (**Scheme 4c**).

Scheme 4: Control experiments



Furthermore, we conducted fluorescence quenching experiments of Eosin Y in presence of **1a** using DMSO as solvent (**Figure 2a**) under inert atmosphere. Similarly, under an inert

atmosphere, we performed fluorescence quenching experiments of Eosin Y in presence of DIPEA in DMSO (**Figure 2b**).

We noticed a gradual reduction in the fluorescence emission spectral intensity of Eosin Y as the concentration of **1a** increased in DMSO (**Figure 2a**). In contrast, the presence of DIPEA did not lead to any substantial alteration in the fluorescence intensity of Eosin Y (**Figure 2b**). These findings unequivocally confirm the oxidative quenching of Eosin Y in the presence of **1a**.

We also conducted cyclic voltammetry for **1a** at room temperature (**Figure 2d**). The results from the cyclic voltammogram clearly indicate that the half-wave potential ($E_{1/2}$) of **1a** is -0.76 V vs. SCE. In contrast, the redox potential of the photosensitizer (Eosin Y) is known to be $P.C^{\bullet+}/P.C^{*}$ = -1.11 V vs. SCE based on existing literature data [17]. These experimental and literature-derived values provide strong evidence that excited state of Eosin Y can readily get oxidatively quenched by the presence of **1a**.

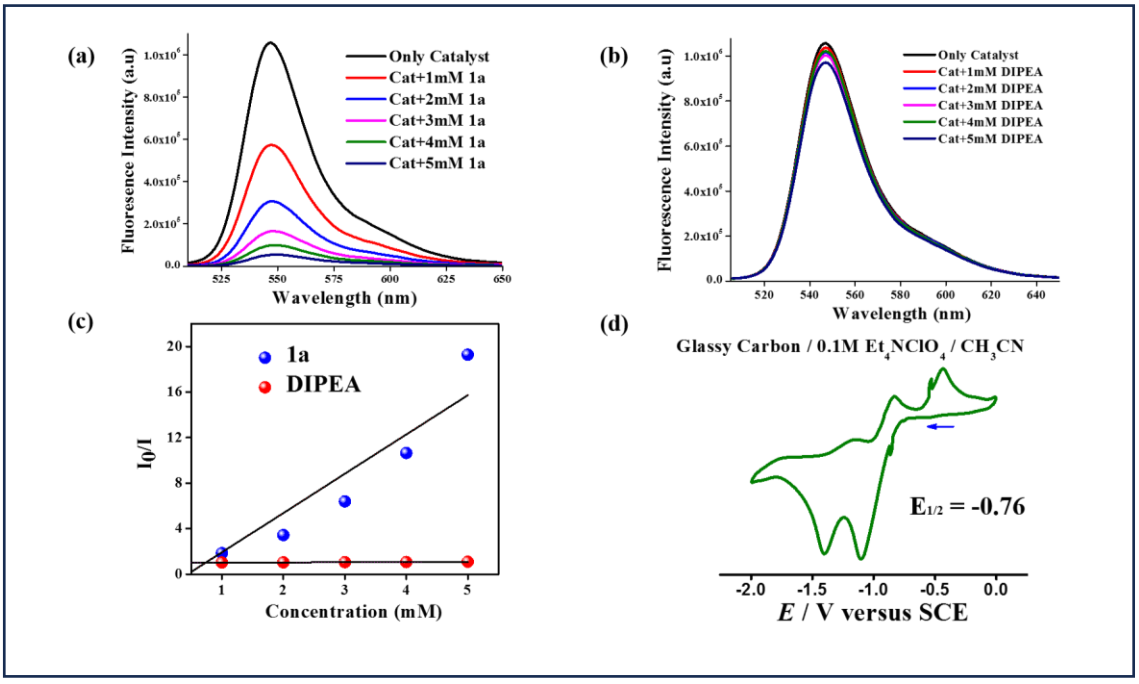
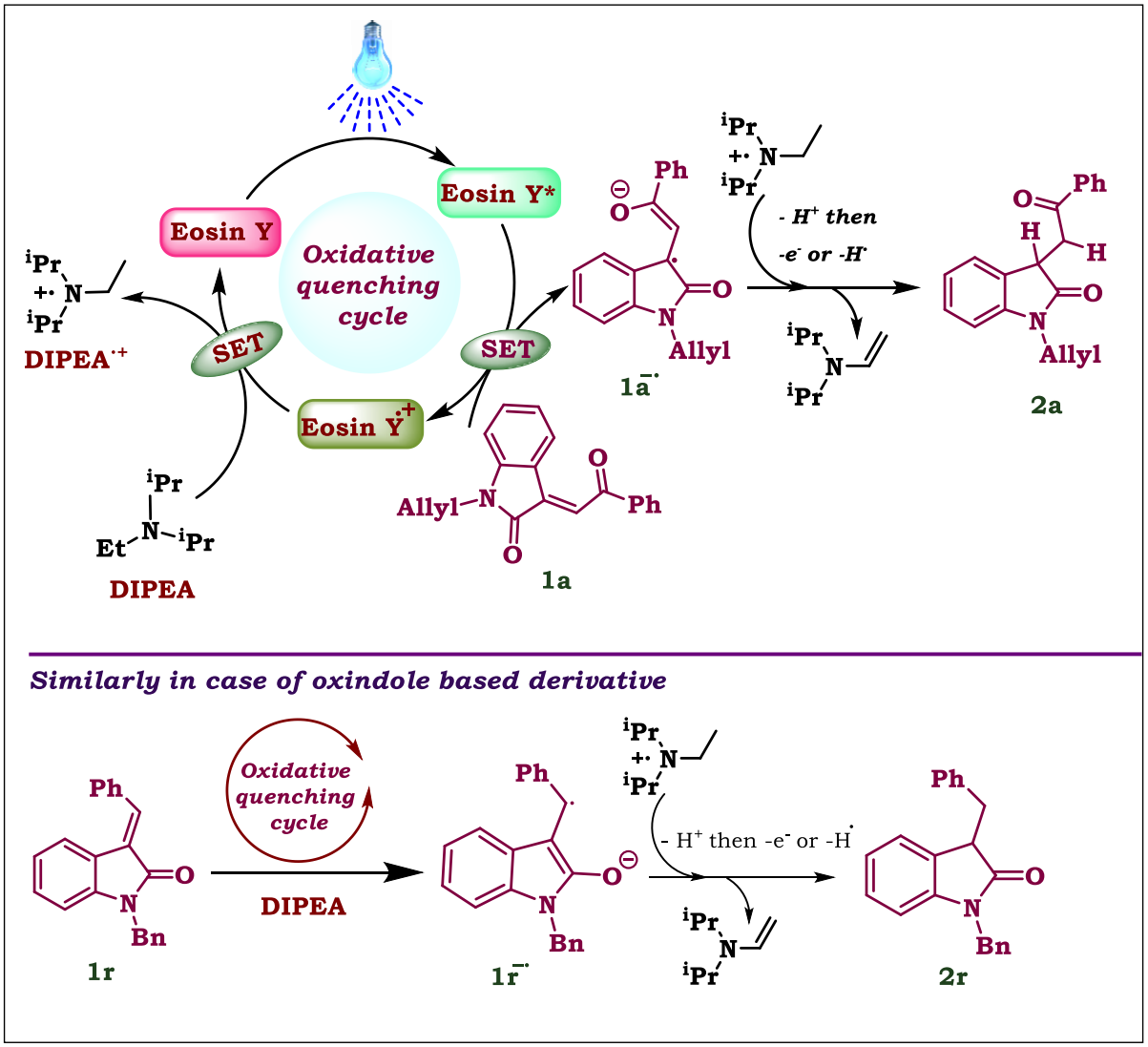


Figure 2: *Fluorescence (emission) and cyclic voltammetry studies to have mechanistic insight (a) Fluorescence quenching experiment of Eosin Y in presence of* ***1a*** *(b) Fluorescence quenching experiment of Eosin Y in presence of DIPEA, (c) Stern–Volmer plot for the fluorescence quenching experiments Eosin Y in presence of* ***1a*** *and DIPEA, (d) Cyclic-voltammetry plot of* ***1a****.*

Based on our control experiments, mechanistic investigations, and a comprehensive review of the literature, we have proposed a most plausible mechanism for this transformation (**Scheme 5**). When subjected to visible light irradiation, Eosin Y transitions into its excited state, Eosin Y*. This excited state, Eosin Y*, undergoes oxidative quenching by **1a**, resulting in the formation of its radical cationic form, Eosin $Y^{\cdot+}$, while concurrently generating the reduced form $\mathbf{1a}^{\cdot-}$.

Scheme 5: Plausible mechanism



Furthermore, the oxidized form of the photocatalyst, Eosin $Y^{\cdot+}$, acquires an electron from DIPEA (acting as a sacrificial electron donor), leading to the regeneration of the ground state Eosin Y and thereby completing the photoredox catalytic cycle. Finally, $\mathbf{1a}^{\cdot-}$ interacts with DIPEA·+ and abstracts a hydrogen atom, ultimately yielding the desired product, **2a** [18].

In a similar manner, the reduction of the alkene **1r**, which is based on a 2-oxindole framework, may likely produce the corresponding product **2r**, possibly through the formation of a stable radical anion intermediate, $\mathbf{1r}^{\bullet-}$.

3.6. Conclusions:

In summary, we have developed a metal-free, chemo-selective hydrogenation method for activated C-C double bonds found in alkylidene oxindoles and succinimide derivatives, all achieved through visible light exposure. Through a comprehensive mechanistic investigation, we've uncovered that the activated double bond is responsible for oxidatively quenching the photocatalyst. We've utilized DIPEA as a sacrificial electron donor, generating an in-situ cationic radical intermediate that serves as a reductant in this transformation. This protocol accommodates a wide range of substrates, delivering high yields of the corresponding reduced products while harnessing clean energy sources. Importantly, this method is scalable to gram quantities, and we've demonstrated its practical utility by employing the reduced products in further synthetic applications.

3.7. Experimental section:

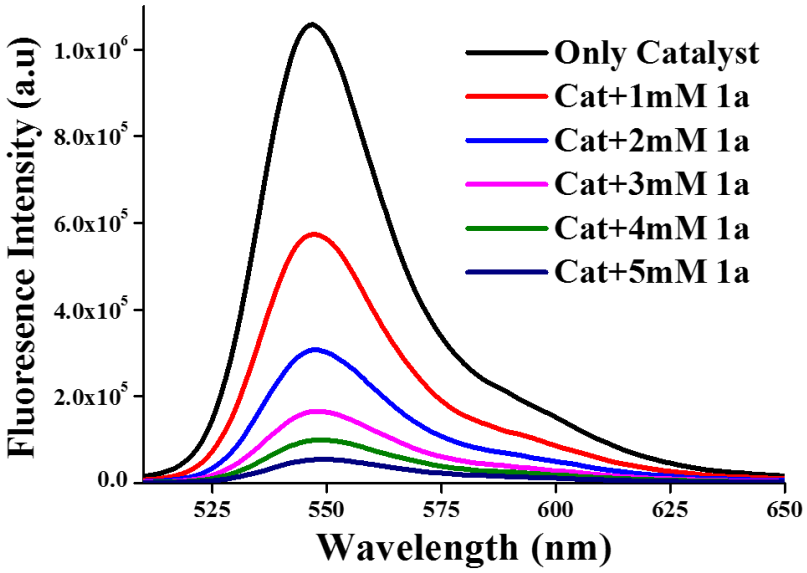
3.7.1. General information:

Unless otherwise noted, all the starting materials and reagents were purchased from commercial suppliers (Aldrich, TCI, and Alfa Aesar) and were used without any further purification. Thin-layer chromatography (TLC) was performed using silica gel 60 GF_{254} pre-coated aluminum backed plates (2.5 mm). Visualization was accomplished by irradiation with UV light at 254 nm. The column chromatography was performed using silica gel (100–200 mesh) eluting with petroleum ether and ethyl acetate. The NMR spectra were recorded using tetramethylsilane as the internal standard. ^{1}H NMR spectra were recorded at 400 MHz and ^{13}C NMR spectra were recorded at 100 MHz (Bruker and Jeol), unless otherwise noted. Chemical shifts (δ) are reported in ppm downfield from $CDCl_3$ (δ = 7.26 ppm) for ^{1}H NMR and relative to the central $CDCl_3$ resonance (δ = 77.16 ppm) for ^{13}C NMR spectroscopy. For ^{1}H NMR, data are reported as follows: chemical shift, multiplicity (s = singlet, d = doublet, dd = double doublet, t = triplet, q = quartet, br = broad, m = multiplet), coupling constants (*J*) are given in Hz and integration. $^{13}C\{^{1}H\}$ NMR spectra were recorded with complete proton decoupling. 19F NMR spectra were recorded at 377 MHz. Mass samples were analyzed by high-resolution mass spectrometry (HRMS)-ESI TOF. Fluorescence spectra were recorded on Fluoromax-4 spectrofluorometer (Horiba Scientific, U.S.A.). All photocatalytic reactions were performed under blue LEDs (IBRA Pure30 W Blue LED Flood Light, IP Rating: IP66). Cyclic voltammetric measurements were done by using a PAR model 273A electrochemistry system.

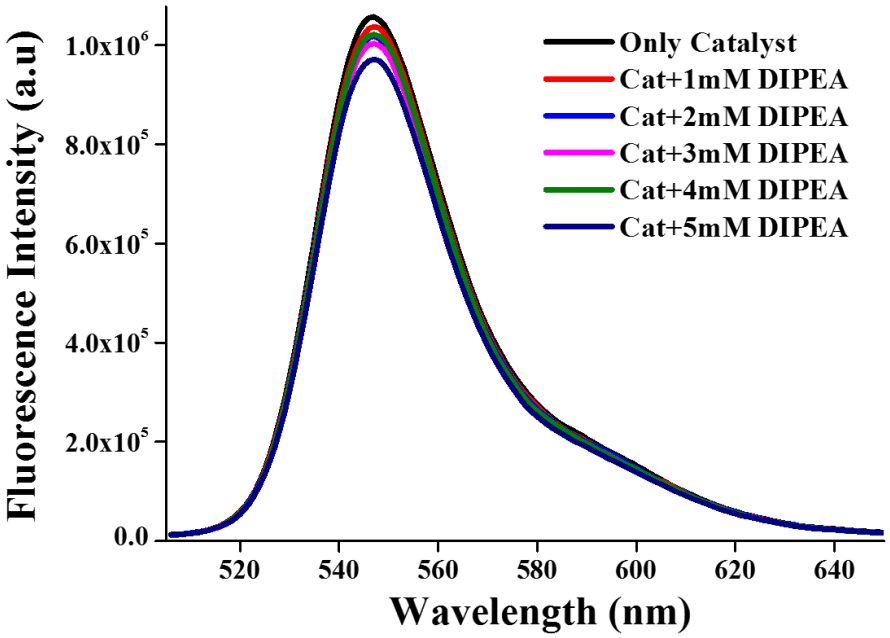
3.7.2. Mechanistic study:

A. Fluorescence Quenching Experiment:

Fluorescence quenching experiment was carried out using Fluorescence spectrophotometer, using 1.0 µM solution of Eosin Y in dry DMSO and variable concentrations of (1 to 5 mM) of (*E*)-1-allyl-3-(2-oxo-2-phenylethylidene)indolin-2-one **1a** in dry DMSO solvent. The sample was prepared in a 3 mL quartz cuvette and the flask was degasified with Argon before the spectra were recorded. The quenching plot of the experiments are given below.



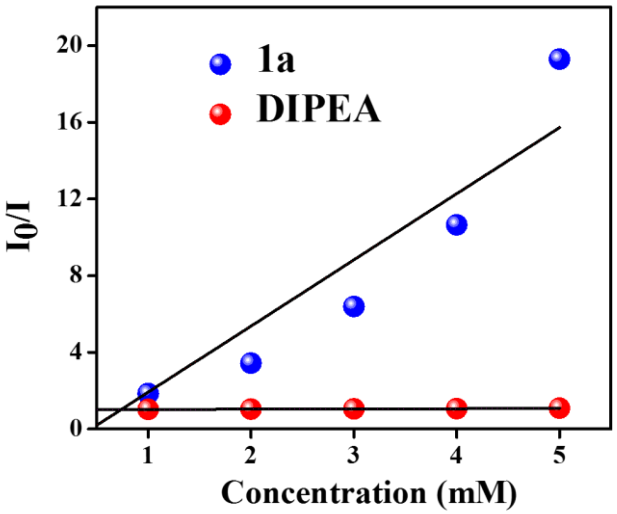
Fluorescence quenching experiment was carried out using Fluorescence spectrophotometer, using 1.0 µM solution of Eosin Y and variable concentrations of (1 to 5 mM) of Diisopropylethylamine (DIPEA) in dry DMSO as solvent. The sample was prepared in a 3 mL quartz cuvette and the flask was degasified with argon before the spectra were recorded. The quenching plot of the experiments are given below.



B. Stern-Volmer plot:

With this fluorescence quenching data, we have drawn the Stern-volmer plot of I0/I vs.

Concentration of the quencher (mM).



Equation	y = a + b*x		
Weight	No Weighting		
Residual Sum of Squares	31.4469		
Pearson's r	0.93216		
Adj. R-Square	0.83615		
		Value	Standard Error
B	Intercept	-1.52922	2.0293
B	Slope	3.45134	0.67025

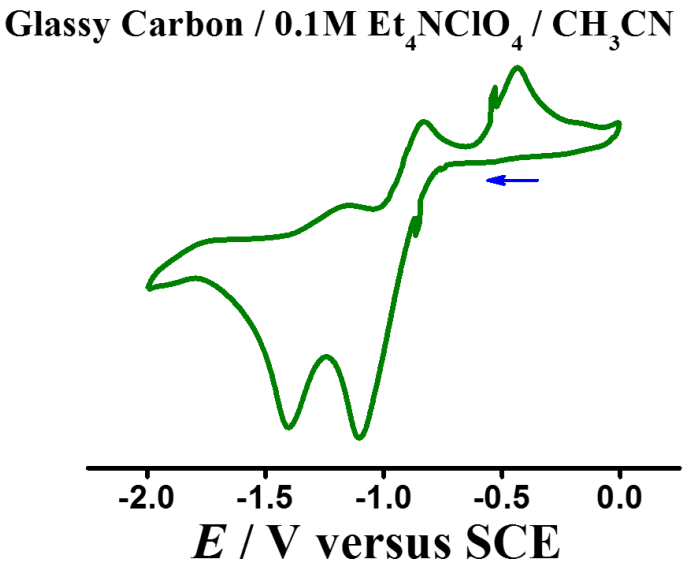
For 1a

Equation	y = a + b*x		
Weight	No Weighting		
Residual Sum of Squares	2.78282E-4		
Pearson's r	0.96935		
Adj. R-Square	0.92456		
		Value	Standard Error
B	Intercept	0.99997	0.00604
B	Slope	0.01573	0.00199

For DIPEA

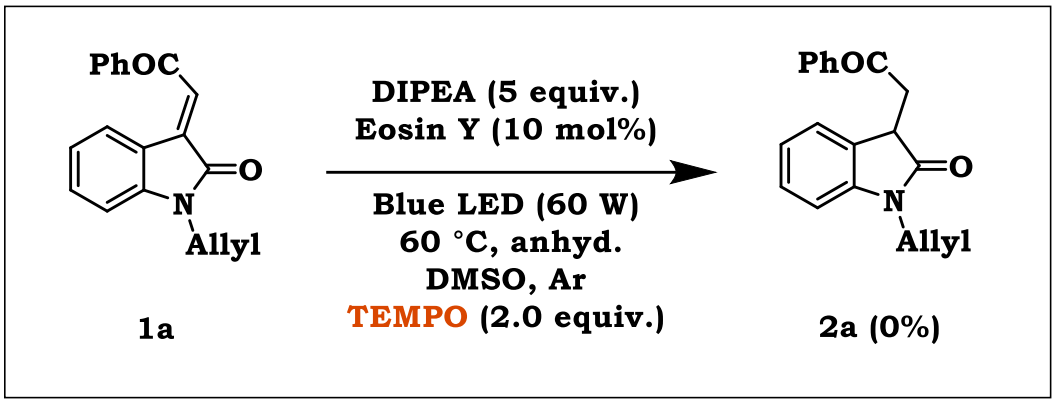
C. Cyclic voltammetry (CV):

Cyclic voltammetric measurement of (*E*)-1-allyl-3-(2-oxo-2-phenylethylidene)indolin-2-one **1a** was done by using a PAR model 273A electrochemistry system. A glassy carbon working electrode, platinum wire auxiliary electrode and a saturated calomel reference electrode (SCE) were used in a standard three-electrode configuration with tetraethylammonium perchlorate (TEAP) as the supporting electrolyte (substrate **1a** concentration $\approx 10^{-3}$ M; standard scan rate 100 mVs^{-1}).



D. Radical trapping experiment:

To an oven dried 10 mL crimp cap vial charged with magnetic stir bar was added 1-allyl-3-(2-oxo-2-phenylethyl)indolin-2-one **1a** (0.35 mmol), Eosin Y (10 mol%) and TEMPO (0.7 mmol) at room temperature under argon atmosphere. The vial was purged with argon again and sealed with aluminium crimp cap using a crimper. Then dry DMSO (3 mL) was added under argon atmosphere. Then the reaction mixture was degasified using argon for 10 min under constant monitoring. After the degasification DIPEA (5 equiv.) was added under inert atmosphere. Then the reaction mixture was irradiated with 60 W blue LED at 60 °C. Even, after 24 h stirring the product the desired product **2a** did not form thus indicating the radical pathway or involving radical intermediate during the course of the reaction.



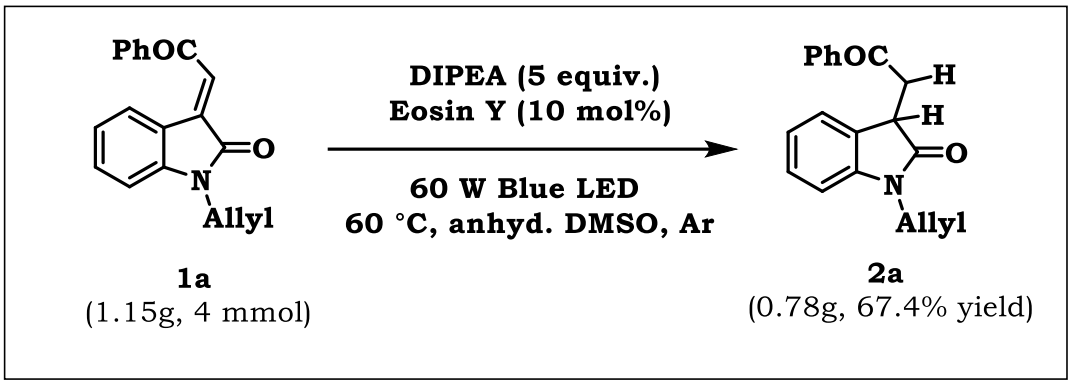
3.7.3. General procedure for the reduction of electron deficient alkenes:

To an oven dried 10 mL crimp cap vial charged with magnetic stir bar was added alkene **1** (0.35 mmol, 1 equiv.), Eosin Y (10 mol%) at room temperature under argon atmosphere. The vial was purged again with argon and sealed with aluminium crimp cap using a crimper. Then dry DMSO (3 mL) was added under argon. Then the reaction mixture was degasified using argon for 10 more minutes under constant monitoring. After the degasification DIPEA (5 equiv.) was added under inert atmosphere. Then the reaction mixture was irradiated with blue LED (60W) at 60 °C stirred for 24 h. After completion of the reaction (monitored by TLC),10 mL of water was added to the reaction mixture and the organic layer was extracted with ethyl acetate (3×10 mL). The combined organic extract was evaporated under reduced pressure and the crude residue was purified by using column chromatography (silica gel 100-200 mesh size, using ethyl acetate / hexane 70:30 system).

3.7.4. General procedure for the reduction of 1a in gram scale:

To an oven dried 10 mL crimp cap vial charged with magnetic stir bar was added alkene **1a** (4 mmol, 1 equiv.), Eosin Y (10 mol%) at room temperature under argon atmosphere. The vial was purged again with argon and sealed with aluminium crimp cap using a crimper. Then dry DMSO (30 mL) was added under argon. Then the reaction mixture was degasified using argon for 10 more minutes under constant monitoring. After the degasification DIPEA (5 equiv.) was added under inert atmosphere. Then the reaction mixture was irradiated with 2* blue LED (60W) at 60 °C stirred for 24 h. After completion of the reaction (monitored by TLC),100 mL of water was added to the reaction mixture and the organic layer was extracted with ethyl acetate (3×100 mL). The combined organic extract was evaporated under reduced pressure and

the crude residue was purified by using column chromatography (silica gel 100-200 mesh size, using hexane:ethyl acetate; 70:30 system) to get **2a** in 67% yield.

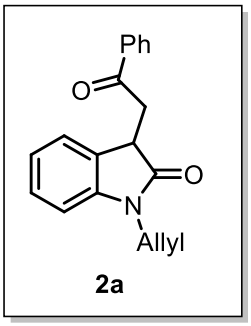


1a
(1.15g, 4 mmol)

2a
(0.78g, 67.4% yield)

3.7.5. Experimental data:

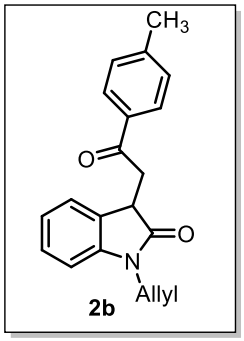
1-allyl-3-(2-oxo-2-phenylethyl) indolin-2-one (2a) [19]



2a

The compound **2a** was prepared following the general procedure **(GP)** White solid (77 mg, 75% yield), R_f = 0.35 (petroleum ether/EtOAc 70:30). **^{1}H NMR (400 MHz, CDCl$_3$)** δ 8.1 – 7.8 (m, 2H), 7.7 – 7.5 (m, 1H), 7.5 (ddd, *J* = 8.3, 6.7, 1.3 Hz, 2H), 7.3 – 7.3 (m, 2H), 7.0 (td, *J* = 7.6, 1.0 Hz, 1H), 6.9 (d, *J* = 7.7 Hz, 1H), 5.9 (ddt, *J* = 17.2, 10.4, 5.3 Hz, 1H), 5.5 – 5.0 (m, 2H), 4.5 (dt, *J* = 5.3, 1.7 Hz, 2H), 4.2 (dt, *J* = 9.0, 2.0 Hz, 1H), 3.9 (dd, *J* = 18.2, 3.0 Hz, 1H), 3.5 (dd, *J* = 18.2, 9.0 Hz, 1H). **^{13}C{^{1}H} NMR (100 MHz, CDCl$_3$)** δ 197.0, 177.6, 143.6, 136.5, 133.6, 131.6, 129.2, 128.8, 128.3, 128.1, 124.5, 122.6, 117.7, 109.0, 42.7, 41.3, 40.2. **HRMS (ESI TOF)** *m/z* calcd. For $C_{19}H_{18}NO_2$ $[M + H]^+$ 292.1398 found 292.1340.

1-allyl-3-(2-oxo-2-(p-tolyl)ethyl)indolin-2-one (2b)

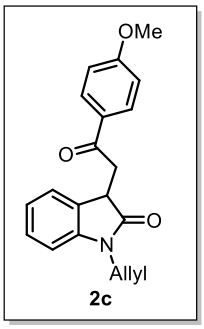


2b

The compound **2b** was prepared following the general procedure **(GP)** White solid (85 mg, 82% yield), R_f = 0.35 (petroleum ether/EtOAc 70:30). **^{1}H NMR (400 MHz, CDCl$_3$)** δ 7.9 (d, *J* = 8.2 Hz, 2H), 7.3 – 7.2 (m, 4H), 7.0 (td, *J* = 7.6, 0.9 Hz, 1H), 6.8 (d, *J* = 7.7 Hz, 1H), 5.9 (ddt, *J* = 17.2, 10.4, 5.3 Hz, 1H), 5.4 – 5.1 (m, 2H), 4.4 (dt, *J* = 5.3, 1.6 Hz, 2H), 4.1 (dd, *J* = 9.1, 2.9 Hz, 1H), 3.8 (dd, *J* = 18.1, 3.0 Hz, 1H), 3.4 (dd, *J* = 18.1, 9.1 Hz, 1H), 2.4 (s, 3H). **^{13}C{^{1}H} NMR (100 MHz, CDCl$_3$)** δ 196.6, 177.7, 144.4, 143.6, 134.0, 131.6,

129.5, 129.3, 128.4, 128.0, 124.6, 122.6, 117.7, 109.0, 42.7, 41.3, 40.1, 21.8. **HRMS (ESI TOF)** *m/z* calcd. For $C_{20}H_{20}NO_2$ $[M + H]^+$ 306.1494 found 306.1490.

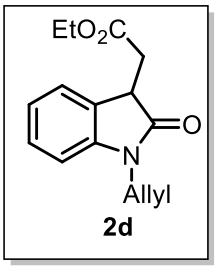
1-allyl-3-(2-(4-methoxyphenyl)-2-oxoethyl)indolin-2-one (2c)



2c

The compound **2c** was prepared following the general procedure **(GP)** White solid (90 mg, 81% yield), R_f = 0.2 (petroleum ether/EtOAc 70:30). **^{1}H NMR (400 MHz, $CDCl_3$)** δ 7.96 (m, 2H), 7.27-7.20 (ddt, *J* = 14.4, 7.7, 1.2 Hz, 2H), 6.99 – 6.84 (m, 4H), 5.89 (ddt, *J* = 17.2, 10.4, 5.3 Hz, 1H), 5.36 – 5.19 (m, 2H), 4.40 (dt, *J* = 5.3, 1.7 Hz, 2H), 4.15 – 4.05 (m, 1H), 3.87 (s, 3H), 3.80 (dd, *J* = 18.0, 3.0 Hz, 1H), 3.37 (dd, *J* = 18.0, 9.1 Hz, 1H). **^{13}C{^{1}H} NMR (100 MHz, $CDCl_3$)** δ 195.4, 177.7, 163.9, 143.6, 131.6, 130.6, 129.6, 129.4, 128.0, 124.6, 122.6, 117.7, 113.9, 109.0, 55.6, 42.6, 41.4, 39.8. **HRMS (ESI TOF)** *m/z* calcd. For $C_{20}H_{20}NO_3$ $[M + H]^+$ 322.1443 found 322.1436.

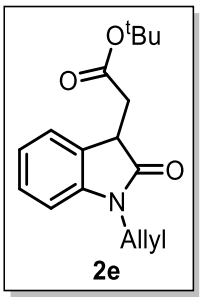
Ethyl 2-(1-allyl-2-oxoindolin-3-yl) acetate (2d)



2d

The compound **2d** was prepared following the general procedure **(GP)** White solid (73 mg, 80% yield), R_f = 0.36 (petroleum ether/EtOAc 70:30). **^{1}H NMR (400 MHz, $CDCl_3$)** δ 7.25 (tt, *J* = 6.8, 1.1 Hz, 2H), 7.02 (td, *J* = 7.5, 1.0 Hz, 1H), 6.85 – 6.82 (m, 1H), 5.85 (ddt, *J* = 17.2, 10.4, 5.3 Hz, 1H), 5.32 – 5.17 (m, 2H), 4.36 (ddt, *J* = 5.1, 3.4, 1.7 Hz, 2H), 4.22 – 4.05 (m, 2H), 3.82 (ddt, *J* = 8.0, 4.6, 1.1 Hz, 1H), 3.09 (dd, *J* = 16.8, 4.5 Hz, 1H), 2.82 (dd, *J* = 16.8, 7.9 Hz, 1H), 1.20 (t, *J* = 7.1 Hz, 3H). **^{13}C{^{1}H} NMR (100 MHz, $CDCl_3$)** δ 176.6, 171.1, 143.7, 131.5, 128.3, 124.0, 122.6, 117.7, 109.1, 61.0, 42.6, 41.9, 35.1, 14.2. **HRMS (ESI TOF)** *m/z* calcd. For $C_{15}H_{18}NO_3$ $[M + H]^+$ 260.1287 found 260.1280.

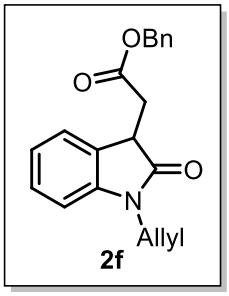
tert-butyl 2-(1-allyl-2-oxoindolin-3-yl)acetate (2e)



2e

The compound **2e** was prepared following the general procedure **(GP)** White solid (79 mg, 78% yield), R_f = 0.38 (petroleum ether/EtOAc 70:30). **^{1}H NMR (400 MHz, CDCl$_3$)** δ 7.32 – 7.16 (m, 2H), 7.03 (td, *J* = 7.5, 1.0 Hz, 1H), 6.83 (d, *J* = 7.8 Hz, 1H), 5.85 (ddt, *J* = 17.2, 10.4, 5.3 Hz, 1H), 5.35 – 5.10 (m, 2H), 4.44 (ddt, *J* = 16.3, 5.2, 1.7 Hz, 1H), 4.26 (ddt, *J* = 16.3, 5.5, 1.6 Hz, 1H), 3.86 – 3.74 (m, 1H), 3.01 (dd, *J* = 16.5, 4.7 Hz, 1H), 2.74 (dd, *J* = 16.5, 7.8 Hz, 1H), 1.36 (s, 9H). **^{13}C{^{1}H} NMR (100 MHz, CDCl$_3$)** δ 176.7, 170.2, 143.7, 131.6, 128.5, 128.2, 124.1, 122.5, 117.7, 109.0, 81.3, 42.6, 42.2, 36.3, 28.0. **HRMS (ESI TOF)** *m/z* calcd. For $C_{17}H_{22}NO_3$ $[M + H]^+$ 288.1600 found 288.1595.

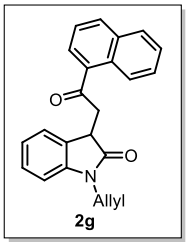
Benzyl 2-(1-allyl-2-oxoindolin-3-yl)acetate (2f)



2f

The compound **2f** was prepared following the general procedure **(GP)** White solid (92 mg, 82% yield), R_f = 0.38 (petroleum ether/EtOAc 70:30). **^{1}H NMR (400 MHz, CDCl$_3$)** δ 7.37 – 7.30 (m, 3H), 7.27 – 7.16 (m, 4H), 6.99 (td, *J* = 7.5, 1.0 Hz, 1H), 6.79 (d, *J* = 7.8 Hz, 1H), 5.79 (ddt, *J* = 17.1, 10.4, 5.3 Hz, 1H), 5.27 – 5.16 (m, 2H), 5.16 – 5.03 (m, 2H), 4.38 – 4.17 (m, 2H), 3.82 (dd, *J* = 7.8, 4.5 Hz, 1H), 3.15 (dd, *J* = 16.9, 4.5 Hz, 1H), 2.89 (dd, *J* = 16.9, 7.8 Hz, 1H). **^{13}C{^{1}H} NMR (100 MHz, CDCl$_3$)** δ 176.4, 170.9, 143.6, 135.6, 131.5, 128.7, 128.4, 128.3, 128.1, 123.9, 122.6, 117.7, 117.7, 109.2, 66.9, 42.5, 41.9, 35.0. **HRMS (ESI TOF)** *m/z* calcd. For $C_{20}H_{20}NO_3$ $[M + H]^+$ 322.1443 found 322.1438.

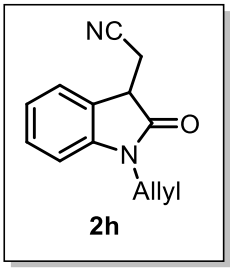
1-allyl-3-(2-(naphthalen-1-yl)-2-oxoethyl)indolin-2-one (2g)



2g

The compound **2g** was prepared following the general procedure **(GP)** White solid (99 mg, 80% yield), R_f = 0.37 (petroleum ether/EtOAc 70:30). **^{1}H NMR (400 MHz, CDCl$_3$)** δ 8.50 (s, 1H), 8.05 (dd, *J* = 8.6, 1.8 Hz, 1H), 7.99 – 7.86 (m, 3H), 7.58 (dddd, *J* = 21.8, 8.3, 6.9, 1.4 Hz, 2H), 7.30 (dd, *J* = 7.4, 1.4 Hz, 1H), 7.23 (dt, *J* = 7.7, 1.1 Hz, 1H), 6.99 (td, *J* = 7.6, 1.1 Hz, 1H), 6.87 (d, *J* = 7.8 Hz, 1H), 5.91 (ddt, *J* = 17.2, 10.4, 5.3 Hz, 1H), 5.37 – 5.19 (m, 2H), 4.43 (dt, *J* = 5.3, 1.7 Hz, 2H), 4.17 (dd, *J* = 9.1, 3.0 Hz, 1H), 4.00 (dd, *J* = 18.1, 3.1 Hz, 1H), 3.58 (dd, *J* = 18.1, 9.1 Hz, 1H). **^{13}C{^{1}H} NMR (100 MHz, CDCl$_3$)** δ 196.9, 177.7, 143.6, 135.9, 133.8, 132.6, 131.6, 130.2, 129.8, 129.2, 128.8, 128.7, 128.1, 127.9, 127.0, 124.6, 122.6, 117.8, 109.1, 42.7, 41.4, 40.3. **HRMS (ESI TOF)** *m/z* calcd. For $C_{23}H_{20}NO_2$ $[M + H]^+$ 342.1494 found 342.1499.

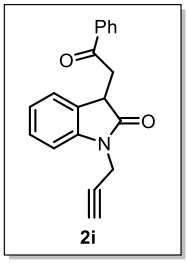
2-(1-allyl-2-oxoindolin-3-yl)acetonitrile (2h)



2h

The compound **2h** was prepared following the general procedure **(GP)** White solid (55 mg, 74% yield), R_f = 0.34 (petroleum ether/EtOAc 70:30). **^{1}H NMR (400 MHz, CDCl$_3$)** δ 7.52 (d, *J* = 7.5 Hz, 1H), 7.35-7.31 (tt, *J* = 7.8, 1.1 Hz, 1H), 7.14-7.10 (td, *J* = 7.6, 1.0 Hz, 1H), 6.88 (d, *J* = 7.9 Hz, 1H), 5.83 (ddt, *J* = 17.2, 10.4, 5.3 Hz, 1H), 5.31 – 5.19 (m, 2H), 4.36 (dq, *J* = 5.1, 1.6 Hz, 2H), 3.71 (dd, *J* = 8.8, 4.6 Hz, 1H), 3.13 (dd, *J* = 16.8, 4.6 Hz, 1H), 2.74 (dd, *J* = 16.8, 8.9 Hz, 1H). **^{13}C{^{1}H} NMR (100 MHz, CDCl$_3$)** δ 174.1, 143.5, 130.9, 129.5, 125.7, 124.4, 123.3, 118.2, 117.2, 109.7, 42.7, 41.5, 19.3. **HRMS (ESI TOF)** *m/z* calcd. For $C_{13}H_{13}N_2O$ $[M + H]^+$ 213.1028 found 213.1020.

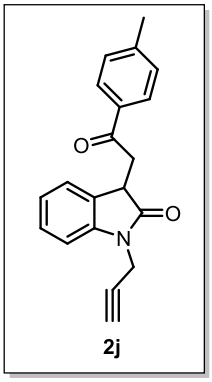
3-(2-oxo-2-phenylethyl)-1-(prop-2-yn-1-yl)indolin-2-one (2i)



2i

The compound **2i** was prepared following the general procedure **(GP)** White solid (78 mg, 77% yield), R_f = 0.35 (petroleum ether/EtOAc 70:30). **^{1}H NMR (400 MHz, $CDCl_3$)** δ 8.00 – 7.95 (m, 2H), 7.61 – 7.55 (m, 1H), 7.50 – 7.42 (m, 2H), 7.34 – 7.28 (m, 1H), 7.27 – 7.24 (m, 1H), 7.10 – 7.06 (m, 1H), 7.02 (td, *J* = 7.6, 1.1 Hz, 1H), 4.57 (qd, *J* = 17.6, 2.6 Hz, 2H), 4.12 (dd, *J* = 9.1, 3.0 Hz, 1H), 3.83 (dd, *J* = 18.2, 3.0 Hz, 1H), 3.43 (dd, *J* = 18.3, 9.1 Hz, 1H), 2.26 (t, *J* = 2.5 Hz, 1H). **^{13}C{^{1}H} NMR (100 MHz, $CDCl_3$)** δ 196.9, 176.9, 142.5, 136.4, 133.6, 129.0, 128.8, 128.3, 128.2, 124.6, 123.0, 109.2, 72.4, 41.2, 40.1, 29.5. **HRMS (ESI TOF)** *m/z* calcd. For $C_{19}H_{16}NO_2$ $[M + H]^+$ 290.1181 found 290.1175.

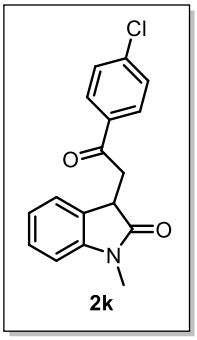
3-(2-oxo-2-(p-tolyl)ethyl)-1-(prop-2-yn-1-yl)indolin-2-one (2j)



2j

The compound **2j** was prepared following the general procedure **(GP)** White solid (83 mg, 79% yield), R_f = 0.35 (petroleum ether/EtOAc 70:30). **^{1}H NMR (400 MHz, $CDCl_3$)** δ 7.87 (d, *J* = 8.3 Hz, 2H), 7.33 – 7.24 (m, 4H), 7.10 – 6.96 (m, 2H), 4.57 (qd, *J* = 17.6, 2.5 Hz, 2H), 4.12 (dd, *J* = 9.2, 3.0 Hz, 1H), 3.80 (dd, *J* = 18.2, 3.0 Hz, 1H), 3.40 (dd, *J* = 18.1, 9.2 Hz, 1H), 2.41 (s, 3H), 2.26 (t, *J* = 2.5 Hz, 1H). **^{13}C{1H} NMR (100 MHz, $CDCl_3$)** δ 196.5, 177.0, 144.5, 142.5, 133.9, 129.5, 129.1, 128.4, 128.2, 124.7, 123.0, 109.1, 72.4, 41.3, 40.0, 29.5, 21.8. **HRMS (ESI TOF)** *m/z* calcd. For $C_{20}H_{18}NO_2$ $[M + H]^+$ 304.1338 found 304.1339.

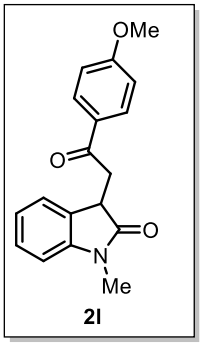
3-(2-(4-chlorophenyl)-2-oxoethyl)-1-methylindolin-2-one (2k)



2k

The compound **2k** was prepared following the general procedure **(GP)** White solid (64 mg, 61% yield), R_f = 0.35 (petroleum ether/EtOAc 70:30). **^{1}H NMR (400 MHz, $CDCl_3$)** δ 8.0 – 7.8 (m, 2H), 7.6 – 7.4 (m, 2H), 7.3 (dt, *J* = 7.7, 1.0 Hz, 1H), 7.2 – 7.2 (m, 1H), 7.0 (td, *J* = 7.6, 1.0 Hz, 1H), 6.9 (d, *J* = 7.8 Hz, 1H), 4.1 (dd, *J* = 9.1, 3.0 Hz, 1H), 3.8 (dd, *J* = 18.2, 3.1 Hz, 1H), 3.4 (dd, *J* = 18.2, 9.1 Hz, 1H), 3.3 (s, 3H). **^{13}C{^{1}H} NMR (100 MHz, $CDCl_3$)** δ 195.9, 177.7, 144.4, 140.1, 134.8, 129.7, 129.2, 129.1, 128.3, 124.5, 122.7, 108.2, 41.3, 40.2, 26.6. **HRMS (ESI TOF)** *m/z* calcd. For $C_{17}H_{15}ClNO_2$ $[M + H]^+$ 300.0791 found 300.0785.

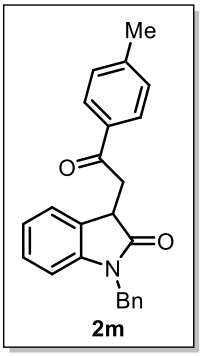
3-(2-(4-methoxyphenyl)-2-oxoethyl)-1-methylindolin-2-one (2l)



2l

The compound **2l** was prepared following the general procedure **(GP)** White solid (74 mg, 72% yield), R_f = 0.2 (petroleum ether/EtOAc 70:30). **^{1}H NMR (400 MHz, $CDCl_3$)** δ 7.98 – 7.92 (m, 2H), 7.28 (dt, *J* = 7.8, 1.1 Hz, 1H), 7.25 (dt, *J* = 2.1, 1.1 Hz, 1H), 6.99 (td, *J* = 7.5, 1.1 Hz, 1H), 6.95 – 6.91 (m, 2H), 6.85 (d, *J* = 7.8 Hz, 1H), 4.08 (dd, *J* = 9.4, 3.0 Hz, 1H), 3.87 (s, 3H), 3.82 – 3.73 (m, 1H), 3.38 – 3.29 (m, 1H), 3.27 (s, 3H). **^{13}C{^{1}H} NMR (100 MHz, $CDCl_3$)** δ 195.6, 178.0, 163.9, 144.4, 130.6, 129.6, 129.4, 128.2, 124.6, 122.6, 114.0, 108.1, 55.6, 41.4, 39.8, 26.5. **HRMS (ESI TOF)** *m/z* calcd. For $C_{18}H_{18}NO_3$ $[M + H]^+$ 296.1287 found 296.1280.

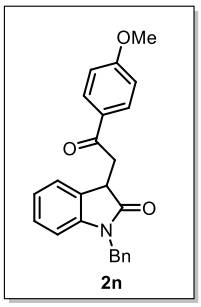
1-benzyl-3-(2-oxo-2-(p-tolyl)ethyl)indolin-2-one (2m) [19]



2m

The compound **2m** was prepared following the general procedure **(GP)** White solid (101 mg, 81% yield), R_f = 0.36 (petroleum ether/EtOAc 70:30). **^{1}H NMR (400 MHz, $CDCl_3$)** δ 7.90 (m, 2H), 7.37 – 7.32 (m, 4H), 7.29 – 7.24 (m, 4H), 7.15 (tt, *J* = 7.8, 1.1 Hz, 1H), 6.95 (td, *J* = 7.5, 1.1 Hz, 1H), 6.74 (dd, *J* = 7.8, 0.9 Hz, 1H), 4.98 (d, *J* = 1.8 Hz, 2H), 4.18 (dd, *J* = 9.1, 2.9 Hz, 1H), 3.87 (dd, *J* = 18.1, 3.1 Hz, 1H), 3.44 (dd, *J* = 18.1, 9.0 Hz, 1H), 2.42 (s, 3H). **^{13}C{^{1}H} NMR (100 MHz, $CDCl_3$)** δ 196.6, 178.0, 144.5, 143.5, 136.1, 134.0, 129.5, 129.3, 128.9, 128.4, 128.1, 127.7, 127.5, 124.6, 122.6, 109.2, 44.1, 41.4, 40.1, 21.8. **HRMS (ESI TOF)** *m/z* calcd. For $C_{24}H_{22}NO_2$ $[M + H]^+$ 356.1651 found 356.1647.

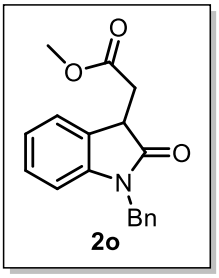
1-benzyl-3-(2-(4-methoxyphenyl)-2-oxoethyl)indolin-2-one (2n) [13]



2n

The compound **2n** was prepared following the general procedure **(GP)** White solid (101 mg, 78% yield), R_f = 0.22 (petroleum ether/EtOAc 70:30). **^{1}H NMR (400 MHz, $CDCl_3$)** δ 8.1 – 7.8 (m, 2H), 7.3 (dd, *J* = 7.2, 1.4 Hz, 2H), 7.3 – 7.3 (m, 2H), 7.3 – 7.2 (m, 1H), 7.2 – 7.0 (m, 2H), 7.0 – 6.8 (m, 3H), 6.7 (d, *J* = 7.8 Hz, 1H), 5.0 (d, *J* = 2.1 Hz, 2H), 4.2 – 4.1 (m, 1H), 3.8 (s, 3H), 3.83 (m, 1H), 3.4 (dd, *J* = 18.0, 9.0 Hz, 1H). **^{13}C{^{1}H} NMR (100 MHz, $CDCl_3$)** δ 195.4, 178.1, 163.8, 143.5, 136.0, 130.6, 129.6, 129.3, 128.9, 128.0, 127.7, 127.4, 124.6, 122.6, 113.9, 109.1, 55.6, 44.0, 41.4, 39.8. **HRMS (ESI TOF)** *m/z* calcd. For $C_{24}H_{22}NO_3$ $[M + H]^+$ 372.1600 found 372.1608.

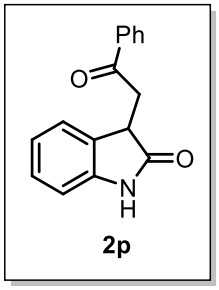
Methyl 2-(1-benzyl-2-oxoindolin-3-yl)acetate (2o)



2o

The compound **2o** was prepared following the general procedure **(GP)** White solid (77 mg, 75% yield), R_f = 0.35 (petroleum ether/EtOAc 70:30). **^{1}H NMR (400 MHz, $CDCl_3$)** δ 7.3 – 7.3 (m, 4H), 7.3 – 7.2 (m, 2H), 7.2 (ddt, *J* = 8.9, 7.8, 1.1 Hz, 1H), 7.0 (td, *J* = 7.5, 1.0 Hz, 1H), 6.8 – 6.6 (m, 1H), 4.9 (dd, *J* = 2.1, 0.8 Hz, 2H), 3.9 (ddt, *J* = 7.8, 4.5, 1.0 Hz, 1H), 3.7 (s, 3H), 3.1 (dd, *J* = 16.9, 4.6 Hz, 1H), 2.9 (dd, *J* = 16.9, 7.9 Hz, 1H). **^{13}C{^{1}H} NMR (100 MHz, $CDCl_3$)** δ 176.8, 171.5, 143.5, 128.8, 128.3, 128.1, 127.7, 127.4, 123.9, 122.6, 109.2, 52.1, 44.0, 41.9, 34.8. **HRMS (ESI TOF)** *m/z* calcd. For $C_{18}H_{18}NO_3$ $[M + H]^+$ 296.1287 found 296.1279.

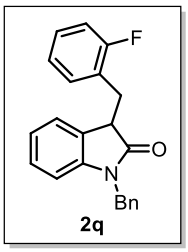
3-(2-oxo-2-phenylethyl)indolin-2-one (2p) [13]



2p

The compound **2p** was prepared following the general procedure **(GP)** White solid (67 mg, 76% yield), R_f = 0.1 (petroleum ether/EtOAc 70:30). **^{1}H NMR (400 MHz, $CDCl_3$)** δ 8.69 (s, 1H), 8.03 – 7.96 (m, 2H), 7.63 – 7.55 (m, 1H), 7.51 – 7.43 (m, 2H), 7.20 (ddt, *J* = 12.6, 7.7, 1.0 Hz, 2H), 7.01 – 6.87 (m, 2H), 4.14 – 4.06 (m, 1H), 3.84 (dd, *J* = 18.2, 3.2 Hz, 1H), 3.47 (dd, *J* = 18.2, 8.8 Hz, 1H). **^{13}C{^{1}H} NMR (100 MHz, $CDCl_3$)** δ 197.0, 180.3, 141.6, 136.4, 133.6, 129.8, 128.9, 128.3, 128.2, 124.7, 122.6, 109.9, 41.8, 40.0. **HRMS (ESI TOF)** *m/z* calcd. For $C_{16}H_{14}NO_2$ $[M + H]^+$ 252.1025 found 252.1022.

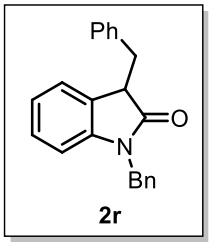
1-benzyl-3-(2-fluorobenzyl)indolin-2-one (2q)



2q

The compound **2q** was prepared following the general procedure **(GP)** White solid (81 mg, 70% yield), R_f = 0.4 (petroleum ether/EtOAc 70:30). **^{1}H NMR (400 MHz, $CDCl_3$)** δ 7.28 – 7.18 (m, 5H), 7.15 – 7.05 (m, 3H), 7.05 – 6.96 (m, 2H), 6.93 – 6.84 (m, 2H), 6.62 (d, *J* = 7.8 Hz, 1H), 4.99 (d, *J* = 15.7 Hz, 1H), 4.78 (d, *J* = 15.7 Hz, 1H), 3.88 (dd, *J* = 8.5, 5.2 Hz, 1H), 3.58 (ddd, *J* = 13.9, 5.1, 1.1 Hz, 1H), 3.07 (ddd, *J* = 13.9, 8.4, 0.9 Hz, 1H). **^{13}C{^{1}H} NMR (100 MHz, $CDCl_3$)** δ 177.05, 161.36 (d, *J* = 246.1 Hz), 143.4, 135.8, 131.8 (d, *J* = 4.5 Hz), 128.8, 128.6, 128.6, 128.1, 127.6, 127.3, 125.1 (d, *J* = 15.3 Hz), 124.7, 124.1 (d, *J* = 3.7 Hz), 122.3, 115.5 (d, *J* = 22.3 Hz), 109.0, 45.9, 43.7, 29.8 (d, *J* = 2.0 Hz). **^{19}F NMR (377 MHz, $CDCl_3$)** δ -116.6. **HRMS (ESI TOF)** *m/z* calcd. For $C_{22}H_{19}FNO$ $[M + H]^+$ 332.1451 found 332.1453.

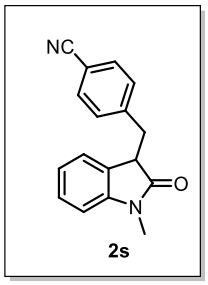
1,3-dibenzylindolin-2-one (2r) [20]



2r

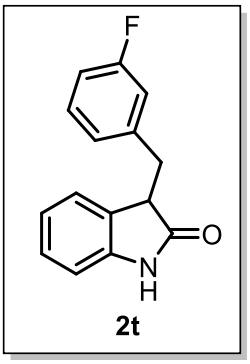
The compound **2r** was prepared following the general procedure **(GP)** White solid (77 mg, 70% yield), R_f = 0.4 (petroleum ether/EtOAc 70:30). **^{1}H NMR (400 MHz, $CDCl_3$)** δ 7.23 – 7.16 (m, 6H), 7.15 – 7.05 (m, 3H), 7.01 – 6.81 (m, 4H), 6.54 (d, *J* = 7.8 Hz, 1H), 5.09 – 4.95 (m, 1H), 4.63 (d, *J* = 15.8 Hz, 1H), 3.84 (dd, *J* = 8.1, 4.3 Hz, 1H), 3.50 (dd, *J* = 13.6, 4.4 Hz, 1H), 3.13 (dd, *J* = 13.6, 8.1 Hz, 1H). **^{13}C{^{1}H} NMR (100 MHz, $CDCl_3$)** δ 177.1, 143.5, 137.5, 135.6, 129.8, 128.8, 128.4, 128.3, 128.0, 127.4, 127.0, 126.8, 124.6, 122.2, 109.2, 47.2, 43.6, 36.6. **HRMS (ESI TOF)** *m/z* calcd. For $C_{22}H_{20}NO$ $[M + H]^+$ 314.1545 found 314.1540.

4-((1-methyl-2-oxoindolin-3-yl)methyl)benzonitrile (2s)



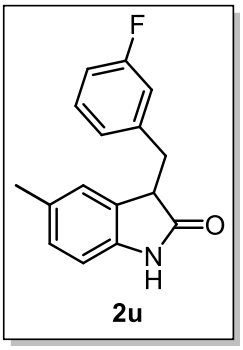
The compound **2s** was prepared following the general procedure **(GP)** White solid (46 mg, 50% yield), R_f = 0.33 (petroleum ether/EtOAc 70:30). **^{1}H NMR (400 MHz, $CDCl_3$)** δ 7.57 – 7.44 (m, 2H), 7.27 – 7.20 (m, 3H), 6.98 (td, *J* = 7.5, 1.0 Hz, 1H), 6.92 – 6.85 (m, 1H), 6.75 (d, *J* = 7.7 Hz, 1H), 3.75 (dd, *J* = 8.0, 4.8 Hz, 1H), 3.45 (dd, *J* = 13.7, 4.8 Hz, 1H), 3.12 (d, *J* = 8.0 Hz, 1H), 3.12 (s, 3H). **^{13}C{^{1}H} NMR (100 MHz, $CDCl_3$)** δ 176.4, 144.3, 143.4, 132.1, 130.3, 128.5, 127.5, 124.3, 122.5, 118.9, 110.7, 108.4, 46.6, 36.7, 26.3. **HRMS (ESI TOF)** *m/z* calcd. For $C_{17}H_{15}N_2O$ $[M + H]^+$ 263.1184 found 263.1176.

3-(3-fluorobenzyl)indolin-2-one (2t)



The compound **2t** was prepared following the general procedure **(GP)** White solid (58 mg, 68% yield), R_f = 0.1 (petroleum ether/EtOAc 70:30). **^{1}H NMR (400 MHz, $CDCl_3$)** δ 9.2 – 8.8 (s, 1H), 7.2 – 7.1 (m, 2H), 7.0 – 6.8 (m, 5H), 6.8 (d, *J* = 7.4 Hz, 1H), 3.7 (dd, *J* = 8.9, 4.7 Hz, 1H), 3.5 (dd, *J* = 13.8, 4.7 Hz, 1H), 3.0 (dd, *J* = 13.8, 8.9 Hz, 1H). **^{13}C{^{1}H} NMR (100 MHz, $CDCl_3$)** δ 179.7, 162.8 (d, *J* = 245.7 Hz), 141.6, 140.4 (d, *J* = 7.3 Hz), 129.9 (d, *J* = 8.4 Hz), 128.7, 128.3, 125.2 (d, *J* = 2.7 Hz), 124.8, 122.3, 116.4 (d, *J* = 21.2 Hz), 113.8 (d, *J* = 21.0 Hz), 110.0, 47.4, 36.3. **^{19}F NMR (377 MHz, $CDCl_3$)** δ -113.3. **HRMS (ESI TOF)** *m/z* calcd. For $C_{15}H_{13}FNO$ $[M + H]^+$ 242.0981 found 242.0983.

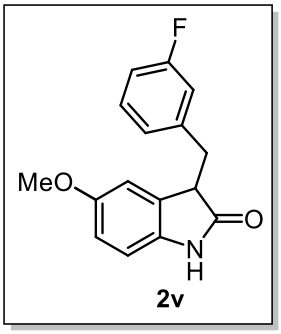
3-(3-fluorobenzyl)-5-methylindolin-2-one (2u)



2u

The compound **2u** was prepared following the general procedure (**GP**) White solid (54 mg, 60% yield), R_f = 0.1 (petroleum ether/EtOAc 70:30. **^{1}H NMR (400 MHz, CDCl$_3$)** δ 8.4 (s, 1H), 7.2 (td, *J* = 7.9, 6.0 Hz, 1H), 7.0 – 6.8 (m, 4H), 6.7 (d, *J* = 7.9 Hz, 1H), 6.6 (s, 1H), 3.7 (dd, *J* = 8.7, 4.7 Hz, 1H), 3.4 (dd, *J* = 13.8, 4.7 Hz, 1H), 3.0 (dd, *J* = 13.8, 8.7 Hz, 1H), 2.2 (s, 3H). **^{13}C{^{1}H} NMR (100 MHz, CDCl$_3$)** δ 179.7, 162.8 (d, *J* = 245.8 Hz), 140.5 (d, *J* = 7.2 Hz), 139.1, 131.7, 129.8 (d, J = 8.2 Hz), 128.8, 128.5, 125.5, 125.2 (d, *J* = 2.8 Hz), 116.4 (d, *J* = 21.2 Hz), 113.7 (d, *J* = 21.0 Hz), 109.7, 47.4, 36.3 (d, *J* = 1.6 Hz), 21.2. **^{19}F NMR (377 MHz, CDCl$_3$)** δ -113.29. **HRMS (ESI TOF)** *m/z* calcd. For $C_{16}H_{15}FNO$ $[M + H]^+$ 256.1138 found 256.1140.

3-(3-fluorobenzyl)-5-methoxyindolin-2-one (2v)

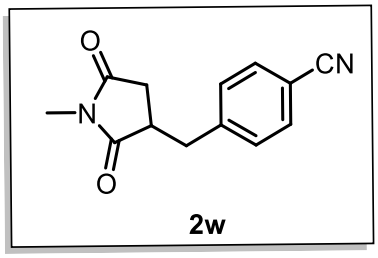


2v

The compound **2v** was prepared following the general procedure (**GP**) White solid (49 mg, 52% yield), R_f = 0.1 (petroleum ether/EtOAc 60:40). **^{1}H NMR (400 MHz, CDCl$_3$)** δ 9.3 (s, 1H), 7.2 (ddd, *J* = 8.9, 7.6, 6.0 Hz, 1H), 7.0 (dt, *J* = 7.6, 1.3 Hz, 1H), 6.9 – 6.9 (m, 2H), 6.8 (d, *J* = 8.4 Hz, 1H), 6.7 (ddd, *J* = 8.5, 2.5, 0.7 Hz, 1H), 6.4 – 6.3 (m, 1H), 3.7 (dd, *J* = 9.1, 4.6 Hz, 1H), 3.7 (s, 3H), 3.5 (dd, *J* = 13.8, 4.7 Hz, 1H), 2.9 (dd, *J* = 13.8, 9.2 Hz, 1H). **^{13}C{^{1}H} NMR (100 MHz, CDCl$_3$)** δ 179.7, 162.8 (d, *J* = 246.0 Hz), 155.5, 140.4 (d, *J* = 7.2 Hz), 135.1, 130.04, 129.9 (d, *J* = 8.2 Hz), 125.3 (d, *J* = 2.9 Hz), 116.4 (d, *J* = 21.1 Hz), 113.8 (d, *J* = 21.1

Hz), 112.9, 111.8, 110.4, 55.7, 47.8, 36.3 (d, *J* = 1.8 Hz). **^{19}F NMR (377 MHz, $CDCl_3$)** δ -113.10. **HRMS (ESI TOF)** *m/z* calcd. For $C_{16}H_{15}FNO_2$ $[M + H]^+$ 272.1087 found 272.1090.

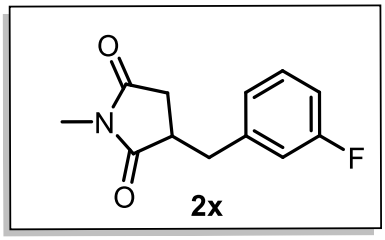
4-((1-methyl-2,5-dioxopyrrolidin-3-yl)methyl)benzonitrile (2w)



2w

The compound **2w** was prepared following the general procedure **(GP)** White solid (72 mg, 90% yield), R_f = 0.25 (petroleum ether/EtOAc 70:30). **^{1}H NMR (400 MHz, $CDCl_3$)** δ 7.61 (d, *J* = 8.3 Hz, 2H), 7.29 (d, *J* = 8.3 Hz, 2H), 3.28 (dd, *J* = 14.0, 4.7 Hz, 1H), 3.14 (tt, *J* = 9.2, 4.8 Hz, 1H), 2.96 (s, 3H), 2.92 (dd, *J* = 14.0, 8.8 Hz, 1H), 2.73 (dd, *J* = 18.3, 9.0 Hz, 1H), 2.37 (dd, *J* = 18.2, 4.9 Hz, 1H). **^{13}C{^{1}H} NMR (100 MHz, $CDCl_3$)** δ 178.7, 175.8, 143.0, 132.7, 129.9, 118.6, 111.3, 41.0, 36.7, 33.4, 25.0. **HRMS (ESI TOF)** *m/z* calcd. For $C_{13}H_{13}N_2O_2$ $[M + H]^+$ 229.0977 found 229.0982.

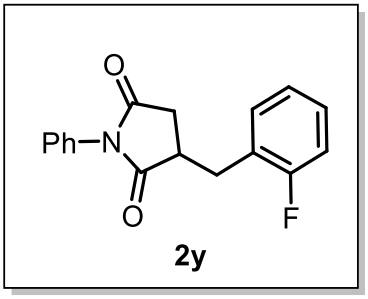
3-(3-fluorobenzyl)-1-methylpyrrolidine-2,5-dione (2x) [15]



2x

The compound **2x** was prepared following the general procedure **(GP)** White solid (60 mg, 78% yield), R_f = 0.3 (petroleum ether/EtOAc 70:30). **^{1}H NMR (400 MHz, $CDCl_3$)** δ 7.30 – 7.22 (m, 1H), 6.99 – 6.83 (m, 3H), 3.23 (dd, *J* = 13.9, 4.5 Hz, 1H), 3.12 (tt, *J* = 9.1, 4.7 Hz, 1H), 2.96 (s, 3H), 2.85 (dd, *J* = 13.9, 8.8 Hz, 1H), 2.71 (dd, *J* = 18.3, 9.0 Hz, 1H), 2.41 (dd, *J* = 18.3, 4.8 Hz, 1H). **^{13}C{^{1}H} NMR (100 MHz, $CDCl_3$)** δ 179.1, 176.2, 163.1 (d, *J* = 246.8 Hz), 139.8 (d, *J* = 7.1 Hz), 130.5 (d, *J* = 8.5 Hz), 124.7 (d, *J* = 2.8 Hz), 115.9 (d, *J* = 21.3 Hz), 114.2 (d, *J* = 21.0 Hz), 41.3, 36.3 (d, *J* = 1.9 Hz), 33.4, 25.0. **^{19}F NMR (377 MHz, $CDCl_3$)** δ -112.5. **HRMS (ESI TOF)** *m/z* calcd. For $C_{12}H_{13}FNO_2$ $[M + H]^+$ 222.0930 found 222.0936.

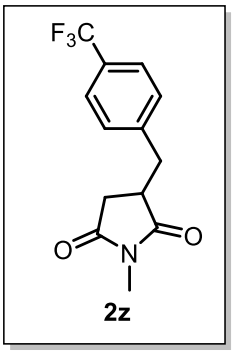
3-(2-fluorobenzyl)-1-phenylpyrrolidine-2, 5-dione (2y)



2y

The compound **2y** was prepared following the general procedure **(GP)** White solid (81 mg, 82% yield), R_f = 0.3 (petroleum ether/EtOAc 70:30). **^{1}H NMR (400 MHz, $CDCl_3$)** δ 7.50 – 7.43 (m, 2H), 7.42 – 7.35 (m, 1H), 7.31 – 7.26 (m, 1H), 7.26 – 7.19 (m, 3H), 7.15 – 7.05 (m, 2H), 3.47 – 3.29 (m, 2H), 3.03 (ddd, *J* = 13.5, 8.1, 1.2 Hz, 1H), 2.90 (dd, *J* = 18.5, 9.1 Hz, 1H), 2.66 (dd, *J* = 18.5, 4.8 Hz, 1H). **^{13}C{^{1}H} NMR (100 MHz, $CDCl_3$)** δ 178.1, 175.3, 161.35 (d, *J* = 245.0 Hz), 131.9, 131.47 (d, *J* = 4.4 Hz), 129.3, 129.2, 128.8, 126.6, 124.68 (d, *J* = 3.7 Hz), 124.17 (d, *J* = 15.6 Hz), 115.89 (d, *J* = 22.3 Hz), 40.7, 33.7 (d, *J* = 1.8 Hz), 30.1 (d, *J* = 1.9 Hz). **^{19}F NMR (377 MHz, $CDCl_3$)** δ -117.2. **HRMS (ESI TOF)** *m/z* calcd. For $C_{17}H_{15}FNO_2$ $[M + H]^+$ 284.1087 found 284.1082.

1-methyl-3-(4-(trifluoromethyl)benzyl)pyrrolidine-2,5-dione (2z)

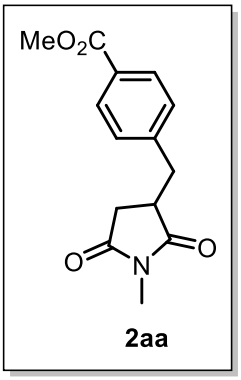


2z

The compound **2z** was prepared following the general procedure **(GP)** White solid (77 mg, 81% yield), R_f = 0.3 (petroleum ether/EtOAc 70:30). **^{1}H NMR (400 MHz, $CDCl_3$)** δ 7.57 (d, *J* = 8.0 Hz, 2H), 7.29 (d, *J* = 8.0 Hz, 2H), 3.30 (dd, *J* = 13.9, 4.6 Hz, 1H), 3.15 (tt, *J* = 9.2, 4.7 Hz, 1H), 2.96 (s, 3H), 2.91 (dd, *J* = 13.9, 9.0 Hz, 1H), 2.72 (dd, *J* = 18.3, 9.0 Hz, 1H), 2.39 (dd, *J* = 18.3, 4.9 Hz, 1H). **^{13}C{^{1}H} NMR (100 MHz, $CDCl_3$)** δ 178.9, 176.0, 141.5, 129.4, 125.9 (q, *J* = 3.8 Hz), 124.2 (d, *J* = 272.1 Hz), 120.1, 41.2, 36.4, 33.4, 25.0. **^{19}F**

NMR (377 MHz, $CDCl_3$) δ -62.6. **HRMS (ESI TOF)** *m/z* calcd. For $C_{13}H_{13}F_3NO_2$ $[M + H]^+$ 272.0898 found 272.0894.

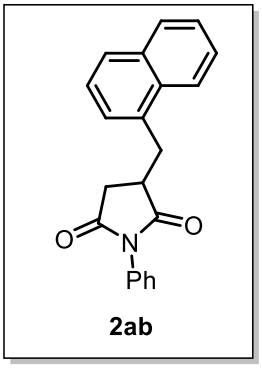
Methyl 4-((1-methyl-2,5-dioxopyrrolidin-3-yl)methyl)benzoate (2aa)



2aa

The compound **2aa** was prepared following the general procedure **(GP)** White solid (63 mg, 69% yield), R_f = 0.25 (petroleum ether/EtOAc 70:30). **^{1}H NMR (400 MHz, $CDCl_3$)** δ 7.97 (d, *J* = 8.3 Hz, 2H), 7.23 (d, *J* = 8.3 Hz, 2H), 3.90 (s, 3H), 3.28 (dd, *J* = 13.8, 4.5 Hz, 1H), 3.15 (tt, *J* = 9.2, 4.6 Hz, 1H), 2.95 (s, 3H), 2.90 (dd, *J* = 13.9, 9.0 Hz, 1H), 2.70 (dd, *J* = 18.3, 9.0 Hz, 1H), 2.39 (dd, *J* = 18.3, 4.8 Hz, 1H). **^{13}C{^{1}H} NMR (100 MHz, $CDCl_3$)** δ 179.0, 176.1, 166.8, 142.7, 130.2, 129.2, 129.1, 52.3, 41.2, 36.6, 33.4, 25.0. **HRMS (ESI TOF)** *m/z* calcd. For $C_{14}H_{16}NO_4$ $[M+H]^+$ 262.1079 found 262.1075.

3-(naphthalen-1-ylmethyl)-1-phenylpyrrolidine-2,5-dione (2ab)

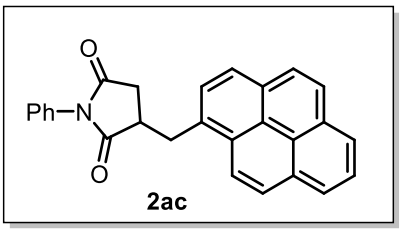


2ab

The compound **2ab** was prepared following the general procedure **(GP)** White solid (86 mg, 78% yield), R_f = 0.3 (petroleum ether/EtOAc 70:30). **^{1}H NMR (400 MHz, $CDCl_3$)** δ 8.12 (dd, *J* = 8.4, 1.2 Hz, 1H), 7.90 (dd, *J* = 8.4, 1.3 Hz, 1H), 7.81 (d, *J* = 8.2 Hz, 1H), 7.63 – 7.49 (m, 2H), 7.54 – 7.40 (m, 3H), 7.45 – 7.32 (m, 2H), 7.32 – 7.20 (m, 2H), 4.05 (dd, *J* = 14.2, 4.2 Hz, 1H), 3.49 (dddd, *J* = 10.2, 9.1, 5.1, 4.1 Hz, 1H), 3.15 (dd, *J* = 14.3, 10.2

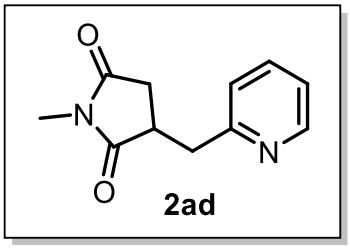
Hz, 1H), 2.77 (dd, *J* = 18.5, 9.0 Hz, 1H), 2.66 (dd, *J* = 18.6, 5.1 Hz, 1H). **$^{13}C\{^{1}H\}$ NMR (100 MHz, $CDCl_3$)** δ 178.5, 175.4, 134.2, 133.6, 132.0, 131.7, 129.3, 129.3, 128.8, 128.3, 127.2, 126.8, 126.6, 126.5, 126.1, 125.6, 123.4, 41.0, 34.5, 34.3. **HRMS (ESI TOF)** *m/z* calcd. For $C_{21}H_{18}NO_2$ $[M + H]^+$ 316.1338 found 316.1336.

1-phenyl-3-(pyren-1-ylmethyl)pyrrolidine-2,5-dione (2ac)



The compound **2ac** was prepared following the general procedure **(GP)** White solid (101 mg, 74% yield), R_f = 0.32 (petroleum ether/EtOAc 70:30). **^{1}H NMR (400 MHz, $CDCl_3$)** δ 8.3 (d, *J* = 9.3 Hz, 1H), 8.2 – 8.1 (m, 3H), 8.1 – 8.1 (m, 2H), 8.0 (dd, *J* = 6.6, 2.1 Hz, 2H), 8.0 (d, *J* = 7.7 Hz, 1H), 7.9 (d, *J* = 7.8 Hz, 1H), 7.5 (td, *J* = 7.3, 6.4, 1.2 Hz, 2H), 7.4 – 7.3 (m, 1H), 7.2 (d, *J* = 3.5 Hz, 1H), 4.3 (dd, *J* = 13.8, 4.0 Hz, 1H), 3.6 – 3.5 (m, 1H), 3.5 (dd, *J* = 13.8, 9.7 Hz, 1H), 2.7 (d, *J* = 1.2 Hz, 1H), 2.7 (s, 1H). **$^{13}C\{^{1}H\}$ NMR (100 MHz, $CDCl_3$)** δ 178.5, 175.3, 132.0, 131.5, 131.2, 130.8, 129.3, 129.1, 128.8, 128.4, 128.0, 127.7, 127.5, 126.6, 126.3, 126.2, 126.1, 125.6, 125.4, 125.0, 124.9, 124.8, 123.2, 122.6, 41.8, 34.5, 34.0. **HRMS (ESI TOF)** *m/z* calcd. For $C_{27}H_{20}NO_2$ $[M + H]^+$ 390.1494 found 390.1491.

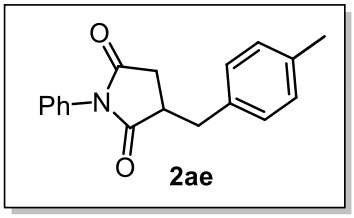
1-methyl-3-(pyridin-2-ylmethyl)pyrrolidine-2,5-dione (2ad)



The compound **2ad** was prepared following the general procedure **(GP)** White solid (74 mg, 80% yield), R_f = 0.31 (petroleum ether/EtOAc 70:30). **^{1}H NMR (400 MHz, $CDCl_3$)** δ 8.45 (ddd, *J* = 4.9, 1.9, 1.0 Hz, 1H), 7.62 – 7.54 (m, 1H), 7.17 – 7.07 (m, 2H), 3.37 – 3.28 (m, 2H), 3.19 – 3.10 (m, 1H), 2.97 (s, 3H), 2.88 – 2.73 (m, 1H), 2.58 (dd, *J* = 18.4, 4.6 Hz, 1H). **$^{13}C\{^{1}H\}$**

NMR (100 MHz, $CDCl_3$) δ 180.0, 177.0, 157.4, 149.5, 136.7, 123.7, 39.4, 37.8, 33.8, 24.9. **HRMS (ESI TOF)** *m/z* calcd. For $C_{11}H_{13}N_2O_2$ $[M + H]^+$ 205.0977 found 205.0969.

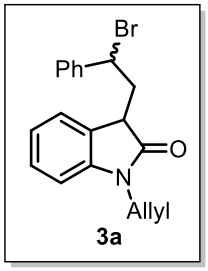
3-(4-methylbenzyl)-1-phenylpyrrolidine-2,5-dione (2ae)



The compound **2ae** was prepared following the general procedure (**GP**) White solid (68 mg, 70% yield), Rf = 0.35 (petroleum ether/EtOAc 70:30). **^{1}H NMR (400 MHz, $CDCl_3$)** δ 7.5 – 7.4 (m, 2H), 7.4 – 7.3 (m, 1H), 7.2 – 7.1 (m, 6H), 3.3 (ddt, *J* = 9.1, 7.9, 4.6 Hz, 1H), 3.2 (dd, *J* = 13.9, 4.6 Hz, 1H), 3.1 (dd, *J* = 13.9, 7.9 Hz, 1H), 2.9 (dd, *J* = 18.5, 9.2 Hz, 1H), 2.6 (dd, *J* = 18.5, 4.7 Hz, 1H), 2.3 (s, 3H). **^{13}C{^{1}H} NMR (100 MHz, $CDCl_3$)** δ 178.51, 175.51, 137.00, 133.63, 131.98, 129.68, 129.27, 129.23, 128.74, 126.59, 41.44, 36.26, 33.40, 21.16. **HRMS (ESI TOF)** *m/z* calcd. For $C_{18}H_{18}NO_2$ $[M + H]^+$ 280.1332 found 280.1338.

3.7.6. Application procedure and Data:

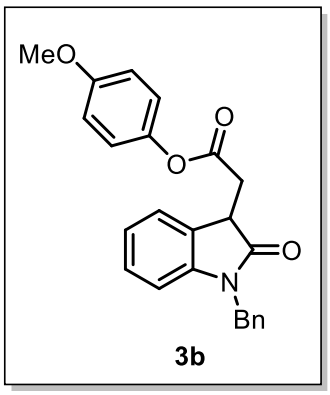
1-Allyl-3-(2-bromo-2-phenylethyl)indolin-2-one (3a)



To an oven dried 10 mL round bottom flask charged with magnetic stir bar was added 1-allyl-3-(2-oxo-2-phenylethyl)indolin-2-one **2a** (0.36 mmol, 1 equiv.), $NaBH_4$ (5 equiv.), THF/H_2O (9:1) 4 mL solution under argon atmosphere. The reaction mixture was stirred at room temperature till the completion of the reaction (monitored by TLC). After which, 10 mL water was added to quench the reaction mixture. The organic layer was extracted with ethyl acetate (3 x10 mL) and the combined extracts was concentrated under reduced pressure. The crude residue was used for the next step without further purification. The residue was further dissolved in dry DCM at 0 ºC under inert condition. To this solution, CBr_4 (1.2 equiv.) and PPh_3 (1.2 equiv.) were added at 0 °C and the reaction mixture was stirred at room temperature for 24 h. After completion of the reaction (monitored by TLC), solvent was removed under

reduced pressure and the crude residue was purified by column chromatography (silica gel 100-200 mesh hexane/ethyl acetate 90: 10) to obtain product **3a** (52 mg, 40% yield) as a white solid. Obtained as diastereomers 80:20 *dr* (inseparable), R_f = 0.6 (petroleum ether/EtOAc 90:10), major diastereomer. **^{1}H NMR (400 MHz, $CDCl_3$)** δ 7.3 – 7.3 (m, 2H), 7.3 – 7.2 (m, 2H), 7.2 – 7.1 (m, 2H), 7.1 (td, *J* = 7.8, 1.2 Hz, 1H), 6.9 (d, *J* = 7.7 Hz, 1H), 6.7 (td, *J* = 7.6, 1.0 Hz, 1H), 6.0 (dd, *J* = 7.5, 1.2 Hz, 1H), 5.9 – 5.8 (m, 1H), 5.3 – 5.2 (m, 2H), 4.5 – 4.4 (m, 2H), 3.4 (t, *J* = 8.6 Hz, 1H), 2.2 (dd, *J* = 9.1, 4.5 Hz, 1H), 2.0 (dd, *J* = 8.0, 4.5 Hz, 1H). **^{13}C{^{1}H} NMR (100 MHz, $CDCl_3$)** δ 176.29, 143.10, 135.23, 131.97, 130.05, 128.49, 128.01, 127.51, 126.57, 121.54, 120.85, 117.51, 108.77, 42.89, 36.14, 33.29, 22.70. **HRMS (ESI TOF)** *m/z* calcd. For $C_{19}H_{19}BrNO$ $[M + H]^+$ 356.0650 found 356.0652.

4-methoxyphenyl 2-(1-benzyl-2-oxoindolin-3-yl)acetate (3b)



3b

To an oven round 10 mL bottom flask charged with magnetic stir bar was added 1-benzyl-3-(2-(4-methoxyphenyl)-2-oxoethyl)indolin-2-one **2l** (0.35 mmol) and CH_2Cl_2/HFIP (2:1, 6 mL). A phosphate buffer (pH 7.6, 0.4 mL) was added to this solution under N_2 atmosphere. Then *m*-CPBA (5 equiv.) was added to the reaction mixture and was stirred at room temperature. After the completion of the reaction (checked by TLC), the solvent was removed under reduced pressure and the crude product was purified by column chromatography (silica gel-100-200 mesh, hexane and ethyl acetate, 80:20) to obtain **3b** as a white solid (68 mg, 50% yield). R_f = 0.5 (petroleum ether/EtOAc 80:20). **^{1}H NMR (400 MHz, $CDCl_3$)** δ 7.36 – 7.32 (m, 1H), 7.32 – 7.27 (m, 2H), 7.25 – 7.17 (m, 4H), 7.03 (td, *J* = 7.6, 1.0 Hz, 1H), 6.84 (s, 4H), 6.73 (d, *J* = 7.8 Hz, 1H), 4.93 (s, 2H), 4.06 – 3.89 (m, 1H), 3.78 (s, 3H), 3.34 (dd, *J* = 16.8, 5.1 Hz, 1H), 3.16 (dd, *J* = 16.8, 7.3 Hz, 1H). **^{13}C{^{1}H} NMR (100 MHz, $CDCl_3$)** δ 176.76, 170.09, 157.4, 144.0, 143.7, 135.7, 128.8, 128.5, 127.8, 127.7, 127.4, 124.1, 122.8, 122.3, 114.5, 109.4, 55.7, 44.1, 42.0, 35.2. **HRMS (ESI TOF)** *m/z* calcd. For $C_{24}H_{22}NO_4$ $[M + H]^+$ 388.1549 found 388.1547.

3.8. Appendix III: ^{1}H, ^{13}C and ^{19}F spectra of representative compounds

Compound No.	Figure AIII.X	Data	Page No.
2a	Figure AIII.1 and AIII.2	^{1}H and ^{13}C	122
2q	Figure AIII.3, AIII.4, AIII.5	^{1}H, ^{13}C, and ^{19}F	123
2w	Figure AIII.6 and AIII.7	^{1}H and ^{13}C	125
3a	Figure AIII.8 and AIII.9	^{1}H and ^{13}C	126
3b	Figure AIII.10 and AIII.11	^{1}H and ^{13}C	127

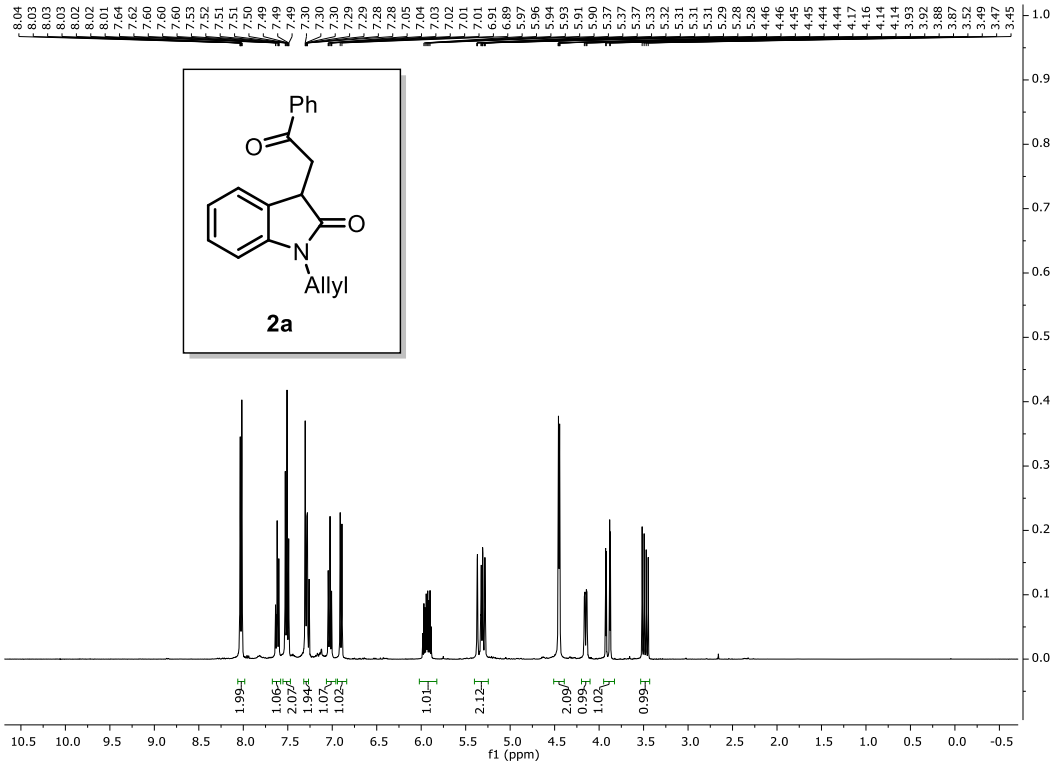


Figure AIII.1 ^{1}H NMR (400 MHz, $CDCl_3$) spectrum of compound **2a**

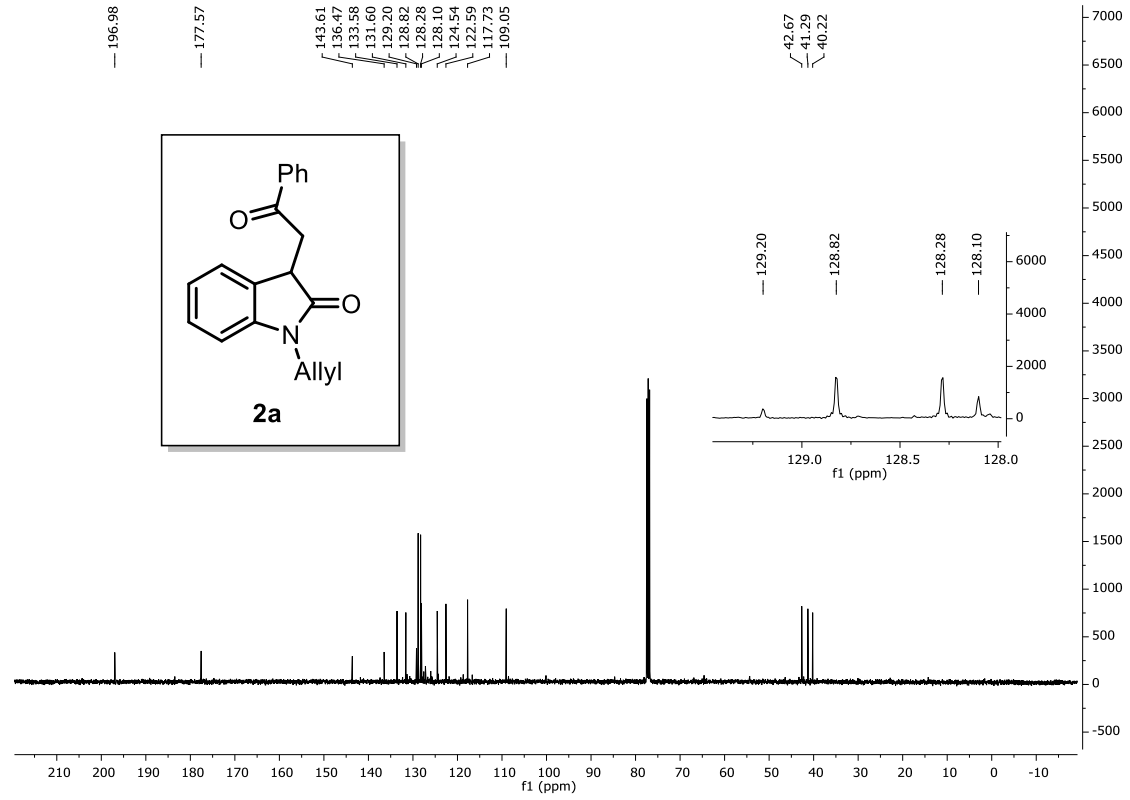


Figure AIII.2 ^{13}C NMR (100 MHz, $CDCl_3$) spectrum of compound **2a**

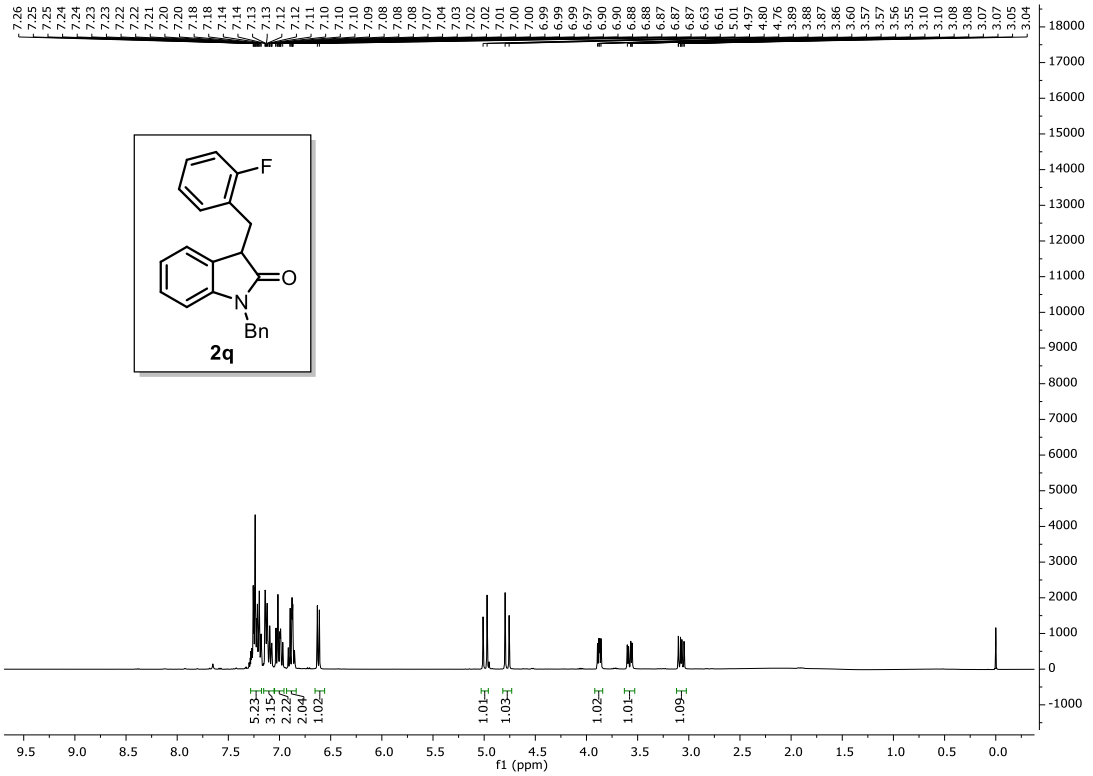


Figure AIII.3 ^{1}H NMR (400 MHz, $CDCl_3$) spectrum of compound **2q**

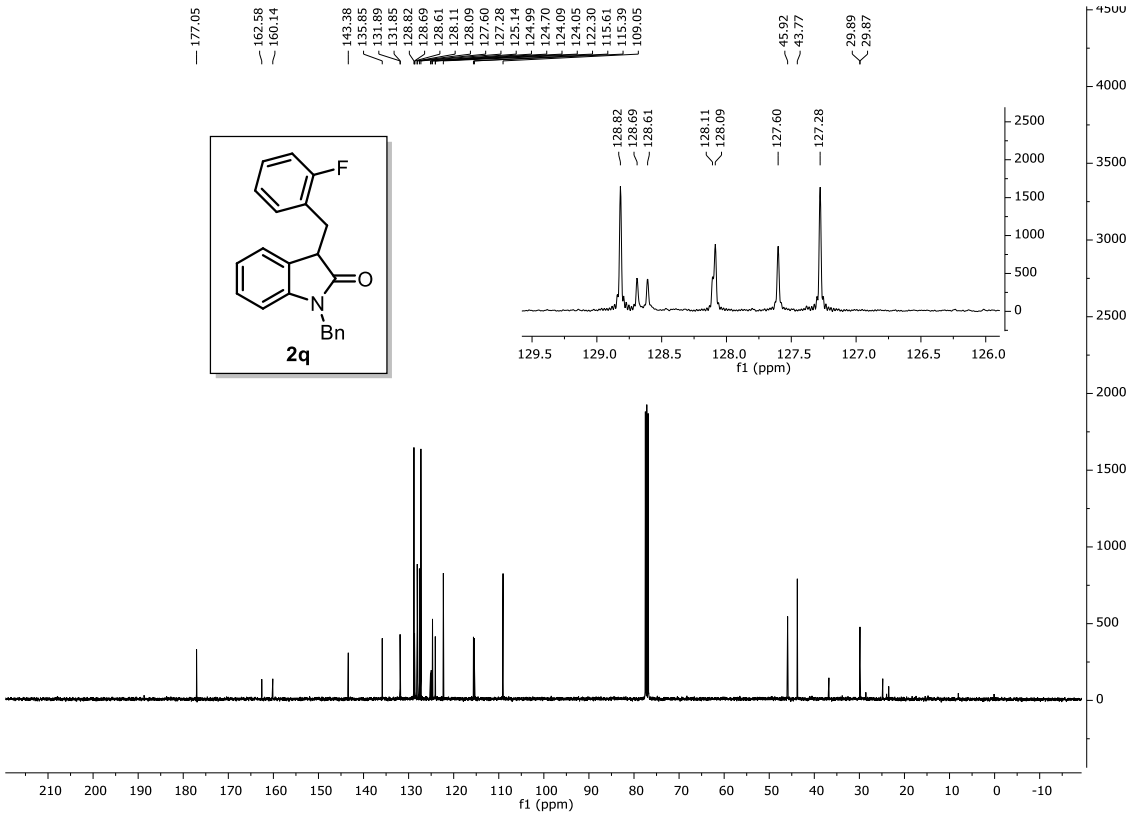


Figure AIII.4 ^{13}C NMR (100 MHz, $CDCl_3$) spectrum of compound **2q**

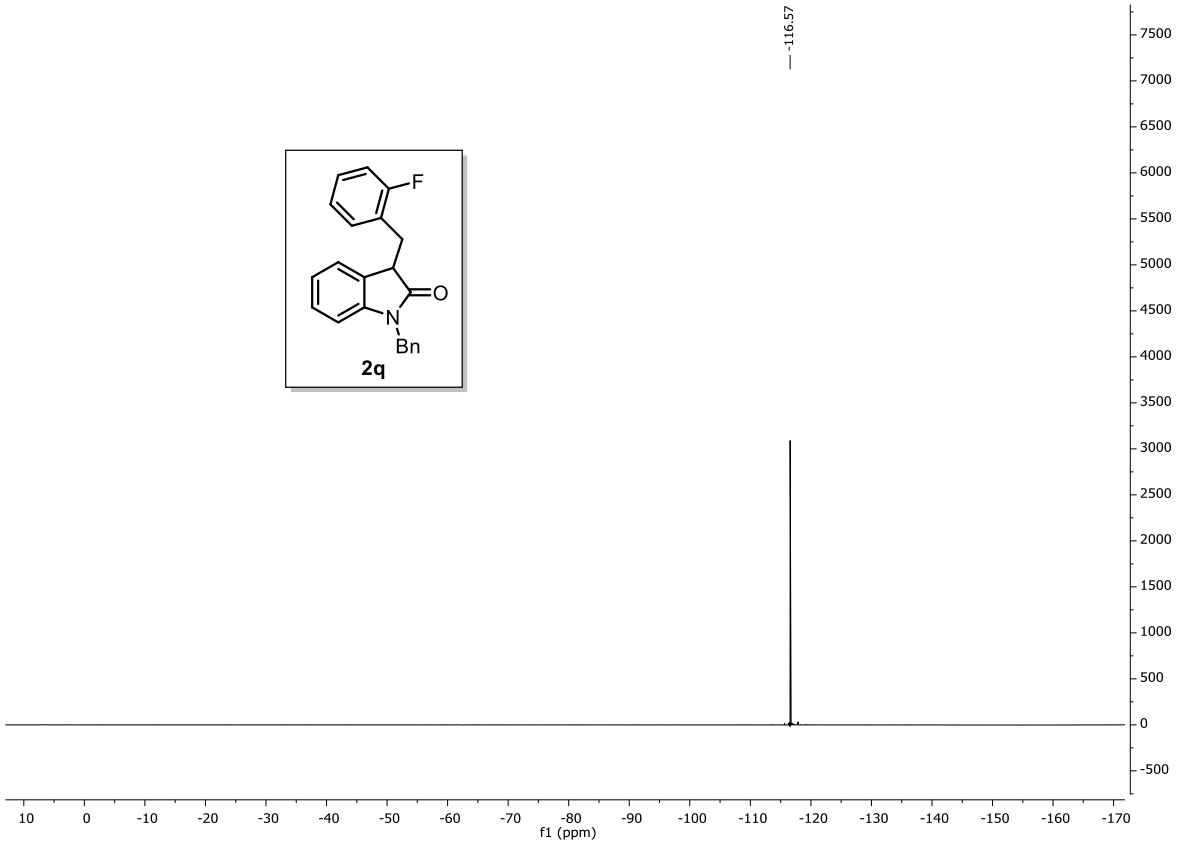


Figure AIII.5 ^{19}F NMR (377 MHz, $CDCl_3$) spectrum of compound **2q**

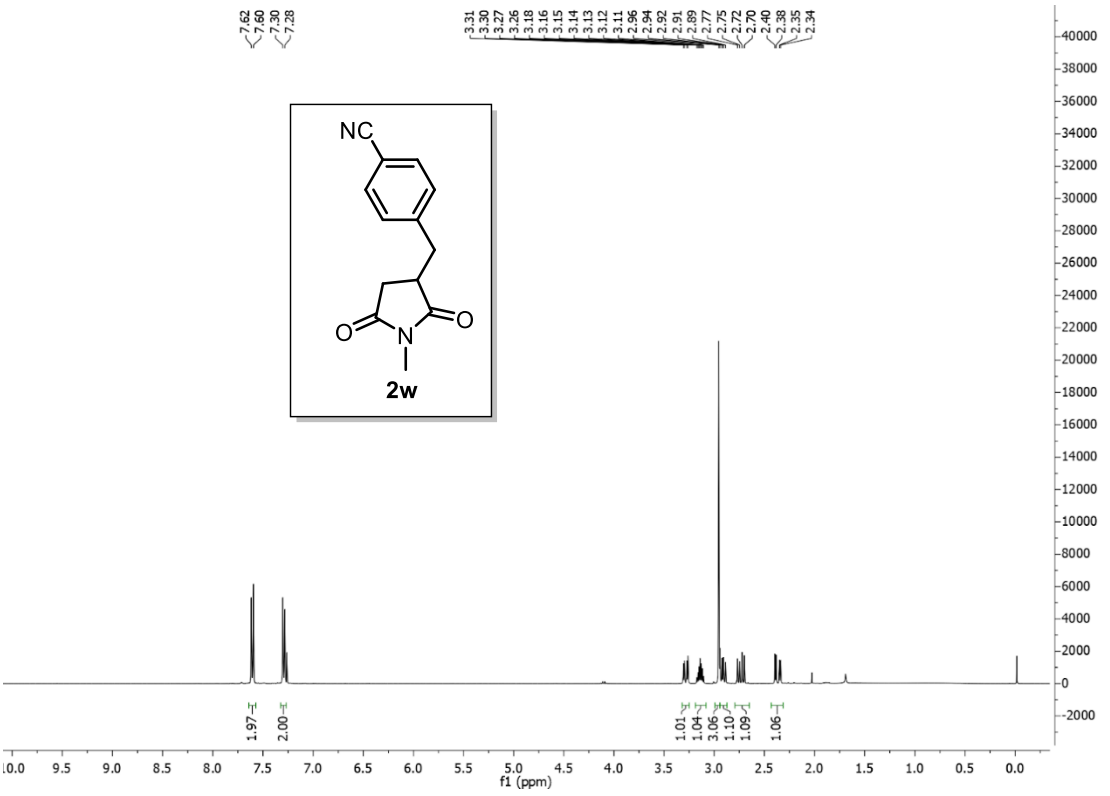


Figure AIII.6 ^{1}H NMR (400 MHz, $CDCl_3$) spectrum of compound **2w**

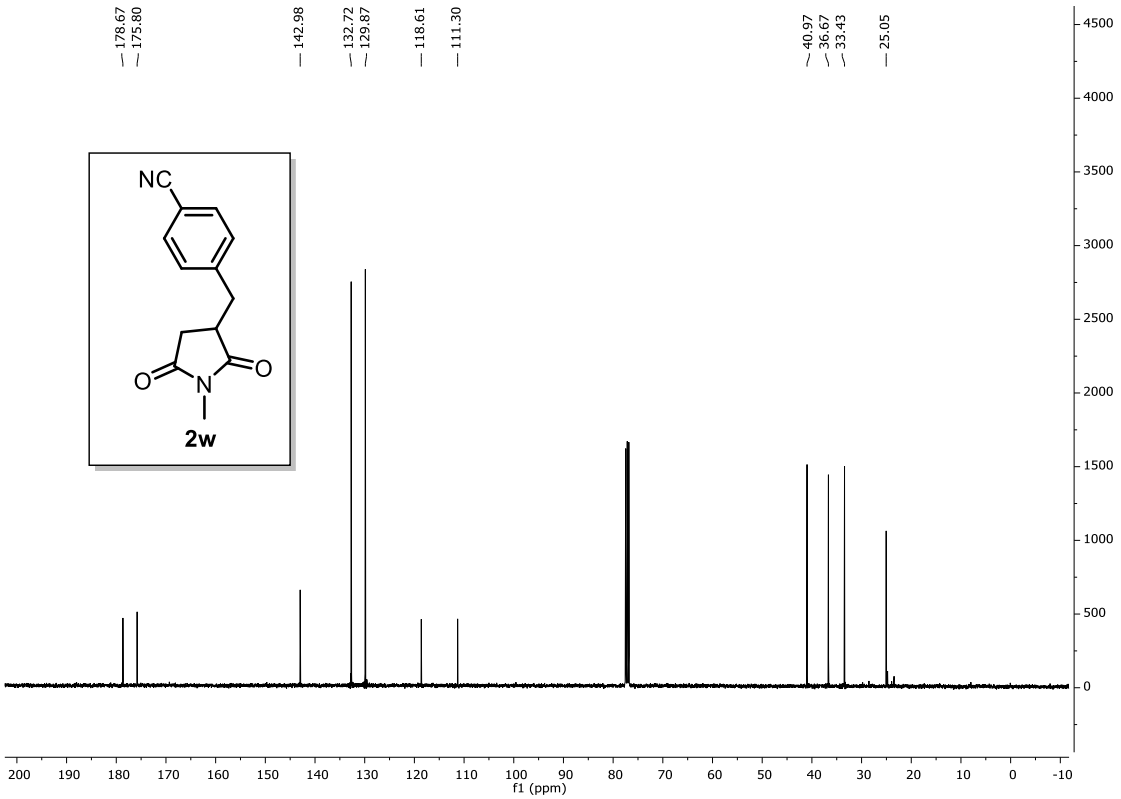


Figure AIII.7 ^{13}C NMR (100 MHz, $CDCl_3$) spectrum of compound **2w**

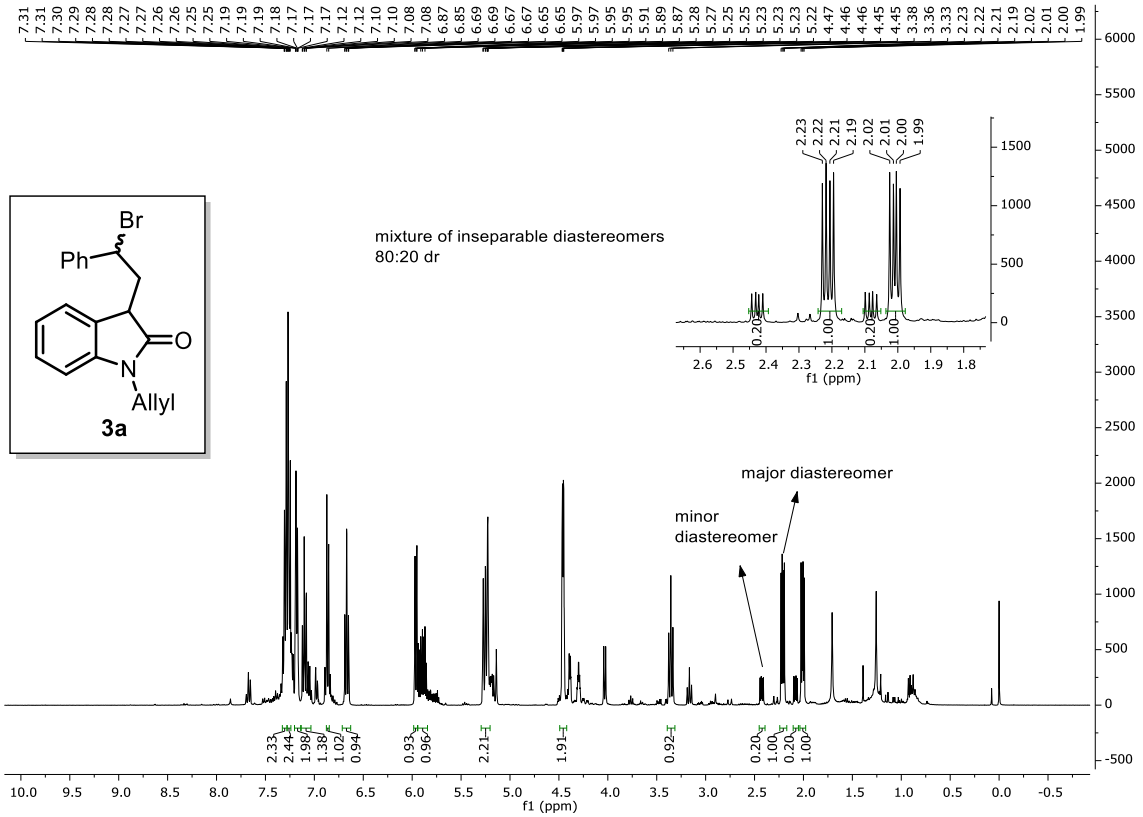


Figure AIII.8 ^{1}H NMR (400 MHz, $CDCl_3$) spectrum of compound **3a**

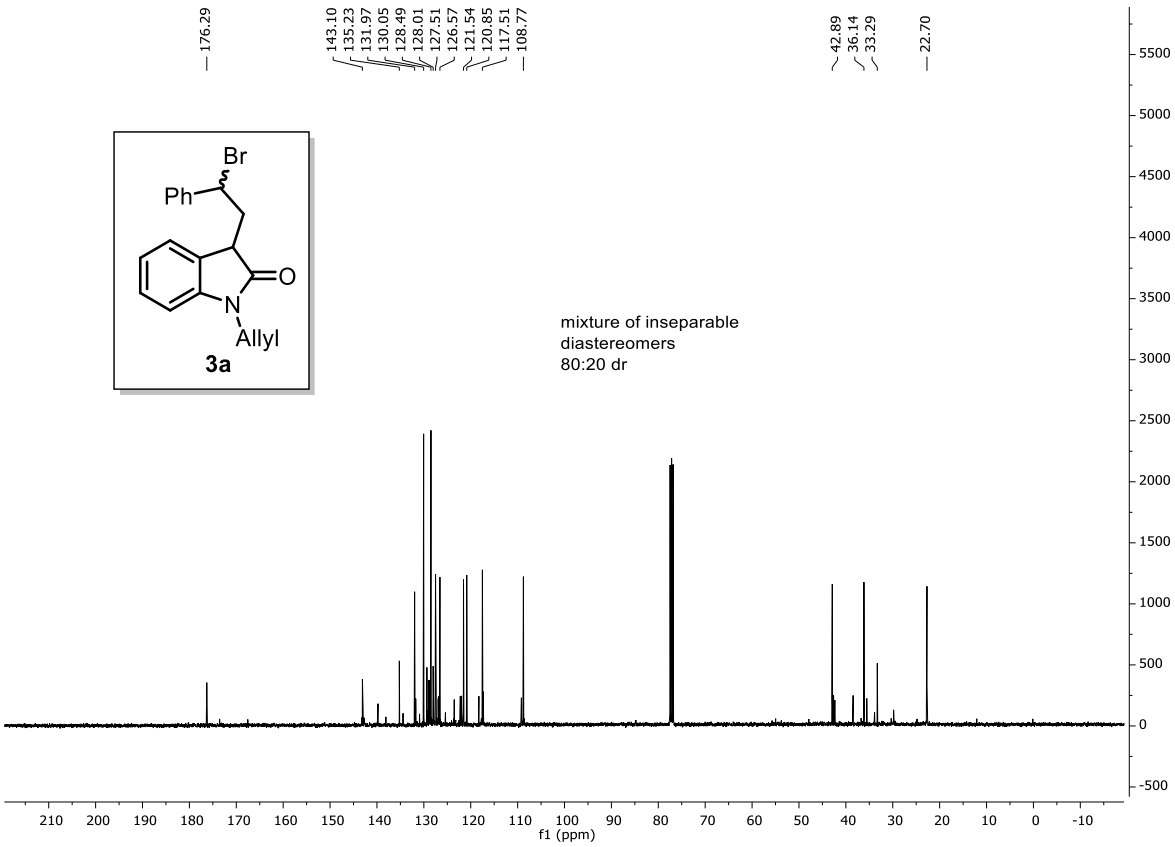


Figure AIII.9 ^{13}C NMR (100 MHz, $CDCl_3$) spectrum of compound **3a**

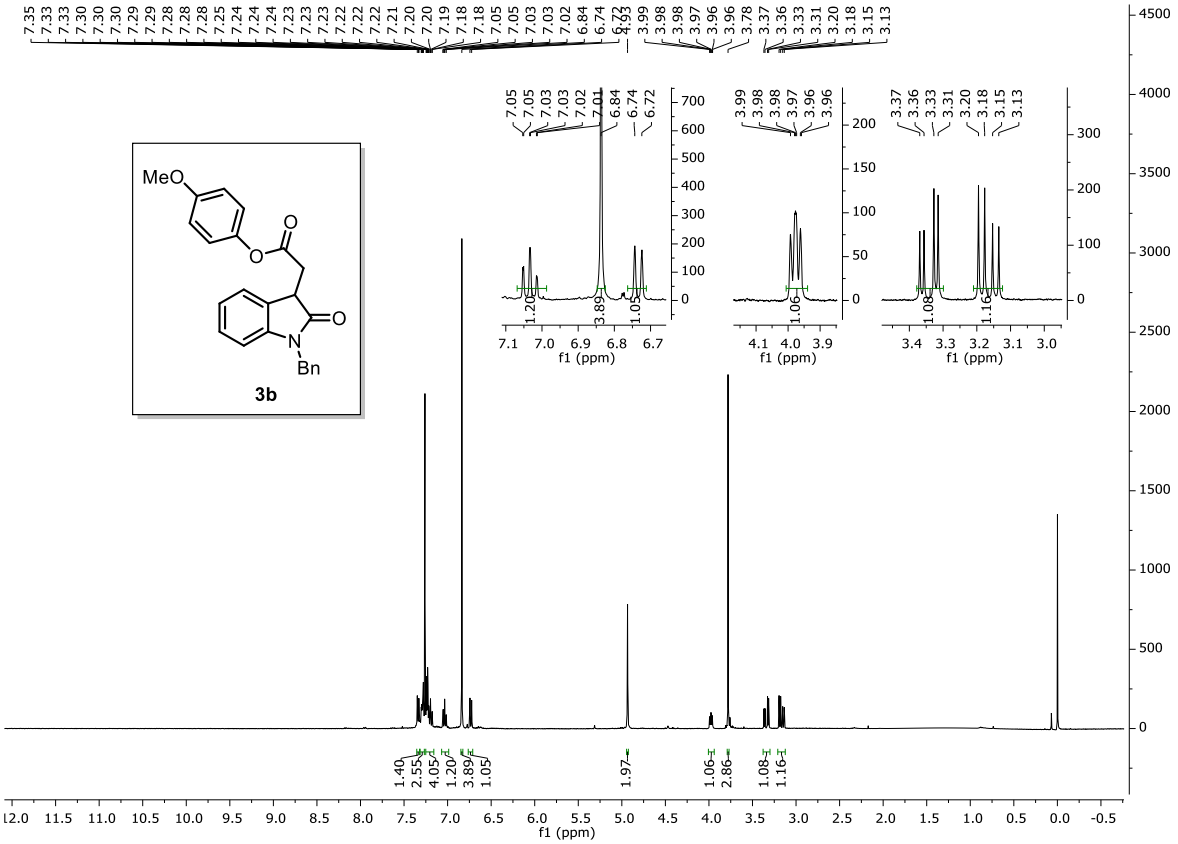


Figure AIII.10 ^{1}H NMR (400 MHz, $CDCl_3$) spectrum of compound **3b**

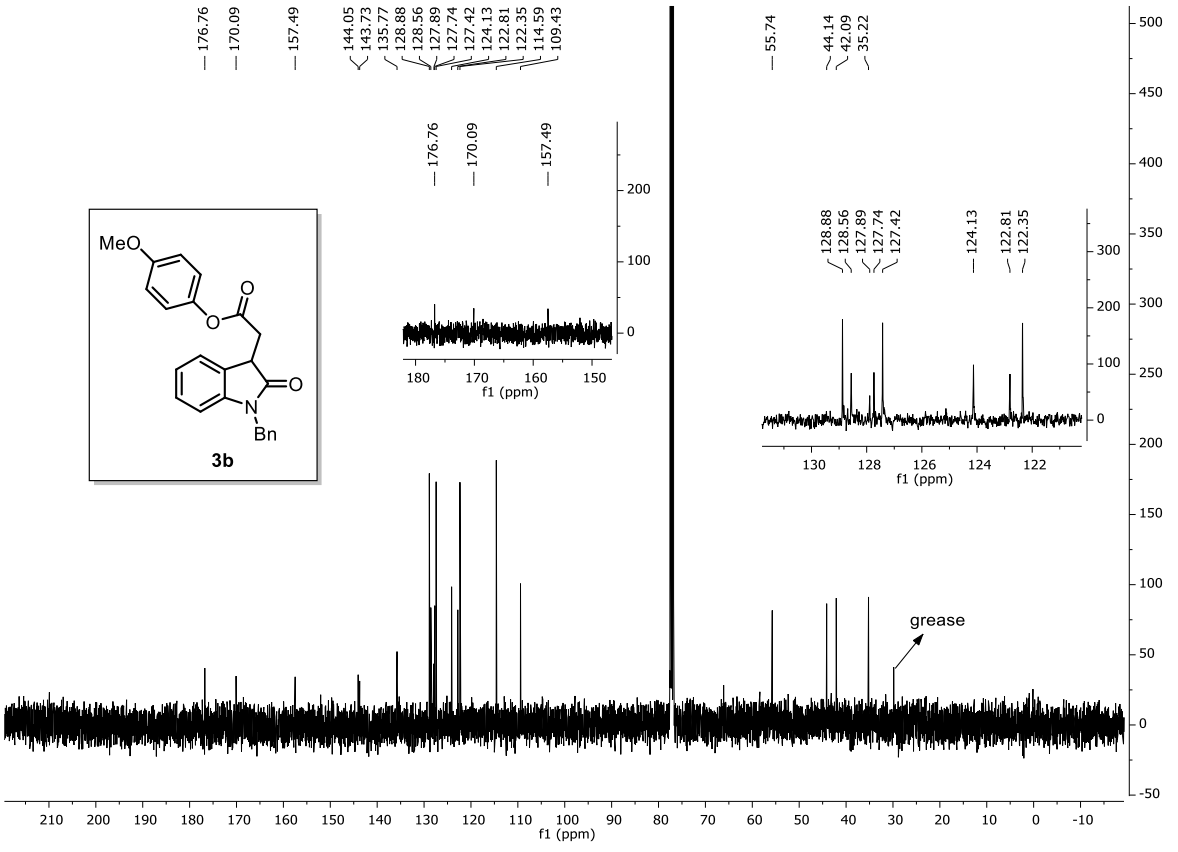


Figure AIII.11 ^{13}C NMR (100 MHz, $CDCl_3$) spectrum of compound **3b**

3.9. References:

[1] (a) Sabatier, P.; Nye, M. J. *Chem. World* **2004**, *1*, 46 –49; (b) Sabatier, P.; La Catalyse en chimie organique, Paris, Branger, **1913**; (c) Wilkinson, G. *Bull. Soc. Chim. Fr*. **1968**, *12*, 5055 – 5058.

[2] Handbook of Homogeneous Hydrogenation (Eds.: de Vries, J. G.; C. J. Elsevier), Wiley-VCH, Weinheim, **2006**.

[3] (a) "Enoate reductase family": Steinbacher, S.; Stumpf, M.; Weinkauf, S.; Rohdich, F.; Bacher, A.; H. Simon in Flavins and Flavoproteins (Eds.: S. K. Chapman, R. N. Perham, N. S. Scrutton, R. Weber), deGruyter, *Berlin*, **2002**, 941–949. (b) Brewster, R. C.; Suitor, J. T.; Bennett, A. W.; Wallace, S. *Angew. Chem. Int. Ed*. **2019**, *58*, 12409–12414.

[4] (a) Hudlický, M. Reductions in Organic Chemistry, 2nd ed., American Chemical Society, Washington, **1996**. (b) Noyori, R. *Angew. Chem*. **2002**, *114*, 2108 – 2123; *Angew.Chem. Int. Ed*. **2002**, *41*, 2008 – 2022; (c) Knowles, W. S. *Angew.Chem*. **2002**, *114*, 2096 – 2107; *Angew. Chem. Int. Ed*. **2002**, *41*,1998 – 2007.

[5] (a) Yutaka, N.; Yasuhiko, M.; Sawako, H.; Akiya, O.; Noboru, S. *Bull. Chem. Soc. Jpn*. **1989**, *62*, 1682–1684, (b) Yang, J. W.; Hechavarria Fonseca, M. T.; List, B. *Angew. Chem. Int. Ed*. **2004**, *43*, 6660–6662; (c) Imada, Y.; Kitagawa, T.; Ohno, T.; Iida, H.; Naota, T. *Org. Lett*. **2010**, *12*, 32–35, (d) Sugiura, M.; Sato, N.; Sonoda, Y.; Kotani, S.; Nakajima, M. *Chem. Asian J*. **2010**, *5*, 478– 481, (e) Xia, X.; Lao, Z.; Toy, P. H. *Synlett* **2019**, *30*, 1100–1104, (f) Sugiura, M.; Ashikari, Y.; Takahashi, Y.; Yamaguchi, K.; Kotani, S.; Nakajima, M. *J. Org. Chem*. **2019**, *84*, 11458–11473.

[6] (a) Rubin, M.; Schwier, T.; Gevorgyan, V. *J. Org. Chem*. **2002**, *67*, 1936–1940; (b) Blackwell, J. M.; Sonmor, E. R.; Scoccitti, T.; Piers, W. E. *Org. Lett*. **2000**, *2*, 3921–3923; (c) Berkefeld, A.; Piers, W. E.; Parvez, M. *J. Am. Chem. Soc*. **2010**, *132*, 10660 10661; (d) Piers, W. E.; Chivers, T. *Chem. Soc. Rev*. **1997**, *26*, 345–354; (e) Piers, W. E.; Marwitz, A. J. V.; Mercier, L. G. *Inorg. Chem*. **2011**, *50*, 12252 – 12262.

[7] Lam, J.; Szkop, K. M.; Mosaferi, E.; Stephan, D. W. *Chem. Soc. Rev*. **2019**, *48*, 3592–3612.

[8] (a) Burnett, M. G.; Oswald, T.; Walker, B. J.*; J. Chem. Soc. Chem. Commun*. **1977**, 155–156. (b) Pal, B.; Pradhan, P. K.; Jaisankar, P.; Giri, V. S. *Synthesis* **2003**, 1549–1552, (c) Cao, S. -H.; Zhang, X. -C.; Wei, Y.; Shi, M. *Eur. J. Org. Chem*. **2011**, 2668–

2672, (d) Kato, T.; Matsuoka, S. -i.; Suzuki, M. *Chem. Commun*. **2015**, *51*, 13906–13909.

[9] (a) Skubi, K. L.; Blum, T. R.; Yoon, T. P. *Chem. Rev*. **2016**, *116*, 10035–10074; (b) Romero, N. A.; Nicewicz, D. A. *Chem. Rev*. **2016**, *116*, 10075–10166, (c) Shaw, M. H.; Twilton, J.; MacMillan, D. W. C. *J. Org. Chem*., **2016**, *81*, 6898–6926, (d) Strieth-Kalthoff, F.; James, M. J.; Teders, M.; Pitzer, L.; Glorius, F. *Chem. Soc. Rev*. **2018**, *47*, 7190–7202.

(e) J. R. Chen, X. Q. Hu, L. Q. Lu, W. J. Xiao, *Chem. Soc. Rev*. **2016**, *45*, 2044-2056; (f) H. Zhao, D. Cheng, X. Xu. *Chin. J. Org. Chem.* **2021**, *41*, 642-660.

[10] (a) Zhong, J. -J.; Wu, C. -J.; MengGao, Q. -Y.; X. -W.; Lei, T.; Tung, C. -H.; Wu, L. -Z. *Adv. Synth. Catal*. **2014**, *356*, 2846– 2852; (b) Zhong, J. -J.; Liu, Q.; Wu, C. -J.; Meng, Q. -Y.; Gao, X. -W.; Li, Z. -J.; Chen, B.; Tung, C. -H.; Wu, L. -Z. *Chem. Commun*. **2016**, *52*, 1800–1803.

[11] (a) Pac, C.; Ihama, M.; Yasuda, M.; Miyauchi, Y.; Sakurai, H. *J. Am. Chem. Soc*. **1981**, *103*, 6495−6497. (b) Pac, C.; Miyauchi, Y.; Ishitani, O.; Ihama, M.; Yasuda, M.; Sakurai, H. *J. Org. Chem*. **1984**, *49*, 26 –34.

[12] (a) Zhou, F.; Liu, Y. -L.; Zhou, J. *Adv. Synth. Catal*. **2010**, *352*, 1381 –1407, (b) Schmid, J.; Junge, T.; Lang, J.; Frey, W.; Peters, R. *Angew. Chem. Int. Ed*. **2019**, *16*, 5447-5451. (c) Galzerano, P.; Bencivenni, G.; Pesciaioli, F.; Mazzanti, A.; Giannichi, B.; Sambri, L.; Bartoli, G.; Melchiorre, P. *Chem. - Eur. J.* **2009**, *15*, 7846−7849; (d) Khetmalis, Y. M.; Shivani, M.; Murugesan, S.; Chandra Sekhar, K. V. G. Biomed. Pharmacother. **2021**, *141*, 111842−111860.

[13] Gandikota, N. M.; Bolla, R. S.; Bandyopadhyay, A.; Kasi Viswanath, I. V. *Russ. J. Org. Chem.* **2019**, *55*, 1197–1203.

[14] Liu, Y.; Mao, Y.; Hu, Y.; Gui, J.; Wang, L.; Wang, W.; Zhang, S. *Adv. Synth. Catal*. **2019**, *361*, 1554−1558.

[15] Liu, Y.; Zhang, W. *Angew. Chem. Int. Ed*. **2013**, *52*, 2203-2206.

[16] (a) Massari, S.; Desantis, J.; Nannetti, G.; Sabatini, S.; Tortorella, S.; Goracci, L.; Cecchetti, V.; Loregian A.; Tabarrini, O. *Org. Biomol. Chem*., **2017**, *15*, 7944–7955; (b) Cao, S. H.; Zhang, X. C.; Wei, Y.; Shi, M. *Eur. J. Org. Chem*. **2011**, 2668-2672; (c) Raji Reddy, C.; Ganesh V.; Singh, A. K. *RSC Adv*., **2020**, *10*, 28630–28634; (d) Laha, D.; Bhat, R. G. *Asian J. Org. Chem*. **2020**, *9*, 918-921.

[17] (a) Srivastava, V.; Singh, P. P. *RSC Adv*. **2017**, *7*, 31377-31392. (b) Hari, D.; König, B. *Chem. Commun.* **2014**, *50*, 6688-6699.

[18] (a) Beatty, J.-W.; Stephenson, C.-R. *Acc. Chem. Res*. **2015**, *48*, 1474−1484. (b) Schmallegger, M.; Gescheidt, G.; *Monatsh. Chem*. **2018**, *149*, 499–504.

[19] Leng, H.; Zhao, Q.; Mao,Q.; Liu, S.; Luo, M.; Qin, R.; Huang, W.; Zhan, G. *Chin. Chem. Lett*. **2021**, *32*, 2567−2571.

[20] Larin, E. M.; Masson-Makdissi, J.; Jin Jang, Y.; Lautens, M. *ACS Catal*. **2022**, *20*, 12744–12749.

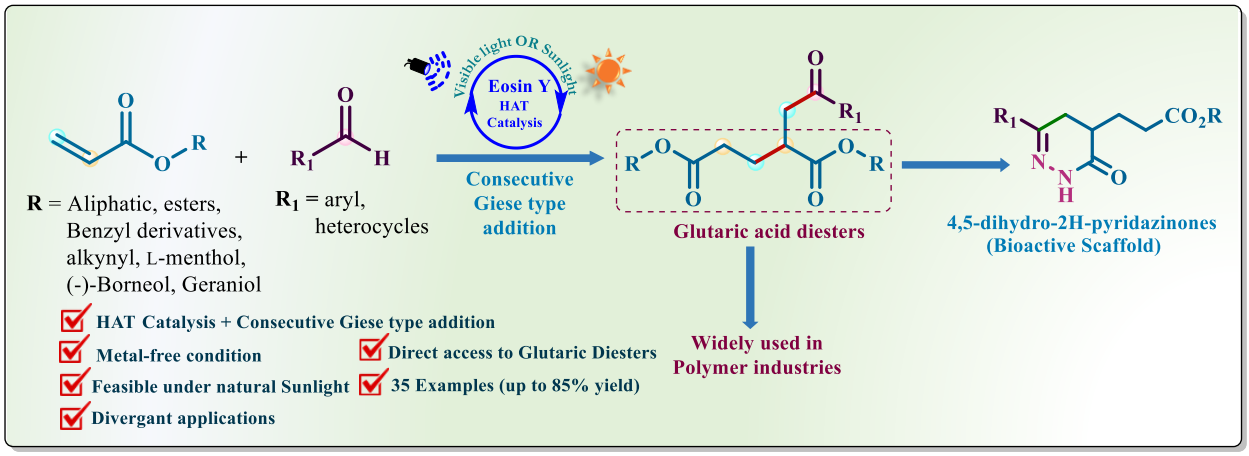
[21]

CHAPTER 4

Synthesis of Industrially Significant Glutaric Acid Diesters from Aldehydes via Sequential Giese-Type Addition Under Visible Light Illumination

Abstract

A direct and practical approach has been devised for obtaining α-substituted glutaric diesters from acrylates and aldehydes by employing visible light, where Eosin Y aids in hydrogen atom transfer (HAT) and subsequent Giese-type addition. Additionally, this method has been investigated for producing substituted 4,5-dihydro-2H-pyridazinones, compounds with promising applications in both biological and industrial fields. Detailed mechanistic studies have been conducted to comprehensively understand the process.



Bhowmick, A.; Chatterjee, A.; Pathaka, S. S.; Bhat, R. G. *Chem. Commun*., **2023**, *59*, 11875-11878.

Synthesis of Industrially Significant Glutaric Acid Diesters from Aldehydes via Sequential Giese-type Addition Under Visible Light Illumination

4.1. Introduction:

Esters represent one of the most prevalent functional groups encountered in both synthetic and naturally existing organic compounds [1]. These compounds and their various derivatives are widely distributed in natural substances, pharmaceuticals, polymer materials, and fine chemicals [2]. Dicarbonyl frameworks are commonly encountered in both bioactive substances and naturally occurring compounds (see figure 1) [3]. Specifically, 1,4-dicarbonyl compounds are prevalent in numerous natural products and bioactive agents [4]. These substances serve as valuable and fundamental components for crafting a variety of biologically active five-membered heterocyclic compounds, including furans, pyrroles, thiophenes, and cyclopentenones [5]. Moreover, 1, 5-dicarbonyl [6] and 1, 6-dicarbonyl compounds [7] also play pivotal roles as crucial intermediates in organic synthesis, enabling the construction of diverse and intricate molecular structures. Notably, glutaric acid and its derivatives have played a significant role as primary starting materials for the synthesis of valuable 1, 5-pentanediols, which hold significant importance in various industrial applications. Through hydrogenation of glutaric diesters, 1, 5-pentanediol is produced and serves as a fundamental raw material for the manufacturing of polyurethane coatings, polyester resins, and polycarbonate diol resins [8]. Glutaric acid is indeed a highly versatile compound, playing a crucial role as a significant precursor for the production of polymers like polyester polyols and polyamides. Furthermore, glutaric diester serves as a important starting material for synthesizing pyrogallol (1, 2, 3-trihydroxybenzene), a commercially important compound with a wide range of applications [9]. Given the extensive uses of 1, 4-, 1, 5-, and 1, 6-dicarbonyl compounds in organic synthesis, substantial efforts have been dedicated to the synthesis of these dicarbonyl compounds as valuable building blocks.

For instance, γ-ketoesters (1, 4-dicarbonyl compounds) have traditionally been synthesized by the conjugate additions of acyl anion equivalents to the Michael acceptors [10]. Alternatively, in recent years, effective strategies such as oxidative couplings [11], umpolung reactions [12a-12c], both homo- and hetero-enolate coupling reactions [12d-12f], and radical-based transformations [12g-12i] have emerged as efficient methods for generating 1, 4-

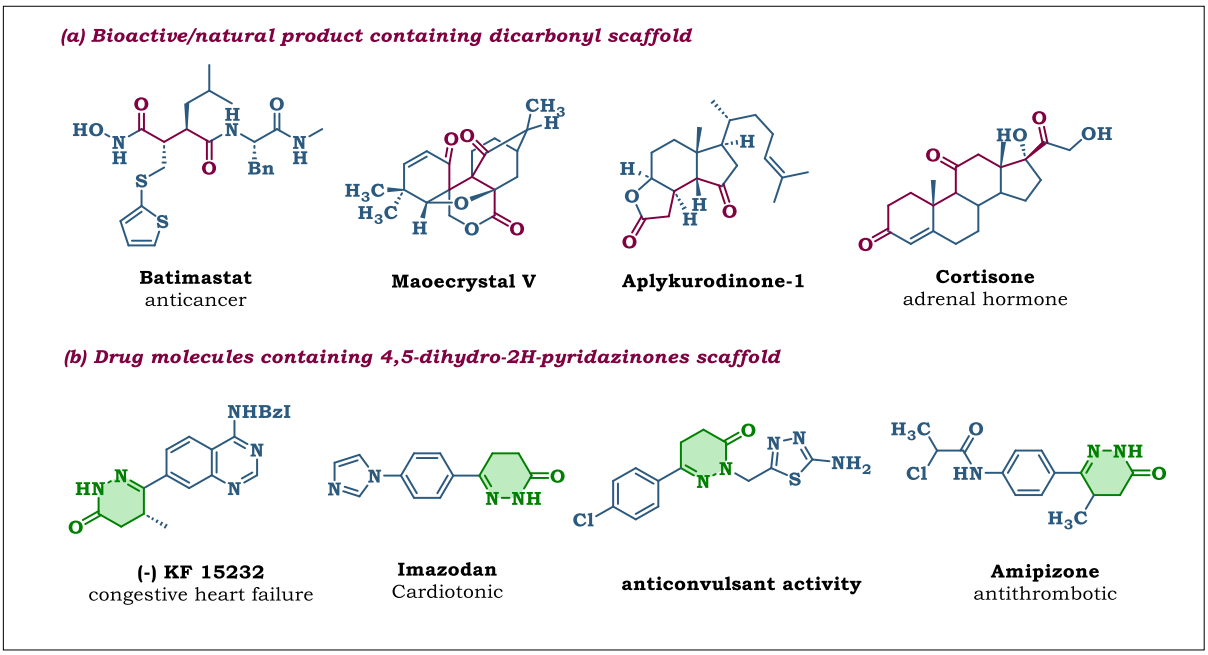


Figure 1. Bioactive compounds containing dicarbonyl and 4, 5-dihydro-2*H*-pyridazinones scaffold

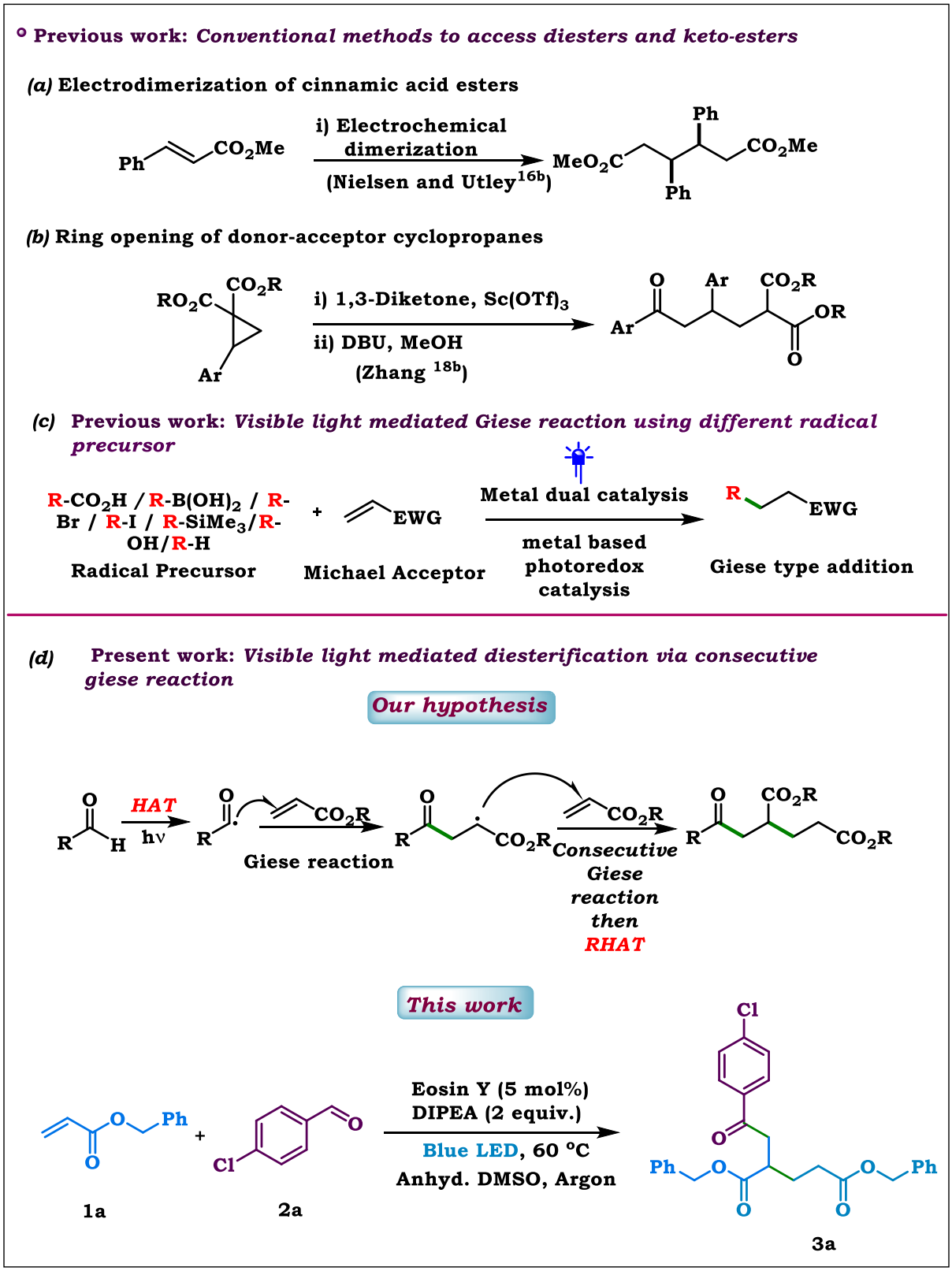
dicarbonyl derivatives. Similarly, the synthesis of glutaric acid (1, 5-dicarbonyl) has been accomplished through the ring-opening reaction of butyrolactone in the presence of potassium cyanide under elevated temperature conditions [13]. Traditionally, the synthesis of 1, 5-dicarbonyl compounds has followed the traditional path of employing the Claisen-Schmidt condensation, followed by the Michael addition of aryl methyl ketones to derivatives of benzaldehyde under alkaline conditions [14]. Similarly, 1, 6-dicarbonyl compounds hold significance as essential intermediates in organic synthesis [15].

4.2. Previous reports on the synthesis of dicarbonyl compounds:

Due to the distinct polarizing effect created by the presence of two carbonyl groups, the retrosynthetic modification of the dicarbonyl scaffold poses a relatively complex challenge. Consequently, numerous synthetic approaches rely on the dimerization of α, β-unsaturated carbonyl compounds as a means to access 1, 6-dicarbonyl compounds (Scheme 1a) [16]. These compounds have been generated through a process that involves the oxidative cleavage of substituted cyclohexene derivatives [17]. However, it's worth noting that this method has its limitations, particularly regarding the range of substrates it can effectively handle. Another efficient approach for building the 1, 6-dicarbonyl framework is through a ring-opening reaction that utilizes donor-acceptor (D-A) cyclopropanes in conjunction with enolate nucleophiles, as depicted in Scheme 1b [18]. While many of the aforementioned methods are intriguing, they

are often constrained by their applicability to only certain substrates, yielding lower results, necessitating harsh reaction conditions, and most notably, relying on the use of

Scheme 1. Access to industrially relevant dicarbonyl compounds and diesters



bulky transition metal reagents. These factors collectively curtail their broader usefulness in organic synthesis.

In the past twenty years, visible light-mediated photoredox catalysis has earned extensive acclaim as a potent technique in organic synthesis. It has proven instrumental in facilitating a multitude of intriguing transformations that were previously challenging or unattainable through conventional synthetic approaches. Photocatalysis encompasses multiple mechanistic pathways, including single-electron transfer (SET), energy transfer (EnT), hydrogen atom transfer (HAT), and proton-coupled electron transfer (PCET) processes. These pathways facilitate the conversion of photon energy into chemical energy, driving various reactions. Recently, diverse photoinduced esterification approaches have been documented [19]. An alternative, convenient, and cost-effective route involves the direct utilization of organic dyes under visible light irradiation.

This approach enables direct C-H bond functionalization without the need for metal catalysts or co-catalysts. Furthermore, appropriate organic dyes or organic photocatalysts are user-friendly, commercially accessible, cost-effective, and environmentally benign due to their non-toxic nature. Notably, there has been recent exploration into leveraging the photocatalytic and hydrogen atom transfer (HAT) capabilities of xanthene-based dyes to achieve successful photoredox catalytic transformations [20].

The Giese reaction, which involves the conjugate addition of alkyl radicals to electron-deficient alkenes, leading to the formation of new $C(sp^3)$-$C(sp^3)$ carbon-carbon bonds, is widely recognized [21]. This radical addition reaction has the distinct advantage of allowing for the selective incorporation of alkyl groups, making it a valuable tool in the synthesis of natural compounds and pharmaceuticals [22]. Of particular note is the visible light-mediated Giese-type reaction, which has garnered significant attention. This reaction facilitates the generation of alkyl or acyl radicals under mild reaction conditions, utilizing readily available pre-functionalized compounds, as depicted in Scheme 1c [23]. The conventional Giese reaction entails the creation of alkyl radicals from pre-functionalized organohalides, employing silyl radicals, stannyl radicals, or transition metal catalysts. However, the reliance on these pre-functionalized starting materials imposes constraints on the broader applicability of these protocols in organic synthesis. Moreover, the generation of alkyl radicals using these starting materials often results in the production of substantial amounts of halogenated waste. Consequently, there is a pronounced need for the design and development of efficient methods capable of generating alkyl radicals from readily accessible starting materials. This would

enable access to synthetically valuable structural frameworks while mitigating the environmental impact associated with halogenated waste production.

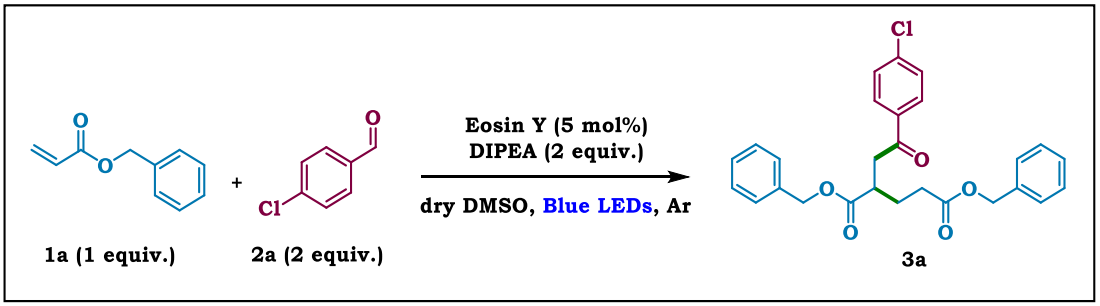
4.3. Our hypothesis and optimization of glutaric acid diester synthesis:

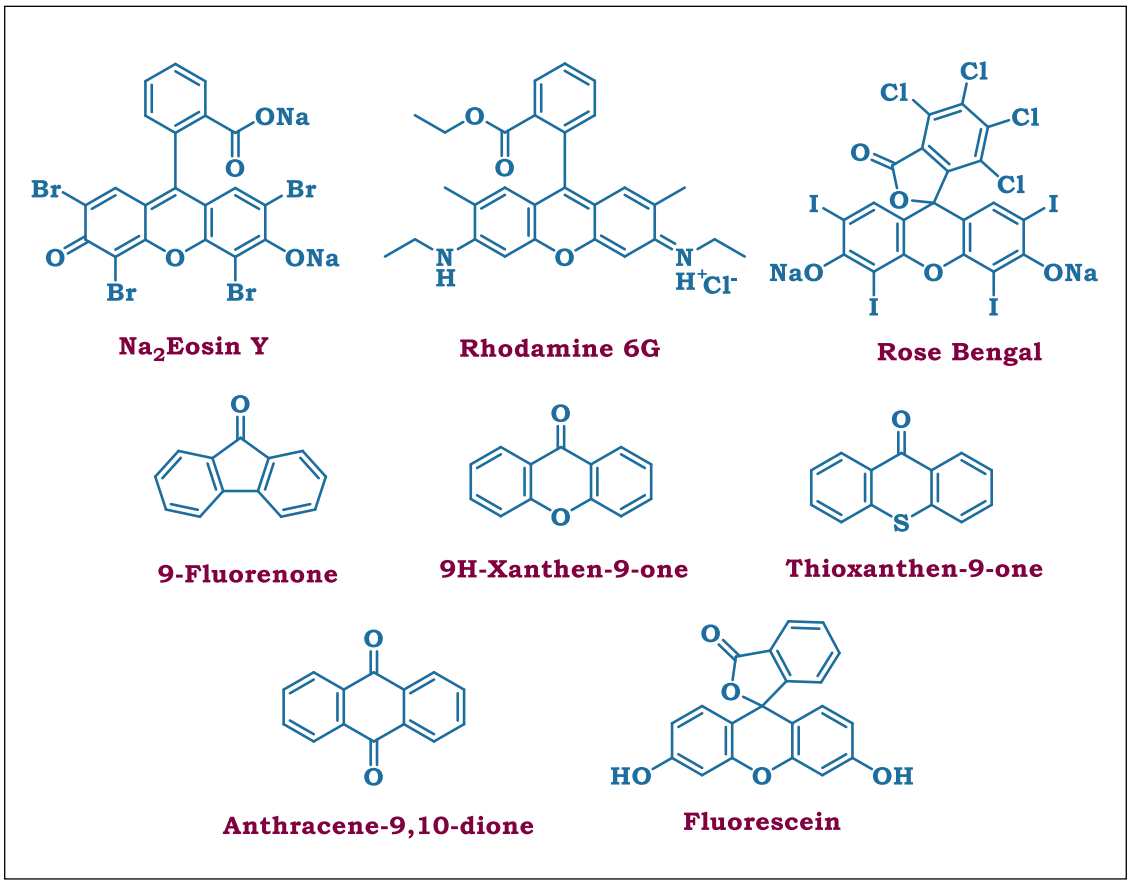
In recent years, our research has been focused on photoredox catalysis, and we've proposed the idea that under appropriate photoredox conditions, acrylates and aldehydes could directly yield valuable diesters through a hydrogen atom transfer (HAT) process. We are pleased to present a innovative procedure, being reported here for the first time, for synthesizing α-aroyl glutaric diesters. This method begins with aldehydes and acrylates, leveraging the HAT capability of Eosin Y, and proceeds with a Giese-type consecutive addition via photoredox catalysis under metal-free conditions, as depicted in Scheme 1d. Notably, these Giese-type reactions result in the formation of two new C-C bonds in a single reaction vessel.

To validate our hypothesis, we initiated our research by conducting optimization studies using benzyl acrylate **1a** and 4-chlorobenzaldehyde **2a** as model substrates. After a thorough and systematic exploration of the photocatalysis process, it was determined that employing Eosin Y as a HAT catalyst, along with DIPEA as an additive, in anhydrous DMSO under an inert atmosphere, and utilizing a blue LED (456 nm) yielded favourable results in obtaining the desired glutaric diester, specifically dibenzyl 2-(2-(4-chlorophenyl)-2-oxoethyl) pentanedioate (**3a**), with a high yield of 80% (as shown in **Table 1**, **Entry 1**). Substituting DIPEA with various other bases in the reaction resulted in a reduction in the yield of the desired product **3a**, as indicated in **Table 1**, **Entries 2-9**. We also noticed that when using other metal-based photocatalysts, the expected product **3a** was not obtained (**Table 1**, **Entries 10-11**). However, when employing various organic photocatalysts, the desired diester **3a** was produced, albeit with reduced yields (**Table 1**, **Entries 12-19**). Subsequently, we conducted a solvent screening experiment under optimized reaction parameters. It became evident that the yield of **3a** decreased significantly with different solvents (**Table 1**, **Entries 20-24**). Among all the solvents tested, anhydrous DMSO emerged as the most favourable choice for achieving a higher yield of **3a** (**Table 1**, **Entry 1**). When we conducted the reaction without DIPEA and with Na_2EosinY as the catalyst instead of Eosin Y, the desired product **3a** was obtained in a very low yield (**Table 1**, **Entry 25**). Similarly, when we used neutral Eosin Y without DIPEA, there was no formation of the desired product **3a** (**Table 1**, **Entry 26**). This observation strongly suggests that the presence of a base is crucial for maintaining the di-anionic form of Eosin Y, which appears to be the active form of the photocatalyst in this reaction.

Under acidic conditions with the presence of TFA, the reaction failed to progress (Table 1, Entry 27). Subsequently, we noted that when the reaction was conducted in the presence of oxygen (air), it also did not proceed (Table 1, Entry 28). Significantly, when the reaction was conducted without exposure to light or the photocatalyst, even at higher temperatures and extended reaction times, no desired product **3a** was obtained (Table 1, Entries 29-30). Detailed information can be found in the Experimental section, Table S4. These outcomes unequivocally demonstrated the essential role of both light and the photocatalyst in facilitating the desired transformation.

Table 1: Optimisation of reaction conditions[a]





Entry	Variation from optimised condition	Yield (%)[b]
1	**None**	**80**
2	DABCO instead of DIPEA	25
3	Triethyl amine instead of DIPEA	59
4	Diisopropyl amine (DIPA) instead of DIPEA	20
5	K_2CO_3 instead of DIPEA	<5
6	Cs_2CO_3 instead of DIPEA	7
7	DBU instead of DIPEA	40
8	DMAP instead of DIPEA	NR
9	HCO_2Na instead of DIPEA	Trace
10	$(Ir[dF(CF_3)ppy]_2(dtbpy))PF_6$ instead of Eosin Y	NR
11	$Ru(bpy)_3(PF_6)_2$ instead of Eosin Y	NR
12	Na_2EosinY instead of Eosin Y	65
13	Thioxanthen-9-one instead of Eosin Y	50
14	Rhodamine 6G instead of Eosin Y	NR
15	Rose Bengal instead of Eosin Y	55
16	9-Fluorenone instead of Eosin Y	Trace
17	9H-Xanthen-9-one instead of Eosin Y	10
18	Anthracene-9,10-dione instead of Eosin Y	NR
19	Fluorescein instead of Eosin Y	45
20	Tert-butanol instead of DMSO	41
21	Acetone instead of DMSO	40
22	Acetonitrile instead of DMSO	60
23	DMF instead of DMSO	62

24	THF instead of DMSO	43
25	Na_2EosinY (instead of Eosin Y) in absence of DIPEA	10
26	No DIPEA	NR
27	TFA instead of DIPEA	NR
28	Open air instead of inert atmosphere	NR
29	No Light	NR
30	No Photocatalyst	NR

***Reaction conditions**: Unless otherwise noted. [a]all the reactions were carried out using Benzyl acrylate **1a** (1 mmol), 4-chlorobenzaldehyde **2a** (2 mmol), Eosin Y (5 mol%), DIPEA (2 mmol), in anhyd. DMSO (3 mL), Kessil Blue LED (456 nm, with 75% intensity temperature around 60 ˚C, switching the fan off), Argon atmosphere; [b] Yields are obtained after the purification over column chromatography.*

Based on our systematic and exhaustive screening, we determined that the optimal reaction conditions for benzyl acrylate **1a** (1.0 mmol) and 4-chlorobenzaldehyde **2a** (2.0 mmol) involved the use of Eosin Y (5 mol%), DIPEA (2.0 mmol), in DMSO, under the illumination of a Blue LED (456 nm, with 75% intensity) at a temperature of approximately 60 °C, with the fan switched off, all under an inert atmosphere.

4.4. Results and Discussion:

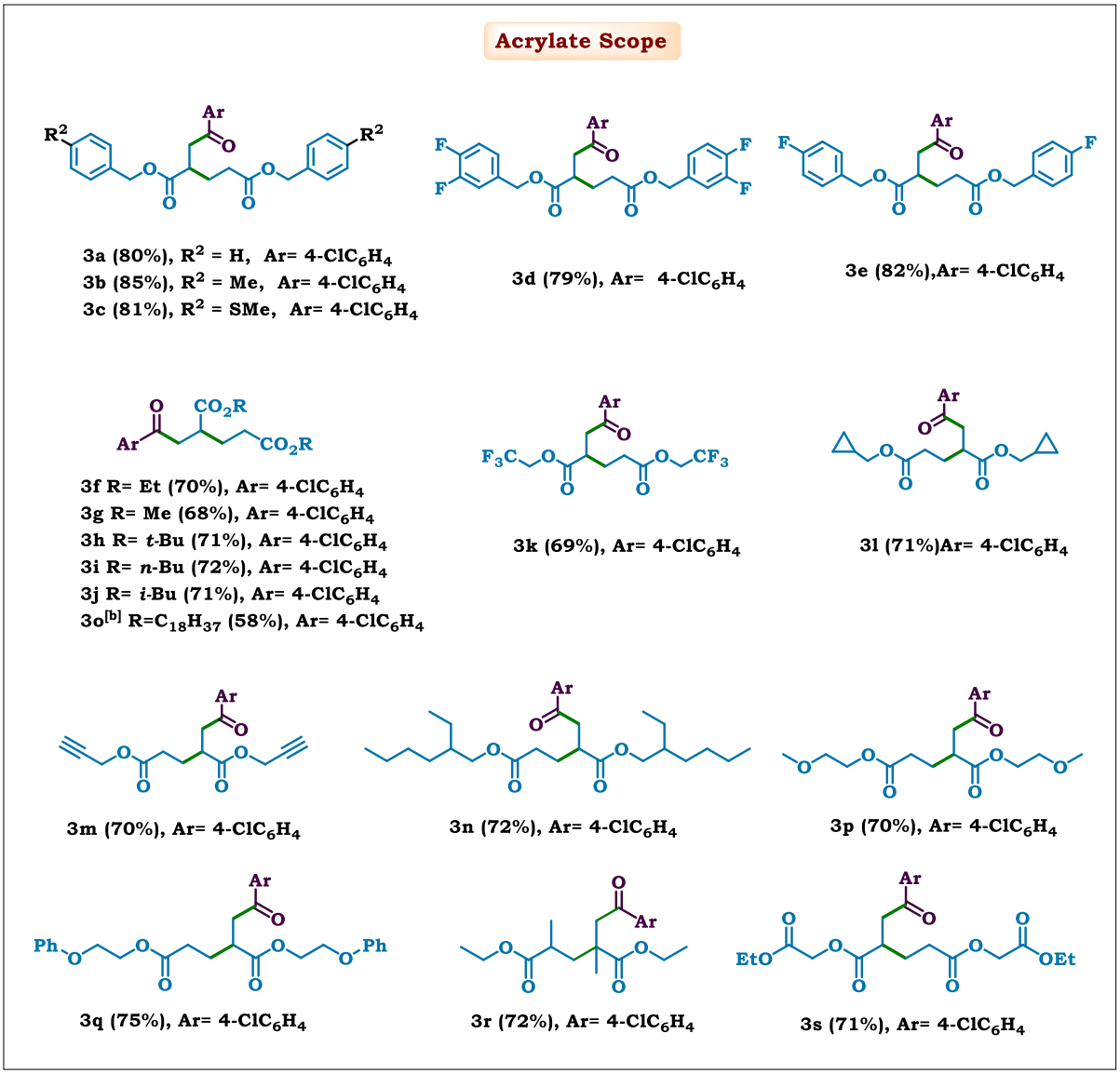
After determining the optimized reaction conditions, we proceeded to expand our investigation by assessing a broader range of substrates to gauge the protocol's generality and gain insights into its reactivity. We initiated our study by investigating the substrate diversity using various aryl/alkyl acrylates (**1a-1s**) while maintaining a constant presence of 4-chlorobenzaldehyde **2a**. Different derivatives of benzyl acrylates (**1a-1e**), featuring both electron-donating and electron-withdrawing groups, consistently yielded the desired products (**3a-3e**) in high yields (up to 85%, **Table 2a**). The acrylates featuring various alkyl groups (**1f-1o**), including ethyl, methyl, branched alkyl, cyclopropyl, propargyl, fluoro-substituted alkyl, and long aliphatic chain (stearyl) groups, exhibited successful reactivity with **2a** under the optimized reaction conditions. This resulted in the formation of α-substituted glutaric diesters (**3f-3o**) in moderate to good yields, (up to 72%, **Table 2a**). Furthermore, the acrylates

incorporating ether or ester functional groups, as well as α-substituted acrylates (**1p-1s**), exhibited efficient reactivity with **2a**, leading to the formation of the desired products (**3p-3s**) in satisfactory yields (up to 75%, **Table 2a)**. Subsequently, we extended our assessment of substrate diversity to encompass various aldehydes (**2t-2ac**) while employing ethyl acrylate **1f** as the reacting partner under the previously optimized reaction conditions. It's worth emphasizing that irrespective of the presence of electron-withdrawing or electron-donating groups on the aryl ring of aldehydes **2**, we consistently obtained the corresponding glutaric diesters (**3t-3z**, **3aa-3ac**) in moderate to good yields (up to 78%, **Table 2b)**. Furthermore, even heterocyclic aldehydes (**2ad-2af)** exhibited efficient reactivity with ethyl acrylate **1f**, yielding the desired products (**3ad-3af**) in moderate yields (up to 65%, as indicated in **Table 2b)**. It is worth noting that even natural products such as *L*-menthol, (-)-borneol, and geraniol-derived acrylates exhibited reactivity with **2a**, leading to the formation of the respective glutaric diesters (**3ag-3ai**) in modest yields (up to 54%, as outlined in **Table 2b)**.

It is important to note that surprisingly the reaction of ^{t}butyl acrylate **1h** and 4-cyano benzaldehyde **2o** afforded the unexpected γ-keto ester **3aj** instead of the substituted glutaric acid diester as a final product (**Table 2c**). The reaction involving methyl acrylate **1g** and 4-cyano benzaldehyde **2o** resulted in an unexpected product, namely, γ-keto ester **3ak**, instead of the anticipated substituted glutaric acid diester as the final product (**Table 2c**). And aliphatic aldehydes (**2p-2r**) and cinnamaldehyde **2s** remains unreactive during the course of the reaction (**Table 2c**).

To illustrate the practical applicability of this approach, we conducted several interesting synthetic transformations using the obtained glutaric diesters **3** (**Scheme 2**). When glutaric diester **3h** was subjected to treatment with a mixture of trifluoroacetic acid (TFA) and dichloromethane (DCM) in a 1:1 ratio, it yielded the corresponding glutaric acid derivative **4a** in an exceptionally high yield (**Scheme 2**, **Eqn. a**). It's worth noting that glutaric acid holds significant importance in the polymer industry. Recognizing its utility, we proceeded to investigate the reaction of glutaric diester **3h** with hydrazine under reflux conditions, resulting in the formation of a 6,4-substituted 4,5-dihydropyridazin-3(2*H*)-one derivative **4b** (**Scheme 2**, **Eqn. b**). It is of utmost significance to highlight that pyridazinone derivatives have garnered substantial attention due to their wide array of biological and pharmacological activities, as depicted in **Figure 1b**. These activities encompass anticonvulsant properties [24], anti-ulcer effects [25], antimicrobial actions [26], and various other bioactive functions [27], as documented in the literature.

Table 2a: Substrate Scope (different acrylate scopes)

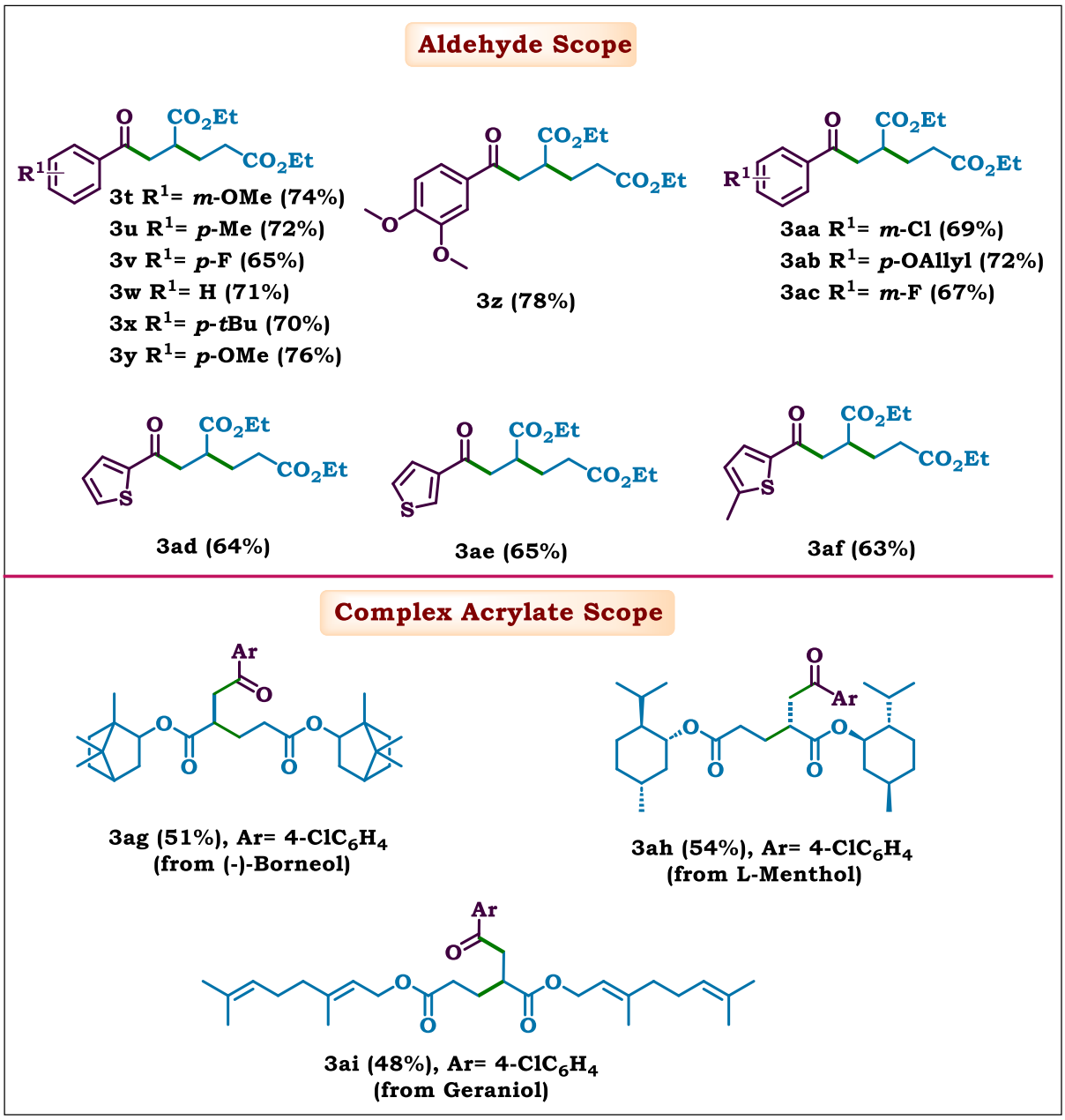


Reaction Conditions: *Unless otherwise noted. [a]all the reactions were carried out using Acrylate* ***1*** *(1 mmol), Aldehyde 2 (2 mmol), Eosin Y (5 mol%), DIPEA (2 mmol), using 456 nm light under inert atmosphere (Ar) (temperature ~ 60 °C, keeping fan switched off) in anhydrous DMSO.*

Moreover, it is crucial to highlight that chiral-substituted 4, 5-dihydro-2*H*-pyridazinones, like KF 15232, have a notable impact on both general efficacy and isozyme selectivity, as illustrated in **Figure 1b**. Similarly, another pyridazinone derivative, **4c**, has been synthesized starting from **3f** (**Scheme 2**, **Eqn. c**). Additionally, a valuable ketoxime derivative, **4d**, has been obtained from **3h** by reacting it with hydroxylamine in tert-butanol (**Scheme 2**, **Eqn. d**). Another key intermediate, γ-keto acid **4e**, has also been successfully synthesized from the glutaric diester derivative **3aj** using a TFA/DCM mixture in a 1:1 ratio (**Scheme 2**, **Eqn. e**). Furthermore, γ-

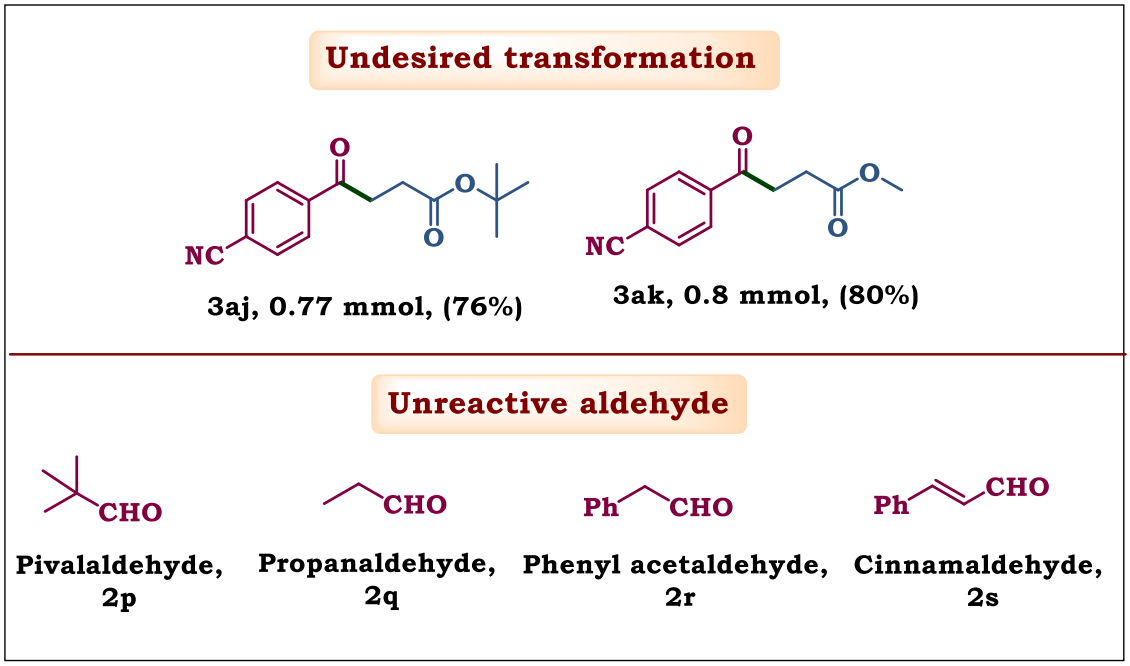
hydroxy ester **4f** was produced by reducing glutaric diester derivative **3ak** with $NaBH_4$ in methanol (**Scheme 2**, **Eqn. f**). To showcase the practical utility of the protocol, we managed to synthesize glutaric diester 3a on a gram scale, achieving a good yield of 75%, as depicted in Scheme 3a. Furthermore, we conducted the reaction under sunlight as the primary light source, resulting in the formation of **3a** in a satisfactory yield of 62% (Scheme 3b).

Table 2b: Substrate Scope (different aldehyde scopes and complexed acrylate scopes)



Reaction Conditions: *Unless otherwise noted. [a]all the reactions were carried out using Acrylate 1 (1 mmol), Aldehyde 2 (2 mmol), Eosin Y (5 mol%), DIPEA (2 mmol), using 456 nm light under inert atmosphere (Ar) (temperature ~ 60 °C, keeping fan switched off) in anhydrous DMSO.*

Table 2c: Undesired transformation and unreactive aldehydes



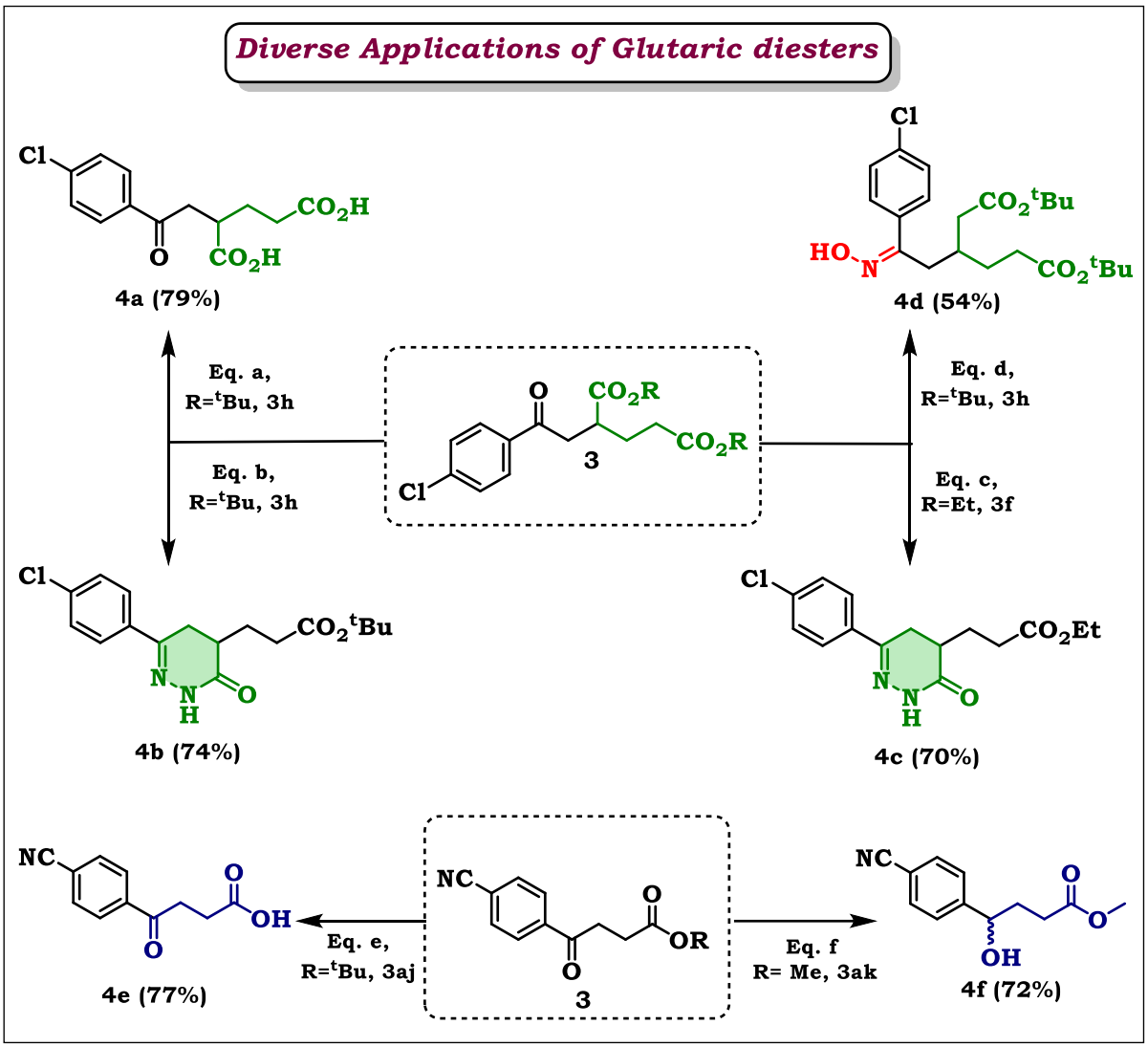
Reaction Conditions: *Unless otherwise noted. [a]all the reactions were carried out using Acrylate 1 (1 mmol), Aldehyde 2 (2 mmol), Eosin Y (5 mol%), DIPEA (2 mmol), using 456 nm light under inert atmosphere (Ar) (temperature ~ 60 °C, keeping fan switched off) in anhydrous DMSO.*

4.5. Control experiments and mechanistic study:

To gain further insights into the potential reaction pathway, we systematically conducted a series of controlled experiments. Our initial experiment involved reacting ethyl acrylate **1f** with deuterated aldehyde **2a-D** under carefully optimized standard reaction conditions. This reaction resulted in significant deuteration at the C4-position of **3f-D**, with an incorporation rate of 85%. This compelling outcome solidifies the argument that the reaction proceeds via a 'reverse hydrogen atom transfer (RHAT) process' within the catalytic cycle, as depicted in **Scheme 4a**. Additionally, when we conducted the reaction of **1f** and **2a** in DMSO-D6 while keeping all other conditions unchanged, we did not obtain any deuterated product **3f** (as depicted in **Scheme 4b**). This outcome serves as conclusive evidence that the solvent itself is not the source of proton incorporation in the final product. Subsequently, upon adding D_2O to the reaction mixture of **1f** and **2a**, we observed the formation of the deuterium-incorporated product **3a-D2** (as shown in **Scheme 4c**). It's worth noting that only two relatively more acidic protons within the product underwent deuteration, likely due to the presence of a base. Interestingly, the relatively less

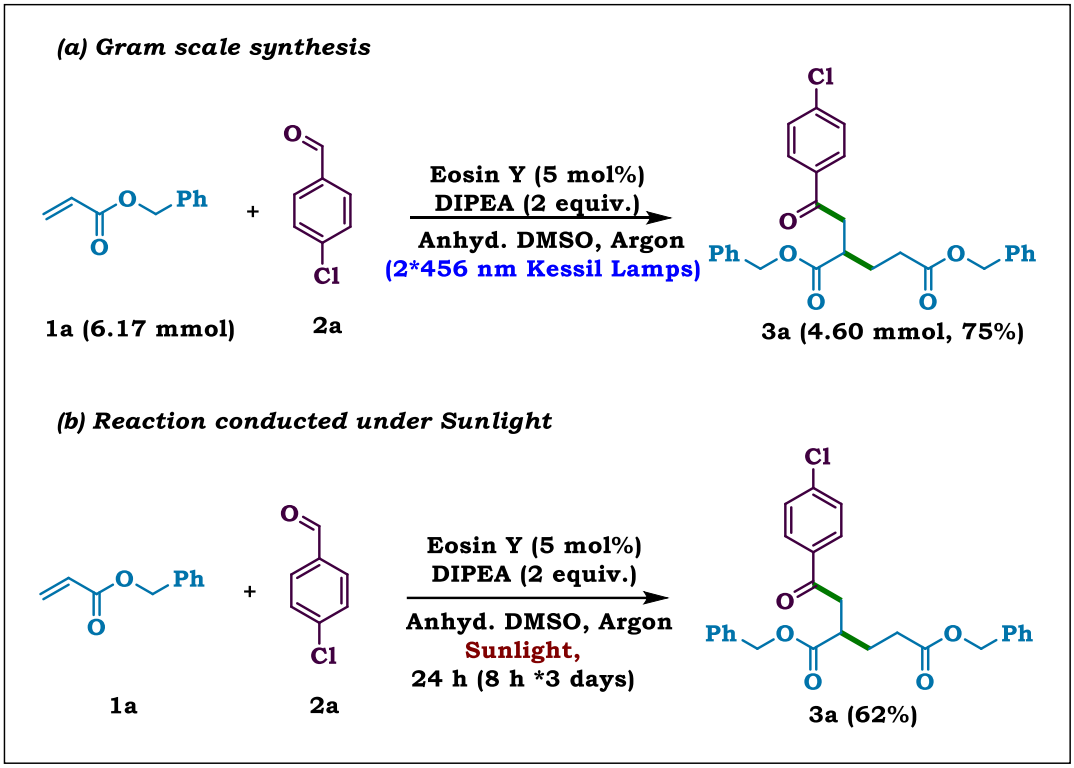
acidic C4-H of product **3a** remained unaffected by deuteration, indicating the absence of any hydrogen-deuterium exchange phenomenon during the catalytic cycle.

Scheme 2: Post synthetic modifications of glutaric diesters

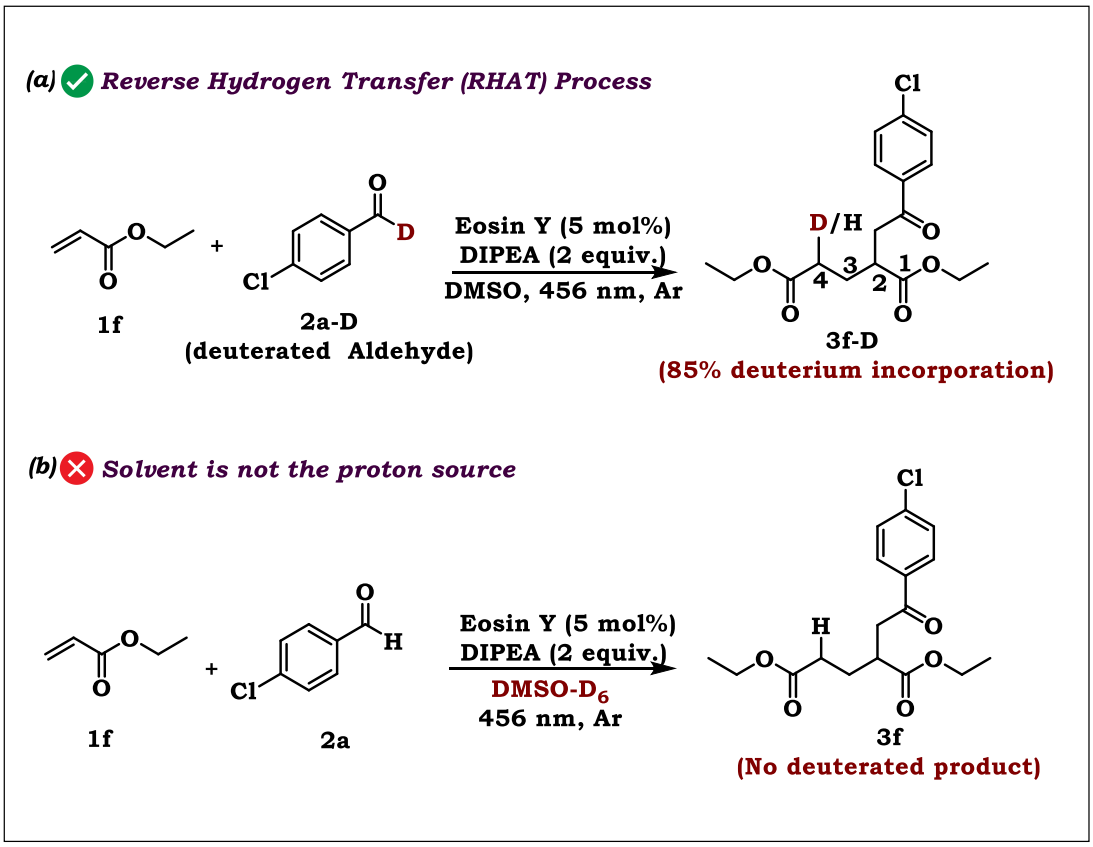


***Reaction conditions**: a) **3h** (0.5 mmol), Trifluoroacetic acid (TFA) / DCM (1:1, 2mL v/v); b) 3h (0.5 mmol), NH_2NH_2 (10 mmol, 0.5 mL) reflux; c) **3f** (0.5 mmol), NH_2NH_2 (10 mmol, 0.5 mL), reflux; d) **3h** (0.5 mmol), NH_2OH (1.5 mmol) in tert-butanol (2 mL), reflux; e) **3aj** (1 mmol), Trifluoroacetic acid (TFA)/DCM (1:1, 2 v/v); f) **3ak** (1 mmol), $NaBH_4$ (2 equiv. 2 mmol) in methanol (2 mL).*

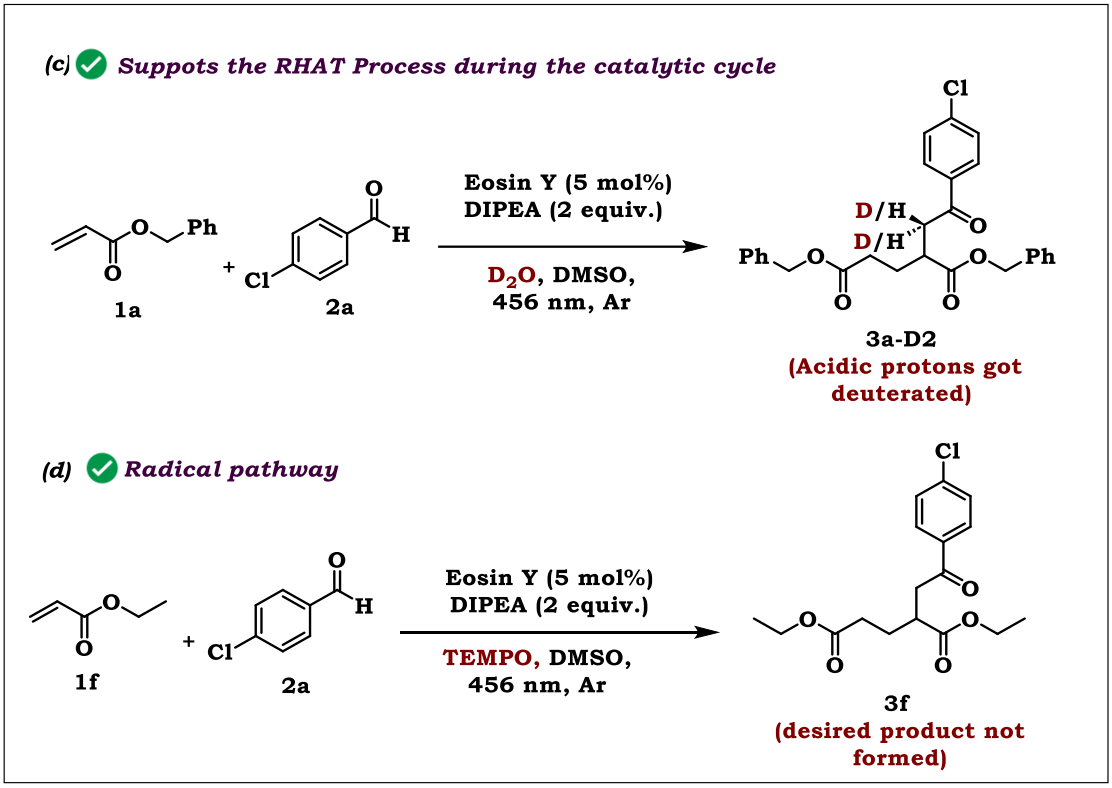
Scheme 3. Gram scale and reaction under sunlight



Scheme 4. Control experiments (a-b)



Scheme 4. Control experiments (c-d)



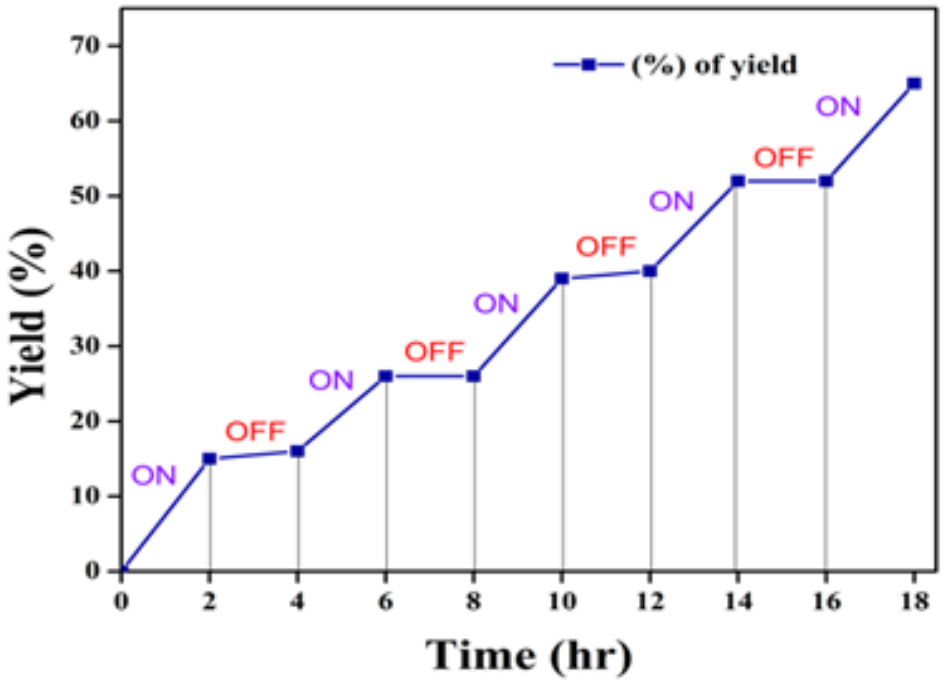


Figure 2: Light switch ON/OFF experiments of the transformation

Furthermore, when we attempted the reaction in the presence of TEMPO (1.0 equiv.), a radical scavenger, it did not yield the desired **3f** product. This result supports the involvement of a radical pathway during the catalytic cycle (as illustrated in **Scheme 4d**).

Subsequently, we conducted light-switch on/off experiments (**Figure 2**) and determined the quantum yield (Φ = 0.56) through calculations (*See Experimental section, page 166-168*). The experimental findings conclusively demonstrate that the transformation does not follow a radical chain-type mechanism.

Furthermore, we conducted fluorescence quenching experiments to gain insights into the reaction mechanism (**Figure 3**). Notably, the fluorescence intensity of Eosin Y remained unaltered in the presence of 4-chlorobenzaldehyde **2a** (refer to the ESI for data), ethyl acrylate **1f** (refer to the ESI for data), or DIPEA (refer to the ESI for data) individually, as shown in **Figure 3-I**. Additionally, the fluorescence intensity of Eosin Y remained unchanged when both aldehyde **2a** and DIPEA were present (refer to the ESI for data).

Figure 3-I **Figure 3-II**

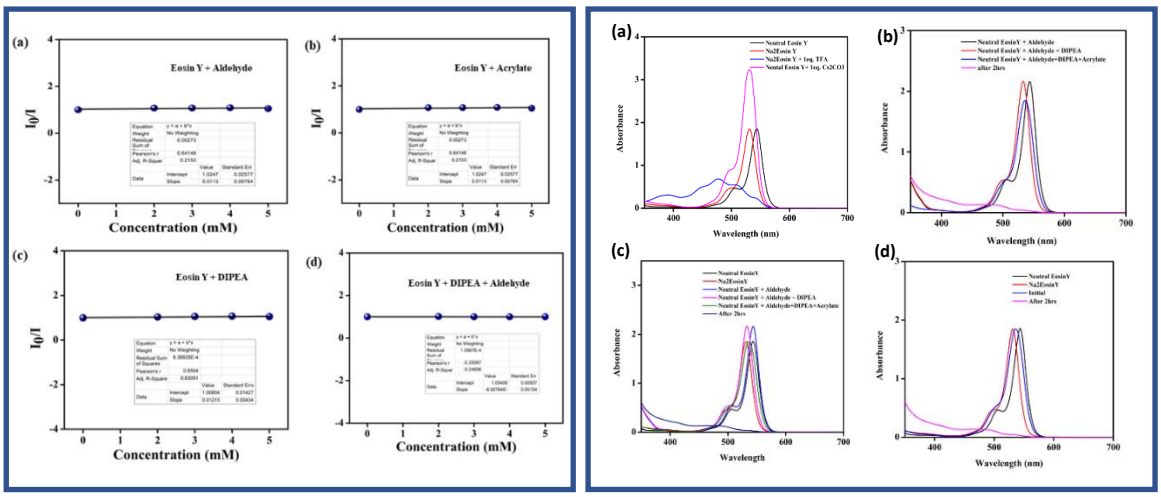


Figure 3-I: Stern-Volmer plot of the fluorescence quenching study (a) Eosin Y in presence of 4-Chlorobenzaldehyde **2a**; (b) Eosin Y in presence of Ethyl acrylate **1f** (c) Eosin Y in presence of DIPEA, (d) Eosin Y in presence of 4-Chlorobenzaldehyde **2a** + DIPEA.

Figure 3-II. (a) UV-Visible absorption of different form of Eosin Y in DMSO. 20 μM neutral Eosin Y, 20 μM Na_2Eosin Y, 20 μM Na_2Eosin Y + 20 μM TFA, 20 μM neutral Eosin Y + 20 μM Cs_2CO_3. **(b)** 20 μM neutral Eosin Y + 1 equiv. 4-chloro benzaldehyde, 20 μM neutral Eosin Y + 1 equiv. 4-chloro benzaldehyde + 1 equiv. DIPEA, 20 μM neutral Eosin Y + 1 equiv. 4-chlorobenzaldehyde aldehyde+ 1 equiv. DIPEA + 1equiv. ethyl acrylate, after 2 hr of the reaction, in DMSO solvent. **(c)** 20 μM neutral Eosin Y, 20μM Na_2EosinY, 20 μM neutral Eosin Y + 1 equiv. 4-chloro benzaldehyde, 20 μM neutral Eosin Y + 1 equiv. 4-chloro benzaldehyde+ 1equiv. DIPEA, 20 μM neutral Eosin Y + 1 equiv. 4-chlorobenzaldehyde + 1 eq. DIPEA + 1 equiv. Ethyl Acrylate **1f**, after 2 h of the reaction, in DMSO solvent. **(d)** 20 μM neutral Eosin Y, 20 μM Na_2EosinY, absorption was recorded before the irradiation of light (reaction at 0 hr). Later, the absorption was recorded after 2 hr of the reaction.

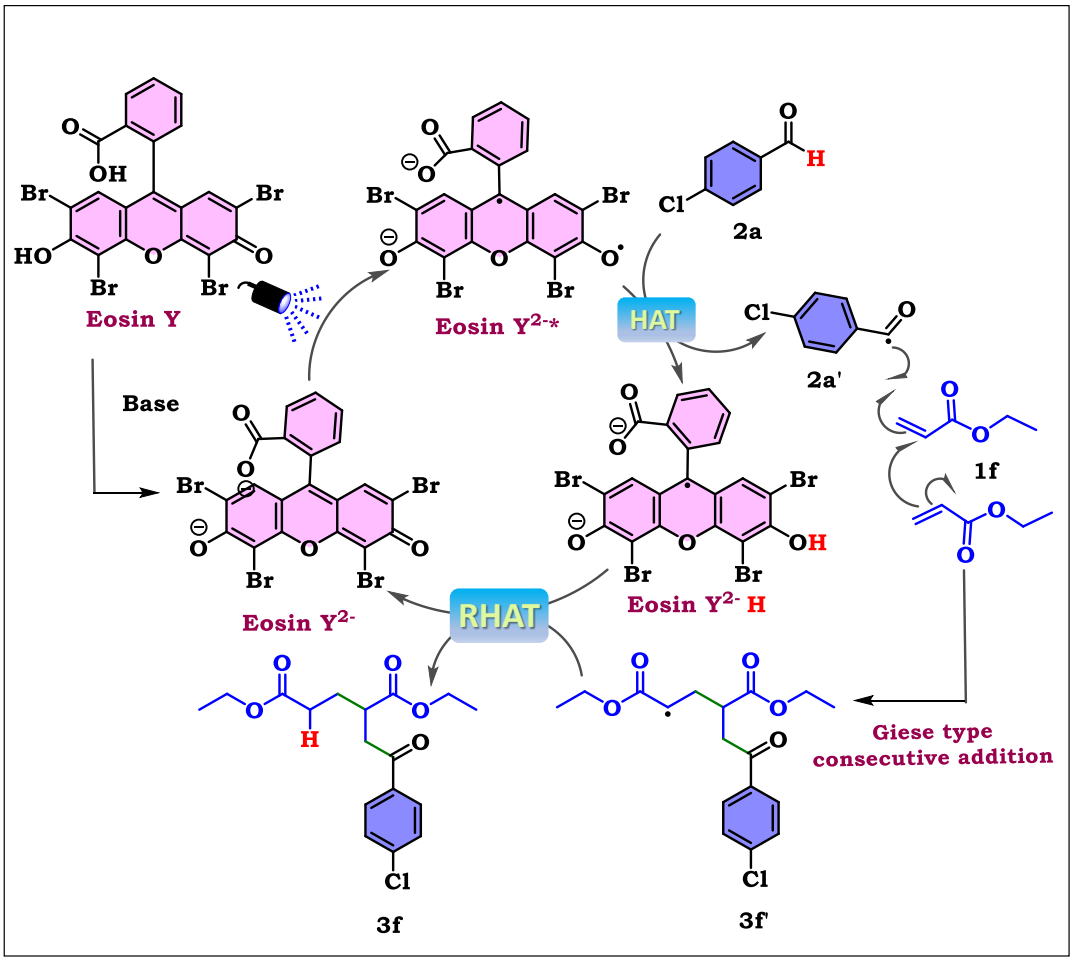
Based on the Stern-Volmer plot data, we have ruled out the possibility of a PCET (Proton Coupled Electron Transfer) process occurring during the course of the reaction pathway (**Figure 3**). The fluorescence quenching experiment and the Stern-Volmer plot collectively suggest that neither a SET (Single Electron Transfer) process nor a PCET process is involved in the reaction. Considering our previously described experimental results and other supporting evidence, our proposed mechanism posits that Eosin Y functions as a HAT (Hydrogen Atom Transfer) catalyst to drive the reaction.

Furthermore, based on our prior experimental findings (specifically, **Entry 11** and **Entry 12** of **Table 1**), we are inclined to believe that the di-anionic form of Eosin Y is the active state of Eosin Y throughout the reaction. We posit that DIPEA may be maintaining the basicity of the reaction environment to ensure the continuous presence of the di-anionic form of Eosin Y. To substantiate this hypothesis, we conducted measurements of the pH of the reaction under different conditions throughout the transformation. Additionally, we recorded UV data under varying conditions (refer to **Figure 3-II**).

Based on the comprehensive experimental results, we have proposed the most plausible reaction mechanism for this transformation, as illustrated in **Scheme 5**. Initially, neutral Eosin Y, in the presence of the base DIPEA, transforms into the corresponding di-anionic form, Eosin Y^{2-} (as shown in **Scheme 5**). In the photoexcited state of Eosin Y^{2-*}, a hydrogen atom is abstracted, facilitated by HAT catalysis, from aldehyde **2a**, resulting in the formation of an acyl radical intermediate **2a'**. This intermediate subsequently engages in a Giese addition process with ethyl acrylate 1f and further reacts with another molecule of ethyl acrylate **1f**, generating a radical

intermediate 3f'. This highly reactive radical intermediate then abstracts a hydrogen atom from Eosin $Y^{2-}H$ through reverse hydrogen atom transfer (RHAT) catalysis, ultimately producing the desired product 3f. This step completes the catalytic cycle by regenerating Eosin Y2-.

Scheme 5. Plausible Reaction Mechanism involving RHAT process



4.6. Conclusions:

In summary, we have developed an innovative method for the direct one-pot synthesis of α-substituted glutaric diesters using readily available aldehydes and acrylates. This process operates without the need for metal catalysts, utilizing visible light for irradiation. Our approach exhibits tolerance for a broad range of functional groups, leading to the formation of various α-substituted glutaric diester derivatives in moderate to good yields. Notably, we have successfully employed acrylates derived from natural products such as menthol, borneol, and geraniol to access valuable glutaric diester derivatives. This protocol offers a convenient and novel route to industrially relevant glutaric acid derivatives. Moreover, we have demonstrated the versatility of these glutaric acid derivatives in synthesizing valuable compounds, including 4,5-pyridazinone derivatives such as dihydro-2*H*-pyridazinones known for their biological activities. Our method is amenable to scale-up for gram-scale production. Furthermore, we have explored the potential of commercially viable Eosin Y as a catalyst for hydrogen atom transfer (HAT) to activate the aldehyde. Our comprehensive investigations, including controlled experiments, deuterium labeling studies, light-switch experiments, fluorescence quenching experiments, and quantum yield calculations, have shed light on the most plausible reaction mechanism for this transformation.

4.7. Experimental section:

4.7.1. General information:

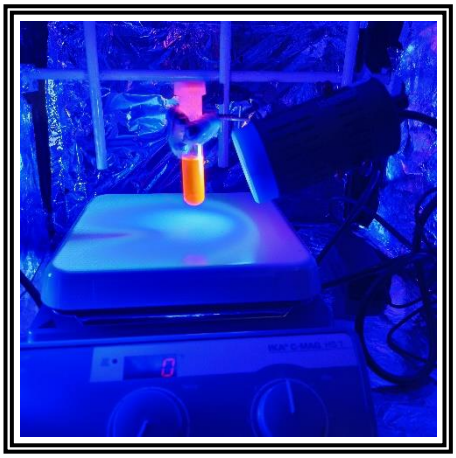
Unless otherwise noted, all the starting materials and reagents were purchased from commercial suppliers (Aldrich, TCI, and Alfa Aesar) and were used without any further purification. Thin-layer chromatography (TLC) was performed using silica gel 60 GF_{254} pre-coated aluminium backed plates (2.5 mm). Visualization was accomplished by the irradiation with UV light at 254 nm. The column chromatography was performed using silica gel (100–200 mesh) eluting with petroleum ether and ethyl acetate. The NMR spectra were recorded using tetramethylsilane as the internal standard. ^{1}H NMR spectra were recorded at 400 MHz and $^{13}C\{^{1}H\}$ NMR spectra were recorded at 100 MHz (Bruker and Jeol) unless otherwise noted. Chemical shifts (δ) are reported in ppm downfield from $CDCl_3$ (δ = 7.26 ppm) for ^{1}H NMR and relative to the central $CDCl_3$ resonance (δ = 77.16 ppm) for $^{13}C\{^{1}H\}$ NMR spectroscopy. For ^{1}H NMR, data are reported as follows: chemical shift, multiplicity (s = singlet, d = doublet, dd = double doublet, t = triplet, q = quartet, br = broad, m = multiplet), coupling constants (*J*) are given in Hz and integration. $^{13}C\{^{1}H\}$ NMR spectra were recorded with complete proton decoupling. ^{19}F NMR spectra were recorded at 377 MHz. Mass samples were analyzed by high-resolution mass spectrometry (HRMS)-ESI TOF. Fluorescence spectra were recorded on Fluoromax-4 spectrofluorometer (Horiba Scientific, U.S.A.). UV absorption was performed using Shimadzu, UV-2600 UV spectrophotometer. All photocatalytic reactions were performed under blue LEDs (Kessil PR160L series Blue LEDs, and IBRA Pure 60 W Blue LED Flood Light, IP Rating: IP66).

4.7.2. General procedure for the synthesis of 3 (GP1):

To an oven dried 10 mL crimp capped vial charged with magnetic stir bar was added aldehyde **2** (2 mmol, 2 equiv.), Eosin Y (5 mol%) and DIPEA (2 mmol, 2 equiv.) at room temperature under argon atmosphere. The vial was purged again with argon and sealed with aluminum crimp cap using a crimper. Then anhydrous DMSO (3 mL) was added under argon. Then the reaction mixture was degasified using argon for 30 minutes under constant purging and monitoring. After the degasification acrylates **1** (1 mmol, 1 equiv.) was added under inert atmosphere. Then the reaction mixture was irradiated with 456 nm Kessil Lamp (Blue LED) with 75% intensity (the temperature turns around 60 °C measured by IR-thermometer, by keeping the fan switch off/ No other external heating source was applied) stirred for 24 h. After the completion of the reaction (monitored by TLC), 10 mL of water was added to the reaction mixture and was

extracted with ethyl acetate (3 × 10 mL). The combined organic extracts were evaporated under reduced pressure and the crude residue was purified by using column chromatography (Silica gel 100–200 mesh size, using ethyl acetate/Pet-Ether as eluent system).

Reaction setup under visible light (Kessils lamp)



4.7.3. General procedure for the synthesis of 3 under sunlight:

To an oven dried 10 mL reaction tube charged with magnetic stir bar was added aldehyde **2** (2 mmol, 2 equiv.), Eosin Y (5 mol%) and DIPEA (2 mmol, 2 equiv.) at room temperature under argon atmosphere. The reaction tube was purged again with argon and sealed with rubber septum. Then anhydrous DMSO (3 mL) was added under argon. Then the reaction mixture was degasified using argon for 30 minutes under constant purging and monitoring. After the degasification acrylates **1** (1 mmol, 1 equiv.) was added under inert atmosphere. Then the reaction mixture was kept under sunlight (around 40 °C) for 24 h. After the completion of the reaction (monitored by TLC), 10 mL of water was added to the reaction mixture and was extracted with ethyl acetate (3 × 10 mL). The combined organic extracts were evaporated under reduced pressure and the crude residue was purified by using column chromatography (Silica gel 100–200 mesh size, using ethyl acetate/Pet-Ether as eluent system).

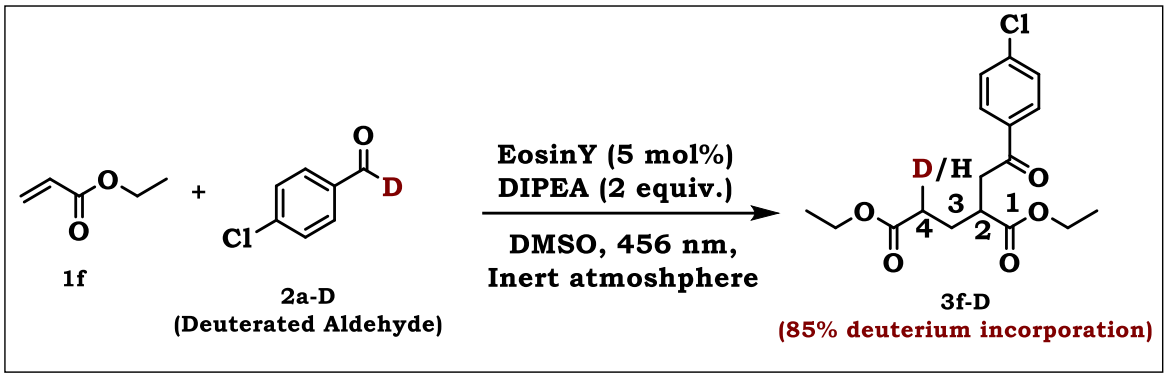
Reaction setup under sunlight



4.7.4. Control Experiments:

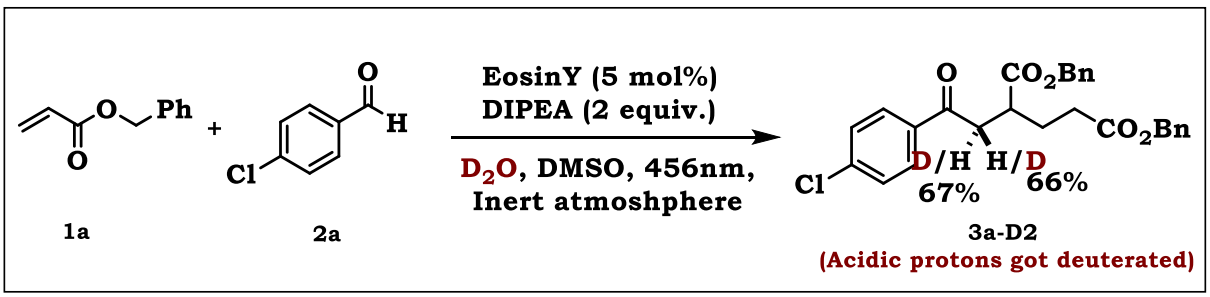
4.7.4.1. Procedure for the preparation of 3f-D:

To an oven dried 10 mL crimp cap vial charged with magnetic stir bar was added deuterated 4-chlorobenzaldehyde **2a-D** [30] (2 mmol, 2 equiv., 283 mg), Eosin Y (5 mol%) and DIPEA (2 mmol, 2 equiv.) at room temperature under argon atmosphere. The vial was purged with argon and sealed with an aluminium crimp cap using a crimper. Then anhydrous DMSO (3 mL) was added under argon. Then the reaction mixture was degasified using argon for 30 minutes under constant purging and monitoring. After the degasification ethyl acrylate **1f** (1 mmol, 1 equiv., 100 mg) was added under inert atmosphere. The reaction mixture was irradiated with 456 nm Kessil lamp (Blue LED) with 75% intensity (the temperature turns around 60 °C-external temperature-measured by IR-thermometer, by keeping the fan switched off) stirred for 24 h. After completion of the reaction (monitored by TLC), 10 mL of water was added to the reaction mixture and was extracted with ethyl acetate (3 × 10 mL). The combined organic extracts were evaporated under reduced pressure and the crude residue was purified by using column chromatography (Silica gel 100–200 mesh size, using ethyl acetate/Petroleum ether as eluent system) to afford the desired product **3f-D** in 65% yield and the deuterium incorporation was observed in C4-carbon of **3f-D** with 85% yield.



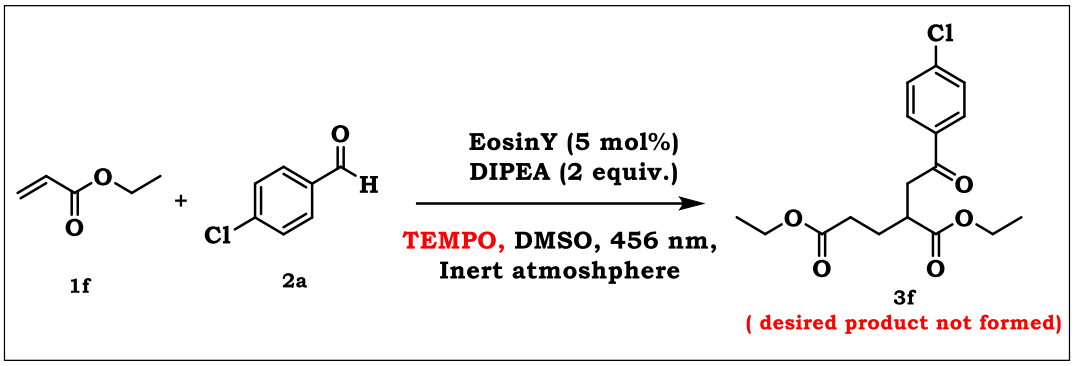
4.7.4.2. Procedure for the preparation of 3a-D_2:

To an oven dried 10 mL crimp cap vial charged with magnetic stir bar was added 4-chlorobenzaldehyde **2a** (2 mmol, 2 equiv., 281 mg), Eosin Y (5 mol%), DIPEA (2 mmol, 2 equiv.) and D_2O (300 µL) at room temperature under argon atmosphere. The vial was purged again with argon and then sealed with aluminium crimp cap using a crimper. Then anhydrous DMSO (3 mL) was added under argon. Then the reaction mixture was degasified using argon for 30 minutes under constant purging and monitoring. After the degasification, the benzyl acrylate **1a** (1 mmol, 1 equiv., 162 mg) was added under inert atmosphere. Then the reaction mixture was irradiated with 456 nm Kessil Lamp (Blue LED) with 75% intensity (the temperature turns around 60 °C-external temperature-measured by IR-thermometer, by keeping the fan switched off) and stirred for 24 h. After completion of the reaction (monitored by TLC), 10 mL of water was added to the reaction mixture and was extracted with ethyl acetate (3 × 10 mL). The combined organic extracts were evaporated under reduced pressure and the crude residue was purified over column chromatography (Silica gel 100–200 mesh size, using ethyl acetate/Petroleum ether as an eluent system) to afford the desired product **3a-D_2** in 45%.



4.7.4.3. Procedure for the reaction using TEMPO:

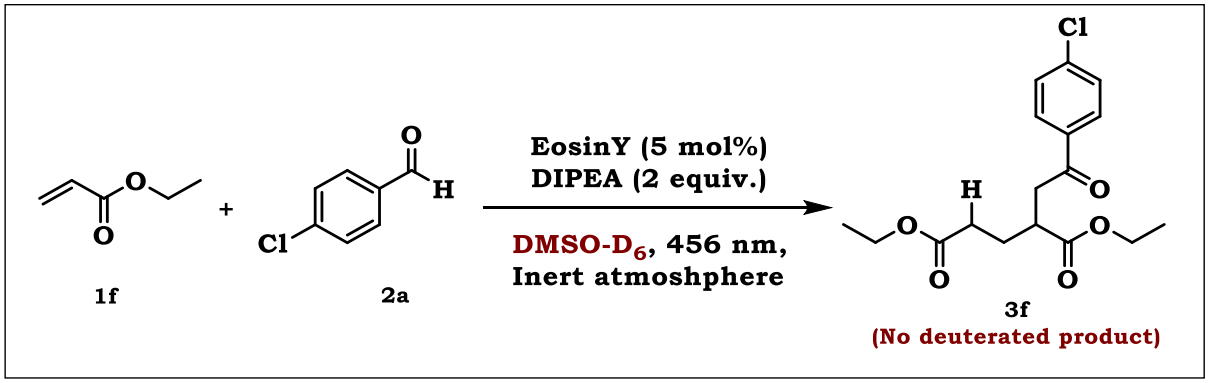
To an oven dried 10 mL crimp cap vial charged with magnetic stir bar was added aldehyde **2a** (2 mmol, 2 equiv., 281 mg), Eosin Y (5 mol%) and DIPEA (2 mmol, 2 equiv.) and TEMPO (2 mmol, 2 equiv.,) at room temperature under argon atmosphere. The vial was then purged again with argon and sealed with aluminium crimp cap using a crimper. Then anhydrous DMSO (3 mL) was added under argon atmosphere. Then the reaction mixture was degasified again using argon for 30 minutes under constant purging and monitoring. After the degasification acrylate **1f** (1 mmol, 1 equiv., 100 mg) was added dropwise under inert atmosphere. Then the reaction mixture was irradiated with 456 nm Kessil lamp (Blue LED) with 75% (the temperature turns around 60 °C-external temperature-measured by IR-thermometer, by keeping the fan switched off) and stirred for 24 h. Even after prolonged reaction time, the compound **3f** was not formed.



4.7.4.4. Procedure for the reaction using DMSO-D$_6$:

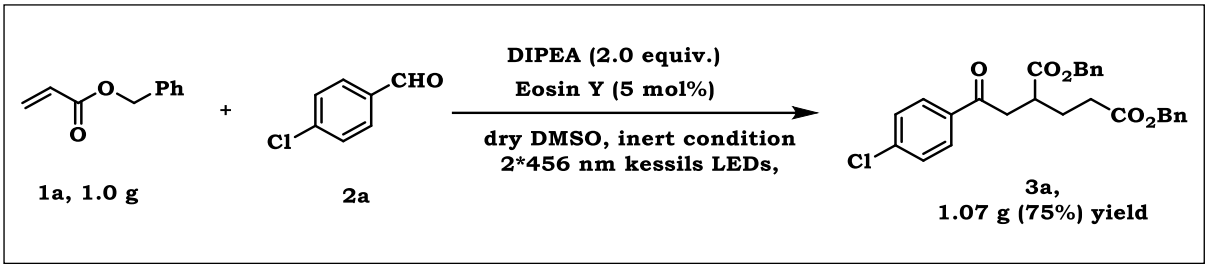
To an oven dried 10 mL crimp cap vial charged with magnetic stir bar was added 4-chlorobenzaldehyde **2a** (2 mmol, 2 equiv., 281 mg), Eosin Y (5 mol%) and DIPEA (2 mmol, 2 equiv.) at room temperature under argon atmosphere. The vial was purged again with argon and sealed with aluminium crimp cap using a crimper. Then anhydrous DMSO-D6 (3 mL) was added under argon atmosphere. Then the reaction mixture was degasified using argon for 30 minutes under constant monitoring. After the degasification ethyl acrylate **1f** (1 mmol, 1 equiv., 100 mg) was added under inert atmosphere. Then the reaction mixture was irradiated with 456 nm Kessil lamp (Blue LED) with 75% intensity (the temperature turns around 60 °C-external temperature-measured by IR-thermometer, by keeping the fan switched off) stirred for 24 h. After completion of the reaction (monitored by TLC), 10 mL of water was added to the reaction mixture and was extracted with ethyl acetate (3 × 10 mL). The combined organic extract was evaporated under reduced pressure and the crude residue was purified by using column chromatography (Silica gel 100–200 mesh size, using ethyl acetate/Petroleum ether as an eluent

system) to afford the product **3f** in 68% yield and the deuterated incorporation was not observed in the product **3f**.



4.7.5. Procedure for the gram scale synthesis of 3a:

To an oven dried 100 mL round bottomed flask aldehyde **2a** (12.33 mmol, 2 equiv., 1.73 g), Eosin Y (5 mol%) and DIPEA (12.33 mmol, 2 equiv.) was added at room temperature under argon atmosphere. The round bottomed flask equipped with rubber septum was flushed with argon (three times). Then anhydrous DMSO (30 mL) was added under argon. Then the reaction mixture was degasified using argon for 1 h under constant purging and monitoring. After the degasification benzyl acrylate **1a** (6.17 mmol, 1 equiv., 1 g) was added under inert atmosphere. Then the reaction mixture was irradiated with 2 * 456 nm Kessil Lamps with 75% intensity (the temperature turns around 60 °C-external temperature-measured by IR-thermometer, by keeping the fan switched off) and stirred for 36 h. After the completion of the reaction (monitored by TLC), 100 mL of water was added to the reaction mixture and was extracted with ethyl acetate (3 × 100 mL). The combined organic extracts were evaporated under reduced pressure and the crude residue was purified by using column chromatography over silica gel (100–200 mesh size) using ethyl acetate/petroleum ether as an eluent system).



4.7.6. Mechanistic study:

4.7.6.1. Fluorescence Quenching Experiment and Stern-Volmer plot:

Fluorescence quenching experiment was carried out using Fluorescence spectrophotometer, using 1.0 µM solution of Eosin Y in dry DMSO and variable concentrations of (2 to 5 mM) of 4-chlorobenzaldehyde **2a** in dry DMSO solvent. The sample was prepared in 3 mL quartz cuvette and the flask was degasified with Argon before the spectra were recorded. The quenching plot of the experiments are given below in **Figure 4**.

Fluorescence quenching experiment was carried out using Fluorescence spectrophotometer, using 1.0 µM solution of Eosin Y in dry DMSO and variable concentrations of (2 to 5 mM) of ethyl acrylate **1f** in dry DMSO solvent. The sample was prepared in a 3 mL quartz cuvette and the flask was degasified with Argon before the spectra were recorded. The quenching plot of the experiments are given below (**Figure 5**).

Fluorescence quenching experiment was carried out using Fluorescence spectrophotometer, using 1.0 µM solution of Eosin Y in dry DMSO and variable concentrations of (2 to 5 mM) of diisopropyl ethylamine (DIPEA) in dry DMSO solvent. The sample was prepared in 3 mL quartz cuvette and the flask was degasified with Argon before the spectra were recorded. The quenching plot of the experiments are given below (**Figure 6**).

Fluorescence quenching experiment was carried out using Fluorescence spectrophotometer, using 1.0 µM solution of Eosin Y in dry DMSO and variable concentrations of (2 to 5 mM) each of diisopropyl ethylamine (DIPEA) + 4-Chlorobenzaldehyde **2a** in dry DMSO solvent. The sample was prepared in a 3 mL quartz cuvette and the flask was degasified with Argon before the spectra were recorded. The quenching plot of the experiments are given below (**Figure 7**).

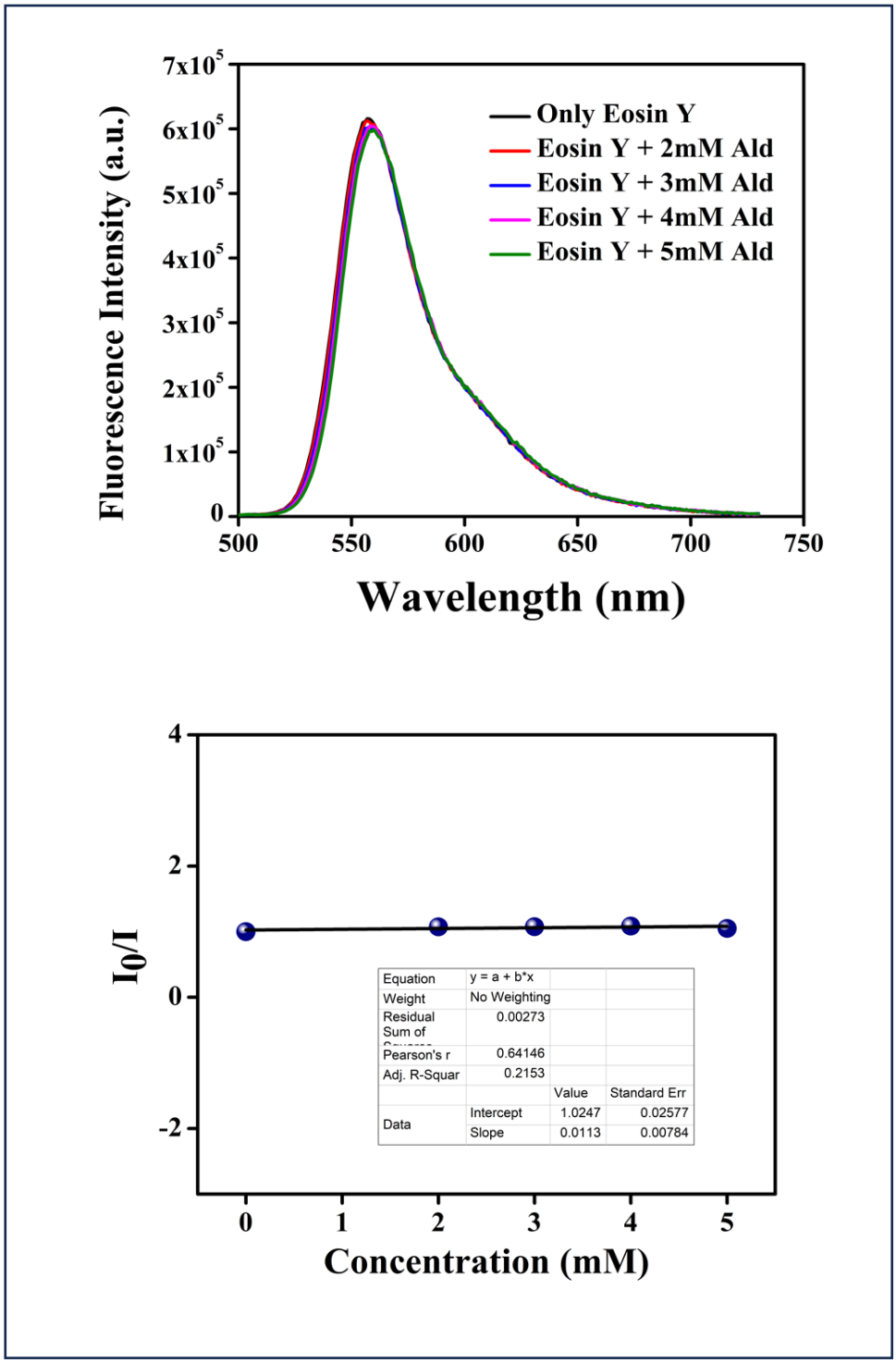


Figure 4. Fluorescence quenching experiments and Stern-Volmer plot of Eosin Y in presence of aldehyde **2a**

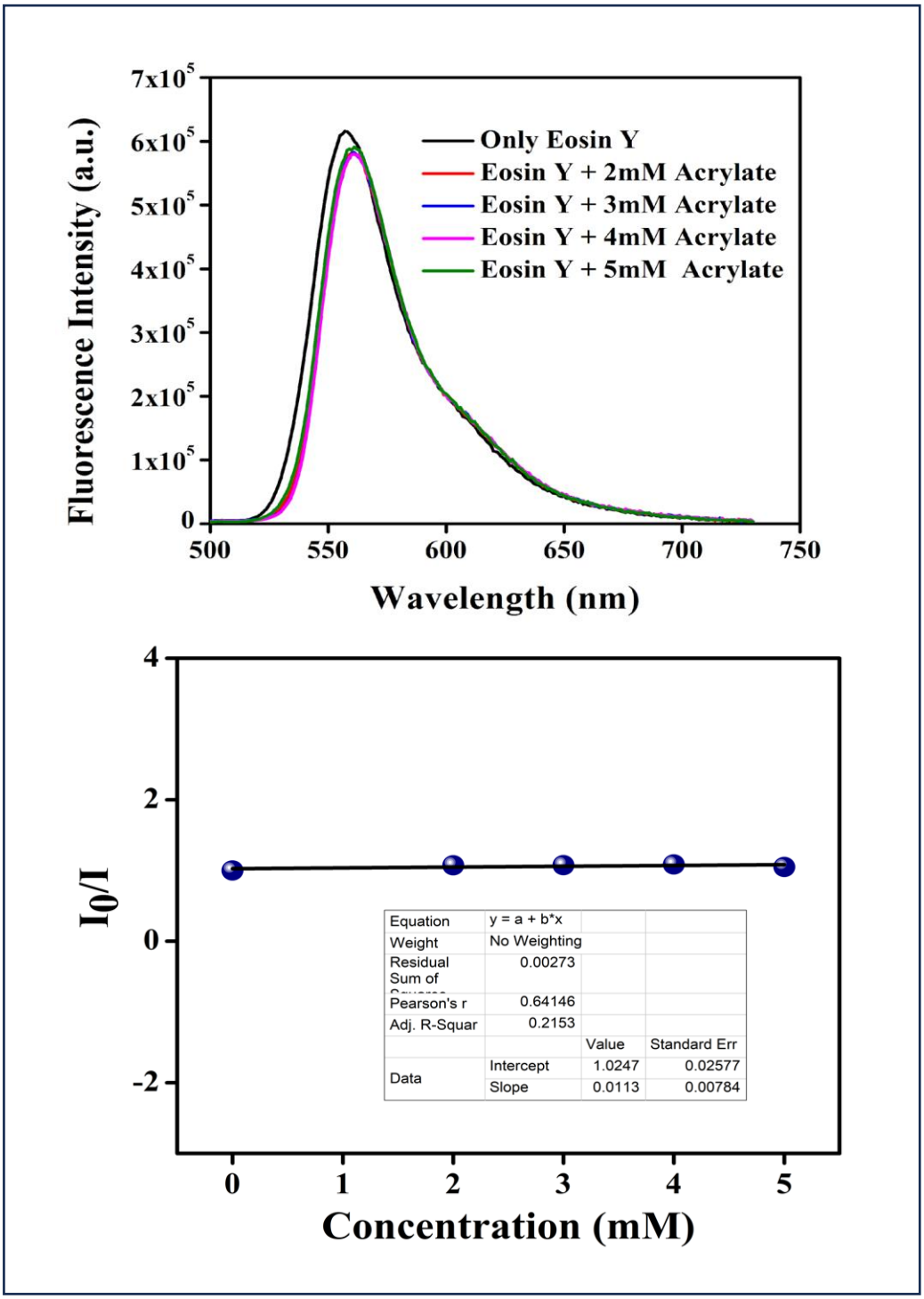


Figure 5. Fluorescence quenching experiments and Stern-Volmer plot of Eosin Y in presence of ethyl acrylate **1f**

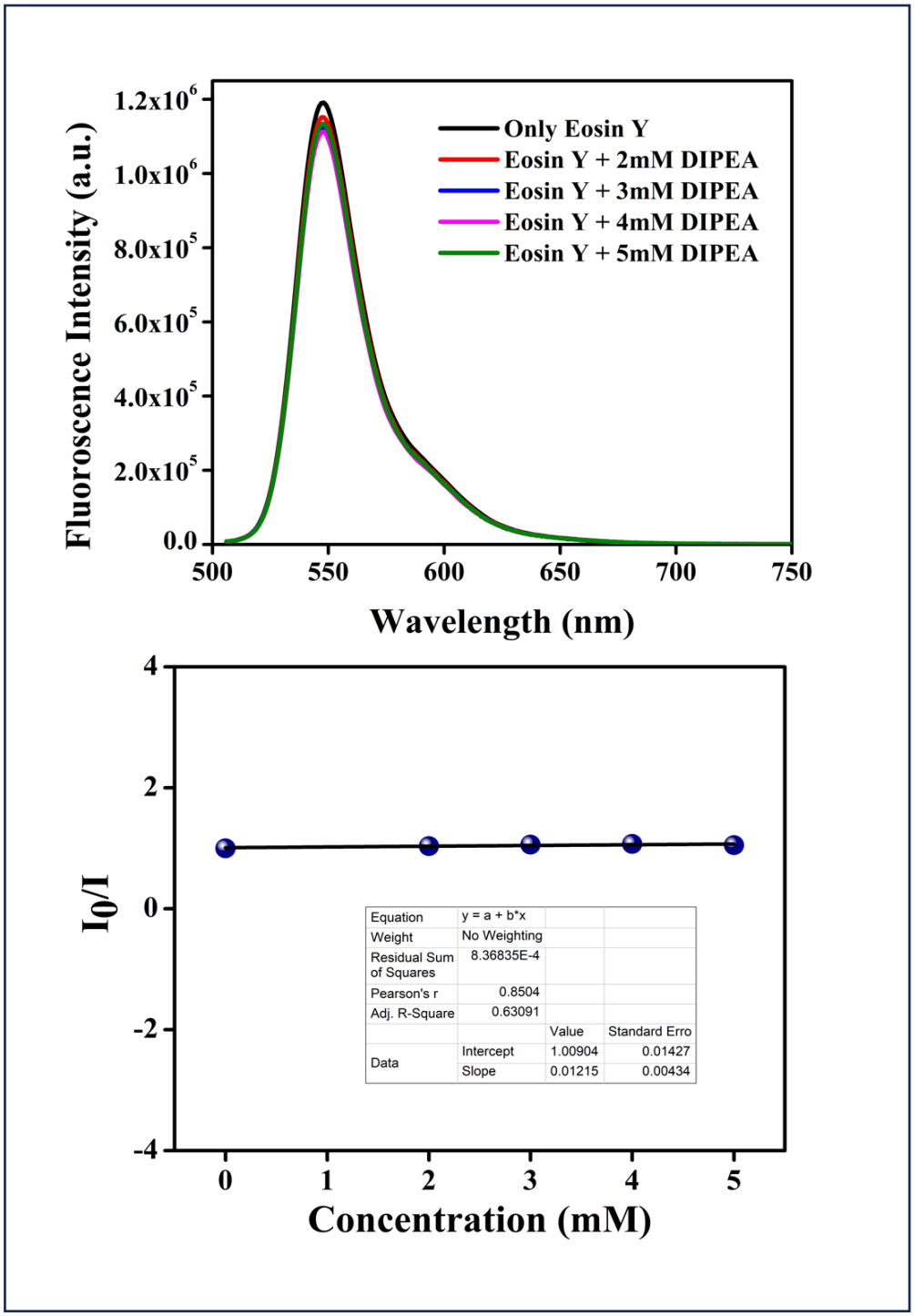


Figure 6. Fluorescence quenching experiments and Stern-Volmer plot of Eosin Y in presence of DIPEA

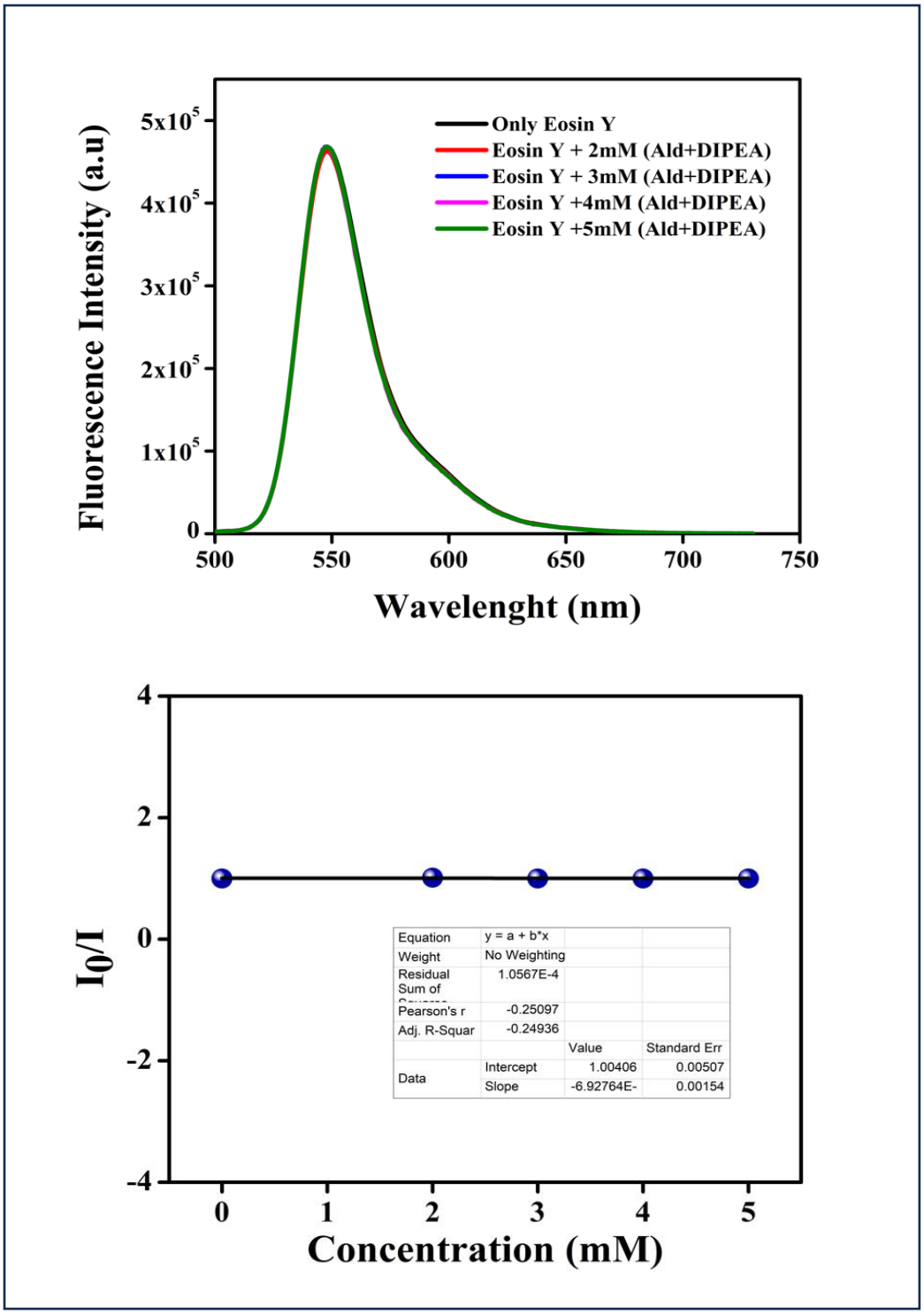


Figure 7. Fluorescence quenching experiments and Stern-Volmer plot of Eosin Y in presence of 4-cholorobenzaldehyde + DIPEA.

4.7.6.2. UV-Visible absorption of Eosin Y and reaction mixture:

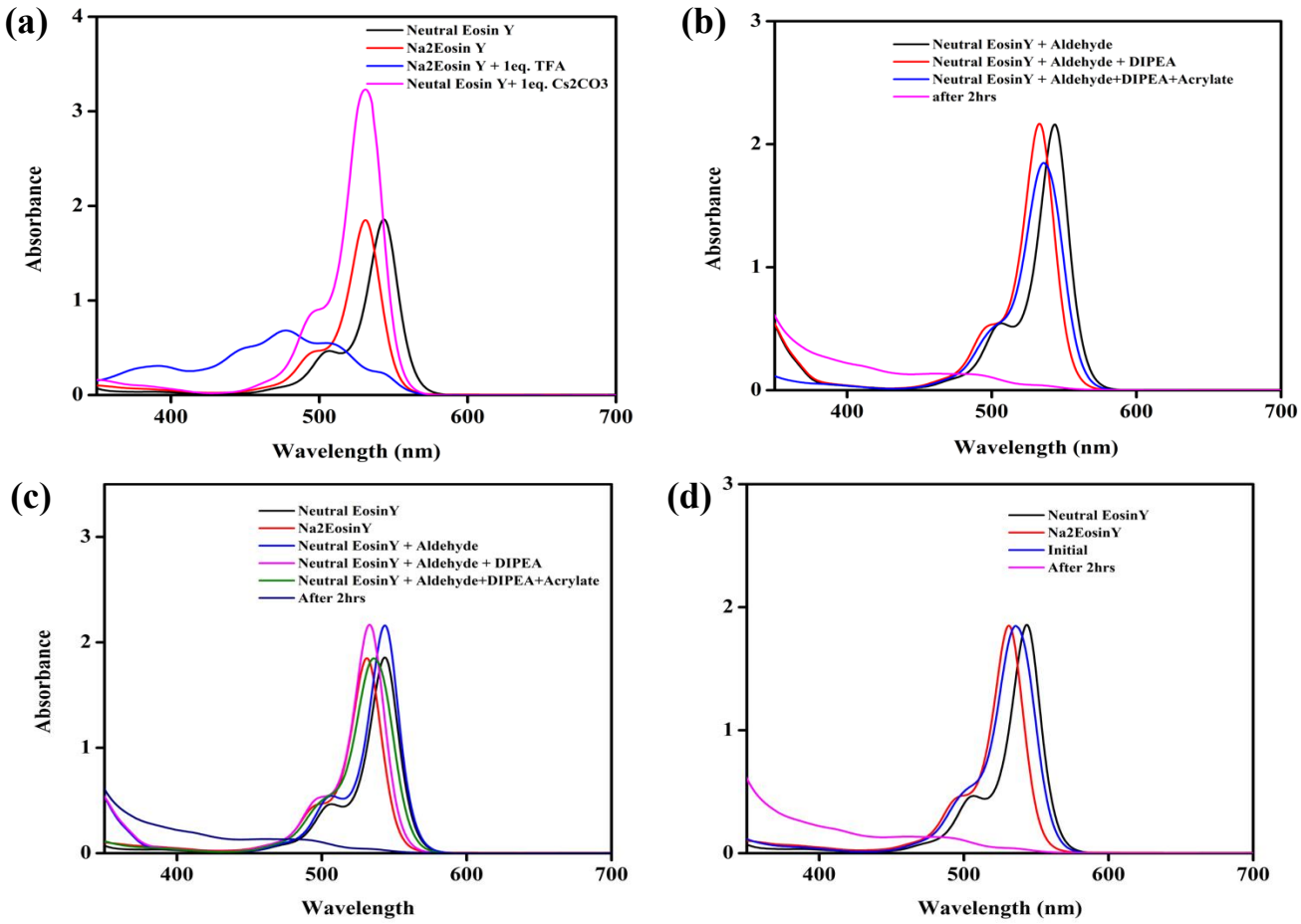


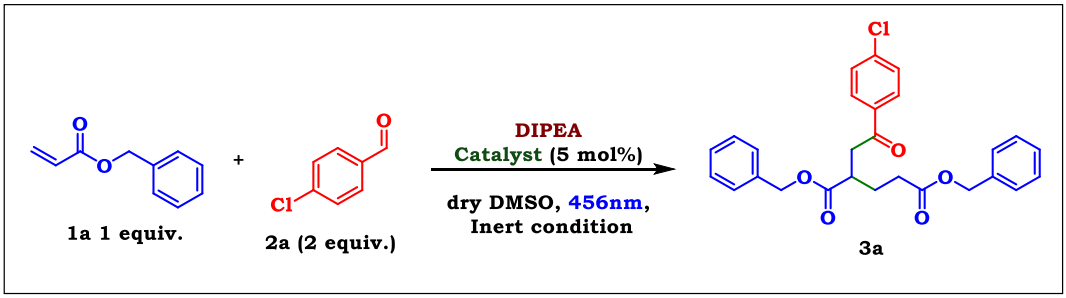
Figure 8. (a) UV-Vis absorption of different form of Eosin Y in DMSO. 20µM neutral Eosin Y, 20µM Na2Eosin Y, 20µM Na2Eosin Y+ 20µM TFA, 20µM neutral Eosin Y + 20µM Cs_2CO_3. **(b)** 20µM neutral Eosin Y + 1 equiv. 4-chloro benzaldehyde, 20µM neutral EosinY + 1 equiv. 4-chloro benzaldehyde + 1 equiv. DIPEA, 20µM neutral Eosin Y+ 1 equiv. 4-chlorobenzaldehyde aldehyde + 1 equiv. DIPEA + 1equiv. ethyl acrylate, after 2 hr of the reaction, in DMSO solvent. **(c)** 20µM neutral Eosin Y, 20µM Na2EosinY, 20µM neutral Eosin Y + 1 equiv. 4-chloro benzaldehyde, 20 µM neutral Eosin Y + 1 equiv. 4-chloro benzaldehyde+ 1equiv. DIPEA, 20 µM neutral Eosin Y + 1 equiv. 4-chlorobenzaldehyde + 1 eq. DIPEA + 1 equiv. Ethyl Acrylate **1f**, after 2 h of the reaction, in DMSO solvent. **(d)** 20 µM neutral Eosin Y, 20 µM Na2EosinY, absorption was recorded before the irradiation of light (reaction at 0 hr). Later, the absorption was recorded after 2 hr of the reaction.

Neutral Eosin Y in DMSO has a maximum absorption at 543 nm. Na_2Eosin Y in DMSO shows maximum absorption at 531 nm. 20µM neutral EosinY + 20µM Cs_2CO_3 in DMSO showed maximum absorption at 531 nm. 20µM Na_2EosinY+ 20 µM TFA in DMSO has maximum absorption at 542 nm. 20µM neutral Eosin Y + 1 equiv. 4-chloro benzaldehyde shows at maximum absorption at 543 nm. 20µM neutral EosinY + 1 equiv. 4-chloro benzaldehyde + 1equiv. DIPEA has a maximum absorption at 533nm. 20 µM neutral EosinY + 1equiv. 4-chloro benzaldehyde + 1 eq. DIPEA + 1 equiv. ethyl acrylate **1f** showed the maximum absorption at 535 nm.

At the beginning the reaction mixture shows maximum absorption at 536 nm. After 2 h of reaction, an absorption hump was observed at 530 nm. It showed that the reaction mixture has maximum absorption nearly equal to the absorption of Na_2Eosin Y and this proved that in the reaction mixture there must be a dianionic form of Eosin Y which is acting as the active form of the catalyst in the catalytic cycle.

4.7.6.3. pH study of the reaction mixture during the course of the reaction:

Table 4.7.6.3.1: pH of different reaction conditions:



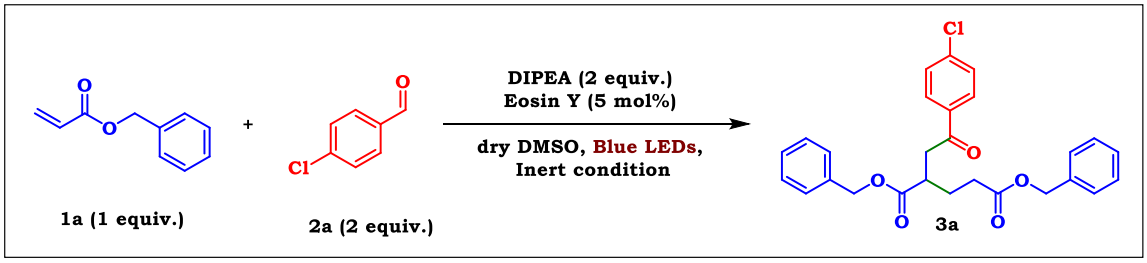
Entry	Reaction condition	pH	Yield (%)
1.	Initially, reaction mixture without DIPEA using Eosin Y	4.33	0
2.	After completion of the reaction, reaction mixture without DIPEA using Eosin Y	2.2	NR
3.	Initially, reaction mixture without DIPEA using Na_2Eosin Y	5.37	0
4.	After completion of the reaction, reaction mixture without DIPEA using Na_2Eosin Y	3.6	10
5.	Initially, reaction mixture with 1 equiv. DIPEA using Eosin Y	7.33	0

6.	After completion of the reaction, reaction mixture with 1 equiv. DIPEA using Eosin Y	4.9	40
7.	Initially, reaction mixture with 1 equiv. DIPEA using Na_2Eosin Y	8.84	0
8.	After completion of the reaction, reaction mixture with 1 equiv. DIPEA using Na_2Eosin Y	5.2	41
9.	Initially, reaction mixture with 2 equiv. DIPEA using Eosin Y	9.25	0
10.	After completion of the reaction, reaction mixture with 2 equiv. DIPEA using Eosin Y	7.2	80
11.	Initially, reaction mixture with 2 equiv. DIPEA using Na_2Eosin Y	8.56	0
12.	After completion of the reaction, reaction mixture with 2 equiv. DIPEA using Na_2Eosin Y	7.1	65

We observed that in the absence of DIPEA, Na_2Eosin Y afforded the product **3a** in 10% yield (*Table 4.7.6.3.1, Entry 4, Page 164).* While the reaction in the absence of DIPEA and neutral Eosin Y didn't proceed at all (Table 1, Entry 2, Page S14). Based on the pH values (measured using pH meter), we observed that the during the course of the transformation the pH of the reaction medium is getting lowered. This might be probably due to the hydrogen atom abstraction during the catalytic cycle. Around pH 7 the maximum yield of the product **3a** was formed (Table 1, Entry 10,12, page S14) as compared to the other conditions having different pH values (see Table 1). Based on these results, we concluded that the DIPEA is essentially maintaining the pH of the reaction to keep the active dianionic form available for the catalytic cycle.

4.8. Optimization table:

Table 4.8.1: Screening of different Blue LEDs

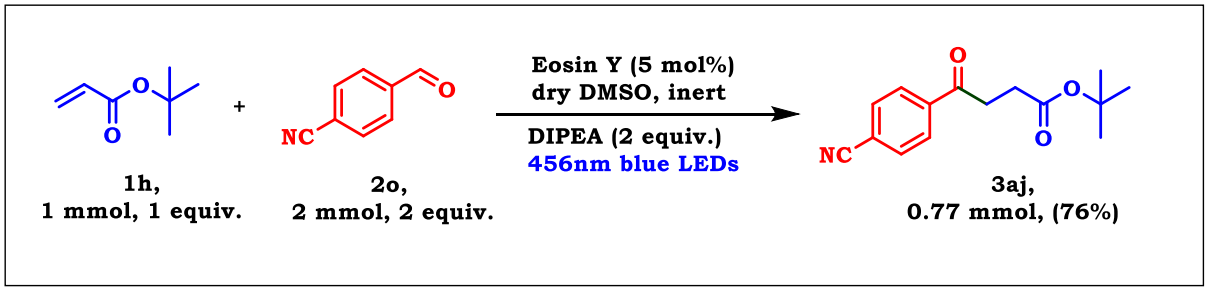


Entry	Lights	Temperature	Yield(%)[b]
1	525 nm (100% intensity)	40 °C	40
2	467 nm (100% intensity)	55 °C	42
3	456 nm (100% intensity)	70 °C	52
4	440 nm (100% intensity)	80 °C	40
5	456 nm (75% intensity)	60 °C	80
6	456 nm (50% intensity)	50 °C	55
7	456 nm (25% intensity)	40 °C	35
8[c]	2 * 456 nm (75% intensity)	25 °C	20
9[c]	2 * 456 nm (100% intensity)	35 °C	61
10[d]	60 W Blue LEDs	60 °C	76

Reaction conditions: *Unless otherwise noted. [a]all the reactions were carried out using Benzyl acrylate* ***1a*** *(1 mmol), 4-chloro benzaldehyde* ***2a*** *(2 mmol), DIPEA (2 mmol), Eosin Y (5 mol%), using a single Kessil Lamp (Blue LED) under inert atmosphere in dry DMSO keeping the fan switched off. [b] Yields are calculated after purification using column chromatography. [c] used 2 Kessil LED lamps with fan switched on. [d] 60 W Blue LED has been used with external temperature 60 °C, instead of Kessils light.*

4.9. Undesired transformation:

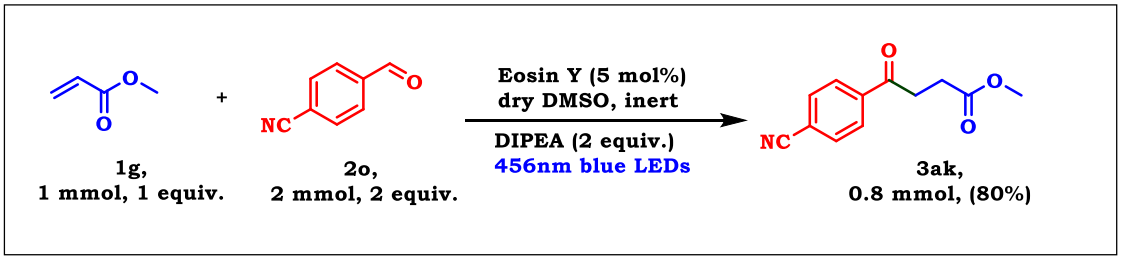
It is important to note that surprisingly the reaction of ^{t}butyl acrylate **1h** and 4-cyano benzaldehyde **2o** afforded the unexpected γ-keto ester **3aj** instead of the substituted glutaric acid diester as a final product. The compound **3aj** was obtained as off-white solid following the general procedure (GP1) (174 mg, 80% yield), R_f = 0.25 (Petroleum ether/EtOAc 70:30).



The reaction of **1g** and **2o** following the the general procedure (**GP1**) afforded the corresponding compound **3ak** as off-white solid (174 mg, 80% yield), R_f = 0.2 (Petroleum ether/EtOAc 70:30).

4.10. Light Switch ON/OFF Experiment:

In order to understand and evaluate the impact of light and heat on the outcome of the yield of the product **3f** and also examine whether or not the reaction is proceeding via radical chain mechanism Light ON/OFF experiment has been carried out.



To an oven dried 10 mL crimp cap vial charged with magnetic stir bar was added 4-chloro benzaldehyde **2a** (2 mmol, 2 equiv.), Eosin Y (5 mol%) and DIPEA (2 mmol, 2 equiv.) at room temperature under argon atmosphere. The vial was sealed with aluminium crimp cap using a crimper and was purged again with argon. Then anhydrous DMSO (3 mL) was added under argon. The reaction mixture was degasified using argon for 30 minutes under constant purging and monitoring. After the degasification ethyl acrylate **1f** (1 mmol, 1 equiv.) was added under inert atmosphere. A total of 9 vials containing the above-mentioned reactants were set up. All the 9 vials were irradiated with 456 nm Kessil LED with 75% intensity (the temperature turns around 60 $^{\circ}$C-external temperature-measured by IR-thermometer, by keeping the fan switched off).

After stirring the reaction mixture for 2 h, one of the reaction vials was taken out and subjected to purification (following the General Procedure-1, using column chromatography) to calculate the yield (see Fig. 3). While the rest of 8 reaction vials were stirred under dark for next 2 h. After the stirring for a total of 4 h (with and without light), one more vial was taken out and subjected to purification (following the General Procedure-1, using column chromatography) to calculate the yield. While the remaining 7 reaction vials were kept under irradiation again for next 2 h and we followed the same procedure of switching off/on LED for remaining all the vials of an interval 2 h over a period of total 18 h for the last vial. The yield for all the reaction vials were calculated after the purification using column chromatography. The detailed results are given below in a bar diagram.

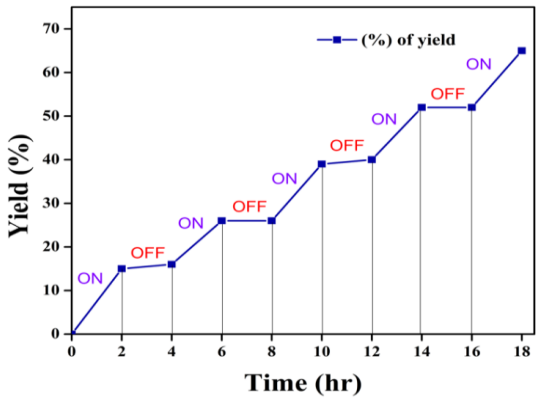


Figure 3: Light Switch ON/OFF experiment

Based on the above results, we concluded that the reaction does not proceed via radical-chain mechanism and in order to support the observation further we calculated the quantum yield of **3f**.

4.11. Quantum yield calculation of 3f:

a) Determination of quantum yield by standard ferrioxalate actinometry

Determination of the light intensity at 450 nm:

Yoon's procedure was followed to calculate the photon flux of the spectrophotometer by standard ferrioxalate actinometry. A 0.15 M solution of ferrioxalate was prepared by dissolving 2.21 g of potassium ferrioxalate hydrate in 30 mL of 0.05 M H_2SO_4. A buffered solution of phenanthroline was prepared by dissolving 50 mg of phenanthroline and 11.25 g of sodium acetate in 50 mL of 0.5 M H_2SO_4. Both solutions were stored under dark. To determine the photon flux of the spectrophotometer, 2.0 mL of the ferrioxalate solution was placed in a cuvette and irradiated for 60 seconds at λ = 456 nm with an emission slit width at 10.0 nm. After irradiation, 0.35 mL of the phenanthroline solution was added to the cuvette. The solution was then allowed to rest for 1 hour to allow the ferrous ions to completely coordinate to the phenanthroline. The absorbance of the solution was measured at 510 nm. A non-irradiated sample was also prepared and the absorbance at 510 nm measured. Conversion was calculated using Eq. (1).

$$\text{Mol } Fe^{2+} = \frac{V.\Delta A}{l.\varepsilon} \qquad \text{Eq.(1)}$$

Where V is the total volume (0.00235 L) of the solution after addition of phenanthroline, ΔA is the difference in absorbance at 510 nm between the irradiated and non-irradiated solutions, l is

the path length (1.000 cm), and ε is the molar absorptivity at 510 nm (11,100 L mol–1 cm–1). The photon flux can be calculated using Eq (2).

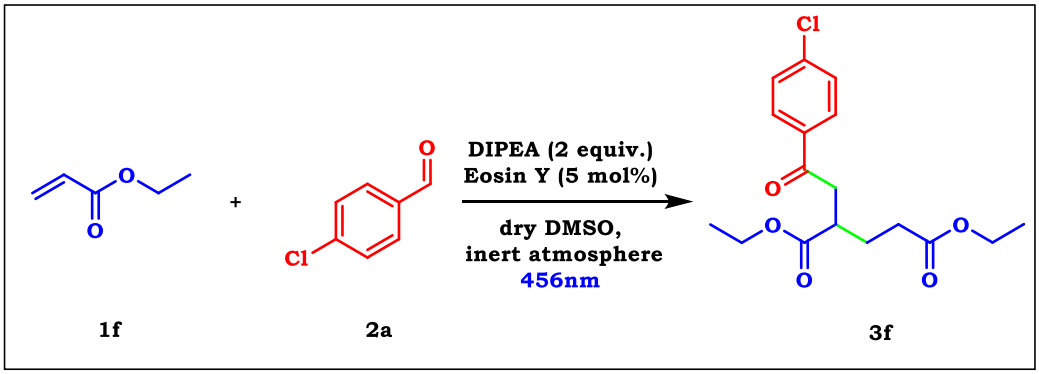
$$\text{Photon flux} = \frac{mol\ Fe^{2+}}{\phi.t.f} \qquad \text{Eq.(2)}$$

Where Φ is the quantum yield for the ferrioxalate actinometer (1.01 for a 0.15 M solution at λ = 450 nm), t is the time (60 seconds), and f is the fraction of light absorbed at λ = 450 nm (0.8979, vide infra). The photon flux was calculated (average of three experiments) to be 1.55 × 10^{-9} einstein s^{-1}.

$$\text{Mol } Fe^{2+} = \frac{0.00235\ L.(1.730-1.332)}{1.00\ cm.11100\ Lcm^{-1}mol^{-1}} = 8.426*10^{-8}\ \text{mol}$$

$$\text{Proton flux} = \frac{8.426*10^{-8}\ mol}{1.01.60s.0.8979} = 1.55\ *10^{-9}\ \text{einstein}\ s^{-1}$$

Determination of quantum yield:

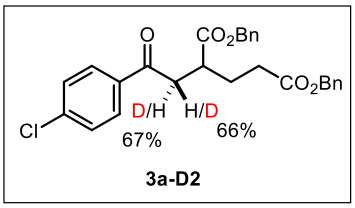


The sample was stirred and irradiated (λ = 456 nm, slit width = 10.0 nm) for 14400 s (4 h). After irradiation, the solvent was removed. The yield of product formed was determined as 5% by crude ^{1}H NMR based on a 1,3,5-trimethoxylbenzene standard. The quantum yield was determined using Eq. (3). Essentially all incident light (f > 0.999, vide infra) is absorbed by the eosin Y at the reaction conditions described above. Φ (5% NMR yield of **3f**) = 0.56.

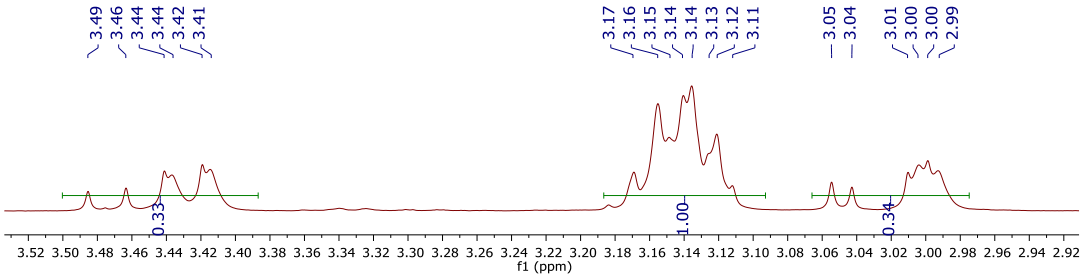
$$\phi = \frac{mol\ product}{flux.t.f} \qquad \text{Eq. (3)}$$

$$= \frac{12.47*10^{-6}}{1.55*10^{-9}\ einstein\ s^{-1}.14400s.1} = \mathbf{0.56}$$

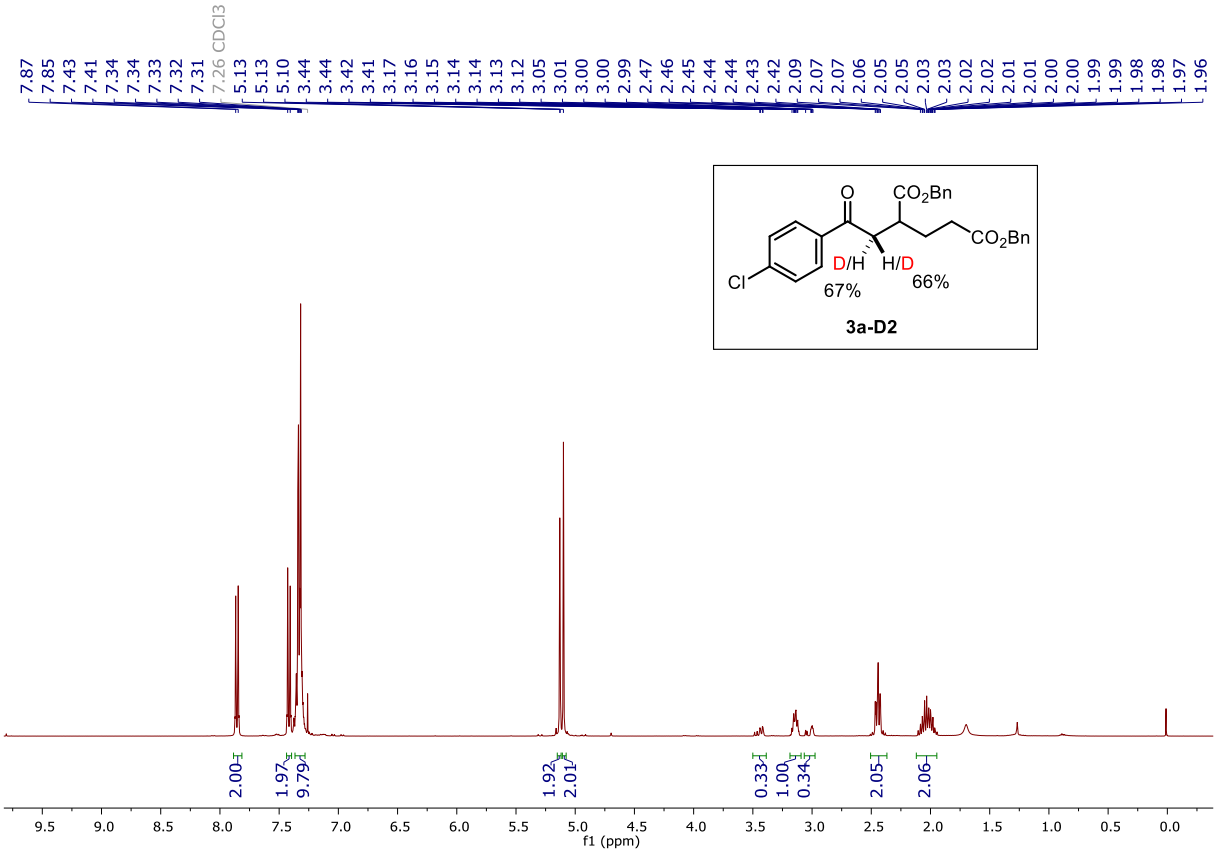
4.12. NMR data of reaction of 2a and 1a in D_2O (3a-D2):



^{1}H NMR (400 MHz, $CDCl_3$) δ 7.86 (d, *J* = 8.58 Hz, 2H), 7.42 (d, *J* = 8.62 Hz, 2H), 7.37 – 7.27 (m, 10H), 5.13 (d, *J* = 1.25 Hz, 2H), 5.10 (s, 2H), 3.44 (m, 0.33H), 3.15 (dt, *J* = 8.06, 5.77 Hz, 1H), 3.02 (m, 0.34H), 2.44 (m, 2H), 2.03 (m, 2H).



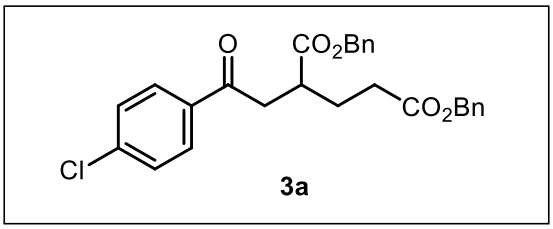
Expansion of **3a-D$_2$** ^{1}H NMR spectra



^{1}H NMR spectra of **3a-D$_2$,** $CDCl_3$, 400 MHz

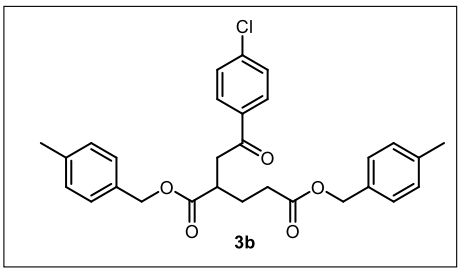
4.13. Experimental data:

Dibenzyl 2-(2-(4-chlorophenyl)-2-oxoethyl)pentanedioate (3a)



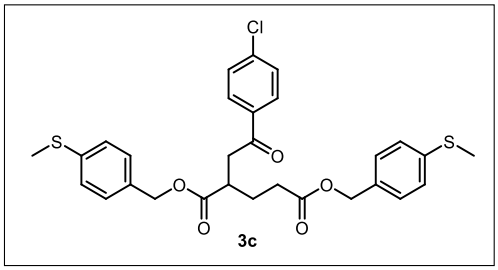
The title compound **3a** was prepared according to the general procedure (**GP1**) starting from benzyl acrylate **1a** (1 mmol) and 4-Chlorobenzaldehyde **2a** (2 mmol). White solid (185 mg, 80% yield), R_f = 0.2 (petroleum ether/EtOAc 80:20). **IR** (neat): 1731, 1686, 1589, 1455, 1157, 1091, 995, 818, 745, 697 cm^{-1}. **^{1}H NMR (400 MHz, $CDCl_3$)** δ 7.77 (d, *J* = 8.68 Hz, 2H), 7.32 (d, *J* = 8.68 Hz, 2H), 7.25 (m, 10H), 5.06 (s, 2H), 5.02 (s, 2H), 3.37 (dd, *J* = 17.73, 8.93 Hz, 1H), 3.08 (tt, *J* = 8.44, 4.22 Hz, 1H), 2.94 (dd, *J* = 17.73, 4.65 Hz, 1H), 2.37 (td, *J* = 7.40, 2.14 Hz, 2H), 1.96 (m, 2H). **^{13}C {^{1}H} NMR (100 MHz, $CDCl_3$)** δ 196.4, 174.4, 172.4, 139.6, 135.8, 135.7, 134.7, 129.4, 128.8, 128.5, 128.5, 128.2, 128.2, 128.1, 128.1, 66.5, 66.3, 40.2, 39.6, 31.7, 26.9. **HRMS (ESI TOF)** *m/z* calcd. For $C_{27}H_{26}ClO_5$ $[M + H]^+$ 465.1463 found 465.1468.

Bis(4-methylbenzyl) 2-(2-(4-chlorophenyl)-2-oxoethyl)pentanedioate (3b)



The title compound **3b** was prepared according to the general procedure (**GP1**) starting from substituted benzyl acrylate **1b** (1 mmol) and 4-Chlorobenzaldehyde **2a** (2 mmol). semi solid (209 mg, 85% yield), R_f = 0.22 (petroleum ether/EtOAc 80:20). **^{1}H NMR (400 MHz, $CDCl_3$)** δ 7.85 (d, *J* = 8.58 Hz, 2H), 7.42 (d, *J* = 8.59 Hz, 2H), 7.22 (dd, *J* = 8.20, 6.70 Hz, 4H), 7.14 (dd, *J* = 13.96, 7.84 Hz, 4H), 5.09 (d, *J* = 1.80 Hz, 2H), 5.06 (s, 2H), 3.44 (dd, *J* = 17.59, 8.80 Hz, 1H), 3.18 – 3.08 (m, 1H), 3.01 (dd, *J* = 17.57, 4.76 Hz, 1H), 2.47 – 2.40 (m, 2H), 2.35 (s, 3H), 2.34 (s, 3H), 2.10 – 1.92 (m, 2H). **^{13}C {^{1}H} NMR (100 MHz, $CDCl_3$)** δ 196.6, 174.5, 172.7, 139.8, 138.1, 134.9, 132.9, 132.8, 129.6, 129.4, 129.3, 129.0, 128.5, 128.4, 66.7, 66.5, 40.3, 39.8, 31.9, 27.0, 21.3. **HRMS (ESI TOF)** *m/z* calcd. For $C_{29}H_{30}ClO_5$ $[M + H]^+$ 493.1776 found 493.1770.

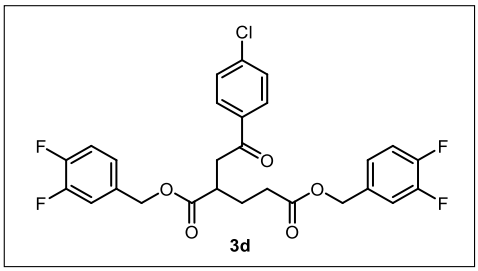
Bis(4-(methylthio)benzyl) 2-(2-(4-chlorophenyl)-2-oxoethyl)pentanedioate (3c)



3c

The title compound **3c** was prepared according to the general procedure (**GP1**) starting from substituted benzyl acrylate **1c** (1 mmol) and 4-Chlorobenzaldehyde **2a** (2 mmol). semi solid (224 mg, 81% yield), R_f = 0.2 (petroleum ether/EtOAc 70:30). **^{1}H NMR (400 MHz, $CDCl_3$)** δ 7.87 – 7.81 (m, 2H), 7.42 (d, *J* = 8.56 Hz, 2H), 7.25 – 7.21 (m, 6H), 7.20 (s, 2H), 5.07 (s, 2H), 5.04 (s, 2H), 3.43 (dd, *J* = 17.60, 8.82 Hz, 1H), 3.12 (tdd, *J* = 8.33, 5.75, 4.62 Hz, 1H), 3.00 (dd, *J* = 17.60, 4.66 Hz, 1H), 2.47 (s, 3H), 2.47 (s, 3H), 2.45 – 2.38 (m, 2H), 2.09 – 1.90 (m, 2H). **^{13}C {^{1}H} NMR (100 MHz, $CDCl_3$)** δ 196.6, 174.5, 172.6, 139.9, 132.6, 132.6, 129.6, 129.1, 129.0, 126.6, 126.6, 66.4, 66.2, 40.4, 39.8, 31.9, 27.0, 15.8. **HRMS (ESI TOF)** *m/z* calcd. For $C_{29}H_{30}ClO_5S_2$ $[M + H]^+$ 557.1218 found 557.1221.

Bis (3,4-difluorobenzyl) 2-(2-(4-chlorophenyl)-2-oxoethyl)pentanedioate (3d)

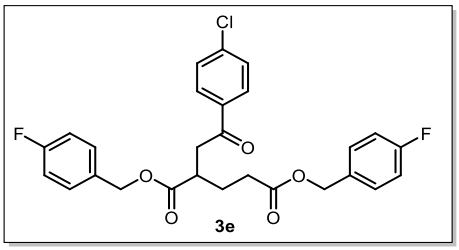


3d

The title compound **3d** was prepared according to the general procedure (**GP1**) starting from substituted benzyl acrylate **1d** (1 mmol) and 4-Chlorobenzaldehyde **2a** (2 mmol). semi solid (210 mg, 79% yield), R_f = 0.22 (petroleum ether/EtOAc 80:20). **^{1}H NMR (400 MHz, $CDCl_3$)** δ 7.92 – 7.82 (m, 2H), 7.47 – 7.41 (m, 2H), 6.86 (ddtd, *J* = 8.94, 6.75, 4.73, 2.40 Hz, 4H), 6.74 (tdq, *J* = 7.96, 6.16, 1.95 Hz, 2H), 5.10 (d, *J* = 4.42 Hz, 2H), 5.07 (s, 2H), 3.51 – 3.41 (m, 1H), 3.20 – 3.11 (m, 1H), 3.08 (dd, *J* = 17.54, 4.53 Hz, 1H), 2.49 (td, *J* = 7.37, 1.51 Hz, 2H), 2.13 – 1.98 (m, 2H). **^{13}C {^{1}H} NMR (100 MHz, $CDCl_3$)** δ 196.4, 174.3, 172.2, 163.23 (d, *J* = 250 Hz), 163.22 (d, *J* = 245Hz), 163.1 (d, *J* = 250 Hz), 163.10 (d, *J* = 245 Hz), 140.1, 139.67 (td, *J* = 9.23, 1.10 Hz), 134.7, 129.6, 129.1, 110.73 (d, *J*= 26 Hz), 110.73 (d, *J*= 12 Hz), 110.71 (d, *J*= 25 Hz), 110.71 (d, *J*= 11 Hz), 103.74 (t, *J*= 25 Hz), 103.69 (t, *J*= 25 Hz), 102.82 (t, *J* = 25.39

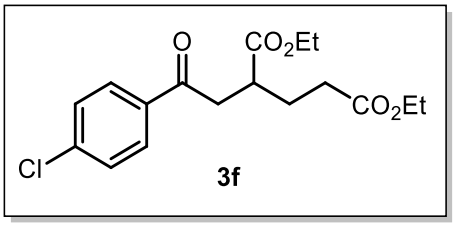
Hz), 65.3, 65.3, 65.3, 65.1, 65.1, 65.1, 40.5, 39.7, 31.7, 26.9. **^{19}F NMR (377 MHz, $CDCl_3$)** δ -109.17, -109.20, -109.73. **HRMS (ESI TOF)** *m/z* calcd. For $C_{27}H_{22}ClF_4O_5$ $[M + H]^+$ 537.1086 found 537.1080.

Bis(4-fluorobenzyl) 2-(2-(4-chlorophenyl)-2-oxoethyl)pentanedioate (3e):



The title compound **3e** was prepared according to the general procedure (**GP1**) starting from substituted benzyl acrylate **1e** (1 mmol) and 4-Chlorobenzaldehyde **2a** (2 mmol). semi solid (205 mg, 82% yield), R_f = 0.22 (petroleum ether/EtOAc 80:20). **^{1}H NMR (400 MHz, $CDCl_3$)** δ 7.89 – 7.79 (m, 2H), 7.44 – 7.37 (m, 2H), 7.30 (ddd, *J* = 8.8, 5.3, 2.2 Hz, 4H), 7.01 (dt, *J* = 13.3, 8.7 Hz, 4H), 5.06 (d, *J* = 12.6 Hz, 4H), 3.43 (dd, *J* = 17.6, 8.8 Hz, 1H), 3.16 – 2.96 (m, 2H), 2.45 – 2.36 (m, 2H), 2.07 – 1.91 (m, 2H). **^{13}C {^{1}H} NMR (100 MHz, $CDCl_3$)** δ 196.40, 174.40, 172.40, 162.7 (d, *J* = 249 Hz), 162.65 (d, *J* = 241 Hz), 139.85, 134.72, 131.6 (t, *J*= 2.8 Hz), 130.3 (d, *J*= 4 Hz), 130.2 (d, *J*= 4 Hz), 129.44, 129.42, 128.98, 128.95, 128.93, 115.49 (d, *J* = 28 Hz), 115.49 (d, *J*= 15 Hz), 65.92, 65.72, 40.30, 39.63, 31.71, 26.92. **^{19}F NMR (377 MHz, $CDCl_3$)** δ -113.42, -113.54. **HRMS (ESI TOF)** *m/z* calcd. For $C_{27}H_{24}ClF_2O_5$ $[M + H]^+$ 501.1275 found 501.1277.

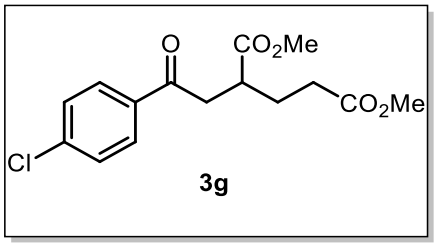
Diethyl 2-(2-(4-chlorophenyl)-2-oxoethyl)pentanedioate (3f)



The title compound **3b** was prepared according to the general procedure (**GP1**) starting from ethyl acrylate **1f** (1 mmol) and 4-Chlorobenzaldehyde **2a** (2 mmol). Colorless liquid (119 mg, 70% yield), R_f = 0.22 (petroleum ether/EtOAc 80:20). **^{1}H NMR (400 MHz, $CDCl_3$)** δ 7.88 (d, *J* = 8.6 Hz, 2H), 7.43 (d, *J* = 8.6 Hz, 2H), 4.20 – 4.10 (m, 4H), 3.44 (q, *J* = 8.6, 8.1 Hz, 1H), 3.09 – 2.97 (m, 2H), 2.40 (ddd, *J* = 7.9, 7.0, 2.1 Hz, 2H), 2.07 – 1.86 (m, 2H), 1.25 (td, *J* = 7.2,

0.8 Hz, 6H). **^{13}C{^{1}H} NMR (100 MHz, $CDCl_3$)** δ 196.7, 174.8, 172.9, 139.9, 135.0, 129.6, 129.1, 60.9, 60.7, 40.5, 39.8, 32.0, 27.2, 14.3, 14.3. **HRMS (ESI TOF)** *m/z* calcd. For $C_{17}H_{22}ClO_5$ $[M + H]^+$ 341.1150 found 341.1156.

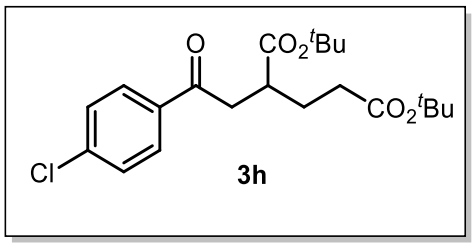
Dimethyl 2-(2-(4-chlorophenyl)-2-oxoethyl)pentanedioate (3g)



3g

The title compound **3g** was prepared according to the general procedure (**GP1**) starting from methyl acrylate **1g** (1 mmol) and 4-Chlorobenzaldehyde **2a** (2 mmol). Colorless liquid (106 mg, 68% yield), R_f = 0.15 (petroleum ether/EtOAc 80:20). **^{1}H NMR (400 MHz, $CDCl_3$)** δ 7.92 – 7.86 (m, 2H), 7.46 – 7.42 (m, 2H), 3.71 (s, 3H), 3.68 (s, 3H), 3.54 – 3.36 (m, 1H), 3.17 – 2.97 (m, 2H), 2.52 – 2.33 (m, 2H), 2.11 – 1.89 (m, 2H). **^{13}C {^{1}H} NMR (100 MHz, $CDCl_3$)** δ 196.6, 175.2, 173.2, 139.9, 134.8, 129.5, 129.1, 52.1, 51.8, 40.5, 39.6, 31.7, 27.1. **HRMS (ESI TOF)** *m/z* calcd. For $C_{15}H_{17}ClO_5Na^+$ $[M + Na]^+$ 335.0657 found 335.0664.

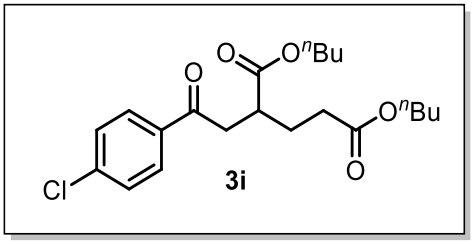
Di-tert-butyl 2-(2-(4-chlorophenyl)-2-oxoethyl)pentanedioate (3h)



3h

The title compound **3h** was prepared according to the general procedure (**GP1**) starting from tert-butyl acrylate **1h** (1 mmol) and 4-Chlorobenzaldehyde **2a** (2 mmol). Colorless liquid (140 mg, 71% yield), R_f = 0.3 (petroleum ether/EtOAc 80:20). **^{1}H NMR (400 MHz, $CDCl_3$)** δ 7.91 – 7.85 (m, 2H), 7.44 – 7.39 (m, 2H), 3.37 (dd, *J* = 18.5, 10.1 Hz, 1H), 3.00 – 2.83 (m, 2H), 2.31 (ddd, *J* = 8.3, 7.2, 1.8 Hz, 2H), 1.96 – 1.80 (m, 2H), 1.43 (s, 9H), 1.43 (s, 9H). **^{13}C{^{1}H} NMR (100 MHz, $CDCl_3$)** δ 196.9, 174.1, 172.3, 139.7, 135.2, 129.6, 129.0, 81.0, 80.6, 40.7, 40.5, 33.1, 28.2, 28.1, 27.4. **HRMS (ESI TOF)** *m/z* calcd. For $C_{21}H_{30}ClO_5$ $[M + H]^+$ 397.1776 found 397.1780.

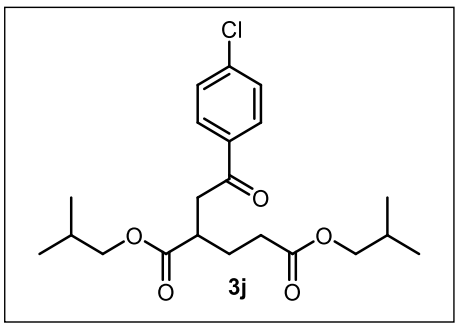
Dibutyl 2-(2-(4-chlorophenyl)-2-oxoethyl)pentanedioate (3i)



3i

The title compound **3i** was prepared according to the general procedure (**GP1**) starting from n-butyl acrylate **1i** (1 mmol) and 4-Chlorobenzaldehyde **2a** (2 mmol). Colorless liquid (142 mg, 72% yield), R_f = 0.27 (petroleum ether/EtOAc 80:20). **^{1}H NMR (400 MHz, CDCl$_3$)** δ 7.93 – 7.86 (m, 2H), 7.49 – 7.39 (m, 2H), 4.09 (dt, *J* = 7.8, 6.7 Hz, 4H), 3.50 – 3.41 (m, 1H), 3.13 – 2.97 (m, 2H), 2.42 (ddd, *J* = 7.9, 7.0, 2.1 Hz, 2H), 2.07 – 1.89 (m, 2H), 1.65 – 1.57 (m, 4H), 1.41 – 1.32 (m, 4H), 0.92 (td, *J* = 7.4, 5.3 Hz, 6H). **^{13}C {^{1}H} NMR (100 MHz, CDCl$_3$)** δ 196.7, 174.9, 173.0, 139.8, 135.0, 129.6, 129.0, 64.8, 64.6, 40.4, 39.8, 32.0, 30.7, 30.7, 27.2, 19.2, 19.2, 13.8, 13.8. **HRMS (ESI TOF)** *m/z* calcd. For $C_{21}H_{30}ClO_5$ $[M + H]^+$ 397.1776 found 397.1774.

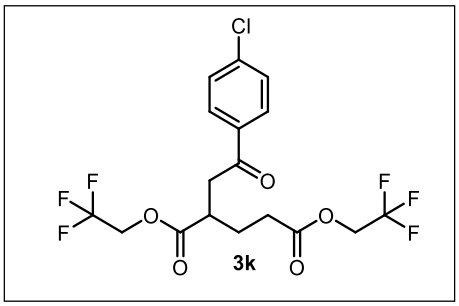
Diisobutyl 2-(2-(4-chlorophenyl)-2-oxoethyl)pentanedioate (3j)



3j

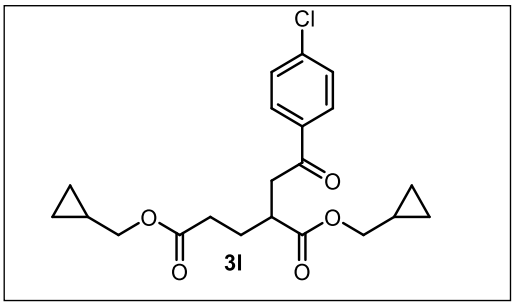
The title compound **3j** was prepared according to the general procedure (**GP1**) starting from iso-butyl acrylate **1j** (1 mmol) and 4-Chlorobenzaldehyde **2a** (2 mmol). Colorless liquid (140 mg, 71% yield), R_f = 0.28 (petroleum ether/EtOAc 80:20). **^{1}H NMR (400 MHz, CDCl$_3$)** δ 7.88 (d, J = 8.53 Hz, 2H), 7.42 (d, *J* = 8.53 Hz, 2H), 3.88 – 3.83 (m, 4H), 3.45 (dd, *J* = 17.34, 8.57 Hz, 1H), 3.12 – 2.96 (m, 2H), 2.47 – 2.39 (m, 2H), 2.07 – 1.83 (m, 4H), 0.92 (d, *J* = 1.85 Hz, 6H), 0.90 (d, *J* = 1.86 Hz, 6H). **^{13}C {^{1}H} NMR (100 MHz, CDCl$_3$)** δ 196.6, 174.8, 172.9, 139.8, 134.9, 129.6, 129.0, 71.1, 70.8, 40.4, 39.9, 32.0, 27.8, 27.2, 19.2, 19.2. **HRMS (ESI TOF)** *m/z* calcd. For $C_{21}H_{29}ClO_5Na^+$ $[M + Na]^+$ 419.1596 found 419.1600.

Bis(2,2,2-trifluoroethyl) 2-(2-(4-chlorophenyl)-2-oxoethyl)pentanedioate (3k)



The title compound **3k** was prepared according to the general procedure (**GP1**) starting from 2,2,2-trifluoroethyl acrylate **1k** (1 mmol) and 4-Chlorobenzaldehyde **2a** (2 mmol). Colorless liquid (154 mg, 69% yield), R_f = 0.25 (petroleum ether/EtOAc 80:20). **IR** (neat): 1753, 1687, 1591, 1404, 1278, 1140, 1092, 975, 818, 665 cm^{-1}. **^{1}H NMR (400 MHz, $CDCl_3$)** δ 7.88 (d, *J* = 8.66 Hz, 2H), 7.45 (d, *J* = 8.67 Hz, 2H), 4.59 (dq, *J* = 12.59, 8.40 Hz, 1H), 4.52 – 4.40 (m, 3H), 3.54 – 3.40 (m, 1H), 3.22 – 3.09 (m, 2H), 2.60 – 2.54 (m, 2H), 2.11 – 1.99 (m, 2H). **^{13}C{^{1}H} NMR (100 MHz, $CDCl_3$)** δ 196.0, 173.1, 171.1, 140.2, 134.6, 129.6, 129.2, 124.4, 124.4, 121.6, 121.6, 118.9, 61.2, 61.1, 60.9, 60.7, 60.5, 60.4, 60.1, 59.9, 40.4, 39.3, 31.1, 26.5. ^{19}F NMR (377 MHz, $CDCl_3$) δ -73.8, -73.9. **HRMS (ESI TOF)** *m/z* calcd. For $C_{17}H_{16}ClF_6O_5$ $[M + H]^+$ 449.0585 found 449.0588.

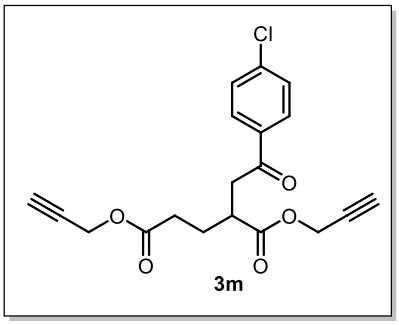
Bis(cyclopropylmethyl) 2-(2-(4-chlorophenyl)-2-oxoethyl)pentanedioate (3l)



The title compound **3l** was prepared according to the general procedure (**GP1**) starting from cyclopropylmethyl acrylate **1l** (1 mmol) and 4-Chlorobenzaldehyde **2a** (2 mmol). Colorless liquid (141 mg, 71% yield), R_f = 0.25 (petroleum ether/EtOAc 80:20). **^{1}H NMR (400 MHz, $CDCl_3$)** δ 7.92 – 7.85 (m, 2H), 7.46 – 7.38 (m, 1H), 3.99 – 3.85 (m, 4H), 3.46 (dd, *J* = 17.41, 8.66 Hz, 1H), 3.14 – 2.94 (m, 2H), 2.46 (ddd, *J* = 8.37, 7.18, 1.77 Hz, 2H), 2.09 – 1.91 (m, 3H), 1.19 – 1.04 (m, 2H), 0.58 – 0.50 (m, 4H), 0.26 (tdd, *J* = 5.38, 4.17, 2.51 Hz, 4H). **^{13}C {^{1}H} NMR (100 MHz, $CDCl_3$)** δ 196.7, 174.91, 173.0, 139.8, 134.9, 129.6, 129.1, 69.7, 69.5,

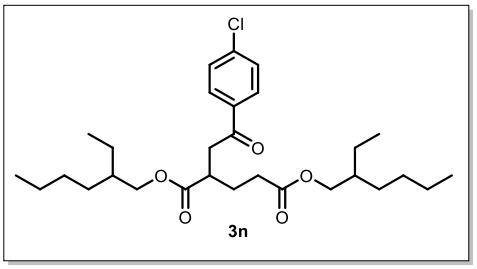
40.5, 39.9, 31.9, 27.2, 9.9, 9.9, 3.4, 3.4, 3.3. **HRMS (ESI TOF)** *m/z* calcd. For $C_{21}H_{25}ClO_5Na^+$ $[M + Na]^+$ 415.1283 found 415.1292.

Di(prop-2-yn-1-yl) 2-(2-(4-chlorophenyl)-2-oxoethyl)pentanedioate (3m)



The title compound **3m** was prepared according to the general procedure (**GP1**) starting from prop-2-yn-1-yl acrylate **1m** (1 mmol) and 4-chlorobenzaldehyde **2a** (2 mmol). Colorless liquid (126 mg, 70% yield), R_f = 0.24 (petroleum ether/EtOAc 80:20). **^{1}H NMR (400 MHz, $CDCl_3$)** δ 7.88 (d, *J* = 8.74 Hz, 2H), 7.43 (d, *J* = 8.64 Hz, 2H), 4.78 – 4.63 (m, 4H), 3.51 – 3.40 (m, 1H), 3.19 – 2.96 (m, 2H), 2.54 – 2.45 (m, 4H), 2.10 – 1.93 (m, 2H). **^{13}C{^{1}H} NMR (100 MHz, $CDCl_3$)** δ 196.3, 174.0, 172.0, 140.0, 134.8, 129.6, 129.1, 77.6, 77.6, 75.2, 75.1, 52.5, 52.2, 40.4, 39.5, 31.6, 26.8. **HRMS (ESI TOF)** *m/z* calcd. For $C_{19}H_{17}ClO_5Na^+$ $[M + Na]^+$ 383.0662 found 361.0664.

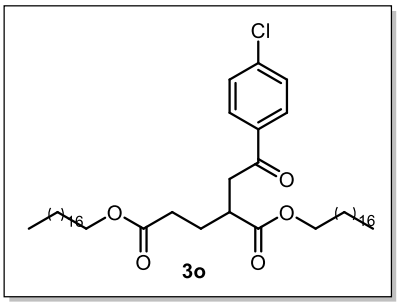
Bis(2-ethylhexyl) 2-(2-(4-chlorophenyl)-2-oxoethyl)pentanedioate (3n)



The title compound **3n** was prepared according to the general procedure (**GP1**) starting from 2-ethylhexyl acrylate **1n** (1 mmol) and 4-Chlorobenzaldehyde **2a** (2 mmol). Off-white Semi-solid (182 mg, 72% yield), R_f = 0.35 (petroleum ether/EtOAc 80:20). **^{1}H NMR (400 MHz, $CDCl_3$)** δ 7.9 (d, *J* = 8.5 Hz, 2H), 7.4 (d, *J* = 8.5 Hz, 2H), 4.0 (ddd, *J* = 9.9, 5.8, 3.6 Hz, 4H), 3.4 (dd, *J* = 17.3, 8.5 Hz, 1H), 3.1 – 3.0 (m, 2H), 2.4 (ddd, *J* = 8.2, 7.0, 2.4 Hz, 2H), 2.1 – 1.9 (m, 2H), 1.6 – 1.5 (m, 2H), 1.4 – 1.3 (m, 16H), 0.9 (ddd, *J* = 6.2, 4.0, 1.9 Hz, 12H). **^{13}C{^{1}H}**

NMR (100 MHz, $CDCl_3$) δ 196.6, 174.9, 173.1, 139.8, 135.0, 129.6, 129.1, 67.3, 67.26, 67.2, 40.4, 39.9, 38.8, 38.8, 32.0, 30.5, 30.5, 30.4, 29.0, 29.0, 27.2, 23.8, 23.1, 23.1, 14.2, 11.1, 11.00. **HRMS (ESI TOF)** *m/z* calcd. For $C_{29}H_{46}ClO_5$ $[M + H]^+$ 509.3028 found 509.3033.

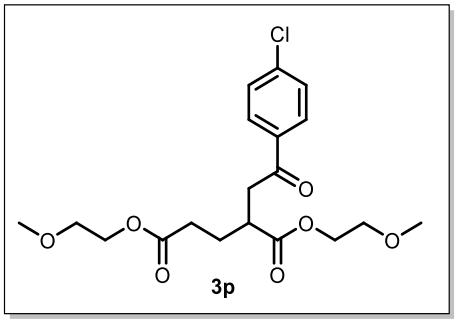
Dioctadecyl 2-(2-(4-chlorophenyl)-2-oxoethyl)pentanedioate (3o)



3o

The title compound **3o** was prepared according to the general procedure (**GP1**) starting from Stearyl Acrylate **1o** (1 mmol) and 4-Chlorobenzaldehyde **2a** (2 mmol). White solid (235 mg, 60% yield), R_f = 0.5 (petroleum ether/EtOAc 85:15). **^{1}H NMR (400 MHz, $CDCl_3$)** δ 7.89 (d, *J* = 8.61 Hz, 2H), 7.43 (d, *J* = 8.56 Hz, 2H), 4.07 (q, *J* = 6.82 Hz, 4H), 3.50 – 3.39 (m, 1H), 3.14 – 2.95 (m, 2H), 2.46 – 2.37 (m, 2H), 2.06 – 1.89 (m, 2H), 1.61 – 1.57 (m, 4H), 1.25 (s, 60H), 0.87 (d, *J* = 7.06 Hz, 6H). **^{13}C{^{1}H} NMR (100 MHz, $CDCl_3$)** δ 196.7, 174.9, 173.0, 139.9, 135.0, 129.6, 129.1, 65.2, 65.0, 40.5, 32.1, 32.0, 29.9, 29.8, 29.8, 29.8, 29.7, 29.5, 29.4, 28.7, 28.7, 27.2, 26.1, 26.0, 22.8. **HRMS (ESI TOF)** *m/z* calcd. For $C_{49}H_{86}ClO_5$ $[M + H]^+$ 789.6158 found 789.6155.

Bis(2-methoxyethyl) 2-(2-(4-chlorophenyl)-2-oxoethyl) pentanedioate (3p)

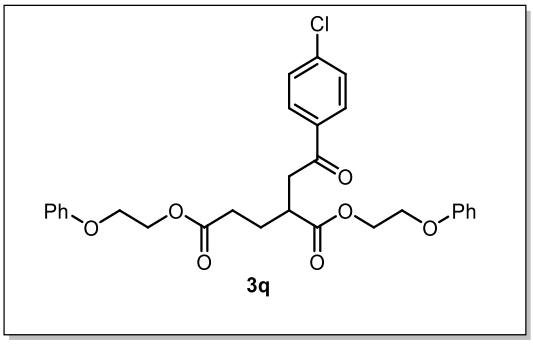


3p

The title compound **3p** was prepared according to the general procedure (**GP1**) starting from 2-methoxyethyl acrylate **1p** (1 mmol) and 4-Chlorobenzaldehyde **2a** (2 mmol). White semi-solid (146 mg, 73% yield), R_f = 0.2 (petroleum ether/EtOAc 75:25). **^{1}H NMR (400 MHz,**

$CDCl_3$) δ 7.87 (d, *J* = 8.79 Hz, 2H), 7.41 (d, *J* = 8.31 Hz, 2H), 4.29 – 4.17 (m, 4H), 3.59 – 3.53 (m, 4H), 3.47 – 3.39 (m, 1H), 3.35 (d, *J* = 0.55 Hz, 3H), 3.33 (d, *J* = 0.55 Hz, 3H), 3.10 – 2.98 (m, 2H), 2.47 (ddd, *J* = 8.08, 7.02, 2.34 Hz, 2H), 2.04 – 1.91 (m, 2H). **$^{13}C\{^1H\}$ NMR (100 MHz, $CDCl_3$)** δ 196.6, 174.7, 172.9, 139.8, 134.9, 129.5, 129.0, 70.5, 70.4, 63.7, 63.7, 59.0, 58.9, 40.4, 39.7, 31.7, 27.0. **HRMS (ESI TOF)** *m/z* calcd. For $C_{19}H_{26}ClO_7Na^+$ $[M + Na]^+$ 423.1186 found 423.1189.

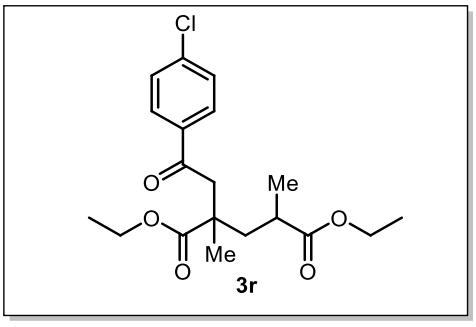
Bis(2-phenoxyethyl) 2-(2-(4-chlorophenyl)-2-oxoethyl)pentanedioate (3q)



3q

The title compound **3q** was prepared according to the general procedure (**GP1**) starting from 2-phenoxyethyl acrylate **1q** (1 mmol) and 4-Chlorobenzaldehyde **2a** (2 mmol). Off-white solid (196 mg, 75% yield), R_f = 0.23 (petroleum ether/EtOAc 75:25). **^1H NMR (400 MHz, $CDCl_3$)** δ 7.89 – 7.78 (m, 2H), 7.39 (d, *J* = 8.63 Hz, 2H), 7.32 – 7.21 (m, 5H), 6.95 (dt, *J* = 8.62, 1.11 Hz, 2H), 6.90 – 6.83 (m, 3H), 4.55 – 4.36 (m, 4H), 4.16 – 4.10 (m, 4H), 3.45 (dd, *J* = 17.57, 8.64 Hz, 1H), 3.19 – 2.94 (m, 2H), 2.56 – 2.45 (m, 2H), 2.12 – 1.92 (m, 2H). **$^{13}C\{^1H\}$ NMR (100 MHz, $CDCl_3$)** δ 196.5, 174.6, 172.8, 158.6, 139.9, 134.8, 129.7, 129.6, 129.6, 129.1, 121.3, 121.2, 114.7, 114.7, 65.8, 65.7, 63.2, 63.1, 40.5, 39.7, 31.7, 27.0. **HRMS (ESI TOF)** *m/z* calcd. For $C_{29}H_{30}ClO_7$ $[M + H]^+$ 525.1675 found 525.1678.

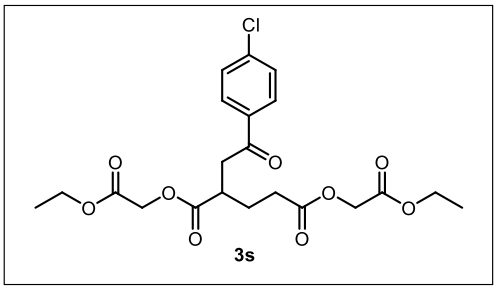
Diethyl 2-(2-(4-chlorophenyl)-2-oxoethyl)-2,4-dimethylpentanedioate (3r)



3r

The title compound **3r** was prepared according to the general procedure (**GP1**) starting from ethyl methacrylate **1r** (1 mmol) and 4-Chlorobenzaldehyde **2a** (2 mmol). Colorless liquid (133 mg, 72% yield), R_f = 0.25 (petroleum ether/EtOAc 80:20). **^{1}H NMR (400 MHz, $CDCl_3$)** δ 7.85 (d, *J* = 8.63 Hz, 2H), 7.41 (d, *J* = 8.56 Hz, 2H), 4.15 – 4.01 (m, 4H), 3.40 (t, *J* = 17.40 Hz, 1H), 3.08 (dd, *J* = 17.71, 4.75 Hz, 1H), 2.57 (dtd, *J* = 8.79, 7.04, 3.23 Hz, 1H), 2.25 (m, 1H), 1.71 (m, 1H), 1.3-1.1 (m, 12H). **^{13}C{^{1}H} NMR (100 MHz, $CDCl_3$)** δ 196.3, 196.2, 177.1, 176.9, 176.3, 176.0, 139.7, 139.6, 135.5, 135.4, 129.4, 129.0, 60.8, 60.8, 60.6, 60.6, 47.4, 46.3, 43.5, 43.5, 42.9, 42.7, 35.9, 35.9, 23.0, 21.5, 20.2, 19.9, 14.3, 14.2, 14.2, 14.1. **HRMS (ESI TOF)** *m/z* calcd. For $C_{19}H_{25}ClO_5Na^+$ $[M + Na]^+$ 391.1283 found 391.1287.

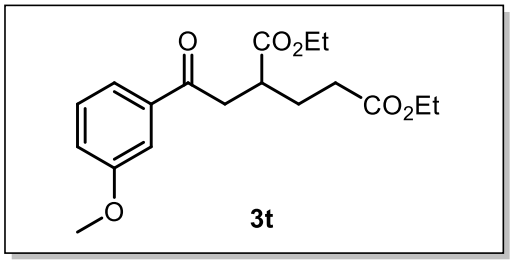
Bis(2-ethoxy-2-oxoethyl) 2-(2-(4-chlorophenyl)-2-oxoethyl)pentanedioate (3s)



3s

The title compound **3s** was prepared according to the general procedure (**GP1**) starting from 2-ethoxy-2-oxoethyl acrylate **1s** (1 mmol) and 4-Chlorobenzaldehyde **2a** (2 mmol). Colorless liquid (162 mg, 71% yield), R_f = 0.3 (petroleum ether/EtOAc 80:20). **^{1}H NMR (400 MHz, $CDCl_3$)** δ 7.90 (d, *J* = 8.64 Hz, 2H), 7.44 (d, *J* = 8.59 Hz, 2H), 4.72 (d, *J* = 15.85 Hz, 1H), 4.61 (d, *J* = 2.08 Hz, 2H), 4.56 (d, *J* = 15.88 Hz, 1H), 4.21 (qd, *J* = 7.17, 2.00 Hz, 4H), 3.52 (dd, *J* = 17.84, 8.75 Hz, 1H), 3.29 – 3.18 (m, 1H), 3.10 (dd, *J* = 17.87, 4.74 Hz, 1H), 2.73 – 2.63 (m, 2H), 2.19 – 2.01 (m, 2H), 1.28 (td, *J* = 7.12, 3.63 Hz, 6H). **^{13}C{^{1}H} NMR (100 MHz, $CDCl_3$)** δ 196.4, 174.2, 172.4, 167.9, 167.8, 139.9, 134.8, 129.6, 129.1, 126.8, 61.6, 61.5, 61.1, 60.9, 40.4, 39.3, 31.3, 26.8, 14.2, 14.2. **HRMS (ESI TOF)** *m/z* calcd. For $C_{21}H_{26}ClO_9$ $[M + H]^+$ 457.1260 found 457.1264.

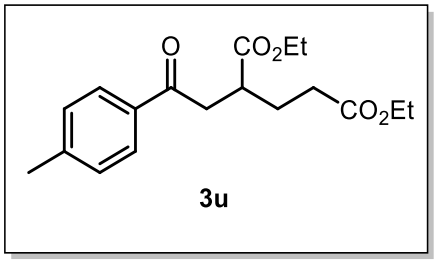
Diethyl 2-(2-(3-methoxyphenyl)-2-oxoethyl)pentanedioate (3t)



3t

The title compound **3t** was prepared according to the general procedure (**GP1**) starting from ethyl acrylate **1f** (1 mmol) and 3-methoxybenzaldehyde **2b** (2 mmol). Colorless liquid (124 mg, 74% yield), R_f = 0.3 (petroleum ether/EtOAc 70:30). **^{1}H NMR (400 MHz, $CDCl_3$)** δ 7.51 (ddd, *J* = 7.7, 1.6, 1.0 Hz, 1H), 7.45 (dd, *J* = 2.7, 1.5 Hz, 1H), 7.34 (t, *J* = 7.9 Hz, 1H), 7.08 (ddd, *J* = 8.2, 2.7, 1.0 Hz, 1H), 4.12 (dq, *J* = 11.3, 7.1 Hz, 4H), 3.82 (s, 3H), 3.44 (dd, *J* = 18.8, 9.8 Hz, 1H), 3.12 – 2.95 (m, 2H), 2.39 (ddd, *J* = 8.0, 7.1, 2.0 Hz, 2H), 2.03 – 1.88 (m, 2H), 1.23 (td, *J* = 7.2, 2.4 Hz, 6H). **^{13}C{^{1}H} NMR (100 MHz, $CDCl_3$)** δ 197.7, 174.8, 172.8, 159.9, 138.0, 129.7, 120.7, 119.9, 112.2, 60.8, 60.6, 55.5, 40.6, 39.8, 32.0, 27.1, 14.3, 14.2. **HRMS (ESI TOF)** *m/z* calcd. For $C_{18}H_{25}O_6$ $[M + H]^+$ 337.1646 found 337.1650.

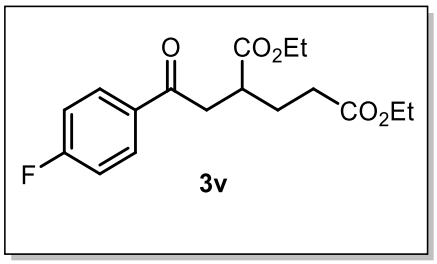
Diethyl 2-(2-oxo-2-(p-tolyl)ethyl)pentanedioate (3u)



3u

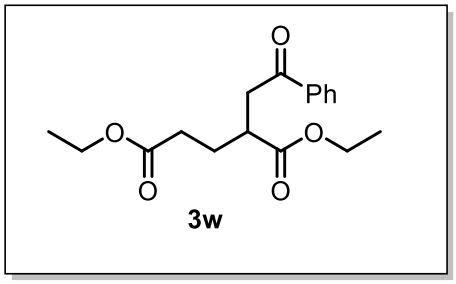
The title compound **3u** was prepared according to the general procedure (**GP1**) starting from ethyl acrylate **1f** (1 mmol) and 4-methylbenzaldehyde **2c** (2 mmol). Colorless liquid (115 mg, 72% yield), R_f = 0.4 (petroleum ether/EtOAc 80:20). **^{1}H NMR (400 MHz, $CDCl_3$)** δ 7.85 (d, *J* = 8.3 Hz, 2H), 7.25 (d, *J* = 7.9 Hz, 2H), 4.14 (dq, *J* = 10.1, 7.1 Hz, 4H), 3.45 (dd, *J* = 18.7, 9.8 Hz, 1H), 3.10 – 2.99 (m, 2H), 2.45 – 2.34 (m, 5H), 2.06 – 1.85 (m, 2H), 1.29 – 1.21 (m, 6H). **^{13}C{^{1}H} NMR (100 MHz, $CDCl_3$)** 197.5, 174.9, 172.9, 144.1, 134.2, 129.4, 128.2, 125.8, 60.8, 60.6, 40.4, 39.9, 32.0, 27.2, 21.7, 14.3, 14.3. **HRMS (ESI TOF)** *m/z* calcd. For $C_{18}H_{25}O_5$ $[M + H]^+$ 321.1697 found 321.1699.

Diethyl 2-(2-(4-fluorophenyl)-2-oxoethyl)pentanedioate (3v)



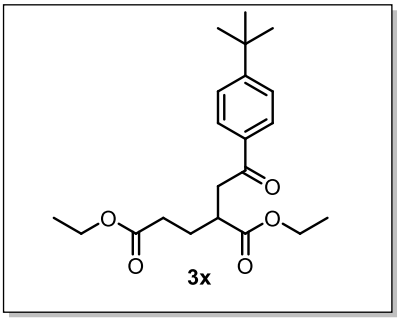
The title compound **3v** was prepared according to the general procedure (**GP1**) starting from ethyl acrylate **1f** (1 mmol) and 4-fluorobenzaldehyde **2d** (2 mmol). Colorless liquid (105 mg, 65% yield), R_f = 0.3 (petroleum ether/EtOAc 80:20**). ^{1}H NMR (400 MHz, CDCl$_3$)** δ 7.97 (dd, *J* = 8.9, 5.4 Hz, 2H), 7.11 (dd, *J* = 8.9, 8.3 Hz, 2H), 4.16 – 4.09 (m, 4H), 3.48 – 3.39 (m, 1H), 3.09 – 2.96 (m, 2H), 2.40 (ddd, *J* = 7.9, 7.1, 2.1 Hz, 2H), 2.06 – 1.88 (m, 2H), 1.24 (td, *J* = 7.1, 1.3 Hz, 6H). **^{13}C{^{1}H} NMR (100 MHz, CDCl$_3$)** δ [1] 196.2, 174.7, 172.8, 165.8 (d, *J* = 255.0 Hz), 133.0 (d, *J* = 3.0 Hz), 130.7 (d, *J* = 9.3 Hz), 115.7 (d, *J* = 21.9 Hz), 60.8, 60.5, 40.3, 39.7, 31.9, 27.0, 14.2, 14.2. **^{19}F NMR (377 MHz, CDCl$_3$)** δ -111.75. **HRMS (ESI TOF)** *m/z* calcd. For $C_{17}H_{22}FO_5$ $[M + H]^+$ 325.1446 found 325.1450.

Diethyl 2-(2-oxo-2-phenylethyl)pentanedioate (3w)



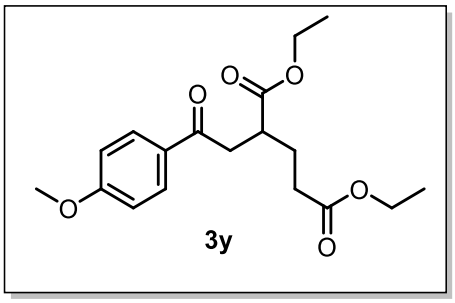
The title compound **3w** was prepared according to the general procedure (**GP1**) starting from ethyl acrylate **1f** (1 mmol) and benzaldehyde **2e** (2 mmol). Colorless liquid (108 mg, 71% yield), R_f = 0.3 (petroleum ether/EtOAc 80:20). **^{1}H NMR (400 MHz, CDCl$_3$)** δ 7.93 (ddd, *J* = 7.51, 1.42, 0.73 Hz, 2H), 7.58 – 7.51 (m, 1H), 7.44 (ddt, *J* = 8.42, 7.74, 0.75 Hz, 2H), 4.13 (dqd, *J* = 10.73, 7.12, 0.77 Hz, 4H), 3.46 (ddd, *J* = 18.78, 9.80, 0.74 Hz, 1H), 3.10 – 3.00 (m, 2H), 2.44 – 2.37 (m, 2H), 2.06 – 1.85 (m, 2H), 1.24 (tdd, *J* = 7.08, 1.29, 0.72 Hz, 6H). **^{13}C{^{1}H} NMR (100 MHz, CDCl$_3$)** δ 197.8, 174.9, 172.9, 136.6, 133.3, 128.7, 128.1, 60.8, 60.6, 40.5, 39.8, 32.0, 27.1, 14.3, 14.2. **HRMS (ESI TOF)** *m/z* calcd. For $C_{17}H_{23}O_5$ $[M + H]^+$ 307.1540 found 307.1543.

Diethyl 2-(2-(4-(tert-butyl)phenyl)-2-oxoethyl)pentanedioate (3x)



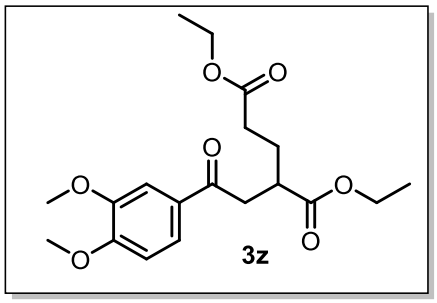
The title compound **3x** was prepared according to the general procedure (**GP1**) starting from ethyl acrylate **1f** (1 mmol) and 4-tert-butyl benzaldehyde **2f** (2 mmol). Colorless liquid (126 mg, 70% yield), R_f = 0.2 (petroleum ether/EtOAc 85:15). **^{1}H NMR (400 MHz, $CDCl_3$)** δ 7.88 (d, *J* = 8.47 Hz, 2H), 7.46 (d, *J* = 8.60 Hz, 2H), 4.13 (dq, *J* = 9.97, 7.13 Hz, 4H), 3.45 (dd, *J* = 18.73, 9.82 Hz, 1H), 3.11 – 2.99 (m, 2H), 2.40 (ddd, *J* = 8.60, 7.14, 2.28 Hz, 2H), 1.98 (qt, *J* = 13.31, 6.73 Hz, 2H), 1.33 (s, 9H), 1.24 (t, *J* = 7.14 Hz, 6H). **^{13}C{^{1}H} NMR (100 MHz, $CDCl_3$)** δ 197.5, 175.0, 172.9, 157.1, 134.1, 128.1, 125.7, 60.8, 60.6, 40.5, 39.9, 35.2, 32.1, 31.2, 27.2. **HRMS (ESI TOF)** *m/z* calcd. For $C_{21}H_{31}O_5$ $[M + H]^+$ 363.2166 found 363.2169.

Diethyl 2-(2-(4-methoxyphenyl)-2-oxoethyl)pentanedioate (3y)



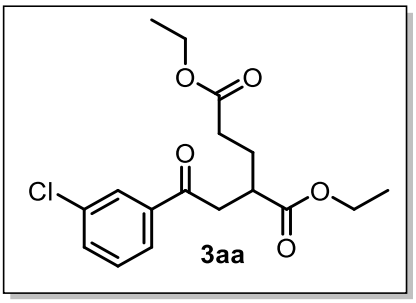
The title compound **3y** was prepared according to the general procedure (**GP1**) starting from ethyl acrylate **1f** (1 mmol) and 4-methoxybenzaldehyde **2g** (2 mmol). Colorless liquid (128 mg, 76% yield), R_f = 0.3 (petroleum ether/EtOAc 70:30). **^{1}H NMR (400 MHz, $CDCl_3$)** δ 7.92 (d, *J* = 8.62 Hz, 2H), 6.92 (d, *J* = 8.66 Hz, 2H), 4.18 – 4.09 (m, 4H), 3.86 (s, 3H), 3.46 – 3.36 (m, 1H), 3.08 – 2.97 (m, 2H), 2.40 (ddd, *J* = 8.58, 7.01, 2.19 Hz, 2H), 2.05 – 1.89 (m, 2H), 1.24 (tdd, *J* = 7.19, 1.11, 0.54 Hz, 6H). **^{13}C{^{1}H} NMR (100 MHz, $CDCl_3$)** δ 196.4, 175.0, 172.9, 163.7, 130.4, 129.8, 113.8, 60.8, 60.6, 55.6, 40.2, 39.9, 32.1, 27.2, 14.3, 14.3. **HRMS (ESI TOF)** *m/z* calcd. For $C_{18}H_{25}O_6$ $[M + H]^+$ 337.1646 found 337.1648.

Diethyl 2-(2-(3,4-dimethoxyphenyl)-2-oxoethyl)pentanedioate (3z)



The title compound **3z** was prepared according to the general procedure (**GP1**) starting from ethyl acrylate **1f** (1 mmol) and 3,4-dimethoxybenzaldehyde **2h** (2 mmol). Colorless liquid (143 mg, 78% yield), R_f = 0.3 (petroleum ether/EtOAc 65:35). **IR** (neat): 1727, 1674, 1594, 1514, 1462, 1418, 1375, 1262, 1148, 1021, 856, 808, 764, 630 cm^{-1}. **^{1}H NMR (400 MHz, $CDCl_3$)** δ 7.58 (dd, *J* = 8.36, 2.04 Hz, 1H), 7.49 (d, *J* = 2.01 Hz, 1H), 6.87 (d, *J* = 8.40 Hz, 1H), 4.13 (dq, *J* = 11.69, 7.13 Hz, 4H), 3.93 (s, 3H), 3.91 (s, 3H), 3.42 (dd, *J* = 18.50, 9.89 Hz, 1H), 3.08 – 2.99 (m, 2H), 2.40 (ddd, *J* = 8.12, 7.06, 2.14 Hz, 2H), 2.04 – 1.88 (m, 2H), 1.24 (td, *J* = 7.14, 3.17 Hz, 6H). **^{13}C{^{1}H} NMR (100 MHz, $CDCl_3$)** δ 196.4, 175.0, 172.9, 153.5, 149.1, 129.9, 122.8, 110.1, 110.1, 60.8, 60.6, 56.2, 56.1, 40.1, 40.0, 32.1, 27.2, 14.3, 14.3. **HRMS (ESI TOF)** *m/z* calcd. For $C_{19}H_{27}O_7$ $[M + H]^+$ 367.1751 found 367.1755.

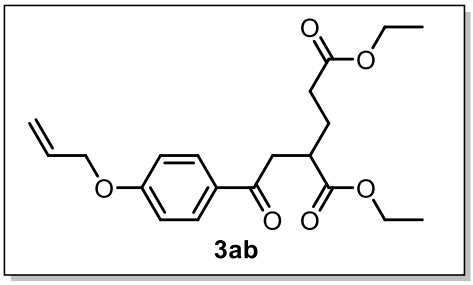
Diethyl 2-(2-(3-chlorophenyl)-2-oxoethyl)pentanedioate (3aa)



The title compound **3aa** was prepared according to the general procedure (**GP1**) starting from ethyl acrylate **1f** (1 mmol) and 3-Chlorobenzaldehyde **2i** (2 mmol). Colorless liquid (118 mg, 69% yield), R_f = 0.22 (petroleum ether/EtOAc 80:20). **^{1}H NMR (400 MHz, $CDCl_3$)** δ 7.91 (t, *J* = 1.88 Hz, 1H), 7.81 (dt, *J* = 7.76, 1.38 Hz, 1H), 7.52 (ddd, *J* = 7.95, 2.10, 1.05 Hz, 1H), 7.39 (t, *J* = 7.87 Hz, 1H), 4.14 (dq, *J* = 8.85, 7.12 Hz, 4H), 3.49 – 3.40 (m, 1H), 3.10 – 2.94 (m, 2H), 2.44 – 2.37 (m, 2H), 2.06 – 1.88 (m, 2H), 1.25 (td, *J* = 7.13, 0.91 Hz, 6H). **^{13}C{^{1}H}**

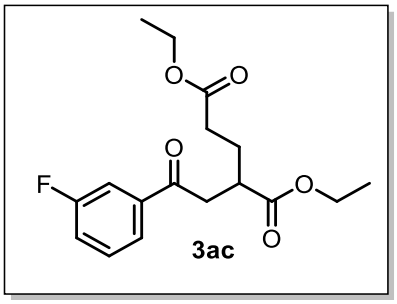
NMR (100 MHz, $CDCl_3$) δ 196.7, 174.7, 172.8, 138.1, 135.1, 133.3, 130.1, 128.3, 126.2, 61.0, 60.7, 40.6, 39.7, 32.0, 27.1, 14.3, 14.3. **HRMS (ESI TOF)** *m/z* calcd. For $C_{17}H_{22}ClO_5$ $[M + H]^+$ 341.1150 found 341.1154.

Diethyl 2-(2-(4-(allyloxy)phenyl)-2-oxoethyl)pentanedioate (3ab)



The title compound **3ab** was prepared according to the general procedure (**GP1**) starting from ethyl acrylate **1f** (1 mmol) and 4-(allyloxy)benzaldehyde **2j** (2 mmol). Colorless liquid (131 mg, 72% yield), R_f = 0.3 (petroleum ether/EtOAc 70:30). **^{1}H NMR (400 MHz, $CDCl_3$)** δ 7.92 (d, *J* = 8.96 Hz, 2H), 6.93 (d, *J* = 8.94 Hz, 2H), 6.04 (ddt, *J* = 17.24, 10.54, 5.29 Hz, 1H), 5.48 – 5.26 (m, 2H), 4.60 (dt, *J* = 5.27, 1.53 Hz, 2H), 4.19 – 4.10 (m, 4H), 3.48 – 3.35 (m, 1H), 3.10 – 2.96 (m, 2H), 2.40 (ddd, *J* = 8.20, 7.06, 2.12 Hz, 2H), 2.06 – 1.90 (m, 2H), 1.25 (td, *J* = 7.10, 1.01 Hz, 6H). **^{13}C{^{1}H} NMR (100 MHz, $CDCl_3$)** δ 196.4, 175.0, 173.0, 162.7, 132.6, 130.4, 129.8, 118.3, 114.5, 69.0, 60.8, 60.6, 40.2, 39.9, 32.1, 27.2, 14.3, 14.3. **HRMS (ESI TOF)** *m/z* calcd. For $C_{20}H_{27}O_6$ $[M + H]^+$ 363.1802 found 363.1805.

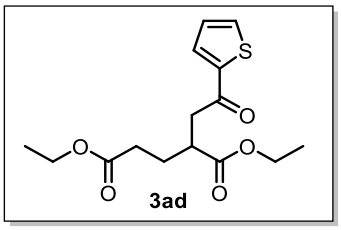
Diethyl 2-(2-(3-fluorophenyl)-2-oxoethyl)pentanedioate (3ac)



The title compound **3ac** was prepared according to the general procedure (**GP1**) starting from ethyl acrylate **1f** (1 mmol) and 3-fluorobenzaldehyde **2k** (2 mmol). Colorless liquid (108 mg, 67% yield), R_f = 0.22 (petroleum ether/EtOAc 80:20). **^{1}H NMR (400 MHz, $CDCl_3$)** δ 7.73 (dt, *J* = 7.81, 1.19 Hz, 1H), 7.62 (ddd, *J* = 9.41, 2.58, 1.51 Hz, 1H), 7.44 (td, *J* = 8.01, 5.51 Hz, 1H),

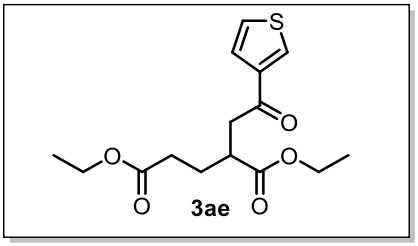
7.29 – 7.23 (m, 1H), 4.14 (dq, *J* = 9.68, 7.17 Hz, 4H), 3.51 – 3.38 (m, 1H), 3.12 – 2.97 (m, 2H), 2.45 – 2.37 (m, 2H), 2.05 – 1.89 (m, 2H), 1.25 (td, *J* = 7.11, 1.17 Hz, 6H). **$^{13}C\{^{1}H\}$ NMR (100 MHz, $CDCl_3$)** δ 196.7, 196.7, 174.8, 172.9, 163.0 (d, *J* = 248.2 Hz), 138.7 (d, *J* = 6.2 Hz), 130.4 (d, *J* = 7.7 Hz), 123.9 (d, *J* = 2.9 Hz), 120.4 (d, *J* = 21.6 Hz), 114.9 (d, *J* = 22.5 Hz), 61.0, 60.7, 40.7, 39.8, 32.0, 27.1, 14.3, 14.3. **^{19}F NMR (377 MHz, $CDCl_3$)** δ -111.7. **HRMS (ESI TOF)** *m/z* calcd. For $C_{17}H_{22}FO_5$ $[M + H]^+$ 325.1446 found 325.1449.

Diethyl 2-(2-oxo-2-(thiophen-2-yl)ethyl)pentanedioate (3ad)



The title compound **3ad** was prepared according to the general procedure (**GP1**) starting from ethyl acrylate **1f** (1 mmol) and thiophene-2-carbaldehyde **2l** (2 mmol). Colorless liquid (100 mg, 64% yield), R_f = 0.3 (petroleum ether/EtOAc 70:30). **^{1}H NMR (400 MHz, $CDCl_3$)** δ 7.73 (dd, *J* = 3.80, 1.14 Hz, 1H), 7.63 (dd, *J* = 4.92, 1.11 Hz, 1H), 7.12 (dd, *J* = 4.93, 3.79 Hz, 1H), 4.13 (p, *J* = 7.16 Hz, 4H), 3.44 – 3.33 (m, 1H), 3.09 – 2.96 (m, 2H), 2.48 – 2.34 (m, 2H), 1.98 (tt, *J* = 14.18, 6.56 Hz, 2H), 1.24 (td, *J* = 7.10, 3.37 Hz, 6H). **$^{13}C\{^{1}H\}$ NMR (100 MHz, $CDCl_3$)** δ 190.8, 174.7, 172.9, 143.8, 133.9, 132.2, 128.3, 61.0, 60.7, 41.0, 39.9, 32.0, 27.1, 14.3, 14.3. **HRMS (ESI TOF)** *m/z* calcd. For $C_{15}H_{21}O_5S$ $[M + H]^+$ 313.1104 found 313.1109.

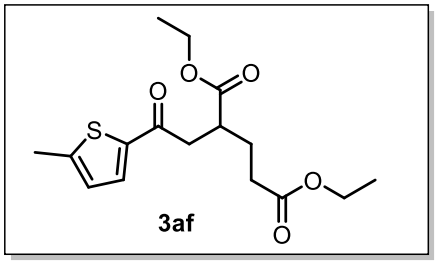
Diethyl 2-(2-oxo-2-(thiophen-3-yl)ethyl)pentanedioate (3ae)



The title compound **3ae** was prepared according to the general procedure (**GP1**) starting from ethyl acrylate **1f** (1 mmol) and thiophene-3-carbaldehyde **2m** (2 mmol). Colorless liquid (101 mg, 65% yield), R_f = 0.3 (petroleum ether/EtOAc 70:30). **^{1}H NMR (400 MHz, $CDCl_3$)** δ 8.06

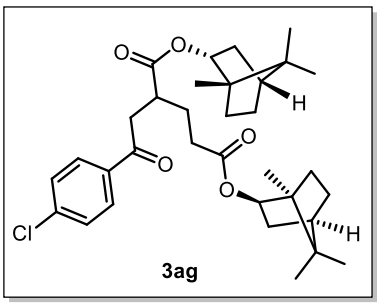
(dd, *J* = 2.87, 1.27 Hz, 1H), 7.53 (dd, *J* = 5.08, 1.25 Hz, 1H), 7.31 (dd, *J* = 5.11, 2.91 Hz, 1H), 4.13 (dq, *J* = 8.68, 7.15 Hz, 4H), 3.37 (dd, *J* = 16.90, 8.22 Hz, 1H), 3.08 – 2.94 (m, 2H), 2.40 (ddd, *J* = 8.06, 7.01, 2.47 Hz, 2H), 2.09 – 1.84 (m, 2H), 1.24 (t, *J* = 7.14 Hz, 6H). **^{13}C{^{1}H} NMR (100 MHz, $CDCl_3$)** δ 192.2, 174.9, 172.9, 141.9, 132.2, 126.9, 126.6, 60.9, 60.7, 41.6, 39.8, 32.0, 27.1, 14.3, 14.3. **HRMS (ESI TOF)** *m/z* calcd. For $C_{15}H_{20}O_5SNa^+$ $[M + Na]^+$ 335.0928 found 335.0926.

diethyl 2-(2-(5-methylthiophen-2-yl)-2-oxoethyl)pentanedioate (3af)



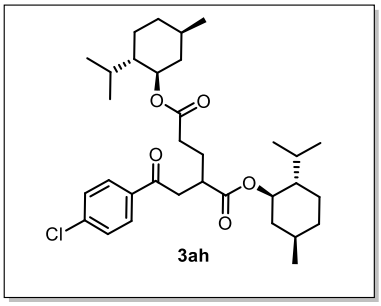
The title compound **3af** was prepared according to the general procedure (**GP1**) starting from ethyl acrylate **1f** (1 mmol) and 5-methylthiophene-2-carbaldehyde **2n** (2 mmol). Colorless liquid (103 mg, 63% yield), R_f = 0.32 (petroleum ether/EtOAc 70:30). **^{1}H NMR (400 MHz, $CDCl_3$)** δ 7.54 (d, *J* = 3.72 Hz, 1H), 6.78 (dd, *J* = 3.79, 1.05 Hz, 1H), 4.17 – 4.13 (m, 2H), 4.12 – 4.09 (m, 2H), 3.32 (dd, *J* = 16.67, 8.39 Hz, 1H), 3.07 – 2.89 (m, 2H), 2.52 (d, *J* = 1.05 Hz, 3H), 2.43 – 2.34 (m, 2H), 2.05 – 1.87 (m, 2H), 1.28 – 1.21 (m, 6H). **^{13}C{^{1}H} NMR (100 MHz, $CDCl_3$)** δ 190.3, 174.7, 172.9, 150.0, 141.6, 132.8, 126.9, 60.9, 60.6, 40.6, 40.0, 32.0, 27.1, 16.1, 14.3, 14.3. **HRMS (ESI TOF)** *m/z* calcd. For $C_{16}H_{23}O_5S$ $[M + H]^+$ 327.1261 found 327.1258.

Bis ((1*S*,2*R*,4*R*)-1,7,7-trimethylbicyclo[2.2.1]heptan-2-yl) 2-(2-(4-chlorophenyl)-2oxoethyl)pentanedioate (3ag)



The title compound **3ag** was prepared according to the general procedure (**GP1**) starting from borneol derived acrylate **1t** (1 mmol) and 4-chlorobenzaldehyde **2a** (2 mmol). White solid (103 mg, 63% yield), R_f = 0.3 (petroleum ether/EtOAc 80:20). **^{1}H NMR (400 MHz, CDCl$_3$)** δ 7.91 – 7.86 (m, 2H), 7.42 (d, *J* = 8.60 Hz, 2H), 4.95 – 4.83 (m, 2H), 3.46 (ddd, *J* = 17.40, 8.90, 4.24 Hz, 1H), 3.16 – 3.04 (m, 1H), 3.05 – 2.97 (m, 1H), 2.50 – 2.42 (m, 2H), 2.34 (dddt, *J* = 13.18, 9.95, 5.16, 2.75 Hz, 2H), 2.10 – 1.83 (m, 4H), 1.74 – 1.65 (m, 4H), 1.35 – 1.00 (m, 6H), 0.90 – 0.87 (m, 6H), 0.86 (d, *J* = 4.14 Hz, 6H), 0.84 – 0.79 (m, 6H). **^{13}C{^{1}H} NMR (100 MHz, CDCl$_3$)** δ 196.63, 196.6, 196.6, 175.0, 174.9 173.1, 139.8, 135.0, 129.6, 129.6, 129.1, 80.62, 80.53, 80.26, 80.24, 49.0, 48.9, 48.9, 48.0, 48.0, 45.0, 45.0, 40.4, 40.1, 40.0, 37.0, 36.9, 36.7, 32.4, 32.3, 28.1, 28.1, 28.08, 27.40, 27.35, 27.31, 27.23, 19.81, 19.80, 19.78, 18.95, 13.65, 13.54. **HRMS (ESI TOF)** *m/z* calcd. For $C_{33}H_{46}ClO_5$ $[M + H]^+$ 557.3028 found 557.3033.

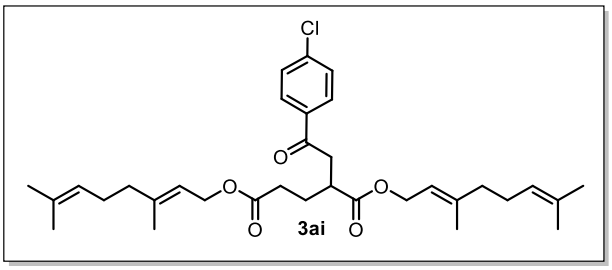
Bis ((1*R*, 2*S*, 5*R*)-2-isopropyl-5-methylcyclohexyl) 2-(2-(4-chlorophenyl)-2-oxoethyl) pentanedioate-(3ah)



3ah

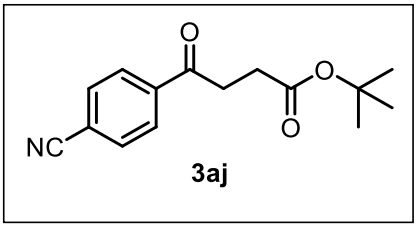
The title compound **3ah** was prepared according to the general procedure (**GP1**) starting from menthol derived acrylate **1u** (1 mmol) and 4-chlorobenzaldehyde **2a** (2 mmol). Semi solid (151 mg, 54% yield), R_f = 0.3 (petroleum ether/EtOAc 80:20). **^{1}H NMR (400 MHz, CDCl$_3$)** δ 7.92 – 7.85 (m, 2H), 7.43 (dd, *J* = 8.58, 1.44 Hz, 2H), 4.67 (dddt, *J* = 14.35, 6.72, 4.79, 2.44 Hz, 2H), 3.44 (dt, *J* = 17.30, 9.57 Hz, 1H), 3.10 – 2.89 (m, 2H), 2.38 (dddd, *J* = 10.41, 8.12, 4.86, 3.02 Hz, 2H), 2.08 – 1.78 (m, 6H), 1.70 – 1.64 (m, 4H), 1.54 – 1.44 (m, 2H), 1.40 – 1.31 (m, 2H), 1.10 – 0.93 (m, 4H), 0.88 (ddd, *J* = 7.11, 4.00, 2.64 Hz, 12H), 0.83 (d, *J* = 7.01 Hz, 2H), 0.76 – 0.70 (m, 6H). **^{13}C{^{1}H} NMR (100 MHz, CDCl$_3$)** δ 196.70, 196.5, 174.3, 174.3, 172.5, 139.8, 139.7, 135.2, 135.1, 129.6, 129.6, 129.0, 129.0, 75.0, 74.8, 74.5, 47.1, 47.1, 47.0, 41.1, 41.1, 40.9, 40.7, 40.4, 40.3, 40.2, 40.1, 34.4, 34.3, 34.4, 32.3, 31.5, 31.5, 31.5, 27.5, 27.2, 26.5, 26.4, 26.2, 26.1, 23.6, 23.5, 23.4, 23.1, 22.2, 22.1, 21.0, 20.9, 20.9, 20.9, 16.5, 16.4, 16.2, 15.9. **HRMS (ESI TOF)** *m/z* calcd. For $C_{33}H_{50}ClO_5$ $[M + H]^+$ 561.3341 found 561.3344.

Bis((*E*)-3,7-dimethylocta-2,6-dien-1-yl)2-(2-(4-chlorophenyl)-2-oxoethyl)pentanedioate-(3ai)



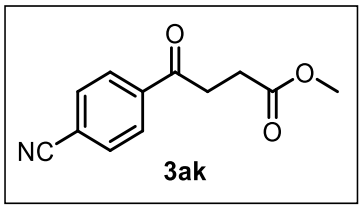
The title compound **3ai** was prepared according to the general procedure (**GP1**) starting from geraniol derived acrylate **1v** (1 mmol) and 4-chlorobenzaldehyde **2a** (2 mmol). Semi solid (134 mg, 48 % yield), R_f = 0.3 (petroleum ether/EtOAc 70:30). **^{1}H NMR (400 MHz, CDCl$_3$)** δ 7.9 – 7.8 (m, 2H), 7.4 (d, *J* = 8.6 Hz, 2H), 5.3 (tq, *J* = 7.1, 1.4 Hz, 2H), 5.1 (tt, *J* = 6.7, 1.5 Hz, 2H), 4.6 (dd, *J* = 11.3, 6.9 Hz, 4H), 3.4 (dd, *J* = 17.2, 8.3 Hz, 1H), 3.1 – 3.0 (m, 2H), 2.4 (td, *J* = 8.2, 7.5, 2.3 Hz, 2H), 2.1 – 2.0 (m, 10H), 1.7 (dd, *J* = 5.6, 1.4 Hz, 12H), 1.6 (d, *J* = 1.4 Hz, 6H). **^{13}C{^{1}H} NMR (100 MHz, CDCl$_3$)** δ 196.7, 174.8, 172.9, 142.6, 142.5, 139.8, 135.0, 132.0, 131.9, 129.6, 129.1, 123.9, 123.9, 118.3, 61.9, 61.7, 40.5, 39.9, 39.7, 39.6, 32.1, 32.0, 29.8, 29.5, 27.2, 26.5, 26.4, 25.8, 22.8, 17.8, 16.6, 16.6, 14.3. **HRMS (ESI TOF)** *m/z* calcd. For $C_{33}H_{46}ClO_5$ $[M + H]^+$ 557.3028 found 493.1770.

tert-butyl 4-(4-cyanophenyl)-4-oxobutanoate (3aj)



The compound **3aj** was prepared according to the general procedure (**GP1**) starting from tert-butyl acrylate **1h** (1 mmol) and 4-cyano benzaldehyde **2o** (2 mmol). Off-white solid (198 mg, 76% yield), R_f = 0.25 (petroleum ether/EtOAc 70:30). **^{1}H NMR (400 MHz, CDCl$_3$)** δ 8.03 (d, *J* = 8.59 Hz, 2H), 7.74 (d, *J* = 8.60 Hz, 2H), 3.22 (t, *J* = 6.45 Hz, 2H), 2.67 (t, *J* = 6.47 Hz, 2H), 1.41 (s, 9H). **^{13}C{^{1}H} NMR (100 MHz, CDCl$_3$)** δ 197.2, 171.8, 139.7, 132.5, 128.5, 118.0, 116.4, 80.9, 33.8, 29.2, 28.1. **HRMS (ESI TOF)** *m/z* calcd. For $C_{15}H_{18}NO_3$ $[M + H]^+$ 260.1281 found 260.1285.

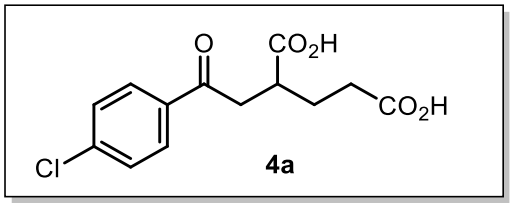
Methyl 4-(4-cyanophenyl)-4-oxobutanoate (3ak)



3ak

The compound **3ak** was prepared according to the general procedure (**GP1**) starting from methyl acrylate **1g** (1 mmol) and 4-cyano benzaldehyde **2o** (2 mmol). Off-white solid (175 mg, 80% yield), R_f = 0.2 (petroleum ether/EtOAc 70:30). **^{1}H NMR (400 MHz, $CDCl_3$)** δ 8.06 (d, *J* = 8.55 Hz, 1H), 7.86 – 7.58 (m, 1H), 3.70 (s, 2H), 3.30 (t, *J* = 6.48 Hz, 1H), 2.78 (t, *J* = 6.44 Hz, 2H). **^{13}C{^{1}H} NMR (100 MHz, $CDCl_3$)** δ 197.0, 173.1, 139.5, 132.6, 128.6, 118.0, 116.6, 52.1, 33.8, 27.9. **HRMS (ESI TOF)** *m/z* calcd. For $C_{12}H_{12}NO_3$ $[M + H]^+$ 218.0812 found 218.0816.

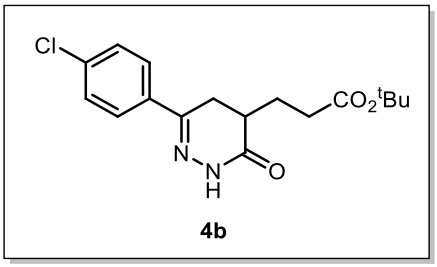
2-(2-(4-chlorophenyl)-2-oxoethyl)pentanedioic acid (4a)



4a

To a solution of ester **3h** (100 mg, 0.251mmol) in dichloromethane (3 mL) was added trifluoroacetic acid (3 mL). The mixture was stirred at room temperature for 2 h. The mixture was evaporated and partitioned between dichloromethane and water. The aqueous layer was washed with dichloromethane (10 mLx3), combined the organic layers, dried over sodium sulfate, then filtered and concentrated in vacuum afford the title compound **4a** as brown solid (57mg, 79% yield). **^{1}H NMR (400 MHz, CD_3OD)** δ 7.98 (d, *J* = 8.62 Hz, 1H), 7.50 (d, *J* = 8.60 Hz, 1H), 3.46 (dd, *J* = 18.07, 9.37 Hz, 1H), 3.14 (dd, *J* = 18.02, 4.36 Hz, 1H), 3.00 (dddd, *J* = 9.33, 7.60, 6.22, 4.33 Hz, 1H), 2.44 (ddd, *J* = 8.17, 6.98, 2.97 Hz, 1H), 2.08 – 1.81 (m, 1H). **^{13}C{^{1}H} NMR (100 MHz, CD_3OD)** δ 198.9, 178.4, 176.7, 140.6, 136.6, 130.8, 129.9, 41.3, 41.0, 32.5, 28.1. **HRMS (ESI TOF)** *m/z* calcd. For $C_{13}H_{14}ClO_5$ $[M + H]^+$ 285.0524 found 285.0520.

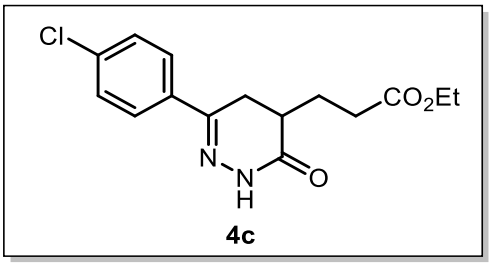
***t*ert-butyl 3-(6-(4-chlorophenyl)-3-oxo-2,3,4,5-tetrahydropyridazin-4-yl)propanoate (4b)**



4b

In 20 mL round bottomed flask the ester derivative **3h** (100 mg, 0.251mmol) was taken. To this 5 mL of hydrazine hydrate was added at room temperature. Then the reaction mixture was reflux for 10 h. After that the solvent was evaporated under reduce pressure. The residue was purified by silica gel column chromatography to give **4b** as white semi-solid. **^{1}H NMR (400 MHz, $CDCl_3$)** δ 8.71 (s, 1H), 7.65 (d, *J* = 8.69 Hz, 2H), 7.38 (d, *J* = 8.68 Hz, 2H), 3.06 (dd, *J* = 16.51, 6.57 Hz, 1H), 2.69 (dd, *J* = 16.51, 10.65 Hz, 1H), 2.62 – 2.51 (m, 1H), 2.45 (ddd, *J* = 7.92, 6.96, 4.16 Hz, 2H), 2.13 (ddt, *J* = 13.96, 8.01, 6.83 Hz, 1H), 1.81 (tt, *J* = 14.04, 6.74 Hz, 1H), 1.43 (s, 9H). **^{13}C{^{1}H} NMR (100 MHz, $CDCl_3$)** δ 172.4, 169.5, 149.6, 136.1, 134.2, 129.0, 127.2, 80.8, 35.2, 32.8, 28.2, 28.2, 25.2. **HRMS (ESI TOF)** *m/z* calcd. For $C_{17}H_{22}ClN_2O_5$ $[M + H]^+$ 337.1313 found 337.1309.

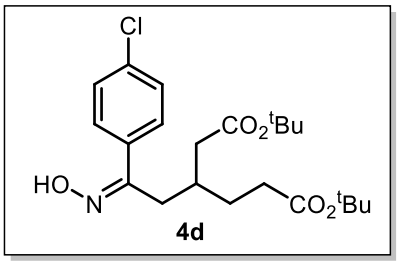
Ethyl 3-(6-(4-chlorophenyl)-3-oxo-2,3,4,5-tetrahydropyridazin-4-yl)propanoate (4c)



4c

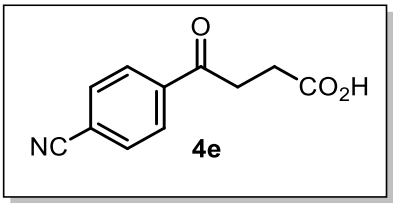
In 20 mL round bottomed flask the ester derivative **3f** (100 mg, 0.251mmol) was taken. To this 5 mL of hydrazine hydrate was added at room temperature. Then the reaction mixture was reflux for 10 h. After that the solvent was evaporated under reduce pressure. The residue was purified by silica gel column chromatography to obtain **4d** as white semi-solid. **^{1}H NMR (400 MHz, $CDCl_3$)** δ 8.88 (s, 1H), 7.68 – 7.62 (m, 2H), 7.40 – 7.35 (m, 2H), 4.12 (q, *J* = 7.16 Hz, 2H), 3.06 (dd, *J* = 16.48, 6.51 Hz, 1H), 2.70 (dd, *J* = 16.45, 10.66 Hz, 1H), 2.65 – 2.49 (m, 3H), 2.16 (dtd, *J* = 14.16, 7.78, 6.73 Hz, 1H), 1.85 (dtd, *J* = 13.86, 7.58, 6.07 Hz, 1H), 1.24 (t, *J* = 7.12 Hz, 3H). **^{13}C{^{1}H} NMR (100 MHz, $CDCl_3$)** δ 173.1, 169.6, 149.6, 136.1, 134.2, 129.0, 127.2, 60.7, 35.1, 31.7, 28.2, 25.2, 14.3. **HRMS (ESI TOF)** *m/z* calcd. For $C_{15}H_{18}ClN_2O_3$ $[M + H]^+$ 309.1000 found 309.1004.

Di-tert-butyl (*Z*)-3-(2-(4-chlorophenyl)-2-(hydroxyimino)ethyl)hexanedioate (4d)



A mixture di-tert-butyl 2-(2-(4-chlorophenyl)-2-oxoethyl)pentanedioate **3h** (0.251 mmol), hydroxylamine hydrochloride (0.753 mmol) and pyridine in (0.753 mmol) in tert-butanol (3 mL) was stirred at 80 °C for 24 h until completion of the reaction as determined by TLC. The solvent was removed in vacuo. Water (10 mL) was added and the mixture was extracted three times with ethyl acetate. The combined organic layers were washed with brine, dried over Na_2SO_4, filtered, and the solvent was removed under reduced pressure to provide the glutarate substituted ketoximes **4c** as off-white semi solid (56 mg, 54% yield). **^{1}H NMR (400 MHz, $CDCl_3$)** δ 8.71 (s, 1H), 7.54 (d, *J* = 8.68 Hz, 2H), 7.33 (d, *J* = 8.64 Hz, 2H), 3.04 – 2.94 (m, 2H), 2.72 – 2.62 (m, 1H), 2.35 – 2.12 (m, 2H), 1.94 – 1.84 (m, 1H), 1.84 – 1.73 (m, 2H), 1.45 (dt, *J* = 7.87, 3.13 Hz, 1H), 1.40 (s, 9H), 1.32 (s, 9H). **^{13}C{^{1}H} NMR (100 MHz, $CDCl_3$)** δ 173.9, 172.4, 156.7, 135.5, 134.0, 128.9, 128.0, 42.8, 33.1, 28.4, 28.2, 28.0, 27.9. **HRMS (ESI TOF)** *m/z* calcd. For $C_{22}H_{33}ClNO_5$ $[M + H]^+$ 426.2042 found 426.2038.

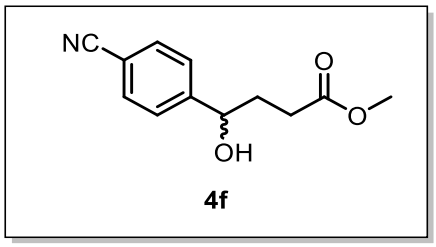
4-(4-cyanophenyl)-4-oxobutanoic acid (4e)



To a solution of ester **3ai** (50 mg, 0.192 mmol) in dichloromethane (1.5 mL) was added trifluoroacetic acid (1.5 mL). The mixture was stirred at room temperature for 2 h. The mixture was evaporated and partitioned between dichloromethane and water. The aqueous layer was washed with dichloromethane (10 mLx3), combined the organic layers, dried over sodium sulfate, then filtered and concentrated in vacuum afford the title compound **4e** as brown solid (30 mg, 77% yield). **^{1}H NMR (400 MHz, Methanol-*d*$_4$)** δ 8.15 – 8.08 (m, 2H), 7.88 – 7.83 (m, 2H), 3.34 – 3.30 (m, 2H), 2.76 – 2.65 (m, 2H). **^{13}C{^{1}H} NMR (100 MHz, Methanol-*d*$_4$)** δ

199.2, 176.3, 141.2, 133.7, 129.7, 119.0, 117.3, 34.7, 28.7. **HRMS (ESI TOF)** *m/z* calcd. For $C_{11}H_{10}NO_3$ $[M + H]^+$ 204.0655 found 204.0657.

Methyl 4-(4-cyanophenyl)-4-hydroxybutanoate (4f)



4f

To a solution of the keto ester **3aj** (50 mg, 0.192 mmol) in methanol (2 mL), sodium borohydride (2 equiv.) was added portion wise at 0 ˚C. The reaction mixture was allowed to warm up to room temperature. When the reduction was completed (according to the TLC) the solvent was carefully evaporated under reduced pressure. The residue was purified by silica gel column chromatography to obtain **4f** (36.5 mg, 72% yield, dr= 3:1). (Major diastereomer).
^{1}H NMR (400 MHz, $CDCl_3$) δ 7.66 – 7.61 (m, 2H), 7.47 (d, *J* = 8.10 Hz, 2H), 4.85 (dd, *J* = 7.97, 4.37 Hz, 1H), 3.68 (s, 3H), 2.46 (q, *J* = 6.75 Hz, 2H), 2.11 – 1.96 (m, 2H). **^{1}H NMR (400 MHz, $CDCl_3$)** (Minor diastereomer) 2.81 – 2.62 (m, 2H). **^{13}C {^{1}H} NMR (100 MHz, $CDCl_3$)** (Major diastereomer) δ 174.5, 149.6, 132.5, 126.6, 118.9, 111.4, 72.8, 52.1, 33.8, 30.2. **^{13}C NMR (100 MHz, $CDCl_3$)** (Minor diastereomer) δ 176.2, 144.8, 132.8, 125.9, 118.5, 112.5, 80.0, 31.0, 28.8. **HRMS (ESI TOF)** *m/z* calcd. For $C_{12}H_{14}NO_3$ $[M + H]^+$ 220.0968 found 220.0965.

4.14 . Appendix IV: ^{1}H, ^{13}C, 2D NMR and IR spectral data of representative compounds

Compound No.	Figure AIII.X	Data	Page No.
3a	Figure AIV. 1 and AIV. 2	^{1}H and ^{13}C	194
3a	Figure AIV. 3	COSY	195
3a	Figure AIV. 4	NOESY	196
3a	Figure AIV. 5	HSQC	197
3a	Figure AIV. 6	HMBC	198
3f	Figure AIV. 7 and AIV. 8	^{1}H and ^{13}C	199
3f	Figure AIV. 9 and AIV. 10	COSY and NOESY	200
3f	Figure AIV. 11 and AIV. 12	HSQC and HMBC	201
3ag	Figure AIV.13 and AIV.14	^{1}H and ^{13}C NMR	202
4a	Figure AIV.15 and AIV.16	^{1}H and ^{13}C NMR	203
4b	Figure AIV.17 and AIV.18	^{1}H and ^{13}C NMR	204
4c	Figure AIV.19 and AIV.20	^{1}H and ^{13}C NMR	205
4d	Figure AIV.21 and AIV.22	^{1}H and ^{13}C NMR	206
4e	Figure AIV.23 and AIV.24	^{1}H and ^{13}C NMR	207
4f	Figure AIV.25 and AIV.26	^{1}H and ^{13}C NMR	208
3a	Figure AIV.27	IR	209
3k	Figure AIV.28	IR	210
3z	Figure AIV.29	IR	211

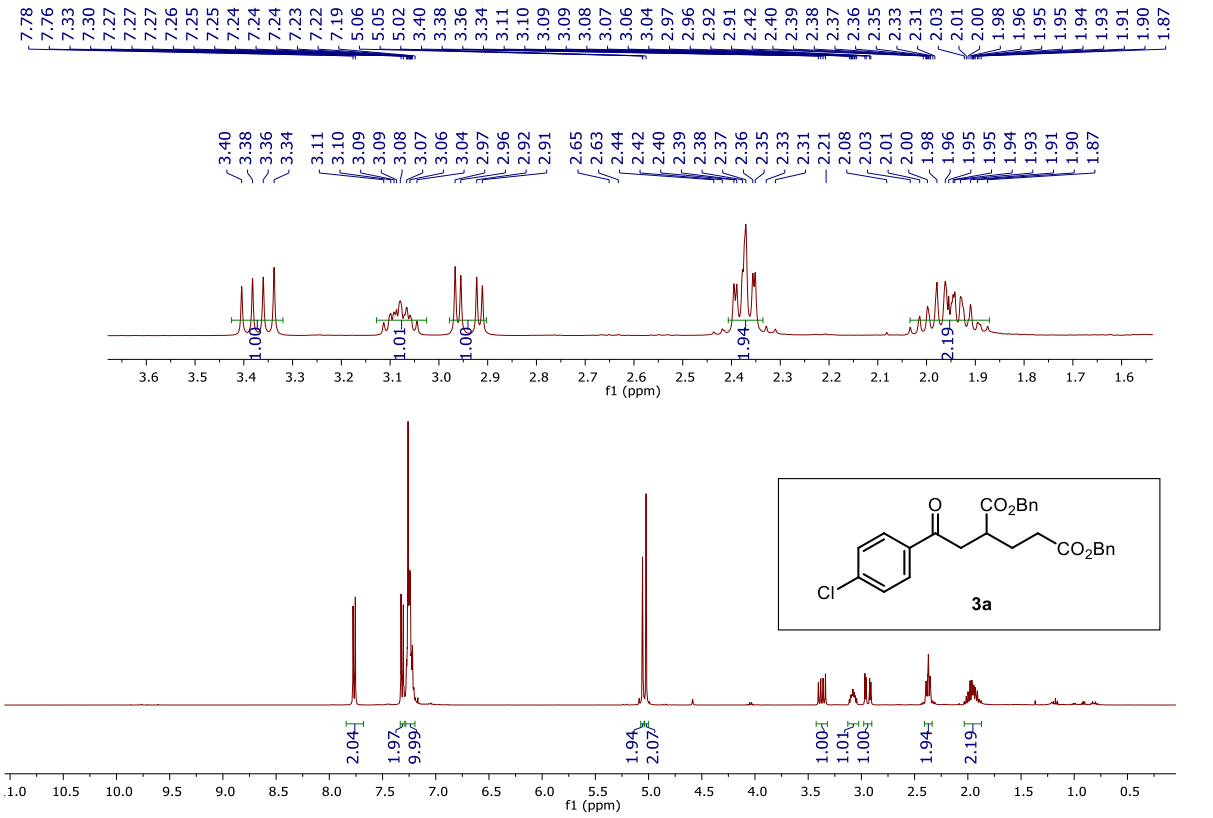


Figure AIV.1 ^{1}H NMR spectrum of **3a**, $CDCl_3$, 400 MHz

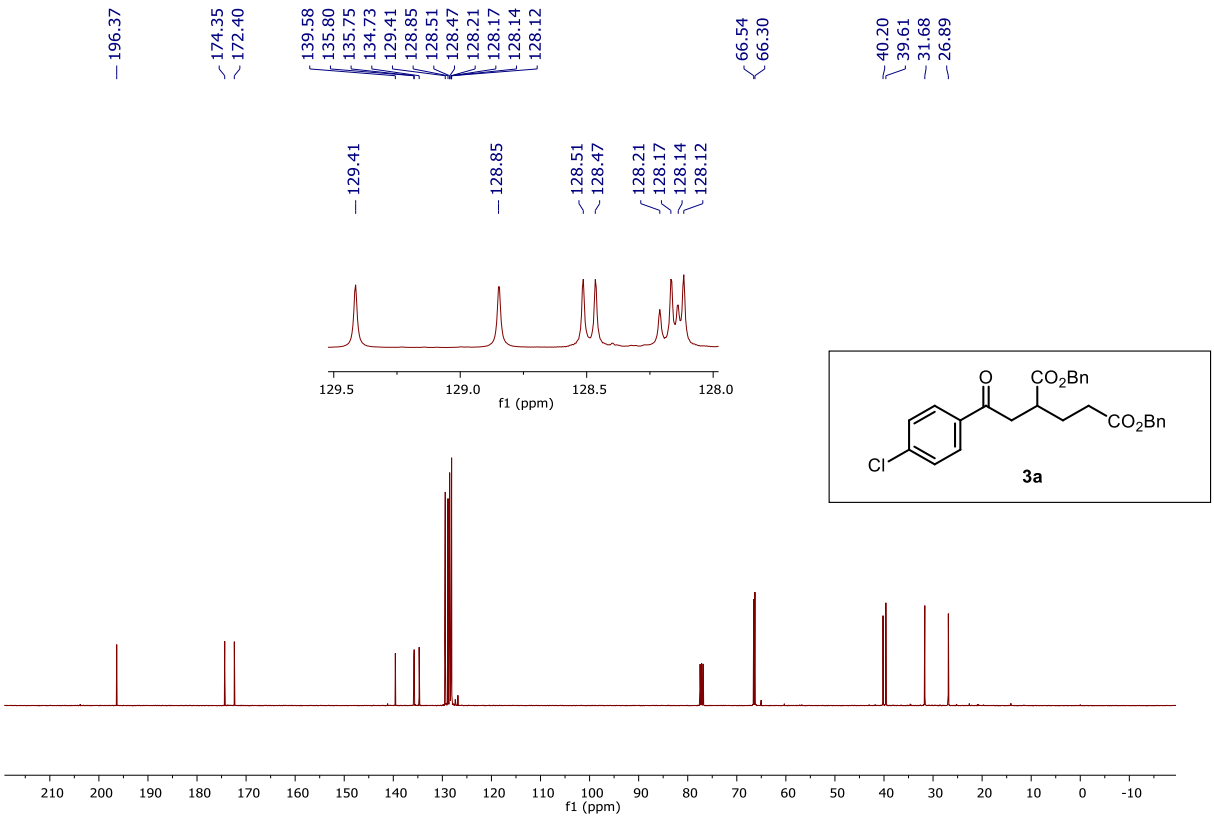


Figure AIV.2 $^{13}C\{^{1}H\}$ NMR spectrum of **3a**, $CDCl_3$, 100 MHz

COSY

^{1}H-^{1}H correlation

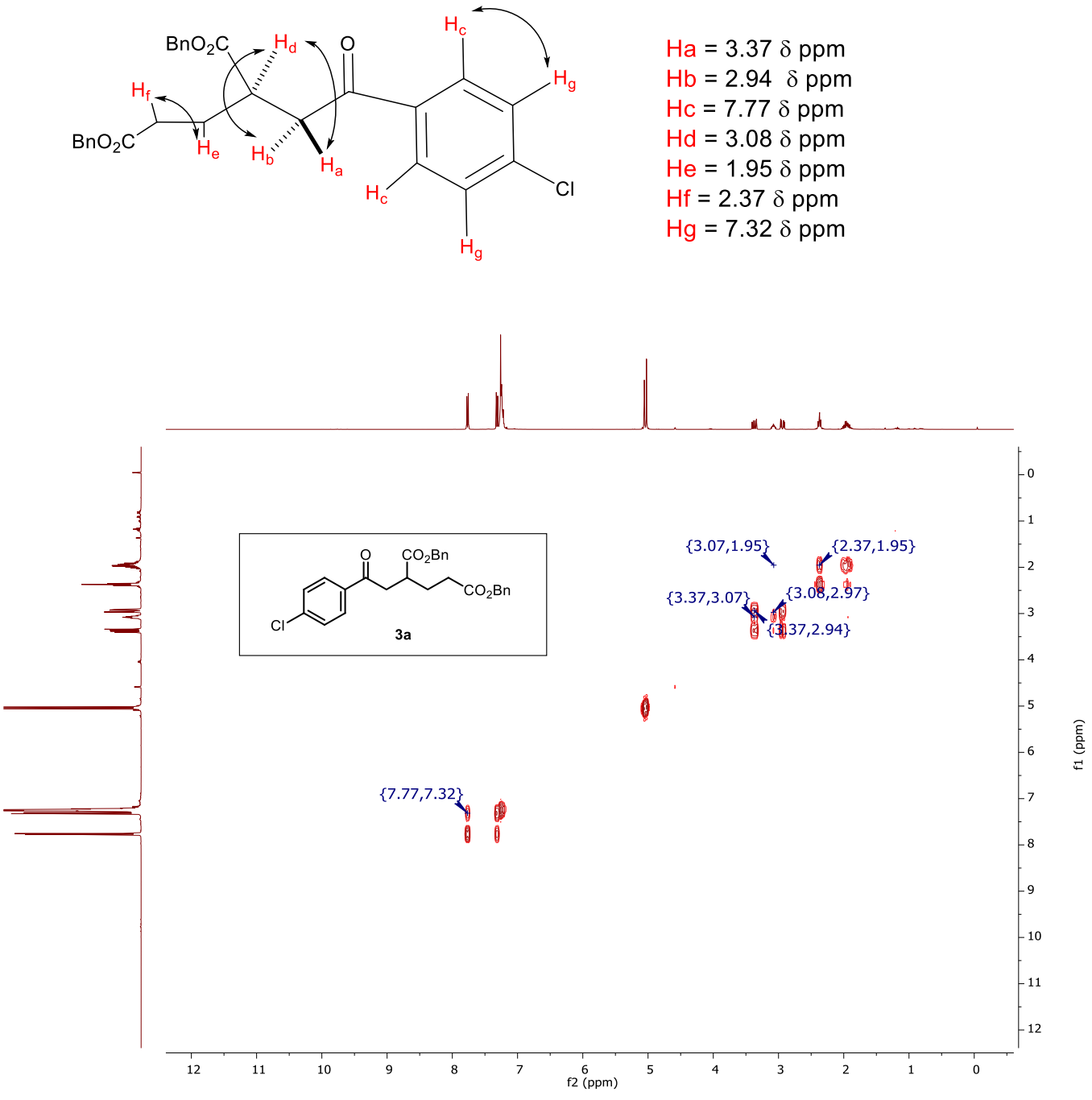
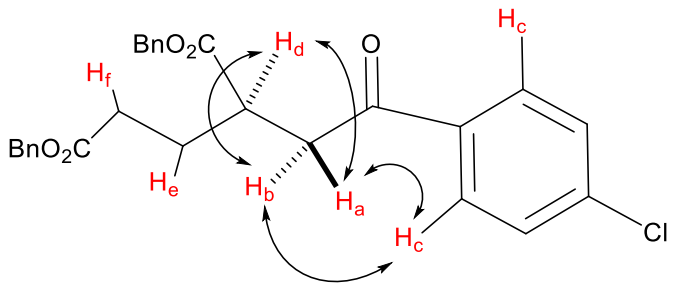


Figure AIV.3 COSY (^{1}H-^{1}H) spectrum of **3a**

NOESY

^{1}H-^{1}H correlation



Ha = 3.37 δ ppm
Hb = 2.94 δ ppm
Hc = 7.77 δ ppm
Hd = 3.08 δ ppm
He = 1.95 δ ppm
Hf = 2.37 δ ppm

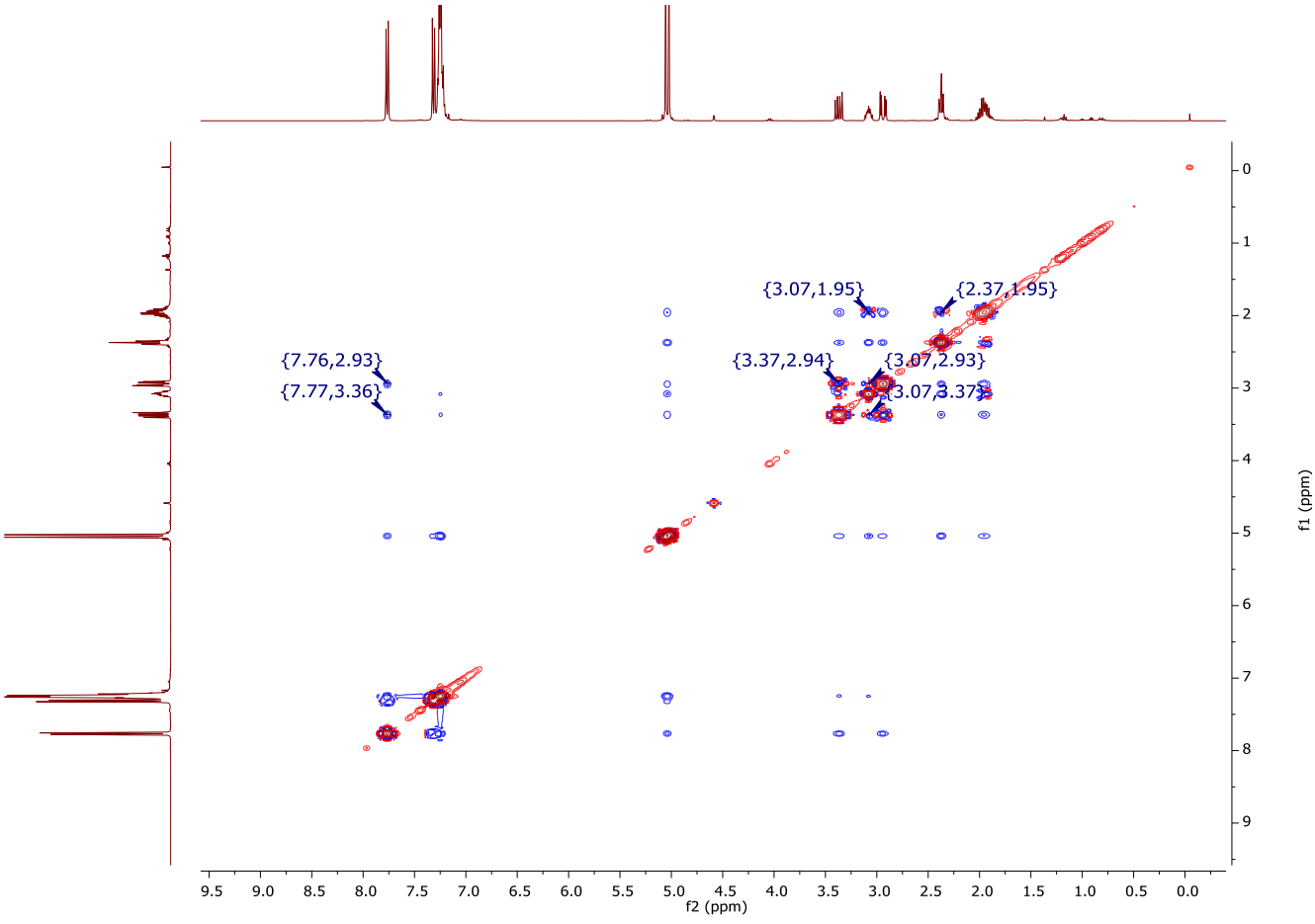


Figure AIV.4 NOESY (^{1}H-^{1}H) spectrum of **3a**

HSQC

^{1}H-^{13}C correlation

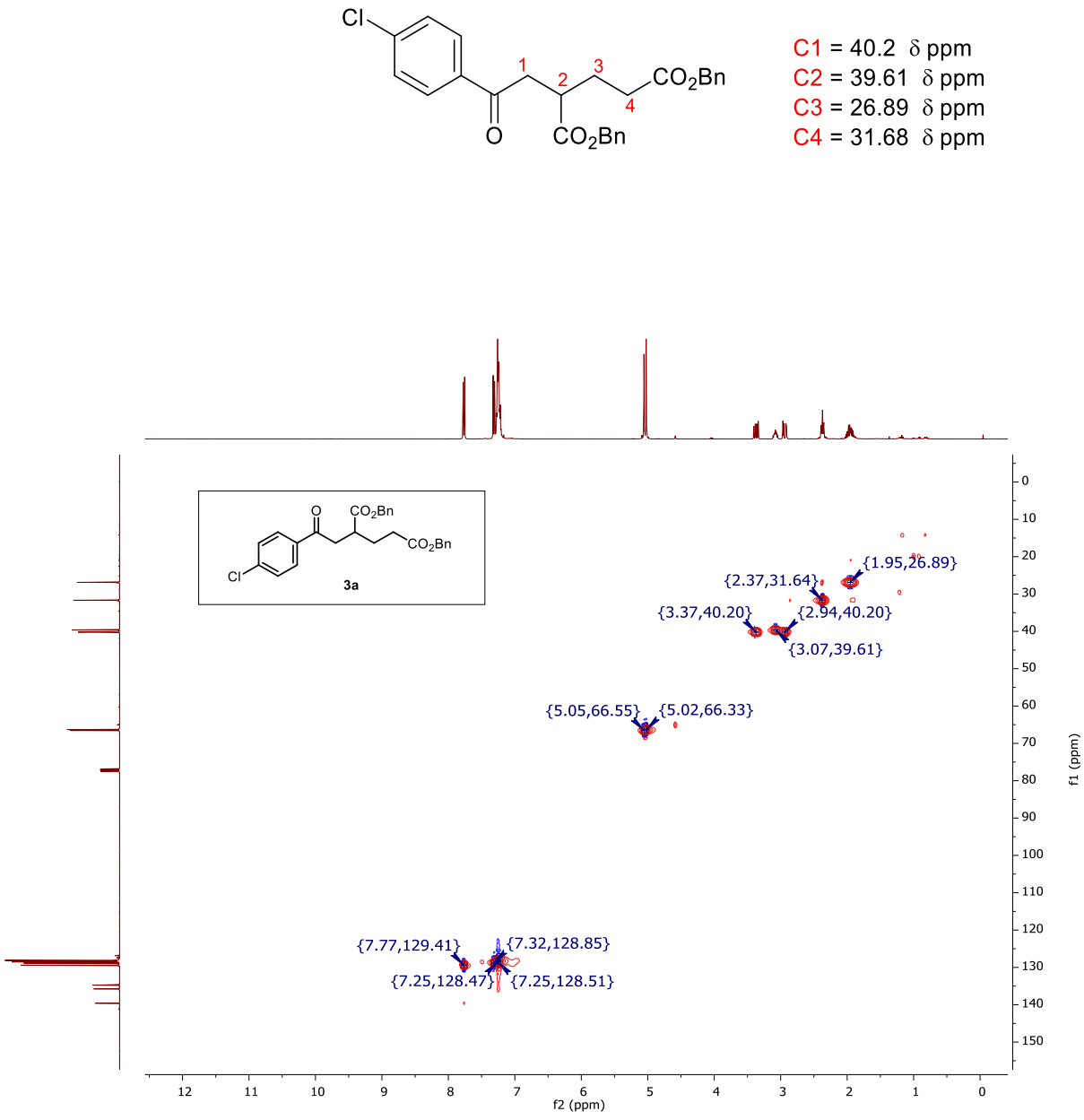


Figure AIV.5 HSQC (^{1}H-^{13}C) spectrum of **3a**

HMBC

^{1}H-^{13}C correlation

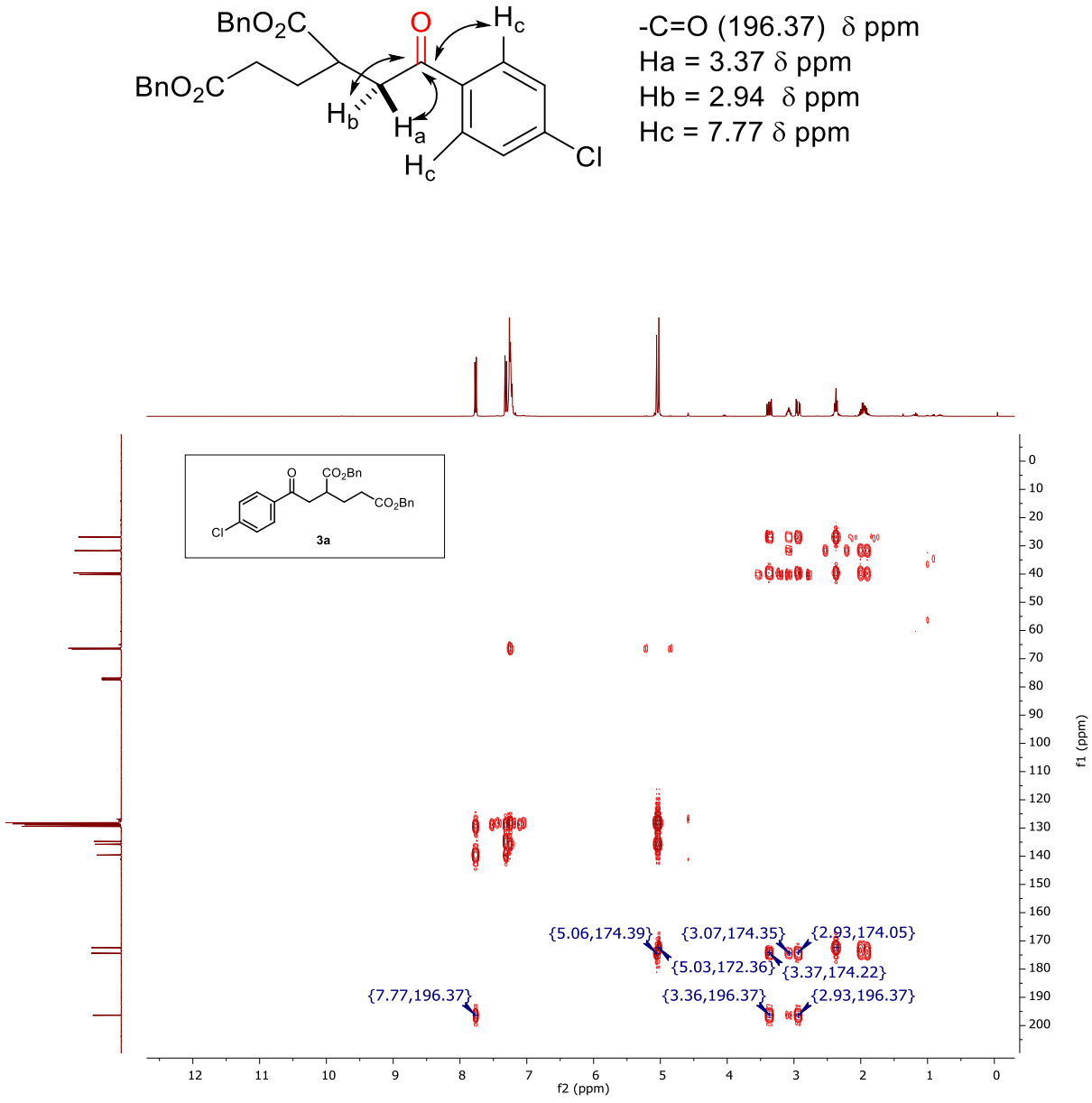


Figure AIV.6 HMBC (^{1}H-^{13}C) spectrum of **3a**

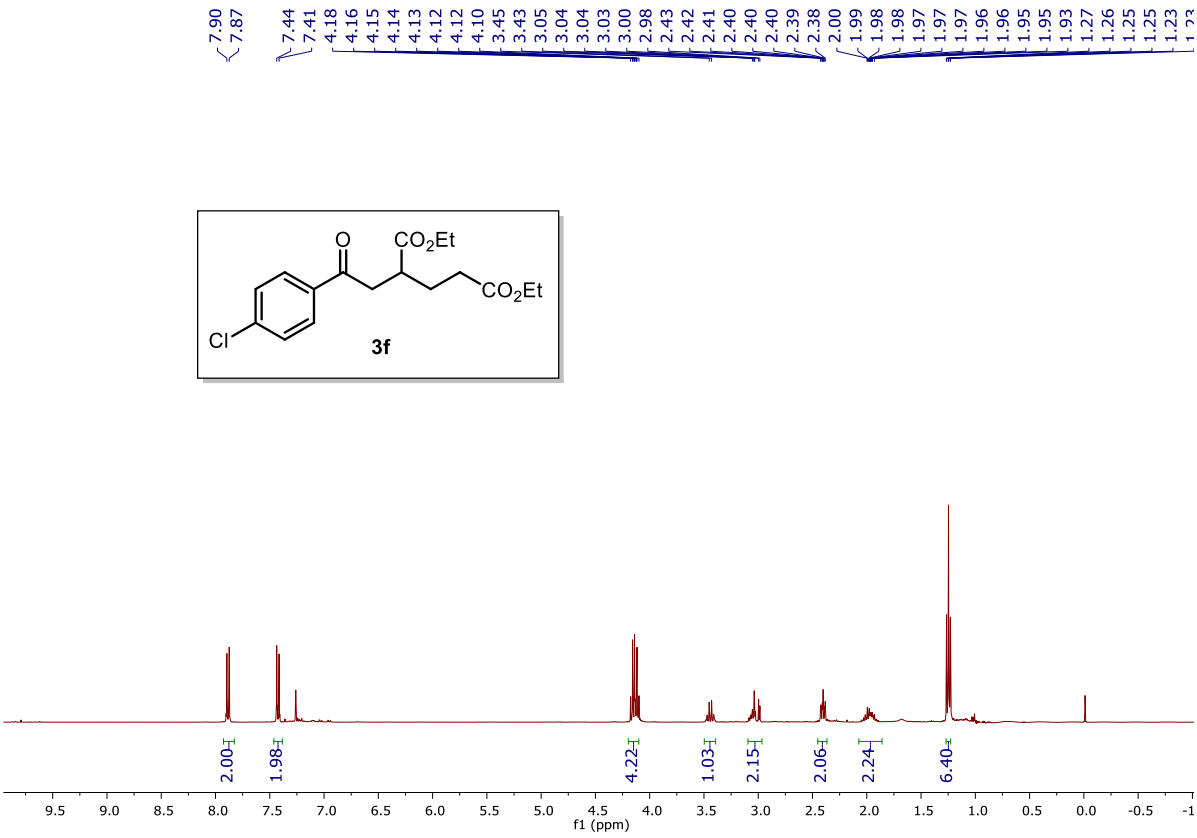


Figure AIV.7 ^{1}H NMR spectrum of **3f**, $CDCl_3$, 400 MHz

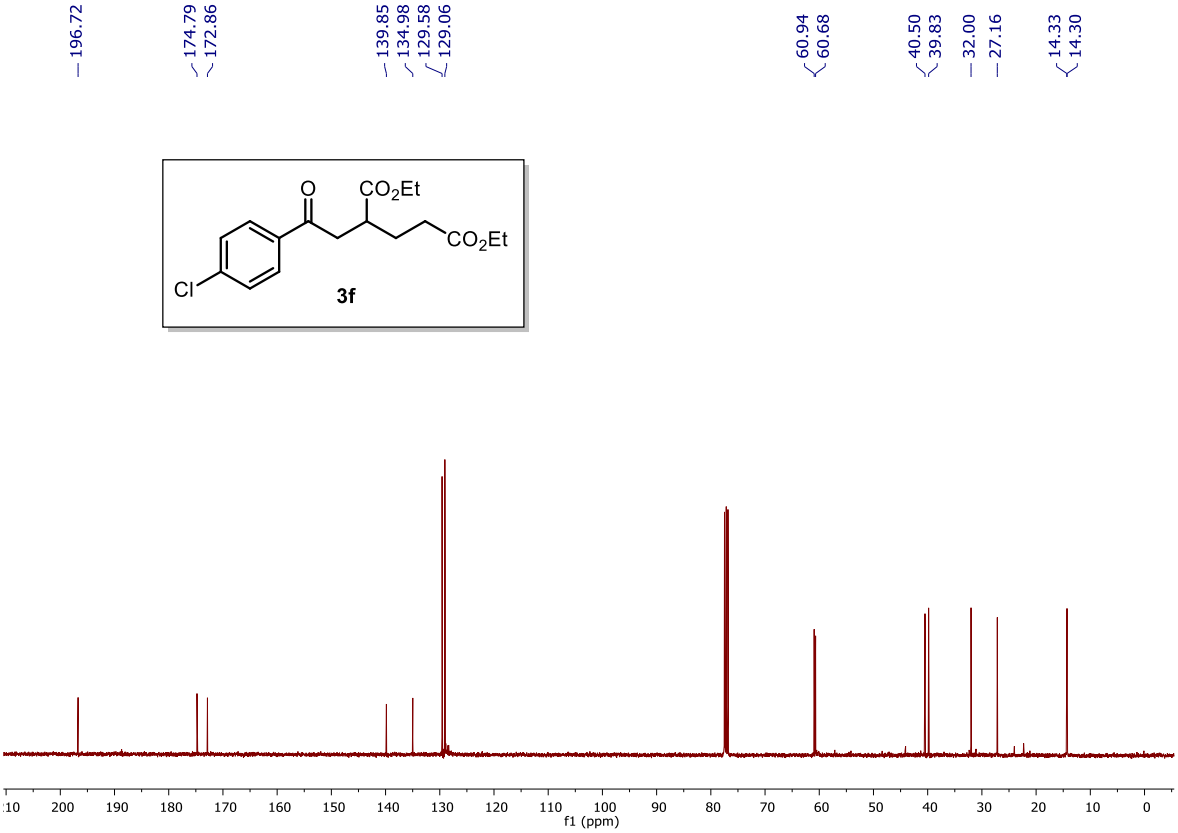


Figure AIV.8 ^{13}C {^{1}H} NMR spectrum of **3f**, $CDCl_3$, 100 MHz

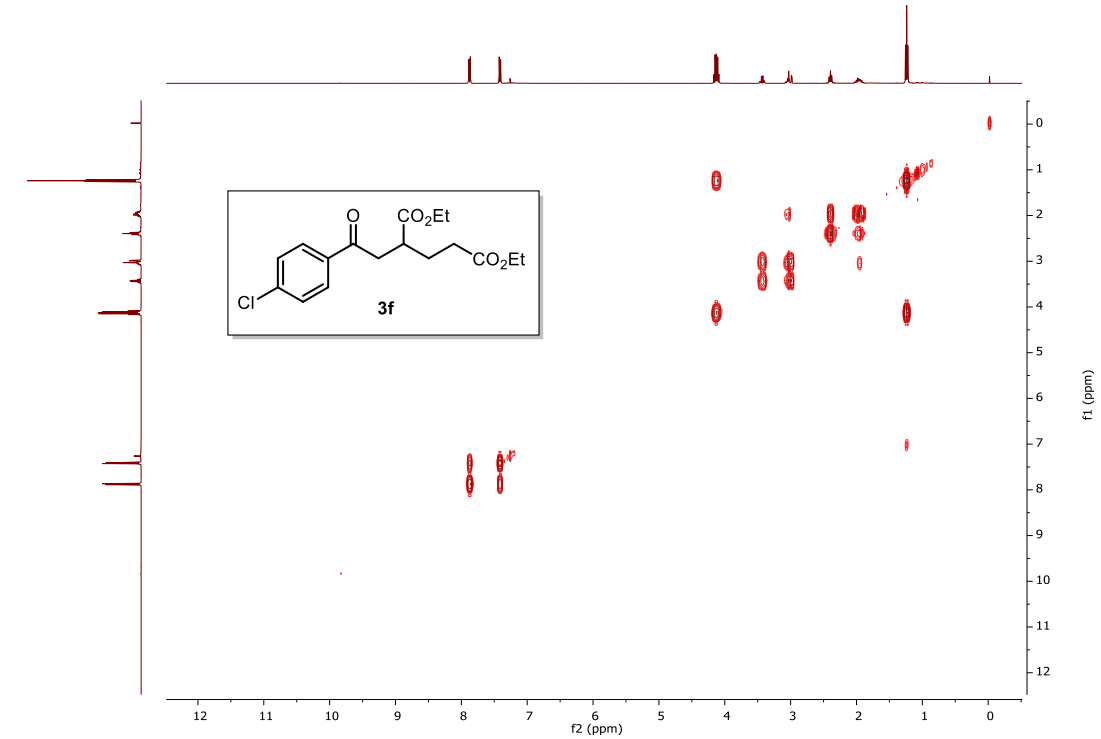


Figure AIV.9 COSY (^{1}H-^{13}C) spectrum of **3f**

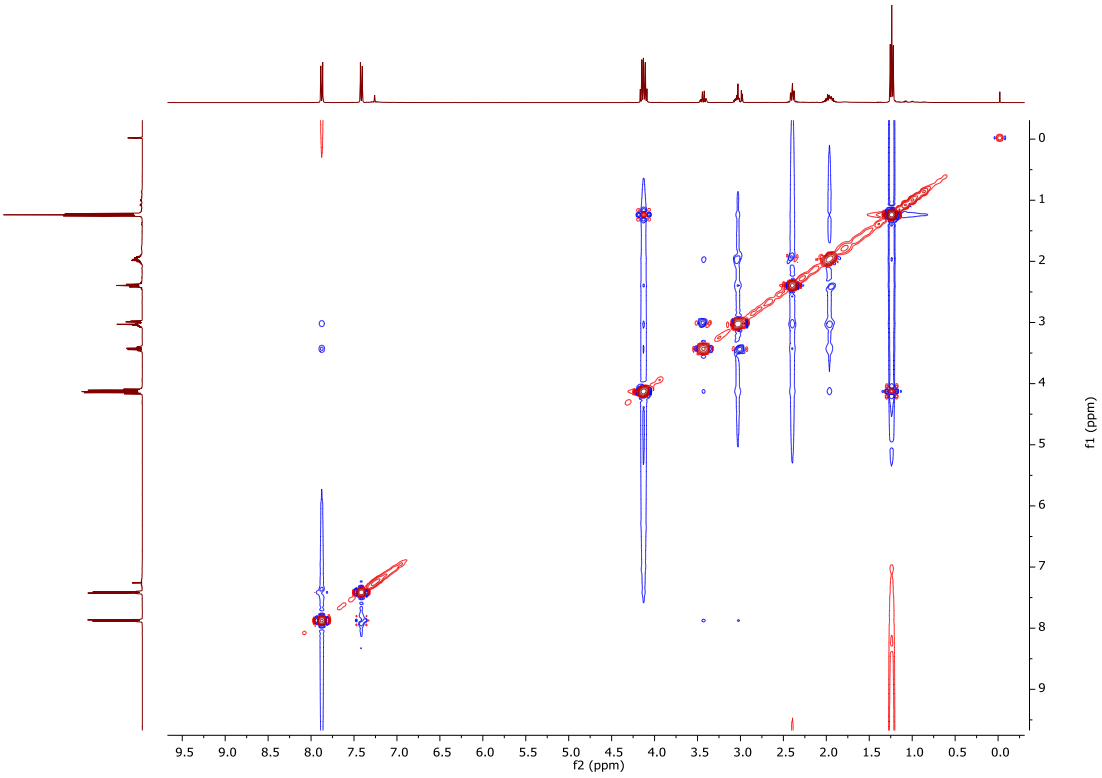


Figure AIV.10 NOESY (^{1}H-^{13}C) spectrum of **3f**

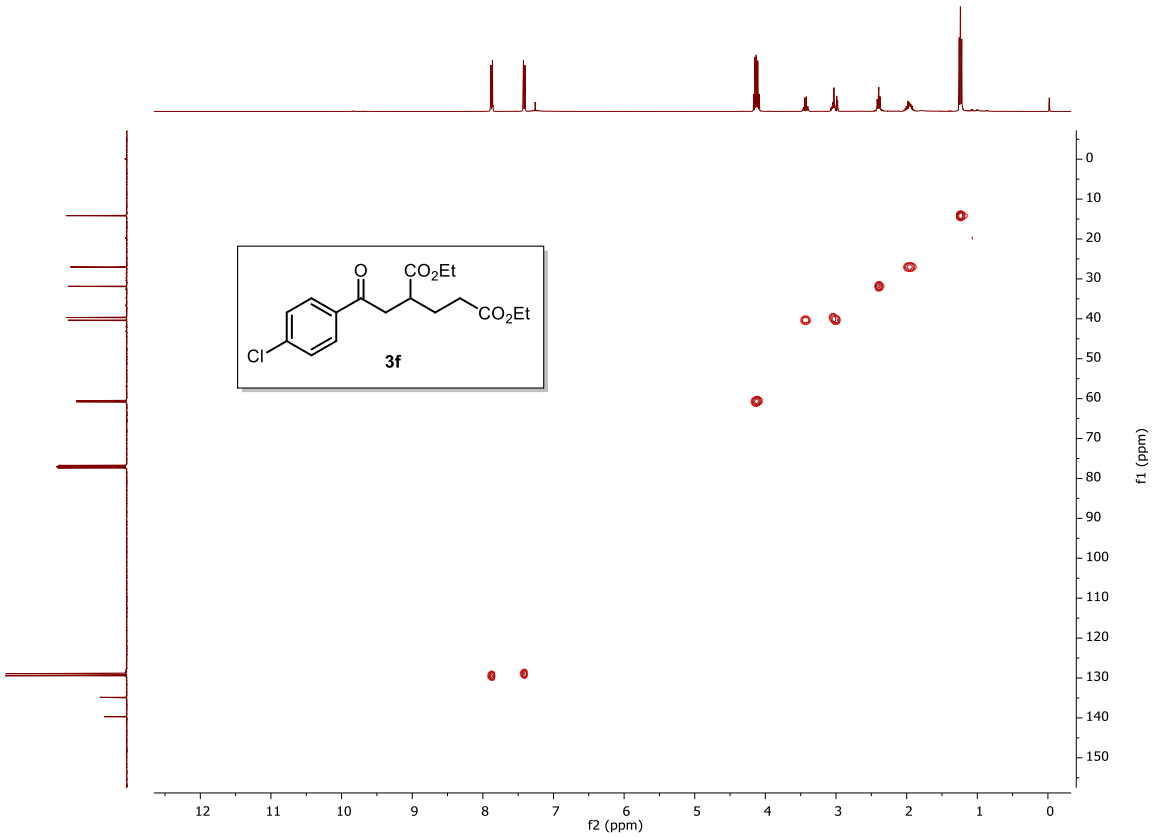


Figure AIV.11 HSQC (^{1}H-^{13}C) spectrum of **3f**

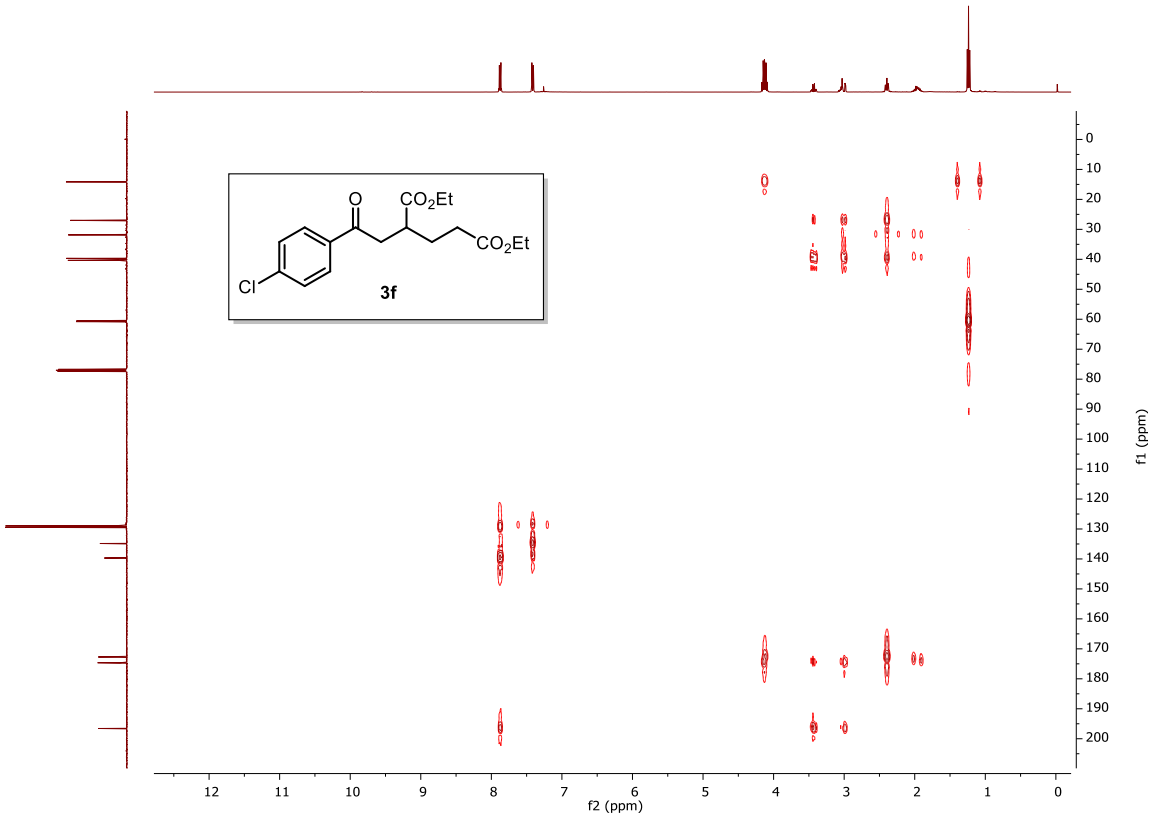


Figure AIV.12 HMBC (^{1}H-^{13}C) spectrum of **3f**

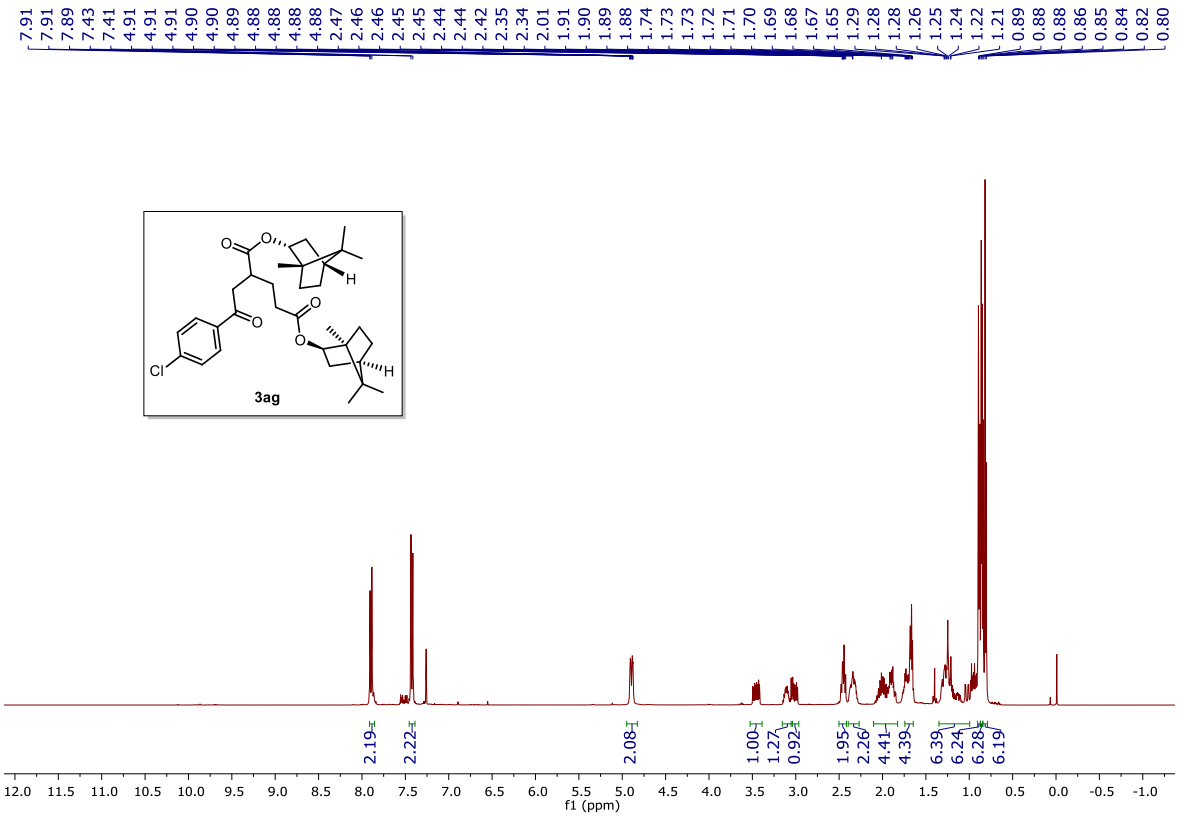


Figure AIV.13 ^{1}H NMR spectrum of **3ag**, $CDCl_3$, 400 MHz

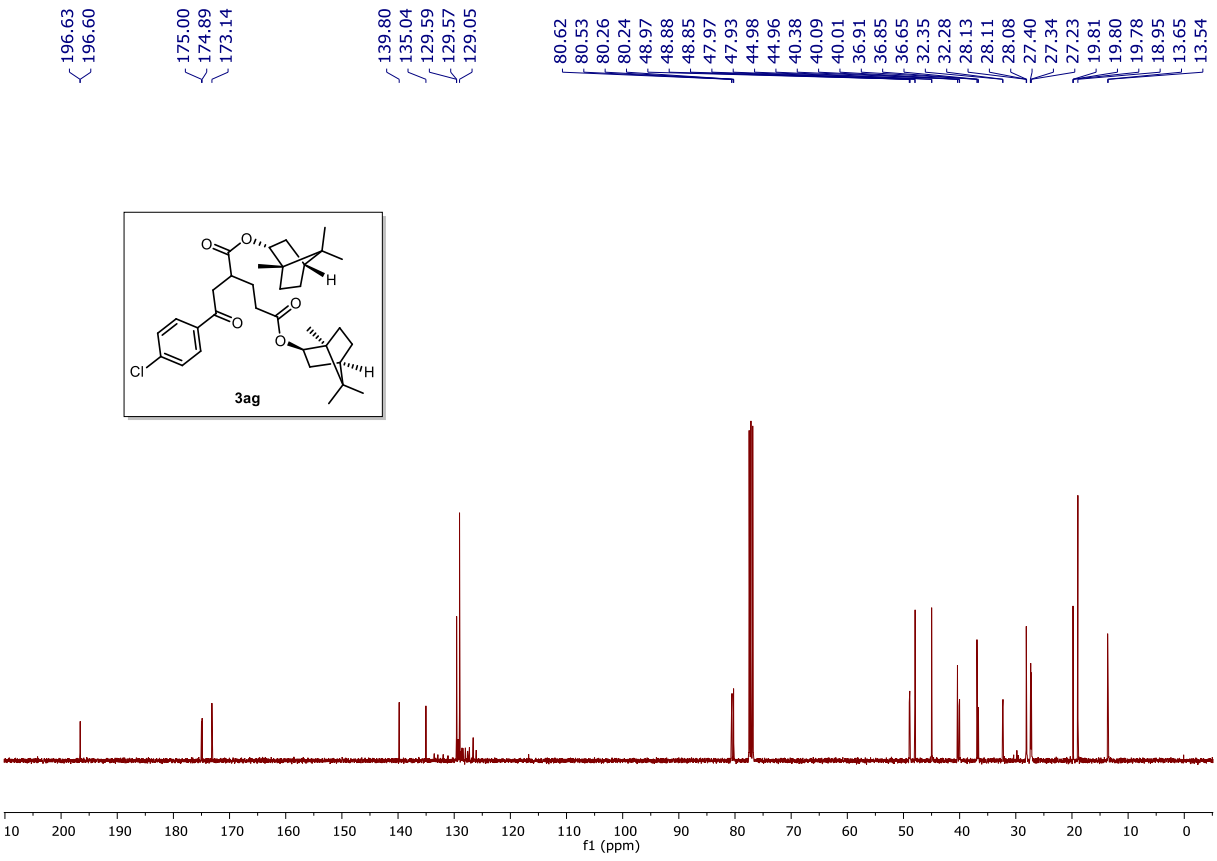


Figure AIV.14 $^{13}C\{^{1}H\}$ NMR spectrum of **3ag**, $CDCl_3$, 100 MHz

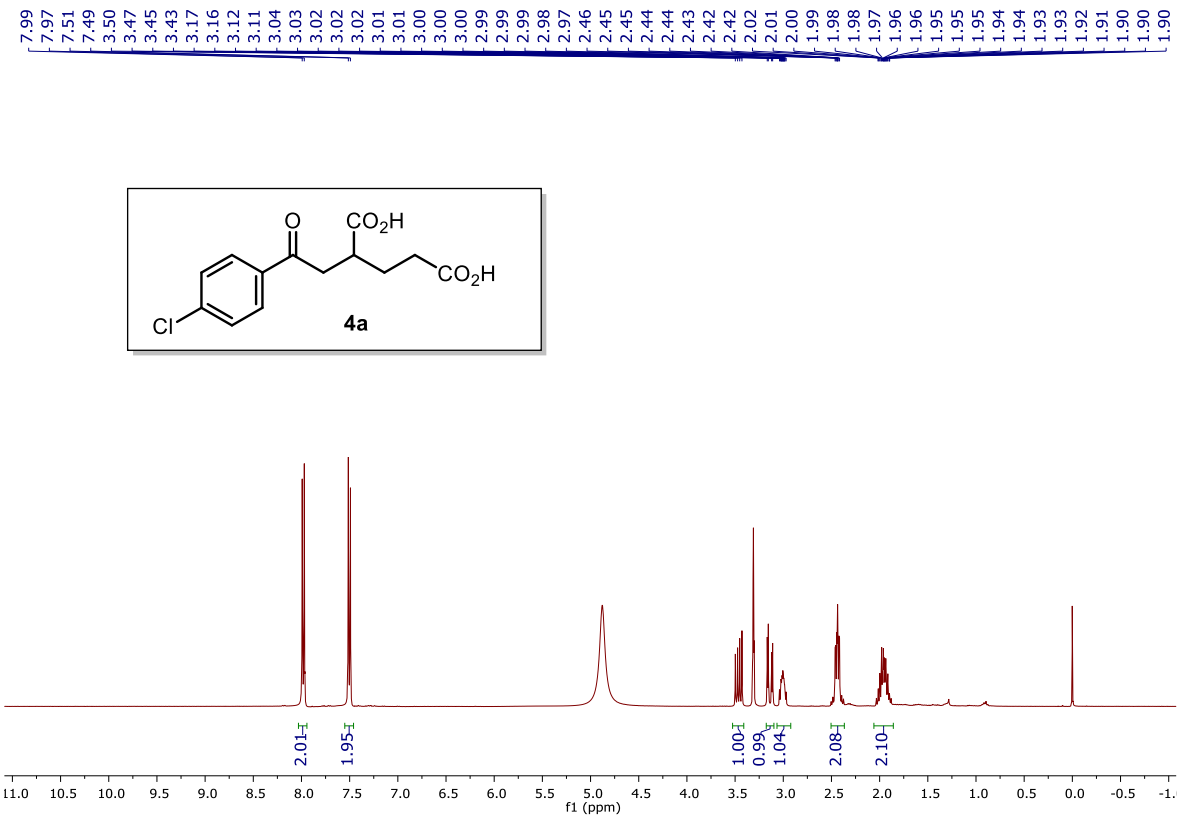


Figure AIV.15 ^{1}H NMR spectrum of **4a**, CD_3OD, 400 MHz

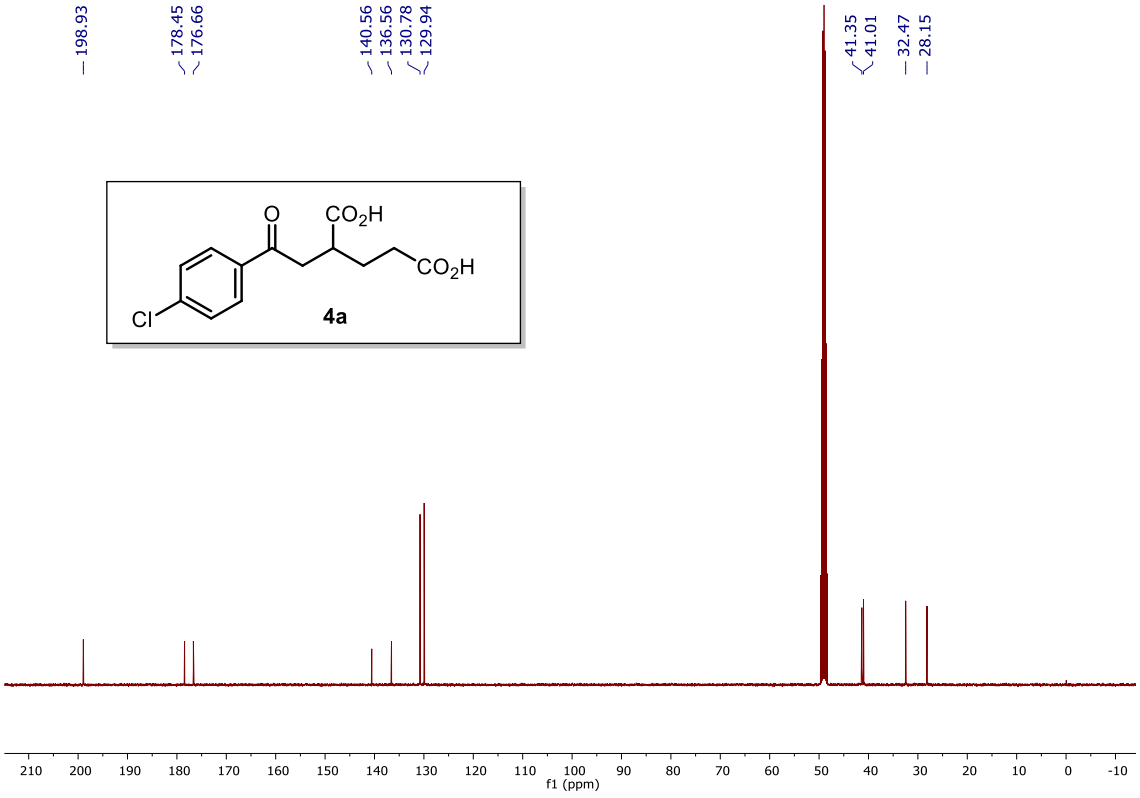


Figure AIV.16 $^{13}C\{^{1}H\}$ NMR spectrum of **4a**, CD_3OD, 100 MHz

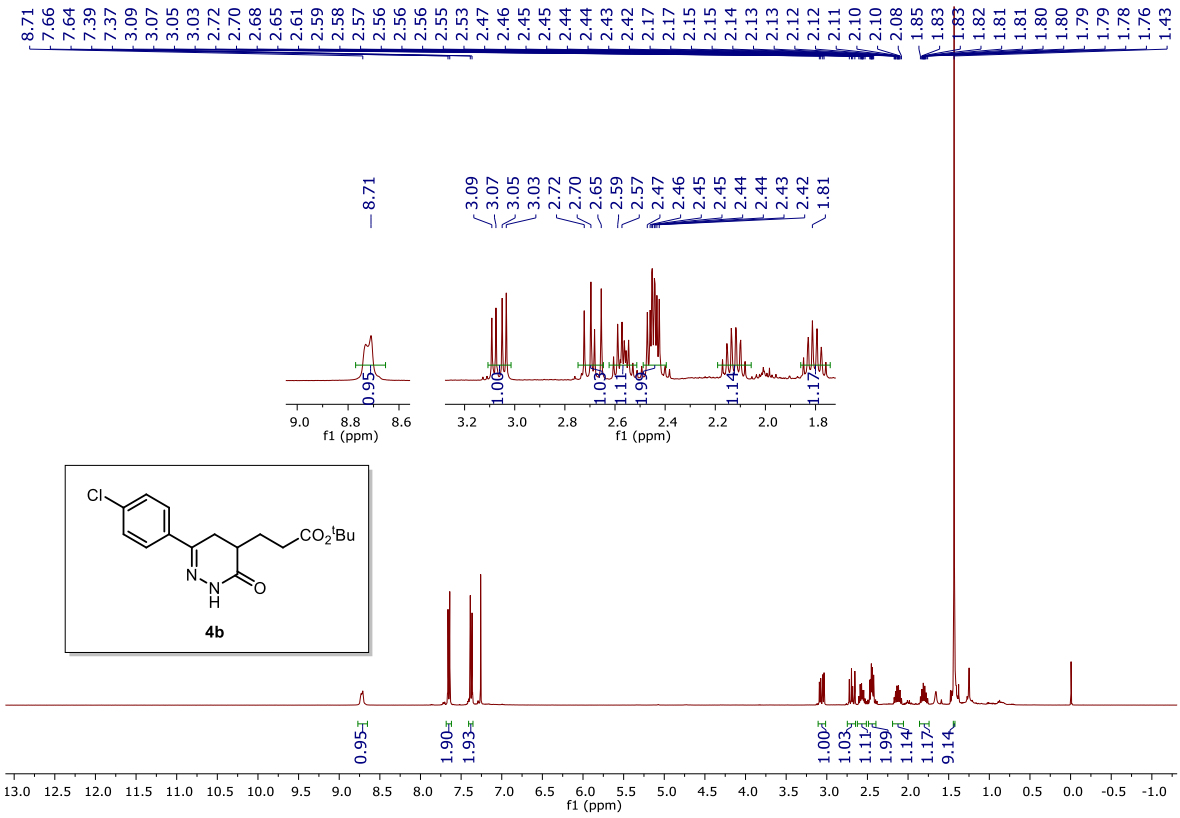


Figure AIV.17 ^{1}H NMR spectrum of **4b**, $CDCl_3$, 400 MHz

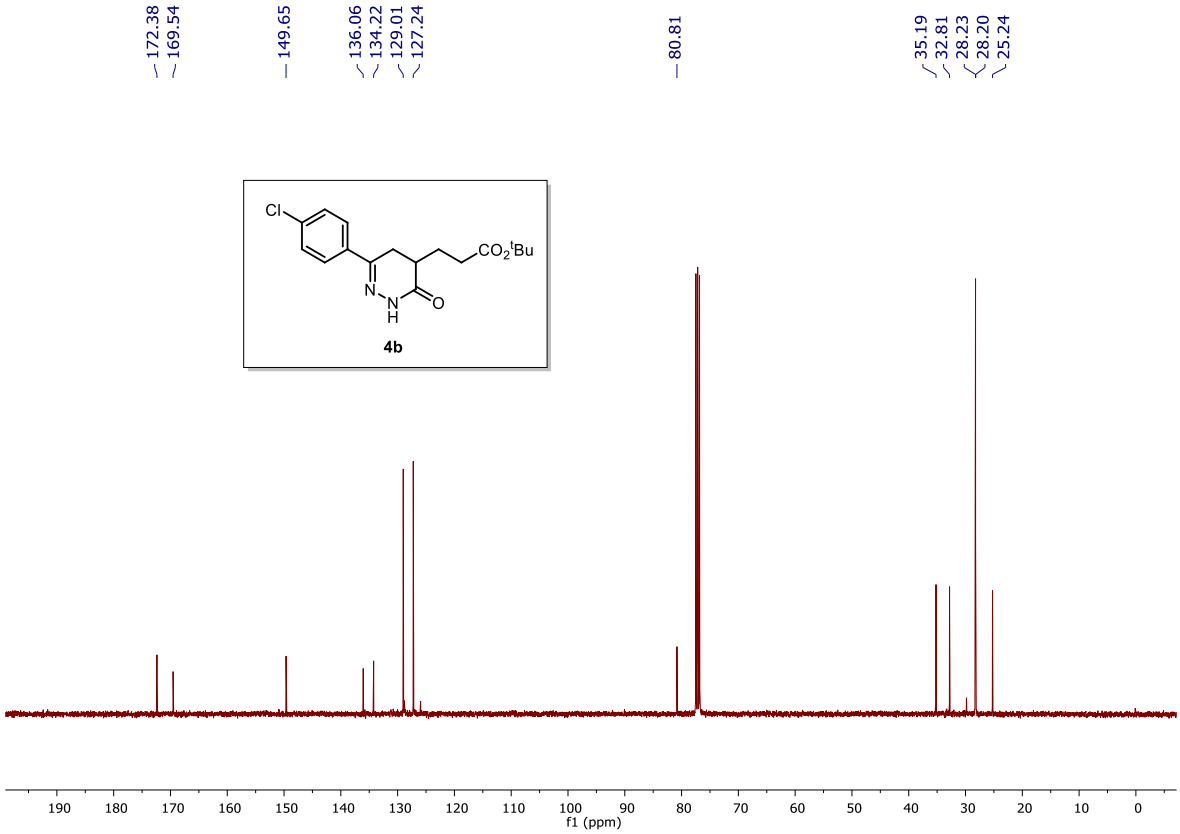


Figure AIV.18 $^{13}C\{^{1}H\}$ NMR spectrum of **4b**, $CDCl_3$, 100 MHz

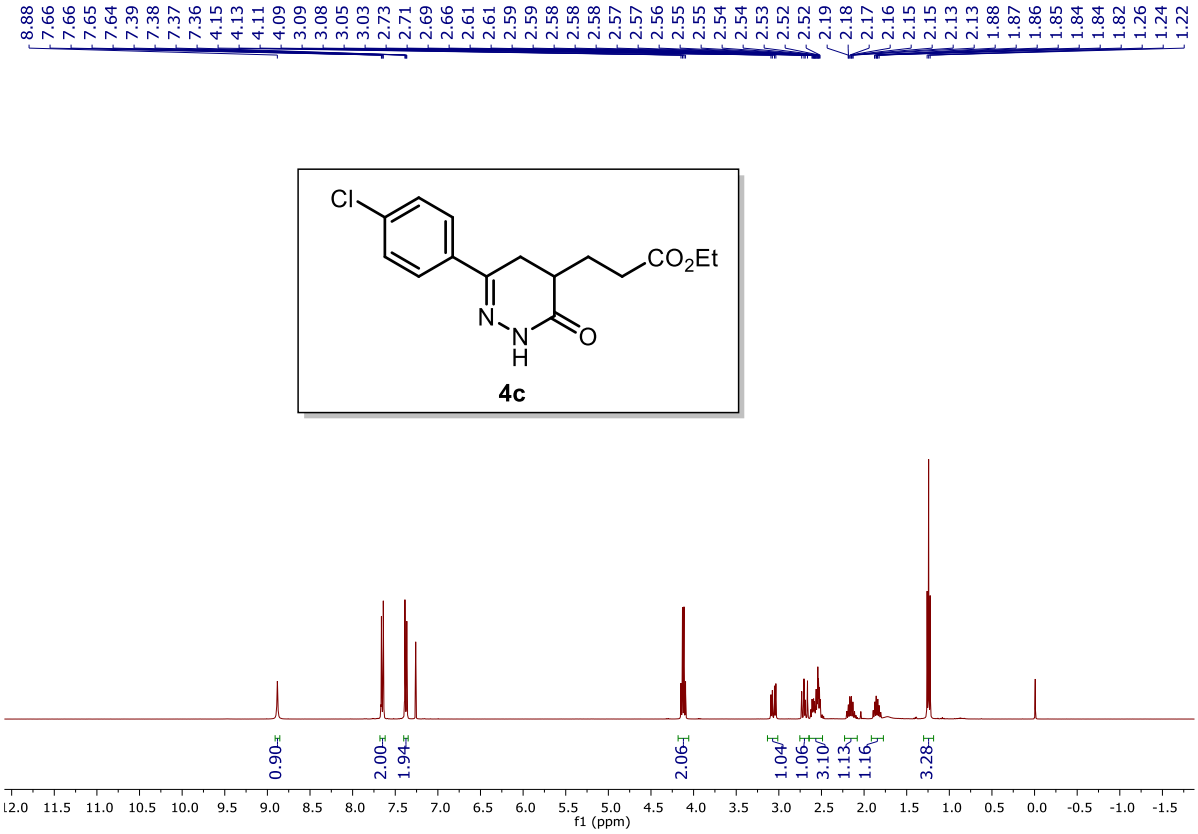


Figure AIV.19 ^{1}H NMR spectrum of **4c**, $CDCl_3$, 400 MHz

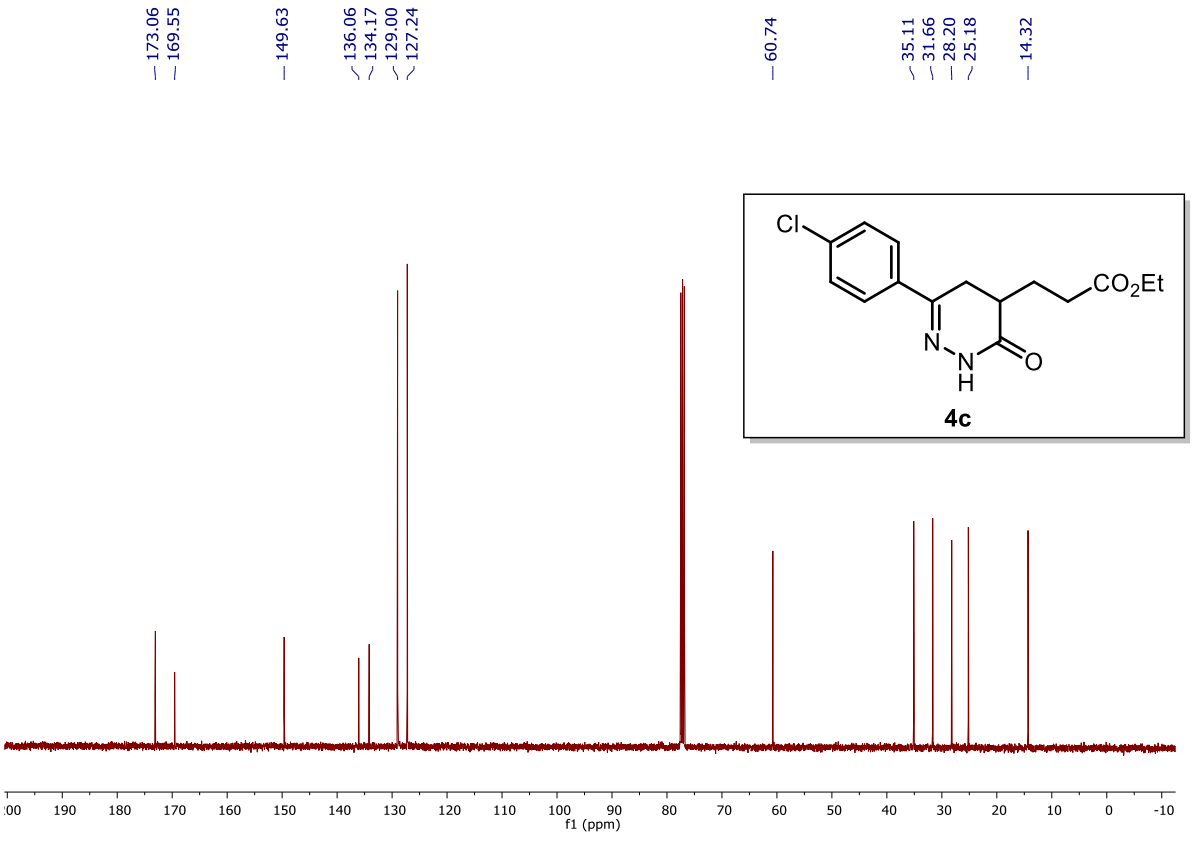


Figure AIV.20 $^{13}C\{^{1}H\}$ NMR spectrum of **4c**, $CDCl_3$, 100 MHz

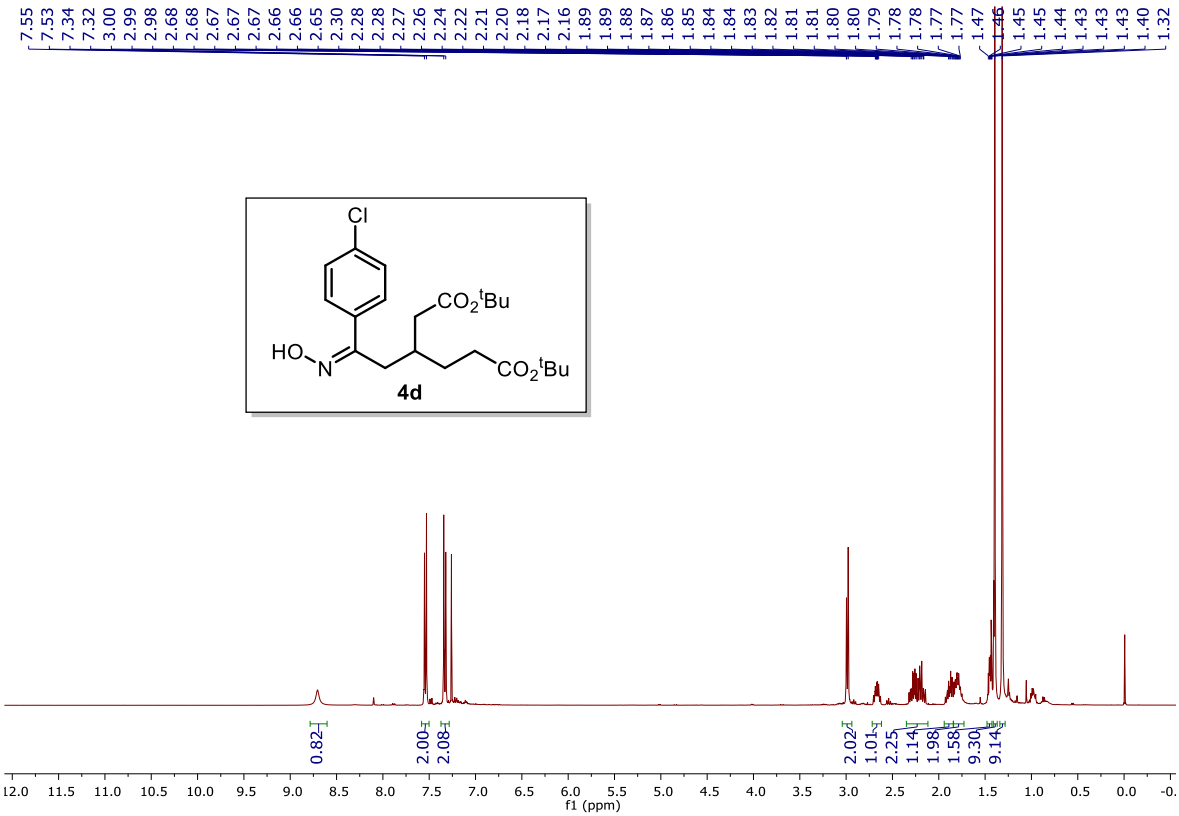


Figure AIV.21 ^{1}H NMR spectrum of **4d**, $CDCl_3$, 400 MHz

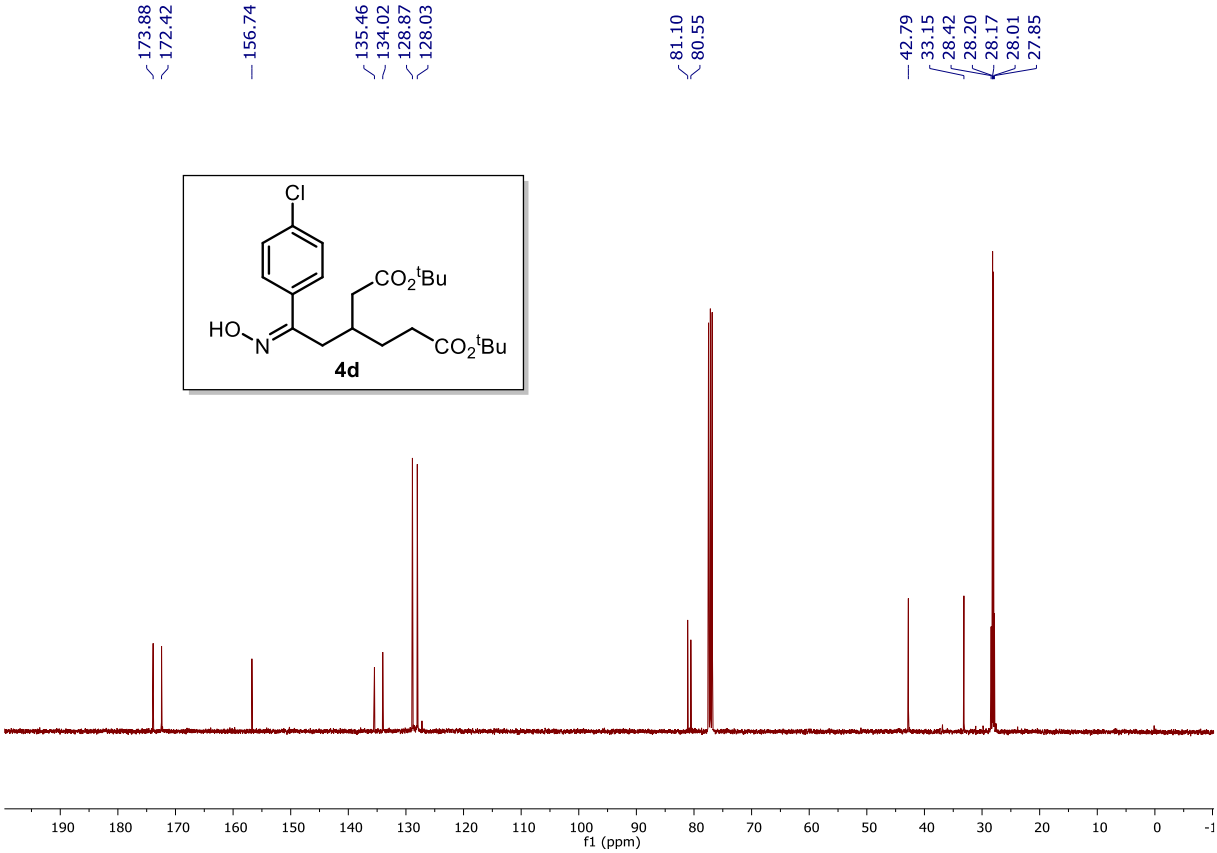


Figure AIV.22 ^{13}C {^{1}H} NMR spectrum of **4d**, $CDCl_3$, 100 MHz

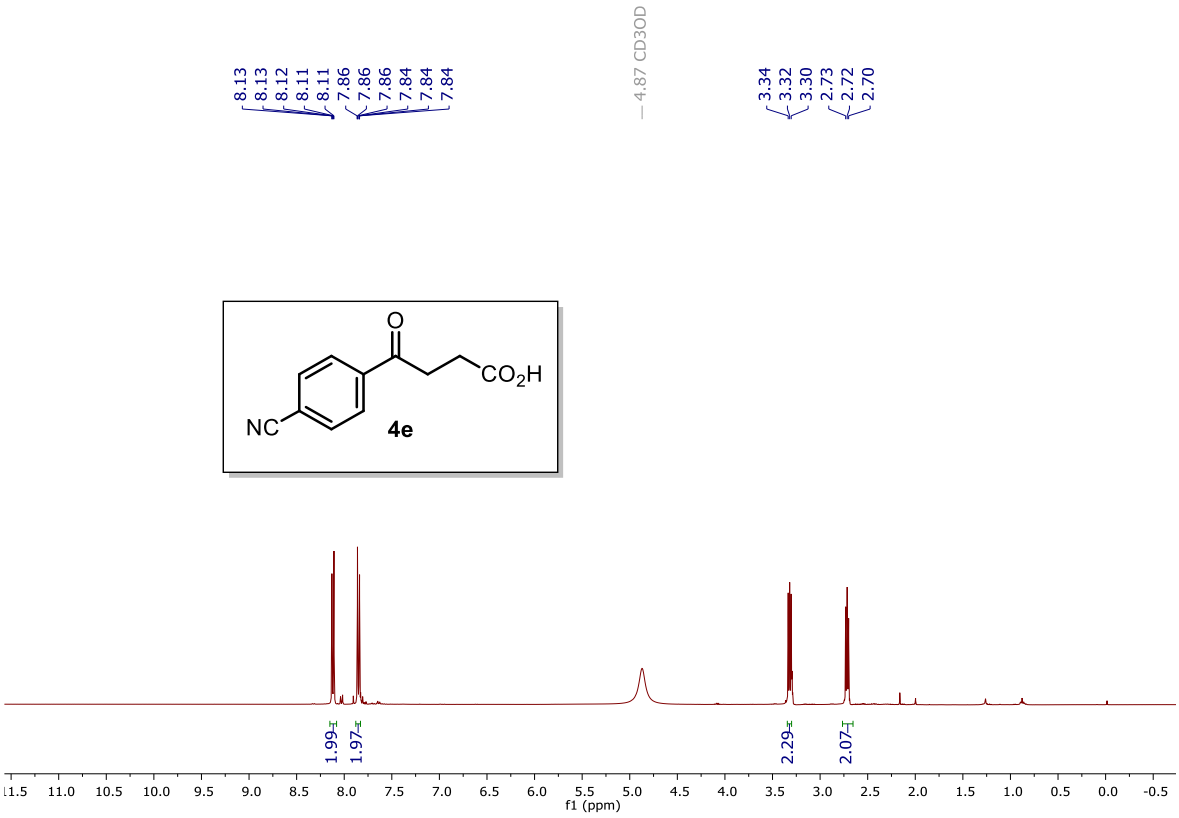


Figure AIV.23 ^{1}H NMR spectrum of **4e**, CD_3OD, 400 MHz

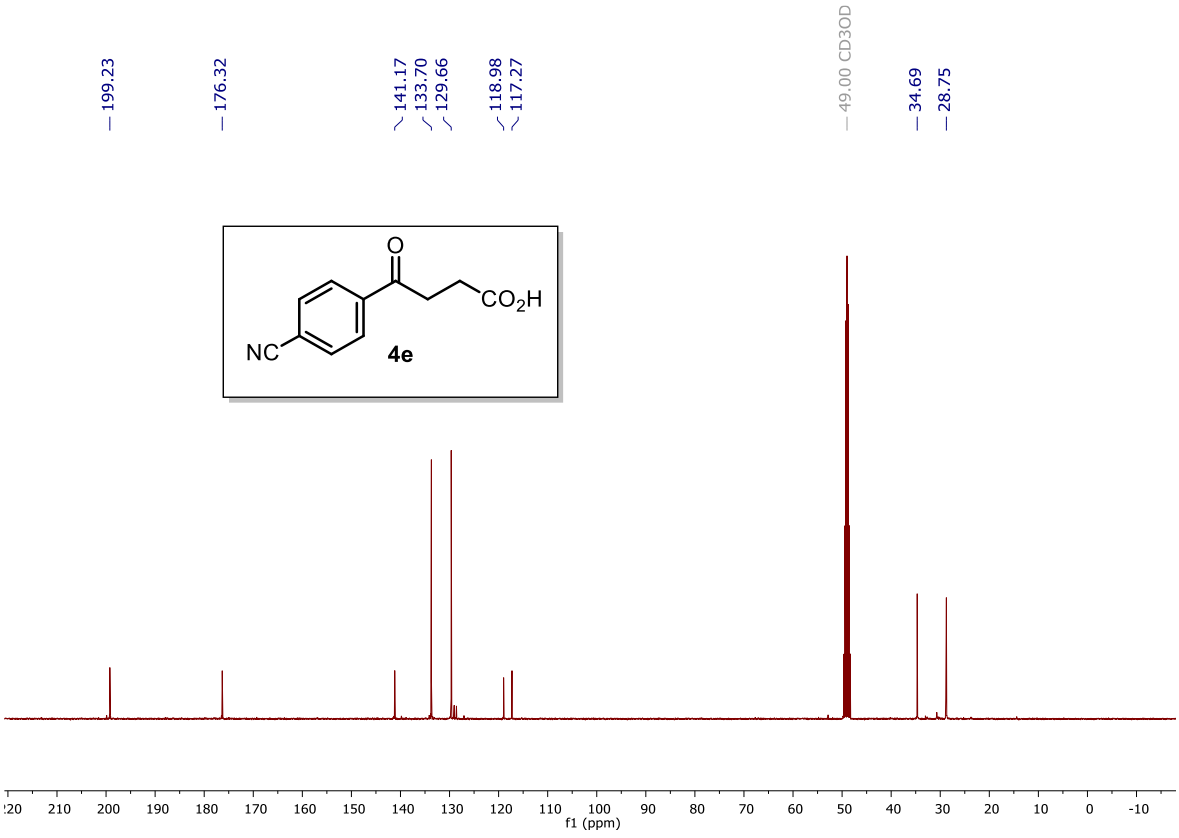


Figure AIV.24 $^{13}C\{^{1}H\}$ NMR spectrum of **4e**, CD_3OD, 100 MHz

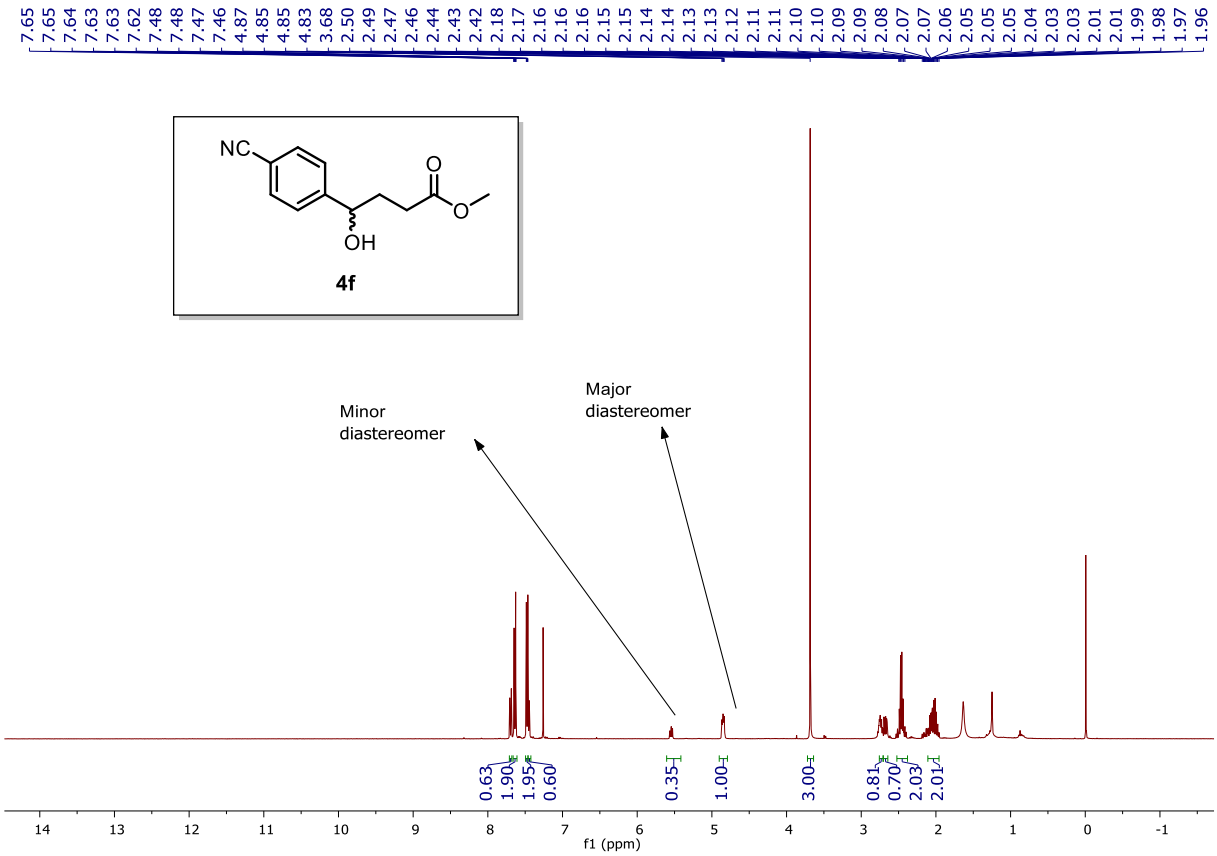


Figure AIV.25 ^{1}H NMR spectrum of **4f**, $CDCl_3$, 400 MHz

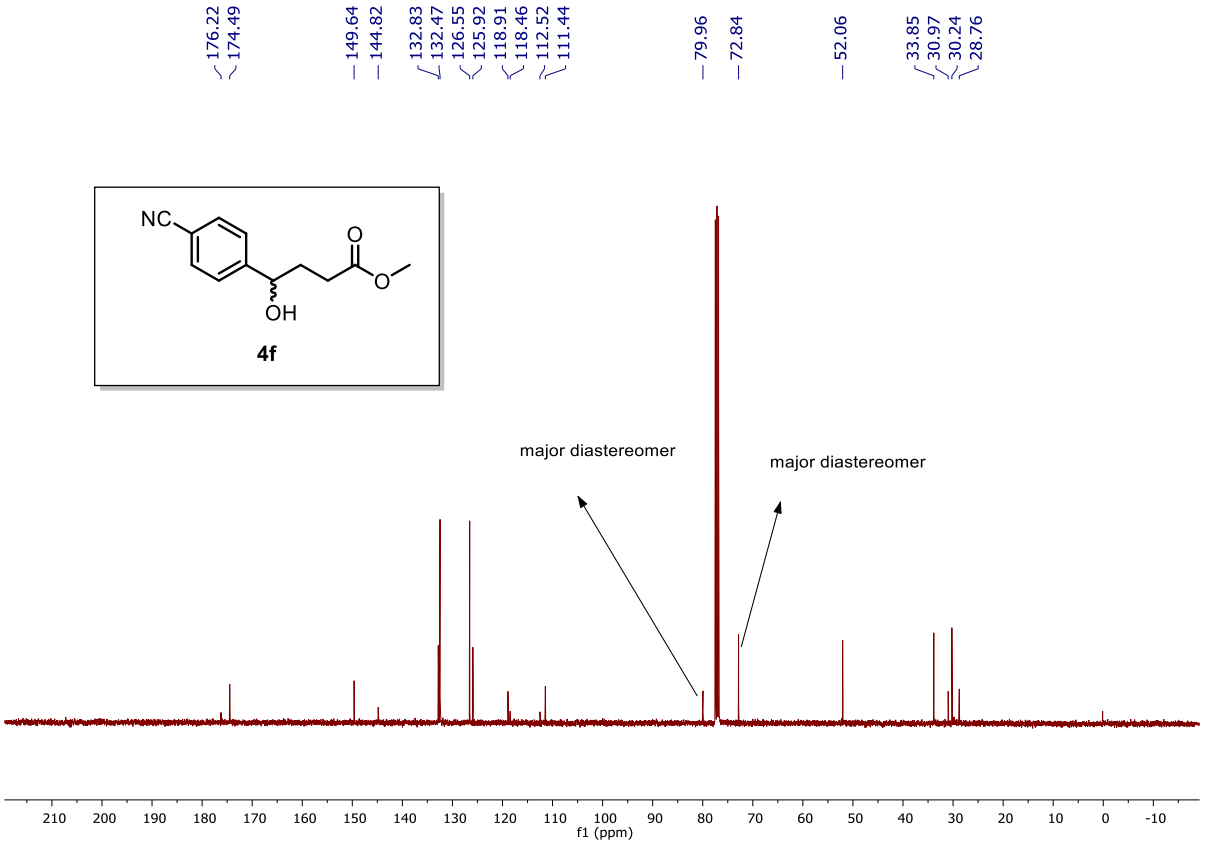


Figure AIV.26 ^{13}C {^{1}H} NMR spectrum of **4f**, $CDCl_3$, 100 MHz

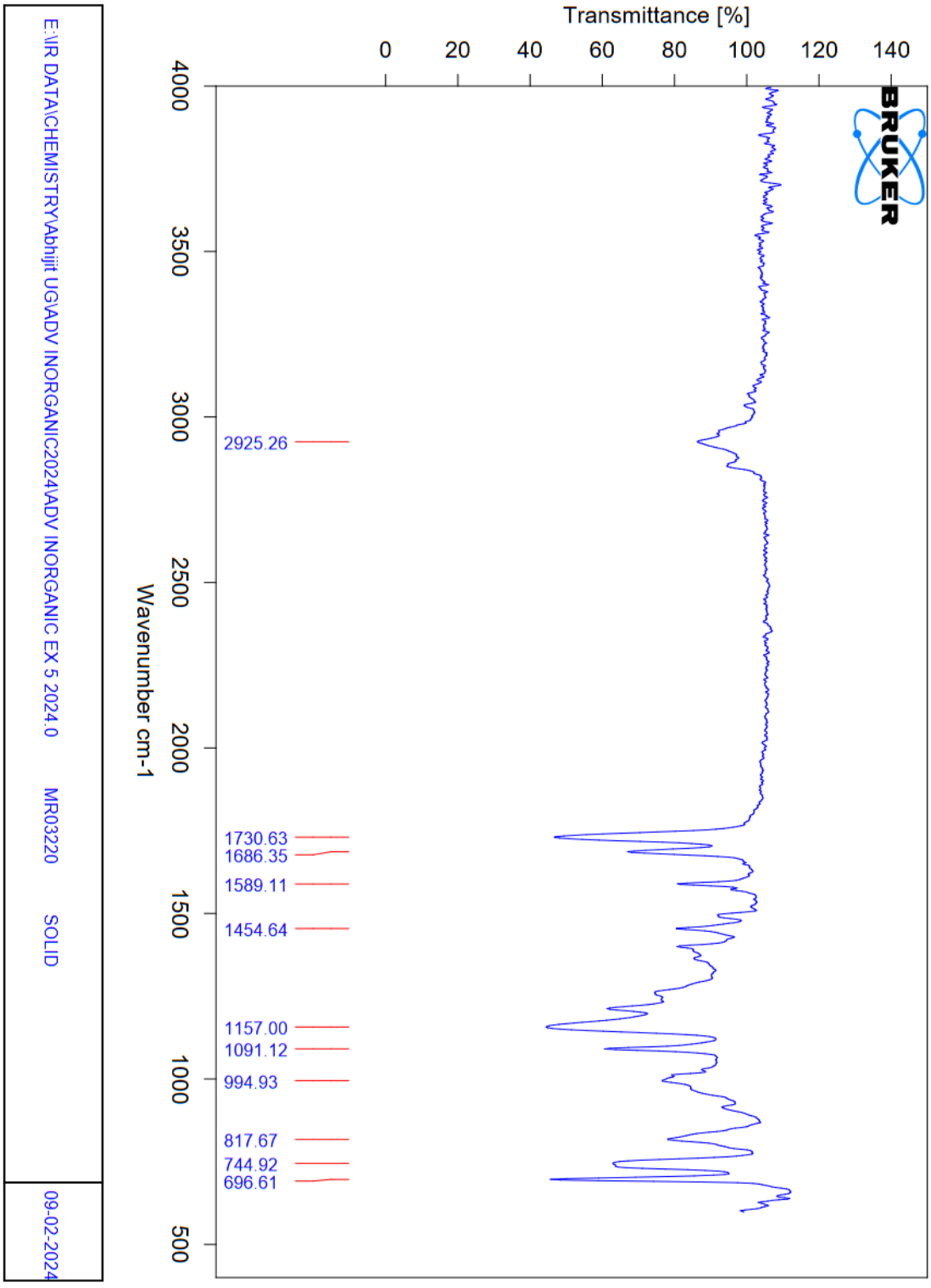


Figure AIV.27 IR spectrum of compound **3a**

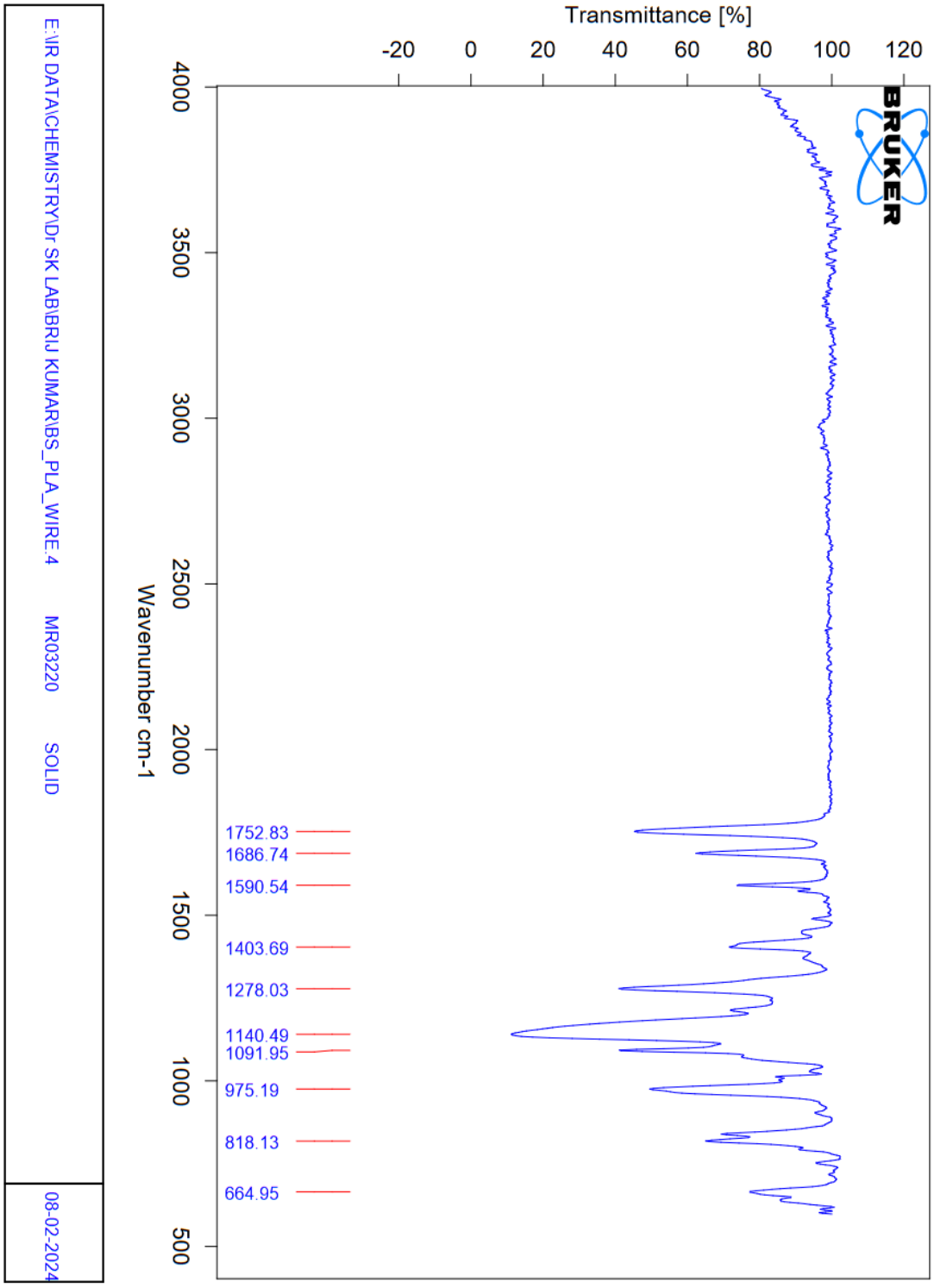


Figure AIV.28 IR spectrum of compound **3k**

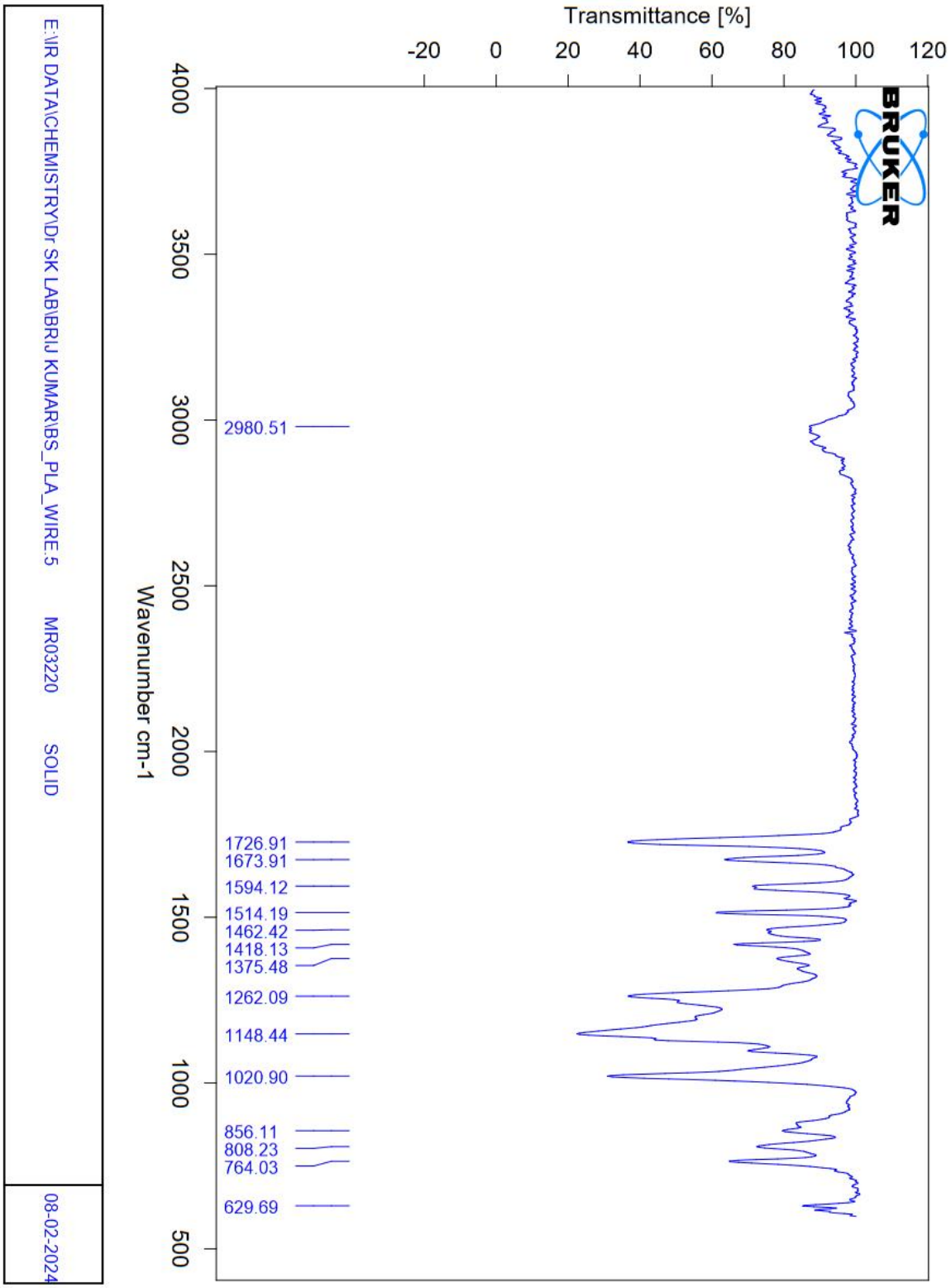


Figure AIV.29 IR spectrum of compound **3z**

4.15 . References:

1. (a) Otera, J.; Nishikido, J. Reaction of Alcohols with Carboxylic Acids and their Derivatives. In Esterification: Methods, Reactions, and Applications, 2nd ed.; Wiley-VCH: Weinheim, Germany, **2010**; pp 3− 157. (b) Siengalewicz, P.; Mulzer, J.; Rinner, U. Synthesis of Esters and Lactones. In Comprehensive Organic Synthesis II, 2nd ed.; Knochel, P., Ed.; Elsevier: Amsterdam, **2014**; Vol. 6, pp 355−410.

2. (a) Gao, W. C.; Liu, J.; Jiang, X. *Org. Chem. Front*. **2021**, *8*, 1275-1279; (b) Valente, E.; Testa, B.; Constantino, L. *Eur. J. Pharm. Sci*. **2021**, *162*, 105831; (c) Wang, Z.; Zhao, Z.; Li, Y.; Zhong, Y.; Zhang, Q.; Liu, Q.; Solan, G. A.; Ma, Y.; Sun, W. H. *Chem. Sci*. **2020**, *11*, 6766–6774.

3. (a) Whittaker, M.; Floyd, C. D.; Brown, P.; Gearing, A. J. H. *Chem. Rev*., **1999**, *99*, 2735–2776; (b) Cernijenko, A.; Risgaard, R.; Baran, P. S. *J. Am. Chem. Soc*., **2016**, *138*, 9425–9428; (c) Woodward, R. B.; Sondheimer, F.; Taub, D. *J. Am. Chem. Soc*., **1951**, *73*, 4057; (d) Xu, B.; Xun, W.; Wang, T.; Qiu, F. G. *Org. Lett*. **2017**, *19*, 4861−4863.

4. (a) Li, S. H.; Wang, J.; Niu, X. M.; Shen, Y. H.; Zhang, H. J.; Sun, H. D.; Li, M. L.; Tian, Q. E.; Lu, Y.; Cao, P.; Zheng, Q. T.; Maoecrystal, V. *Org. Lett*. **2004**, *6*, 4327−4330; (b) Valot, G.; Regens, C. S.; Malley, D. P. O'; Godineau, E.; Takikawa, H.; Fürstner, A. *Angew. Chem. Int. Ed*. **2013**, *52*, 9534−9538; (c) Mukaiyama, T.; Narasaka, K.; Furusato, M. *J. Am. Chem. Soc*. **1972**, *94*, 8641−8642.

5. (a) Eicher, T.; Hauptmann, S.; Speicher, A. The Chemistry of Heterocycles; Wiley-VCH: **2003**. (b) Rao, H. S. P.; Jothilingam, S. *J. Org. Chem*. **2003**, *68*, 5392−5394; (c) Li, C. S.; Tsai, Y. H.; Lee, W. C.; Kuo, W. J. *J. Org. Chem*. **2010**, *75*, 4004−4013; (d) Guo, F.; Konkol, L. C.; Thomson, R. J. *J. Am. Chem. Soc*. **2011**, *133*, 18−20.

6. (a) Che, C.; Qian, Z.; Wu, M.; Zhao, Y.; Zhu, G. *J. Org. Chem*. **2018**, *83*, 5665− 5673; (b) Kirsch, S. F. *Org. Biomol. Chem*. **2006**, *4*, 2076−2080. (c) Bellina, F.; Rossi, R. *Tetrahedron* **2006**, *62*, 7213−7256.

7. Organic Synthesis: The Disconnection Approach, ed. Warren, S.; Wyatt, P. Wiley **2008**, p. 199. (b) Sarkar, S.; Baneriee, A.; Yao, W.; Patterson, E. V.; Ngai, M.-Y. *ACS. Catal*., **2019**, *9*, 10358–10364; (c) Pati, B. V.; Ghosh, A.; Ravikumar, P. C. *Org. Lett*. **2020**, *22*, 2854−2860.

8. Peter Werle and Marcus Morawietz "Alcohols, Polyhydric" in Ullmann's Encyclopedia of Industrial Chemistry: **2002**, Wiley-VCH: Weinheim. DOI 10.1002/14356007.a01_305].

9. Shipchandler, Mohammed T., "Method of synthesis of pyrogallol ' US 4046817).

10. For a representative example, see: (a) Miura, K.; Tojino, M.; Fujisawa, N.; Hosomi, A.; Ryu, I. *Angew. Chem. Int. Ed*. **2004**, *43*, 2423; (b) Nemoto, H.; Kawamura, T.; Miyoshi, N. *J. Am.*

Chem. Soc. **2005**, *127*, 14546; (c) Myers, M. C.; Bharadwaj, A. R.; Milgram, B. C.; Scheidt, K. A. *J. Am. Chem. Soc*. **2005**, *127*, 14675; (d) Enders, D.; Han, J.; Henseler, A. *Chem. Commun*. **2008**, *34*, 3989; (e) DiRocco, D. A.; Oberg, K. M.; Dalton, D. M.; Rovis, T. *J. Am. Chem. Soc*. **2009**, *131*, 10872; (f) Biju, A. T.; Wurz, N. E.; Glorius, F. *J. Am. Chem. Soc*. **2010**, *132*, 5970.

11. (a) Ito, Y.; Konoike, T.; Saegusa, T. *J. Am. Chem. Soc*. **1975**, *97*, 649−651; (b) Ito, Y.; Konoike, T.; Harada, T.; Saegusa, T. *J. Am. Chem. Soc*. **1977**, *99*, 1487−1493; (c) Baran, P. S.; DeMartino, M. P. *Angew. Chem., Int. Ed*. **2006**, *45*, 7083−7086; (d) Clift, M. D.; Taylor, C. N.; Thomson, R. J. *Org. Lett*. **2007**, *9*, 4667−4669.

12. (a) Enders, D.; Han, J.; Henseler, A. *Chem. Commun*. **2008**, 3989−3991. (b) Liu, Q.; Perreault, S.; Rovis, T. *J. Am. Chem. Soc*. **2008**, *130*, 14066−14067. (c) Chen, X.-Y.; Enders, D. *Angew. Chem. Int. Ed*. **2019**, *58*, 6488−6490. (d) Yasuda, M.; Tsuji, S.; Shigeyoshi, Y.; Baba, A. *J. Am. Chem. Soc*. **2002**, *124*, 7440−7447. (e) Luo, J.; Jiang, Q.; Chen, H.; Tang, Q. *RSC Adv*. **2015**, *5*, 67901−67908. (f) Kaiser, D.; Teskey, C. J.; Adler, P.; Maulide, N. *J. Am. Chem. Soc*. **2017**, *139*, 16040−16043. (g) Jang, H.-Y.; Hong, J.-B.; MacMillan, D. W. C. *J. Am. Chem. Soc*. **2007**, *129*, 7004−7005; (h) Yasu, Y.; Koike, T.; Akita, M. *Chem. Commun*. **2012**, *48*, 5355−5357; (i) Kuang, Y.; Wang, K.; Shi, X.; Huang, X.; Meggers, E.; Wu, J. *Angew. Chem. Int. Ed*. **2019**, *58*, 16859−16863.

13. Danheiser DL (**2011**) Organic syntheses: the “Gold Standard” in experimental synthetic organic chemistry. Org Synth 88:1-3.

14. (a) Liu, L.; Feng, S.; Li, C. A. *RSC Adv*. **2015**, *5*, 56949−56953; (b) Takahashi, H.; Arai, T.; Yanagisawa, A. *Synlett* **2006**, 2833−2835. (c) Yanagisawa, A.; Takahashi, H.; Arai, T. *Tetrahedron* **2007**, *63*, 8581−8585. (d) Zhang, Y.; Yang, X.; Zhou, H.-C. *Dalton Trans*. **2018**, *47*, 11806−11811.

15. Seebach, D. *Angew. Chem. Int. Ed*., **1979**, *18*, 239.

16. (a) Maekawa, H.; Nakano, K.; Hirashima, T.; Nishiguchi, I. *Chem. Lett*. **1991**, 20, 1661; (b) Fussing, I.; Hammerich, O.; Hussain, A.; Nielsen, M. F.; Utley, J. H. P. *Acta Chem. Scand*. **1998**, *52*, 328.

17. (a) Plavac, F.; Heathcock, C. H. *Tetrahedron Lett*. **1979**, 2115. (b) Eschenmoser, A.; Winter, C. E. *Science* **1977**, *196*, 1410; (c) McMurry, J. E. *J. Org. Chem*. **1987**, *52*, 4885; (d) Iwata, C.; Takemoto, Y.; Doi, M.; Imanishi, T. *J. Org. Chem*. **1988**, *53*, 1623.

18. (a) Qu, J. P.; Deng, C.; Zhou, J.; Sun, X. L.; Tang, Y. *J. Org. Chem*. **2009**, *74*, 7684; (b) Zhang, D.; Cai, H.; Chen, Y.; Yin, L.; Zhong, J.; Zhang, Y.; Zhang, Q. F. *J. Org. Chem*. **2020**, *85*, 14262; (c) Fang, J.; Ren, J.; Wang, Z. *Tetrahedron Lett*. **2008**, *49*, 6659; (d) For a review, see Schneider, T. F.; Kaschel, J.; Werz, D. B. *Angew. Chem. Int. Ed*. **2014**, *53*, 5504e.

19. (a) Maeda, B.; Sakakibara, Y.; Murakami, K.; Itami, K. *Org. Lett*. **2021**, *23*, 5113−5117; (b) Zhang, Y.; Jiang, Y.; Wang, Y.; Sun, T.; Meng, Y.; Huang, Y.; Lv, X.; Gao, J.; Zhang, X.; Zhang, S.; Liu, S. *Org. Lett*. **2022**, *24*, 2679−2683; (c) Bhowmick, A.; Warghude, P. K.; Dharpure, P. D.; Bhat, R. G. *Org. Chem. Front*. **2021**, *8*, 4777−4784.

20. (a) Nicewicz, D. A.; Nguyen, T. M. *ACS Catal*. **2014**, *4*, 355−360; (b) Bhowmick, A.; Warghude, P. K.; Bhat, R. G. *Asian J. Org. Chem*. **2022**, *11*, e202200205. (c) Majek, M.; Jacobi von Wangelin, A. *Acc. Chem. Res*. **2016**, *49*, 2316−2327; (d) Fan, X. Z.; Rong, J. W.; Wu, H. L.; Zhou, Q.; Deng, H. P.; Tan, J. D.; Wu, J. *Angew. Chem. Int. Ed*. **2018**, *57*, 8514; (e) Singla, D.; Luxami, V.; Paul, K. *Org. Chem. Front*. **2023**, *10*, 237.

21. Giese, B.; Gonz´alez-G´omez, J. A.; Witzel, T. *Angew. Chem., Int. Ed*., **1984**, *23*, 69–70.

22. (a) Srikanth, G. S. C.; Castle, S. L. *Tetrahedron* **2005**, *61*, 10377–10441; (b) Streuff, J.; Gans¨auer, A. *Angew. Chem., Int. Ed*., **2015**, *54*, 14232–14242; (c) Lovinger, G. J.; Morken, J. P. *Eur. J. Org. Chem*., **2020**, 2362–2368.

23. (a) Mistry, S.; Kumar, R.; Lister, A.; Gaunt, M. J. *Chem. Sci*., **2022**, *13*, 13241−13247; (b) ElMarrouni, A.; Ritts, C. B.; Balsells, J. *Chem. Sci*., **2018**, *9*, 6639–6646; (c) Gualandi, A.; Matteucci, E.; Monti, F.; Baschieri, A.; Armaroli, N.; Sambri, L.; Cozzi, P. G. *Chem. Sci*., **2017**, *8*, 1613; (d) Lima, F.; Sharma, U. K.; Grunenberg, L.; Saha, D.; Johannsen, S.; Sedelmeier, J.; Van der Eycken, E. V.; Ley, S. V. *Angew. Chem., Int. Ed*., **2017**, *56*, 15136; (e) Ramirez, N. P.; Gonzalez-Gomez, J. C. *Eur. J. Org. Chem*., **2017**, 2154–2163; (f) Rostoll-Berenguer, J.; Blay, G.; Pedro, J. R.; Vila, C. *Org. Lett*., **2020**, *22*, 8012–8017; (g) Chinchole, A.; Henriquez, M. A.; Cortes-Arriagada, D.; Cabrera, A. R.; Reiser, O. *ACS Catal*., **2022**, *12*, 13549−13554; (h) Silvi, M.; Verrier, C.; Rey, Y. P.; Buzzetti, L.; Melchiorre, P. *Nat. Chem*., **2017**, *9*, 868; (i) Nawrat , C.; Jamison, C. R.; Slutskyy, Y.; MacMillan, D. W. C.; Overman, L. E. *J. Am. Chem. Soc*., **2015**, *137* , 11270.

24. (a) Siddiqui, A. A.; Islam, M.; Asif, M.; Asthana, C. *J. Ultra Fine Chem*. **2007**, *3*, 173; (b) Asif, M.; Singh, A. *Open Pharma. Sci. J*. **2016**, *3*, 203.

25. Asif, M. Mini Rev. *Med. Chem*. **2015**, *14*, 1093.

26. Chen, G.-H.; Ren, Z.; Yang, Y. *Chinese J. Antibiot*. **2009**, *34*, 479.

27. (a) Asif, M.; Singh, D.; Singh, A. *Global J. Pharmacol*. **2011**, *5*, 18; (b) Bialer, M. *Expert Opin. Investig. Drugs* **2006**, *15*, 637.

28. (a) Owings, F. F.; Fox, M.; Kowalski, C. J.; Baine, N. H. *J. Org. Chem*. **1991**, *56*, 1963. (b) Lim, Y. J.; Angela, M.; Buonora, P. T. *Tetrahedron Lett*. **2003**, *44*, 7799−7801.

29. (a) Westfall, M. V.; Wahler, G. M.; Solaro, R. J. *Bio- chemistry* **1993**, *32*, 10464; (b) Lues, I.; Beier, N.; Jonas, R.; Klockow, M.; Haeusler, G. J. *Card. Pharm*. **1993**, *21*, 883; (c) Akhtar,

W.; Shaquiquzzaman, M.; Akhter, M.; Verma, G.; Khan, M. F.; Alam, M. M. *Eur. J. Med. Chem*., **2016**, *123*, 256−281; (d) Zhou, Y.; Zhou, H.; Xu, J. *J. Org. Chem*. **2022**, *87*, 3677−3685.

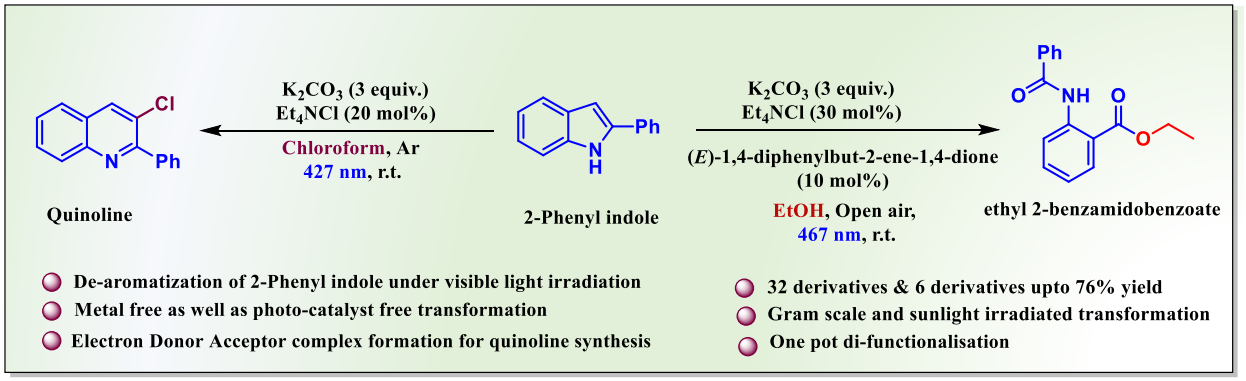
30. Mahesh, S. K.; Nanubolu, J. B.; Sudhakar, G. *J. Org. Chem*. **2019**, *84*,7815-7828.

CHAPTER 5

Photocatalyst-Free Visible Light-Driven Synthesis of Anthranilic Acid and Quinoline Derivatives from 2-Phenylindole

Abstract

In this chapter, we have developed methodologies that are adaptable to different solvents for the direct synthesis of anthranilic acid derivatives and quinoline derivatives from 2-phenylindole under visible light irradiation, without the need for any photocatalyst. The reaction of 2-phenylindoles with alcohols results in the formation of corresponding anthranilic acid derivatives, showcasing a broad substrate scope. Similarly, when 2-phenylindole is subjected to chloroform under visible light irradiation, the corresponding quinoline derivatives are obtained in moderate to good yields.



Bhowmick, A.; Pathak, S. S.; Kahde, V. V.; Bhat, R. G. *Manuscript under preparation.*

Photocatalyst-Free Visible Light-Driven Synthesis of Anthranilic Acid and Quinoline Derivatives from 2-Phenylindole

5.1. Introduction:

Anthranilic acid and its analogues hold a significant position as core elements within various bioactive compounds and approved drugs. Furthermore, their derivatives exhibit a broad spectrum of biological activities, playing a crucial role in managing several diseases and regulating pathways that contribute to disease onset [1]. From an industrial standpoint, anthranilic acid serves as a crucial intermediate in the manufacturing of azo dyes and saccharin [2]. Significantly, Methyl anthranilate (MANT) is extensively utilized for its grape-like aroma, enhancing flavours in foods and drugs [3a]. Its pleasant scent makes it valuable in perfumes and cosmetics. Additionally, MANT serves as a bird repellent, oxidation inhibitor, and is integral in producing various chemicals, dyes, and pharmaceuticals [3b]. Benzoxazinones stand as vital fused heterocycles within a multitude of biological compounds and pharmaceutical drugs [4].

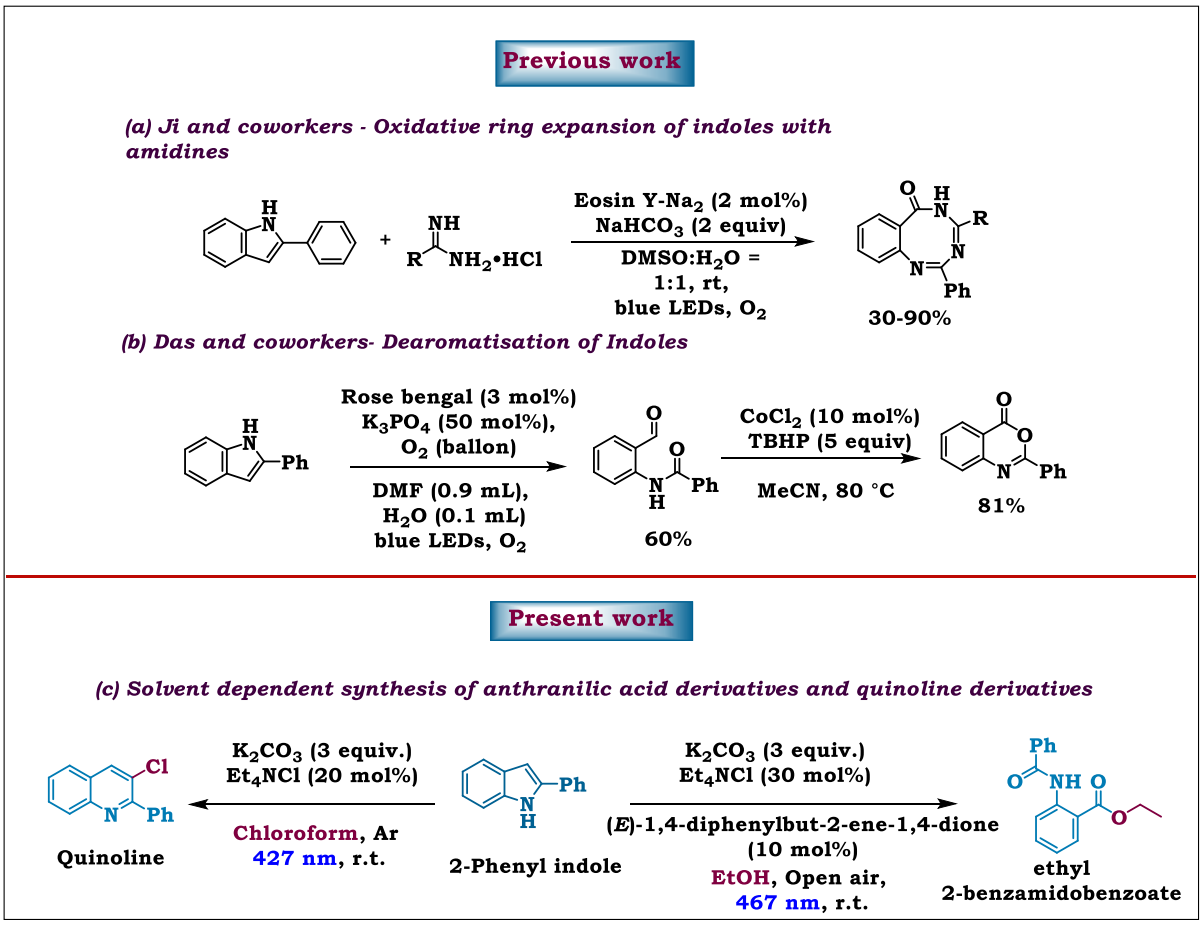
The quinoline structural motif is present in a variety of naturally-occurring bioactive compounds, such as quinine, chloroquine, bulaquine, primaquine, and tafenoquine, all of which are derived from Cinchona alkaloids [5]. Moreover, modified quinoline structures represent crucial pharmacophoric elements, possessing undeniable therapeutic potential due to their well-documented array of biological and pharmacological effects. These effects encompass anticancer [6], antimicrobial [7], anti-inflammatory [8], antioxidant [9], antitubercular [10], antimalarial [11], among others.

Dearomatizing heteroaromatic compounds to produce important products having represents a robust approach for synthesizing pharmaceuticals and bioactive compounds [12]. Indeed, the majority of natural products comprise heteroaromatic nuclei like indole, pyrrole, and similar structures [13]. Significantly, the de-aromatization of indole nuclei to produce difunctional enriched products is of considerable significance, particularly when conducted under mild reaction conditions. Given their significant aromatic resonance energy, precise modulation of catalysts and reaction conditions becomes exceptionally crucial [14]. Drawing from this concept, the de-aromatization of indole derivatives has been successfully accomplished through various methods including borylation, hydrosilylation, trifluoromethylation, arylation, allylation, and more [15]. However, the methods outlined

above are subject to overarching limitations, including the generation of significant metal waste, the utilization of stoichiometric oxidants, or the necessity for elevated temperatures.

In light of the worldwide energy crisis and environmental preservation challenges, there is a compelling demand for ecologically sustainable synthetic methods. Visible light, acknowledged as an economical and environmentally-friendly energy resource, is commonly seen as an excellent catalyst for driving organic transformations. In recent years, there has been a substantial rise in the utilization of visible-light-mediated photochemistry for synthesis. This surge is attributed to significant advancements in photoredox catalysis, energy transfer, and atom transfer processes [16]. In recent years, there has been notable progress in employing visible light to trigger de-aromatization of indole within organic synthesis. In the year 2019, Ji and co-workers reported oxidative ring expansion of indole with amidines in aqueous phase under visible light irradiation **Scheme 1a** [17a].

Scheme 1: De-aromatization of 2-phenyl indole under visible light irradiation

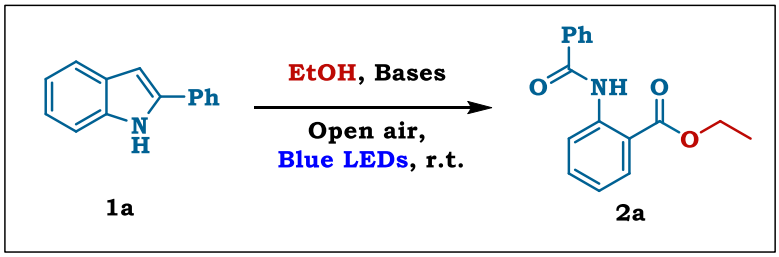


In 2020, Das and co-workers developed visible light induced de-aromatization of indole to their corresponding isatin derivatives **Scheme 1b** [17b]. Yet, the viability of these reactions predominantly relies on the presence of a photocatalyst [17-18]. However, the methods reported in the literature relies on the photocatalyst for the smooth transformation. Looking at the literature, we planned to explore and develop the photocatalyst free strategy for the dearomatization. In a pioneering effort, we have developed a photocatalyst-free method for the dearomatization of 2-phenylindole. This method has been achieved by oxidizing the 2,3-double bonds (also referred to as Wiktop oxidation) followed by nucleophilic reopening, enabling the synthesis of anthranilic acid derivatives in a one-pot process under visible light irradiation in open air. For the first time, we have established a protocol for synthesizing quinoline derivatives from 2-phenylindole using chloroform as a solvent under visible light irradiation in inert conditions.

5.2. Results and Discussion:

We commenced with the model reaction by employing 2-Phenylindole **1a** as the substrate in presence of DBU as a base and ethanol as a solvent as well nucleophile under open-air using Blue LEDs (467 nm) at room temperature. Gratifyingly, we successfully obtained the dearomatized oxidative ring-opened product, ethyl 2-benzamidobenzoate **2a** in modest yield (35%, **Table 1, Entry 1**). Encouraged by the initial results, we further carried out the optimization by testing various bases (**Table 1**, **Entries 1-12**). Among all the K_2CO_3 emerged as the optimized base for the transformation (**Table 1, Entry 6**).

Table 1: Screening of bases and light wavelengths[a]

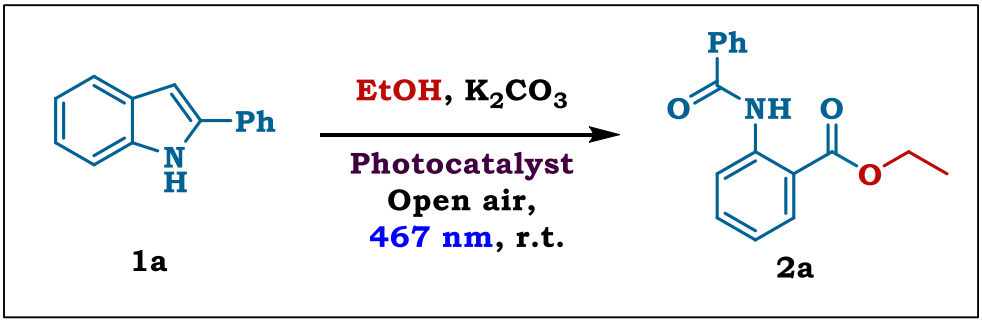


Entry	Bases (1 equiv.)	Light (nm)	Yield of 2a (%)[b]
1	DBU	467	35
2	Et_3N	467	15
3	DIPEA	467	12

4	DMAP	467	N. R
5	DABCO	467	N.R
6	K_2CO_3	467	42
7	Cs_2CO_3	467	23
8	Na_2CO_3	467	35
9	$K_3PO_4.H_2O$	467	34
10	$HK_2PO_4.H_20$	467	33
11	$H_2KPO_4.H_20$	467	28
12	N-Methylmorpholine	467	N. R
13	K_2CO_3 (0.5 equiv)	467	28
14	K_2CO_3 (2 equiv.)	467	46
15	K_2CO_3 (3 equiv.)	467	58
16	K_2CO_3 (4 equiv.)	467	46
17	K_2CO_3 (3 equiv.)	370	34
18	K_2CO_3 (3 equiv.)	427	43
19	K_2CO_3 (3 equiv.)	440	42
20	K_2CO_3 (3 equiv.)	456	45
21	K_2CO_3 (3 equiv.)	525	N. R.

***Reaction conditions**: Unless otherwise noted. [a]all the reactions were carried out using **1a** (0.3 mmol) in ethanol (3 mL) under open air for 24 h at room temperature, [b]Yield is calculated by ^1H NMR spectroscopy using 1,3,5-trimethoxy benzene as internal standard.*

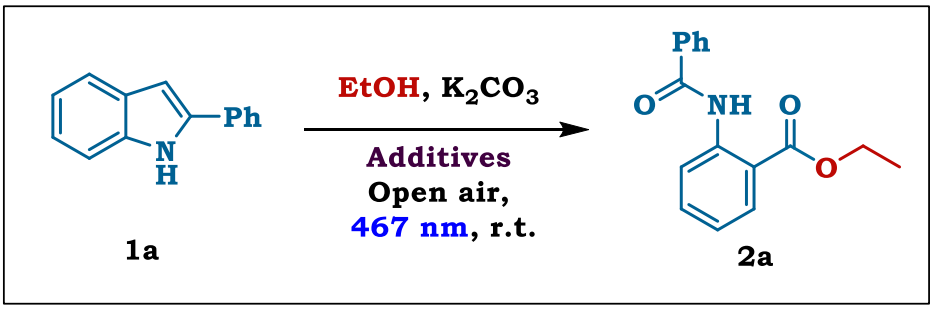
Table 2: Screening of photocatalysts[a]

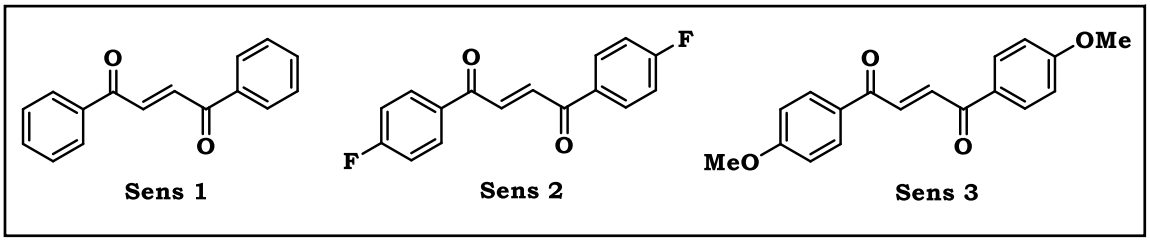


Entry	Bases (3 equiv.)	Photocatalyst (2 mol%)	Yield of 2a[b]
1	K_2CO_3	Rose Bengal	55
2	K_2CO_3	Eosin Y	46
3	K_2CO_3	Na_2Eosin Y	48
4	K_2CO_3	$Ru(BPY)_3Cl_2.6H_2O$	40
5	K_2CO_3	Riboflavin	45
6	K_2CO_3	Rhodamine 6G	32

***Reaction conditions**: Unless otherwise noted. [a]all the reactions were carried out using **1a** (0.3 mmol) in ethanol (3 mL) under open air for 24 hrs at room temperature using 467 nm blue LED, [b]Yield is calculated by ^{1}H NMR spectroscopy using 1,3,5-trimethoxy benzene.*

Table 3: Screening of additives[a]





Entry	Base (3 equiv.)	Light (nm)	Additives 1 (10 mol%)	Additives 2 (10 mol%)	Yield of 2a (%)[b]
1	K_2CO_3	467	$(NH_4)_2S_2O_8$	-	52
2	K_2CO_3	467	$Na_2S_2O_8$	-	55
3	K_2CO_3	467	$K_2S_2O_8$	-	50

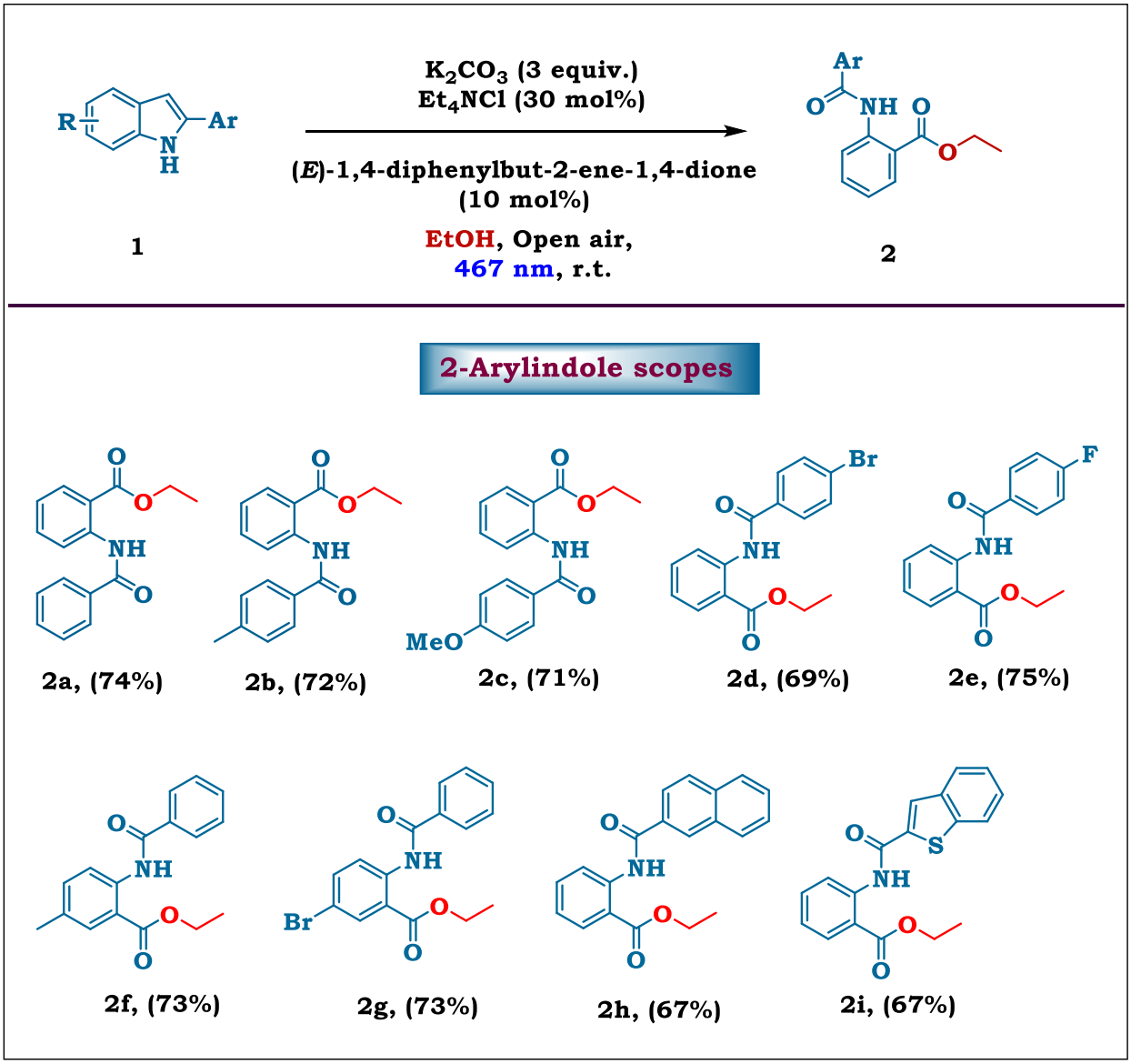
4	K_2CO_3	467	KBr	-	59
5	K_2CO_3	467	nBu_4NCl	-	60
6	K_2CO_3	467	nEt_4NCl	-	66
7	K_2CO_3	467	nBu_4NBr	-	64
8	K_2CO_3	467	nEt_4NCl	Sens 1	72
9	K_2CO_3	467	nEt_4NCl	Sens 2	69
10	K_2CO_3	467	nEt_4NCl	Sens 3	67
11	K_2CO_3	467	nEt_4NCl (20)	Sens 1	76
12	K_2CO_3	467	nEt_4NCl (30)	Sens 1	80 (74%)
13	K_2CO_3	467	nEt_4NCl (40)	Sens 1	73
14	-	467	-	-	N.R
15	K_2CO_3	-	-	-	N.R

***Reaction conditions**: Unless otherwise noted. [a]all the reactions were carried out using **1a** (0.3 mmol) in ethanol (3 mL) under open air for 24 hrs at room temperature using 467nm blue LED, [b]Yield is calculated by ^1H NMR spectroscopy using 1,3,5-trimethoxy benzene.*

Further, we systematically varied the quantity of K_2CO_3 to determine the optimal amount required for the smooth transformation to obtain the desired product in higher yields (**Table 1, Entries 13-16**). Later, we explored different wavelengths of Blue LEDs for the effective transformation and among all 467 nm proved to be the efficient (**Table 1, Entries 17-21**). Our experimentation with various photocatalysts yielded consistent yields, indicating that the desired transformation does not rely on a photocatalyst (**Table 2, Entries 1-6**). Given that the transformation involves oxidative ring opening under open air conditions, we further screened different oxidants and oxygen as an oxidant. However, we did not see any significant changes in the yield of the desired product **2a** (**Table 3, Entries 1-3**). Continuing our investigation, we introduced various additives to enhance the yield further (**Table 3, Entries 4-13**). Notably, the combination of nEt_4NCl and Sens1 [(*E*)-1,4-diphenylbut-2-ene-1,4-dione] proved to be the best to afford the desired product **2a** in highest yield (**Table 3, Entry 12**). Later, we carried out the reaction without Blue LEDs and base. In both the cases, the desired product **2a** did not form thus clearly indicating that both visible light (blue LEDs) and base are essential for this protocol

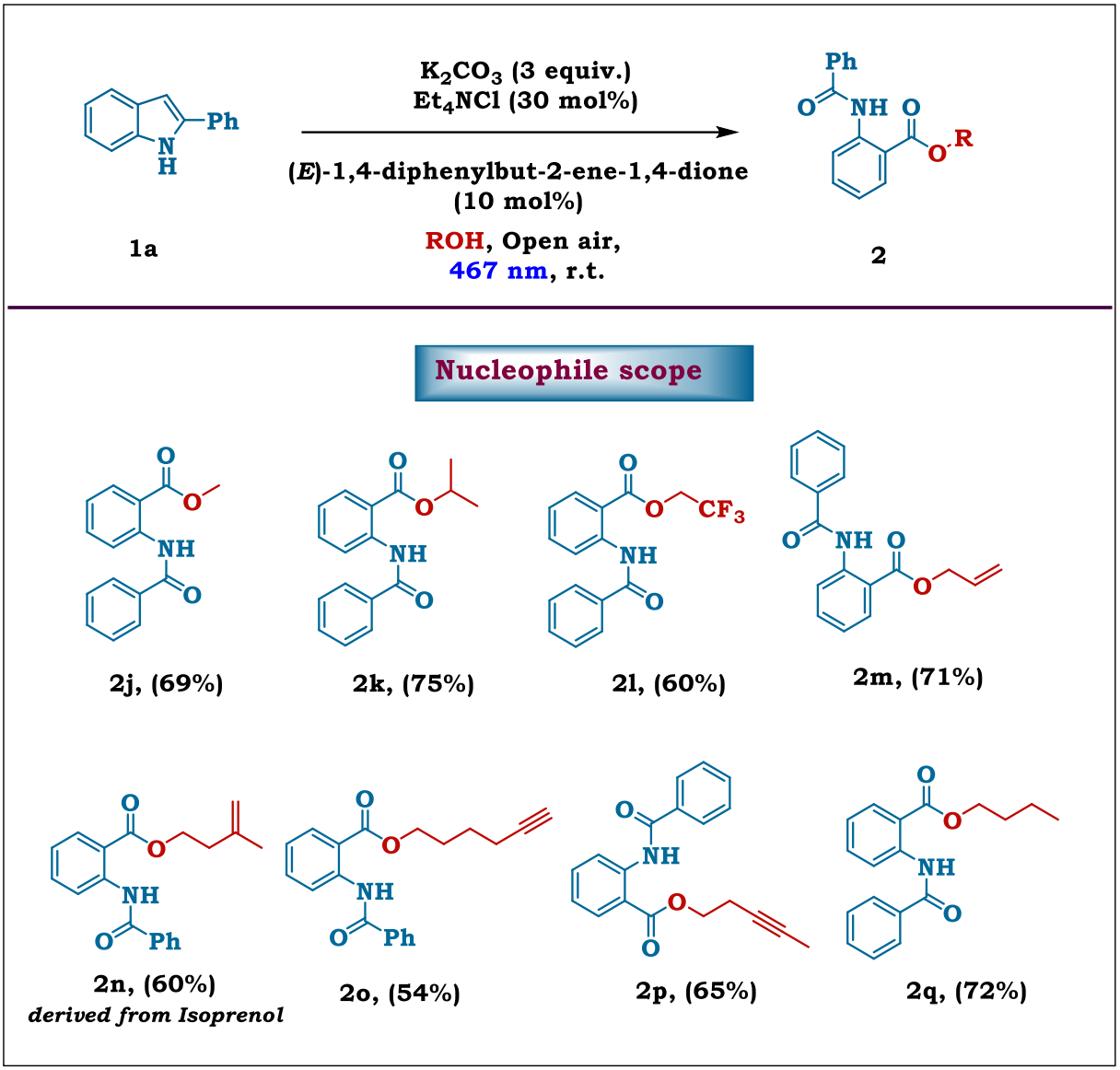
(**Table 3, Entry 14-15**). After a thorough and systematic optimization process, it was determined that employing **1a** along with 3 equivalents of K_2CO_3, 30 mol% of nEt_4NCl and 10 mol% of (*E*)-1,4-diphenylbut-2-ene-1,4-dione in ethanol under open-air conditions and irradiation with 467 nm light proved to be the optimal reaction conditions for achieving the highest yield of the desired product **2a**.

Scheme 2: Substrate scope for anthranilic acid derivatives



Reaction conditions: *Unless otherwise noted. [a]all the reactions were carried out using 0.3 mmol **1**, 0.9 mmol K_2CO_3, 30 mol% nEt_4NCl, 10 mol% (E)-1,4-diphenylbut-2-ene-1,4-dione, in ethanol (3 mL) using 467nm light source at room temperature. Isolated Yield after purification using column chromatography.*

Scheme 2: Substrate scope for anthranilic acid derivatives

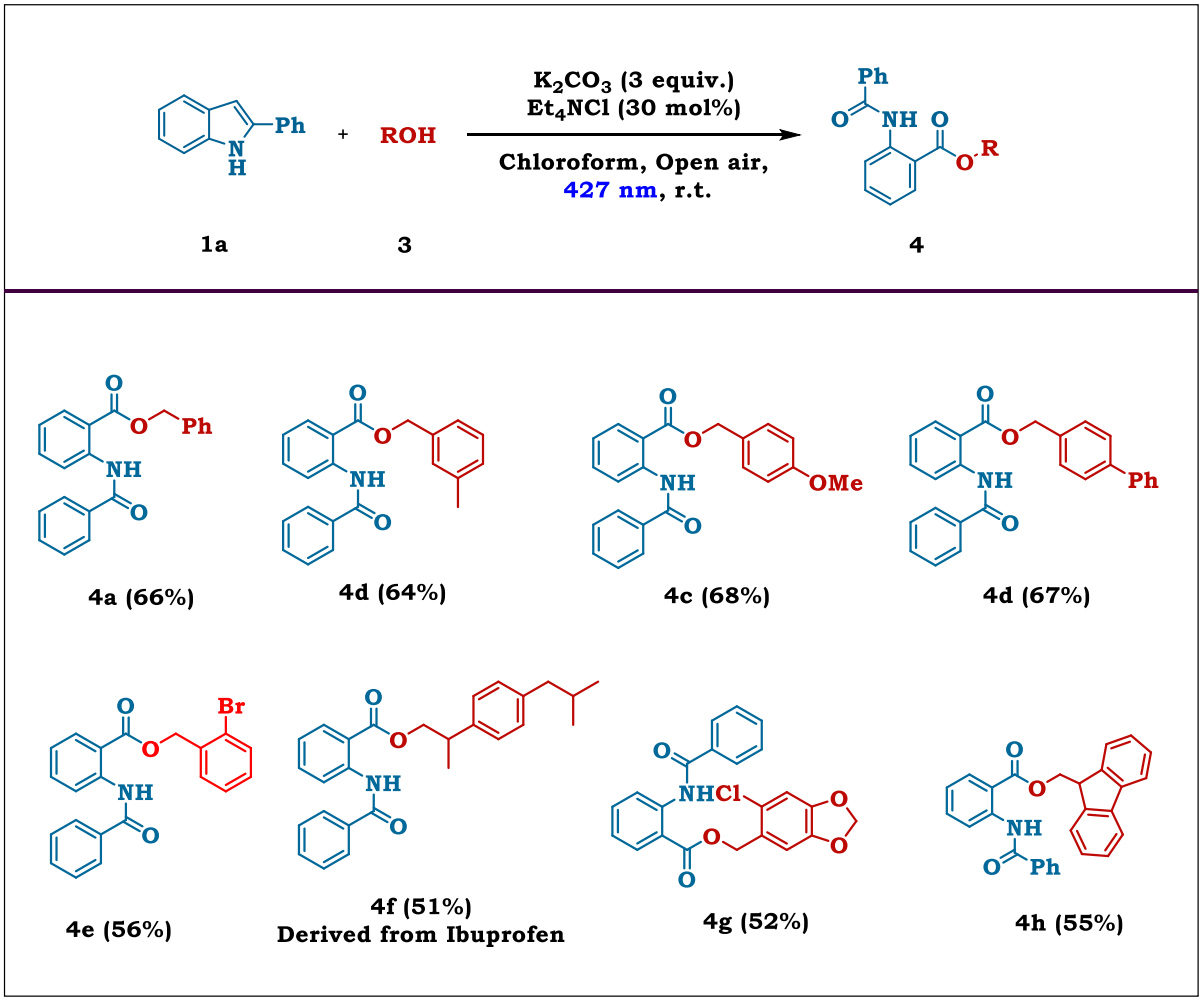


Reaction conditions: *Unless otherwise noted. [a]all the reactions were carried out using* ***1a*** *(0.3 mmol), K_2CO_3 (0.9 mmol), 30 mol% nEt_4NCl, 10 mol% (E)-1,4-diphenylbut-2-ene-1,4-dione, in different alcohols (3 mL) as a nucleophilic source using 467nm light source at room temperature. Isolated yield is calculated by column chromatography.*

Having obtained the optimized reaction condition, we further investigated the substrates that are suitable for this protocol. We conducted the reaction using diverse 2-arylindole derivatives **1** featuring electron-donating groups, halogens, fused aromatic ring, and heterocycle in ethanol to furnish the corresponding desired products in (**2a-2i**) in moderate to good yields (up to 75%, **Scheme 2**). Expanding our inquiry while keeping 2-phenylindole **1a** consistent, we utilized different alcohols as solvent as well as nucleophile to obtain the corresponding anthranilic acid (**2j-2q**) in moderate to good yields (up to 75%, **Scheme 2**).

In this method, alcohols play dual roles as solvents as well as nucleophiles and adaptations are needed for alcohols with elevated boiling points or in solid state form. For that reason, we have separately optimised the reaction condition *(see Experimental section, Table 5.5.7.1, Page 238-239).* Implementing the optimized reaction conditions, we extended the protocol with **1a** with various benzyl alcohol derivatives to obtain the desired products (**4a-4e**) in moderate yields (up to 68%, **Scheme 3**). Employing the optimized reaction conditions, alcohols with elevated boiling points and/or solid-state form reacted with **1a** smoothly to furnish the desired products (**4f-4h)** in moderate to good yields (up to 55%, **Scheme 3,**).

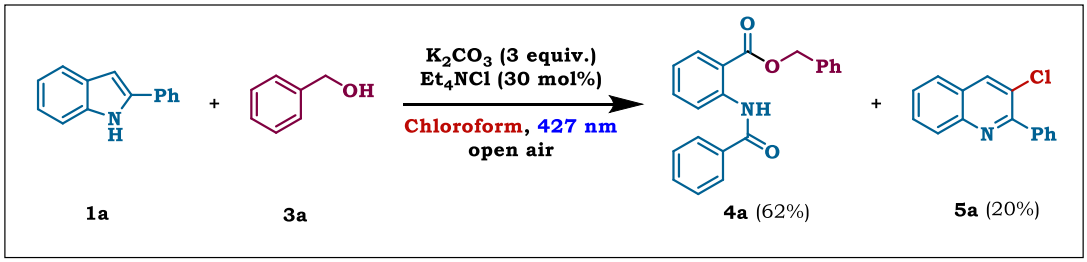
Scheme 3: Substrate scope for anthranilic acid derivatives using non-volatile alcohol as nucleophile



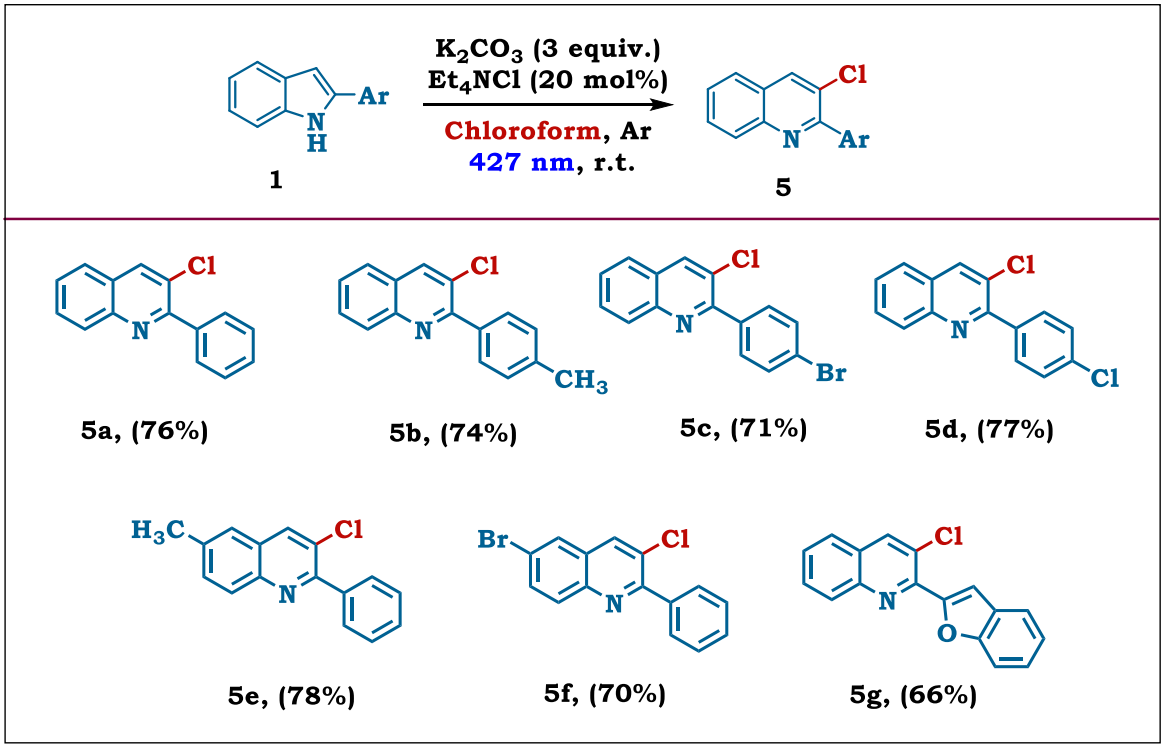
Reaction conditions: *Unless otherwise noted. [a]all the reactions were carried out using 0.3 mmol* ***1a****, 3 mmol alcohol* ***3****, 0.9 mmol K_2CO_3, 30 mol% nEt_4NCl, 10 mol% (E)-1,4-diphenylbut-2-ene-1,4-dione, using 427nm light source at room temperature. Isolated Yield after purification using column chromatography.*

During the solvent optimization process with chloroform, we observed that an unintended side product **5a** was being generated alongside our desired target product **4a** (**Scheme 4**).

Scheme 4: Observation of the initial synthesis of 3-chloro-2-phenylquinoline **5a**



Scheme 5: Substrates scope for the quinoline derivatives



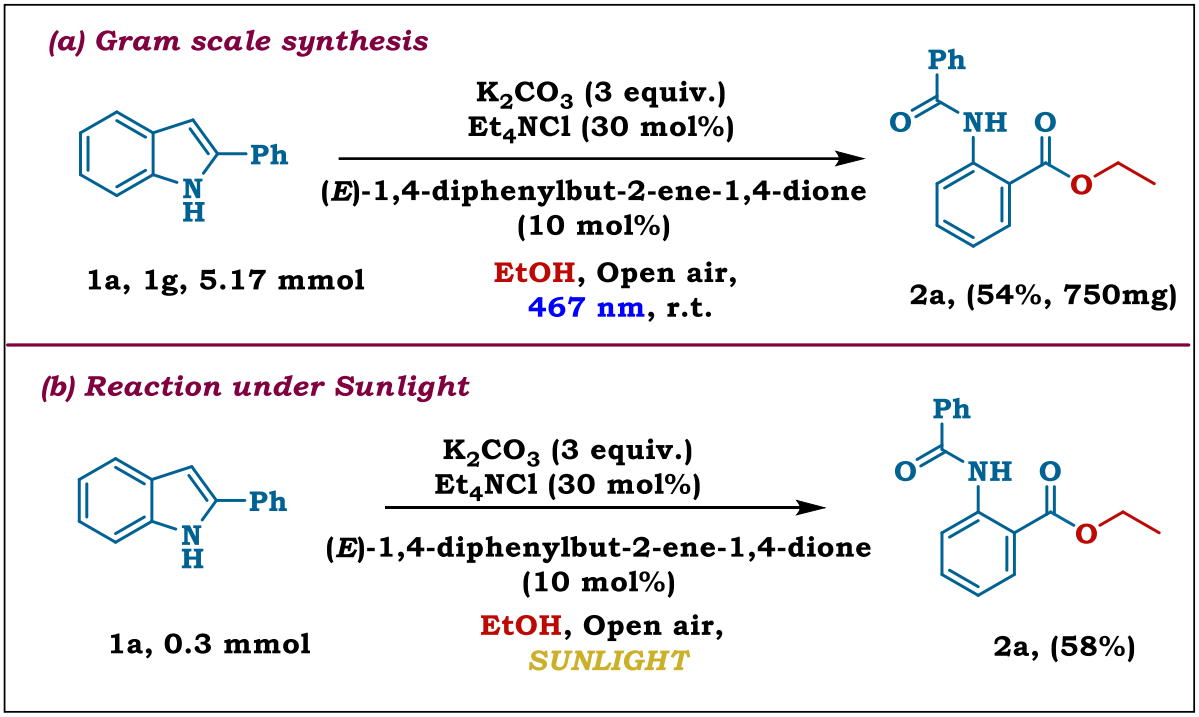
Reaction conditions: *Unless otherwise noted. [a]all the reactions were carried out using 0.3 mmol **1**, 0.9 mmol K_2CO_3, 20 mol% nEt_4NCl, in chloroform, using 427nm light source at room temperature. Isolated Yield after purification using column chromatography.*

Subsequent characterization revealed that the side product identified was 3-chloro-2-phenylquinoline **5a**. Additional comprehensive optimizations have been undertaken to develop the optimum reaction conditions to ensure the maximum yield of 3-chloro-2-phenylquinoline, **5a** derived from 2-phenyl indole **1a** in chloroform, particularly under blue light irradiation (*See*

Experimental Section, Table 5.5.7.2, Page 240-242). After obtaining the optimized protocol in chloroform, we proceeded to examine the substrate scope to assess its tolerance towards various functional groups and its applicability in diverse scenarios. In this regard, in order to generalize the practicality of the protocol, we have synthesised few quinoline derivatives (**5a-5g)** in moderate to good yields (up to 78%, **Scheme 5**).

For the practicability, we further carried out the synthesis of anthranilic acid derivative **2a** starting from **1a** on a gram scale using the optimized conditions (**Scheme 6a**). Later, as an application, we carried out the reactions under sunlight to obtain the desired product **2a** satisfactory yield (**Scheme 6b**).

Scheme 6: Gram scale synthesis and reaction under sunlight



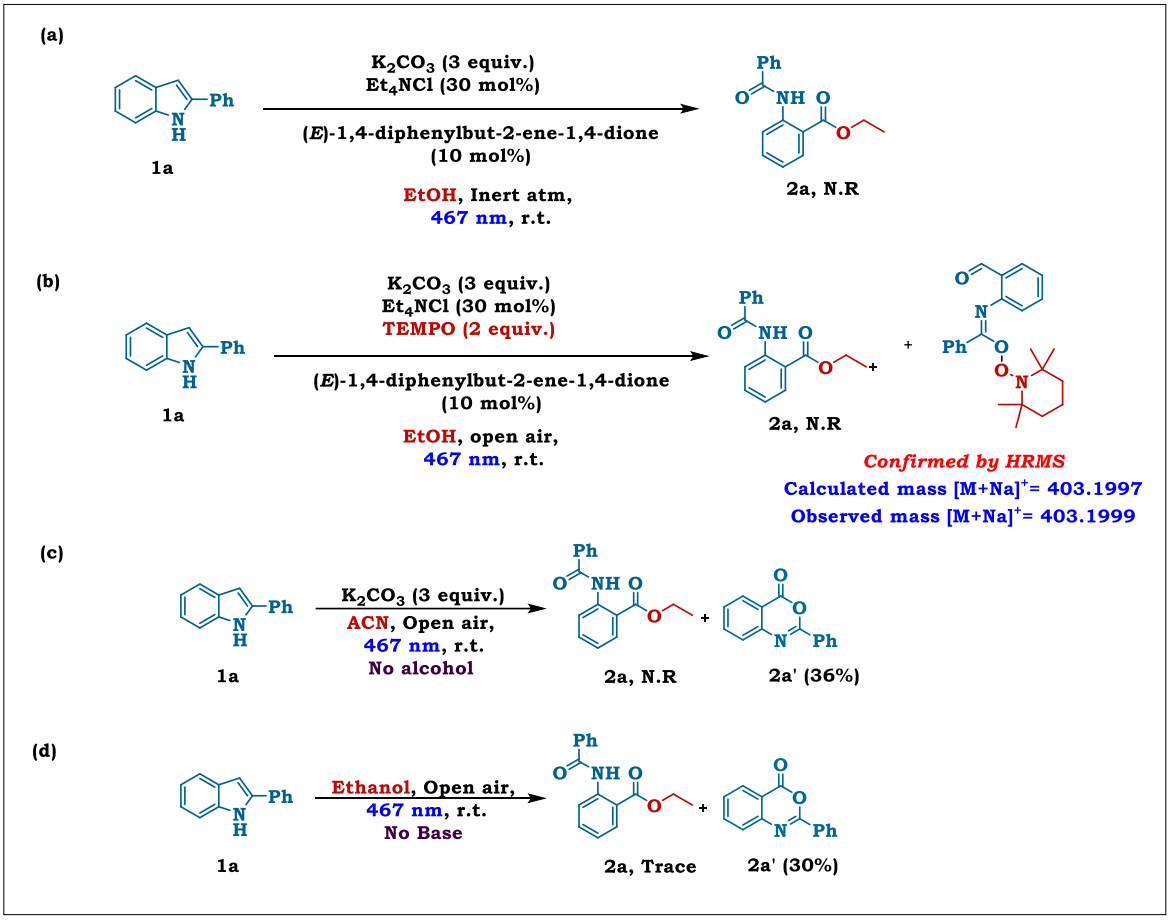
5.3. Control experiments

We have performed a series of controlled experiments in order to prove the mechanism. We conducted control experiments for the two separate protocols in two solvent-dependent protocols in order to have mechanistic insights. As the alcohol-based protocol, worked in presence of oxygen (under open air), we became curious to know the exact role of oxygen if any. The reaction of **1a** under inert condition while maintaining other standard optimized reaction conditions, did not afford the desired product **2a**. This result indicated that the oxygen is essential for this transformation (**Scheme 7a)**. Further, the radical trapping experiment using

the radical quencher - TEMPO was performed and we did not observe any desired product **2a** formation. Also, the TEMPO-trapped radical intermediate has been characterized by the High-Resolution Mass Spectrometry (HRMS) (**Scheme 7b)**. These results clearly support that the radical intermediate is being generated during the course of the reaction. In absence of alcohol as well as base, we did not obtain the desired product **2a** thus proving that both the alocol and base are essential for the transformation (**Scheme 7c-7d)**. Further we have proved the generation of H_2O_2 as a green by product using peroxide detection strips (**Scheme 9)**.

Following that step, in order to identify the active form of oxygen responsible for the reaction, we carried out the reaction of **1a** in presence of singlet oxygen trapping agents such as DABCO and NaN_3 under the optimized reaction conditions **(see, Scheme 8a-8b)**. Interestingly, we did not observe any desired product **2a** indicating that the singlet oxygen is the active form and is driving the reaction.

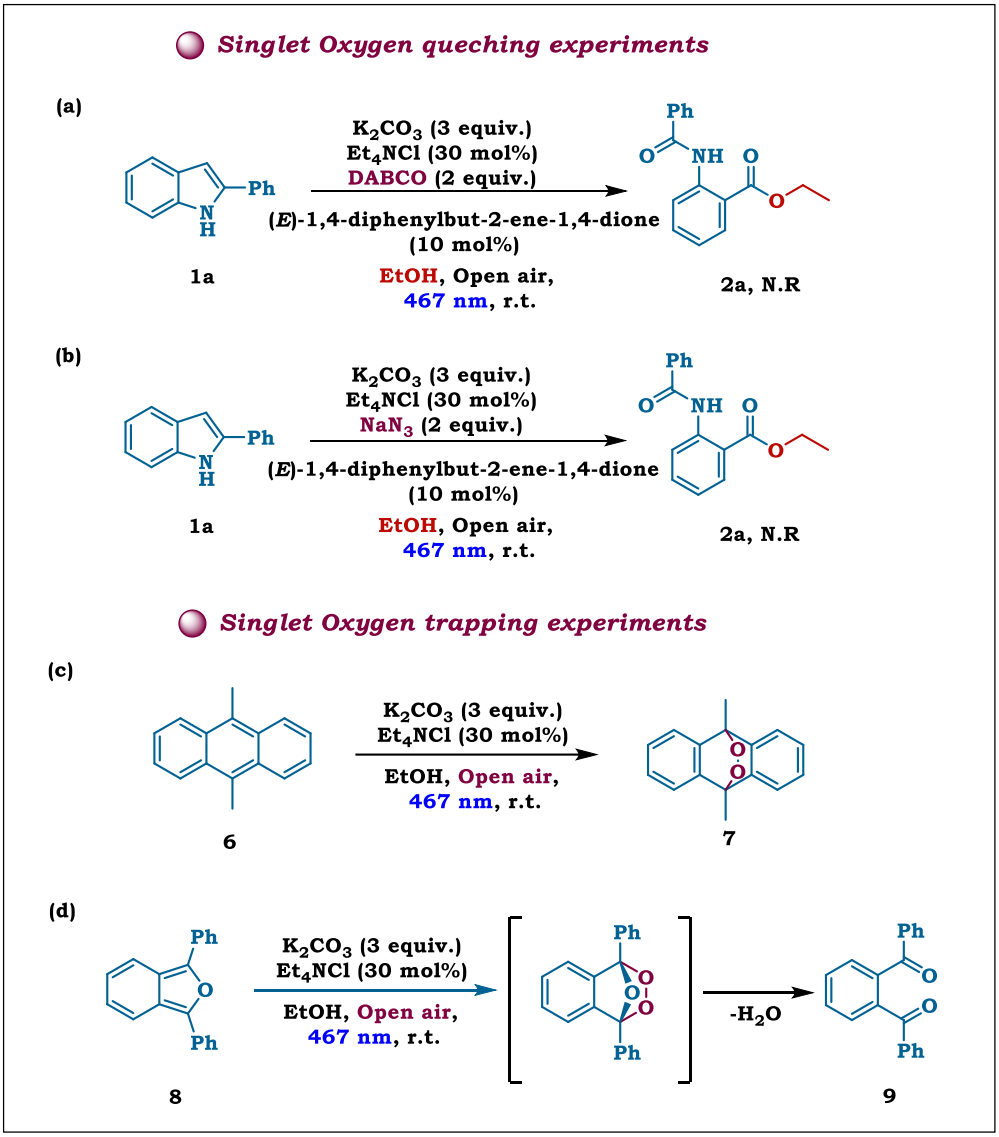
Scheme 7: Control experiments



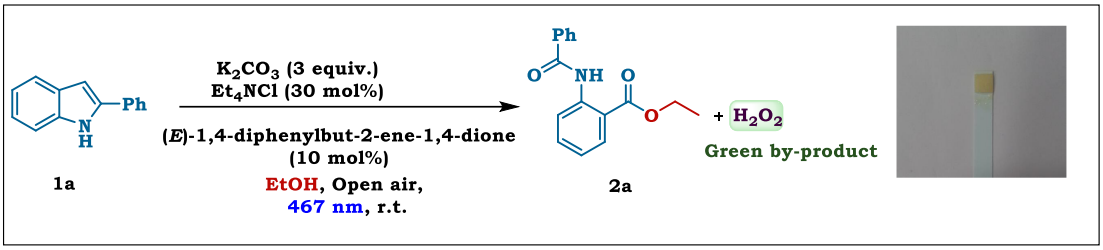
Further, to validate our proposal we have trapped singlet oxygen using singlet oxygen trapping agents during the course of the reaction. In these experiments, we maintained the optimized conditions consistently while substituting **1a** with 9,10-dimethylanthracene **6** and 1,3-diphenylisobenzofuran **8**, a well-known singlet oxygen trapper. Later, we carried out the

reaction of **6** and **8** under light (467 nm, Blue LED) while maintaining the other optimized reaction conditions. Pleasingly, we successfully obtained the corresponding singlet oxygen trapped products **7** and **9** respectively (**Scheme 8c-8d**). This result very clearly supports the formation of active singlet oxygen during the course of the reaction. In order to validate further we have carried out the reaction of 2,2,6,6-Tetramethylpiperidine (TEMP) instead of **1a** while maintaining the other optimized reaction conditions and performed the EPR experiment. We obtained the EPR signal corresponding to the TEMPO [19] (**Figure 1).** This result clearly supported the formation of radical during the course of the reaction.

Scheme 8: Determining the role and the active role of oxygen



Scheme 9: Detection of H_2O_2



Given that the reaction follows a photo-catalyst-free, visible light-induced protocol, we initially conducted an extensive UV-Vis experiment on the reaction mixtures under various conditions. We carried out this study to rule out any possibility of forming Electron Donor-Acceptor (EDA) complexes during the course of the reaction (**Figure 2**).

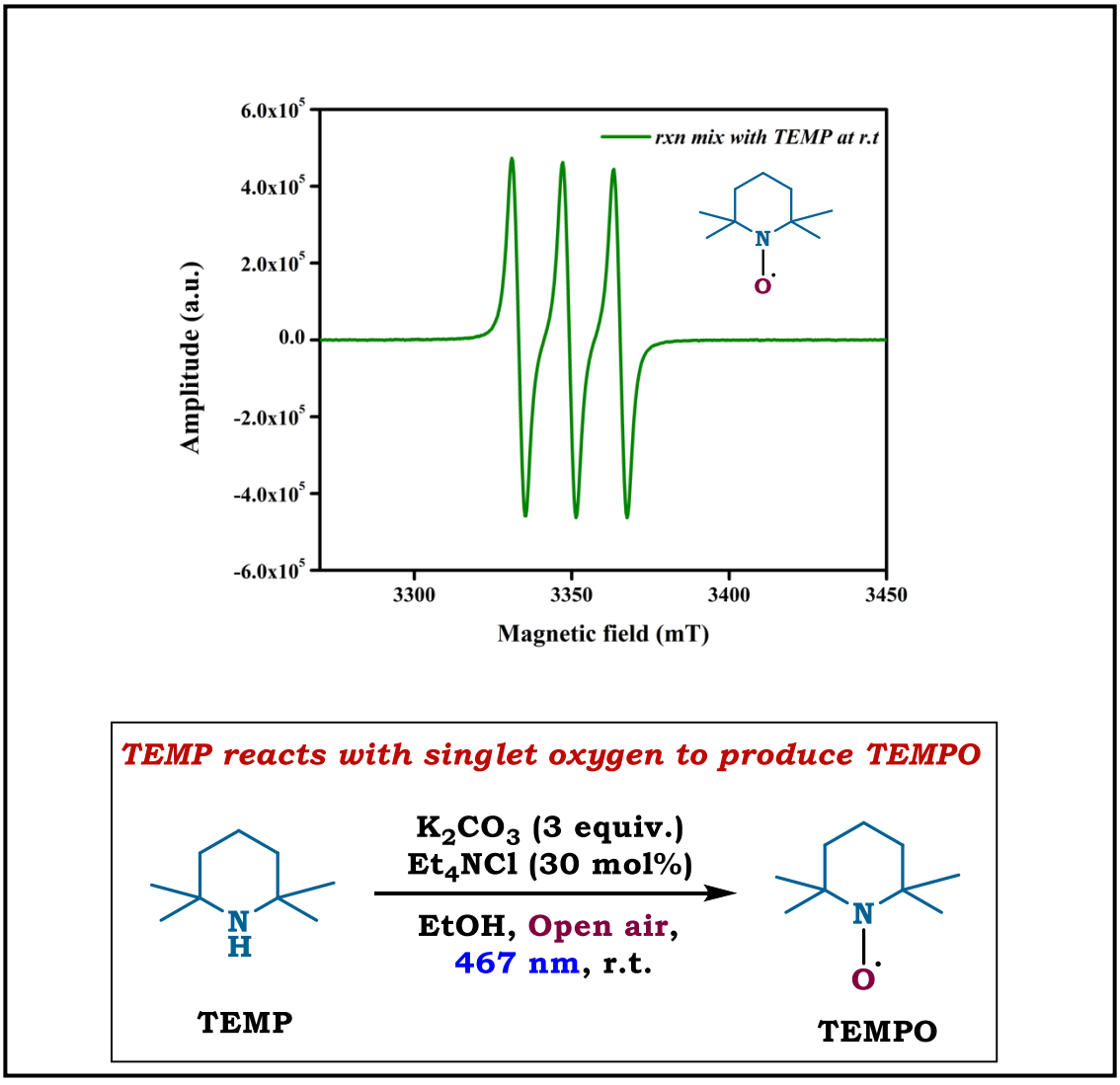
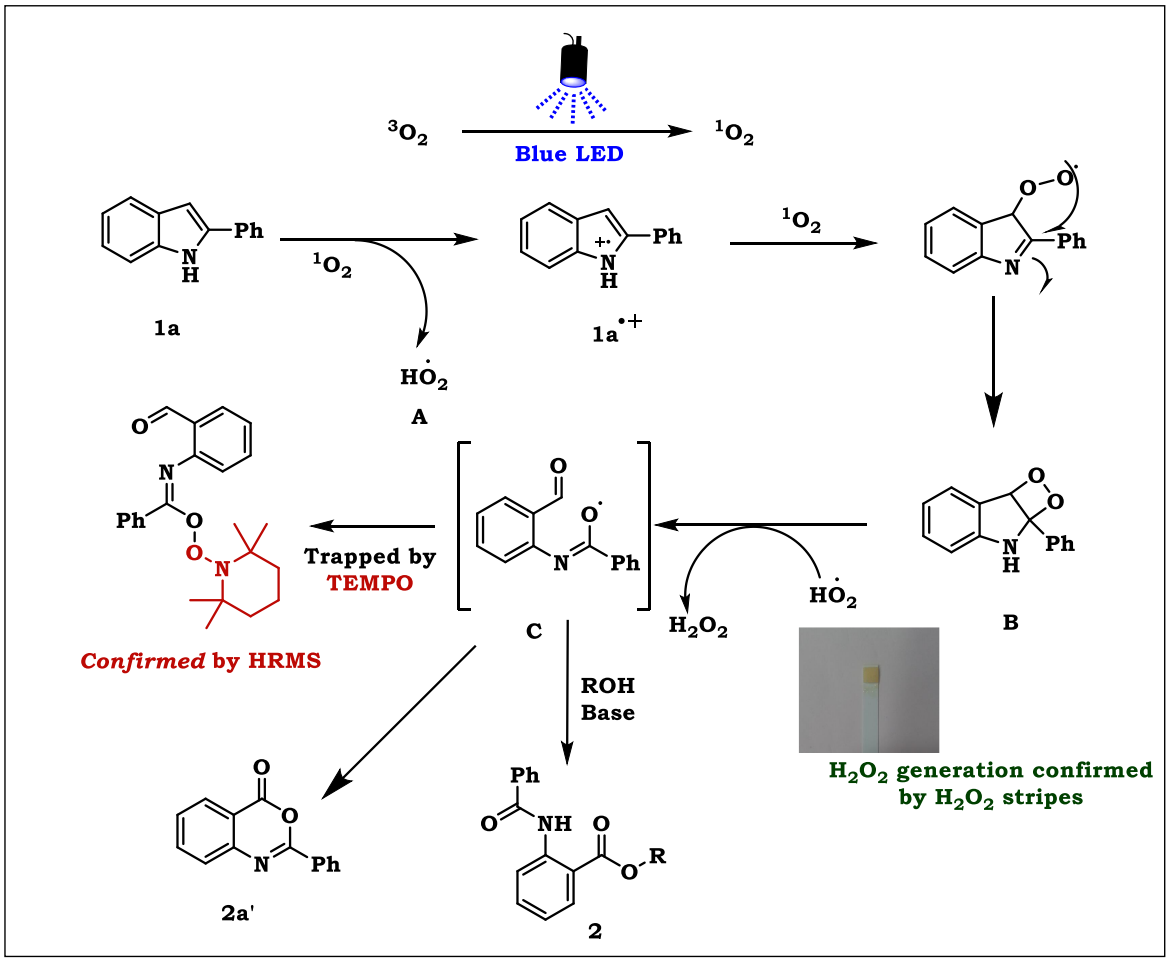


Figure 1: (a) EPR data of the reaction mixture of 2,2,6,6-Tetramethylpiperidine (TEMP) with the optimised reaction condition.

Based on a series of control experiments, the most plausible reaction mechanism has been depicted (**Scheme 10**). Under the optimized reaction conditions when illuminated with visible light (456 nm), oxygen undergoes conversion to singlet oxygen [20]. This singlet oxygen further extracts an electron from 2-phenyl indole **1a**, resulting in the generation of hydroperoxyl radical **A** and **1a**$^{\bullet+}$. Moreover, it is likely that **1a**$^{\bullet+}$ reacts with singlet oxygen, resulting in the formation of cyclic product **B**. Subsequently, through a single electron transfer (SET) with hydroperoxyl radical **A**, the cyclic product **B** transforms into a radical intermediate **C** along with the generation of hydrogen peroxide. The presence of intermediate **C** has been validated (HRMS data), specifically the TEMPO adduct of intermediate **C**. Intermediate **C** further undergoes cyclization to afford the cyclic product **2a'**. However, in the presence of alcohol and base, intermediate **C** transforms into the final desired product **2**.

Scheme 10: Probable mechanism for the synthesis of anthranilic acid derivatives



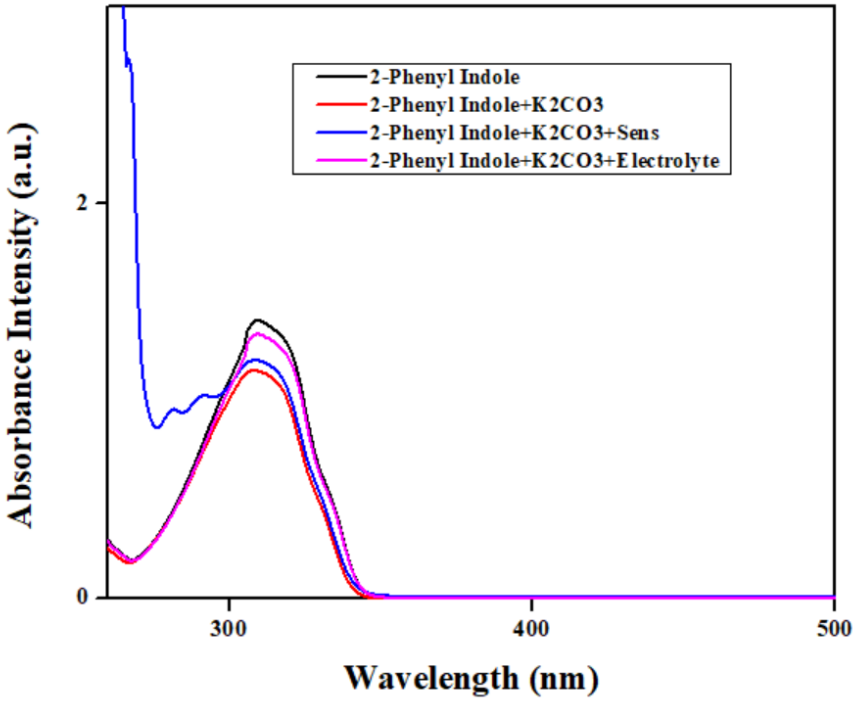
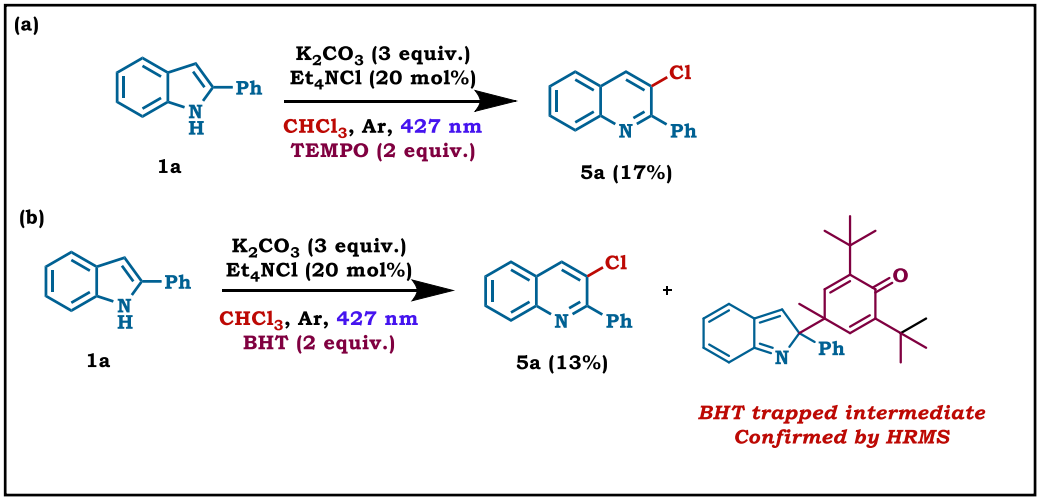


Figure 2: UV-Visible experiments of the reaction mixture in different conditions

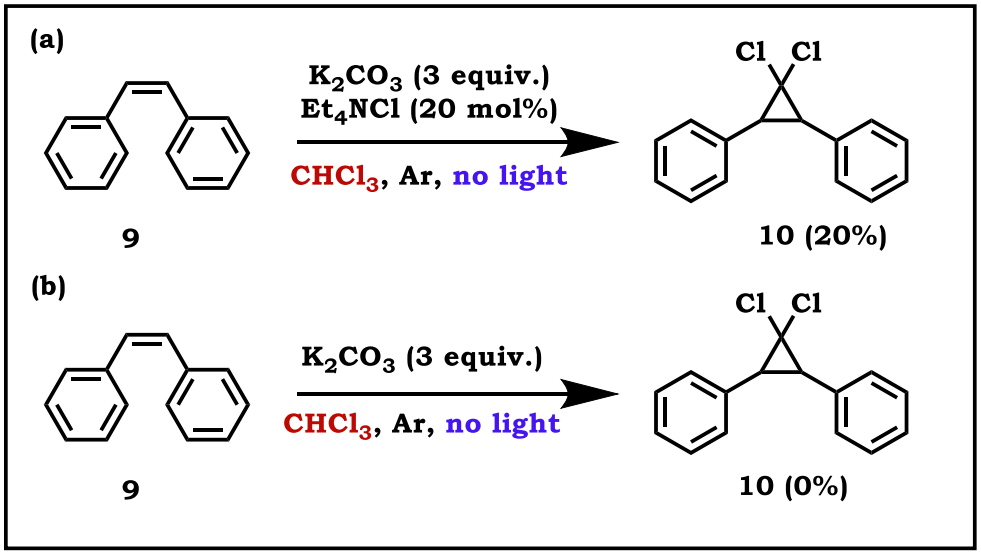
In the chloroform-based protocol, radical quenching experiments were conducted with the inclusion of TEMPO and BHT while maintaining other optimized reaction conditions (**Scheme 11**). These experiments led to a significant decrease in the yield of the intended product **5a**. Subsequently, the identification of the BHT-trapped radical intermediate was accomplished through HRMS analysis (**Scheme 11b**).

Scheme 11: Control experiments



The generation of 3-chloro-2-phenylquinoline **5a** from 2-phenylindole **1a** in chloroform implies the in-situ formation of dichlorocarbene in the reaction medium. Our objective was to investigate the characteristics of the carbene and determine whether its formation is triggered by exposure to light.

Scheme 12: Trapping of singlet carbene



Under identical conditions i.e., in presence of K_2CO_3 and nEt_4NCl in chloroform, we carried out the reaction of *cis*-stilbene **9** as the carbene trapping agent while in the absence of light. Interestingly, we obtained (3,3-dichlorocyclopropane-1,2-diyl)dibenzene **10** as the sole product in modest yield (20%, **Scheme 12a)**. This result clearly supports the generation of a singlet dichlorocarbene during the course of the reaction in the absence of light. Nevertheless, the desired product **10** did not form in the presence of K_2CO_3 in chloroform (in the absence of nEt_4NCl) (**Scheme 12b**). This observation confirms that for the generation of dichlorocarbene K_2CO_3 and nEt_4NCl in chloroform are necessary. Based on the NMR experiments, we surmised that the -NH proton of **1a** is getting abstracted in presence of K_2CO_3, and nEt_4NCl before irradiation of light (**Figure 3**).

In order to further investigate the potential formation of the EDA (Electron Donor-Acceptor) complex during the course of the reaction, UV-Visible experiments were conducted. It was observed that the combination of 2-phenylindole, K_2CO_3, and nEt_4NCl in chloroform, before light irradiation exhibited a new absorbance peak at a longer wavelength in the visible region (**Figure 4**). This peak was not present in other cases, providing evidence for the formation of an EDA complex in the reaction medium prior to exposure to light.

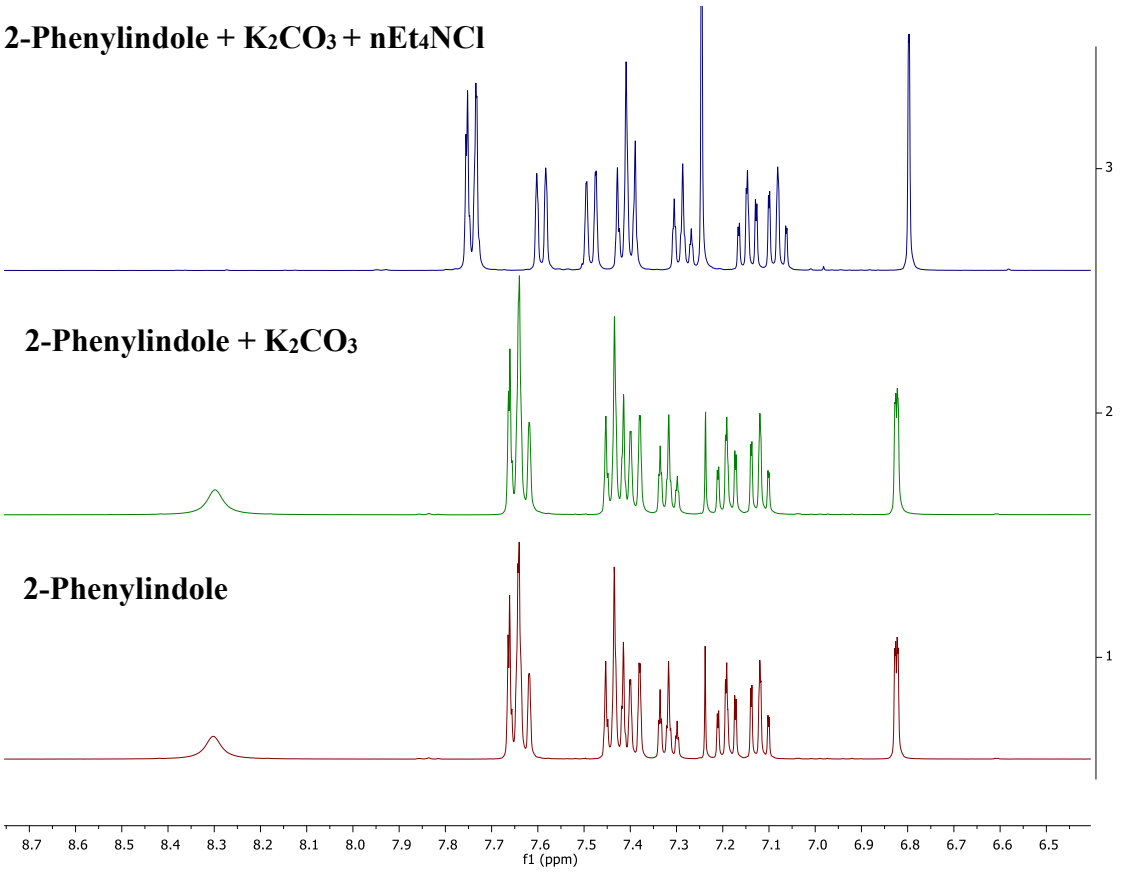


Figure 3: NMR experiments.

Based on a series of control experimental results along with additional observations, the most plausible reaction mechanism has been depicted (**Scheme 13**). The dichlorocarbene is generated from chloroform in the presence of K_2CO_3 and nEt_4NCl while in the absence of light (before the illumination of light). Subsequently, the deprotonated form of 2-phenylindole **1a**$^-$ (which forms in the presence of K_2CO_3 and nEt_4NCl before light irradiation) serves as a donor, while the electron-deficient dichlorocarbene acts as an acceptor, resulting in the formation of a yellow-coloured Electron Donor-Acceptor (EDA) complex in their ground state, with absorption in the visible region. Upon exposure to light, an intermolecular single electron transfer (SET) occurs between **1a**$^-$ and dichlorocarbene, leading to the generation of **1a**$^+$ and **D**. The confirmation of **1a**$^{\bullet+}$ formation is validated by HRMS (BHT adduct intermediate). Subsequent cyclization between **1a**$^+$ and **D**, followed by aromatization, affords the desired product **5a**.

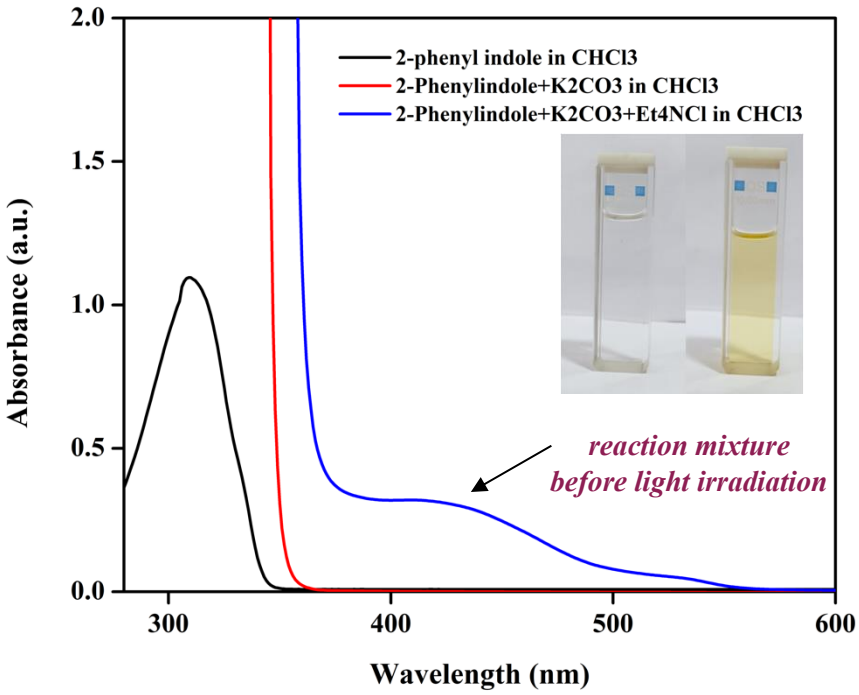
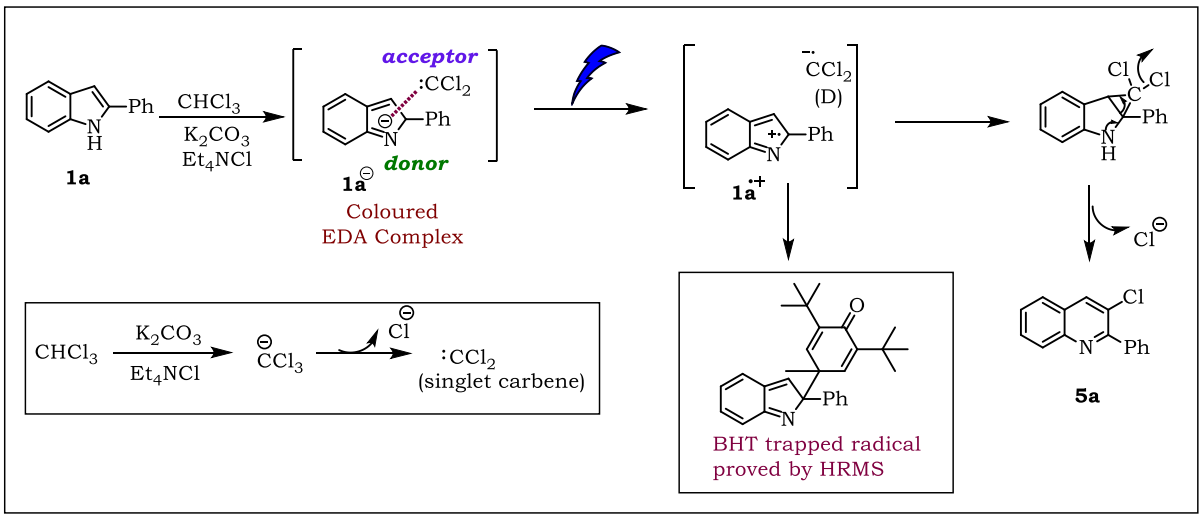


Figure 4: UV-Visible experiments of the reaction mixture

Scheme 13: Probable mechanism for the synthesis of quinoline derivatives



5.4. Conclusions:

In summary, we have developed solvent tunable methodologies for the direct synthesis of anthranilic acid derivatives and quinoline derivatives from 2-phenylindole under visible light irradiation, without employing any photocatalyst. The 2-phenylindoles in the presence of alcohols affords the corresponding anthranilic acid derivatives. A broad substrate scope has been demonstrated. 2-Phenylindole in the presence of chloroform under visible light irradtion afforded the corresponding the quinoline derivatives in moderate to good results. In order to have the mechanistic insights of these two solvent-dependent methodologies, we conducted comprehensive controlled experiments, UV-Vis experiments, and EPR experiments. The mechanistic study indicates that in the alcohol-based protocol, singlet oxygen serves as the active participant, playing a crucial role in the subsequent steps of the mechanism. Conversely, in the chloroform-based protocol, we have demonstrated the formation of an Electron Donor-Acceptor (EDA) complex in the reaction medium, which becomes activated upon exposure to light irradiation.

5.5. Experimental section:

5.5.1. General information:

Unless otherwise noted, all the starting materials and reagents were purchased from commercial suppliers (Aldrich, TCI, and Alfa Aesar) and were used without any further purification. Thin-layer chromatography (TLC) was performed using silica gel 60 GF_{254} pre-coated aluminium backed plates (2.5 mm). Visualization was accomplished by the irradiation with UV light at 254 nm. The column chromatography was performed using silica gel (100–200 mesh) eluting with petroleum ether and ethyl acetate. The NMR spectra were recorded using tetramethylsilane as the internal standard. ^{1}H NMR spectra were recorded at 400 MHz and $^{13}C\{^{1}H\}$ NMR spectra were recorded at 100 MHz (Bruker and Jeol) unless otherwise noted. Chemical shifts (δ) are reported in ppm downfield from $CDCl_3$ (δ = 7.26 ppm) for ^{1}H NMR and relative to the central $CDCl_3$ resonance (δ = 77.16 ppm) for $^{13}C\{^{1}H\}$ NMR spectroscopy. For ^{1}H NMR, data are reported as follows: chemical shift, multiplicity (s = singlet, d = doublet, dd = double doublet, t = triplet, q = quartet, br = broad, m = multiplet), coupling constants (*J*) are given in Hz and integration. $^{13}C\{^{1}H\}$ NMR spectra were recorded with complete proton decoupling. ^{19}F NMR spectra were recorded at 377 MHz. Mass samples were analyzed by high-resolution mass spectrometry (HRMS)-ESI TOF. X-Band EPR measurements for the detection of radical study were carried out using a JON Bruker BioSpin connected to Bruker EMX plus spectrometer. UV absorption was performed using Shimadzu, UV-1900 UV spectrophotometer. All photocatalytic reactions were performed under blue LEDs (Kessil PR160L series Blue LEDs, and IBRA Pure 60 W Blue LED Flood Light, IP Rating: IP66).

5.5.2. General procedure for the synthesis of 2 (GP1):

2-arylindole **1** (0.3 mmol, 1 equiv.), K_2CO_3 (0.9 mmol, 3 equiv.), nEt_4NCl (30 mol%), (E)-1,4-diphenylbut-2-ene-1,4-dione (10 mol%), and alcohols (3 ml) were added to an oven-dried 10 mL glass vial charged with magnetic stir bar. The mixture was agitated for 24 hours at ambient temperature and in the open while being illuminated by a 467nm Kessil lamp (50% intensity). After the completion of the reaction (monitored by TLC), the reaction mixture was purified by using column chromatography (Silica gel 100–200 mesh size, using ethyl acetate/Pet-Ether as eluent system).

5.5.3. General procedure for the synthesis of 4 (GP2):

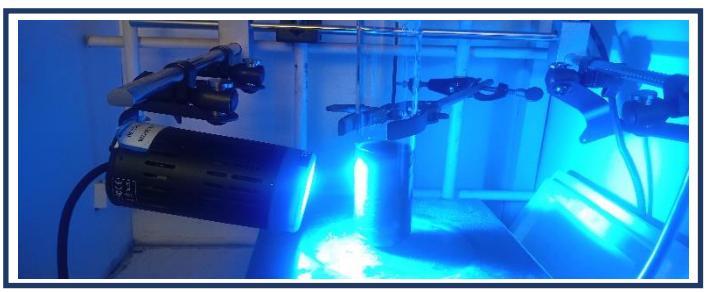
2-arylindole **1** (0.3 mmol, 1 equiv.), K_2CO_3 (0.9 mmol, 3 equiv.), nEt_4NCl (30 mol%), and chloroform (3 ml) were added to an oven-dried 10 mL glass vial charged with magnetic stir bar. To the mixture alcohol **3** (3 mmol, 10 equiv.) was added. The mixture was agitated for 24 hours at ambient temperature and in the open while being illuminated by a 427nm Kessil lamp (50% intensity). After the completion of the reaction (monitored by TLC), the reaction mixture was purified by using column chromatography (Silica gel 100–200 mesh size, using ethyl acetate/Pet-Ether as eluent system).

5.5.4. General procedure for the synthesis of 5 (GP3):

2-arylindole **1** (0.3 mmol, 1 equiv.), K_2CO_3 (0.9 mmol, 3 equiv.), nEt_4NCl (20 mol%), and chloroform (4 ml) were added to an oven-dried 10 mL glass vial charged with magnetic stir bar. Then the reaction mixture was degasified using argon for 30 minutes under constant purging and monitoring. The mixture was agitated for 24 hours at ambient temperature under inert condition while being illuminated by a 427nm Kessil lamp (50% intensity). After the completion of the reaction (monitored by TLC), the reaction mixture was purified by using column chromatography (Silica gel 100–200 mesh size, using ethyl acetate/Pet-Ether as eluent system).

5.5.5. Procedure for the gram scale synthesis of 2a:

2-Phenylindole **1a** (1 gm, 5.17 mmol, 1 equiv.), K_2CO_3 (15.51 mmol, 3 equiv.), nEt_4NCl (30 mol%), (E)-1,4-diphenylbut-2-ene-1,4-dione (10 mol%), and ethanol (30 ml) were added to an oven-dried 100 mL glass vial charged with magnetic stir bar. The mixture was agitated for (24 hours*2 days) at ambient temperature and in the open while being illuminated by a 467nm Kessil lamp (50% intensity). After the completion of the reaction (monitored by TLC), the reaction mixture was purified by using column chromatography (Silica gel 100–200 mesh size, using 4% ethyl acetate/Pet-Ether as eluent system), **2a** was formed in a good yield (750mg, 54%).



GRAM-SCALE SET UP

5.5.6. Procedure for the synthesis of 2a under sunlight:

2-Phenylindole **1a** (0.3 mmol, 1 equiv.), K_2CO_3 (0.9 mmol, 3 equiv.), nEt_4NCl (30 mol%), (E)-1,4-diphenylbut-2-ene-1,4-dione (10 mol%), and ethanol (3 ml) were added to an oven-dried 10 mL glass vial charged with magnetic stir bar. The mixture was agitated for 24 hours (8hrs * 3 days) at ambient temperature and in the open while being irradiated under sunlight. After the completion of the reaction (monitored by TLC), the reaction mixture was purified by using column chromatography (Silica gel 100–200 mesh size, using 4% ethyl acetate/Pet-Ether as eluent system), 2a was formed in a good yield (47mg, 58%).

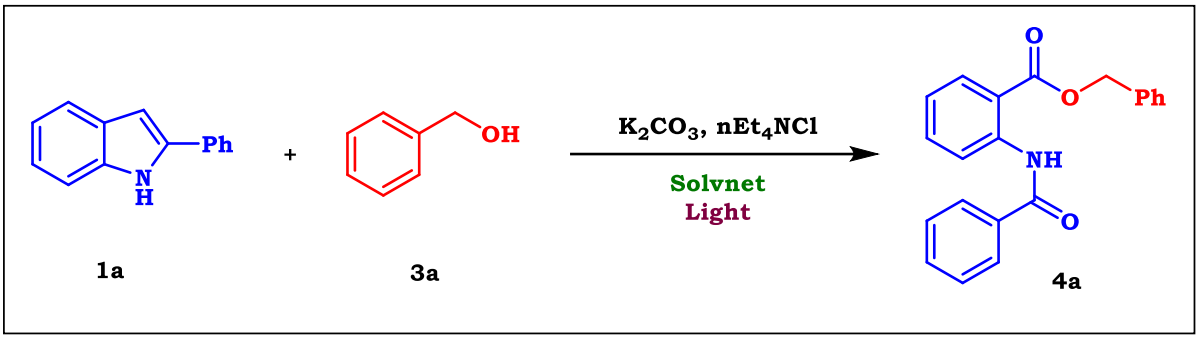


SUNLIGHT REACTION SET UP

5.5.7. Optimisation table:

5.5.7.1. Optimisation table for the synthesis of 4:

In order to get ideal circumstances where alcohols with higher boiling points or solid forms are not suitable solvents, we further optimized the system. In order to ensure optimal performance in these particular instances, the optimization sought to create updated and effective conditions that were specific to these cases.



5.5.7.1.1. Light optimisation table:

Entry	*Solvents*	*Light (nm)*	*Yield (%)[a]*
1	**Acetonitrile**	**467**	**26**
2	**Acetonitrile**	**456**	**36**
3	**Acetonitrile**	**440**	**42**
4	**Acetonitrile**	**427**	**60**
5	**Acetonitrile**	**370**	**43**

Reaction conditions: *0.3 mmol* ***1a****, 10 equiv. of alcohol* ***3a****, 3quiv. K_2CO_3, 30mol% nEt_4NCl in acetonitrile, [a]Yield is calculated by ^1H NMR spectroscopy using 1,3,5-trimethoxy benzene.*

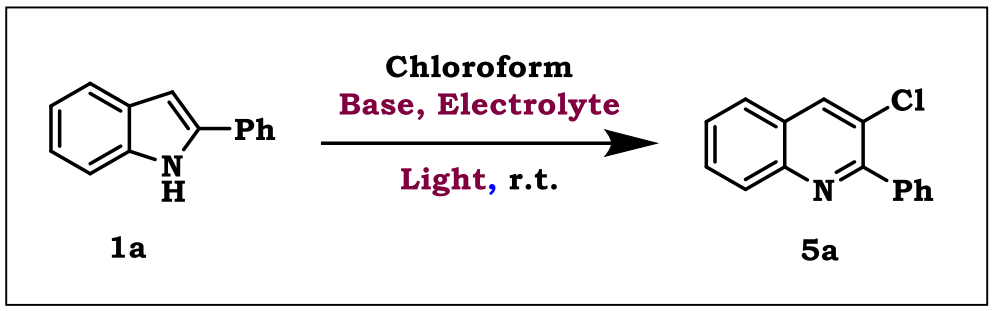
5.5.7.1.2. Solvent optimisation table:

Entry	*Solvents*	*Yield (%)[a]*
1	**Acetonitrile**	**60**
2	**DCM**	**56**
3	**$CHCl_3$**	**72 (66%)**
4	**DMSO**	**Trace**
5	**DMF**	**Trcae**
6	**Toluene**	**N.R**
7	**1,4-Dioxane**	**N.R**
8	**Ethyl acetate**	**N.R**

Reaction conditions: *0.3 mmol* ***1a****, 10 equiv. of alcohol* ***3a****, 3quiv. K_2CO_3, using 427nm. [a]Yield is calculated by ^1H NMR spectroscopy using 1,3,5-trimethoxy benzene.*

5.5.7.2. Optimisation table for the synthesis of quinoline derivative 5:

Particularly, in chloroform we have observed quinoline derivative **5** (3-chloro-2-phenylquinoline, **5a**) was formed. We have further optimised the reaction condition to get the best yield.



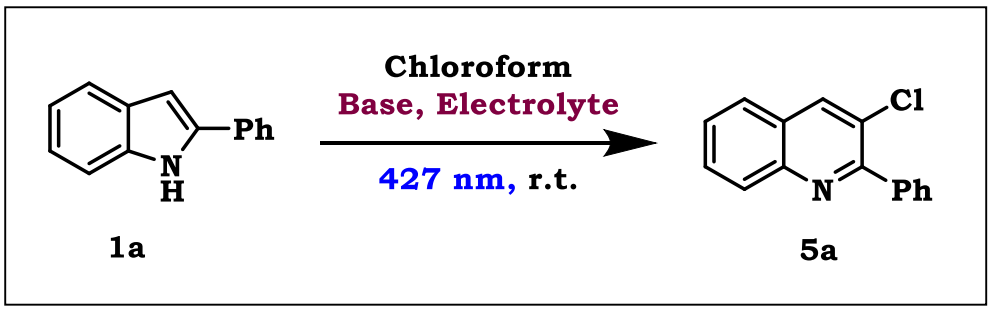
1a 5a

5.5.7.2.1. Light optimisation table:

Entry	*Electrolyte (mol %)*	*Light (nm)*	*Yield (%)[a]*
1	$^{n}(Et)_4NCl$ (20)	427	76
2	$^{n}(Et)_4NCl$ (20)	456	48
3	$^{n}(Et)_4NCl$ (20)	440	65
4	$^{n}(Et)_4NCl$ (20)	467	61
5	$^{n}(Et)_4NCl$ (20)	405	N. R
6	$^{n}(Et)_4NCl$ (20)	N. A	N. R

Reaction conditions: *0.3 mmol* ***1a****, 3quiv.* K_2CO_3*, under inert condition for 24 hrs.* [a]*Yield is calculated by column chromatography.*

5.5.7.2.2. Base optimisation table:

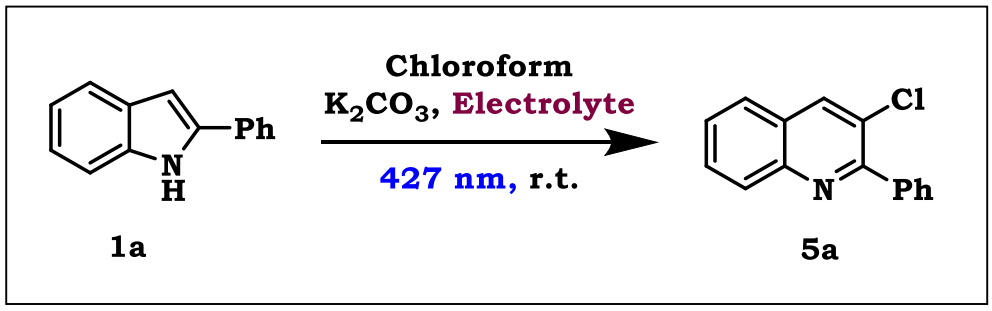


1a 5a

Entry	*Base (3 equiv.)*	*Yield (%)* [a]
1	Cs_2CO_3	60
2	K_2CO_3	76
3	KOH	Trace
4	DBU	30%
5	Na_2CO_3	Trace
6	*t*-BuOK	Trace

Reaction conditions: *0.3 mmol* ***1a****, 20 mol% nEt_4NCl, in chloroform, using 427nm under inert condition for 24 hrs.* [a]*Yield is calculated by column chromatography.*

5.5.7.2.3. Electrolyte optimisation table:



Entry	*Electrolyte (20 mol%)*	*Yield (%)* [a]
1	NA	N. R
2	$^{n}(Et)_4NCl$	76
3	KCl	N. R
4	KBr	N. R
5	NaCl	N. R
6	$C_6H_5CH_2(C_2H_5)_3NCl$	62
7	$^{n}(Bu)_4NBr$	51
8	$^{n}(Bu)_4NI$	43
9	$^{n}(Bu)_4NF$	75

10	$^{n}(Bu)_4NCl$	63
11	$^{n}(Bu)_4NClO_4$	N. R
12	NH_4Cl	N. R

Reaction conditions: *0.3 mmol* ***1a****, 3 equiv, K_2CO_3 in chloroform using 427nm under inert condition for 24 hrs. [a]Yield is calculated by column chromatography.*

5.5.7.2.4. Electrolyte mol% optimisation table:

Entry	***$^{n}(Et)_4NCl$ (mol%)***	***Yield (%)[a]***
1	$^{n}(Et)_4NCl$ (5)	46
2	$^{n}(Et)_4NCl$ (10)	52
3	$^{n}(Et)_4NCl$ (20)	76
4	$^{n}(Et)_4NCl$ (30)	58

Reaction conditions: *0.3 mmol* ***1a****, 3 equiv, K_2CO_3, in chloroform using 427nm under inert condition for 24 hrs. [a]Yield is calculated by column chromatography.*

5.5.7.2.5. Control optimisation table:

Entry	***Base***	***Solvent***	***Electrolyte***	***Light***	***Yield (%) [a]***
1	K_2CO_3	Chloroform	$^{n}(Et)_4NCl$	427	76
2	K_2CO_3	Chloroform	$^{n}(Et)_4NCl$	-	N. R.
3	K_2CO_3	Chloroform	-	427	N. R.
4	K_2CO_3	ACN	$^{n}(Et)_4NCl$	427	N. R.
5	-	Chloroform	$^{n}(Et)_4NCl$	427	N. R.

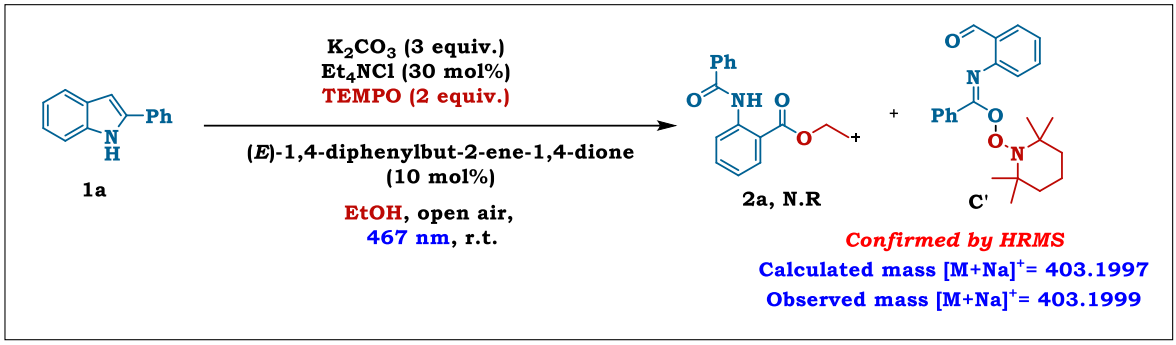
Reaction conditions: *0.3 mmol* ***1a****, 3 equiv, K_2CO_3, 20 mol% nEt4NCl in chloroform using 427nm under inert condition for 24 hrs. [a]Yield is calculated by column chromatography.*

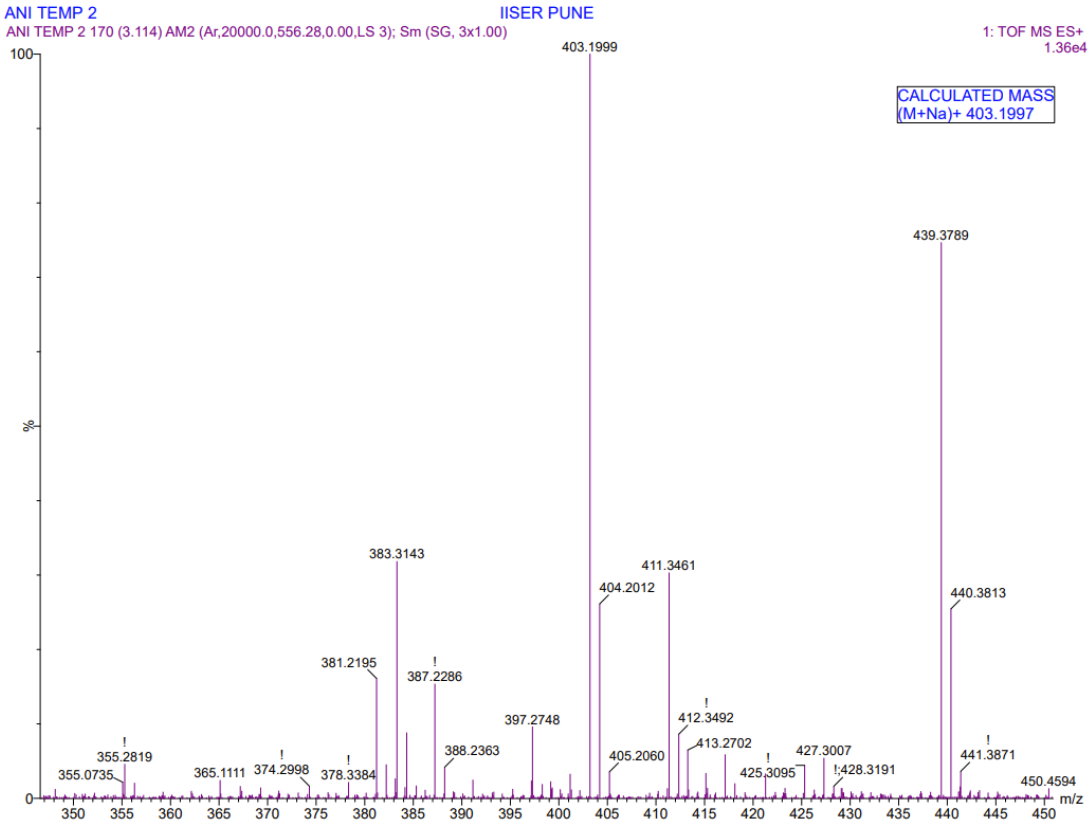
Conclusion: These optimisation table clearly suggests that K_2CO_3, nEt_4NCl, Chloroform and light all are necessary for the transformation.

5.5.8. Control Experiments for the synthesis of anthranilic acid derivatives:

5.5.8.1. Procedure for the radical quenching experiments with TEMPO:

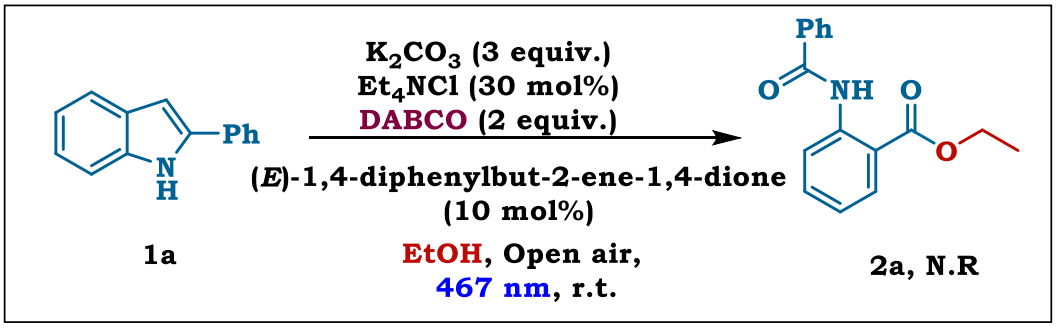
2-Phenylindole **1a** (0.3 mmol, 1 equiv.), K_2CO_3 (0.9 mmol, 3 equiv.), nEt_4NCl (30 mol%), (E)-1,4-diphenylbut-2-ene-1,4-dione (10 mol%), TEMPO (0.6 mmol, 2 equiv.) and ethanol (3 ml) were added to an oven-dried 10 mL glass vial charged with magnetic stir bar. The mixture was agitated for 24 hours at ambient temperature and in the open while being illuminated by a 467nm Kessil lamp (50% intensity). Even after prolonged reaction time, the compound **2a** was not formed. Proved the formation of radical intermediate in-situ in the reaction medium. Gratifyingly, we have observed a TEMPO adduct intermediate **C'** and was confirmed by HRMS analysis. Calcd. Mass $[M + Na]^+ = 403.1997$, found mass $[M + Na]^+ = 403.1999$.



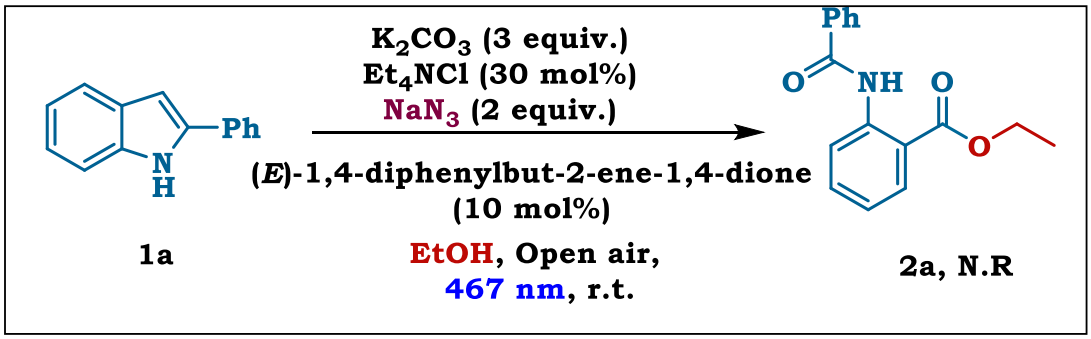


5.5.8.2. Procedure for the singlet oxygen quenching experiments:

2-Phenylindole **1a** (0.3 mmol, 1 equiv.), K_2CO_3 (0.9 mmol, 3 equiv.), nEt_4NCl (30 mol%), (*E*)-1,4-diphenylbut-2-ene-1,4-dione (10 mol%), DABCO (0.6 mmol, 2 equiv.) and ethanol (3 ml) were added to an oven-dried 10 mL glass vial charged with magnetic stir bar. The mixture was agitated for 24 hours at ambient temperature and in the open while being illuminated by a 467nm Kessil lamp (50% intensity). Even after prolonged reaction time, the compound **2a** was not formed. Proved the involvement of singlet oxygen in the reaction medium.



2-Phenylindole **1a** (0.3 mmol, 1 equiv.), K_2CO_3 (0.9 mmol, 3 equiv.), nEt_4NCl (30 mol%), (E)-1,4-diphenylbut-2-ene-1,4-dione (10 mol%), NaN_3 (0.6 mmol, 2 equiv.) and ethanol (3 ml) were added to an oven-dried 10 mL glass vial charged with magnetic stir bar. The mixture was agitated for 24 hours at ambient temperature and in the open while being illuminated by a 467nm Kessil lamp (50% intensity). Even after prolonged reaction time, the compound **2a** was not formed. Proved the involvement of singlet oxygen in the reaction medium.



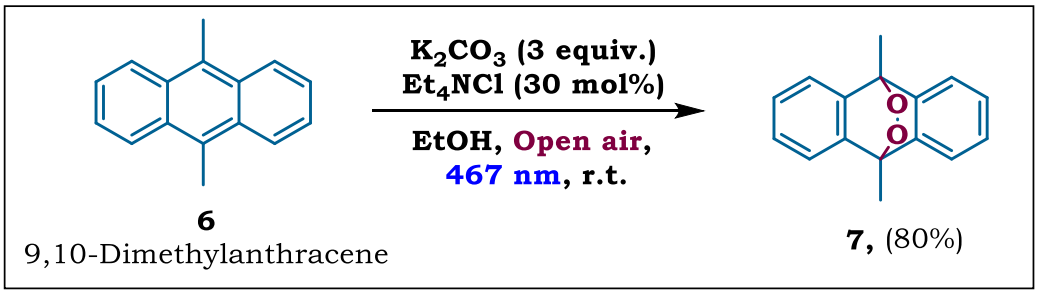
5.5.8.3. Procedure for the singlet oxygen trapping experiments:

5.5.8.3.1. Oxygen trapping reaction with 9,10-Dimethylanthracene:

9,10-Dimethylanthracene **6** (0.3 mmol, 1 equiv.), K_2CO_3 (0.9 mmol, 3 equiv.), nEt_4NCl (30 mol%), and ethanol (3 ml) were added to an oven-dried 10 mL glass vial charged with magnetic stir bar. The mixture was agitated for 24 hours at ambient temperature and in the open while being illuminated by a 467nm Kessil lamp (50% intensity). After the completion of the reaction (monitored by TLC), the reaction mixture was purified by using column chromatography (Silica gel 100–200 mesh size, ethyl acetate/Pet-Ether as eluent system), singlet oxygen trapped product **7** was formed in a good yield (80%).

9,10-dimethyl-4a,9,9a,10-tetrahydro-9,10-epidioxyanthracene (7)

^{1}H NMR (400 MHz, $CDCl_3$) δ 7.4 (dd, *J* = 5.5, 3.2 Hz, 2H), 7.3 (dd, *J* = 5.5, 3.2 Hz, 2H), 2.1 (s, 3H). **^{13}C NMR** (100 MHz, $CDCl_3$) δ 140.91, 127.55, 120.82, 13.86. **HRMS** (ESI TOF) m/z calcd. For $C_{16}H_{15}O_2$ [M + H] + 239.1067 found 239.1075.



6
9,10-Dimethylanthracene

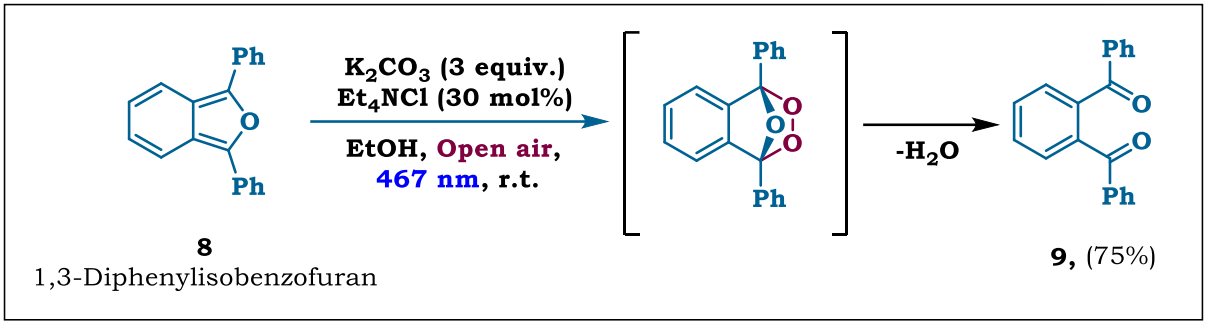
7, (80%)

5.5.8.3.2. Oxygen trapping reaction with 1,3-Diphenylisobenzofuran:

1,3-Diphenylisobenzofuran **8** (0.3 mmol, 1 equiv.), K_2CO_3 (0.9 mmol, 3 equiv.), nEt_4NCl (30 mol%), and ethanol (3 ml) were added to an oven-dried 10 mL glass vial charged with magnetic stir bar. The mixture was agitated for 24 hours at ambient temperature and in the open while being illuminated by a 467nm Kessil lamp (50% intensity). After the completion of the reaction (monitored by TLC), the reaction mixture was purified by using column chromatography (Silica gel 100–200 mesh size, ethyl acetate/Pet-Ether as eluent system), singlet oxygen trapped product **9** was formed in a good yield (75%).

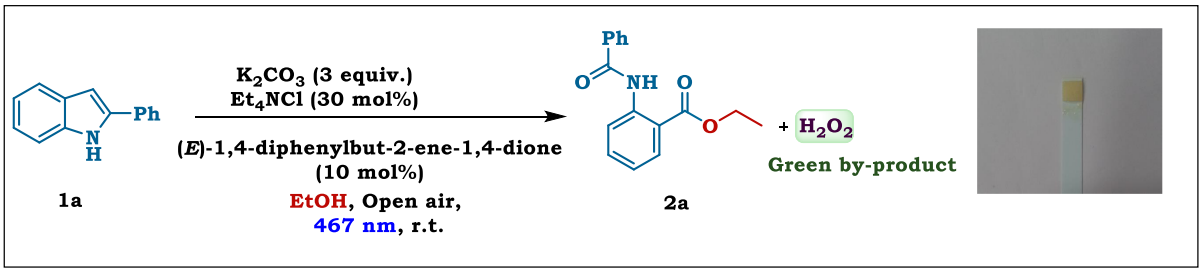
1,2-phenylenebis(phenylmethanone) (9)

^{1}H NMR (400 MHz, $CDCl_3$) δ 7.7 – 7.7 (m, 4H), 7.6 (d, *J* = 1.3 Hz, 4H), 7.6 – 7.5 (m, 2H), 7.4 (dd, *J* = 8.4, 7.1 Hz, 4H). **^{13}C NMR (100 MHz, $CDCl_3$)** δ 196.7, 140.2, 137.3, 133.1, 130.5, 129.96, 129.81, 128.47. **HRMS (ESI TOF)** m/z calcd. For $C_{20}H_{15}O_2$ $[M+H]^+$ 287.1067 found 287.1066.



5.5.8.4. Procedure for the detection of H_2O_2:

An oven-dried 10 mL glass vial charged with a magnetic stir bar was filled with 2-phenylindole **1a** (0.3 mmol, 1 equivalent), K_2CO_3 (0.9 mmol, 3 equivalent), nEt_4NCl (30 mol%), (*E*)-1,4-diphenylbut-2-ene-1,4-dione (10 mol%), and ethanol (3 ml). The mixture was stirred for a whole day at room temperature under an open Kessil lamp with a wavelength of 467 nm and 50% intensity. A hydrogen peroxide test strip is added to the diluted reaction mixture once the reaction is finished, and it is allowed to rest for two seconds. Compare it with the color chart after removing it. We have determined that H_2O_2 was created in the reaction mixture by comparing the color charts.





5.5.9. Mechanistic study:

5.5.9.1. UV-Visible experiment of the reaction mixture of the anthranilic acid derivatives:

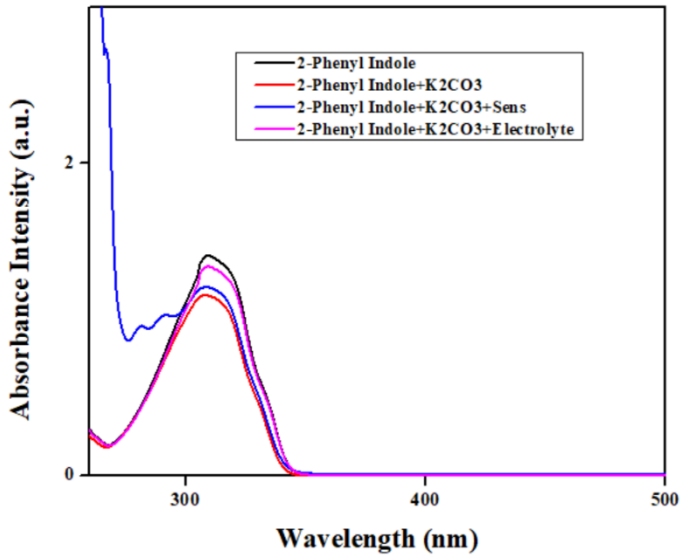


Figure 6: UV-Visible experiments for the (i) 25μM 2-phenyl indole in Ethanol, (ii) 25μM 2-phenyl indole + 3 equiv. K_2CO_3 in Ethanol, (iii) 25μM 2-phenyl indole + 3 equiv. K_2CO_3 + 30 mol% electrolyte (nEt_4NCl) in Ethanol, (iv) 25μM 2-phenyl indole + 3 equiv. K_2CO_3 + 10 mol% Sens ((*E*)-1,4-diphenylbut-2-ene-1,4-dione) in Ethanol.

Explanation:

We have recorded the UV-Visible spectra of 2-phenylindole **1a** and combinations of the **1a** with different reagents present in the reaction medium. We have observed that there was no new absorption peak appeared, which ruled out the possibility of formation of Electron Donor-Acceptor complex (EDA Complex) in-situ in the reaction medium.

5.5.9.2. EPR Study:

X-Band EPR measurements for the detection of radical study were carried out using a JON Bruker BioSpin connected to Bruker EMX plus spectrometer with a radio wave source (9.402995 GHz) at room temperature.

Procedure:

2,2,6,6-tetramethylpiperidine (**TEMP**) (0.3 mmol, 1 equiv.), K_2CO_3 (0.9 mmol, 3 equiv.), nEt_4NCl (30 mol%), and ethanol (3 ml) were added to an oven-dried 10 mL glass vial charged with magnetic stir bar. After the mixture was stirred for an hour at room temperature and under the light of a 467 nm Kessil lamp with 50% intensity, it was transfered to an EPR tube and the EPR measurement was performed on it.

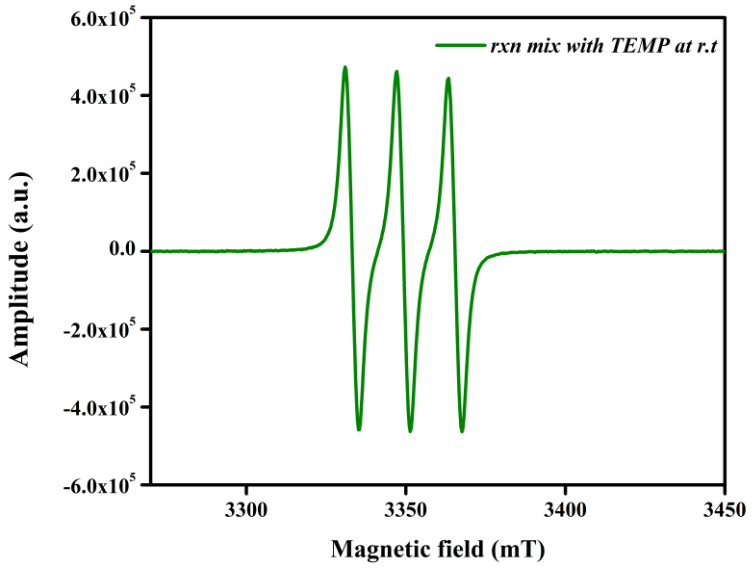
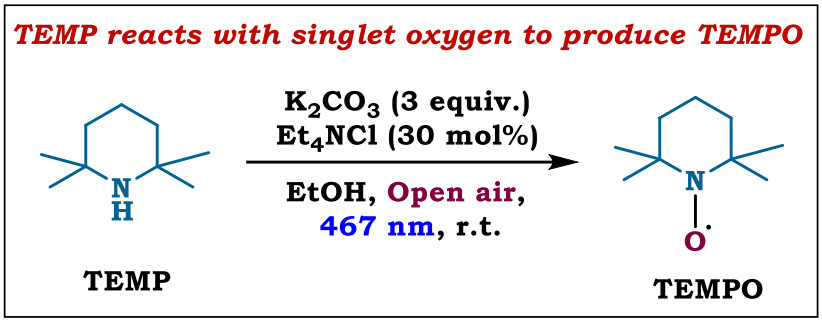


Figure 5: EPR experiments to confirm the generation of singlet oxygen *in-situ* in the reaction medium.



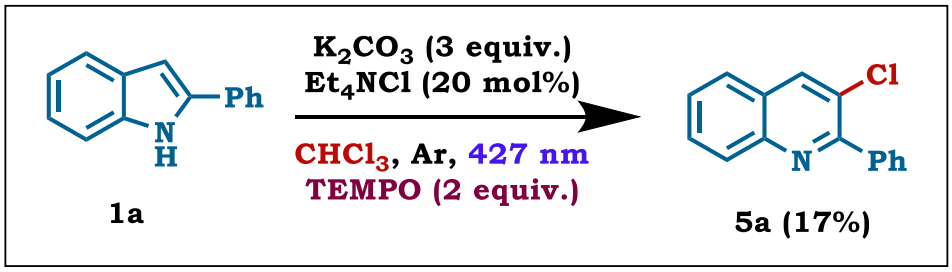
Explanation:

According to a report, **TEMP** is changed into **TEMPO** (2,2,6,6-Tetramethylpiperidine 1-Oxyl; Free Radical), which is EPR active, when singlet oxygen is present. We substituted TEMP for **1a** while maintaining the optimized condition in order to verify the presence of singlet oxygen in the reaction medium. The EPR signal of TEMPO was observed (same as described in other publications [19]). Furthermore, the presence of singlet oxygen in-situ in the reaction medium is demonstrated by this observation.

5.5.10. Control Experiments for the synthesis of quinoline derivatives:

5.5.10.1. Procedure for the radical quenching experiments with TEMPO:

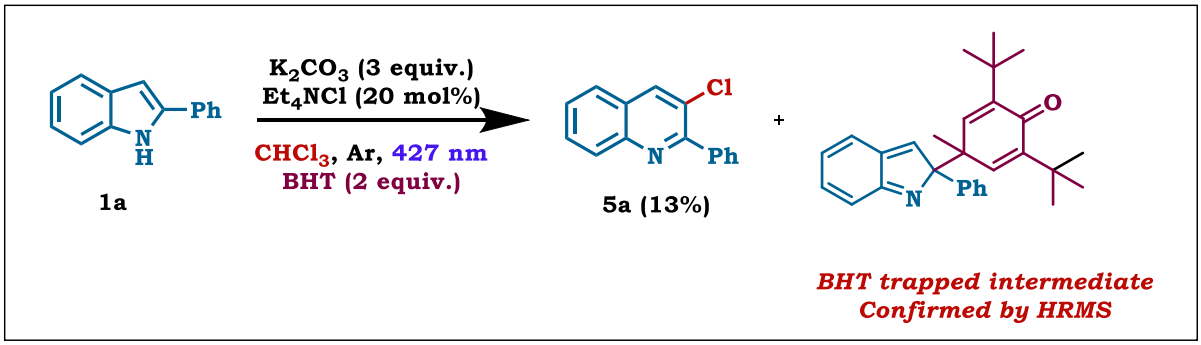
2-Phenyllindole **1a** (0.3 mmol, 1 equiv.), K_2CO_3 (0.9 mmol, 3 equiv.), nEt_4NCl (20 mol%), TEMPO (0.6 mmol, 2 equiv.) and chloroform (4 ml) were added to an oven-dried 10 mL glass vial charged with magnetic stir bar. Then the reaction mixture was degasified using argon for 30 minutes under constant purging and monitoring. The mixture was agitated for 24 hours at ambient temperature under inert atmosphere, while being illuminated by a 427nm Kessil lamp (50% intensity). The reaction produced a trace amount of the product **5a**. Proved the radical pathway of the reaction.

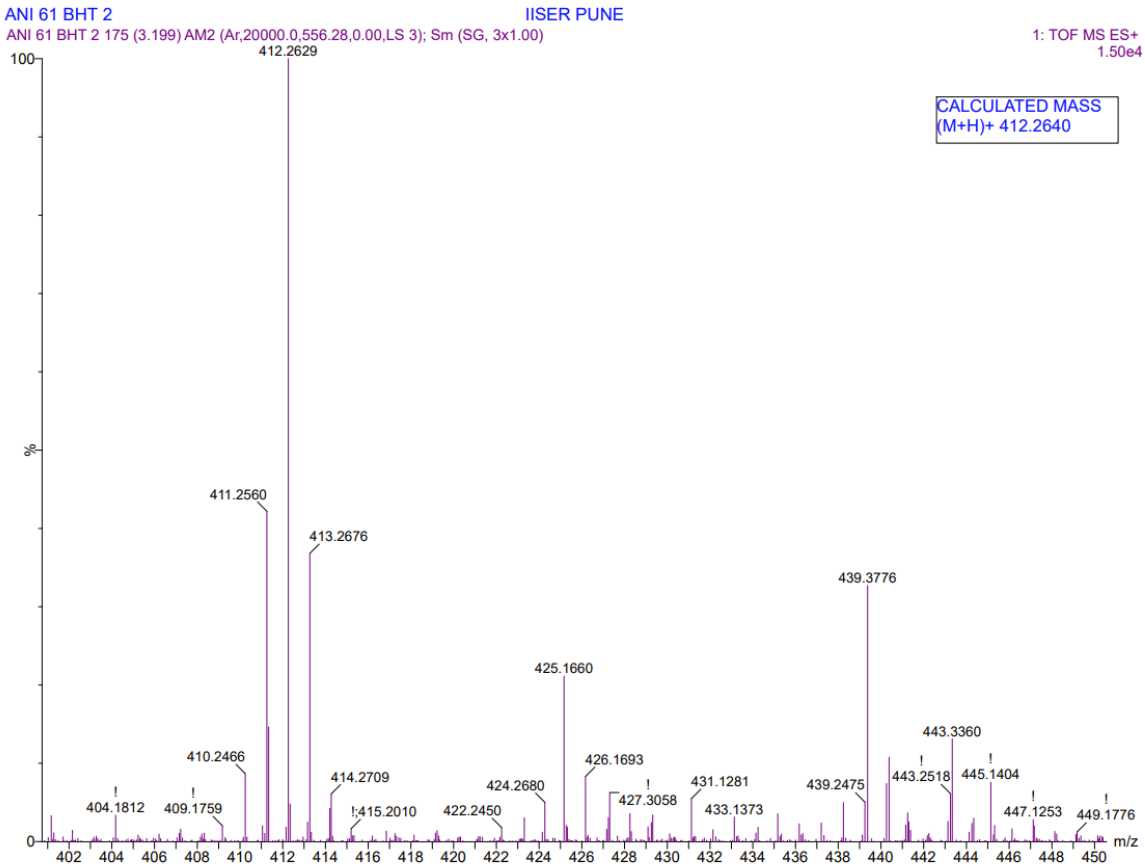


5.5.10.2. Procedure for the radical quenching experiments with BHT:

2-Phenyllindole **1a** (0.3 mmol, 1 equiv.), K_2CO_3 (0.9 mmol, 3 equiv.), nEt_4NCl (20 mol%), BHT (0.6 mmol, 2 equiv.) and chloroform (4 ml) were added to an oven-dried 10 mL glass vial charged with magnetic stir bar. Then the reaction mixture was degasified using argon for 30 minutes under constant purging and monitoring. The mixture was agitated for 24 hours at ambient temperature under inert atmosphere, while being illuminated by a 427nm Kessil lamp (50% intensity). The reaction did not proceed well and a trace amount of **5a** was produced. Proved the involvement of radical intermediate in the reaction medium. By the HRMS analysis we have confirmed the formation of $\mathbf{1a}^{\bullet+}$ in the reaction medium (BHT adduct $\mathbf{1a}^{\bullet+}$).

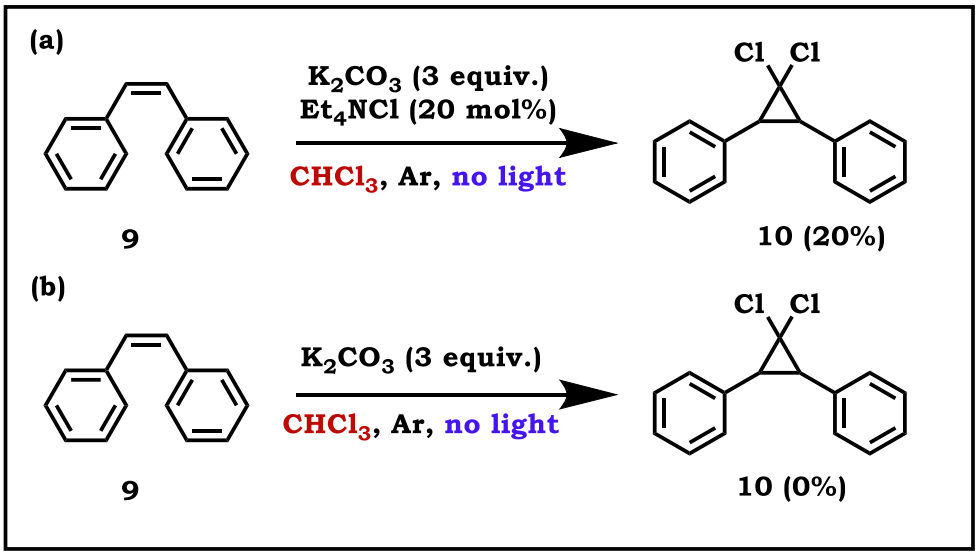
Calcd. Mass $[M+H^+]$ = 412.2640, found mass $[M+H^+]$ = 412.2629.





5.5.10.3. Procedure for the generation and trapping of singlet carbene:

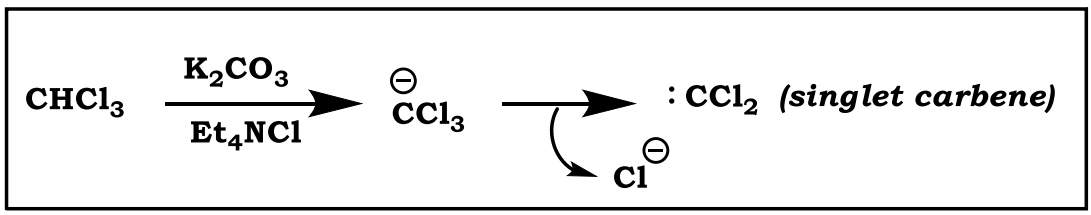
Scheme 14: Reaction of trapping the singlet carbene



Cis-Stibene **9**, K_2CO_3 (3 equiv.) and nEt_4NCl (20 mol%) were taken in a glass vial. Chloroform was added to the reaction mixture and the reaction mixture was stirred at room temperature for 24 hrs (**Scheme 12a**). The reaction produced the carbene trapped product **10** in 20% of yield. Same reaction has been carried out in absence of nEt_4NCl, and after prolonged reaction time, no desired product **10** is formed (**Scheme 12b**).

Conclusion:

The outcomes substantiate the presence of a singlet carbene in the reaction medium. Importantly, the formation of the singlet carbene is independent of the light source. However, it is important to note that the combination of K_2CO_3 and nEt_4NCl is essential for the generation of dichlorocarbene from chloroform in the reaction mixture. Solely relying on K_2CO_3 is insufficient for the formation of dichlorocarbene from chloroform.



5.5.10.4. Procedure for the NMR study:

Procedure:

Initially, 10 mg of 2-Phenylindole 1a was placed in a 0.7 ml $CDCl_3$-containing NMR tube, and the NMR data was recorded. Subsequently, 21 mg of K_2CO_3 (3 equiv.) was introduced into the ^1H NMR tube, and another set of NMR measurements was conducted. Following this, 2.5 mg of Et_4NCl (30 mol%) was added, and additional ^1H NMR data was recorded.

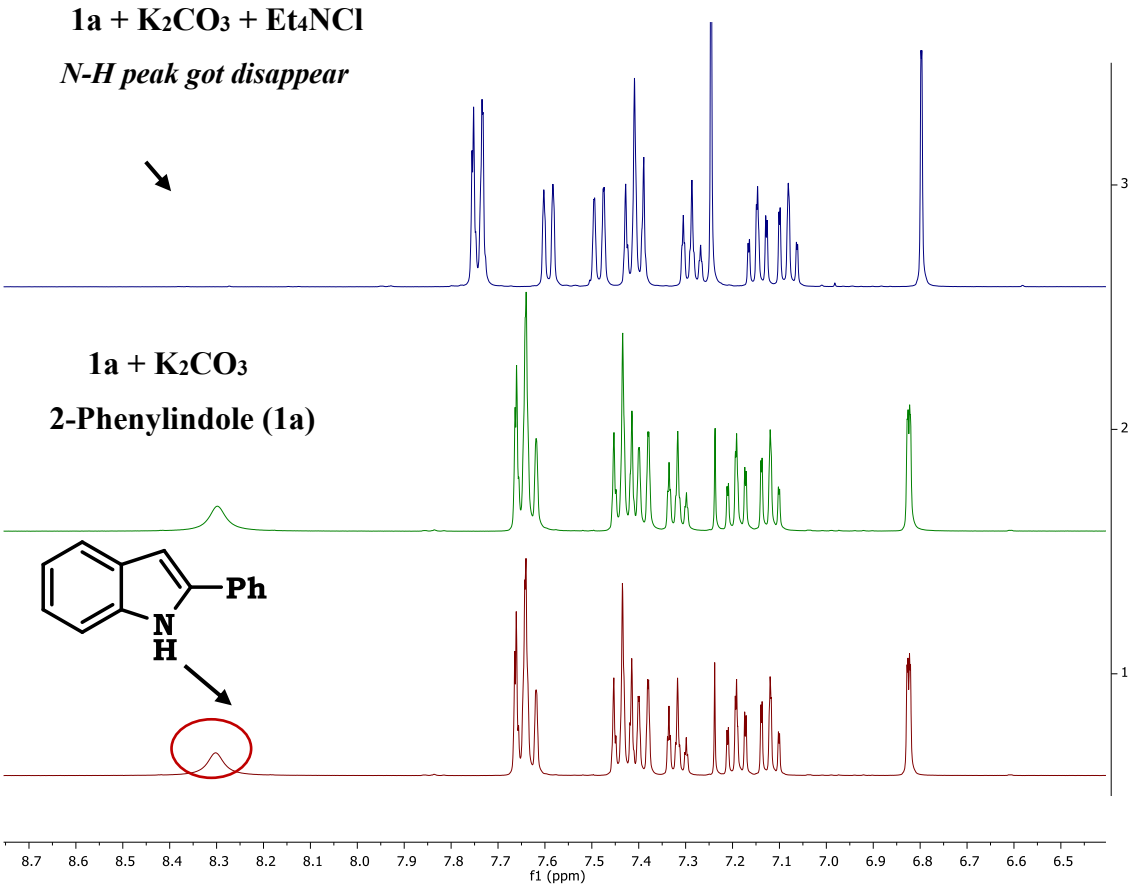


Figure 6: NMR experiments

Conclusion:

Analysis of the ^1H NMR data reveals the disappearance of the N-H peak and the shifting of other peaks in the presence of K_2CO_3 and nEt_4NCl. This observation suggests the abstraction of the N-H proton and the formation of a new intermediate in the presence of K_2CO_3 and nEt_4NCl with **1a** in solution. Importantly, it is noted that K_2CO_3 alone is unable to perform the proton abstraction of the N-H proton of **1a**.

5.5.10.5. UV-Visible experiments of reaction mixture of the quinoline derivatives:

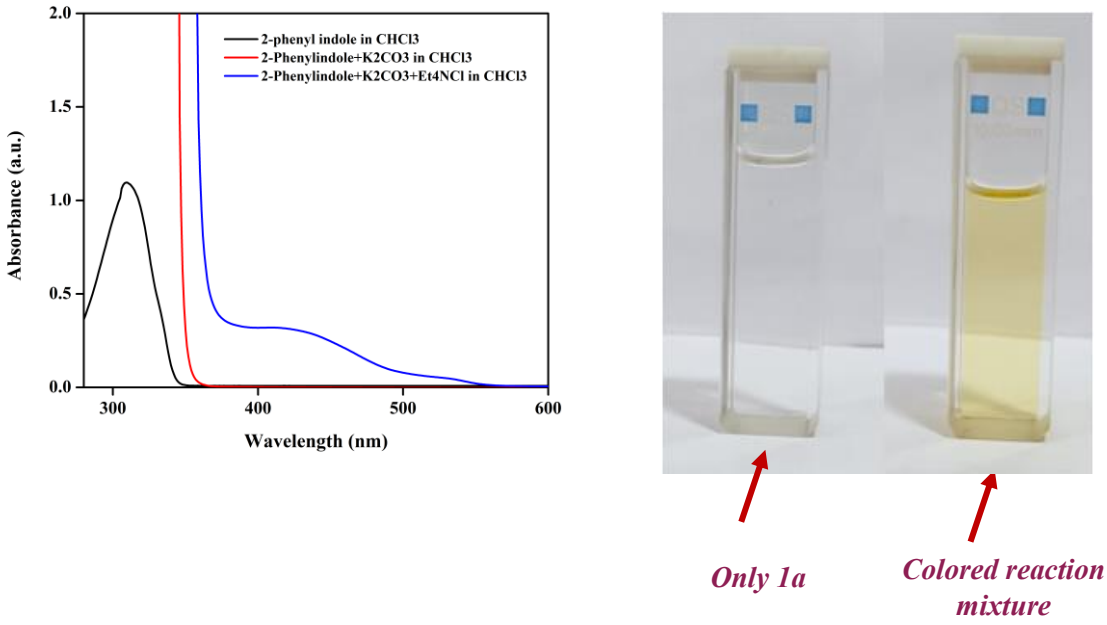


Figure 7: UV-Visible experiment of the reaction mixture (i) 2-Phenylindole in chloroform, (ii) 2-Phenylindole and 3 equiv. K_2CO_3 in chloroform, (iii) reaction mixture of 2-Phenylindole and 3 equiv. K_2CO_3, nEt_4NCl (20 mol%) in chloroform.

Explanation:

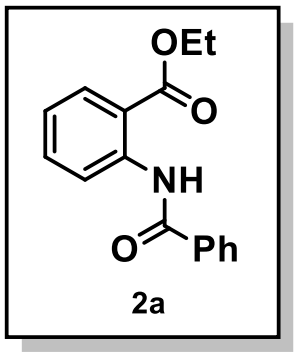
We have recorded the UV-Visible data of 2-Phenylindole **1a**, and a mixture of 2-Phenylindole **1a** and K_2CO_3, and the mixture of 2-Phenylindole **1a**, K_2CO_3 and nEt_4NCl in chloroform.

The combination of 2-Phenylindole **1a**, K_2CO_3, and nEt_4NCl in chloroform results in a solution with a yellow color, and this colored mixture exhibits absorption in the visible region. This provides evidence for the formation of a new complex within the reaction medium.

As previously noted, the generation of a singlet dichlorocarbene was observed even before light irradiation, and a new intermediate was identified to form from **1a**. It is hypothesized that these two reactive intermediates play a crucial role in the formation of the EDA (Electron Donor-Acceptor) complex in the reaction mixture while in their ground state, preceding light irradiation.

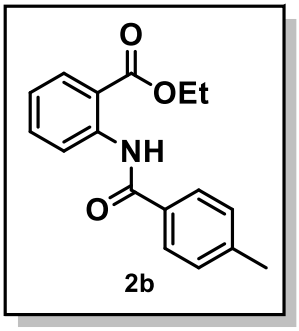
5.6. Experimental data:

Ethyl 2-benzamidobenzoate (2a)



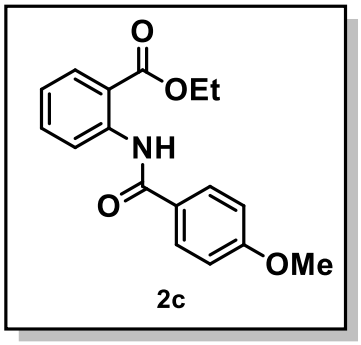
The title compound **2a** was prepared according to the general procedure (**GP1**) starting from 2-Phenylindole **1a** (0.3 mmol). White solid (60 mg, 74% yield), **^{1}H NMR (400 MHz, CDCl$_3$)** δ 12.09 (s, 1H), 8.94 (dd, *J* = 8.5, 1.2 Hz, 1H), 8.11 (dd, *J* = 8.0, 1.7 Hz, 1H), 8.08 – 8.04 (m, 2H), 7.61 (ddd, *J* = 8.7, 7.2, 1.7 Hz, 1H), 7.57 – 7.49 (m, 3H), 7.13 (ddd, *J* = 8.3, 7.3, 1.2 Hz, 1H), 4.43 (q, *J* = 7.2 Hz, 2H), 1.43 (t, *J* = 7.1 Hz, 3H). **^{13}C {^{1}H} NMR (100 MHz, CDCl$_3$)** δ 168.8, 165.9, 142.0, 135.1, 134.8, 132.1, 131.1, 128.9, 127.5, 122.7, 120.6, 115.6, 61.7, 14.4. **HRMS (ESI TOF)** *m/z* calcd. For $C_{16}H_{15}NO_3Na$ $[M + Na]^+$ 292.0950 found 292.0944.

Ethyl 2-(4-methylbenzamido) benzoate (2b)



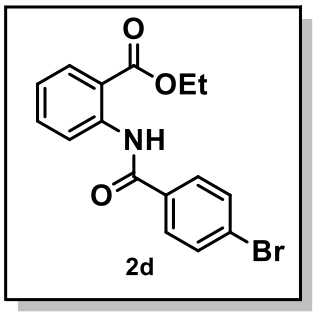
The title compound **2b** was prepared according to the general procedure (**GP1**) starting from 2-(p-tolyl)-1H-indole **1b** (0.3 mmol). White solid (61 mg, 72% yield). **^{1}H NMR (400 MHz, CDCl$_3$)** δ 12.04 (s, 1H), 8.93 (dd, *J* = 8.5, 1.2 Hz, 1H), 8.10 (dd, *J* = 8.0, 1.7 Hz, 1H), 7.99 – 7.89 (m, 2H), 7.63 – 7.56 (m, 1H), 7.32 (d, *J* = 8.0 Hz, 2H), 7.11 (ddd, *J* = 8.2, 7.3, 1.2 Hz, 1H), 4.42 (q, *J* = 7.1 Hz, 2H), 2.43 (s, 3H), 1.43 (t, *J* = 7.1 Hz, 3H). **^{13}C{^{1}H} NMR (100 MHz, CDCl$_3$)** δ 168.6, 165.8, 142.4, 142.0, 134.7, 132.2, 130.9, 129.5, 127.4, 122.4, 120.4, 115.4, 61.5, 21.5, 14.2. HRMS (ESI TOF) *m/z* calcd. For $C_{17}H_{17}NO_3Na$ $[M + Na]^+$ 306.1106 found 306.1109.

Ethyl 2-(4-methoxybenzamido) benzoate (2c)



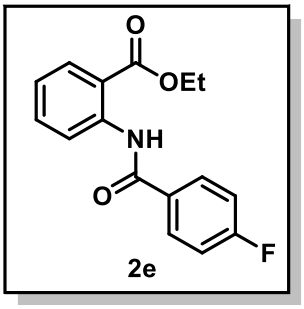
The title compound **2c** was prepared according to the general procedure (**GP1**) starting from 2-(4-methoxyphenyl)-1H-indole **1c** (0.3 mmol). White solid (64 mg, 71% yield). **^{1}H NMR (400 MHz, CDCl$_3$)** δ 12.01 (s, 1H), 8.92 (dd, *J* = 8.5, 1.2 Hz, 1H), 8.09 (dd, *J* = 8.0, 1.7 Hz, 1H), 8.06 – 7.98 (m, 2H), 7.59 (ddd, *J* = 8.7, 7.2, 1.7 Hz, 1H), 7.14 – 7.06 (m, 1H), 7.05 – 6.97 (m, 2H), 4.42 (q, *J* = 7.1 Hz, 2H), 3.88 (s, 3H), 1.43 (t, *J* = 7.1 Hz, 3H). **^{13}C{^{1}H} NMR (100 MHz, CDCl$_3$)** δ 168.7, 165.3, 162.6, 142.2, 134.7, 130.9, 129.3, 127.3, 122.3, 120.4, 115.3, 114.0, 61.5, 55.5, 14.2. **HRMS (ESI TOF)** *m/z* calcd. For $C_{17}H_{17}NO_4Na$ $[M + Na]^+$ 322.1055 found 322.1052.

Ethyl 2-(4-bromobenzamido)benzoate (2d)



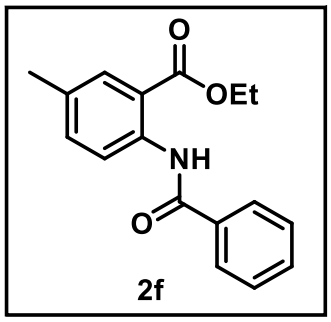
The title compound **2d** was prepared according to the general procedure (**GP1**) starting from 2-(4-bromophenyl)-1H-indole **1d** (0.3 mmol). White solid (72 mg, 69% yield). **^{1}H NMR (400 MHz, CDCl$_3$)** δ 12.12 (s, 1H), 8.89 (dd, *J* = 8.4, 1.1 Hz, 1H), 8.11 (dd, *J* = 8.0, 1.7 Hz, 1H), 7.99 – 7.84 (m, 2H), 7.68 – 7.64 (m, 2H), 7.61 (ddd, *J* = 8.8, 7.3, 1.7 Hz, 1H), 7.14 (ddd, *J* = 8.2, 7.3, 1.2 Hz, 1H), 4.42 (q, *J* = 7.1 Hz, 2H), 1.44 (t, *J* = 7.1 Hz, 3H). **^{13}C{^{1}H} NMR (100 MHz, CDCl$_3$)** δ 168.7, 164.7, 141.7, 134.8, 133.8, 132.1, 131.0, 129.0, 126.8, 122.8, 120.4, 115.5, 61.6, 14.2. **HRMS (ESI TOF)** *m/z* calcd. For $C_{16}H_{15}BrNO_3$ $[M + H]^+$ 348.0235 and 350.0215 found 348.0237 and 350.0217

Ethyl 2-(4-fluorobenzamido)benzoate (2e)



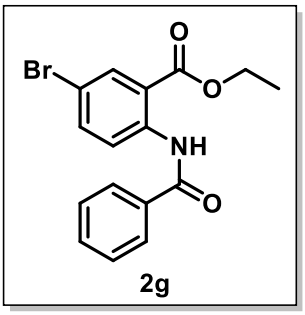
The title compound **2e** was prepared according to the general procedure (**GP1**) starting from 2-(4-fluorophenyl)-1H-indole **1e** (0.3 mmol). White solid (64 mg, 75% yield). **^{1}H NMR (400 MHz, $CDCl_3$)** δ 12.10 (s, 1H), 8.90 (dd, *J* = 8.5, 1.3 Hz, 1H), 8.11 (dd, *J* = 8.0, 1.7 Hz, 1H), 8.09 – 8.05 (m, 2H), 7.61 (ddd, *J* = 8.7, 7.2, 1.7 Hz, 1H), 7.23 – 7.16 (m, 2H), 7.13 (ddd, *J* = 8.3, 7.3, 1.2 Hz, 1H), 4.43 (q, *J* = 7.2 Hz, 2H), 1.44 (t, *J* = 7.1 Hz, 3H). **^{13}C {^{1}H} NMR (100 MHz, $CDCl_3$)** δ 168.8, 166.3, 164.6, 163.8, 141.8, 134.8, 130.9, 129.9, 129.8, 122.7, 120.4, 116.0, 115.8, 115.4, 61.6, 14.2. **^{19}F NMR (377 MHz, $CDCl_3$)** δ -107.62. **HRMS (ESI TOF)** *m/z* calcd. For $C_{16}H_{14}FNO_3Na$ $[M + Na]^+$ 310.0855 found 310.0855.

Ethyl 2-benzamido-5-methylbenzoate (2f)



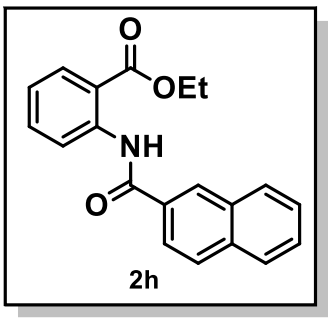
The title compound **2f** was prepared according to the general procedure (**GP1**) starting from 5-methyl-2-phenyl-1H-indole **1f** (0.3 mmol). White solid (62 mg, 73% yield). **^{1}H NMR (400 MHz, $CDCl_3$)** δ 11.98 (s, 1H), 8.82 (d, *J* = 8.6 Hz, 1H), 8.06 – 8.02 (m, 2H), 7.89 (d, *J* = 2.2 Hz, 1H), 7.56 – 7.48 (m, 3H), 7.41 (dd, *J* = 8.6, 2.3 Hz, 1H), 4.41 (q, *J* = 7.2 Hz, 2H), 2.36 (s, 3H), 1.44 (t, *J* = 7.1 Hz, 3H). **^{13}C {^{1}H} NMR (100 MHz, $CDCl_3$)** δ 168.7, 165.6, 139.5, 135.4, 135.1, 132.1, 131.8, 131.0, 128.8, 127.4, 120.4, 115.4, 61.5, 20.8, 14.3. **HRMS (ESI TOF)** *m/z* calcd. For $C_{17}H_{17}NO_3Na$ $[M + Na]^+$ 306.1106 found 306.1104.

Ethyl 2-benzamido-5-bromobenzoate (2g)



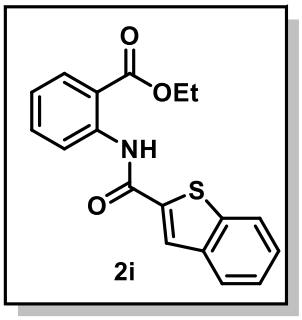
The title compound **2g** was prepared according to the general procedure (**GP1**) starting from 5-bromo-2-phenyl-1H-indole **1g** (0.3 mmol). White solid (77 mg, 73% yield). **^{1}H NMR (400 MHz, $CDCl_3$)** δ 12.0 (s, 1H), 8.9 (d, *J* = 9.1 Hz, 1H), 8.2 (d, *J* = 2.4 Hz, 1H), 8.2 – 7.9 (m, 2H), 7.7 (dd, *J* = 9.1, 2.6 Hz, 1H), 7.7 – 7.4 (m, 3H), 4.4 (q, *J* = 7.2 Hz, 2H), 1.4 (t, *J* = 7.2 Hz, 3H). **^{13}C {^{1}H} NMR (100 MHz, $CDCl_3$)** δ 167.3, 165.5, 140.8, 137.2, 134.4, 133.3, 132.0, 128.7, 127.2, 122.0, 116.8, 114.8, 61.9, 14.0. **HRMS (ESI TOF)** *m/z* calcd. For $C_{16}H_{15}BrNO_3$ $[M + H]^+$ 348.0235 found 348.0237

Ethyl 2-(2-naphthamido)benzoate (2h)



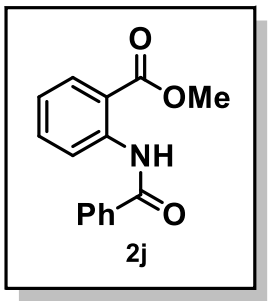
The title compound **2h** was prepared according to the general procedure (**GP1**) starting from 2-(naphthalen-2-yl)-1H-indole **1h** (0.3 mmol). White solid (64 mg, 67% yield). **^{1}H NMR (400 MHz, $CDCl_3$)** δ 12.26 (s, 1H), 8.99 (dd, *J* = 8.5, 1.2 Hz, 1H), 8.59 (dd, *J* = 1.7, 0.8 Hz, 1H), 8.12 (ddd, *J* = 9.8, 8.3, 1.8 Hz, 2H), 8.05 – 8.01 (m, 1H), 7.98 (d, *J* = 8.6 Hz, 1H), 7.92 – 7.89 (m, 1H), 7.61 (dddd, *J* = 19.6, 7.3, 6.2, 1.7 Hz, 3H), 7.15 (ddd, *J* = 8.3, 7.3, 1.2 Hz, 1H), 4.45 (q, *J* = 7.2 Hz, 2H), 1.45 (t, *J* = 7.1 Hz, 3H). **^{13}C{^{1}H} NMR (100 MHz, $CDCl_3$)** δ 168.7, 165.8, 142.0, 135.0, 134.7, 132.8, 132.2, 131.0, 129.4, 128.7, 128.4, 127.9, 127.8, 126.7, 123.7, 122.6, 120.5, 115.6, 61.6, 14.3. **HRMS (ESI TOF)** *m/z* calcd. For $C_{20}H_{17}NO_3Na$ $[M + Na]^+$ 342.1106 found 342.1103.

Ethyl 2-(benzo[b]thiophene-2-carboxamido)benzoate (2i)



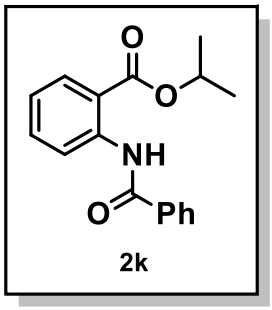
The title compound **2i** was prepared according to the general procedure (**GP1**) starting from 2-(benzo[b]thiophen-2-yl)-1H-indole **1i** (0.3 mmol). White solid (66 mg, 67% yield). **^{1}H NMR (400 MHz, $CDCl_3$)** δ 12.24 (s, 1H), 8.87 (dd, *J* = 8.5, 1.2 Hz, 1H), 8.12 (dd, *J* = 8.0, 1.6 Hz, 1H), 8.03 (d, *J* = 0.8 Hz, 1H), 7.97 – 7.86 (m, 2H), 7.61 (ddd, *J* = 8.7, 7.3, 1.7 Hz, 1H), 7.48 – 7.38 (m, 2H), 7.14 (ddd, *J* = 8.2, 7.3, 1.2 Hz, 1H), 4.47 (q, *J* = 7.1 Hz, 2H), 1.46 (t, *J* = 7.1 Hz, 3H). **^{13}C {^{1}H} NMR (100 MHz, $CDCl_3$)** δ 168.8, 160.9, 141.5, 141.5, 140.0, 139.3, 134.8, 131.0, 126.5, 125.5, 125.4, 124.9, 122.8, 122.8, 120.4, 115.3, 61.7, 14.3. **HRMS (ESI TOF)** *m/z* calcd. For $C_{18}H_{16}NO_3S$ $[M + H]^+$ 326.0851 found 326.0850.

Methyl 2-benzamidobenzoate (2j)



The title compound **2j** was prepared according to the general procedure (**GP1**) starting from 2-Phenylindole **1a** (0.3 mmol) in methanol. White solid (53 mg, 69% yield). **^{1}H NMR (400 MHz, $CDCl_3$)** δ 12.04 (s, 1H), 8.94 (dd, *J* = 8.5, 1.3 Hz, 1H), 8.11 – 8.03 (m, 3H), 7.61 (ddd, *J* = 8.8, 7.3, 1.8 Hz, 1H), 7.57 – 7.49 (m, 3H), 7.12 (ddd, *J* = 8.4, 7.3, 1.2 Hz, 1H), 3.96 (s, 3H). **^{13}C{^{1}H} NMR (100 MHz, $CDCl_3$)** δ 169.1, 165.8, 141.9, 134.9, 134.9, 132.0, 131.0, 128.8, 127.4, 122.6, 120.5, 115.2, 52.5. **HRMS (ESI TOF)** *m/z* calcd. For $C_{15}H_{13}NO_3Na$ $[M + Na]^+$ 320.1262 found 320.1256.

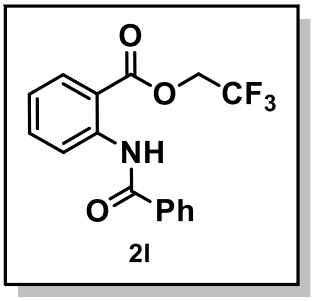
Isopropyl 2-benzamidobenzoate (2k)



2k

The title compound **2k** was prepared according to the general procedure (**GP1**) starting from 2-Phenylindole **1a** (0.3 mmol) in isopropanol. White solid (64 mg, 75% yield). **^{1}H NMR (400 MHz, CDCl$_3$)** δ 12.09 (s, 1H), 8.95 – 8.88 (m, 1H), 8.11 (dd, *J* = 8.0, 1.7 Hz, 1H), 8.08 – 8.03 (m, 2H), 7.61 (ddd, *J* = 8.7, 7.2, 1.7 Hz, 1H), 7.57 – 7.49 (m, 3H), 7.13 (ddd, *J* = 8.3, 7.3, 1.2 Hz, 1H), 4.43 (q, *J* = 7.2 Hz, 2H), 1.43 (t, *J* = 7.1 Hz, 3H). **^{13}C{^{1}H} NMR (100 MHz, CDCl$_3$)** δ 168.3, 165.9, 142.0, 135.1, 134.7, 132.0, 131.1, 128.9, 127.5, 122.7, 120.6, 116.0, 69.3, 22.0. **HRMS (ESI TOF)** *m/z* calcd. For $C_{17}H_{17}NO_3Na$ $[M + Na]^+$ 306.1106 found 306.1113.

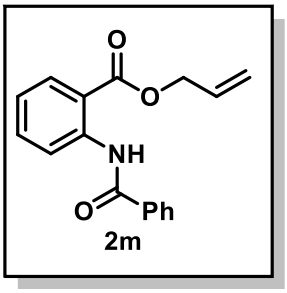
2,2,2-trifluoroethyl 2-benzamidobenzoate (2l)



2l

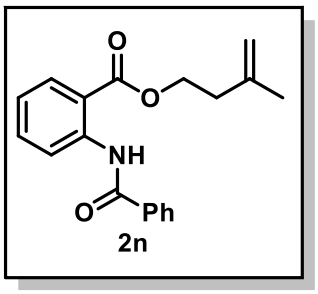
The title compound **2l** was prepared according to the general procedure (**GP1**) starting from 2-Phenylindole **1a** (0.3 mmol) in 2,2,2-trifluoroethanol. White solid (58 mg, 60% yield). **^{1}H NMR (400 MHz, CDCl$_3$)** δ 11.67 (s, 1H), 8.96 (dd, *J* = 8.5, 1.1 Hz, 1H), 8.11 (dd, *J* = 8.0, 1.7 Hz, 1H), 8.04 – 8.00 (m, 2H), 7.65 (ddd, *J* = 8.8, 7.3, 1.7 Hz, 1H), 7.59 – 7.49 (m, 3H), 7.15 (ddd, *J* = 8.3, 7.3, 1.2 Hz, 1H), 4.74 (q, *J* = 8.3 Hz, 2H). **^{13}C{^{1}H} NMR (100 MHz, CDCl$_3$)** δ 167.5, 165.7, 141.0, 137.4, 134.6, 133.4, 132.2, 128.9, 127.4, 122.2, 117.0, 115.0, 62.0, 14.2. **^{19}F NMR (377 MHz, CDCl$_3$)** δ -73.49. **HRMS (ESI TOF)** *m/z* calcd. For $C_{16}H_{12}F_3NO_3Na$ $[M + Na]^+$ 346.0667 found 346.0665.

Allyl 2-benzamidobenzoate (2m)



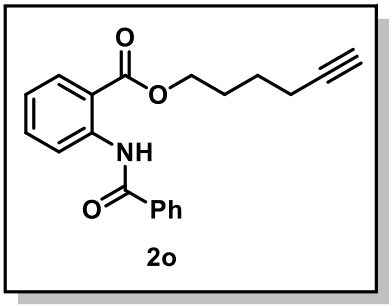
The title compound **2m** was prepared according to the general procedure (**GP1**) starting from 2-Phenylindole **1a** (0.3 mmol) in allyl acohol. White solid (60 mg, 71% yield). **^{1}H NMR (400 MHz, $CDCl_3$)** δ 12.02 (s, 1H), 8.95 (dd, *J* = 8.5, 1.2 Hz, 1H), 8.14 (dd, *J* = 8.0, 1.7 Hz, 1H), 8.09 – 8.01 (m, 2H), 7.62 (ddd, *J* = 8.8, 7.3, 1.7 Hz, 1H), 7.59 – 7.48 (m, 3H), 7.13 (ddd, *J* = 8.3, 7.3, 1.2 Hz, 1H), 6.06 (ddt, *J* = 17.1, 10.4, 5.7 Hz, 1H), 5.45 (dq, *J* = 17.2, 1.5 Hz, 1H), 5.36 – 5.31 (m, 1H), 4.87 (dt, *J* = 5.7, 1.4 Hz, 2H). **^{13}C{^{1}H} NMR (100 MHz, $CDCl_3$)** δ 168.7, 166.2, 142.4, 135.4, 135.3, 132.4, 132.1, 131.4, 129.3, 127.8, 123.1, 121.0, 119.3, 115.6, 66.4. **HRMS (ESI TOF)** *m/z* calcd. For $C_{17}H_{15}NO_3Na$ $[M + Na]^+$ 304.0950 found 304.0951.

3-methylbut-3-en-1-yl 2-benzamidobenzoate (2n)



The title compound **2n** was prepared according to the general procedure (**GP1**) starting from 2-Phenylindole **1a** (0.3 mmol) in isoprenol. White solid (56 mg, 60% yield). **^{1}H NMR (400 MHz, $CDCl_3$)** δ 12.06 (s, 1H), 8.93 (dd, *J* = 8.5, 1.2 Hz, 1H), 8.25 – 7.93 (m, 3H), 7.61 (ddd, *J* = 8.8, 7.4, 1.7 Hz, 1H), 7.57 – 7.50 (m, 3H), 7.12 (ddd, *J* = 8.3, 7.3, 1.2 Hz, 1H), 4.85 (d, *J* = 15.2 Hz, 1H), 4.48 (t, *J* = 6.7 Hz, 2H), 2.52 (d, *J* = 1.2 Hz, 1H), 1.83 (t, *J* = 1.2 Hz, 3H). **^{13}C{^{1}H} NMR (100 MHz, $CDCl_3$)** δ 168.7, 165.9, 142.0, 141.5, 135.1, 134.9, 132.1, 131.1, 129.0, 127.5, 122.8, 120.6, 115.5, 112.8, 63.8, 36.8, 22.7. **HRMS (ESI TOF)** *m/z* calcd. For $C_{19}H_{19}NO_3Na$ $[M + Na]^+$ 332.1262 found 332.1257.

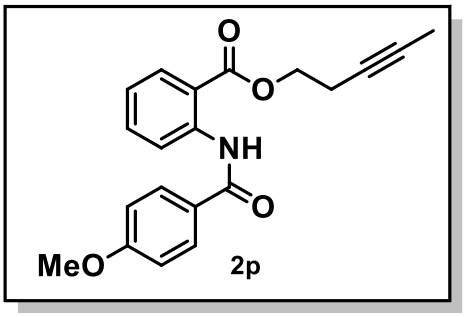
Hex-5-yn-1-yl 2-benzamidobenzoate (2o)



2o

The title compound **2o** was prepared according to the general procedure (**GP1**) starting from 2-Phenylindole **1a** (0.3 mmol) in hex-5-yn-1-ol. White solid (52 mg, 54% yield). **^{1}H NMR (400 MHz, $CDCl_3$)** δ 12.07 (s, 1H), 8.94 (dd, *J* = 8.5, 1.2 Hz, 1H), 8.09 (dd, *J* = 8.0, 1.7 Hz, 1H), 8.07 – 8.03 (m, 2H), 7.61 (ddd, *J* = 8.8, 7.3, 1.7 Hz, 1H), 7.57 – 7.50 (m, 3H), 7.13 (td, *J* = 7.7, 1.2 Hz, 1H), 4.40 (t, *J* = 6.4 Hz, 2H), 2.30 (td, *J* = 7.0, 2.7 Hz, 2H), 1.99 (t, *J* = 2.6 Hz, 1H), 1.94 (dt, *J* = 8.2, 6.6 Hz, 2H), 1.76 – 1.67 (m, 2H). **^{13}C{^{1}H} NMR (100 MHz, $CDCl_3$)** δ 168.8, 165.9, 142.1, 135.0, 135.0, 132.1, 131.0, 129.0, 127.5, 122.7, 120.6, 115.5, 83.8, 69.1, 65.1, 27.7, 25.1, 18.2. **HRMS (ESI TOF)** *m/z* calcd. For $C_{20}H_{19}NO_3Na$ $[M + Na]^+$ 344.1263 found 344.1265.

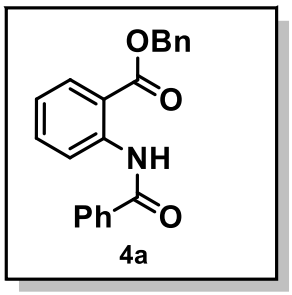
Pent-3-yn-1-yl 2-(4-methoxybenzamido) benzoate (2p)



2p

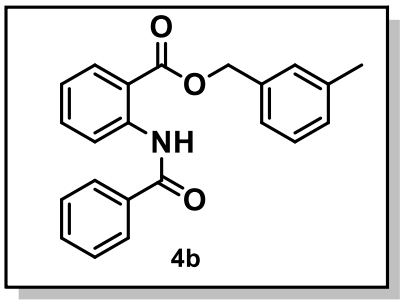
The title compound **2p** was prepared according to the general procedure (**GP1**) starting from 2-Phenylindole **1a** (0.3 mmol) in hex-5-yn-1-ol. White solid (60 mg, 65% yield). **^{1}H NMR (400 MHz, $CDCl_3$)** δ 12.01 (s, 1H), 8.94 (dd, *J* = 8.5, 1.1 Hz, 1H), 8.12 (dd, *J* = 8.0, 1.7 Hz, 1H), 8.08 – 8.01 (m, 2H), 7.61 (ddd, *J* = 8.7, 7.3, 1.7 Hz, 1H), 7.59 – 7.47 (m, 3H), 7.13 (ddd, *J* = 8.3, 7.3, 1.2 Hz, 1H), 4.42 (t, *J* = 6.9 Hz, 2H), 2.64 (tq, *J* = 7.1, 2.6 Hz, 2H), 1.78 (t, *J* = 2.5 Hz, 3H). **^{13}C{^{1}H} NMR (100 MHz, $CDCl_3$)** δ 168.5, 165.8, 142.1, 135.0, 135.0, 132.1, 131.2, 128.9, 127.5, 122.7, 120.6, 115.3, 77.9, 74.4, 63.9, 19.4, 3.6. **HRMS (ESI TOF)** *m/z* calcd. For $C_{20}H_{19}NO_4Na$ $[M + Na]^+$ 360.1212 found 360.1215.

Benzyl 2-benzamidobenzoate (4a)



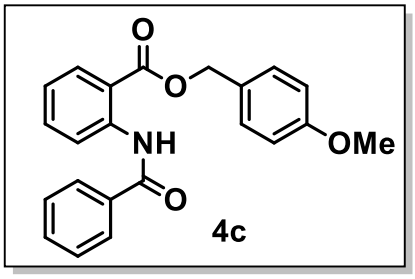
The title compound **4a** was prepared according to the general procedure (**GP2**) starting from 2-Phenylindole **1a** (0.3 mmol) and Benzyl alcohol **3a**. White solid (66 mg, 66% yield).
^{1}H NMR (400 MHz, $CDCl_3$) δ 12.04 (s, 1H), 8.95 (dd, *J* = 8.5, 1.2 Hz, 1H), 8.14 (dd, *J* = 8.0, 1.7 Hz, 1H), 8.09 – 8.04 (m, 2H), 7.65 – 7.52 (m, 4H), 7.48 – 7.38 (m, 5H), 7.12 (ddd, *J* = 8.3, 7.3, 1.2 Hz, 1H), 5.41 (s, 2H). **^{13}C{^{1}H} NMR (100 MHz, $CDCl_3$)** δ 168.4, 165.8, 142.0, 135.4, 135.0, 134.9, 132.0, 131.1, 128.8, 128.8, 128.6, 128.2, 127.4, 122.7, 120.5, 115.2, 67.1. **HRMS (ESI TOF)** *m/z* calcd. For $C_{21}H_{18}NO_3$ $[M + H]^+$ 332.1283 found 332.1284.

3-methylbenzyl 2-benzamidobenzoate (4b)



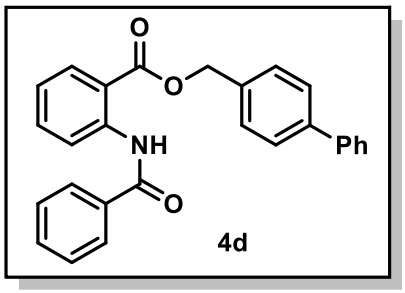
The title compound **4b** was prepared according to the general procedure (**GP2**) starting from 2-Phenylindole **1a** (0.3 mmol) and 3-methylbenzyl alcohol **3b**. White solid (66 mg, 64% yield).
^{1}H NMR (400 MHz, $CDCl_3$) δ 12.05 (s, 1H), 8.96 (dd, *J* = 8.6, 1.1 Hz, 1H), 8.15 (dd, *J* = 8.0, 1.7 Hz, 1H), 8.11 – 8.04 (m, 2H), 7.65 – 7.51 (m, 4H), 7.34 – 7.25 (m, 3H), 7.22 – 7.17 (m, 1H), 7.13 (ddd, *J* = 8.2, 7.3, 1.2 Hz, 1H), 5.38 (s, 2H), 2.40 (s, 3H). **^{13}C{^{1}H} NMR (100 MHz, $CDCl_3$)** δ 168.4, 165.8, 142.0, 138.5, 135.3, 134.9, 134.9, 132.0, 131.1, 129.3, 129.0, 128.8, 128.7, 127.4, 125.3, 122.7, 120.5, 115.3, 67.2, 21.4. **HRMS (ESI TOF)** *m/z* calcd. For $C_{22}H_{20}NO_3$ $[M + H]^+$ 346.1443 found 346.1445.

4-methoxybenzyl 2-benzamidobenzoate (4c)



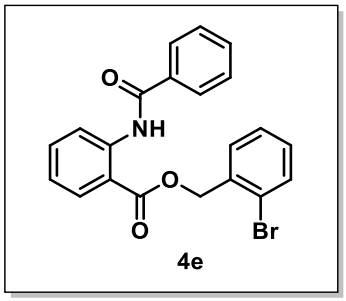
The title compound **4c** was prepared according to the general procedure (**GP2**) starting from 2-Phenylindole **1a** (0.3 mmol) and 4-methoxybenzyl alcohol **3c**. White solid (74 mg, 68% yield).**^{1}H NMR (400 MHz, CDCl$_3$)** δ 12.05 (s, 1H), 8.94 (dd, *J* = 8.5, 1.2 Hz, 1H), 8.10 (dd, *J* = 8.1, 1.6 Hz, 1H), 8.08 – 8.05 (m, 2H), 7.63 – 7.59 (m, 1H), 7.56 – 7.50 (m, 3H), 7.43 – 7.38 (m, 2H), 7.10 (ddd, *J* = 8.3, 7.3, 1.2 Hz, 1H), 6.96 – 6.91 (m, 2H), 5.34 (s, 2H), 3.82 (s, 3H). **^{13}C{^{1}H} NMR (100 MHz, CDCl$_3$)** δ 168.2, 165.5, 159.7, 141.7, 134.7, 134.6, 131.7, 130.9, 129.9, 128.6, 127.2, 122.4, 120.2, 115.1, 113.9, 66.8, 55.1. **HRMS (ESI TOF)** *m/z* calcd. For $C_{22}H_{19}NO_4Na$ $[M + Na]^+$ 384.1211 found 384.1203.

[1,1'-biphenyl]-4-ylmethyl 2-benzamidobenzoate (4d)



The title compound **4d** was prepared according to the general procedure (**GP2**) starting from 2-Phenylindole **1a** (0.3 mmol) and 4-phenylbenzyl alcohol **3d**. White solid (82 mg, 67% yield). **^{1}H NMR (400 MHz, CDCl$_3$)** δ 12.05 (s, 1H), 8.97 (dd, *J* = 8.6, 1.2 Hz, 1H), 8.17 (dd, *J* = 8.0, 1.7 Hz, 1H), 8.12 – 8.05 (m, 2H), 7.66 – 7.60 (m, 5H), 7.60 – 7.49 (m, 5H), 7.51 – 7.42 (m, 2H), 7.42 – 7.33 (m, 1H), 7.14 (ddd, *J* = 8.3, 7.2, 1.2 Hz, 1H), 5.46 (s, 2H). **^{13}C {^{1}H} NMR (100 MHz, CDCl$_3$)** δ 168.51, 165.86, 142.13, 141.64, 140.64, 135.09, 134.99, 134.41, 132.09, 131.20, 128.96, 128.94, 128.83, 127.67, 127.57, 127.53, 127.24, 122.78, 120.64, 115.28, 67.00. **HRMS (ESI TOF)** *m/z* calcd. For $C_{27}H_{21}NO_3Na$ $[M + Na]^+$ 430.1418 found 430.1416.

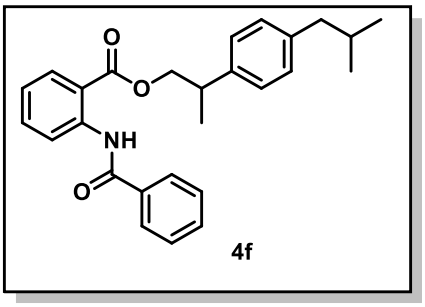
2-bromobenzyl 2-benzamidobenzoate (4e)



4e

The title compound **4e** was prepared according to the general procedure (**GP2**) starting from 2-Phenylindole **1a** (0.3 mmol) and 2-bromobenzyl alcohol **3e**. White solid (69 mg, 56% yield). **^{1}H NMR (400 MHz, $CDCl_3$)** δ 11.99 (s, 1H), 8.95 (dd, *J* = 8.5, 1.2 Hz, 1H), 8.17 (dd, *J* = 8.0, 1.6 Hz, 1H), 8.06 (dd, *J* = 8.1, 1.6 Hz, 2H), 7.66 – 7.60 (m, 2H), 7.58 – 7.47 (m, 4H), 7.36 (td, *J* = 7.6, 1.3 Hz, 1H), 7.24 (dd, *J* = 7.6, 1.7 Hz, 1H), 7.14 (ddd, *J* = 8.2, 7.3, 1.2 Hz, 1H), 5.49 (s, 2H). **^{13}C {^{1}H} NMR (100 MHz, $CDCl_3$)** δ 168.3, 165.9, 142.2, 135.2, 135.0, 134.9, 133.20, 132.1, 131.3, 130.2, 130.1, 129.0, 127.8, 127.6, 123.7, 122.9, 120.7, 115.2, 66.8. **HRMS (ESI TOF)** *m/z* calcd. For $C_{21}H_{16}BrNO_3Na$ $[M + Na]^+$ 432.0211 found 432.0214.

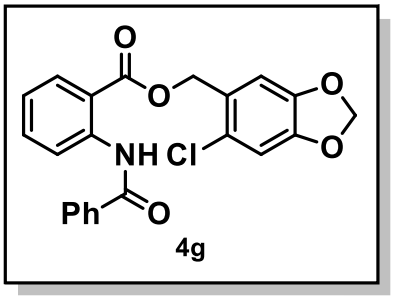
2-(4-isobutylphenyl)propyl 2-benzamidobenzoate (4f)



4f

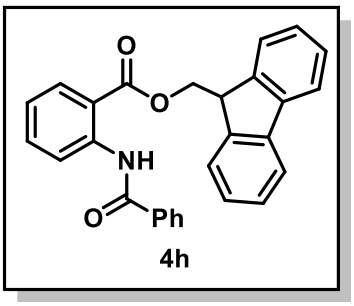
The title compound **4f** was prepared according to the general procedure (**GP2**) starting from 2-Phenylindole **1a** (0.3 mmol) and 2-(4-isobutylphenyl)propan-1-ol **3f**. White solid (64 mg, 51% yield). **^{1}H NMR (400 MHz, $CDCl_3$)** δ 12.04 (s, 1H), 8.93 (dd, *J* = 8.5, 1.2 Hz, 1H), 8.08 – 8.02 (m, 2H), 7.98 (dd, *J* = 8.0, 1.7 Hz, 1H), 7.60 (ddd, *J* = 8.8, 7.3, 1.7 Hz, 1H), 7.57 – 7.49 (m, 3H), 7.22 – 7.18 (m, 2H), 7.14 – 7.06 (m, 3H), 4.49 – 4.38 (m, 2H), 3.25 (h, *J* = 7.0 Hz, 1H), 2.45 (d, *J* = 7.2 Hz, 2H), 1.85 (dp, *J* = 13.5, 6.7 Hz, 1H), 1.42 (d, *J* = 7.0 Hz, 3H), 0.89 (d, *J* = 6.6 Hz, 6H). **^{13}C {^{1}H} NMR (100 MHz, $CDCl_3$)** δ 168.5, 165.7, 141.9, 140.3, 140.0, 134.9, 134.8, 131.9, 130.9, 129.3, 128.8, 127.4, 127.0, 122.6, 120.5, 115.4, 70.5, 45.0, 38.6, 30.2, 22.39, 22.36, 18.1. **HRMS (ESI TOF)** *m/z* calcd. For $C_{27}H_{21}NO_3Na$ $[M + Na]^+$ 415.2147 found 415.2149.

(6-chlorobenzo[d][1,3]dioxol-5-yl)methyl 2-benzamidobenzoate (4g)



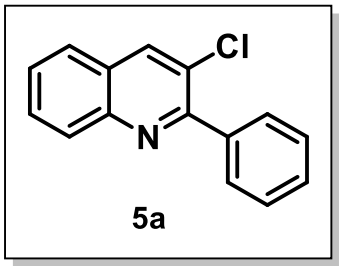
The title compound **4g** was prepared according to the general procedure (**GP2**) starting from 2-Phenylindole **1a** (0.3 mmol) and (6-chlorobenzo[*d*][1, 3]dioxol-5-yl)methanol **3g**. White solid (64 mg, 52% yield). **^{1}H NMR (400 MHz, $CDCl_3$)** δ 11.98 (s, 1H), 8.94 (dd, *J* = 8.5, 1.2 Hz, 1H), 8.12 (dd, *J* = 8.0, 1.7 Hz, 1H), 8.08 – 8.03 (m, 2H), 7.65 – 7.61 (m, 1H), 7.61 – 7.59 (m, 3H), 7.12 (ddd, *J* = 8.3, 7.3, 1.2 Hz, 1H), 6.98 (s, 1H), 6.90 (s, 1H), 6.00 (s, 2H), 5.40 (s, 2H). **^{13}C{^{1}H} NMR (100 MHz, $CDCl_3$)** δ 168.2, 165.7, 148.5, 146.8, 142.0, 135.0, 134.8, 132.0, 131.1, 128.8, 127.4, 126.4, 126.0, 122.7, 120.5, 115.0, 110.1, 109.9, 102.0, 64.5. **HRMS (ESI TOF)** *m/z* calcd. For $C_{22}H_{16}ClNO_5Na$ $[M + Na]^+$ 432.0615 found 432.0619.

(9*H*-fluoren-9-yl)methyl 2-benzamidobenzoate (4h)



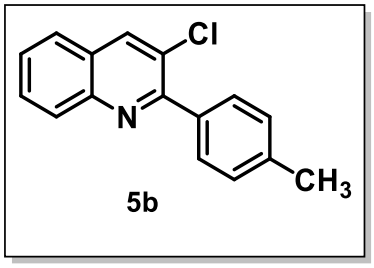
The title compound **4h** was prepared according to the general procedure (**GP2**) starting from 2-Phenylindole **1a** (0.3 mmol) and (9H-fluoren-9-yl)methanol **3h**. White solid (69 mg, 55% yield). **^{1}H NMR (400 MHz, $CDCl_3$)** δ 12.04 (s, 1H), 8.97 (dd, *J* = 8.5, 1.2 Hz, 1H), 8.14 (dd, *J* = 8.0, 1.7 Hz, 1H), 8.07 – 8.00 (m, 2H), 7.81 (dt, *J* = 7.6, 1.0 Hz, 2H), 7.68 – 7.62 (m, 3H), 7.56 – 7.48 (m, 3H), 7.43 (tt, *J* = 7.5, 0.9 Hz, 2H), 7.34 (td, *J* = 7.5, 1.2 Hz, 2H), 7.22 – 7.15 (m, 1H), 4.66 (d, *J* = 7.2 Hz, 2H), 4.42 (t, *J* = 7.2 Hz, 1H). **^{13}C{^{1}H} NMR (100 MHz, $CDCl_3$)** δ 168.6, 165.8, 143.5, 142.2, 141.4, 135.0, 134.8, 132.0,130.8, 128.8, 128.0, 127.4, 127.3, 125.0, 122.8, 120.6, 120.2, 115.1, 67.5, 46.8. **HRMS (ESI TOF)** *m/z* calcd. For $C_{28}H_{21}NO_3Na$ $[M + Na]^+$ 442.1419 found 442.1423.

3-chloro-2-phenylquinoline (5a)



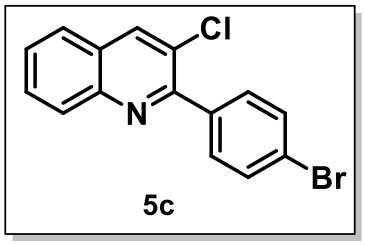
The title compound **5a** was prepared according to the general procedure (**GP3**) starting from 2-Phenylindole **1a** (0.3 mmol). White solid (55 mg, 76% yield). **^{1}H NMR (400 MHz, $CDCl_3$)** δ 8.28 (d, *J* = 0.8 Hz, 1H), 8.15 (dq, *J* = 8.5, 0.9 Hz, 1H), 7.82 – 7.8 (m, 3H), 7.73 (ddd, *J* = 8.4, 6.9, 1.5 Hz, 1H), 7.6 (ddd, *J* = 8.1, 6.9, 1.2 Hz, 1H), 7.54 – 7.5 (m, 3H). **^{13}C {^{1}H} NMR (100 MHz, $CDCl_3$)** δ 157.2, 146.5, 138.7, 136.4, 130.0, 129.7, 129.7, 129.1, 128.2, 128.0, 127.6, 127.6, 126.7. **HRMS (ESI TOF)** *m/z* calcd. For $C_{15}H_{11}ClN$ $[M + H]^+$ 240.0580 found 240.0578.

3-chloro-2-(p-tolyl)quinoline (5b)



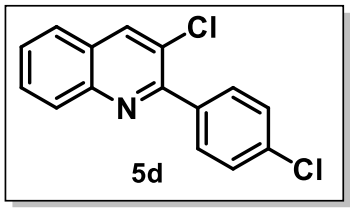
The title compound **5b** was prepared according to the general procedure (**GP3**) starting from 2-(p-tolyl)-1H-indole **1b** (0.3 mmol). White solid (56 mg, 74% yield). **^{1}H NMR (400 MHz, $CDCl_3$)** δ 8.26 (d, *J* = 0.8 Hz, 1H), 8.14 (dd, *J* = 8.6, 1.1 Hz, 1H), 7.78 (dd, *J* = 8.2, 1.4 Hz, 1H), 7.75 – 7.67 (m, 3H), 7.56 (ddd, *J* = 8.1, 6.9, 1.2 Hz, 1H), 7.32 (d, *J* = 7.9 Hz, 2H), 2.45 (s, 3H). **^{13}C {^{1}H} NMR (100 MHz, $CDCl_3$)** δ 157.2, 146.5, 139.1, 136.3, 135.9, 129.9, 129.6, 129.6, 128.9, 127.9, 127.6, 127.4, 126.6, 21.5. **HRMS (ESI TOF)** *m/z* calcd. For $C_{16}H_{13}ClN$ $[M + H]^+$ 254.0737 found 254.0736.

2-(4-bromophenyl)-3-chloroquinoline (5c)



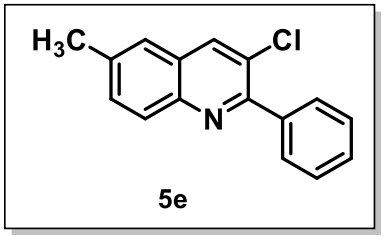
The title compound **5c** was prepared according to the general procedure (**GP3**) starting from 2-(4-bromophenyl)-1H-indole **1d** (0.3 mmol). White solid (68 mg, 71% yield). **^{1}H NMR (400 MHz, $CDCl_3$)** δ 8.28 (d, *J* = 0.9 Hz, 1H), 8.12 (dq, *J* = 8.6, 0.9 Hz, 1H), 7.80 (dd, *J* = 8.1, 1.4 Hz, 1H), 7.74 (ddd, *J* = 8.5, 6.9, 1.5 Hz, 1H), 7.71 – 7.70 (m, 2H), 7.66 – 7.62 (m, 2H), 7.70 (ddd, *J* = 8.1, 6.9, 1.2 Hz, 1H). **^{13}C{^{1}H} NMR (100 MHz, $CDCl_3$)** δ 156.3, 146.8, 137.9, 136.9, 131.8, 131.7, 130.5, 130.0, 128.4, 128.2, 127.6, 127.0, 124.0. **HRMS (ESI TOF)** *m/z* calcd. For $C_{15}H_{10}BrClN$ $[M + H]^+$ 317.9685 found 317.9686.

3-chloro-2-(4-chlorophenyl) quinoline (5d)



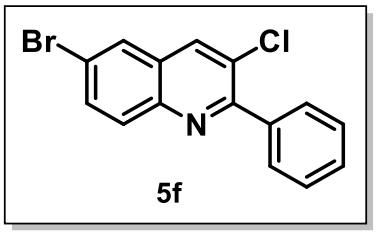
The title compound **5d** was prepared according to the general procedure (**GP3**) starting from 2-(4-bromophenyl)-1H-indole **1j** (0.3 mmol). White solid (64 mg, 77% yield). **^{1}H NMR (400 MHz, $CDCl_3$)** δ 8.28 (d, *J* = 0.9 Hz, 1H), 8.13 (dq, *J* = 8.5, 1.0 Hz, 1H), 7.81 – 7.71 (m, 4H), 7.59 (ddd, *J* = 8.1, 6.9, 1.2 Hz, 1H), 7.51 – 7.46 (m, 2H). **^{13}C{^{1}H} NMR (100 MHz, $CDCl_3$)** δ 155.6, 146.2, 136.8, 136.3, 135.0, 130.8, 129.9, 129.3, 128.2, 127.7, 127.5, 127.0, 126.4. **HRMS (ESI TOF)** *m/z* calcd. For $C_{15}H_{10}Cl_2N$ $[M + H]^+$ 274.0190 found 274.0193.

3-chloro-6-methyl-2-phenylquinoline (5e)



The title compound **5e** was prepared according to the general procedure (**GP3**) starting from 2-Phenylindole **1a** (0.3 mmol). White solid (59 mg, 78% yield). **^{1}H NMR (400 MHz, $CDCl_3$)** δ 8.17 (d, *J* = 0.8 Hz, 1H), 8.04 (d, *J* = 8.5 Hz, 1H), 7.84 – 7.75 (m, 2H), 7.61 – 7.45 (m, 6H), 2.55 (d, *J* = 0.9 Hz, 3H). **^{13}C{^{1}H} NMR (100 MHz, $CDCl_3$)** δ 156.5, 145.4, 139.1, 138.0, 136.0, 132.7, 130.0, 129.6, 129.3, 128.5, 128.4, 127.8, 125.7, 22.1 **HRMS (ESI TOF)** *m/z* calcd. For $C_{16}H_{13}ClN$ $[M + H]^+$ 254.0737 found 254.0736.

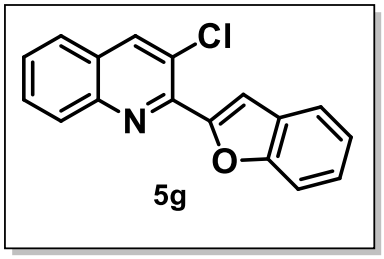
6-bromo-3-chloro-2-phenylquinoline (5f)



5f

The title compound **5a** was prepared according to the general procedure (**GP3**) starting from 5-methyl-2-phenyl-1H-indole **1f** (0.3 mmol). White solid (69 mg, 55% yield). **^{1}H NMR (400 MHz, $CDCl_3$)** δ 8.19 (s, 1H), 8.00 (d, *J* = 9.0 Hz, 1H), 7.95 (d, *J* = 2.2 Hz, 1H), 7.82 – 7.75 (m, 3H), 7.53 – 7.48 (m, 3H). **^{13}C{^{1}H} NMR (100 MHz, $CDCl_3$)** δ 157.9, 145.4, 138.6, 135.7, 133.9, 131.7, 129.9, 129.7, 129.3, 129.0, 128.9, 128.6, 122.0 **HRMS (ESI TOF)** *m/z* calcd. For $C_{15}H_{10}BrClN$ $[M + H]^+$ 317.9685 found 317.9688.

2-(benzofuran-2-yl)-3-chloroquinoline (5g)

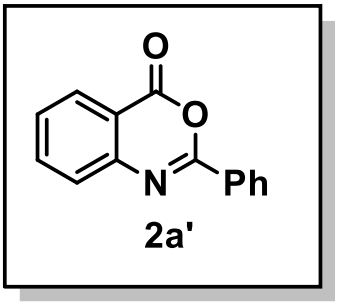


5g

The title compound **5a** was prepared according to the general procedure (**GP3**) starting from 2-(benzofuran-2-yl)-1H-indole **1k** (0.3 mmol). White solid (55 mg, 66% yield).
^{1}H NMR (400 MHz, $CDCl_3$) δ 8.31 – 8.23 (m, 2H), 7.90 (d, *J* = 0.9 Hz, 1H), 7.78 – 7.68 (m, 4H), 7.58 (ddd, *J* = 7.9, 6.8, 1.2 Hz, 1H), 7.41 (ddd, *J* = 8.2, 7.2, 1.3 Hz, 1H), 7.33 – 7.27 (m, 1H). **^{13}C{^{1}H} NMR (100 MHz, $CDCl_3$)** δ 155.2, 152.0, 146.3, 146.0, 137.3, 130.4, 129.9,

128.5, 128.1, 127.7, 126.6, 126.2, 126.1, 123.4, 122.2, 112.2, 111.7. **HRMS (ESI TOF)** *m/z* calcd. For $C_{17}H_{11}ClNO$ $[M + H]^+$ 280.0529 found 280.0527.

2-phenyl-4H-benzo[d][1,3]oxazin-4-one (2a')



^{1}H NMR (400 MHz, $CDCl_3$) δ 8.35 – 8.29 (m, 2H), 8.25 (dd, *J* = 7.9, 1.5 Hz, 1H), 7.84 (ddd, *J* = 8.1, 7.3, 1.6 Hz, 1H), 7.70 (dd, *J* = 7.9, 1.2 Hz, 1H), 7.61 – 7.55 (m, 1H), 7.52 (dddd, *J* = 8.3, 6.6, 2.5, 1.3 Hz, 4H). **^{13}C{^{1}H} NMR (100 MHz, $CDCl_3$)** δ 159.60, 157.16, 147.02, 136.59, 132.64, 130.27, 128.81, 128.77, 128.63, 128.34, 128.28, 127.25, 117.05. **HRMS (ESI TOF)** *m/z* calcd. For $C_{14}H_{10}NO_2$ $[M + H]^+$ 224.0711 found 224.0704.

5.7. Appendix V: ^{1}H, ^{13}C spectral data of representative compounds

Compound No.	Figure AIII.X	Data	Page No.
2a	Figure AV.1 and AV.2	^{1}H and ^{13}C	271
4a	Figure AV.3, AV.4,	^{1}H and ^{13}C	272
5a	Figure AV.5 and AV.6	^{1}H and ^{13}C	273
7	Figure AV.7 and AV.8	^{1}H and ^{13}C	274
9	Figure AV.9 and AV.10	^{1}H and ^{13}C	275
2a'	Figure AV.11 and AV.12	^{1}H and ^{13}C	276

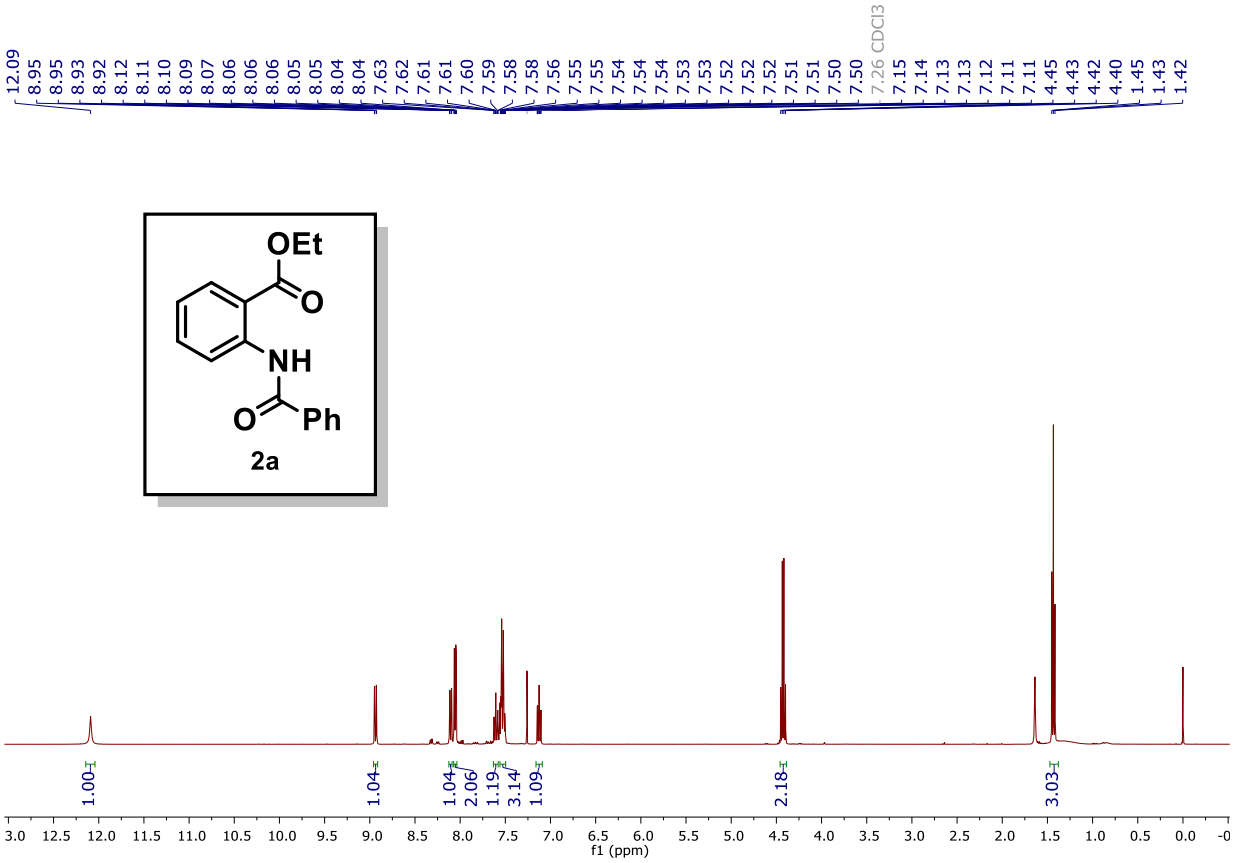


Figure AV.1: ^{1}H NMR spectrum of **2a**, $CDCl_3$, 400 MHz

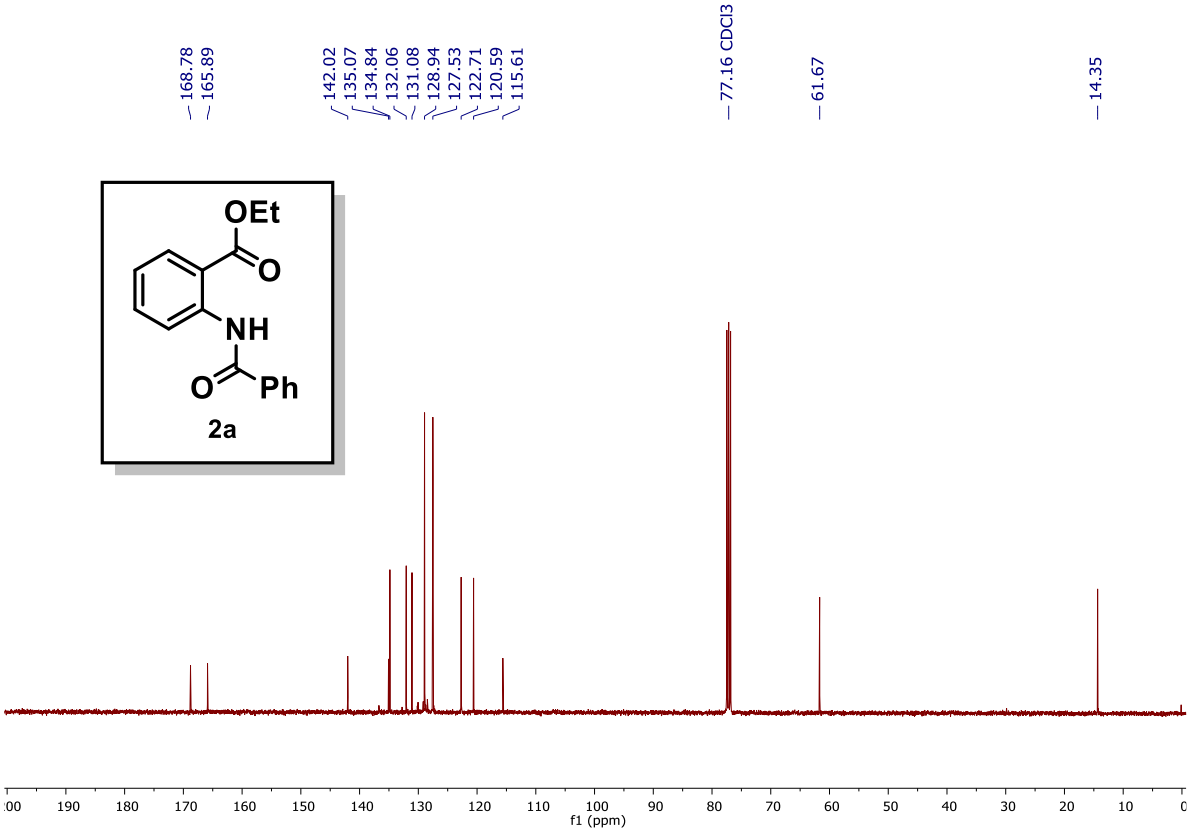


Figure AV.2: $^{13}C\{^{1}H\}$ NMR spectrum of **2a**, $CDCl_3$, 100 MHz

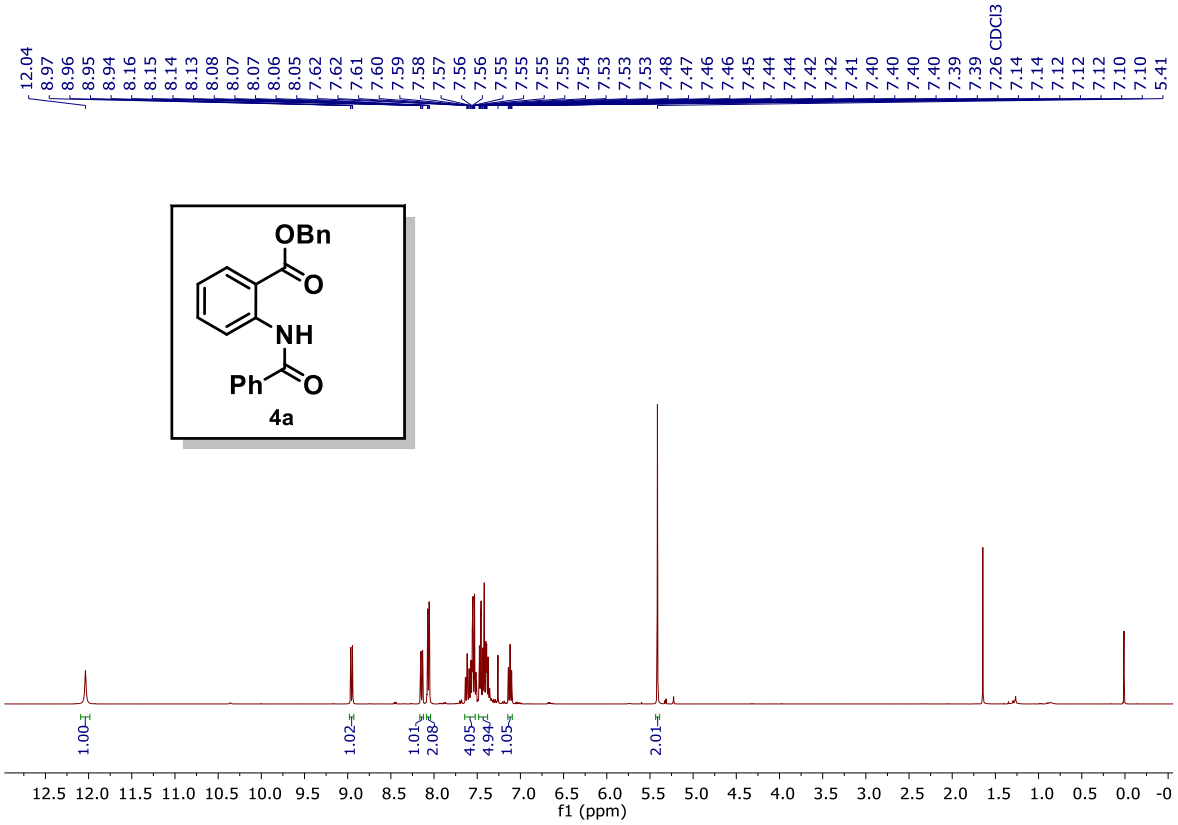


Figure AV.3: ^{1}H NMR spectrum of **4a**, $CDCl_3$, 400 MHz

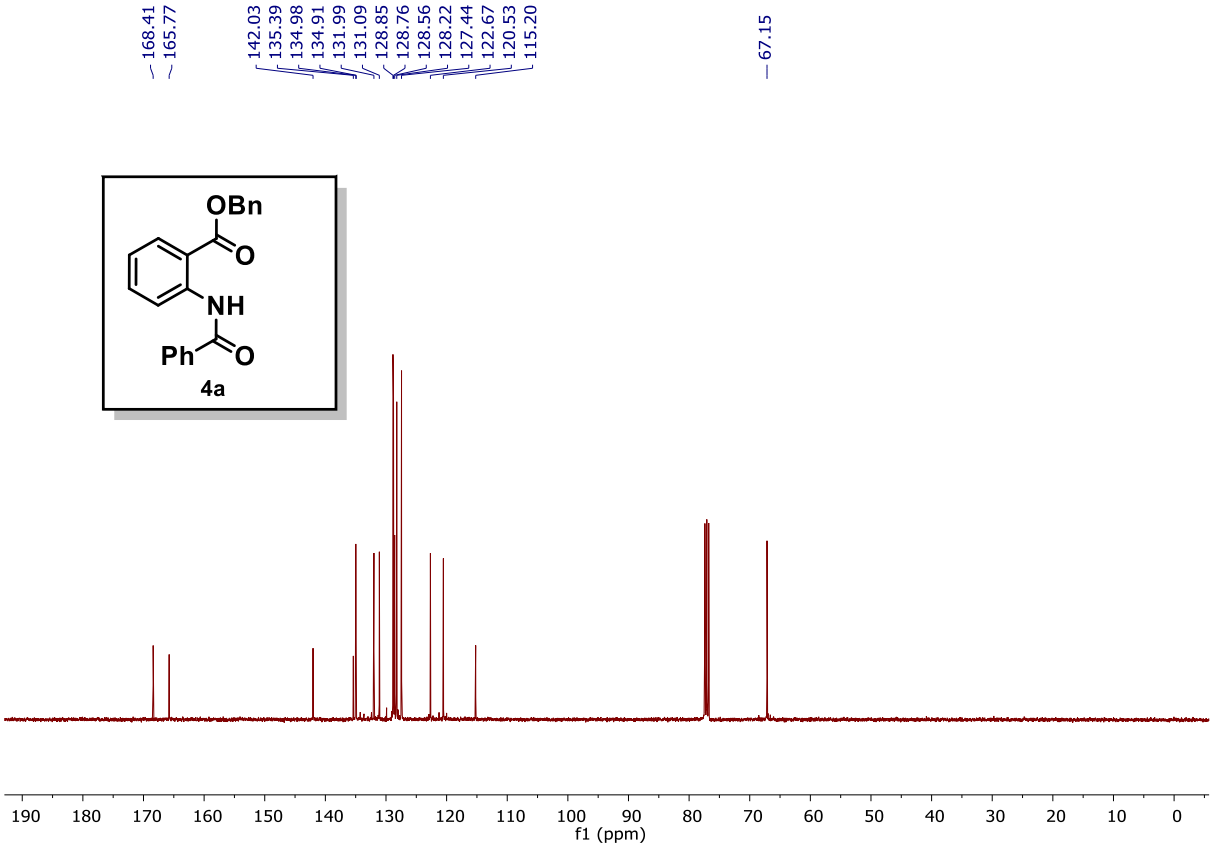


Figure AV.4: $^{13}C\{^{1}H\}$ NMR spectrum of **4a**, $CDCl_3$, 100 MHz

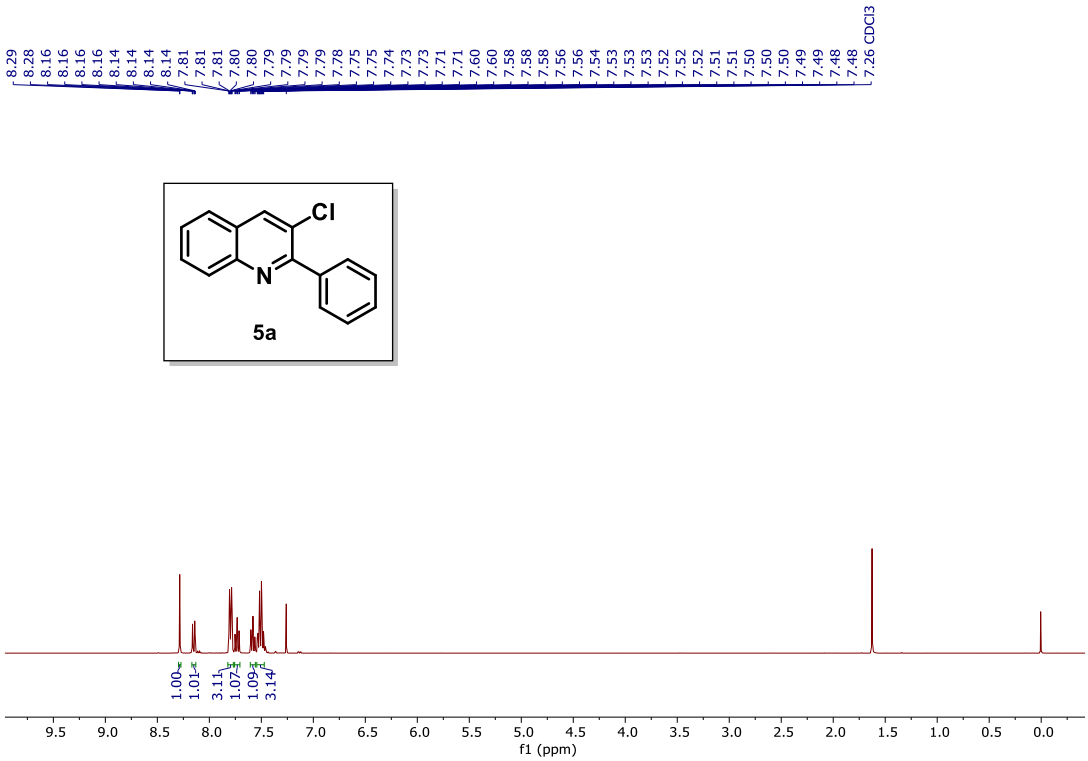


Figure AV.5: ^{1}H NMR spectrum of **5a**, $CDCl_3$, 400 MHz

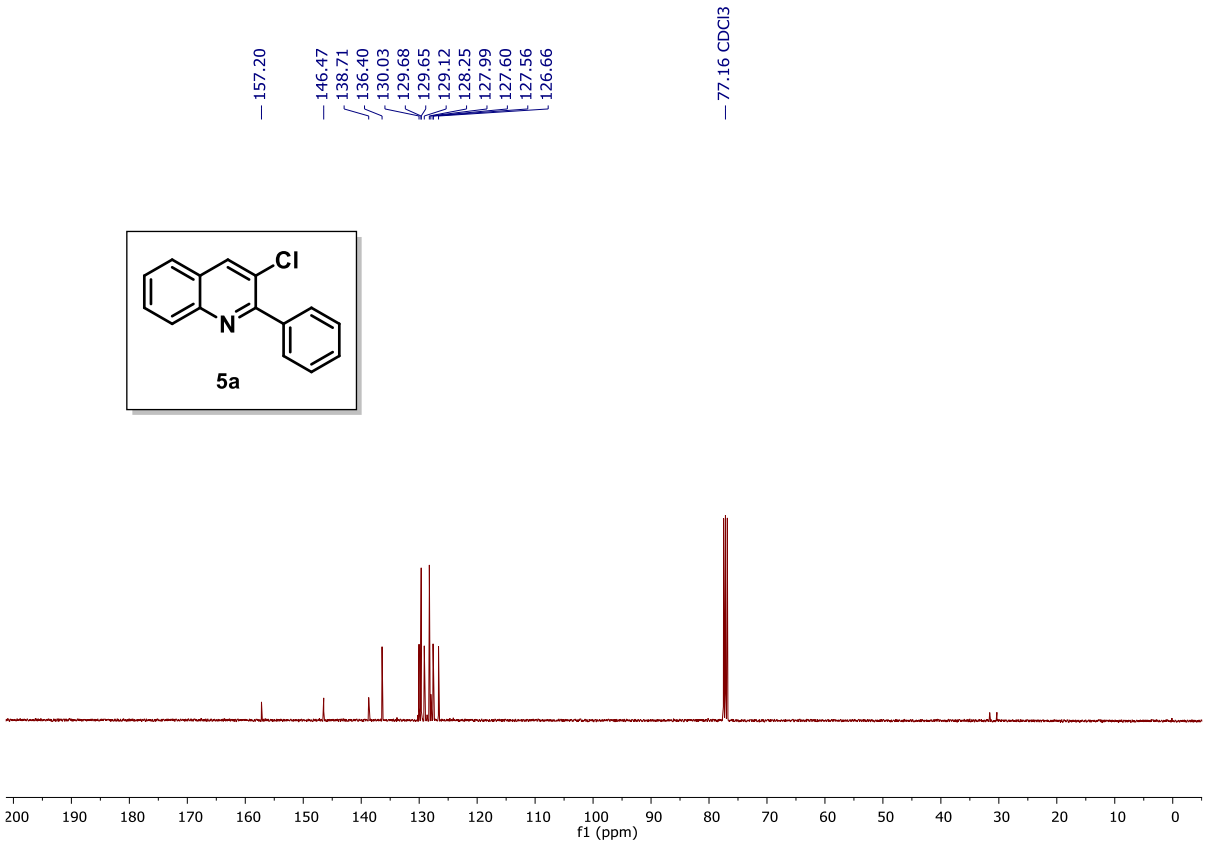


Figure AV.6: ^{13}C NMR spectrum of **5a**, $CDCl_3$, 100 MHz

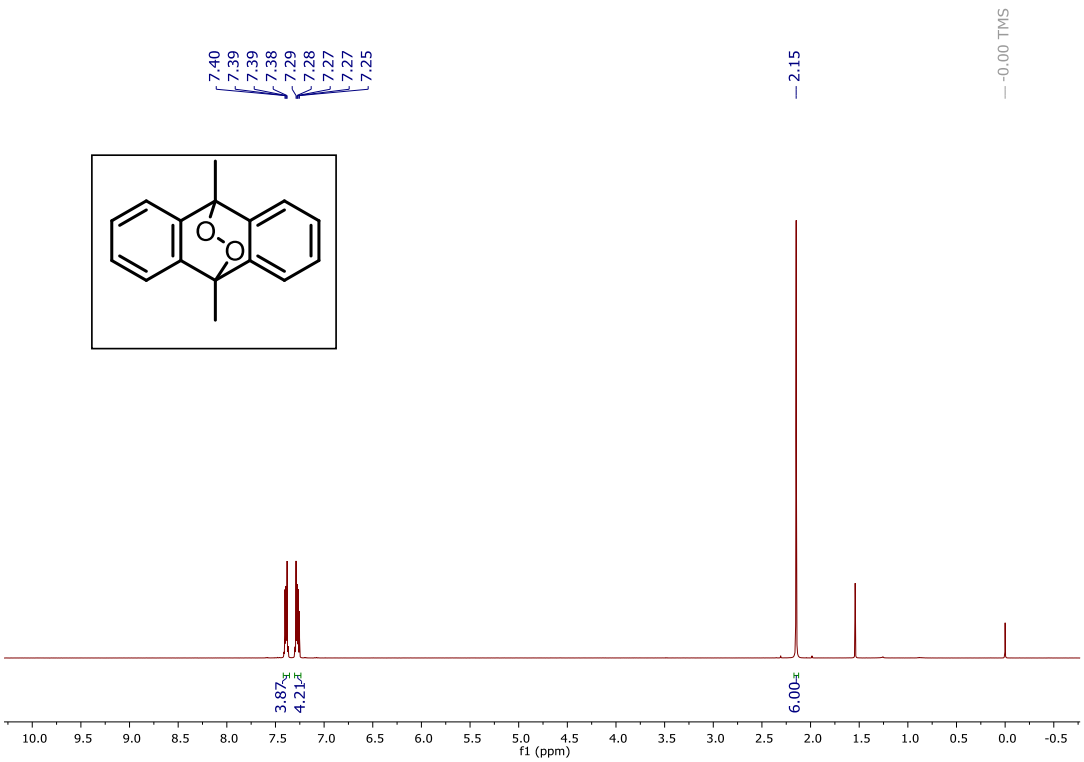


Figure AV.7: ^{1}H NMR spectrum of **7**, $CDCl_3$, 400 MHz

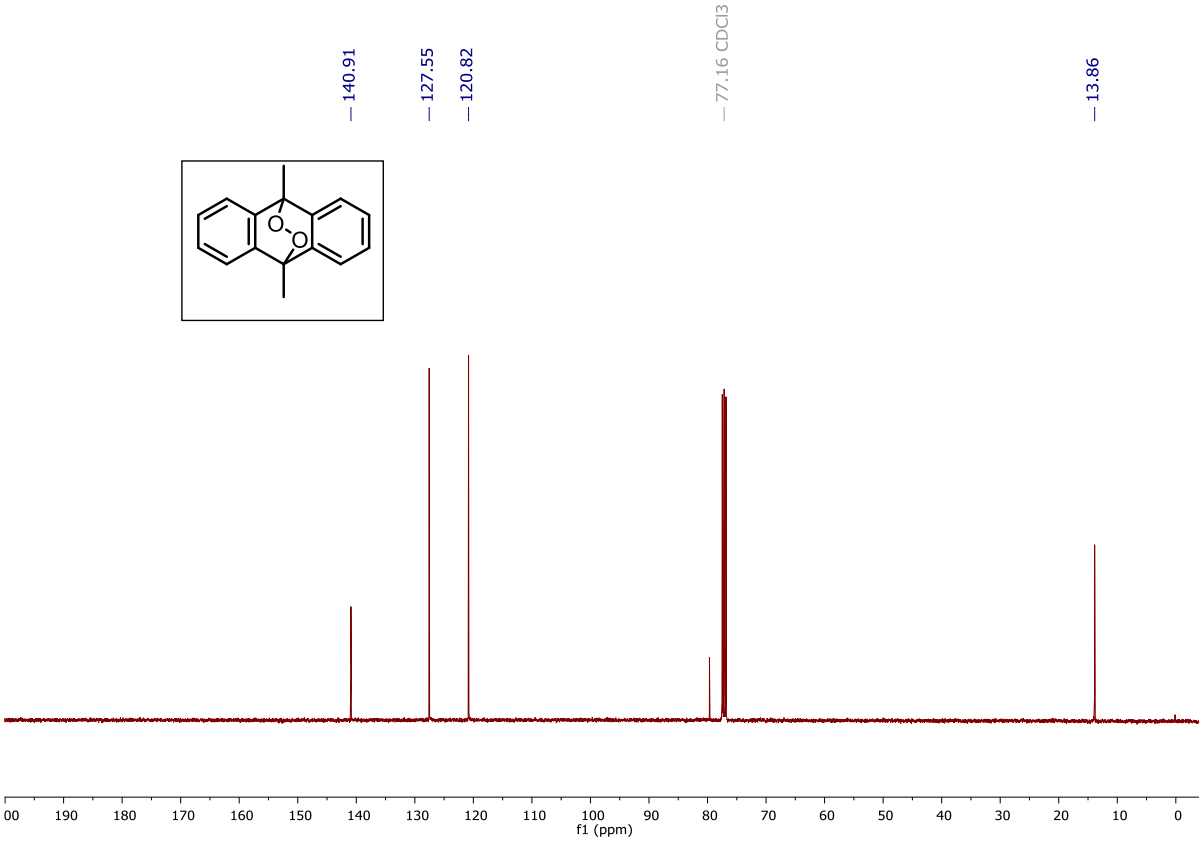


Figure AV.8: ^{13}C NMR spectrum of **7**, $CDCl_3$, 100 MHz

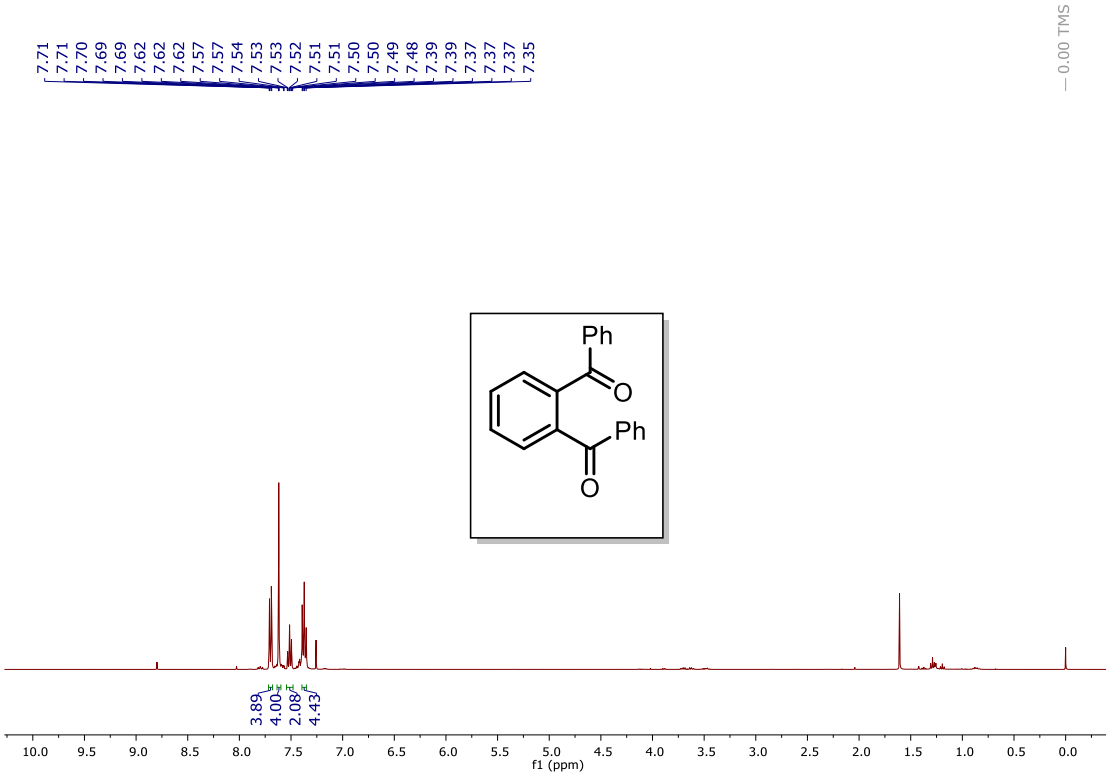


Figure AV.9: ^{1}H NMR spectrum of **9**, $CDCl_3$, 400 MHz

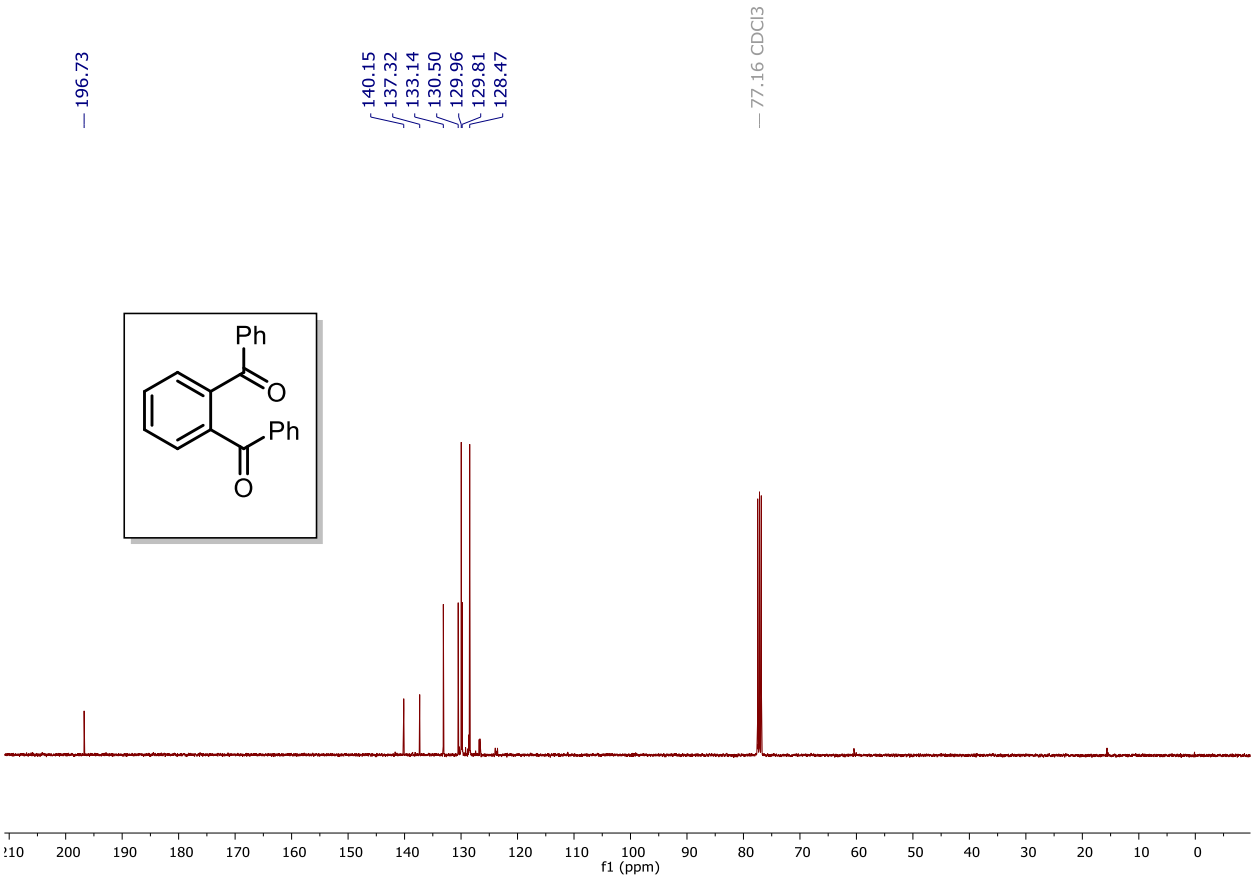


Figure AV.10: ^{13}C NMR spectrum of **9**, $CDCl_3$, 100 MHz

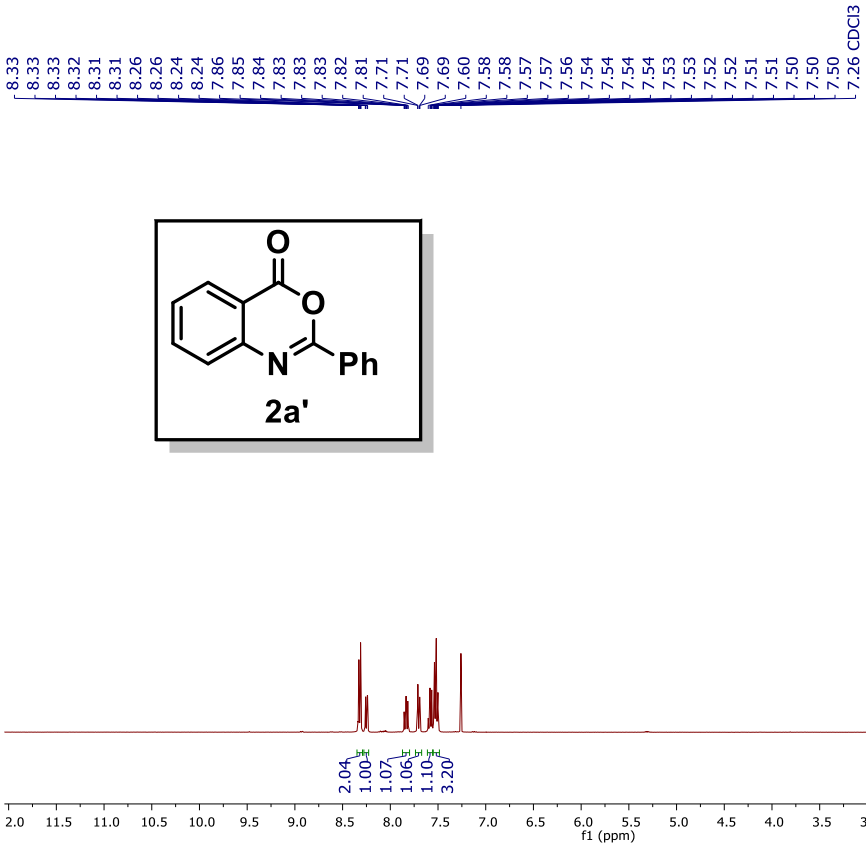


Figure AV.11: ^{1}H NMR spectrum of **2a'**, $CDCl_3$, 400 MHz

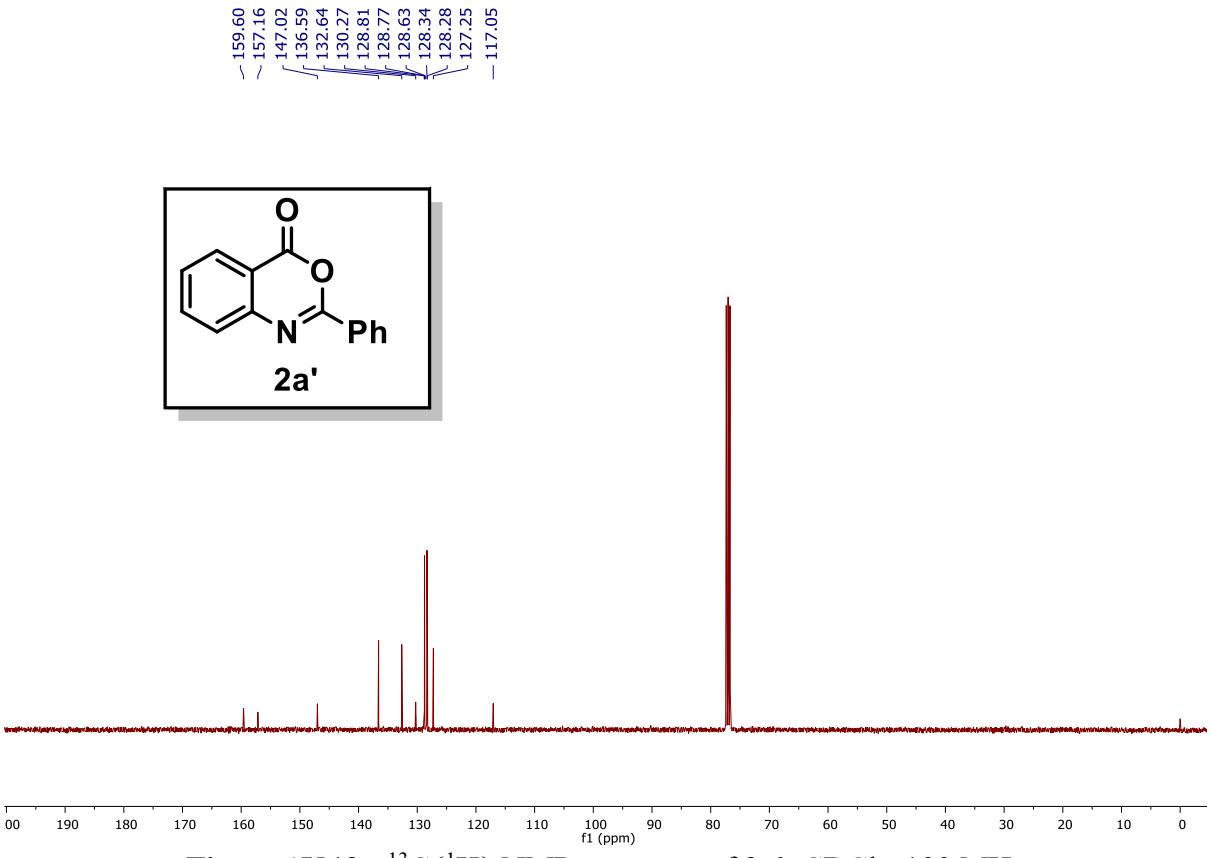


Figure AV.12: $^{13}C\{^{1}H\}$ NMR spectrum of **2a'**, $CDCl_3$, 100 MHz

5.8. References:

1. a) Elshaarawy, R. F. M., & Janiak, C. Antibacterial susceptibility of new copper (II) N-pyruvoyl anthranilate complexes against marine bacterial strains—In search of new antibiofouling candidate. *Arabian Journal of Chemistry*, **2016**, *9*, 825–834. b) Jayanthi, M., & Rajakumar, P. Synthesis and antimicrobial activity of unsymmetrical dendrimers with indazole, salicylates and anthranilates as surface units. *Journal of Heterocyclic Chemistry*, **2017**, *54*, 1963–1973. c) Prasher, P.; Sharma, M. Medicinal Chemistry of Anthranilic Acid Derivatives: A Mini Review. *Drug. Dev. Res*. **2021**, *82*, 945−958.
2. von Rymon Lipinski, G.-W.. Sweeteners. In Ullmann's Encyclopedia of Industrial Chemistry; American Cancer Society, 2015; pp 1−25. DOI: 10.1002/14356007.a26_023.pub2.
3. a) Luo, Z. W., Cho, J. S., and Lee, S. Y. Microbial production of methyl anthranilate, a grape flavour compound. *Proc. Natl. Acad. Sci*. U. S. A. **2019**, *116*, 10749–10756. b) Wang J, De Luca V (2005) The biosynthesis and regulation of biosynthesis of Concord grape fruit esters, including "foxy" methyl anthranilate. Plant J44: 606–619.
4. (a) A. Krantz, R. W. Spencer, T. F. Tam, T. J. Liak, L. J. Copp, E. M. Thomas and S. P. Rafferty, *J. Med. Chem*., **1990**, *33*, 464–479; (b) R. Padwal, *Curr. Opin. Invest. Drugs*, **2008**, *9*, 414–421.
5. (a) O. A. Olateju, C. P. Babalola, O. O. Olubiyi, O. A. Kotila, D. A. Kwasi, A. O. Oaikhena and I. N. Okeke, Quinoline antimalarials increase the antibacterial activity of ampicillin, *Front. Microbiol*., **2021**, *12*, 556550; (b) V. Sharma, D. K. Mehta and R. Das, Synthetic methods of quinoline derivatives as potent anticancer agents, Mini-Rev. *Med. Chem*., **2017**, *17*, 1557–1572.
6. K. Govindarao, N. Srinivasan, R. Suresh, R. K. Raheja, S. Annadurai, R. R. Bhandare and A. B. Shaik, Quinoline conjugated 2-azetidinone derivatives as prospective antibreast cancer agents: in vitro antiproliferative and anti-EGFR activities, molecular docking and in-silico drug likeliness studies, *J. Saudi Chem. Soc*., **2022**, *26*, 101471, DOI: 10.1016/j.jscs.2022.101471.
7. A. Kania, W. Tejchman, A. M. Pawlak, K. Mokrzynski, ´ B. R´ozanowski, B. M. Musielak and M. Greczek-Stachura, Preliminary studies of antimicrobial activity of new synthesized hybrids of 2-thiohydantoin and 2-quinolone derivatives activated with blue light, *Molecules*, **2022**, *27*, 1069, DOI: 10.3390/molecules27031069.

8. K. L. Ji, W. Liu, W. H. Yin, J. Y. Li and J. M. Yue, Quinoline alkaloids with anti-in ammatory activity from Zanthoxylum avicennae, *Org. Biomol. Chem*., **2022**, *20*, 4176–4182.
9. M. V. V. V. Prasad, R. H. R. Rao, V. Veeranna, V. S. Chennupalli and B. Sathish, Novel quinolone derivatives: synthesis and antioxidant activity, *Russ. J. Gen. Chem*., **2021**, *91*, 2522–2526.
10. R. Moodley, C. Mashaba, G. H. Rakodi, N. B. Ncube, M. V. Maphoru, M. O. Balogun, A. Jordan, D. F. Warner, R. Khan and M. Tukulula, New quinoline–urea– benzothiazole hybrids as promising antitubercular agents: synthesis, in vitro antitubercular activity, cytotoxicity studies, and in silico ADME profiling, *Pharmaceuticals*, **2022**, *15*, 576, DOI: 10.3390/ph15050576.
11. K. Murugan, C. Panneerselvam, J. Subramaniam, M. Paulpandi, R. Rajaganesh, M. Vasanthakumaran, J. Madhavan, S. S. Shafi, M. Roni, J. S. Portilla-Pulido, S. C. Mendez, J. E. Duque, L. Wang, A. T. Aziz, B. Chandramohan, D. Dinesh, S. Piramanayagam and J. S. Hwang, Synthesis of new series of quinoline derivatives with insecticidal effects on larval vectors of malaria and dengue diseases, *Sci. Rep*., **2022**, *12*, 4765, DOI: 10.1038/s41598-022-08397-5.
12. a) T. Eicher, S. Hauptmann, A. Speicher, The Chemistry of Heterocycles: Structures, Reactions, Synthesis and Applications, Wiley-VCH, Weinheim, **2013**; b) S. W. Pelletier, Alkaloids: Chemical and Biological Perspective, Springer, Vol. 13,**1999**.
13. a) D. Lachkar, N. Denizot, G. Bernadat, K. Ahamada, M. A. Beniddir, V. Du-montet, V. Gallard, J.-F. Guillot, K. Leblanc, E. O. N'nang, V. Turpin, C. Kouklovsky, E. Poupon, L. Evanno, G. Vincent, Nat. Chem. **2017**, *9*, 793–798; b) T. Tomakinian, R. Guillot, C. Kouklovsky, G. Vinvent, *Angew. Chem. Int. Ed*. **2014**, *53*, 11881–11885. c) H. Ding, P. L. DeRoy, C. Perreault, A. LarivØe, A. Siddiqui, C. G. Caldwell, S. Harran, P. G. Harran, Angew. Chem. Int. Ed. **2015**, *54*, 4818–4822.
14. a) A. T. Balaban, D. C. Oniciu, A. R. Katritzky, Chem. Rev. **2004**, *104*, 2777–2812; b) T. M. Krygowski, M. K. Cyran´ski, *Chem. Rev*. **2001**, *101*, 1385–1420.
15. a) L. Chen, J.-J. Shen, Q. Gao, S. Xu, *Chem. Sci*. **2018**, *9*, 5855–5859; b) A. Jayaraman, L. C. M. Castro, V. Desrosiers, F.-G. Fontaine, Chem. Sci. **2018**, *9*, 5057–5063; c) Y.-C. Xiao, C. Wang, Y. Yao, J. Sun, Y.-C. Chen, *Angew. Chem. Int. Ed*. **2011**, *50*, 10661–10664; d) G. Han, Q. Wang, L. Chen, Y. Liu, Q. Wang, *Adv. Synth. Catal*. **2016**, *358*, 561–566; e) C. Shen, R.-R. Liu, R.-J. Fan, Y.-L. Li, T.-F. Xu, J.-R.Gao, Y.-X. Jia, *J. Am. Chem. Soc*.

2015, *137*, 4936–4939; f) M. Kimura, M.Futamata, R. Mukai, Y. Tamaru, *J. Am. Chem. Soc*. **2005**, *127*, 4592–4593. g) Lian, X. L.; Lei, H.; Quan, X. J.; Ren, Z. H.; Wang, Y. Y.; Guan, Z. H. *Chem. Commun*. **2013**, *49*, 8196.

16. For selected reviews of visible light photocatalysis, see: (a) T. P. Yoon, M. A. Ischay and J. Du, *Nat. Chem*., **2010**, *2*, 527; (b) D. P. Hari and B. König, *Angew. Chem., Int. Ed*., **2013**, *52*, 4734; (c) M. D. Kärkäs, J. A. Porco Jr and C. R. J. Stephenson, *Chem. Rev*., **2016**, *116*, 9683; (d) D. Ravelli, S. Protti and M. Fagnoni, *Chem. Rev*., **2016**, *116*, 9850.

17. a) Zhang, L.-L.; Cao, W.-B.; Xu, X.-P.; Ji, S.-J. *Org. Chem. Front*. **2019**, *6*, 1787. b) Schilling, W.; Zhang, Y.; Riemer, D.; Das, S. Visible-Light-Mediated Dearomatisation of Indoles and Pyrroles to Pharmaceuticals and Pesticides. *Chem.−Eur. J*. **2020**, *26*, 390−395.

18. a) Y.-Z. Cheng, Q.-R. Zhao, X. Zhang and S.-L. You, *Angew. Chem., Int. Ed*., **2019**, *58*, 18069–18074; b) Chen, S.; Van Meer velt, L.; Van der Eycken, E. V.; Sharma, U. K. Visible-light-driven palladium-catalyzed radical tandem dearomatization of indoles with unactivated alkenes. *Org. Lett*. **2022**, *24*, 1213−1218.

19. Nardi, G.; Manet, I.; Monti, S.; Miranda, M. A.; Lhiaubet-Vallet, V. Scope and limitations of the TEMPO/EPR method for singlet oxygen detection: the misleading role of electron transfer. Free Radical Biology and Medicine **2014**, *77*, 64–70.

20. a) Liu, L.-H.; Wu, D.; Xia, S.-H.; Cui, G. Theoretical Study on Photooxidation Mechanism ofRuthenium Complex [Ru(II)- (Bpy)2(Tmbiimh2)]2+with Molecular Oxygen. *J. Comput. Chem*. **2016**, *37*, 2212−2219. b) Li, G.; Yan, Q.; Gong, X.; Dou, X.; Yang., D. Photocatalyst-Free Regioselective C–H Thiocyanation of 4-Anilinocoumarins under Visible Light. *ACS Sustainable Chemistry & Engineering* **2019**, *7*, 14009-14015.

Summary

Photoredox catalysis has emerged as a powerful and versatile tool in organic synthesis, enabling diverse chemical transformations that were previously challenging or inaccessible. This thesis explores the principles, applications, and recent advancements in photoredox catalysis to address contemporary challenges in the field of synthetic chemistry. The introductory section provides an overview of the fundamental concepts underlying photoredox catalysis, elucidating the mechanisms involved in light-induced electron transfer processes and their significance in promoting a wide array of organic reactions. Emphasis is placed on the unique ability of photoexcited catalysts to access high-energy intermediates and drive reactions under mild conditions, facilitating the construction of complex molecular architectures with enhanced efficiency and selectivity. Subsequent chapters showcase various protocols developed within photoredox catalysis. One such method demonstrates a versatile protocol for synthesizing α-acyloxy esters and ketones from aldehydes under visible light conditions, highlighting its adaptability to various aldehydes and functional groups, which underscores its broad applicability and robustness. Additionally, a metal-free, chemo-selective hydrogenation method for activated C-C double bonds using visible light exposure is presented. The mechanistic investigation reveals the role of activated double bonds in oxidatively quenching the photocatalyst, employing DIPEA as a sacrificial electron donor. Furthermore, an innovative one-pot synthesis of α-substituted glutaric diesters from readily available aldehydes and acrylates under visible light, without metal catalysts, is introduced. This approach demonstrates tolerance for diverse functional groups and explores the derivatives' versatility in synthesizing biologically relevant compounds.

Moreover, solvent-tunable methodologies for synthesizing anthranilic acid derivatives and quinoline derivatives from 2-phenylindole under visible light irradiation, without photocatalysts, are developed. The alcohol-based protocol involves singlet oxygen, while the chloroform-based method forms an Electron Donor-Acceptor (EDA) complex, both activated by light exposure.

ORGANIC CHEMISTRY FRONTIERS

RESEARCH ARTICLE

View Article Online
View Journal | View Issue

Published on 17 June 2021. Downloaded by Indian Institute of Science Education & Research Pune on 12/25/2023 4:35:44 AM.

Check for updates

Cite this: *Org. Chem. Front.*, 2021, **8**, 4777

Direct access to α-acyloxycarbonyl compounds and esters *via* oxidative esterification of aldehydes under visible light†‡

Anindita Bhowmick, Prakash K. Warghude, § Pankaj D. Dharpure§ and Ramakrishna G. Bhat *

Received 11th May 2021,
Accepted 10th June 2021

DOI: 10.1039/d1qo00731a

rsc.li/frontiers-organic

Herein we report the efficient synthesis of α-acyloxycarbonyl compounds and esters starting directly from aldehydes and α-bromocarbonyl compounds/benzyl bromide derivatives and bromo nitriles using an organic photocatalyst in combination with silver tetrafluoroborate under visible light at room temperature. The reaction is compatible with a variety of functional groups and has been successfully applied to the synthesis of various molecules. The strength of this protocol was effectively demonstrated by utilising both aromatic and aliphatic aldehydes. The detailed controlled studies including the labeling experiment and fluorescence spectroscopic data clearly revealed the reductive quenching of the photoredox catalytic cycle.

α-Acyloxycarbonyl compounds and esters are found in various natural products and bioactive molecules.[1] This class of compounds is well known for their antimicrobial,[2] antifungal,[3] and antiviral properties.[4] These are very useful precursors and have been explored to synthesize complex chiral molecules *via* stereoselective addition in a chelation-controlled manner.[5] Likewise, α-acyloxy ketones have been explored for the synthesis of useful heterocyclic compounds such as imidazole and oxazole derivatives.[6] Similarly, furans, cyclobutanes, and hydroxyketones have been constructed using α-acyloxycarbonyl compounds.[7] It has been demonstrated that α-acyloxy ketones are useful intermediates for synthesizing anti-inflammatory drugs.[8] Many bioactive molecules have an α-acyloxy ketone functionality in their structures (Fig. 1).[7b]

Owing to the importance of α-acyloxycarbonyl compounds and esters, efforts have been made to synthesize them through various routes. Some of the conventional methods rely on the reaction of alkaline carboxylate or carboxylic acids with α-halocarbonyl compounds[6a]/α-diazoesters.[9] Some of these methods have a narrow substrate scope and others require the preparation of starting materials. The classic esterification methods such as the Mitsunobu and Steglich reactions generate a large amount of by-product waste. In another method, the oxidative homocoupling of aryl ketones has been explored.[10] Similarly, hypervalent iodine catalysts have also been explored for the direct oxidative coupling of ketones with carboxylic acids in the presence of co-oxidants to access α-acyloxy ketones.[11] Over the years, esters have also been directly accessed starting from aldehydes as commercially viable and easily available starting materials in order to minimize the number of steps.[12]

Sudalai and co-workers have disclosed the synthesis of α-acyloxy ketones starting from aldehydes and alkenes *via* NHC catalysis under an oxygen atmosphere (Scheme 1A).[13] The visible light mediated synthesis of organic compounds has attracted the attention of the synthetic organic community due to its eco-friendly and sustainable reaction conditions.[14] A few elegant methods have been reported for the one pot synthesis of esters starting from aldehydes under visible light conditions. In 2014, for the first time, Zhu and co-workers proposed gold nanoparticle supported esterification of aldehydes under visible light.[15] In 2017, Jain and co-workers reported an esterification of aromatic aldehyde in the presence of visible

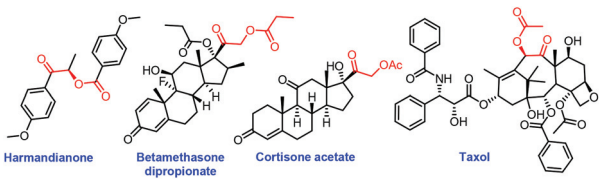


Fig. 1 Bioactive compounds containing the α-acyloxy ketone moiety.

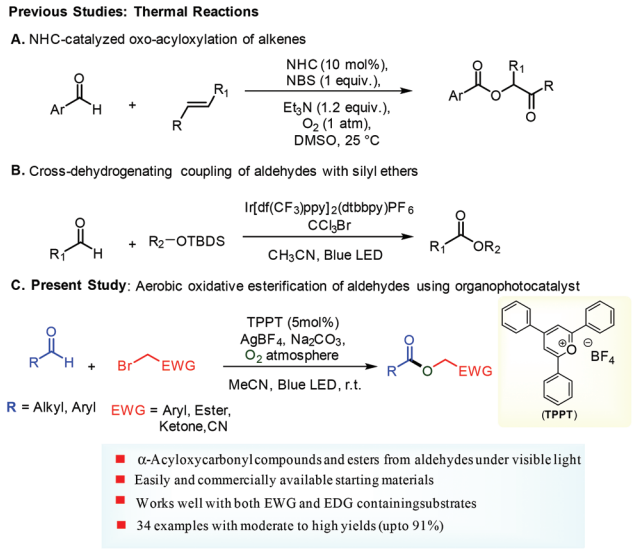
Department of Chemistry, Indian Institute of Science Education and Research (IISER) Pune, Dr. Homi Bhabha Road, Pashan, 411008 Maharashtra, India.
E-mail: rgb@iiserpune.ac.in

† Dedicated to Professor S. Chandrasekaran on the occasion of his 75th birthday.

‡ Electronic supplementary information (ESI) available. See DOI: 10.1039/d1qo00731a

§ These authors contributed equally to this work.

Published on 17 June 2021. Downloaded by Indian Institute of Science Education & Research Pune on 12/25/2023 4:35:44 AM.



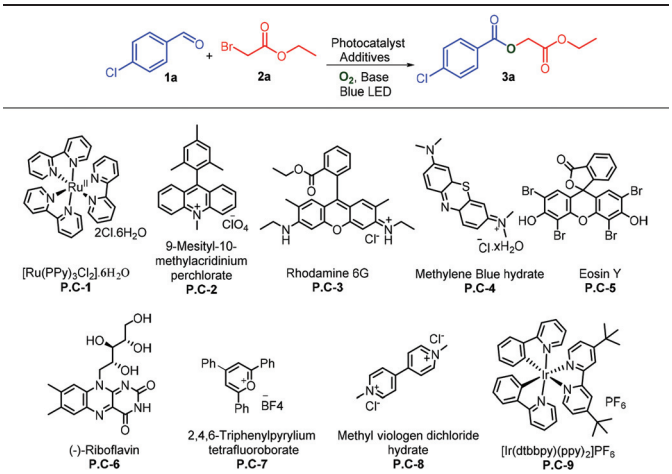
Scheme 1 Access to α-acyloxycarbonyl compounds and esters.

light and a carbon nitride based cobalt complex (Co@npg-C3N4) as a photocatalyst.[16] In 2018, Pandey and co-workers demonstrated a protocol to synthesize esters from aldehyde and silyl ethers (R-OTBS) in a cross dehydrogenating coupling manner in the presence of an iridium photocatalyst under visible light (Scheme 1B).[17] Recently, Luca and co-workers developed a visible light mediated esterification of aldehyde using trichloroisocyanuric acid (TCCA) in which the reaction proceeded through an acyl chloride intermediate.[18] Although there are very few available literature reports for the visible light mediated esterification of aldehydes, yet to the best of our knowledge, the synthesis of α-acyloxycarbonyl compounds directly from aldehyde in the presence of visible light has not been developed to date.

We hypothesized that α-acyloxycarbonyl compounds and esters could be prepared from aldehydes and α-bromocarbonyl compounds under suitable photocatalytic conditions. Herein, we wish to report the direct synthesis of different α-acyloxycarbonyl compounds starting from aldehydes under visible light conditions.

In order to validate the hypothesis, we commenced with the reaction using 4-chlorobenzaldehyde **1a** and ethyl bromoacetate **2a** as model substrates. Initially, we explored the reaction of **1a** and **2a** using PC-1 [$Ru(PPy)_3Cl_2$] as a photoredox catalyst in DMF in the presence of DIPEA (2 equiv.) under blue LED irradiation. To our delight, we obtained the desired product **3a** albeit in a poor yield and unreacted aldehyde **1a** was recovered (Table 1, entry 1). Encouraged by this initial result, we planned to screen different suitable catalysts and additives in order to optimize the reaction conditions under blue LED irradiation. We screened the reaction of **1a** and **2a** using different photoredox catalysts and DIPEA (2 equiv.) in DMF (Table 1, entries 2–9). We observed that among all the photoredox catalysts that were screened, 2,4,6-triphenylpyrylium tetrafluoroborate (**TPPT**; PC-7) proved to be relatively promising by affording the

Table 1 Optimization of reaction conditions[a]



Entry	Solvent	Catalyst	Base	Additive	Yield[e] (%)
1	DMF	PC-1	DIPEA	—	6
2	DMF	PC-2	DIPEA	—	6
3	DMF	PC-3	DIPEA	—	Trace
4	DMF	PC-4	DIPEA	—	N.R.
5	DMF	PC-5	DIPEA	—	Trace
6	DMF	PC-6	DIPEA	—	N.R.
7	DMF	PC-7	DIPEA	—	9
8	DMF	PC-8	DIPEA	—	N.R.
9	DMF	PC-9	DIPEA	—	7
10	MeCN	PC-7	DIPEA	—	15
11	$CHCl_3$	PC-7	DIPEA	—	11
12	Dioxane	PC-7	DIPEA	—	12
13	Toluene	PC-7	DIPEA	—	13
14	MeCN	PC-7	Et_3N	—	11
15	MeCN	PC-7	Na_2CO_3	—	20
16	MeCN	PC-7	K_2CO_3	—	17
17	MeCN	PC-7	Na_2CO_3	$LiBF_4$	27
18	MeCN	PC-7	Na_2CO_3	$NaBF_4$	23
19	MeCN	PC-7	Na_2CO_3	$Sc(OTf)_3$	37
20	MeCN	PC-7	Na_2CO_3	$AgSbF_6$	60
21	MeCN	PC-7	Na_2CO_3	$AgBF_4$	82
22	MeCN	PC-7	Na_2CO_3	$AgNO_3$	30
23	MeCN	PC-7	Na_2CO_3	Ag_2CO_3	50
24[b]	MeCN	PC-7	Na_2CO_3	$AgBF_4$(1)	70
25[c]	MeCN	PC-7	Na_2CO_3	$AgBF_4$(0.5)	50
26[b]	MeCN	PC-7	Na_2CO_3	$AgBF_4(H_2O)$	Trace
27[b]	MeCN	PC-7	Na_2CO_3	$AgBF_4(O_2)$	85
28	MeCN	—	Na_2CO_3	$AgBF_4$	N.R.
29	MeCN	PC-7	—	$AgBF_4$	N.R.
30[d]	MeCN	PC-7	Na_2CO_3	$AgBF_4$	N.R.

[a] Reaction conditions: Unless otherwise noted, all the reactions were carried out using 0.712 mmol of **1a**, 1.07 mmol of **2a**, 1.42 mmol of additive, 1.42 mmol of base and 0.0356 mmol (5 mol%) of photocatalyst under blue LED (15 W) irradiation at room temperature for 48 h. [b] Additive (1 equiv. of $AgBF_4$). [c] Additive (0.5 equiv. of $AgBF_4$). All the reactions were carried out under blue LED (15 W) irradiation at room temperature (monitored). [d] The reaction was carried out in the dark (no light). [e] Isolated yield after purification by column chromatography. N.R. = no reaction.

desired product **3a** in 9% yield (Table 1, entry 7). Next, acetonitrile proved to be the optimum solvent among all the solvents that were screened for the desired transformation by affording compound **3a** in 15% yield (Table 1, entries 10–13). In order to improve the yield of **3a**, we examined the effect of

 This journal is © the Partner Organisations 2021

Published on 17 June 2021. Downloaded by Indian Institute of Science Education & Research Pune on 12/25/2023 4:35:44 AM.

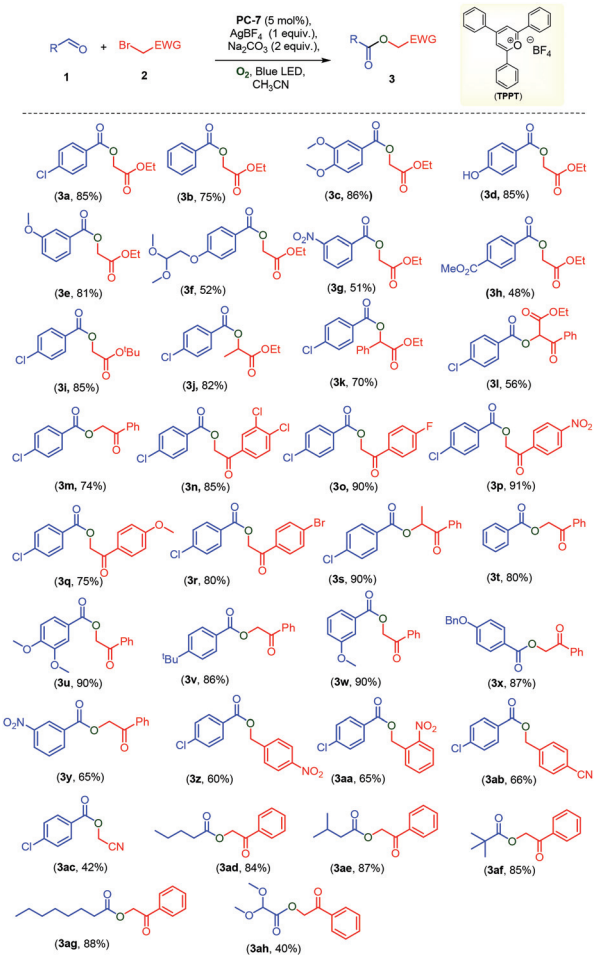
different bases on the desired transformation (Table 1, entries 14–16). We observed an incremental improvement in the yield of **3a** (20%) when Na_2CO_3 was used as a base (Table 1, entry 15). Furthermore, we switched our attention to explore the use of suitable additives for optimizing the reaction conditions. The reaction of **1a** and **2a** in the presence of a photocatalyst (**TPPT**, PC-7) in acetonitrile was screened using different additives (Table 1, entries 17–23). Gratifyingly, we observed an overwhelming increase in the yield of **3a** along with the complete consumption of aldehyde **1a** when we used $AgBF_4$ as an additive in the presence of **TPPT** in acetonitrile (82% yield, Table 1, entry 21).

Further reduction in the amount of $AgBF_4$ decreased the yield of **3a** significantly (Table 1, entries 24 and 25). In order to understand the role of moisture if any, the reaction was carried out in the presence of $AgBF_4$ and H_2O (Table 1, entry 26). Interestingly, the presence of H_2O afforded the desired product **3a** in a trace amount. As we had performed all the screening reactions under open air, we became curious to know if there is any significant role of oxygen in the reaction. In this regard, we carried out the reaction under an oxygen atmosphere (O_2 balloon) with a lower additive loading of $AgBF_4$ (1 equiv.). Interestingly, the reaction was completed in a relatively shorter time (15 h) to afford the desired product **3a** in a very good yield (85%, Table 1, entry 27).

The controlled experiments in the absence of a photoredox catalyst, a base and light (blue LED) did not succeed (Table 1, entries 28–30). These results unambiguously supported the necessity of a photoredox catalyst, a base and light for the desired transformation. Based on the exhaustive screening, 4-chlorobenzaldehyde **1a**, ethyl bromoacetate **2a**, 5 mol% of **TPPT** (PC-7), $AgBF_4$ (1 equiv.) as an additive, Na_2CO_3 (2 equiv.) in acetonitrile under an oxygen atmosphere and blue LED irradiation at room temperature proved to be the optimum reaction conditions (Table 1, entry 27).

Having obtained the standard optimized reaction conditions, we planned to explore the substrate scope for the generality of the protocol. In order to access different α-acyloxy esters, we treated ethyl bromoacetate **2a** with a variety of aldehydes **1** under the optimized reaction conditions. Aromatic aldehydes containing electron-donating groups (**1b–1f**) reacted smoothly with ethyl bromoacetate **2a** under the optimized reaction conditions to afford the corresponding α-acyloxy esters (**3b–3f**) in very good yields (up to 86%, Scheme 2), while the aromatic aldehydes containing electron-withdrawing/-deactivating groups (**1g** and **1h**) afforded the desired products (**3g and 3h**) in moderate yields (Scheme 2). It is very interesting to note that this protocol provides an access to a diester (**3h**) directly in one pot from an aldehyde which otherwise may not be accessible very easily. We observed that aromatic aldehydes containing electron-donating groups gave relatively much better yields than the compounds containing electron-withdrawing groups. This is probably due to the fact that aromatic aldehydes containing electron-withdrawing groups usually have an overall higher oxidation potential making it difficult to undergo further oxidation.[19]

In order to explore the practicality of the protocol, we treated different α-bromoesters (**2b–2e**) with 4-chlorobenzaldehyde **1a**. The corresponding α-acyloxy esters (**3i–3l**) were formed in moderate to very good yields (up to 85%, Scheme 2). We further switched our attention towards the synthesis of α-acyloxy ketones starting from different phenacyl bromides. Gratifyingly, the reaction of 4-chlorobenzaldehyde **1a** with different phenacyl bromides (**2f–2l**) proceeded smoothly to afford the corresponding α-acyloxy ketones (**3m–3s**) in good to excellent yields (up to 91%, Scheme 2). Later, in order to examine the reactivity of aldehydes, we treated phenacyl bromide **2f** with different aromatic aldehydes (**1b**, **1c**, **1e**, **1g**, **1i**, **1j**) to afford the desired products (**3t–3y**) in moderate to excellent yields (up to 90%, Scheme 2). We further explored the strength of the protocol by treating 4-chlorobenzaldehyde **1a** with different benzylic bromides (**2m–2o**). To our delight, we obtained the corresponding benzyl esters (**3z**, **3aa and 3ab**)

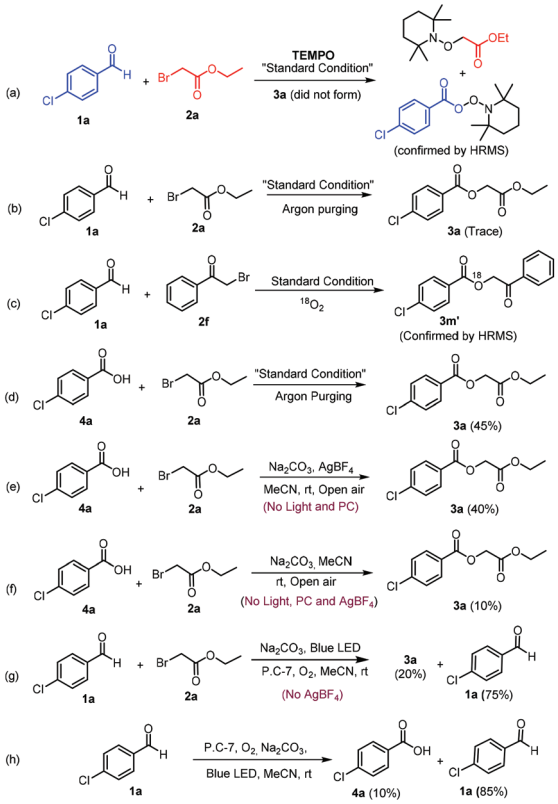


Scheme 2 Substrate scope for α-acyloxycarbonyl compounds and esters. Reaction conditions: Unless otherwise noted, all the reactions were carried out using 50 mg of **1**, 1.5 equiv. of **2**, 1 equiv. of additive $AgBF_4$, 2 equiv. of Na_2CO_3 and 5 mol% of photoredox catalyst (**TPPT**) under blue LED (15 W) irradiation at room temperature for 15–24 h (in the case of **3m** to **3y** and **3ad** to **3ah**, 1.1 equiv. of **2** were used). All the reactions were carried out under blue LED (15 W) irradiation at room temperature; yields were calculated after the purification of the product by column chromatography.

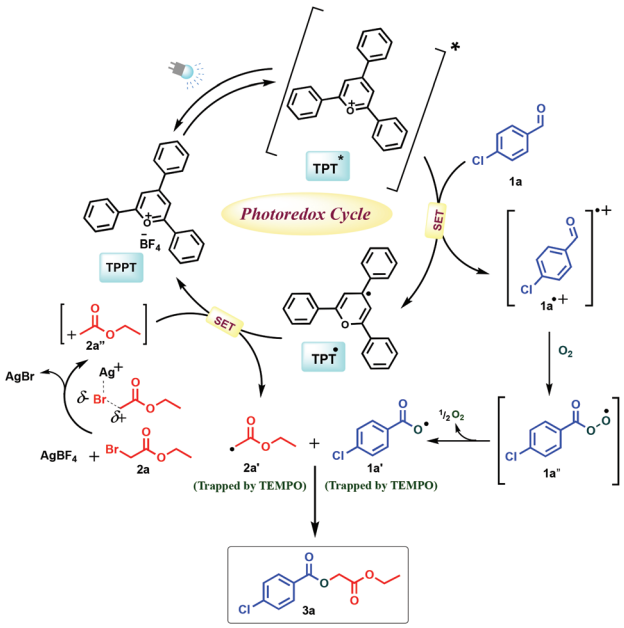
Published on 17 June 2021. Downloaded by Indian Institute of Science Education & Research Pune on 12/25/2023 4:35:44 AM.

in moderate yields. We observed that under the reaction conditions, even bromoacetonitrile (**2p**) reacted smoothly with 4-chlorobenzaldehyde **1a** to give cyanomethyl ester **3ac** in a satisfactory yield (Scheme 2).

This protocol also worked effectively with aliphatic aldehydes (**1k–1o**) to furnish the corresponding α-acyloxy ketones (**3ad–3ah**) in modest to very good yields (up to 88%, Scheme 2). To demonstrate the practicality of the protocol, the gram scale synthesis of **3m** was successfully demonstrated starting from **1a** under the optimized reaction conditions with 72% yield (see the ESI, page S24‡). In order to obtain some insight into the reaction pathway, several control experiments were carried out systematically. Initially, the reaction of **1a** and **2a** in the presence of the radical scavenger TEMPO did not afford the desired product **3a**, thus indicating the involvement of a radical intermediate during the course of the reaction (Scheme 3a). In addition, TEMPO trapped radical intermediates were confirmed by HRMS (see the ESI, pages S4 and S5‡). These results supported the *in situ* generation of carboxyl radical **1a′** as well as ethyl acetate radical **2a′** starting from aldehyde and ethyl bromoacetate respectively during the course of the reaction (see also Scheme 4). Later, we observed that the desired product **3a** was formed in a trace amount under inert atmospheric conditions thus proving the requirement of an oxygen atmosphere for the desired transformation (Scheme 3b). Furthermore, the reaction in the presence of ^{18}O labelled oxygen afforded the product **3m′** with the incorporation of labelled oxygen (Scheme 3c, for more details, see the ESI, page S6‡). This result strongly supported that oxygen is essential for the desired transformation. In order to verify the possible formation of carboxylic acid, if any, *in situ* (starting from aldehyde), we treated 4-chlorobenzoic acid **4a** with **2a** under the standard conditions as well as under an argon atmosphere independently (absence of oxygen). We observed that the desired product **3a** was formed in a modest yield (43–45%, Scheme 3d). It is evident from this result that the reaction may not be proceeding *via* the oxidation of an aldehyde to carboxylic acid followed by the substitution of ethyl bromoacetate **2a.**



Scheme 3 Control experiments.



Scheme 4 Plausible mechanism for the oxidative esterification of aldehydes.

In order to prove that this transformation was indeed a photocatalytic oxidative alkylation and not the photocatalytic oxidation of an aldehyde to carboxylic acid followed by the nucleophilic substitution of ethyl bromoacetate, we planned to carry out a few more control experiments. To begin with, we performed a reaction of 4-chlorobenzoic acid **4a** and ethyl bromoacetate **2a** under the standard conditions but in the absence of blue LED irradiation and photocatalyst PC-7. We observed that the desired product **3a** was formed in a modest yield (Scheme 3e). Next we carried out the reaction of 4-chlorobenzoic acid **4a** and ethyl bromoacetate **2a** under the standard conditions but in the absence of $AgBF_4$, blue LED irradiation and photocatalyst PC-7. To our surprise, we obtained the desired product **3a** in a very poor yield (10%, Scheme 3f). Later, the reaction of 4-chlorobenzaldehyde **1a** and ethyl bromoacetate **2a** under the standard conditions (but in the absence of $AgBF_4$) furnished the corresponding product **3a** in a poor yield and the unreacted 4-chlorobenzaldehyde **1a** was isolated in 75% yield (Scheme 3g). Finally, the reaction of

This journal is © the Partner Organisations 2021

Published on 17 June 2021. Downloaded by Indian Institute of Science Education & Research Pune on 12/25/2023 4:35:44 AM.

4-chlorobenzaldehyde **1a** in the absence of **2a** and $AgBF_4$ under an oxygen atmosphere at room temperature furnished the corresponding 4-chlorobenzoic acid **4a** in a trace amount and the unreacted 4-chlorobenzaldehyde **1a** was recovered in 85% (Scheme 3h).

Based on the observed experimental results (Scheme 3e–h), it is quite clear that a photocatalyst, light, oxygen and $AgBF_4$ are absolutely essential for the desired transformation. Also, it is evident from the results that $AgBF_4$ plays a greater role (not just reacting as a Lewis acid) and indeed it drives and sustains the photocatalytic cycle. These results strongly support the photocatalytic oxidative alkylation and not just the usual photocatalytic oxidation of an aldehyde.

Based on the previous literature reports,[20] it is known that 2,4,6-triphenylpyrylium tetrafluoroborate (**TPPT**, PC-7) catalysed reactions proceed only through the reductive quenching cycle as the catalyst is electron deficient in nature. The oxidation potential of aldehyde is +1.34 V (ref. 21) and the excited state of **TPT*** is E^*_{red} (^{3}**TPT**$^{+}$*/**TPT**$^{\bullet}$) = *ca.* +1.9 V.[20] These data suggest that the excited state of the photocatalyst can easily oxidise the aldehyde and in turn gets reduced. It is well known in the literature that the formation of $^1O_2$ from $^3O_2$ *via* energy transfer from the triplet excited species ^{3}**TPT**$^{+}$* is not possible as the electron donor (aldehyde) present in the reaction mixture can easily quench the triplet excited state ^{3}**TPT**$^{+}$* much faster than $^3O_2$.[20]

In order to obtain further insight into the detailed mechanism, we performed fluorescence quenching experiments in the presence of argon as well as oxygen independently. We observed that in both the cases, the fluorescence intensity of catalyst PC-7 was reduced with the increase in the concentration of 4-chlorobenzaldehyde **1a** and also there was no significant difference in both the fluorescence spectra (see the ESI, page S3‡). On the other hand, we did not observe any reduction in the fluorescence intensity of catalyst PC-7 in the presence of ethyl bromoacetate **2a** (see the ESI, page S4‡). This result clearly indicated that oxygen is not directly involved during the reductive quenching cycle thus supporting the significant role of 4-chlorobenzaldehyde **1a** in the reductive quenching. The reduction potentials of ethyl bromoacetate and **TPPT** are −1.08 V and −0.28 V *vs.* SCE respectively.[22] These values signify that it is almost difficult for the catalyst **TPPT** to reduce ethyl bromoacetate. However, to our surprise, we observed that the yield of the desired product **3a** was increased by the addition of $AgBF_4$. Based on this experimental result, we can surmise that $AgBF_4$ might be lowering the reduction potential of ethyl bromoacetate probably either *via* generation of the corresponding short-lived ethyl acetate cation **2a**$^+$ or by the enhancement of the electrophilicity of **2a** through coordination (see Scheme 4). Based on the reduction potential, we believe that possibly **TPT**$^{\bullet}$ may be reducing the cationic species **2a**″ or highly polarised ethyl acetate *via* the SET mechanism to generate ethyl acetate radical **2a**′ (see Scheme 4).

Based on the previous literature reports[21] and the control experiments that we have carried out, the most probable photoredox catalytic cycle is proposed in Scheme 4. Upon visible light irradiation, the catalyst **TPPT** (PC-7) gets excited to **TPT***. This in turn gets reductively quenched by 4-chlorobenzaldehyde **1a** *via* a single electron transfer (SET) mechanism leading to the formation of a carbonyl radical cation intermediate (**1a**$^{\bullet+}$) along with the generation of reduced **TPT**$^{\bullet}$. Furthermore, the radical cation (**1a**$^{\bullet+}$) reacts with oxygen to form the reactive carboxyl radical **1a**′ probably *via* the formation of 4-chlorobenzoylperoxy radical **1a**″. It is proposed that in the presence of $AgBF_4$, ethyl bromoacetate **2a** is believed to get reduced to ethyl acetate radical **2a**′ (most probably *via* cationic species **2a**″ or highly polarised ethyl acetate) by interacting with **TPT**$^{\bullet}$ *via* a SET mechanism to complete the photoredox catalytic cycle. Finally, the radical–radical coupling of **1a**′ and **2a**′ furnishes the desired product **3a**.[23]

In summary, we have successfully demonstrated the synthesis of α-acyloxycarbonyl compounds and esters starting directly from aldehydes under visible light. The generality of the protocol was demonstrated by the synthesis of various α-acyloxy esters and α-acyloxy ketones. Aromatic as well as aliphatic aldehydes worked efficiently and different functional groups tolerated the reaction conditions. We have successfully demonstrated the strength of the protocol by exploring a wide range of substrates containing different functional groups to access useful compounds using a clean energy source. Based on systematic controlled experiments and other observations, a reductive quenching photoredox catalytic cycle for this transformation has been proposed.

Conflicts of interest

There are no conflicts to declare.

Acknowledgements

R. G. B. thanks the Science and Engineering Research Board, Department of Science and Technology (SERB-DST), New Delhi, Government of India (File no: CRG/2019/005753) for the generous research grant. A. B. and P. D. D. thank the CSIR, New Delhi for the fellowship. P. K. W. thanks the UGC, New Delhi for the fellowship. The authors thank Dr Utpal Das for providing ^{18}O labelled oxygen. The authors thank IISER Pune for the financial assistance. The authors also thank Mr Abhijit Chatterjee, IISER Pune for helping in obtaining the fluorescence spectra and for the useful discussions.

Notes and references

1 (*a*) S. Murahashi, T. Saito, H. Hanaoka, Y. Murakami, T. Naota, H. Kumobayashi and S. Akutagawa, Ruthenium-catalyzed oxidative transformation of alkenes to alpha.-ketols with peracetic acid. Simple synthesis of cortisone acetate, *J. Org. Chem.*, 1993, **58**, 2929–2930; (*b*) J. M. Gao, S. X. Yang and J. C. Qin, Azaphilones: Chemistry and

Published on 17 June 2021. Downloaded by Indian Institute of Science Education & Research Pune on 12/25/2023 4:35:44 AM.

Biology, *Chem. Rev.*, 2013, **113**, 4755–4811; (*c*) C. Sun, D. K. Hunt, C. L. Chen, Y. Deng, M. He, R. B. Clark, C. Fyfe, T. H. Grossman, J. A. Sutcliffe and X. Y. Xiao, Design, synthesis, and biological evaluation of hexacyclic tetracyclines as potent, broad spectrum antibacterial agents, *J. Med. Chem.*, 2015, **58**, 4703–4712; (*d*) J. A. Vida, C. M. Samour, M. H. O'Dea and T. S. T. Wang, Analgesics. 2. Selected 5-substituted 5-(1-phenylethyl)-barbituric acids, *J. Med. Chem.*, 1974, **17**, 1194–1197; (*e*) J. A. Vida, C. M. Samour, M. H. O'Dea, T. S. T. Wang, W. R. Wilber and J. F. Reinhard, Analgesics. 1. Selected 5-substituted 5- propionoxybarbituric acids, *J. Med. Chem.*, 1974, **17**, 732–736.

2 (*a*) Y. Che, J. B. Gloer, B. Koster and D. Malloch, Decipinin A and Decipienolides A and B: New bioactive metabolites from the coprophilous fungus Podospora decipiens, *J. Nat. Prod.*, 2002, **65**, 916–919; (*b*) X. Wang, J. G. Sena Filho, A. R. Hoover, J. B. King, T. K. Ellis, D. R. Powell and R. H. Cichewicz, Chemical epigenetics alters the secondary metabolite composition of guttate excreted by an atlantic-forest-soil-derived Penicillium citreonigrum, *J. Nat. Prod.*, 2010, **73**, 942–948; (*c*) P. Wang, W. Kim, L. B. Pickens, X. Gao and Y. Tang, Heterologous expression and manipulation of three tetracycline biosynthetic pathways, *Angew. Chem., Int. Ed.*, 2012, **51**, 11136–11140; (*d*) Z. Wang, Y. Sheng, H. Duan, Q. Yu, W. Shi and S. Zhang, New haptens synthesis, antibody production and comparative molecular field analysis for tetracyclines, *RSC Adv.*, 2014, **4**, 53788–53794.

3 (*a*) T. Fukuda, A. Matsumoto, Y. Takahashi, H. Tomoda and S. Omura, Phenatic acids A and B, new potentiators of antifungal miconazole activity produced by Streptomyces sp. K03–0132, *J. Antibiot.*, 2005, **58**, 252–259; (*b*) L. Lin, N. Mulholland, Q.-Y. Wu, D. Beattie, S.-W. Huang, D. Irwin, J. Clough, Y.-C. Gu and G.-F. Yang, Synthesis and antifungal activity of novel sclerotiorin analogues, *J. Agric. Food Chem.*, 2012, **60**, 4480–4491; (*c*) H. Yamazaki, S. Omura and H. Tomoda, 6′-Hydroxy-3′-methoxymitorubrin, a new potentiator of antifungal miconazole activity, produced by Penicillium radicum FKI-3765–2, *Chem. Pharm. Bull.*, 2010, **58**, 829–832.

4 (*a*) H. Wang, Y. Wang, W. Wang, P. Fu, P. Liu and W. Zhu, Antiinfluenza virus polyketides from the acid-tolerant fungus Penicillium purpurogenum JS03–21, *J. Nat. Prod.*, 2011, **74**, 2014–2018; (*b*) X.-L. Sun, T. Hiroaki, M. Keiichi, T. Haruo, F. Kimio and O. Satoshi, Synthesis and inhibitory activities of isochromophilone analogues against gp120-CD4 binding, *J. Antibiot.*, 1996, **49**, 689–692.

5 M. Yasuda, K. Okamoto, T. Sako and A. Baba, Highly stereoselective addition to alkoxy or hydroxy ketones using an α-stannyl ester–stannous chloride system in a chelation-controlled manner, *Chem. Commun.*, 2001, **2**, 157–158.

6 (*a*) L. Liu, S. Feng and C. Li, Practical Approach for Quantitative Green Esterifications, *ACS Sustainable Chem. Eng.*, 2016, **4**, 6754–6762; (*b*) P. F. Carneiro, B. Gutmann, R. O. M. A. de Souza and C. O. Kappe, Process Intensified Flow Synthesis of 1H-4-Substituted Imidazoles: Toward the Continuous Production of Daclatasvir, *ACS Sustainable Chem. Eng.*, 2015, **3**, 3445–3453.

7 (*a*) G. Cignarella, D. Barlocco, D. Pocar, F. Clerici, M. M. Curzu, G. L. Gessa, F. Fadda, M. Serra and G. Biggio, Synthesis and pharmacological evaluation of a new series of substituted benzoyl-γ-butyrolactone derivatives, *Eur. J. Med. Chem.*, 1995, **30**, 721–726; (*b*) P. K. Prasad, R. N. Reddi and A. Sudalai, Recent methods for the synthesis of α-acyloxy ketones, *Org. Biomol. Chem.*, 2018, **16**, 9334–9348.

8 (*a*) J. Chen, D. Liu, N. Butt, C. Li, D. Fan, Y. Liu and W. Zhang, Palladium–Catalyzed Asymmetric Hydrogenation of α–Acyloxy–1—arylethanones, *Angew. Chem., Int. Ed.*, 2013, **52**, 11632–11636; (*b*) B. Vigante, M. Rucins, A. Plotniece, K. Pajuste, I. Luntena, B. Cekavicus, E. Bisenieks, R. Smits, G. Duburs and A. Sobolev, Direct Aminolysis of Ethoxycarbonylmethyl 1, 4-Dihydropyridine-3-carboxylates, *Molecules*, 2015, **20**, 20341–20354.

9 (*a*) L. Dumitrescu, K. Azzouzi-Zriba, D. Bonnet-Delpon and B. Crousse, Nonmetal Catalyzed Insertion Reactions of Diazocarbonyls to Acid Derivatives in Fluorinated Alcohols, *Org. Lett.*, 2011, **13**, 692–695; (*b*) Y. Wang, H. Cui, L. Zhang and C.-Y. Su, An Acid Stable Metal–Organic Framework as an Efficient and Recyclable Catalyst for the O—H Insertion Reaction of Carboxylic Acids, *ChemCatChem*, 2018, **17**, 3901–3906.

10 L. Tan, C. Chen and W. Liu, α-Acetoxyarone synthesis via iodine-catalyzed and tert-butyl hydroperoxide-mediateded self-intermolecular oxidative coupling of aryl ketones, *Beilstein J. Org. Chem.*, 2017, **13**, 1079–1084.

11 (*a*) R. N. Reddi, P. K. Prasad and A. Sudalai, I_2-Catalyzed Regioselective Oxo- and Hydroxy-acyloxylation of Alkenes and Enol Ethers: A Facile Access to α-Acyloxyketones, Esters, and Diol Derivatives, *Org. Lett.*, 2014, **16**, 5674–5677; (*b*) T. Dohi, A. Maruyama, M. Yoshimura, K. Morimoto, H. Tohma and Y. Kita, Versatile hypervalent-iodine(III) catalyzed oxidations with m-chloroperbenzoic acid as a co-oxidant, *Angew. Chem., Int. Ed.*, 2005, **44**, 6193–6196; (*c*) M. Ochiai and K. Miyamoto, Catalytic Version of and Reuse in Hypervalent Organo-λ3 - and -λ5-iodane Oxidation, *Eur. J. Org. Chem.*, 2008, 4229–4239; (*d*) J. Huang, L.-T. Li, H.-Y. Li, E. Husan, P. Wang and B. Wang, Bu_4NI-catalyzed benzylic acyloxylation of alkylarenes with aromatic aldehydes, *Chem. Commun.*, 2012, **48**, 10204–10206; (*e*) M. Uyanik, D. Suzuki, T. Yasui and K. Ishihara, In Situ Generated (Hypo)Iodite Catalysts for the Direct α-Oxyacylation of Carbonyl Compounds with Carboxylic Acids, *Angew. Chem., Int. Ed.*, 2011, **50**, 5331–5334; (*f*) S. Guo, J. T. Yu, Q. Dai, H. Yang and J. Cheng, The Bu_4I-catalyzed alfa-acyloxylation of ketones with benzylic alcohols, *Chem. Commun.*, 2014, **50**, 6240–6242.

12 (*a*) K. Ekoue-Kovi and C. Wolf, One–Pot Oxidative Esterification and Amidation of Aldehydes, *Chem. – Eur. J.*, 2008, **21**, 6302–6315; (*b*) J. B. Feng, J. L. Gong and X. F. Wu, Calcium and magnesium chlorides-catalyzed oxidative esterification of aromatic aldehydes, *Tetrahedron Lett.*,

 This journal is © the Partner Organisations 2021

Published on 17 June 2021. Downloaded by Indian Institute of Science Education & Research Pune on 12/25/2023 4:35:44 AM.

2014, **9**, 1657–1659; (*c*) R. A. Green, D. Pletcher, S. G. Leach and R. C. D. Brown, N-Heterocyclic Carbene-Mediated Oxidative Electrosynthesis of Esters in a Microflow Cell, *Org. Lett.*, 2015, **17**, 3290–3293; (*d*) S. Gaspa, A. Porcheddu and L. De Luca, Recent developments in oxidative esterification and amidation of aldehydes, *Tetrahedron Lett.*, 2016, **31**, 3433–3440; (*e*) D. J. Jeong, S. B. Lee and J. C. Lee, Direct Oxidation of Aldehydes to Methyl Esters with Urea Hydrogen Peroxide and *p*-Toluenesulfonyl Chloride, *Lett. Org. Chem.*, 2017, **10**, 725–728; (*f*) E. E. Finney, K. A. Ogawa and A. J. Boydston, Organocatalyzed Anodic Oxidation of Aldehydes, *J. Am. Chem. Soc.*, 2012, **134**, 12374–12377; (*g*) B. E. Marki and K. A. Scheidt, N-Heterocyclic Carbene-Catalyzed Oxidation of Unactivated Aldehydes to Esters, *Org. Lett.*, 2008, **10**, 4331–4334; (*h*) D. Talukdar, K. Sharma, S. K. Bharadwaj and A. J. Thakur, $VO(acac)_2$: An Efficient Catalyst for the Oxidation of Aldehydes to the Corresponding Acids in the Presence of Aqueous H_2O_2, *Synlett*, 2013, 963–966; (*i*) N. Mori and H. Togo, Facile oxidative conversion of alcohols to esters using molecular iodine, *Tetrahedron*, 2005, **61**, 5915–5925; (*j*) B. R. Travis, M. Sivakumar, G. O. Hollist and B. Borhan, Facile Oxidation of Aldehydes to Acids and Esters with Oxone, *Org. Lett.*, 2003, **5**, 1031–1034; (*k*) S. Gaspa, A. Porcheddu and L. De Luca, Metal-Free Direct Oxidation of Aldehydes to Esters Using TCCA, *Org. Lett.*, 2015, **17**, 3666–3669; (*l*) Y. Zhu, H. Yan, L. Lu, D. Liu, G. Rong and J. Mao, Copper-Catalyzed Methyl Esterification Reactions via C-C Bond Cleavage, *J. Org. Chem.*, 2013, **78**, 9898–9905; (*m*) S. De Sarkar, S. Grimme and A. Studer, NHC Catalyzed Oxidations of Aldehydes to Esters: Chemoselective Acylation of Alcohols in Presence of Amines, *J. Am. Chem. Soc.*, 2010, **132**, 1190–1191; (*n*) S. K. Rout, S. Guin, K. K. Ghara, A. Banerjee and B. K. Patel, Copper Catalyzed Oxidative Esterification of Aldehydes with Alkylbenzenes via Cross Dehydrogenative Coupling, *Org. Lett.*, 2012, **14**, 3982–3985; (*o*) R. Lerebours and C. Wolf, Chemoselective Nucleophilic Arylation and Single-Step Oxidative Esterification of Aldehydes Using Siloxanes and a Palladium–Phosphinous Acid as a Reaction Switch, *J. Am. Chem. Soc.*, 2006, **128**, 13052–13053.

13 R. N. Reddi, P. V. Malekar and A. Sudalai, N-Heterocyclic carbene catalyzed regioselective oxo-acyloxylation of alkenes with aromatic aldehydes: a high yield synthesis of α-acyloxy ketones and esters, *Org. Biomol. Chem.*, 2013, **11**, 6477–6482.

14 (*a*) Q. Liu and L.-Z. Wu, Recent advances in visible-light-driven organic reactions, *Natl. Sci. Rev.*, 2017, **4**, 359–380; (*b*) L. Marzo, S. K. Pagire, O. Reiser and B. König, Visible-Light Photocatalysis: Does It Make a Difference in Organic Synthesis?, *Angew. Chem., Int. Ed.*, 2018, **57**, 10034–10072; (*c*) C. R. J. Stephenson, T. P. Yoon and D. W. C. MacMillan, *Visible light photocatalysis in organic chemistry*, Wiley-VCH, Weinheim, 2017; (*d*) B. König, Photocatalysis in Organic Synthesis – Past, Present, and Future, *Eur. J. Org. Chem.*, 2017, 1979–1981; (*e*) M. Tavakolian and M. Hosseini-Sarvari, Catalyst-Free Organic Transformations under Visible-Light, *ACS Sustainable Chem. Eng.*, 2021, **9**, 4296–4323; (*f*) Z. Gan, G. Li, X. Yang, Q. Yan, G. Xu, G. Li, Y.-Y. Jiang and D. Yang, Visible-light-induced regioselective cross-dehydrogenative coupling of 2-isothiocyanato naphthalenes with amines using molecular oxygen, *Sci. China: Chem.*, 2020, **63**, 1652–1658; (*g*) W.-M. Cheng and R. Shang, Transition Metal-Catalyzed Organic Reactions under Visible Light: Recent Developments and Future Perspectives, *ACS Catal.*, 2020, **10**, 9170–9196; (*h*) L.-Y. Xie, Y.-S. Bai, X.-Q. Xu, X. Peng, H.-S. Tang, Y. Huang, Y.-W. Lin, Z. Cao and W.-M. He, Visible-light-induced decarboxylative acylation of quinoxalin-2(1H)-ones with α-oxo carboxylic acids under metal-, strong oxidant- and external photocatalyst-free conditions, *Green Chem.*, 2020, **22**, 1720–1725.

15 Y. L. Zhang, Q. Xiao, Y. S. Bao, Y. J. Zhang, S. Bottle, S. Sarina, B. Zhaorigetu and H. Y. Zhu, Direct Photocatalytic Conversion of Aldehydes to Esters Using Supported Gold Nanoparticles under Visible Light Irradiation at Room Temperature, *J. Phys. Chem. C*, 2014, **118**, 19062–19069.

16 A. Kumar, P. Kumar, A. K. Pathak, A. N. Chokkapu and S. L. Jain, Carbon Nitride Grafted Cobalt Complex (Co@npg–C3N4) for Visible Light–Assisted Esterification of Aldehydes, *ChemistrySelect*, 2017, **2**, 3437–3443.

17 G. Pandey, S. Koley, R. Talukdar and P. K. Sahani, Cross-Dehydrogenating Coupling of Aldehydes with Amines/R-OTBS Ethers by Visible-Light Photoredox Catalysis: Synthesis of Amides, Esters, and Ureas, *Org. Lett.*, 2018, **20**, 5861–5865.

18 S. Gaspa, I. Raposo, L. Pereira, G. Mulas, P. C. Ricci, A. Porcheddu and L. De Luca, Visible light-induced transformation of aldehydes to esters, carboxylic anhydrides and amides, *New J. Chem.*, 2019, **43**, 10711–10715.

19 K. M. Pelzer, L. Cheng and L. A. Curtiss, Effects of Functional Groups in Redox-Active Organic Molecules: A High-Throughput Screening Approach, *J. Phys. Chem. C*, 2017, **121**, 237–245.

20 (*a*) N. A. Romero and D. A. Nicewicz, Organic Photoredox Catalysis, *Chem. Rev.*, 2016, **116**, 10075–10166, and references cited therein. (*b*) E. Alfonzo, F. S. Alfonso and A. B. Beeler, Redesign of a Pyrylium Photoredox Catalyst and Its Application to the Generation of Carbonyl Ylides, *Org. Lett.*, 2017, **19**, 2989–2992.

21 H. Adkins, R. M. Elofson, A. G. Rossow and C. C. Robinson, The Oxidation Potentials of Aldehydes and Ketones, *J. Am. Chem. Soc.*, 1949, **71**, 3622–3629.

22 H. G. Roth, N. A. Romero and D. A. Nicewicz, Experimental and Calculated Electrochemical Potentials of Common Organic Molecules for Applications to Single-Electron Redox Chemistry, *Synlett*, 2016, 714–723.

23 For radical–radical coupling reactions under visible light, see: (*a*) M. S. Santos, A. G. Corrêa, M. W. Paixão and B. König, $C(sp^3)$–$C(sp^3)$ Cross-Coupling of Alkyl Bromides and Ethers Mediated by Metal and Visible Light Photoredox Catalysis, *Adv. Synth. Catal.*, 2020, **362**, 2367–

Published on 17 June 2021. Downloaded by Indian Institute of Science Education & Research Pune on 12/25/2023 4:35:44 AM.

2372; (*b*) A. L. Berger, K. Donabauer and B. Konig, Photocatalytic Barbier reaction – visible-light induced allylation and benzylation of aldehydes and ketones, *Chem. Sci.*, 2018, **9**, 7230; (*c*) J. L. Jeffrey, F. R. Petronijevic and D. W. MacMillan, Selective Radical–Radical Cross-Couplings: Design of a Formal β-Mannich Reaction, *J. Am. Chem. Soc.*, 2015, **137**, 8404–8407; (*d*) J. D. Cuthbertson and D. W. MacMillan, The direct arylation of allylic sp^3 C–H bonds via organic and photoredox catalysis, *Nature*, 2015, **519**, 74–77.

This journal is © the Partner Organisations 2021

Check for updates

ACES Asian Chemical Editorial Society

doi.org/10.1002/ajoc.202200205

ASIAN JOURNAL OF ORGANIC CHEMISTRY
Research Article

www.asianjoc.org

Visible Light Promoted Metal-Free Sustainable Reduction of α-Alkylidene Oxindoles/Succinimides

Anindita Bhowmick, Prakash K. Warghude, and Ramakrishna G. Bhat*[a]

Abstract: Visible light promoted chemoselective metal free hydrogenation of activated double bond has been achieved via photoredox catalysis. Eosin Y has proved to be an efficient catalyst for the effective reduction of C–C double bonds of alkylidene oxindoles and succinimides under visible light. Commercially viable DIPEA has been employed as a sacrificial electron donor and it's in-situ generated cationic radical acts as reductant in this transformation. The method proved to be practical as a broad range of substrates containing activated double bond were easily reduced. The method proved to be scalable on a gram quantity and the reduced product has been utilized successfully for the further synthetic application. The systematic and detailed mechanistic studies reveal the oxidative quenching of the photocatalyst by the activated double bond.

The hydrogenation of unsaturated organic compounds is one of the most important and key transformations in organic synthesis till date.[1] The hydrogenation is indispensable to synthetic community and this process has been widely employed for a range of applications in the chemical, biochemical, food, agrochemical, polymer and pharmaceutical industries.[2] The selective reduction is a key process in many biosynthetic pathways. During the biosynthesis of fatty acids, the selective reduction of activated carbon-carbon double bonds is achieved by enoate reductases (in living microorganism) that are abundant in mother nature.[3] However, in organic synthesis traditionally the hydrogenation reactions are carried out using hydrogen gas in presence of catalytic amount of transition metals or stoichiometric amount of metal hydrides.[4] In this regard, eco-friendly transition metal-free reduction protocols have been discovered that are relatively safer than the processes that involve transition metals and reactive hydrogen gas. Hantzsch ester,[5] silanes[6] have also been used as the reactive organic reducing agent for the hydrogenation of carbon-carbon double bonds. Hydrogenation has also been achieved using frustrated Lewis pairs (FLPs).[7] There are also examples of chemoselective hydrogenation of unsaturated carbonyl compounds using alkyl phosphines and *N*-heterocyclic carbenes.[8] However, most of the hydrogenation strategies rely either on the heavy transition metals and hydrogen or on stoichiometric amount of expensive, pyrophoric as well as toxic metal based reducing agents.

Therefore, to develop an efficient and metal free protocol for the reduction of C–C double bond is highly demanding and challenging to pursue.

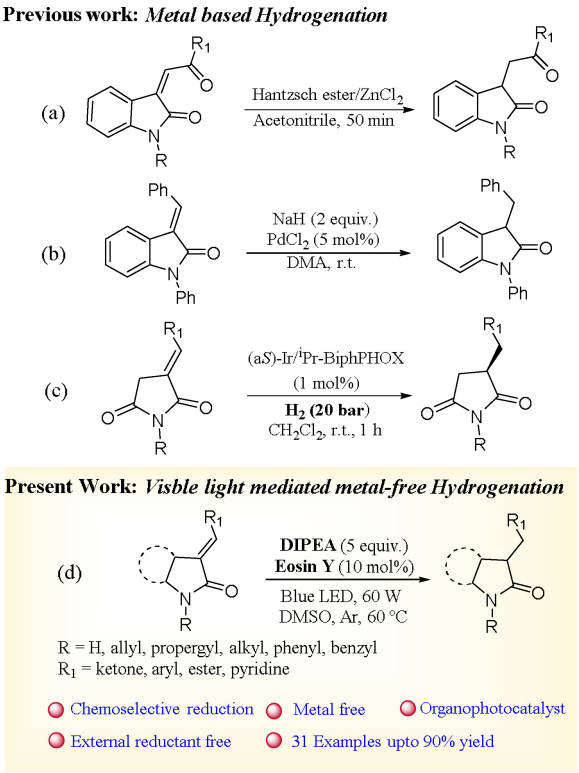
Over the last few years, the visible light photoredox catalysis has been progressing very rapidly as a promising field in organic synthesis. Photoredox catalysis has been emerging as a safer alternative strategy for some of the transformations that are tedious to be realized by traditional routes. Very importantly, the visible light mediated transformations are usually non-toxic, eco-friendly and easy to handle with lesser waste.[9] Very recently, very few visible light-mediated cascade cross-coupling hydrogenation reactions have been reported that avoid the use of any sacrificial oxidants. However, these transfer hydrogenation/semihydrogenation strategies solely rely on the metal complexes under visible light conditions to generate hydrogen in situ.[10] In 1980's Sakurai group developed visible light mediated reduction protocols of alkenes with 1-benzyl-1,4-dihydronicotinamide in presence of Ru catalyst.[11] Despite these advances, a metal free hydrogenation under visible light irradiation is highly desirable and required.

It is also highly challenging and demanding to enable the selective hydrogenation of electron deficient carbon-carbon double bond in a molecule. Among the molecules containing electron deficient carbon-carbon double bonds, the α-alkylidene oxindole and succinimide based unsaturated compounds have a broad range of application in the organic synthesis as precursors of many natural products and bioactive compounds.[12] In this regard, efforts have been made to reduce the electron deficient or activated carbon- carbon double bond selectively by few research groups. In 2019, Kasi Viswanath and co-workers described a chemoselective reduction of 3-phenacylideneoxindoles by using Hantzsch ester and $ZnCl_2$ (Scheme 1a).[13] In the same year, Zhang and co-workers developed a palladium catalysed hydrogenation for the α,β-unsaturated compounds using sodium hydride as a Michael donor (Scheme 1b).[14] In 2013, Zhang and co-workers have disclosed an iridium catalysed asymmetric hydrogenation of α-alkylidene succinimides derivatives under very high pressure (H_2, 20 bar Scheme 1c).[15] However, all of these methods relied on the use of metal catalysts, strong bases or hydrogen gas at very high pressure. The usefulness of these methods is limited due to the drastic reaction conditions and hazard associated with them. It would be really interesting to investigate the reduction of activated C–C double bond of alkylidene oxin-

[a] *A. Bhowmick, Dr. P. K. Warghude, Prof. Dr. R. G. Bhat*
Department of Chemistry, Indian Institute of Science Education and Research (IISER)-Pune, Dr. Homi Bhabha Road, Pashan, 411008 Pune, Maharashtra, India
E-mail: rgb@iiserpune.ac.in

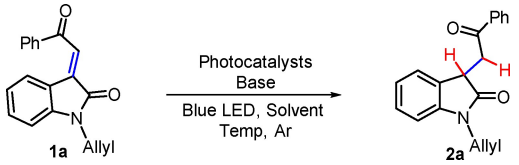
Supporting information for this article is available on the WWW under https://doi.org/10.1002/ajoc.202200205

© 2022 Wiley-VCH GmbH



Scheme 1. Methods for the hydrogenation of different electron deficient alkene.

Table 1. Optimization of Reaction Conditions[a]



Entry	Photocatalyst	Base	Solvent	Yield [%][f]
1	$Ru(bpy)_3Cl_2$	DIPEA	MeCN	50
2	*fac*-Ir(PPy_3)	DIPEA	MeCN	54
3	Eosin Y	DIPEA	MeCN	64
4	4CzIPN	DIPEA	MeCN	32
5	Rhodamine 6G	DIPEA	MeCN	NR
6	Acridinium	DIPEA	MeCN	NR
7	Eosin Y	DBU	MeCN	NR
8	Eosin Y	DABCO	MeCN	NR
9	Eosin Y	Et_3N	MeCN	46
10	Eosin Y	DIPEA	DMF	50
11	Eosin Y	DIPEA	THF	18
12	**Eosin Y**	**DIPEA**	**DMSO**	**75**
13	Eosin Y	^tBuOK	DMSO	NR
14	Eosin Y	Cs_2CO_3	DMSO	NR
15[b]	Eosin Y	DIPEA	DMSO	35
16[c]	–	DIPEA	DMSO	NR
17[d]	Eosin Y	–	DMSO	NR
18[e]	Eosin Y	DIPEA	DMSO	NR

Reaction Condition: Unless otherwise noted. [a] all the reactions were carried out using 0.350 mmol of **1a**, 1.75 mmol of base and 35 µmol (10 mol%) of photocatalyst under blue LED (60 W) irradiation at 60 °C for 24 h. (1–5 mol% Eosin Y gave lower yield of **2a**, see S6, ESI for details); [b] 10 equivalent of H_2O was added to the reaction mixture (1–3, 5 equiv. of water slightly improved the yield in comparsion to 10 equiv. of H_2O, dry DMSO worked the best), [c] in absence of photocatalyst, [d] in absence of DIPEA, [e] in absence of light (in dark). [f] Isolated yield after the purification by column chromatography. Acridinium = 9-Mesityl- 10-methylacridinium perchlorate.

doles/succinimides under completely metal free conditions. It is also important that some of these scaffolds containing activated double bond are routinely explored as intermediates in many transformations and also, they are easy to be synthesized for the synthetic applications.

Herein we wish to report metal free sustainable reduction of activated C–C double bonds of α-alkylidene oxindoles/succinimides under visible light using DIPEA as a sacrificial electron donor as well as reducing agent and Eosin Y as a photocatalyst (Scheme 1d).

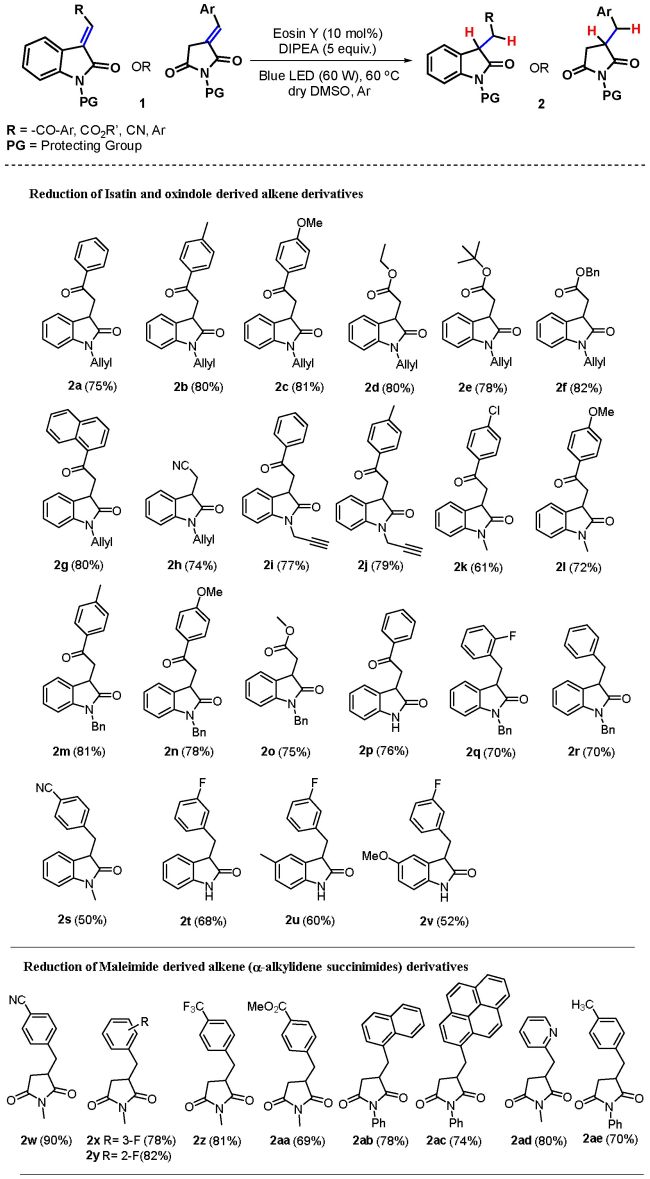
Initial screening of the reaction at a range of temperatures (rt to 50 °C) did not give any satisfactory results.[16] Later we commenced with the reaction of **1a** using DIPEA in presence of ruthenium catalyst (Ru Cat.) in anhydrous acetonitrile under blue LED (60 W) at 60 °C using inert atmosphere. Gratifyingly, we obtained the desired reduction product **2a** in moderate yield (50%, Table 1, Entry 1). Later, we screened the reaction of **1a** with different photocatalysts in presence of DIPEA (Table 1, Entries 2–6). Among all photocatalysts explored, Eosin Y proved to be most efficient by affording the desired reduced product **2a** in 64% yield (Table 1, Entry 3). This result encouraged us to optimize the reaction condition further and, in this regard, we screened the reaction with different organic as well as inorganic bases. We observed that among all the bases, DIPEA proved to be efficient in affording the desired product **2a** (Table 1, Entries 2, 7–9, 13–14). Having optimized the photocatalyst and base, we further screened the reaction using different solvents to enhance the yield of desired product **2a** (Table 1, Entries 10–12). Gratifyingly, the reaction worked smoothly in dry DMSO to afford the desired reduction product **2a** in good yield (75% yield, Table 1, Entry 12). In order to verify the role of water if any, we carried out the reaction of **1a** in presence of Eosin Y, DIPEA in DMSO along with H_2O (10 equiv.). The presence of water reduced the yield of **2a** significantly (Table 1, Entry 15). We carried out the optimization further by systematically screening reactions at different temperatures, variable wavelength of visible light (LEDs) and other reaction conditions (ESI for details). We further confirmed that photocatalyst, base as well as light are essential for the desired transformation to obtain desired product **2a** (Table 1, Entries 16–18). Based on the exhaustive screening, compound **1a**, Eosin Y (10 mol%), DIPEA (5 equiv.) in dry DMSO under blue light irradiation (60 W) at 60 °C under inert atmosphere proved to be the optimum reaction condition to obtain the desired product **2a** in higher yield.

Having optimized the reaction condition in hand, we set out to explore the substrate scope of this visible light mediated hydrogenation of electron deficient alkenes. To begin with, we synthesized different isatin based alkene derivatives (**1a**–**1p**) to investigate their reactivity and broad substrate scope of the protocol (See ESI S2). We observed that all the substrates (**1a**–**1p**) reacted smoothly under the optimized reaction condition to furnish the corresponding reduced products (**2a**–**2p**) in

© 2022 Wiley-VCH GmbH

21935815, 2022, 8, Downloaded from https://onlinelibrary.wiley.com/doi/10.1002/ajoc.202200205 by Indian Institute Of Science Education And Research Pune, Wiley Online Library on [24/12/2023]. See the Terms and Conditions (https://onlinelibrary.wiley.com/terms-and-conditions) on Wiley Online Library for rules of use; OA articles are governed by the applicable Creative Commons License

moderate to good yields (Scheme 2). It is important to note that all the substrates containing *N*-allyl as well as *N*-propargyl protecting groups reacted easily to afford the corresponding reduced products (**2a**–**2j**) in very good yields (up to 82% yield). Under the reaction conditions, we observed the selective reduction of electron-deficient alkene and the *N*-allyl or *N*-propargyl groups were intact. Moreover, *N*-methyl as well as *N*-benzyl protected isatin derivatives have also reacted efficiently to furnish the desired reduced products (**2k**–**2o**) in moderate to good yields (up to 81% yield, Scheme 2). It is highly remarkable to note that the substrate with unprotected nitrogen worked smoothly under the optimized reaction condition to afford the corresponding reduction product in **2p** good yield and we did not observe any side product (Scheme 2).



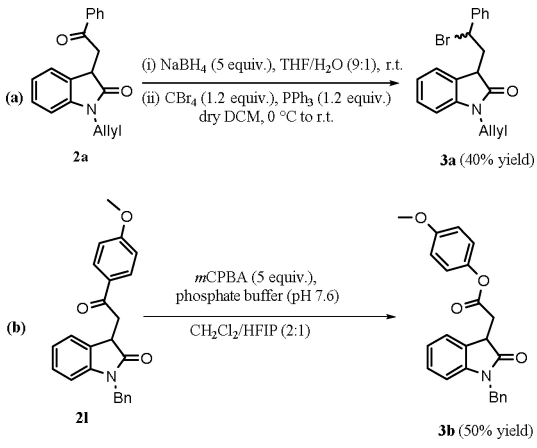
Scheme 2. Substrate scope of the reduction protocol. **Reaction Condition**: Unless otherwise noted. [a] all the reactions were carried out using 0.350 mmol of **1**, 1.75 mmol of base and 35 µmol, Eosin Y (10 mol%) in dry DMSO under blue LED (60 W) irradiation at 60 °C for 24 h.

Later we turned our attention to explore the applicability of the protocol for the reduction of a variety of alkylidene 2-oxindoles with different protecting groups as well as electron withdrawing substituents. Under the reaction conditions 2-oxindole based alkenes (**1q**–**1v**) furnished the corresponding reduced products (**2q**–**2v**) in moderate to good yields (up to 70% yield, Scheme 2). After the initial success, we planned to apply this photocatalyzed hydrogenation protocol for the reduction of α-alkylidene succinimides (derived from maleimides). We explored the reactivity of different α-alkylidene succinimides (**1w**–**1ae**) under optimized reaction condition.

Further, as an extension of this strategy we have performed different transformations using the final products (**2a**, **2l**) to demonstrate its synthetic utility (Scheme 3).

At first, we have carried out the chemoselective reduction followed by bromination of the ketone moiety of **2a** to obtain the corresponding bromo product **3a** (Scheme 3a). Next, we performed a Baeyer–Villiger oxidation of compound **2l** to obtain the corresponding ester **3b** as a final product (Scheme 3b).

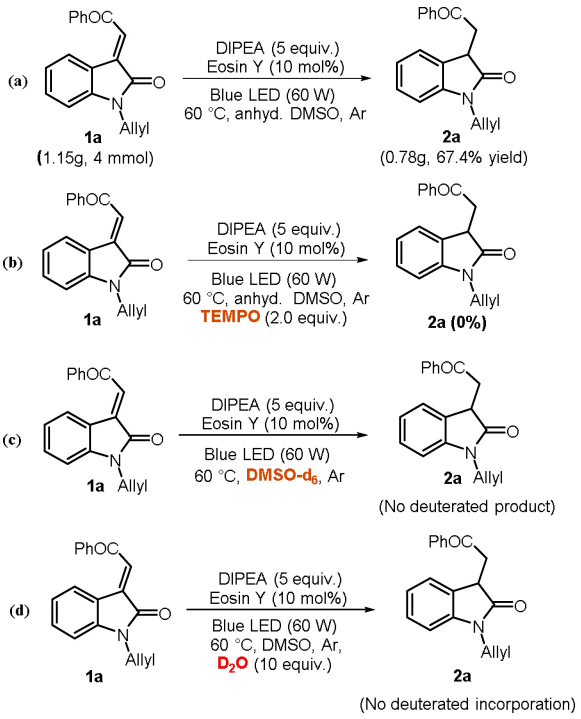
Further, in order to generalize the practicality of the protocol, gram scale synthesis of **2a** has been achieved (0.78 g, 67.4% yield, Scheme 4a). In order to have the mechanistic insight into this transformation, we systematically performed few control experiments. To begin with we carried out a radical quenching experiment of **1a** in presence of TEMPO under the optimized reaction conditions. The desired product **2a** did not form even after prolonged reaction time thus supporting the involvement of radical intermediate during the course of the reaction (Scheme 4b). Further to prove the source of hydrogen in the reduction process, we carried out the reaction of **1a** under optimized conditions using DMSO-d_6 as a solvent (Scheme 4c). However, we did not obtain any deuterated reduced product instead we exclusively obtained **2a** and this unambiguously proved that the solvent is not the source of hydrogen (Scheme 4c). Later, to check the possibility of visible light photoredox catalyzed successive single electron transfer process, we carried out the reaction of **1a** with D_2O (10 equiv.) while maintaining the optimized reaction conditions under inert atmosphere. However, we did not observe any deuterium



Scheme 3. Synthetic Utility.

© 2022 Wiley-VCH GmbH

21935815, 2022, 8, Downloaded from https://onlinelibrary.wiley.com/doi/10.1002/ajoc.202200205 by Indian Institute Of Science Education And Research Pune, Wiley Online Library on [24/12/2023]. See the Terms and Conditions (https://onlinelibrary.wiley.com/terms-and-conditions) on Wiley Online Library for rules of use; OA articles are governed by the applicable Creative Commons License



Scheme 4. Control experiments and gram scale synthesis.

incorporation in the reduced product **2a** thus ruling out the possibility of carbanion intermediate (Scheme 4d).

Further, we have carried out fluorescence quenching experiment of Eosin Y in DMSO and **1a** (Figure 1a). Likewise, the fluorescence quenching experiment of Eosin Y in DMSO and DIPEA was carried out under inert atmospheric condition (Figure 1b).

We observed that the fluorescence emission spectral intensity of Eosin Y was reduced gradually with the increasing concentration of **1a** in DMSO (Figure 1a). However, we did not observe any significant change in the fluorescence intensity of Eosin Y in presence of DIPEA (Figure 1b). These results un-

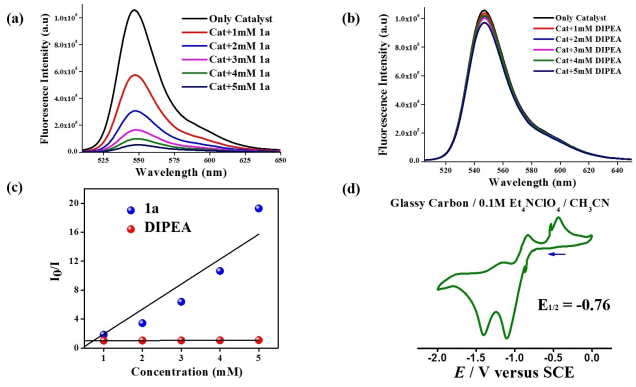
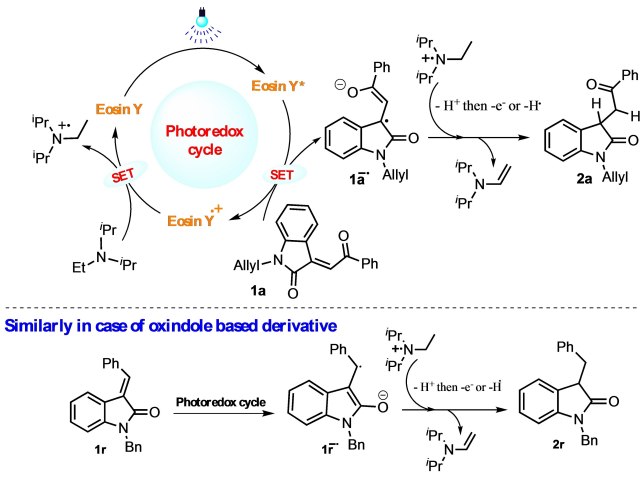


Figure 1. Fluorescence (emission) and cyclic voltammetry studies to have mechanistic insight (a) Fluorescence quenching experiment of Eosin Y in presence of **1a** (b) Fluorescence quenching experiment of Eosin Y in presence of DIPEA, (c) Stern–Volmer plot for the fluorescence quenching experiments Eosin Y in presence of **1a** and DIPEA, (d) Cyclic- voltammetry plot of **1a**.



Scheme 5. Plausible mechanistic cycle.

ambiguously support the oxidative quenching of Eosin Y in presence of **1a**. We have also carried out the cyclic voltammetry of **1a** at room temperature (Figure 1d).

Based on cyclic voltammogram, it was very clear that $E_{1/2}$ of **1a** is −0.76 V vs. SCE. While P.C (Eosin Y) has a redox potential $P.C^{\bullet+}/P.C = -1.11$ V vs. SCE based on the available data.[17] It is very clear from the experiments and literature value that **1a** can be easily reduced by the excited state of photocatalyst P.C (Eosin Y). Further, the oxidized form of the photocatalyst Eosin $Y^{\bullet+}$ abstracts an electron from DIPEA (a sacrificial electron donor) to generate the ground state Eosin Y thus completing the photoredox catalytic cycle. Finally, the radical anion intermediate $\mathbf{1a}^{\bullet-}$ interacts with $DIPEA^{\bullet+}$ to abstract hydrogen atom by affording the desired product **2a** (Scheme 5).[18] Likewise, the reduction of 2-oxindole based alkene **1r** may form the corresponding product **2r** probably via the stable radical anion intermediate $\mathbf{1r}^{\bullet-}$ (Scheme 5).

In summary, we have developed a chemo-selective metal-free hydrogenation of activated C–C double bond of alkylidene oxindoles and succinimide derivatives under visible light irradiation. Further a detailed mechanistic study revealed the oxidative quenching of the photocatalyst by the activated double bond. DIPEA has been used as a sacrificial electron donor and it's in-situ generated cationic radical intermediate acts as a reductant for this transformation. A broad range of substrates were employed in this protocol to obtain the corresponding reduced products in high yields using clear energy. The method proved to be scalable on a gram quantity and we have also employed reduced products for the further synthetic utility to demonstrate synthetic application.

Experimental Section

General procedure for the reduction

To an oven dried 10 mL crimp cap vial charged with magnetic stir bar was added alkene 1 (0.35 mmol, 1 equiv.), Eosin Y (10 mol%) at

© 2022 Wiley-VCH GmbH

21935815, 2022, 8, Downloaded from https://onlinelibrary.wiley.com/doi/10.1002/ajoc.202200205 by Indian Institute Of Science Education And Research Pune, Wiley Online Library on [24/12/2023]. See the Terms and Conditions (https://onlinelibrary.wiley.com/terms-and-conditions) on Wiley Online Library for rules of use; OA articles are governed by the applicable Creative Commons License

room temperature under argon atmosphere. The vial was purged again with argon and sealed with aluminium crimp cap using a crimper. Then dry DMSO (3 mL) was added under argon. Then the reaction mixture was degasified using argon for 10 more minutes under constant monitoring. After the degasification DIPEA (5 equiv.) was added under inert atmosphere. Then the reaction mixture was irradiated with blue LED (60 W) at 60 °C stirred for 24 h. After completion of the reaction (monitored by TLC), 10 mL of water was added to the reaction mixture and was extracted with ethyl acetate (3×10 mL). The combined organic extract was evaporated under reduced pressure and the crude residue was purified by using column chromatography (Silica gel 100–200 mesh size, using ethyl acetate/hexane as eluent system).

Acknowledgements

R. G. B. thanks Science and Engineering Research Board, Department of Science and Technology (SERB-DST), New Delhi, Government of India (File no: CRG/2019/005753), for the generous research grant. A. B. thank CSIR, New Delhi for the fellowship. P. K. W. thanks UGC, New Delhi for the fellowship. Authors also thank Mr. Abhijit Chatterjee, IISER Pune for helping in obtaining the fluorescence spectra and for the useful discussions.

Conflict of Interest

The authors declare no conflict of interest.

Data Availability Statement

The data that support the findings of this study are available in the supplementary material of this article.

Keywords: Eosin Y · Metal-Free · Reduction · Stern-Volmer plot · Visible Light

[1] a) P. Sabatier, M. J. Nye, *Chem. World* **2004**, *1*, 46–49; b) P. Sabatier, in *La Catalyse en chimie organique*, Paris, Branger, 1913; c) G. Wilkinson, *Bull. Soc. Chim. Fr.* **1968**, *12*, 5055–5058.
[2] J. G. de Vries, C. J. Elsevier, in *Handbook of Homogeneous Hydrogenation*, Wiley-VCH, Weinheim, **2006**.
[3] a) S. Steinbacher, M. Stumpf, S. Weinkauf, F. Rohdich, A. Bacher, H. Simon, in *"Enoate reductase family": Flavins and Flavoproteins* (Eds.: S. K. Chapman, R. N. Perham, N. S. Scrutton, R. Weber), deGruyter, *Berlin*, **2002**, 941–949; b) R. C. Brewster, J. T. Suitor, A. W. Bennett, S. Wallace, *Angew. Chem. Int. Ed.* **2019**, *58*, 12409–12414; *Angew. Chem.* **2019**, *131*, 12539–12544.
[4] a) M. Hudlický, in *Reductions in Organic Chemistry, 2nd ed.*, American Chemical Society, Washington, **1996**; b) R. Noyori, *Angew. Chem.* **2002**, *114*, 2108–2123; *Angew. Chem. Int. Ed.* **2002**, *41*, 2008–2022; c) W. S. Knowles, *Angew. Chem.* **2002**, *114*, 2096–2107; *Angew. Chem. Int. Ed.* **2002**, *41*,1998–2007.
[5] a) N. Yutaka, M. Yasuhiko, H. Sawako, O. Akiya, S. Noboru, *Bull. Chem. Soc. Jpn.* **1989**, *62*, 1682–1684; b) J. W. Yang, M. T. Hechavarria Fonseca, B. List, *Angew. Chem. Int. Ed.* **2004**, *43*, 6660–6662; *Angew. Chem.* **2004**, *116*, 6829–6832; c) Y. Imada, T. Kitagawa, T. Ohno, H. Iida, T. Naota, *Org. Lett.* **2010**, *12*, 32–35; d) M. Sugiura, N. Sato, Y. Sonoda, S. Kotani, M. Nakajima, *Chem. Asian J.* **2010**, *5*, 478–481; e) X. Xia, Z. Lao, P. H. Toy, *Synlett* **2019**, *30*, 1100–1104; f) M. Sugiura, Y. Ashikari, Y. Takahashi, K. Yamaguchi, S. Kotani, M. Nakajima, *J. Org. Chem.* **2019**, *84*, 11458–11473.
[6] a) M. Rubin, T. Schwier, V. Gevorgyan, *J. Org. Chem.* **2002**, *67*, 1936–1940; b) J. M. Blackwell, E. R. Sonmor, T. Scoccitti, W. E. Piers, *Org. Lett.* **2000**, *2*, 3921–3923; c) A. Berkefeld, W. E. Piers, M. Parvez, *J. Am. Chem. Soc.* **2010**, *132*, 10660 10661; d) W. E. Piers, T. Chivers, *Chem. Soc. Rev.* **1997**, *26*, 345–354; e) W. E. Piers, A. J. V. Marwitz, L. G. Mercier, *Inorg. Chem.* **2011**, *50*, 12252–12262.
[7] J. Lam, K. M. Szkop, E. Mosaferi, D. W. Stephan, *Chem. Soc. Rev.* **2019**, *48*, 3592–3612.
[8] a) M. G. Burnett, T. Oswald, B. J. Walker, *J. Chem. Soc. Chem. Commun.* **1977**, 155–156; b) B. Pal, P. K. Pradhan, P. Jaisankar, V. S. Giri, *Synthesis* **2003**, 1549–1552; c) S.-H. Cao, X.-C. Zhang, Y. Wei, M. Shi, *Eur. J. Org. Chem.* **2011**, *2011*, 2668–2672; d) T. Kato, S.-i. Matsuoka, M. Suzuki, *Chem. Commun.* **2015**, *51*, 13906–13909.
[9] a) K. L. Skubi, T. R. Blum, T. P. Yoon, *Chem. Rev.* **2016**, *116*, 10035–10074; b) N. A. Romero, D. A. Nicewicz, *Chem. Rev.* **2016**, *116*, 10075–10166; c) M. H. Shaw, J. Twilton, D. W. C. MacMillan, *J. Org. Chem.* **2016**, *81*, 6898–6926; d) F. Strieth-Kalthoff, M. J. James, M. Teders, L. Pitzer, F. Glorius, *Chem. Soc. Rev.* **2018**, *47*, 7190–7202; e) J. R. Chen, X. Q. Hu, L. Q. Lu, W. J. Xiao, *Chem. Soc. Rev.* **2016**, *45*, 2044–2056; f) H. Zhao, D. Cheng, X. Xu, *Chin. J. Org. Chem.* **2021**, *41*, 642–660.
[10] a) J.-J. Zhong, C.-J. Wu, Q.-Y. Meng, X.-W. Gao, T. Lei, C.-H. Tung, L.-Z. Wu, *Adv. Synth. Catal.* **2014**, *356*, 2846–2852; b) J.-J. Zhong, Q. Liu, C.-J. Wu, Q.-Y. Meng, X.-W. Gao, Z.-J. Li, B. Chen, C.-H. Tung, L.-Z. Wu, *Chem. Commun.* **2016**, *52*, 1800–1803.
[11] a) C. Pac, M. Ihama, M. Yasuda, Y. Miyauchi, H. Sakurai, *J. Am. Chem. Soc.* **1981**, *103*, 6495–6497; b) C. Pac, Y. Miyauchi, O. Ishitani, M. Ihama, M. Yasuda, H. Sakurai, *J. Org. Chem.* **1984**, *49*, 26–34.
[12] a) F. Zhou, Y.-L. Liu, J. Zhou, *Adv. Synth. Catal.* **2010**, *352*, 1381–1407; b) J. Schmid, T. Junge, J. Lang, W. Frey, R. Peters, *Angew. Chem. Int. Ed.* **2019**, *16*, 5447–5451; c) P. Galzerano, G. Bencivenni, F. Pesciaioli, A. Mazzanti, B. Giannichi, L. Sambri, G. Bartoli, P. Melchiorre, *Chem. Eur. J.* **2009**, *15*, 7846–7849.
[13] N. M. Gandikota, R. S. Bolla, A. Bandyopadhyay, I. V. Kasi Viswanath, *Russ. J. Org. Chem.* **2019**, *55*, 1197–1203.
[14] Y. Liu, Y. Mao, Y. Hu, J. Gui, L. Wang, W. Wang, S. Zhang, *Adv. Synth. Catal.* **2019**, *361*, 1554–1558.
[15] Y. Liu, W. Zhang, *Angew. Chem. Int. Ed.* **2013**, *52*, 2203–2206; *Angew. Chem.* **2013**, *125*, 2259–2262.
[16] The initial attempts to optimize the reaction conditions at room temperature using different photocatalysts and bases were unsuccessful. The reaction was optimized after screening different LEDs with varying intensites, by changing the mol% of photocatalyst (see page S6, ESI for more details).
[17] a) V. Srivastava, P. P. Singh, *RSC Adv.* **2017**, *7*, 31377–31392; b) D. Hari, B. König, *Chem. Commun.* **2014**, *50*, 6688–6699.
[18] a) J.-W. Beatty, C.-R. Stephenson, *Acc. Chem. Res.* **2015**, *48*, 1474–1484; b) M. Schmallegger, G. Gescheidt, *Monatsh. Chem.* **2018**, *149*, 499–504.

Manuscript received: April 15, 2022
Revised manuscript received: June 16, 2022
Accepted manuscript online: June 24, 2022
Version of record online: July 7, 2022

© 2022 Wiley-VCH GmbH

21935815, 2022, 8, Downloaded from https://onlinelibrary.wiley.com/doi/10.1002/ajoc.202200205 by Indian Institute Of Science Education And Research Pune, Wiley Online Library on [24/12/2023]. See the Terms and Conditions (https://onlinelibrary.wiley.com/terms-and-conditions) on Wiley Online Library for rules of use; OA articles are governed by the applicable Creative Commons License

Published on 29 August 2023. Downloaded by Indian Institute of Science Education & Research Pune on 12/25/2023 4:40:20 AM.

ChemComm

COMMUNICATION

View Article Online
View Journal | View Issue

Check for updates

Cite this: *Chem. Commun.*, 2023, 59, 11875

Received 26th May 2023,
Accepted 24th August 2023

DOI: 10.1039/d3cc02557h

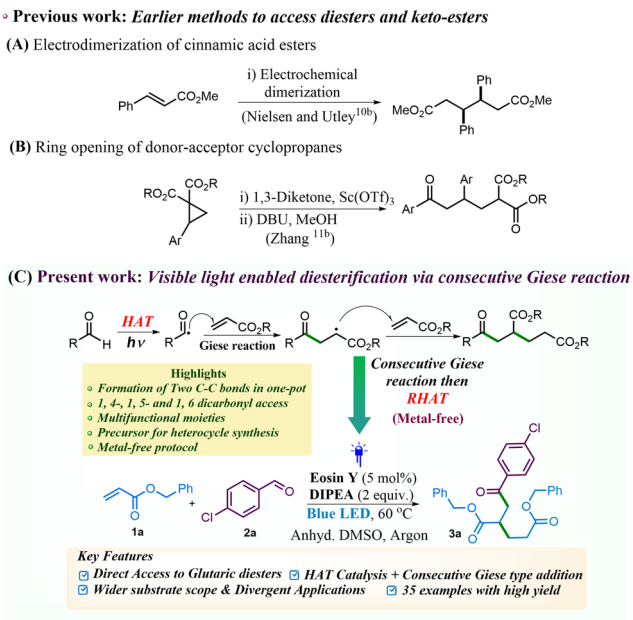
rsc.li/chemcomm

A visible light-driven direct synthesis of industrially relevant glutaric acid diesters from aldehydes†

Anindita Bhowmick, Abhijit Chatterjee, Sidharth S. Pathak and Ramakrishna G. Bhat *

A straightforward and practical method has been developed to access α-substituted glutaric diesters from acrylates and aldehydes using visible light, with Eosin Y facilitating hydrogen atom transfer (HAT) and subsequent Giese-type addition. Also, sunlight has been successfully used as an alternative sustainable light source. The method has also been explored to access substituted 4,5-dihydro-2H-pyridazinones, which have potential biological and industrial applications. Comprehensive mechanistic investigations have been carried out.

Esters and their derivatives are ubiquitous in natural products, pharmaceuticals, polymer materials, and fine chemicals.[1,2] Similarly, the dicarbonyl scaffolds are also abundant in bioactive and natural products.[3] In particular, 1,4-dicarbonyl compounds are widespread in a large number of natural products and bioactive compounds.[4] In addition, 1,5-dicarbonyl[5] and 1,6-dicarbonyl compounds[6] also serve as important intermediates in organic synthesis for constructing different complex molecular architectures. Glutaric diesters (1,5-dicarbonyl) under hydrogenation conditions furnish 1,5-pentanediol, which is used as a raw material for the production of polyurethane coatings, polyester resins, and polycarbonate diol resins.[7] The glutaric acid is a very useful compound and it also serves as an important precursor for the synthesis of polymers such as polyester polyols, and polyamides. Glutaric acid (1,5-dicarbonyl) has been synthesized *via* the ring opening reaction of butyrolactone and potassium cyanide under heating conditions.[8] Likewise, 1,6-dicarbonyl compounds are important intermediates in organic synthesis. Due to the "dissonant" polarizing effect generated by the two carbonyl groups,[9] the dicarbonyl scaffold is relatively challenging to be tailored retrosynthetically into its classical synthons. In view of this, various synthetic methods rely on the dimerization of



Scheme 1 Access to industrially relevant dicarbonyl compounds and diesters.

α,β-unsaturated carbonyl compounds to access 1,6-dicarbonyl molecules (Scheme 1A).[10] The 1,6-dicarbonyl skeleton has been efficiently constructed *via* the ring-opening reaction of donor–acceptor (D–A) cyclopropanes with enolate nucleophiles (Scheme 1B).[11]

Though most of the highlighted methods are interesting, they are limited by few specific substrates, lower yields and harsh reaction conditions, and more importantly many rely on the use of heavy transition metal reagents.

Over the last two decades, visible light mediated photoredox catalysis has gained widespread recognition as a powerful tool in organic synthesis. Photocatalysis comprises several mechanistic pathways such as single-electron transfer (SET), energy transfer (EnT), hydrogen atom transfer (HAT) and proton-coupled electron

Department of Chemistry, Indian Institute of Science Education and Research (IISER) Pune, Dr. Homi Bhabha Road, Pashan, 411008, Maharashtra, India. E-mail: rgb@iiserpune.ac.in

† Electronic supplementary information (ESI) available. See DOI: https://doi.org/10.1039/d3cc02557h

Published on 29 August 2023. Downloaded by Indian Institute of Science Education & Research Pune on 12/25/2023 4:40:20 AM.

transfer (PCET) processes through which photonic energy is converted into chemical energy to drive the reactions. Very recently, different types of photoinduced esterification strategies have been reported.[12] Recently, the photocatalytic as well as HAT properties of xanthene-based dyes have been explored for realizing successful photoredox catalytic transformations.[13]

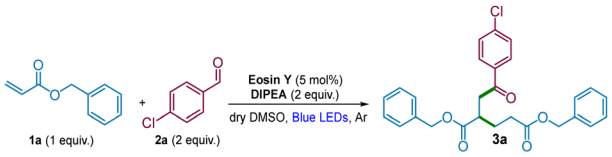
The visible light-mediated Giese-type reaction has gained tremendous interest as it generates reactive radicals either from the pre-functionalized starting materials, or using expensive metal photocatalysts, or metal dual catalysis using UV light.[14] In this regard, the design and development of efficient methods for the generation of alkyl radicals from commercially available starting materials under metal-free conditions is highly desirable.

Herein for the very first time, we wish to report a novel protocol for the synthesis of the α-aroyl glutaric diesters starting from aldehyde and acrylates by exploring the HAT property of Eosin Y followed by the Giese type 'consecutive addition' *via* photoredox catalysis under metal-free conditions (Scheme 1C). The resulting Giese-type reactions involved the formation of two new C–C bonds in one pot.

We commenced our reaction optimization studies with benzyl acrylate **1a** and 4-chlorobenzaldehyde **2a** as model substrates. Upon systematic and detailed investigation for the photocatalysis, Eosin Y as a HAT catalyst and DIPEA as an additive in anhydrous DMSO using blue LEDs (456 nm) under an inert atmosphere turned out to be advantageous for accessing the desired glutaric diester **3a** in very good yield (80%, Table 1, entry 1), while the reaction in the presence of different bases (instead of DIPEA) led to a decrease in the yield of the desired product **3a** (Table 1, entries 2–4 and see ESI,† S16, Table S1). We also observed that metal-based photocatalysts did not afford the corresponding desired product **3a** (Table 1, entries 5 and 6), while the reaction in the presence of different organic photocatalysts afforded the desired diester **3a** albeit in lower yield (Table 1, entries 7–9, and see ESI,† S17, Table S2). Later, we screened different solvents and observed that the yield of **3a** was lowered significantly (Table 1, entries 10 and 11 and see ESI,† S18, Table S3 for details) and among all, anhydrous DMSO proved to be the most advantageous to obtain **3a** in higher yield (Table 1, entry 1). The reaction in the presence of Na_2EosinY as a catalyst (instead of Eosin Y) and in the absence of DIPEA afforded the desired product **3a** in a very low yield (Table 1, entry 12), while the use of neutral Eosin Y, in the absence of DIPEA, did not furnish any desired product **3a** (Table 1, entry 13). This observation clearly indicated that the base is very essential to maintain the anionic form of Eosin Y and this might be the active form of the photocatalyst in this reaction.

The reaction under acidic conditions did not proceed (Table 1, entry 14). Later we also observed that the reaction in the presence of oxygen (air) did not proceed as well (Table 1, entry 15). Notably, the reaction in the absence of light as well as photocatalyst did not afford any desired product **3a** even at higher temperature and prolonged reaction time (Table 1, entries 16 and 17, see ESI,† S19, Table S4 for details).

Table 1 Optimization of the reaction conditions[a]



Entry	Variation from the optimised condition	Yield[b] (%)
1	**None**	**80**
2	DABCO instead of DIPEA	25
3	Triethyl amine instead of DIPEA	59
4	HCO_2Na instead of DIPEA	Trace
5	$(Ir[dF(CF_3)ppy]_2(dtbpy))PF_6$ instead of Eosin Y	NR
6	$Ru(bpy)_3(PF_6)_2$ instead of Eosin Y	NR
7	Na_2EosinY instead of Eosin Y	65
8	Thioxanthen-9-one instead of Eosin Y	50
9	Rhodamine 6G instead of Eosin Y	NR
10	*tert*-Butanol instead of DMSO	41
11	Acetone instead of DMSO	40
12	Na_2EosinY (instead of Eosin Y) in the absence of DIPEA	10
13	No DIPEA	NR
14	TFA instead of DIPEA	NR
15	Open air instead of inert atmosphere	NR
16	No light	NR
17	No photocatalyst	NR

Standard reaction conditions: [a] Benzyl acrylate **1a** (1 mmol), 4-chlorobenzaldehyde **2a** (2 mmol), Eosin Y (5 mol%), DIPEA (2 mmol), in anhyd. DMSO (3 mL), Kessil Blue LED (456 nm with 75% intensity temperature around 60 °C, switching the fan off), argon atmosphere. [b] Yields are obtained after purification over column chromatography.

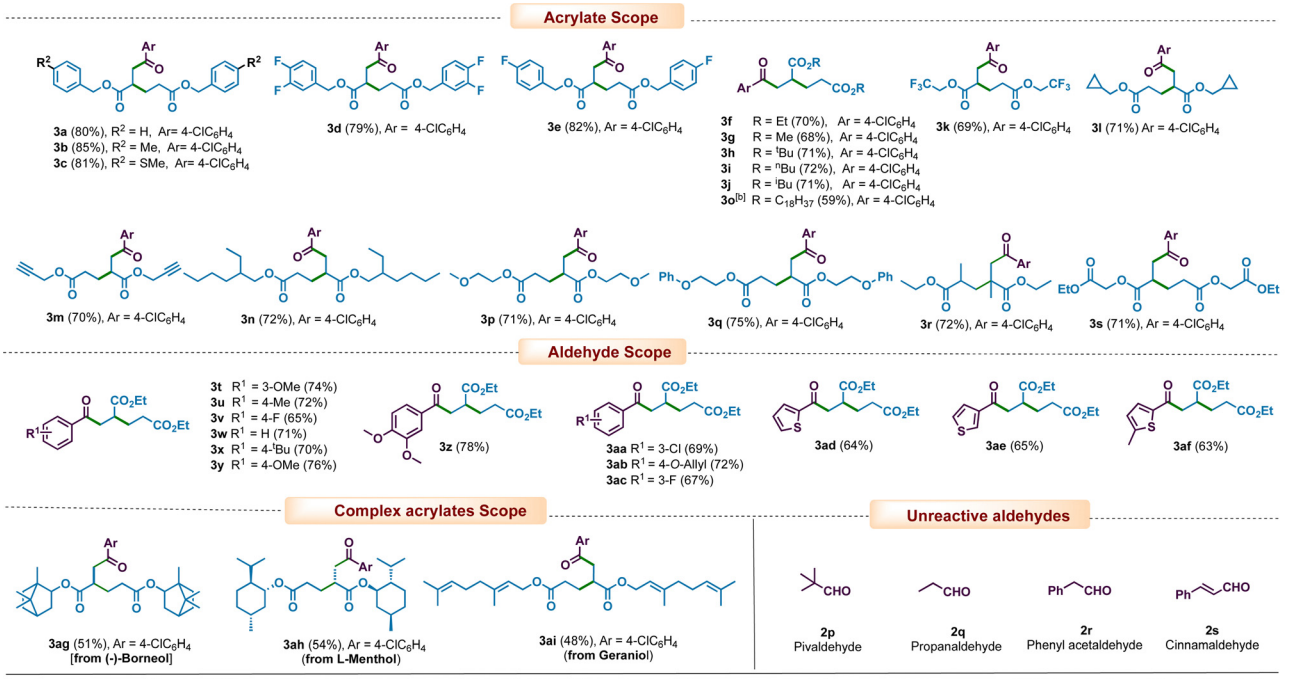
Furthermore, these results clearly proved the necessity of light as well as photocatalyst for the desired transformation. Based on the systematic and exhaustive screening, benzyl acrylate **1a** (1 mmol), 4-chlorobenzaldehyde **2a** (2 mmol), Eosin Y (5 mol%), DIPEA (2 mmol), in DMSO, Blue LED (456 nm) under an inert atmosphere proved to be the optimum reaction conditions.

Having established the optimized reaction conditions, we further evaluated the wider substrate scope of this HAT-catalysed consecutive Giese-type protocol. To begin with we have explored the substrate scope for the different aryl/alkyl acrylates (**1a–1s**) while keeping the 4-chlorobenzaldehyde **2a** as a constant. Different derivatives of benzyl acrylates (**1a–1e**) containing electron-donating as well as electron-withdrawing groups delivered the corresponding desired products (**3a–3e**) in very good yields (up to 85%, Table 2), while the acrylates bearing different alkyl groups (**1f–1o**) such as ethyl, methyl, branched alkyl, cyclopropyl, propargyl, fluoro containing alkyl and long aliphatic chain (stearyl) groups reacted smoothly with **2a** under the optimized reaction conditions to afford the corresponding products (**3f–3o**) in moderate to good yields (up to 72%, Table 2). Even the acrylates containing ether as well as ester moieties and α-substituted acrylates (**1p–1s**) reacted efficiently with **2a** to furnish the desired products (**3p–3s**) in good yields (up to 75%, Table 2). Aromatic aldehydes with electron donating as well as deactivating groups (**2b–2l**) afforded the desired products (**3t–3ac**) in moderate to good yields (Table 2). Moreover, heteroaromatic aldehydes (**2m–2o**) also reacted

 This journal is © The Royal Society of Chemistry 2023

Published on 29 August 2023. Downloaded by Indian Institute of Science Education & Research Pune on 12/25/2023 4:40:20 AM.

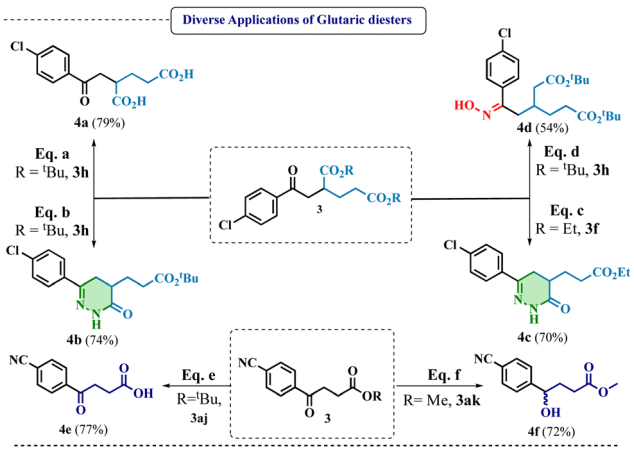
Table 2 Substrate scope



Reaction Conditions: [a]Acrylate **1** (1 mmol), Aldehyde **2** (2 mmol), Eosin Y (5 mol%), DIPEA (2 mmol), using 456 nm light under inert atmosphere (Ar) (temperature ~ 60 °C, keeping fan switched off) in anhydrous DMSO; [b]Anhydrous THF is used instead of DMSO due to lesser solubility.

efficiently with **1f** to furnish the corresponding desired products (**3ad–3af)** in moderate yields (up to 65%, Table 2). Unfortunately, some of the aliphatic aldehydes (**2p–2s**) did not afford the desired products under the reaction conditions (complex mixture observed, Table 2). Gratifyingly, the natural product [L-menthol, (−)-borneol and geraniol] derived acrylates reacted with **2a** to afford the corresponding diesters (**3ag–3ai**) in modest yields (up to 54%, Table 2).

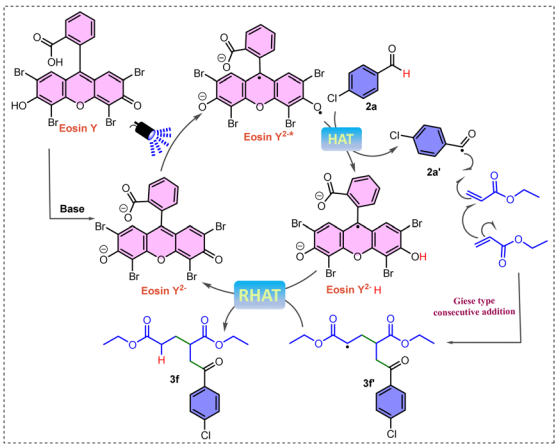
In order to demonstrate the synthetic utility, we further carried out a few transformations utilizing the glutaric diesters **3** (Scheme 2). The diester **3h** upon treatment with TFA/DCM (1 : 1) delivered the corresponding glutaric acid derivative **4a** in a very high yield (Scheme 2, eqn (a)). We further explored the reaction of glutaric diester **3h** and hydrazine under reflux conditions to access 6,4-substituted 4,5-dihydropyridazin-3(2*H*)-one derivative **4b** (Scheme 2, eqn (b)). It is very important to note that pyridazinone derivatives are known for their diverse range of biological and pharmacological activities.[15] Similarly, another pyridazinone derivative **4c** has been synthesized from **3f** (Scheme 2, eqn (c)). Likewise, useful ketoxime derivative **4d** has been synthesized starting from **3h** and hydroxyl amine in *tert*-butanol (Scheme 2, eqn (d)). Furthermore, γ-keto acid **4e** has also been synthesized from glutaric diester derivative **3aj** using TFA/DCM (1 : 1) (Scheme 2, eqn (e)). In order to demonstrate the practical utility of the protocol glutaric diester **3a** has been synthesized in a gram quantity in a good yield (75%, ESI,† S8). We have also performed the reaction under the direct exposure of natural sunlight as a light source, which afforded **3a** in a satisfactory yield (62%, see ESI,† S4). To shed light on the plausible reaction pathway, we carried out



Scheme 2 Post synthetic modifications of glutaric diesters. **Reaction conditions**: (a) **3h** (0.5 mmol), trifluoroacetic acid (TFA)/DCM (1 : 1, 2 mL v/v); (b) **3h** (0.5 mmol), NH_2NH_2 (10 mmol, 0.5 mL) reflux; (c) **3f** (0.5 mmol), NH_2NH_2 (10 mmol, 0.5 mL), reflux; (d) **3h** (0.5 mmol), NH_2OH (1.5 mmol) in *tert*-butanol (2 mL), reflux; (e) **3aj** (1 mmol), trifluoroacetic acid (TFA)/DCM (1 : 1, 2 v/v); (f) **3ak** (1 mmol), $NaBH_4$ (2 equiv. 2 mmol) in methanol (2 mL).

a few control experiments. To begin with we performed the reaction of ethyl acrylate **1f** with deuterated aldehyde **2a-D** under the standard optimized reaction conditions. This led to the deuteration at the C4-position of **3f-D** (85% deuterium incorporation) thus proving that the reaction involves a reverse hydrogen atom transfer (RHAT) process in the catalytic cycle (see ESI,† S5, Scheme S1a). Furthermore, the reaction of **1f** and **2a** in DMSO-D_6 did not furnish any deuterated product **3f**

Published on 29 August 2023. Downloaded by Indian Institute of Science Education & Research Pune on 12/25/2023 4:40:20 AM.



Scheme 3 Plausible reaction mechanism.

(ESI,† S6) proving that the solvent is not the proton source for the desired transformation (see ESI,† S5, Scheme S1b).

Later the addition of D_2O in the reaction mixture of **1f** and **2a** resulted in the deuterium incorporated product **3a-D2** (see Scheme S1c, ESI,†, S5). Interestingly, two relatively more acidic protons of the product got deuterated and this is probably due to the presence of a base. Also, C4-H of product **3a** did not get deuterated and this indicated that no hydrogen–deuterium exchange phenomenon occurred during the catalytic cycle (Scheme S1c, ESI†). Furthermore, the reaction in the presence of TEMPO (1 equiv.) did not work to afford the desired **3f** thus supporting the radical pathway involved during the catalytic cycle (see Scheme S1d, ESI,† S5).

Later, we carried out the light switch on/off experiments (Fig. 3, see ESI,† S21) and calculated the quantum yield (ϕ = 0.56) (see ESI,† S20–S23). These experimental observations proved that the transformation does not involve a radical chain-type mechanism. Furthermore, we performed fluorescence quenching experiments to understand the reaction mechanism (see ESI†, S8–S12). The fluorescence quenching experiment and the Stern–Volmer plot clearly suggested that neither the SET process nor the PCET process is involved during the course of the reaction. Based on the experimental results and other supporting evidence, we proposed that Eosin Y must be acting as a HAT catalyst to drive the reaction. Furthermore, based on our earlier experimental results (Table 1, entries 11 and 12) we believe that the anionic form of Eosin Y must be the active form of Eosin Y during the reaction. We believe that DIPEA might be maintaining the basicity of the reaction medium to ensure the constant availability of the anionic form of Eosin Y. In order to validate this claim, we further measured the pH of the reaction in different conditions during the course of the transformation and also recorded the UV data under different conditions (see ESI,† S6.2, S6.3 and S13–S16).

Based on these detailed experimental results, the most plausible reaction mechanism of the transformation has been depicted in Scheme 3. Neutral Eosin Y in the presence of base DIPEA forms the corresponding di-anionic Eosin Y (Eosin Y^{2-}) (Scheme 3). The photoexcited state of Eosin Y^{2-*} further abstracts a hydrogen (*via* HAT catalysis) from the aldehyde **2a** to form an acyl radical intermediate **2a′**. This intermediate further attacks the ethyl acrylate **1f** *via* a Giese addition manner and consecutively attacks another **1f** molecule to form a radical intermediate **3f′**. This **3f′** further abstracts a hydrogen atom from the EosinY^{2-}-H *via* RHAT catalysis to furnish the desired product **3f** and completes the catalytic cycle by regenerating the Eosin Y^{2-}.

In summary, we have developed a metal-free protocol for synthesizing α-substituted glutaric diesters directly from aldehydes and acrylates. Also method gave an access to 6,4-substituted 4,5-dihydropyridazin-3(2*H*)-one derivatives. It's also scalable on gram quantity and can be carried out under sunlight for sustainability. Our investigation involved various experiments to have an insight into the mechanism.

R. G. B. thanks the Science and Engineering Research Board, Department of Science and Technology (SERB-DST), New Delhi, Government of India (File no. CRG/2019/005753), for the generous research grant. A. B. thanks CSIR, New Delhi for the senior research fellowship. A. C. thanks IISER Pune for the fellowship. S. S. P. thanks UGC, New Delhi for the junior research fellowship.

Conflicts of interest

There are no conflicts to declare.

Notes and references

1 J. Otera and J. Nishikido, Reaction of Alcohols with Carboxylic Acids and their Derivatives, *Esterification: Methods, Reactions, and Applications*, Wiley-VCH, Weinheim, Germany, 2nd edn, 2010, pp. 3–157.
2 (*a*) W. C. Gao, *et al.*, *Org. Chem. Front.*, 2021, **8**, 1275–1279; (*b*) Z. Wang, *et al.*, *Chem. Sci.*, 2020, **11**, 6766–6774.
3 (*a*) M. Whittaker, *et al.*, *Chem. Rev.*, 1999, **99**, 2735–2776; (*b*) A. Cernijenko, *et al.*, *J. Am. Chem. Soc.*, 2016, **138**, 9425–9428; (*c*) R. B. Woodward, *et al.*, *J. Am. Chem. Soc.*, 1951, **73**, 4057.
4 (*a*) S. H. Li, *et al.*, *Org. Lett.*, 2004, **6**, 4327–4330; (*b*) G. Valot, *et al.*, *Angew. Chem., Int. Ed.*, 2013, **52**, 9534–9538.
5 (*a*) C. Che, *et al.*, *J. Org. Chem.*, 2018, **83**, 5665–5673; (*b*) S. F. Kirsch, *Org. Biomol. Chem.*, 2006, **4**, 2076–2080.
6 (*a*) S. Sarkar, *et al.*, *ACS Catal.*, 2019, **9**, 10358–10364; (*b*) B. V. Pati, *et al.*, *Org. Lett.*, 2020, **22**, 2854–2860.
7 P. Werle and M. Morawietz, Alcohols, Polyhydric, *Ullmann's Encyclopedia of Industrial Chemistry*, Wiley-VCH, Weinheim, 2002, DOI: 10.1002/14356007.a01_305.
8 D. L. Danheiser, Organic syntheses: the "Gold Standard" in experimental synthetic organic chemistry, *Org. Synth.*, 2011, **88**, 1–3.
9 D. Seebach, *Angew. Chem., Int. Ed. Engl.*, 1979, **18**, 239.
10 (*a*) H. Maekawa, *et al.*, *Chem. Lett.*, 1991, 1661; (*b*) I. Fussing, *et al.*, *Acta Chem. Scand.*, 1998, **52**, 328.
11 (*a*) J. P. Qu, *et al.*, *J. Org. Chem.*, 2009, **74**, 7684; (*b*) D. Zhang, *et al.*, *J. Org. Chem.*, 2020, **85**, 14262.
12 (*a*) B. Maeda, *et al.*, *Org. Lett.*, 2021, **23**, 5113–5117; (*b*) Y. Zhang, *et al.*, *Org. Lett.*, 2022, **24**, 2679–2683; (*c*) A. Bhowmick, *et al.*, *Org. Chem. Front.*, 2021, **8**, 4777–4784.
13 (*a*) D. A. Nicewicz and T. M. Nguyen, *ACS Catal.*, 2014, **4**, 355–360; (*b*) A. Bhowmick, *et al.*, *Asian J. Org. Chem.*, 2022, **11**, e202200205; (*c*) D. Singla, *et al.*, *Org. Chem. Front.*, 2023, **10**, 237.
14 (*a*) S. Mistry, *et al.*, *Chem. Sci.*, 2022, **13**, 13241–13247; (*b*) A. ElMarrouni, *et al.*, *Chem. Sci.*, 2018, **9**, 6639–6646; (*c*) A. Gualandi, *et al.*, *Chem. Sci.*, 2017, **8**, 1613.
15 (*a*) Y. J. Lim, *et al.*, *Tetrahedron Lett.*, 2003, **44**, 7799–7801; (*b*) W. Akhtar, *et al.*, *Eur. J. Med. Chem.*, 2016, **123**, 256–281; (*c*) Y. Zhou, *et al.*, *J. Org. Chem.*, 2022, **87**, 3677–3685.

 This journal is © The Royal Society of Chemistry 2023

Tetrahedron Letters 61 (2020) 151407

Contents lists available at ScienceDirect

Tetrahedron Letters

journal homepage: www.elsevier.com/locate/tetlet

Visible-light mediated facile dithiane deprotection under metal free conditions

Pankaj D. Dharpure, Anindita Bhowmick, Prakash K. Warghude, Ramakrishna G. Bhat *

Department of Chemistry, Indian Institute of Science Education and Research (IISER)-Pune, Dr. Homi Bhabha Road, Pashan, 411008 Pune, Maharashtra, India

ARTICLE INFO

Article history:
Received 20 August 2019
Revised 13 November 2019
Accepted 14 November 2019
Available online 18 November 2019

Keywords:
Dithiane
Deprotection
Visible-light
Eosin Y

ABSTRACT

Visible light mediated facile and selective dithiane deprotection under metal free conditions is developed. Eosin Y (1 mol%) proved to be an effective catalyst for the dithiane deprotection under the ambient photoredox conditions. The standard household compact fluorescent light source (CFL bulb) proved to be effective under open-air conditions in aqueous acetonitrile at room temperature. The protocol that exhibits a broad substrate scope and functional group tolerance has been shown to expand to a range of transformations for the electron-rich and -deficient thioacetals and thioketals. The synthetic utility of this protocol has also been demonstrated by gram-scale application.

© 2019 Elsevier Ltd. All rights reserved.

Introduction

The dithiane deprotection is one of the most crucial steps in the multistep synthesis of complex molecules. The dithiane protection has been widely explored for altering and masking the reactivity of carbonyl functionality [1]. Due to its high stability under both acidic as well as basic conditions and simple user friendly protection conditions [1,2], dithiane protection has been widely utilized in the synthetic transformations. However, over the years selective deprotection of dithiane under practical and environmentally viable conditions has been a topic of interest for the synthetic community [3]. Many methods have been developed for the dithiane deprotection over the years. Most of these rely on heavy and toxic metals due to their high affinity towards thiols [3–12]. Alternatively, halogenation reagents such as NBS (*N*-bromosuccinimide) [13,14], NCS(*N*-chlorosuccinimide) [13,15] and hypervalent iodine [16] have been explored. Some of the dithiane deprotection protocols have been achieved by using alkylation, [17] oxone [18], selectfluor [19], nitrogen oxide, [20] Dess-Martin periodinane [21] and clayfen [22]. However, some of these methods are either health hazardous and highly oxidizing or require the use of stoichiometric or excess amount of reagents. Similarly, imidazolium ion based organocatalytic deprotection of thioacetals and thioketals require higher temperature and have proven to be inefficient for the sterically crowded thioacetals [23]. In parallel, efforts have also been focused on avoiding the use of heavy metals and strong oxidizing agents by exploring light mediated deprotection of dithianes. UV light has been utilized for the deprotection of dithiane using catalytic amount of methylene blue along with $MgClO_4$ [3b]. Likewise, recently UV light mediated deprotection using excess amount of H_2O_2 in aqueous acetonitrile has been reported [24]. However, unfortunately these protocols are not suitable for sensitive molecules under high energetic UV light thus leading to desired products in moderate yields along with the side products. Kamata and co-workers explored the high intensity xenon and mercury lamps for the dithiane deprotection using different photosensitizers such as 9,10-dicyanoanthracene, methylene green, *meso*-tetraphenylporphine with the limited substrate scope (Scheme 1a) [25–29]. Unfortunately, some of these methods suffer due to their practical limitations to achieve the wider utility of variety of substrates. Interestingly, further efforts have not been devoted to overcome some of these perennial problems. Even though very recently blue LED mediated dithiane and acetal protection of aldehydes and ketones has been reported [30–32], the development of metal free-visible light mediated practical protocol for the dithiane deprotection remains a great challenge.

Visible light mediated metal-free photocatalysis is an emerging area to access useful synthetic precursors under milder reaction conditions [33]. Herein, we report the visible light mediated facile and selective dithiane deprotection under metal-free conditions using Eosin Y (1 mol %) in aqueous acetonitrile at room temperature.

* Corresponding author.
E-mail address: rgb@iiserpune.ac.in (R.G. Bhat).

https://doi.org/10.1016/j.tetlet.2019.151407
0040-4039/© 2019 Elsevier Ltd. All rights reserved.

Tetrahedron Letters 97 (2022) 153791

Contents lists available at ScienceDirect

Tetrahedron Letters

journal homepage: www.elsevier.com/locate/tetlet

Direct access to spirooxindole dihydropyrrole fused pyrazolones and bis-spiropyrazolone derivatives

Prakash K. Warghude, Anindita Bhowmick, Ramakrishna G. Bhat *

Department of Chemistry, Indian Institute of Science Education and Research (IISER)-Pune, Dr. Homi Bhabha Road, Pashan, Pune 411008, Maharashtra, India

ARTICLE INFO

Article history:
Received 24 January 2022
Revised 24 March 2022
Accepted 7 April 2022
Available online 14 April 2022

Keywords:
Annulation
Bis-spiropyrazolones
Diastereoselective
MBH carbonate
Spirooxindole

ABSTRACT

A highly regio- and diastereo-selective [3 + 2] annulation of Morita–Baylis–Hillman carbonates of isatins/pyrazolones with pyrazolone derived ketimines has been developed to access spiroheterocycles. The protocol worked effectively to construct spirooxindole dihydropyrrole fused pyrazolone and bis-spiropyrazolone dihydropyrrole derivatives bearing two vicinal quaternary spirocentres in good to excellent yields with very high diastereoselectivities under mild catalytic condition at room temperature. The protocol proved to be efficient with diverse MBH carbonates and ketimine derivatives. The method has successfully demonstrated the utility of DMAP as the commercially viable catalyst for this transformation.
© 2022 Elsevier Ltd. All rights reserved.

Introduction

Over the years, tremendous efforts have been made to develop new therapeutic agents in modern drug discovery research. The modification of existing pharmacophores by merging two or more biologically active fragments gives an access to new scaffold known as a hybrid molecule [1]. The various hybrid molecules are being explored for their pharmacological properties using *in silico* molecular modelling. Some of the hybridization strategies have contributed to the development of hybrid molecules as new antimicrobials with an ability to overcome resistance [2a], multi-targeted agents for cancer [2b], Alzheimer's [2c] and Plasmodium elicited infections [2d]. The spiroheterocycles have drawn the attention of synthetic organic as well as medicinal chemists due to their biological significane [3]. Among the various spirocyclic compounds, the multi-functional spirooxindoles, spiropyrazolones and spirooxindole fused pyrazolones have gained the greater importance owing to their unique structural framework. A large number of natural products and synthetic products containing the spirocyclic scaffold are known to exhibit remarkable biological activities (Fig. 1) [4–6].

Over the last few years, enormous efforts have been made on the design and synthesis of these structurally diverse and valuable spirocyclic scaffolds in diastereoselective as well as enantioselective manner [7,8]. In 2013, Wang and co-workers have reported the very first organocatalytic Michael–cyclization cascade reaction between 3 and isothiocyanato oxindoles and unsaturated pyrazolones to construct spirooxindole fused pyrazolone compounds via enantioselective [3 + 2] cyclization using chiral tertiary amine derived thiourea catalyst (Scheme 1a) [9]. Subsequent year, Yuan and co-workers have reported a similar protocol to access spirooxindole fused pyrazolones under quinine catalysis [10]. Later, in 2015, Du and co-workers have disclosed the diastereoselective Michael/alkylation cascade reaction of 3-chlorooxindoles and arylidenepyrazolones to achieve the spiropyrazolone-cyclopropane-oxindole derivatives [11]. In 2018, Bao et al. have developed the organocatalytic asymmetric [3 + 2] cyclization for the synthesis of spirooxindole fused pyrazolones using isatin-derived ketimines and 4-isothiocyanato pyrazolones [12]. In 2019, Liu et al. have reported the organocatalytic double Michael tandem strategy for the synthesis of bis-spirocarbocyclic pyrazolones utilizing 3-substituted methyleneoxindole/methylene benzofuranone and bifunctional pyrazolone–chromones (Scheme 1b) [13]. Recently, Du (Scheme 1c) [14] Wang/Yan [15] and Zhong [16] research groups have employed the [3 + 2] annulation strategy to construct the spirooxindole fused spiropyrazonole derivatives. Very recently, our research group [17] has also developed the method for the synthesis of spirooxindole fused spiropyrazolone scaffolds under organocatalytic conditions.

Despite these recent advances in the synthesis of spirooxindole fused pyrazolone derivatives, interestingly, very few methods have been disclosed for the construction of scaffold embedded with three different moieties such as oxindole, dihydropyrrole and pyra-

* Corresponding author.
E-mail address: rgb@iiserpune.ac.in (R.G. Bhat).

https://doi.org/10.1016/j.tetlet.2022.153791
0040-4039/© 2022 Elsevier Ltd. All rights reserved.

Downloaded via IISER PUNE on December 25, 2023 at 04:44:08 (UTC). See https://pubs.acs.org/sharingguidelines for options on how to legitimately share published articles.

JOC The Journal of Organic Chemistry

pubs.acs.org/joc Article

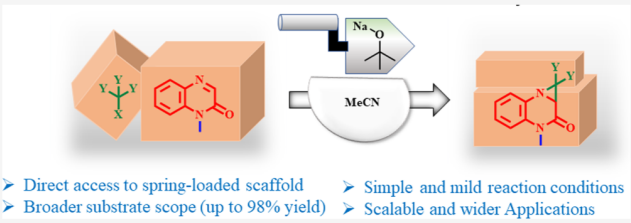
Direct Access to Strained Fused Dihalo-Aziridino Quinoxalinones via C3-Alkylation Followed by Tandem Cyclization

Vikas V. Khade, Anindita Bhowmick, Archana S. Thube, and Ramakrishna G. Bhat*

Cite This: J. Org. Chem. 2023, 88, 8010–8023 Read Online

ACCESS | Metrics & More | Article Recommendations | Supporting Information

ABSTRACT: Quinoxalinones are a privileged class of compounds, and their structural framework is found in many bioactive compounds, natural compounds, and pharmaceuticals. Quinoxalinone is a promising scaffold for different types of functionalization, and the slight modification of the quinoxalinone skeleton is known to offer a wide range of compounds for drug discovery. Owing to the importance of the quinoxalinone scaffold, we have developed a base-mediated protocol for the C3-alkylation of quinoxalinone followed by tandem cyclization to access novel types of strenuous and fused dihalo-aziridino-quinoxalinone heterocycles via the construction of C−C and C−N bonds. The protocol proved to be simple and practical to access desired fused quinoxalinone heterocycles in excellent yields (up to 98% yield). As an application, the highly functionalized fused dihalo-aziridino-quinoxalinone molecule has been further utilized for monodehalogenation under visible light irradiation and selective amide reduction. Moreover, the protocol has also been demonstrated on a gram scale.



INTRODUCTION

Quinoxalin-2(1*H*)-one is one of the important classes of bioactive frameworks that is commonly found in many pharmaceutical compounds. Quinoxalin-2(1*H*)-one-derived compounds are known for their anticonvulsant,[1] antidepression,[2] antibacterial,[3] antiviral,[4] anti-inflammatory,[5] antiallergy,[6] antithrombosis,[7] anti-diabetes,[8] and anti-oxidation[9] properties (Figure 1). Additionally, some of the fused quinoxalin-2(1*H*)-one-derived compounds are also known as kinase inhibitors and antitumor, anticancer, and hepatoprotective agents.[32] Looking at their exceptional biological importance, and in drug discovery and development, even the little modification of the quinoxalin-2(1*H*)-one backbone has been considered as useful as it leads to a wide variety of new chemical entities (NCE) with potential bioactivities. Owing to this, in recent years, the direct C3-H functionalization of quinoxalinone has gained great attention to access novel compounds and to explore potential biological activity for newer targets.[10]

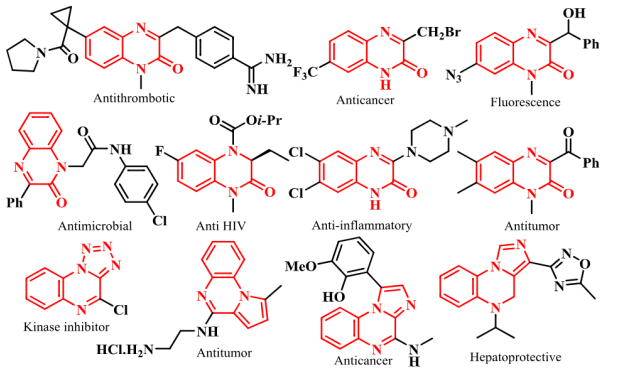


Figure 1. Representative quinoxalin-2(1*H*)-one derivatives with varied biological properties.

Similarly, three-membered *N*-heterocyclic compounds such as aziridines are also known for their intrinsic reactivity due to their steric strain. Aziridines are also widely present in many natural products and biomolecules. They have been utilized in various organic transformations due to their inherent reactivity and to access many interesting compounds.[11] Considering the importance of the quinoxalin-2(1*H*)-one skeleton, many researchers have dedicated their efforts to directly functionalize the quinoxalin-2(1*H*)-one moiety to access different quinoxalinone derivatives.

Many novel, efficient, and sustainable synthetic strategies have been reported for the C3-arylation of quinoxalinones using different reagents such as aryl boronic acids,[12a] arylhydrazines,[12b] diaryliodonium salts,[12c] arylamines,[12d,e] aryl diazonium salts,[12f] and simple arenes (Scheme 1a). The metal-mediated and metal-free approaches have been explored for

Received: January 7, 2023
Published: June 1, 2023



ACS Publications © 2023 American Chemical Society

https://doi.org/10.1021/acs.joc.3c00033
J. Org. Chem. 2023, 88, 8010−8023

RESEARCH ARTICLE doi.org/10.1002/adsc.202300528 Advanced Synthesis & Catalysis

Transient Directing Group Enabled *C3*-(sp^2)–H Alkenylation of Five Membered Heterocyclic Aldehydes: An Access to Mechanochromic Luminogen

Javed Y. Shaikh,[a] Anindita Bhowmick,[a] Abhijit Chatterjee,[a] Nitin A. Thombare,[a] and Ramakrishna G. Bhat[a,*]

[a] Department of Chemistry, Indian Institute of Science Education and Research (IISER)-Pune, Dr. Homi Bhabha Road, Pashan, 411008, Pune, Maharashtra, India
E-mail: rgb@iiserpune.ac.in

Manuscript received: May 19, 2023; Revised manuscript received: July 8, 2023;
Version of record online: August 1, 2023

Supporting information for this article is available on the WWW under https://doi.org/10.1002/adsc.202300528

Abstract: The palladium (II) catalyzed direct C3-(sp^2)–H alkenylation of five membered heterocyclic aldehydes has been developed using 3-aminobutanoic acid as a catalytic transient directing group. A wide range of heterocyclic aldehydes reacted with various acrylates to afford highly site-selective C3-alkenylated products. This method features an exclusive *E*-selective alkenylation at the C3-position of heterocyclic aldehydes with a broad substrate scope. The protocol also proved to be useful to construct the mechanochromic luminogen.

Keywords: Palladium; C–H activation; alkenylation; heterocyclic aldehydes; mechanochromism

Introduction

The alkenyl substituted five membered heterocyclic scaffolds are widely present in a large number of natural products, pharmaceutically active compounds, polymers, dyes and organic functional materials (Figure 1).[1,2] Owing to the importance of this scaffold in organic synthesis and medicinal chemistry, great efforts have been devoted for the development of efficient and succinct protocols for the construction as well as functionalization of heterocyclic scaffolds. In recent years, the transition metal catalyzed alkenylation of five membered heterocyclic scaffolds has become one of the important and most atom- and step-economical approaches in organic synthesis.[3]

The selective C3-alkenylation of five membered heterocyclic scaffolds is quite challenging due to the intrinsic low reactivity at this position. Generally, the palladium catalyzed alkenylation of five membered heterocyclic compounds occurs at C2 and/or C5 positions (α-positions) because five membered heterocyclic rings are chemically more reactive at this position.[4]

In spite of the great significance of C3 alkenylated heterocyclic scaffolds, interestingly only a few literature reports are available for the synthesis of C3 or β-alkenylated five membered heterocyclic derivatives. Some of these protocols relied on cross coupling reactions,[5] C–H activation strategy using different directing groups (fixed at C2 position) such as carboxylic acid,[6] acyl moiety[6] for the direct alkenylation of

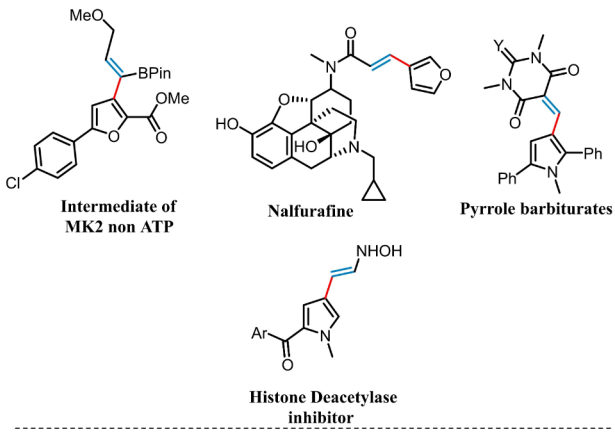


Figure 1. Representative compounds with C3-alkenylated heterocyclic scaffold.

© 2023 Wiley-VCH GmbH

Palladium Catalyzed C3-(sp^2)-H Alkenylation of Pyrroles: A Direct Access to Novel Organic Thermally Activated Delayed Fluorescence (TADF) Materials

Javed Y. Shaikh,[a] Anindita Bhowmick[a,†] Abhijit Chatterjee[a,†] Debasish Laha[a] and Ramakrishna G. Bhat[a]*

Department of Chemistry, Indian Institute of Science Education and Research (IISER) Pune, Dr. Homi Bhabha Road, Pashan, 411008, Pune, Maharashtra, India.
E-mail:rgb@iiserpune.ac.in

Abstract: A Pd (II)-catalyzed direct C3-(sp^2)-H alkenylation of heteroarenes using benzothiazole as a directing group has been successfully achieved. A wide range of 2-*N*-alkylpyrroles undergo an oxidative coupling with a variety of acrylates to furnish highly regio- and chemo-selective *E*-alkenylation products at C3 position. An important intermediate complex has been isolated and characterized so as to have an insight into the mechanism. This convenient protocol proved to practical to access novel thermally activated delayed fluorescence materials (TADF). These molecules proved to be blue emitting TADF materials (~ms life time). A detailed and systematic investigation has been carried out to study the photophysical properties and this has been further validated by the time dependent (TD) density functional theory (DFT) calculations.

Introduction

The five membered heterocyclic scaffold has a great significance as it is found in many pharmaceutically active compounds and therapeutic agents.[1] Among many heteroarenes, pyrrole is one of the most important core scaffolds that is prominently present in pharmaceutically active compounds, marketed drugs such as tolmetin, atorvastatin and ketorolac. Also, many natural products, bioactive molecules, polymers, dyes contain pyrole as a core scaffold.[2,3] Importantly, the histone deacetylase inhibitor and pyrrole barbiturates contain the C3-alkenylated pyrrole core as well.[2,3] Few organic functional materials also contain pyrrole framework.[2,3] Interestingly, benzothiazole derived compounds are known to be biologically active [4] and core to some of the pharmaceuticals. Also, due to fluorescence properties, the benzothiazole scaffold has been explored in optical research and utilized in florescence probes.[5,6] Looking at the importance and applications of these compounds, we planned to design and synthesize the hybrid molecules containing both pyrrole and benzothiazole moieties. We also hypothesized that having an extended delocalization by introducing an olefinic moiety may enhance the photophysical properties of this hybrid core scaffold (Scheme 1b).

In order to construct this proposed hybrid framework, we planned to build the pyrrole-benzothiazole core first followed by the alkenylation based on few parameters. Along with its biological potency and optical properties, benzothiazole has also been explored as a directing group (DG) for C-H activation.[4,7] In this regard, we planned to build the pyrrole-benzothiazole hybrid framework and explore the strength of benzothiazole (as a DG) for the direct alkenylation at suitable position. In the last few years, the transition metal catalyzed alkenylation of five membered heteroarenes have emerged among the most atom- and step-economical approaches in organic synthesis.[8] However, the selective C3-alkenylation of the pyrrole derivatives is relatively difficult due to its low reactivity at this position compared to more reactive C2 and C5 positions as they are located at α-position of the nitrogen in pyrroles.[9] Despite their high significance in pharmaceuticals and their utility in organic synthesis, only a few literature reports are available for the direct C3-alkenylated pyrrole derivatives.[7,10-12] Though some of these methods have their own merits, however some of these have limitations such as relying on pre-functionalized starting materials, necessity of bulky group on the nitrogen and multi-step approaches to access target compounds.[7,10-12]

Interestingly, the alkenylation of the pyrroles by using benzothiazole moiety as a directing group has been rarley explored in the literature. Also there are limited reports on the use of benzothiazole moiety as a directing group for the C-H bond functionalization of aromatic/heteroaromatic compounds.[4,7] In 2017, Peng and coworkers disclosed the *ortho*-alkenylation of the aromatic compounds using benzothiazole as a directing group.[4]

Looking at the limited synthetic strategies using benzothiazole moiety as a directing group, we became more interested to construct the pyrrole-benzothioazole hybrid molecule along with the alkenyl functionality. This would give an opportunity to develop synthetic strategy as well as furnish novel compounds with an extended delocalization to harness the photophysical properties and possible potent bioactivity.

However, the transition metal catalyzed C3-(sp^2)-H alkenyaltion of 2-*N*-alkylpyrrole benzo[d]thiazoles with a variety of acrylates using benzothiazole moiety as a directing group is

https://doi.org/10.26434/chemrxiv-2023-z95xl **ORCID:** https://orcid.org/0000-0002-7739-9553 Content not peer-reviewed by ChemRxiv. **License:** CC BY-NC-ND 4.0